Chapter 11: Weather and climate extreme events in a changing climate

Coordinating Lead Authors:
Sonia I. Seneviratne (Switzerland), Xuebin Zhang (Canada)

Lead Authors:
Muhammad Adnan (Pakistan), Wafae Badi (Morocco), Claudine Dereczynski (Brazil), Alejandro Di Luca (Australia/Argentina), Subimal Ghosh (India), Iskhaq Iskandar (Indonesia), James Kossin (USA), Sophie Lewis (Australia), Friederike Otto (UK/Germany), Izidine Pinto (Mozambique), Masaki Satoh (Japan), Sergio M. Vicente-Serrano (Spain), Michael Wehner (USA), Botao Zhou (China)

Contributing Authors:
Lisa V. Alexander (Australia), Richard Allan (UK), Mansour Almazroui (KSA), Margot Bador (France/Australia), Markus Donat (Germany/Spain), Robert Dunn (UK), Hayley Fowler (UK), Nathan Gillett (Canada), Peter Greve (Germany/Austria), Lofti Halimi (Algeria), Zhenyu Han (China), Mathias Hauser (Switzerland), Yeon-Hee Kim (South Korea), Megan Kirchmeier-Young (Canada/USA), Thomas Knutson (USA), Chao Li (China), Georges-Noel Longandjo (Democratic Republic of Congo), Kathleen McInnes (Australia), Tim R. McVicar (Australia), Seung-Ki Min (Korea), Lincoln Muniz Alvez (Brazil), Jonathan Spinoni (Italy), Qiaohong Sun (Canada/China), Ying Sun (China), Mouhamadou Bamba Sylla (Rwanda/Senegal), Wim Thiery (Belgium), Jessica Tierney (USA), Maarten K. van Aalst (Netherlands), Seth Westra (Australia), Jakob Zscheischler (Germany/Switzerland)

Review Editors:
Johnny Chan (China), Asgeir Sorteberg (Norway), Carolina Vera (Argentina)

Chapter Scientists:
Mathias Hauser (Switzerland), Megan Kirchmeier-Young (Canada/USA), Hui Wan (Canada)

Date of Draft:
01/03/2020

Note:
TSU compiled version

Table Of Content

Executive Summary

This chapter assesses changes in weather and climate extremes with a regional focus, including observed and projected changes, as well as their attribution. The considered extremes include temperature extremes, rainfall extremes, floods, droughts, storms (including tropical cyclones), as well as compound events. Changes in marine extremes, including marine heatwaves, extreme ocean waves and sea level are addressed in Chapter 9 and Cross-chapter Box 9.1. Reliable observations with global coverage are available only after 1950 and for this reason, assessments of past changes and their causes are also from 1950 onward, unless indicated otherwise. Because of the close connection between regional changes in extremes and the level of global warming, future projections are provided as a function of global warming levels. The timing at which global warming levels are reached under different emission scenarios is assessed in Chapter 4. {11.1, 11.2}

There have been major new developments and knowledge advances on changes in weather and climate extremes since the AR5. Evidence of observed changes in extremes and their attribution to human influence have strengthened since the AR5, in particular for extreme precipitation, droughts, tropical cyclones, and compound extremes. There is evidence of an increase in the land area affected by concurrent extremes. {11.1, 11.3, 11.4, 11.5, 11.6, 11.7, 11.8, Box 11.3}

Many of the observed changes in extremes will continue in the future. An additional half degree of global warming would be sufficient to cause further detectable changes in temperature extremes (*virtually certain*) and precipitation extremes (*very likely*) at the global scale. Accumulating evidence continues strengthening our understanding that many of the observed changes in extremes will continue in the future, but future changes in extreme events will be limited if global warming is stabilized to 1.5°C compared to 2°C or higher levels of global warming. Climate models are overall suitable for projections of changes in extremes, but their accuracy depends on the considered extreme. {11.1, 11.3, 11.4, 11.5, 11.6, 11.7}

Temperature extremes

It is *virtually certain* that there has been an increase in the likelihood and severity of hot extremes and a decrease in the likelihood and severity of cold extremes on global scale since 1950. Evidence of changes include an increase in the number of warm days and nights, an increase in the intensity and duration of heatwaves, and a decrease in the number of cold days and nights (*virtually certain)*. Both the coldest extremes and hottest extremes display increasing temperatures (*virtually certain*). The observed trends depend on the observed extreme indices and are clearest for the number of hot days, on all continents (*high confidence*). Trends in temperature extremes are generally larger (by ca. 50% to 200%) than those in global mean temperature, due to larger warming on land and additional feedback effects (*high confidence*). Trends on regional to continental scales are generally consistent with the global-scale trends (*high confidence)*. In a few regions, trends are difficult to assess due to limited data availability, in particular in parts of Africa and Southern America. {11.3, 11.9}

It is *extremely likely* that human influence is the main contributor to the observed increase in the likelihood and severity of hot extremes and the observed decrease in the likelihood and severity of cold extremes on global scales. It is *very likely* that this also applies on continental scale. The available evidence suggests that some recent extreme events could not have occurred without human influence (*medium confidence*). The effect of enhanced greenhouse gas concentrations on extreme temperature are moderated, counteracted or amplified at the regional scale due to feedbacks or forcings such as regional land use and land cover changes, or aerosols. Urbanization has exacerbated the effects of global warming in cities (*high confidence*). Changes in aerosol concentrations have affected trends in hot extremes in some regions, with the presence of aerosols leading to attenuated warming, in particular from 1950-1980. Irrigation and crop expansion have attenuated increases in summer hot extremes in some regions, such as the central North America (*medium confidence)*. {1.3}

It is *virtually certain* that further increases in the likelihood and severity of hot extremes and decreases in the likelihood and severity of cold extremes will occur throughout the 21st century. Such changes are expected at both global and continental scales, and in nearly all inhabited regions[1], if global warming increases to +1.5°C or higher above the preindustrial level, with stronger increases at higher levels of global warming. It is *virtually certain* that the number of hot days and hot nights and the length, frequency, and/or intensity of warm spells or heat waves (defined with respect to late 20th century conditions) will increase over most land areas. In most regions, changes in the magnitude of temperature extremes are proportional to global warming levels (*high confidence*). The likelihood of temperature extremes generally increases exponentially with increasing global warming levels (*high confidence*). {11.3, 11.9}

Heavy precipitation

There is *high confidence* that heavy precipitation has intensified on global scale over land regions. It is *likely* that, since 1950, the annual maximum amount of precipitation falling in a day or over five consecutive days has increased in more regions than it has decreased, over land regions with sufficient observation coverage for assessment. This is also the case at the continental scale over three continents, including North America, Europe, and Asia. Larger percentage increases in heavy precipitation have been observed in the northern high-latitudes in all seasons, as well as in the mid-latitudes in the cold season (*high confidence*). Regional increases in the frequency and/or in the intensity of heavy rainfall have also been observed in i) most parts of Asia, northwest Australia, northern Europe, southeast South America, north South America and most of the United States (*high confidence*), and ii) west and southern Africa, central Europe, eastern Mediterranean region, Mexico (*medium confidence*). Elsewhere, there is generally *low confidence* in observed trends in heavy precipitation due to data limitations. {11.4, 11.9}

It is *likely* that anthropogenic influence is the main cause of the observed intensification of heavy precipitation in land regions.The evidence includes attribution of the observed global increase in annual maximum one-day and five-day precipitation to human influence (*high confidence*), a large fraction of land showed enhanced extreme precipitation, and larger probability in record-breaking one-day precipitation. At continental and regional scales, human influence on extreme precipitation is less detectable because of higher variability, but evidence is emerging. There is evidence of human influence on intensification of extreme precipitation in North America, and a human contribution to the increase in the probability or magnitude of some individual extreme precipitation events in different parts of the world. {11.4}

Over almost all land regions, it is *very likely* thatextreme precipitation will be more intense and more frequent in a warmer world. The increase in the magnitude of extreme precipitation will be, in general, proportional to the global warming level, with an increase of 7% and a slightly smaller rate in the 50-yr event of annual maximum 1-day and 5-day precipitation per 1°C warming, respectively (*high confidence*). The increase in the likelihood of extreme precipitation will *very likely*accelerate with increased global warming, with larger incremental increases at higher global warming levels, and for rarer events. There can be large differences in the increase regionally. {11.4}

Floods and water logging

There is *high confidence* that the seasonality of flood has changed in cold regions where snow-melt is involved. There is *high confidence* that significant trends in peak streamflow have been observed in some regions over the past decades, including increases in parts of northern Asia, southern South America, northeast US, UK, and the Amazon and decreases in parts of the Mediterranean, northeastern Brazil, southern Australia, central China, southeastern US. There is *low confidence* in attributing changes in the probability or magnitude of individual floods to human influences. {11.5}

There is *high confidence* in an increase in flood potential in urban areas where extreme precipitation is projected to increase, especially at high global warming levels. Global hydrological models project a

[1] See Figure 1.16 in Chapter 1 for definition.

larger fraction of the land areas to be affected by an increase in river floods than by a decrease in river floods (*medium confidence)*. There is *medium confidence* that river floods will increase in the western Amazon, the Andes, and northern Eurasia. Regional changes in river floods are more uncertain because complex hydrological processes are involved. {11.5}

Droughts

Different drought types (related to precipitation deficits, soil moisture deficits, streamflow deficits or increased atmospheric evaporative demand) are associated with different impacts and respond differently to increased greenhouse gas forcing. Observed trends in drought measures are highly regional, with increases in some regions and decreases in others. Atmospheric evaporative demand displays a global drying tendency over continents, and there is an observed tendency towards increased drying in the dry season since the beginning of the 20th century, when aggregated on global scale. There is *high confidence* (*medium confidence*) that precipitation deficits have increased since the mid 20th century in west Africa, central Africa, and southern Africa (Northeastern Brazil). There is *medium confidence* that soil moisture deficits have increased in east Asia, central Europe, the Mediterranean region, and northwest North America. There is *medium confidence* that some regions show more frequent hydrological droughts (e.g., southern Africa, southern North America, the Mediterranean region). There is *medium confidence* that trends in potential evaporation have exceeded trends in precipitation in some regions and seasons. There is overall *medium confidence* in the ability of available models (climate, land surface or hydrological models) to simulate trends and anomalies in precipitation deficits, soil moisture deficits, streamflow deficits, or atmospheric dryness on global and regional scales. {11.6}

There is *high confidence* that human influence has increased the potential for worsening of drought conditions and increased the tendency towards drying in the dry season since the beginning of the 20th century, when aggregated on the global scale. The drying tendency is dominated by warming- and radiation-induced increase in evaporative demand rather than by changes in precipitation. At local to regional scales, human influence on drought and water scarcity is complex, as it includes climate forcing, land use changes, water management, and socio-economical influences. There is *low confidence* in the contribution of greenhouse gas forcing to changes in atmospheric circulation processes affecting drought.{11.6}

There is *high confidence* that atmospheric evaporative demand will continue to increase with increasing global warming and lead to further drying tendencies in some regions. There is *medium confidence* in projected increases in the frequency and severity of precipitation, soil moisture, and streamflow deficits in the Mediterranean region, southern Africa, southern North America, central America and northeastern Brazil. While there is high agreement among climate models, there are uncertainties in drought representation in climate models, the use of drought metrics in projections, and a lack of observations in several regions to evaluate models. In addition, there is *medium confidence* that soil moisture and streamflow deficits may also be affected by physiological CO_2 effects on plants' transpiration under enhanced CO_2 concentrations. Projections of soil moisture deficits show stronger increases in drought area and severity than projections of changes in precipitation deficits (*medium confidence*). These projections are strongly dependent on the warming scenario considered, with stronger drought trends for higher warming levels, even for changes as small as 0.5°C in global warming (*high confidence*). Some regions with humid or transitional climate characteristics in the 20th century are projected to become drier (*medium confidence*). {11.6}

Storms

There is *medium confidence* that the global proportion of stronger tropical cyclones (TCs) has increased detectably over the past 40 years. The average location of peak TC wind-intensity has migrated poleward in the western North Pacific Ocean since the 1940s, substantially increasing TC exposure at higher latitudes. It is unlikely that the observational evidence for a migration is the result of data artefacts, and there is *medium confidence* that it cannot be explained by natural variability

{11.7.1}. There is *medium confidence* that TC forward motion (translation speed) has slowed detectably over the U.S. since 1900, but *low confidence* for a global signal because of the potential for data heterogeneity {11.7.1}. There is *low confidence* in the cause of the slowdown in any region due to a lack of robust agreement among models that simulate TCs, although the slowdown is consistent with theory and modelling studies that indicate a general slowing of atmospheric circulation with warming {11.7.1}. There is *low confidence* in past trends in characteristics of severe convective storms such as hail and severe thunderstorm winds {11.7.3}.

There is *high confidence* that average peak TC wind speeds and the proportion of Category 4-5 TCs will increase globally with warming {11.7.1}. There is *medium confidence* that the average location where TCs reach their maximum wind-intensity will migrate poleward in the western North Pacific Ocean as the tropics expand with warming {11.7.1}. There is *medium confidence* that the global frequency of TCs over all categories will decrease or remain unchanged {11.7.1}. There is *medium confidence* that wind speeds associated with extratropical cyclones will change following changes in the storm tracks, with increases/decreases depending on the region being considered {11.7.2}. There is *medium confidence* that the frequency of springtime severe convective storms will increase, leading to a lengthening of the severe convective storm season {11.7.3}.

There is *high confidence* that the average and maximum rain-rates associated with tropical and extratropical cyclones, atmospheric rivers and severe convective storms will increase as atmospheric water vapour increases with warming {11.7.1, 11.7.2, 11.7.3}. There is *medium confidence* that peak TC rain-rates will increase at greater than the Clausius-Clapeyron scaling rate of 7% per °C of warming in some regions due to increased low-level moisture convergence caused by regional increases in TC windintensity {11.7.1}. There is *high confidence* that the magnitude of the increase in precipitation depends on the horizontal resolution and the specific representation of convective processes in climate models due to the effect of fine-scale dynamical feedbacks {11.7.1, 11.7.2, 11.7.3}.

Compound events

There is *high confidence* that concurrent heatwaves and droughts have become more frequent and that this trend will continue under higher levels of global warming. There is *high confidence* that concurrent extremes events at different locations, but possibly affecting similar sectors (e.g., breadbaskets) in different regions, will become more frequent at higher levels of warming, in particular above 2°C of global warming. There is *medium confidence* that the likelihood of compound flooding (storm surge, extreme rainfall and/or river flow) has increased in some locations, and will continue to increase due to both sea level rise and increases in heavy precipitation. There is *medium confidence* that wildfire (compound hot and dry event) risk has increased in some regions over the last century. There is *medium confidence* that various risks of other compound events will increase under higher levels of global warming. {11.8, Box 11.3, Box 11.4}.

Limits to the assessment

There are currently several knowledge gaps associated with assessments on changes in the dynamics driving extreme events in past and future. Some topics are still insufficiently investigated such as hail, and there are some remaining uncertainties regarding changes in some extremes such as droughts and tropical cyclones, although evidence have become much more robust in these areas compared to the AR5. Also, there is *low confidence* regarding the global warming levels at which possible changes associated with global and regional tipping points (low-probability high-impact events)related to extremes would occur, but these cannot be excluded, especially at high global warming levels (>3°C). Finally, there are still remaining important data and literature gaps in several regions of the world, in particular in Africa and south America. {11.10}

11.1 Framing

11.1.1 Introduction to the chapter

This chapter provides assessments on changes in weather and climate extremes (collectively referred to as extremes) with a focus on the relevance to the Working Group II assessment. Here, we assess observed changes, their attribution to causes, and future projections. The occurrence of extremes in an environment with exposed and vulnerable human and natural systems can lead to disasters (IPCC, 2012). Changes in extremes result in changes in impacts not only as a direct consequence of changes in the magnitude and frequency of extremes (which are termed "hazards" in a risk framework, see also Chapter 12), but also through their influence on exposure and resilience. As such, extremes are an essential component assessed in sucessive IPCC reports. The Special Report on Managing the Risks of Extreme Events and Disasters to Advance Climate Change Adaptation (referred as the SREX report, IPCC, 2012) provided a comprehensive assessment on changes in extremes and how exposure and vulnerability to extremes determine the impacts and likelihood of disasters. Chapter 3 of that report (Seneviratne et al., 2012a, hereafter also referred to as SREX Chapter 3) assessed physical aspects of extremes, and laid a foundation for the follow-up assessments of changes in extremes including the IPCC Working Group I 5th Assessment report (IPCC AR5; IPCC, 2013), and the recent IPCC special reports on 1.5°C global warming (SR1.5, IPCC, 2018), on climate change and land (IPCC, 2019a), and on oceans and the cryosphere (IPCC, 2019b). These assessments are the starting point of the present assessment.

The AR6 WGI report dedicates this chapter to assess past and projected changes in extremes. This chapter is also one of the three "regional chapters" of the WGI report (along with Chapters 10 and 12). We assess changes in extremes from a global and continental perspective to provide a large-scale context, and the assessment also has a regional focus paying particular attention to changes in extremes at regional scales. The approach taken in the AR6 WGI report for the assessment of changes in extremes is different from that in the AR5 WGI report. The assessments in the AR5 were spread throughout various chapters including observed changes (Hartmann et al., 2013), the evaluation of models' performance in simulating extremes (Flato et al., 2013), the detection and attribution of changes in extremes to causes (Bindoff et al., 2013), and long-term projections in extremes (Collins et al., 2013a). The AR5 assessments were also at large scales in general. The types of extremes assessed in the AR5 are similar to those assessed in the SREX Chapter 3. We adapt the general approach used in SREX Chapter 3 regarding the types of extremes assessed and the presentation of the assessment. This provides a traceability and basis for comparison to earlier assessments. Note that this chapter does not assess impacts, which are covered in the WGII report. Chapter 10 of this report provides a framework for understaning regional changes. Chapter 12 translates the assessment of changes in extremes provided here into changes in metrics that quantify impact-relevant hazards, supplemented by assessments of other hazards and supported by the Atlas, providing a key handshake with the WGII report.

This chapter is structured as follows. This Section (11.1) provides a general framing and introduction for the chapter, highlighting key aspects that underlie the confidence and uncertainty in the assessment of changes in extremes, and introducing some main elements of the chapter. Section 11.2 introduces methodological aspects of research on climate extremes. Sections 11.3 to 11.7 assess past changes and their attribution to causes, and projected future changes in extremes, for different types of extremes, such as temperature extremes, heavy precipitation, floods, droughts, and storms in separate sections. Section 11.8 addresses compound events or multivariate extremes. Section 11.9 summarizes regional information on extremes by continents in tables. Finally, Section 11.10 provides a brief summary of current knowledge gaps in the field. The chapter also entails several boxes and FAQs to more specific topics.

11.1.2 What is an extreme event and how is its change studied?

The risk framework defined in the SREX report (IPCC, 2012) articulates clearly that the exposure and vulnerability to hazards such as extremes determine the magnitude of impacts, and that adaptation that reduces exposure and vulnerability will increase resilience resulting in a reduction in impacts. There is thus not always a one-to-one correspondence between the weather and climate extremes and extreme impacts. Consequently, when assessing changes in extremes in this chapter, we focus on physical aspects of extremes rather than on their impacts, which are assessed in the WGII report. Building on the SREX report, the AR5 defined an extreme weather event as "an event that is rare at a particular place and time of year" and an extreme climate event as "a pattern of extreme weather that persists for some time, such as a season" (AR5 Glossary). These definitions are adopted here. Yet, there is no clear-cut distinction between an extreme weather event and an extreme climate event, although usage implies that they are of different space and time scales in general. An extreme weather event typically has a weather scale (from minutes to days, such as a storm) while an extreme climate event typically has a climate scale (months or years, such as a drought). For simplicity, here we collectively refer to weather and climate extremes as "extremes" or "extreme events". The definitions of rare are wide ranging, depending on applications. Some studies consider an event as an extreme if it is unprecedented; on the other hand, other studies consider events that occur several times a year as moderate extreme events. Rarity of an event with a fixed magnitude also changes in the changing climate. For example, the 2013 summer temperature was the hottest on record at the time, but it has a recourrence interval of about 4 years in the climate of 2013 (Sun et al., 2014).

In the literature, an event is generally considered as extreme if the value of a variable exceeds (or lies below) a threshold. The thresholds have been defined in different ways, leading to differences in the meaning of extremes that may share the same name. For example, two sets of frequency of hot/warm days have been used in the literature. One set counts the number of days when maximum daily temperature is above a relative threshold defined as the 90th or higher percentile of maximum daily temperature for the calendar day over a base period. An event based on such a definition can occur during any time of the year and the impact of such an event would differ depending on the season. The other set counts the number of days in which maximum daily temperature is above an absolute threshold such as 35°C, as exceedance of this temperature can sometimes cause health impacts (however, these impacts may depend on location and whether ecosystems and the population are adapted to such temperatures). While both types of hot extreme indices have been used to analyze changes in the frequency of hot/warm events, they represent different events that occur at different times of the year, possibly affected by different types of processes and mechanisms, and possibly also associated with different impacts.

Changes in extremes have also been examined from two perspectives: changes in the frequency for a given magnitude of extremes or changes in the magnitude for a particular return period (frequency). Changes in the probability of extremes (e.g., temperature extremes) are dependent on the rarity of the extreme event that is assessed, with a larger change in the probability associated with a rarer event (e.g., Kharin et al., 2018). On the other hand, changes in the magnitude represented by the return levels of the extreme events may not be as sensitive to the rarity of the event. While the answers to the two different questions are related, their relevance to different audiences may differ. Conclusions regarding the respective contribution of greenhouse gas forcing to changes in magnitude versus frequency of extremes may also differ (Otto et al., 2012). Correspondingly, the sensitivity of changes in extremes to increasing global warming is also dependent on the definition of considered extremes. In the case of temperature extremes, changes in magnitude have been shown to often depend linearly on global temperature (Seneviratne et al., 2016; Wartenburger et al., 2017), while changes in frequency tend to be non-linear and can, for example, be exponential for increasing global warming levels (Fischer and Knutti, 2015; Kharin et al., 2018). When similar damage occurs once a fixed threshold is exceeded, it is more important to ask a question regarding changes in the frequency. But when the exendance of this fixed threshold becomes a normal occurrence in the future, this can lead to a saturation in the change of probability (Harrington and Otto, 2018a). On the other hand, if the impact of an event increases with the intensity of the event, it would be more relevant to examine changes in the magnitude. Finally, adaptation to climate change might change the relevant thresholds over time, although such aspects are still rarely integrated in the assessment of projected changes in extremes. Framing, including how extremes are defined and how the questions are asked in the literature, is considered when forming our assessments.

11.1.3 Types of extremes assessed in this chapter

The types of extremes and phenomena assessed in this chapter include temperature and precipitation extremes, drought, floods, tropical cyclones, and severe convective storms. In addition, we also consider compound events, i.e. bivariate or multivariate extreme events. We consider these types of extremes because of their relevance to impacts as well as the availability of literature on the subject. Most of the considered extremes were also assessed in the SREX and the AR5. Compound events were not assessed in detail in past IPCC reports, although the SREX briefly addressed this topic (SREX Chapter 3). Marine-related extremes such as marine heat waves and extreme sea level, are assessed in Chapter 9 (Cross-chapter box 9.1) of this report.

Extreme phenomena in the atmosphere are of different spatial and temporal scales. Tornadoes have a spatial scale as small as less than 100 meters and a temporal scale as short as a few minutes. In contrast, a drought can last for multiple years, affecting a whole continent. The level of complexity of the involved processes differs from one type of extreme to another, affecting our capability in detecting and attributing, and in projecting changes in weather and climate extremes. Temperature and precipitation extremes studied in the literature are often based on extremes derived from daily values, such as annual maxima or minima of daily temperatures, annual counts of daily temperature above or below certain percentiles, duration of heatwaves based on daily temperature data, annual maximum one-day or five-day precipitation events. Studies of events on longer time scales for both temperature or precipitation, or on sub-daily extremes are scarcer, which generally limits the assessment for such events. Nevertheless, extremes on time scales different from daily are assessed, when possible. We assess drought and tropical and extratropical cyclones as phenomena in general, not limited by their extreme forms, because these phenomena are relevant to impacts. We also consider both precipitation and wind extremes associated with storms.

Multiple stressors can come together to yield more extreme hazards and/or exhaust the adaptative capacity of a system more quickly. For this reason, the occurrence of multiple extremes that are multivariate and/or concurrent and/or in succession, which are the so-called "compound events" (SREX Chapter 3), can lead to impacts that are much larger than the sum of the impacts from the occurrence of individual extremes in isolation (see Section 11.8, and also Chapter 12). For this reason, compound events are assessed in as much depth as the literature allows (Section 11.8).

The assessment of projected future changes is presented as function of different levels of global warming (Section 11.2.6). This is to provide traceability and comparison to the SR15 assessment (Hoegh-Guldberg et al., 2018, hereafter referred to as SR15 Chapter 3). This shall also be useful for decision makers as actionable information, as much of the mitigation policy discussion and adaptation planning can be tied to the level of global warming. For example, regional changes in extremes, and thus their impacts, can be linked to global mitigation efforts. Additionally, there is also an advantage of separating uncertainty in future projections due to natural internal variability from other factors such as differences in model sensitivities and emission scenarios. However, some analyses related to specific emissions scenarios are also provided based on CMIP6 simulations to fascilitate easier comparsion with the AR5 assessment.

A global-scale synthesis of this chapter's assessments is provided in Section 11.1.7. In particular, Tables 11.1 and 11.2 provide a synthesis for observed and attributed changes and projected changes in extremes, respectively, at different levels of global warming. Tables for regional-scale assessments are provided in Section 11.9.

11.1.4 Effects of greenhouse gas and other external forcings on extremes

External forcings such as human emissions of greenhouse gases are the main drivers of the past and future changes in the climate. They are also the main drivers of the changes in extremes, at least globally, as extremes are an integral part of the climate system. The SREX, AR5, and SR15 reports assessed that there is evidence from observations that some extremes have changed since the mid 20[th] century, that some of the changes are a result of anthropogenic influences, and that some observed changes are projected to continue into the future, while other changes are projected to emerge from natural climate variability under enhanced global warming (SREX Chapter 3, AR5 Chapter 10; see also 11.1.3).

At the global and continental scales and at the regional scale to some extent, much of the changes in extremes are a direct consequence of the enhanced radiative forcing, and the associated global warming and/or its resultant increase in the water-holding capacity of the atmosphere as well as changes in vertical statbility and meridional temperature gradients that affect climate dynamics (see Box 11.1 on Thermodynamic vs Dynamic processes). Widespread observed and projected increases in hot extremes and decreases in cold extremes are consistent with global and regional warming (Section 11.3). Increases in the magnitude of annual maximum daily maximum temperatures and in annual minimum daily minimum temperatures scale robustly and in general linearly with the global mean temperature increase across different geographical regions and different emission scenarios (Seneviratne et al., 2016; Wartenburger et al., 2017; Kharin et al., 2018; for more details see Section 11.2.6), whereby extreme temperatures on land tend to increase more than the mean global temperature (Fig 11.1), due in large part to the land-sea contrast, and additionally to regional feedbacks in some regions (Section 11.1.6) The number of heatwave days and the length of heatwave seasons in various regions also scale well, but non-linearly (because of the threshold effect) with global mean temperatures (Wartenburger et al., 2017; Sun et al., 2018a). Changes in annual maximum one-day precipitation are proportional to global mean temperature changes, at about 7% increase per 1°C temperature increase, i.e. following the Clausius-Clapeyron relationship (Box 11.1), in the observations (Westra et al., 2013) and in future projections (Kharin et al., 2013) at the global scale. Extreme short-duration precipitation in North America also scales with global mean temperature (Li et al., 2018a; Prein et al., 2016b). At the local and regional scales, changes in extremes are also strongly modulated and controlled by regional forcings and feedback mechanisms (Section 11.1.6), whereby some regional forcings, e.g., associated with land use/albedo or aerosol emissions, can have non-local or some (non-homogeneous) global-scale effects (Persad and Caldeira, 2018; Seneviratne et al., 2018a). In general, there is *high confidence* in changes in extremes due to global-scale thermodynamic processes (i.e. mean global warming, mean moisterning of the air) as the processes are well understood, while the confidence of those related to dynamic processes or regional and local forcing, including regional and local thermodynamic processes, are much lower due to multiple factors (see two following sub-sections and Box 11.1).

[START FIGURE 11.1 HERE]

Figure 11.1: Time series of temperature anomalies (relative to 1979-2018 mean) for global average annual mean temperature (T_global), land average annual mean temperature (T_land) and extreme temperatures fromCMIP5 and CMIP6 simulations, and from observations and a reanalysis data product. Extreme temperatures include annual maximum daily maximum temperature (TXx) and the annual 95th percentile of daily maximum temperature (TXp95). Grey shading mark the reference period 1979-2018. (a) and (b), temperatures from CMIP5 and CMIP6 simulations, respectively. Solid lines are multi-model averages while the blue shading shows the multiple range of global mean temperature by all models. CMIP5 temperatures include the models' historical simulations and future projection under RCP4.5 forcing scenario. CMIP6 temperatures include the models' historical simulations and future projections under the SSP2-4.5 forcing scenario (note that RCP4.5 and SSP2-4.5 do not share the same forcing). (c) Observed temperatures based on HadCRUT4 and temperatures computed from ERA–Interim reanalysis.

[END FIGURE 11.1 HERE]

Since the AR5, the attribution of extreme weather events, or the investigation of changes in the frequency or magnitude of individual and local- and regional-scale extreme weather events due to various drivers (see Cross Chapter Box 1.4, Section 11.2.5) has provided evidence that greenhouse gases and other external forcings have affected individual extreme weather events. The events that have been studied are geographically uneven. A few events, e.g., extreme rainfall events in the UK (Schaller et al., 2016; Vautard et al., 2016; Otto et al., 2018b) or heat waves in Australia (King et al., 2014; Perkins-Kirkpatrick et al., 2016; Lewis et al., 2017b), have spurred more studies than other events. Many highly impactful extreme weather events have not been studied in the event attribution framework due to various reasons including lack of observational data (Section 11.2), lack of reliable climate models (Section 11.2.3), and lack of scientific capacity (Otto et al., submitted, b). While the events that have been studied are not representative of all extreme events that occurred and results from these studies may also be subject to selection bias, the large number of event attribution studies provide evidence that changes in the properities of these local and individual events are in line with expected consequences of anthropogenic influence on the climate and can be attributed to external drivers. Fig 11.2 provides a synthesized assessment of the existing event attribution literature to date.

[START FIGURE 11.2 HERE]

Figure 11.2: Synthesis of event attribution literature. The symbols depict types of extreme events for which one or more such events have been studied in the event attribution framework (see Appendix A.1). The location of symbols does not indicate the places of the event occurrence as the symbols represent the synthesized assessment of all studies for the same type of events occurring in the region. The arrows indicate the direction of changes in the intensity and likelihood of the events due to anthropogenic climate change. A "mixed signal" indicates that different studies found different results regarding the direction of changes in magnitude and frequency, depending on the definition of the event (Section 11.2.5).

[END FIGURE 11.2 HERE]

[START BOX 11.1 HERE]

BOX 11.1: Thermodynamic and dynamic changes across scales

Changes in weather and climate extremes result from the combined effect of changes related to atmospheric or oceanic motions (dynamic changes) and those associated with local exchanges of heat, moisture, and other quantities (thermodynamic changes). While thermodynamic and dynamic processes are necessarily interconnected, considering them separately may allow disentangling roles of different processes contributing to the changes in climate extremes as a result of greenhouse forcing and internal climate variability (e.g., Shepherd, 2014). The AR5 used the dynamic and thermodynamic framework when placing the level of confidence in the projected patterns of precipitation change (Collins et al., 2013a).

Temperature extremes

An increase in the concentration of greenhouse gases in the atmosphere leads to warming of air and the Earth's surface. This direct thermodynamic effect produces a shift of the temperature distribution towards a warmer state, leading to an increase in the frequency and intensity of warm extremes and a decrease in the frequency and intensity of cold extremes. The initial increase in temperature in turn leads to other thermodynamic responses and feedbacks, such as an increase in the water vapour content of the atmosphere (water vapour feedback, see Section 7.4.2.2) and changes in vertical temperature profiles (e.g., lapse rate feedback, see Section 7.4.2.2). While the water vapour feedback always contributes to temperature increases (positive feedback), the sign and magnitude of the lapse rate feedback depends on the sign of the change in the lapse rate and leads to near-surface temperature increases in mid and high latitudes and decreases in tropical regions (Pithan and Mauritsen, 2014).

The initial temperature increase near the surface can also trigger other positive land surface feedbacks such as the snow-ice albedo feedback (see Section 7.4.2.3) and soil-moisture feedbacks, both of which are characterised by a strong seasonal and regional dependence. For instance, Arctic amplification occurs due to the combined effect of several feedback processes, including snow-ice albedo, water vapour and lapse-rate feedbacks (see Section 7.6.2.1 for details), which leads to increases in winter Arctic temperature extremes being three times as large as global mean changes (*high confidence*, Section 11.3). In some midlatitude areas such as the Mediterranean, temperature increases are amplified by the stabilizing effect of changes in temperature lapse rates (Kröner et al., 2016; Brogli et al., 2018) and by the higher atmospheric moisture demand combined with a decrease in precipitation that results in a drying of the soils leading to enhanced sensible heat fluxes and thus a further heating of the air immediately above. These changes lead to a positive, i.e self-enhancing, soil-moisture temperature feedback process (Seneviratne et al., 2010; Vogel et al., 2017) and thus larger increases in warm temperature extremes and decreases in cold temperature extremes. The soil moisture-temperature feedback can also include further decrease of cloud cover (increasing incident shortwave radiation) as a result of decreased evapotranspiration input from the land surface (Vogel et al., 2018). Greenhouse gases also have direct and indirect radiative forcing on regional land temperatures due to physiological responses of plants to the increase in CO_2(Lemordant et al., 2016; Swann et al., 2016; Section 11.6).

Changes in the spatial distribution of temperatures can in turn lead to changes in the large-scale atmospheric circulation (dynamics) and the characteristics of synoptic perturbations leading to further changes in warm and cold temperature extremes. For example, polar amplification has been linked with a weakening of the summer circulation in the Northern Hemisphere with weaker cyclone activity and an increase in the persistence of heatwaves which could explain some of the summer temperature increases over the last four decades (Coumou et al., 2015, 2018; Mann et al., 2017), although there is only *low confidence* in these changes in atmospheric circulation patterns and their persistence characteristics (Section 11.1.5).

Precipitation extremes

The thermodynamic vs. dynamic decomposition framework has been used to understand the observed and projected future changes in precipitation extremes (Byrne and O'Gorman, 2015; O'Gorman, 2015; Trenberth et al., 2015; Vautard et al., 2016; Pfahl et al., 2017). Changes in water vapour have been shown to be controlled by temperature changes through increases in evaporation and in the water-holding capacity of the atmosphere (e.g., Trenberth, 1999). As a result, water vapour content at the global scale increases roughly following the Clausius-Clapeyron (C-C) relation, with an increase of approximately 7 % for every degree of global-mean surface warming (Held and Soden, 2006; O'Gorman and Schneider, 2009). Nonetheless, increases at regional scales may differ from this C-C rate because regions with temperature increases stronger than the global mean would have larger increases in the atmospheric water-holding capacity. Additionally, regional differences from the global rate may occur because atmospheric moisture over land may be more limited in the future due to decreases in evapotranspiration rates (from land-atmosphere feedbacks and CO_2 effects on photosynthesis, Berg et al. 2016) and decreases in moisture supply from the ocean (Byrne and O'Gorman, 2018)

CMIP3 and CMIP5 models consistently project increases in global-scale atmospheric moisture at a rate close to that determined by the C-C relationship. The thermodynamic contribution would lead to precipitation extremes increasing at a similar rate as atmospheric moisture: around 7 % per degree of surface warming. Some studies (Westra et al., 2013; Fischer and Knutti, 2016) have shown that the observed rate of increase of precipitation extremes is similar to the C-C scaling, but this agreement seems to result from large regional compensations (e.g., Westra et al., 2013). At regional scales, dynamic effects can be substantial and strongly modify the rate of change of extreme precipitation compared to the thermodynamic contribution (Pfahl et al., 2017; Guerreiro et al., 2018b). Dynamic contributions to changes in precipitation extremes are ultimately related to changes in the magnitude and distribution of atmospheric vertical motion. Vertical velocities can be influenced by changes in large-scale conditions (i.e., circulation patterns and static stability) and by changes occurring within the storm (e.g., Pendergrass, 2018). Large-scale changes in the vertical and horizontal distribution of temperature (thermodynamics) lead to modifications in hydrodynamic instabilities affecting atmospheric motions (dynamics) from a range of synoptic and subsynoptic phenomena including tropical cyclones, extratropical cyclones, fronts, mesoscale-convective systems and thunderstorms. There is *medium confidence* in the magnitude and direction of current and future changes in these phenomena. This is because changes in atmospheric circulation occur as an indirect effect of thermodynamic changes. This is also because the circulation effects in synoptic and subsynoptic phenomena are usually complex due to the interplay between several large-scale drivers that often have opposing influences (e.g., Shaw et al., 2016).

Therefore, changes in extremes due to dynamic contributions show large differences across models and are more uncertain than those due to thermodynamic contributions (Shepherd, 2014; Trenberth et al., 2015; Pfahl et al., 2017). Nevertheless, there is consistency among model simulations that dynamic contributions can lead to increases in some regions but decreases in other regions on the backdrop of the thermodynamic contribution (Norris et al., 2019; Pfahl et al., 2017; Tandon et al., 2018).

Box 11.1, Figure 1 shows the fractional change in annual maximum one-day precipitation (Rx1day) together with an estimated decomposition of thermodynamic and dynamic contributions over the period 1950-2100 simulated by 22 CMIP5 models (Pfahl et al., 2017). Precipitation extremes (Box 11.1, Figure 1a) are projected to intensify with global warming over most of the globe, with the exception of some subtropical areas where no changes or even decreases are simulated. The thermodynamic contribution (Box 11.1, Figure 1b) leads to increases everywhere with similar magnitude (mostly between 4 and 8% per degree of warming). The dynamic contribution (Box 11.1, Figure 1c) varies greatly in space with large regions in the subtropics showing substantial decreases and an area in the equatorial Pacific showing substantial increases. Most areas where changes are substantial also show high agreement across models, though in transition areas and most middle and high latitudes the agreement across models is poor. In the subtropics, negative contributions from the dynamic term have been linked with a decrease in the horizontal scale of the ascending motion related to increases in static stability (Tandon et al., 2018b, 2018a).

Extreme precipitation can also be enhanced by dynamic responses and feedbacks occurring within the storms resulting from the extra latent heat released from changes in the thermodynamic contribution (Lackmann, 2013; Willison et al., 2013; Marciano et al., 2015; Nie et al., 2018). The extra latent heat released within the storms has been shown to increase precipitation extremes by strengthening convective updrafts and the intensity of the cyclonic circulation, although weakening effects have also been found in midlatitude cyclones (e.g., Kirshbaum et al., 2017). Additionally, the increase in latent heat can also suppress convection at larger scales due to atmospheric stabilization (Nie et al., 2018; Tandon et al., 2018b; Kendon et al., 2019). As these dynamic effects result from feedback processes within the storms and include convective processes, their proper representation requires models to explicitly represent convective processes, and to have higher horizontal and vertical resolutions than current climate models (i.e., Ban et al., 2015; Kendon et al., 2014; Meredith et al., 2015; Nie et al., 2018; Prein et al., 2015; Westra et al., 2014). Positive dynamic feedbacks, either related to changes in the large scale circulation or within the storm, lead to changes in precipitation extremes that exceed those expected from purely thermodynamic considerations.

In summary, there is *high confidence* that thermodynamic factors will drive an intensification of heavy rainfall events close to 7% per degree of warming, but less certain dynamic changes might exacerbate or mitigate this intensification at regional scales.

[START BOX 11.1, FIGURE 1 HERE]

Box 11.1, Figure 1: Multi-model mean fractional changes in % per degree of warming for (a) annual maximum precipitation (Rx1day), (b) thermodynamic contributions and (c) dynamic contributions estimated using the difference between full changes and changes in thermodynamic contributions. Changes were derived from a linear regression for the period 1950–2100. Stippling indicates that at least 80% of the models agree on the sign of the signal. A more detailed description of the estimation of dynamic and thermodynamic contributions is given in Pfahl et al. (2017).

[END BOX 11.1, FIGURE 1 HERE]

Droughts

Droughts alsoresult from a combination of thermodynamic and dynamic processes (Section 11.6). While greenhouse gas forcing on drought is strongly related to thermodynamic processes (through increased radiation, air temperature, and atmospheric drying, which all increase evaporative demand), it is uncertain how changes in circulation patterns may affect drought occurrence, length, and intensity (Section 11.6).

There is *high confidence* that historical and projected changes in drought pattens cannot be fully encompassed with the simplistic statement "dry-gets-drier, wet-gets-wetter", since many dry or wet regions display uncertain changes, and some humid regions currently display drying trends and/or are projected to become drier (Greve et al., 2014; Byrne and O'Gorman, 2015). This highlights that thermodynamic processes cannot be understood using the C-C relationshipalone because, over continents, limited moisture supply can strongly modify the evaporative demand and contribute to the full response, together with internal climate variability (Kumar et al., 2015).In addition, regional changes in thermodynamic processes affecting droughts display large model variations and thus are only associated with *low* or *medium confidence* (Section 11.6). In particular, observed atmospheric drying in recent decades over land is not well captured in the CMIP5 multi-model ensemble (Douville and Plazzotta, 2017), with possible consequences for drought and heavy precipitation projections.

In summary, both thermodynamic and dynamic processes contribute to the occurrence of climate extremes and their changes. Thermodynamic processes are usually directly related to greenhouse gas forcing and thus are better understood and more easily attributable to human-induced global warming. However, there remain large uncertainties related to regional-scale thermodynamic processes (e.g., snow-albedo temperature feedbacks or soil moisture-evapotranspiration-temperature/precipitation feedbacks). Dynamic processes are usually an indirect response to thermodynamic changes and are also strongly affected by internal climate variability. Contributions from changes in the dynamic processes can be substantial, and can either enhance or counteract the effect of thermodynamic responses.

[END BOX 11.1 HERE]

11.1.5 Effects of large-scale circulation on changes in extremes

Atmospheric large-scale circulation patterns and associated atmospheric dynamics are important determinants of the regional climate (Chapter 10). As a result, they are also important to the occurrence and severity of extremes (see also Box 11.3). Aspects of changes in large-scale circulation patterns are assessed in Chapters 2, 3, 4, and 8. Here we provide some general concepts, through a couple of examples, on why the uncertainty in the response of large-scale circulation patterns to external forcing can cascade to uncertainty in the response of extremes to external forcings. Details for specific types of extremes are covered in the relevant subsections. For example, the occurrence of the El Niño-Southern Oscillation (ENSO) influences precipitation regimes in many areas, favoring droughts in some regions and heavy rains in others (Box 11.3). The extent and strengh of the Hadley circulation influences regions where tropical and extra-tropical cyclones occur, with important consequences for the characteristics of extreme precipitation and winds. The circulation patterns associated with land-ocean heat contrast, which affect the monsoon circulations (Biasutti et al., 2018), lead to heavy precipitation along the coastal regions in East Asia (Freychet et al., 2015). As a result, changes in the spatial and/or temporal variability of the atmospheric circulation in response to warming affect characteristics of weather systems such as tropical cyclones (Sharmila and Walsh, 2018), storm tracks (Shaw et al., 2016), and atmospheric rivers (Waliser and Guan, 2017) (see also Section 11.7). Changes in weather systems in turn affect the frequency and intensity of extreme winds, extreme temperatures, and extreme precipitation, on the backdrop of thermodynamic responses of extremes to warming. Aerosol forcing through changing patterns of sea surface temperatures (SSTs) also affects circulation patterns and tropical cyclone activities (Takahashi et al., 2017).

Changes in atmospheric large-scale circulation due to external forcing are uncertain in general but there are clear signals in some aspects (Chapter 2, 3, 4, and 8). Among them, there is *medium confidence* that the Hadley circulation has expanded poleward (Chapter 3). The poleward expansion affects drought occurrence in some regions (see Section 11.6), and results in poleward shifts of tropical cyclones and storm tracks (see Sections 11.7.1 and 11.7.2). The projection of ENSO events is uncertain (Chapter 4), and this would have implications for projected changes in extreme events affected by ENSO, including droughts over wide areas (Section 11.6 and Box 11.3) and tropical cyclones (see Section 11.7.1). A case study is provided for the intense ENSO in 2015/2016 in Box 11.3 to highlight the influence of ENSO on extremes.

In summary, large-scale atmospheric circulation patterns are important drivers for local and regional extremes, especially on the interannual time scale. There is overall *low confidence* about future changes in the strength of these patterns, which results in uncertainty in projected responses of extremes.

11.1.6 Effects of regional-scale processes and forcings and feedbacks on changes in extremes

At the local and regional scales, changes in extremes are strongly modulated by regional and local feedbacks (Seneviratne et al., 2013; Miralles et al., 2014; Lorenz et al., 2016; Vogel et al., 2017), changes in large-scale circulation patterns (11.1.5), and regional forcings such as changes in land use or aerosol concentrations (Hirsch et al., 2017, 2018; Seneviratne et al., 2018; Thiery et al., 2017; Wang et al., 2017f; Findell et al., 2017). In some cases, such responses may also include non-local effects (e.g., Persad and Caldeira, 2018; Miralles et al., 2019). It should be noted that regional-scale forcing and feedbacks are often found to be asymmetric for temperature distributions, with generally higher effects for the hottest percentiles (Section 11.3).

Land use can affect regional extremes, in particular hot extremes, in several ways (*high confidence*). For instance, cropland intensification has been suggested to be responsible for a cooling of the highest temperature percentiles in the US Midwest (Mueller et al., 2016b). Similarly, irrigation has been shown to be responsible for a cooling of hot temperature extremes of up to 1-2°C in many mid-latitude regions in the present climate (Thiery et al., 2017), a process not represented in state-of-the-art Earth System Model (ESM) simulations of the 5th or 6th phase of the Coupled Model Intercomparison Project (CMIP5, CMIP6). Changes in agricultural management associated with no-till farming, which lead to higher surface albedo after harvest (about +0.1) and reduced surface evaporation, may also asymmetrically cool hot days more than median days, with effects of ca. 1°C (Davin et al., 2014). In addition, the decrease in soil evaporation may also mitigate the onset of drought (Wilhelm et al., 2015). Finally, deforestation has been shown to have substantially contributed to the warming of hot extremes in some mid-latitude regions over the course of the 20th century (Lejeune et al., 2018); it should be noted that this effect is often not well captured in ESMs. While observations show a cooling effect of forest cover compared to non-forest vegetation during daytime (Li et al., 2015), in particular in arid, temperate, and tropical regions (Alkama and Cescatti, 2016), several models simulate a warming of daytime temperatures for regions with forest vs non-forest cover (Lejeune et al., 2017). Overall, the effects of land use forcing may be particularly relevant in the context of low-emissions scenarios, which include large land use modifications, for instance associated with the expansion of biofuels, or biofuels with carbon capture and storage (BECCS) or re-/afforestation to ensure negative emissions, as well as with the expansion of food production (e.g., Seneviratne et al., 2018b, Hirsch et al., 2018).

Aerosol forcing also has a strong regional footprint associated with regional emissions, which affects temperature and precipitation extremes (*high confidence;* see also Sections 11.3 and 11.4). From approximately the 1960s to 1980s, enhanced aerosol loadings led to regional cooling due to decreases in global solar radiation ("global dimming") which was followed by a phase of "global brightening" due to a reduction in aerosol loadings (Chapter 7; Wild et al., 2005). King et al. (2016a) show that aerosol-induced cooling delays the timing of the identification of a significant human contribution to record-breaking heat extremes in some regions. On the other hand, the decreased aerosol loading since the 1990s has led to an accelerated warming of hot extremes in some regions. Based on simulations with an ESM, Dong et al. (2017b) suggest that a substantial fraction of the warming of the annual hottest days in Western Europe since the mid-1990s has been due to decreases in aerosol concentrations in the region. Dong et al. (2016) also identify non-local effects of decreases in aerosol concentrations in Western Europe, which they estimate played a dominant role in the warming of the hottest daytime temperatures in Northeast Asia since the mid-1990s, via induced coupled atmosphere-land surface and cloud feedbacks, rather than through a direct impact of anthropogenic aerosol changes on cloud condensation nuclei.

In addition to regional forcings, regional feedback mechanisms can also substantially affect extremes (*high confidence*). This is the case with soil moisture feedbacks in several mid-latitude regions, which lead to a marked additional warming of hot extremes compared to mean global warming (Seneviratne et al., 2016), which is superimposed on the known land-sea contrast in mean warming (Vogel et al., 2017). These feedbacks are also associated with substantial spread in models, and in some regions can imply more uncertainty for projections in temperature extremes than the spread resulting from the differences in global transient climate responses in climate models (Seneviratne and Hauser, submitted). In addition, there are also feedbacks between soil moisture content and precipitation occurrence, generally characterized by negative spatial feedbacks and positive local feedbacks (Taylor et al., 2012; Guillod et al., 2015). Climate model projections suggest that these feedbacks are relevant for projected changes in heavy precipitation (Seneviratne et al., 2013), however, there is evidence that climate models do not capture the correct sign of the soil moisture-precipitation feedbacks in several regions, in particular spatially and/or in some cases also temporally (Taylor et al., 2012; Moon et al., 2019). In high latitudes of the Northern Hemisphere, the snow- and ice-albedo feedback, along with other factors, is projected to largely amplify temperature increases (e.g., Pithan and Mauritsen, 2014), although the effect on temperature extremes is still unclear. It is also still unclear whether snow-albedo feedbacks in mountainous regions might have an effect on temperature and precipitation extremes (e.g., Gobiet et al., 2014), however these feedbacks play an important role in projections of changes in high-latitude warming (Hall and Qu, 2006), and, in particular, changes in cold extremes in these regions (Section 11.3).

Finally, in some regions, weather and climate extremes may amplify one another. This is, for instance, the case between heatwaves and droughts, with high temperatures leading to drying tendencies on land because of increased evapotranspiration, and drier soil conditions leading later on to decreased evapotranspiration and higher sensible heat flux and hot temperatures (Seneviratne et al., 2013; Vogel et al., 2017; Zscheischler and Seneviratne, 2017; Miralles et al., 2014; see also Box 11.1 and Section 11.8).

In summary, regional forcings and feedbacks, in particular associated with land use and aerosol forcings, and soil moisture-temperature, soil moisture-precipitation, and snow/ice-albedo-temperature feedbacks, play an important role in modulating regional changes in extremes. These can also lead to a higher warming of extreme temperatures compared to mean temperature (*high confidence*), and possibly cooling in some regions (*medium confidence*). However, there is only *medium confidence* in the representation of the associated processes in state-of-the-art Earth System Models.

11.1.7 Global-scale synthesis

Tables 11.1 and 11.2 provide a synthesis for observed and attributed changes in extremes, and projected changes in extremes, respectively, at different levels of global warming.

Figure 11.3 provides a synthesis on the level of confidence in the attribution and projection of changes in extremes, building the assessments from Tables 11.1 and 11.2. In the case where the physical processes underlying the changes in extremes in response to human forcing are well understood and the signal in the observations is still relatively weak, confidence in the projections would be higher than in the attribution because of increase in signal to noise ratio with higher global warming. On the other hand, when the observed signal is already strong and when observational evidence is consistent with model simulated responses, confidence in attribution may be higher than that in projections if certain physical processes could be expected to behave differently in a much warmer world and under much higher greenhouse gas forcing, and if such a behavior is poorly understood.

[START FIGURE 11.3 HERE]

Figure 11.3: Synthesis of confidence in attribution of extremes vs confidence in projection of extremes [PLACEHOLDER: THIS FIGURE WILL BE FURTHER DEVELOPED FOR THE FGD FOR ALL

CONSIDERED EXTREMES, AS WELL AS FOR DIFFERENT SPATIAL SCALES)

[END FIGURE 11.3 HERE]

[START TABLE 11.1 HERE]

Table 11.1: Synthesis table on observed changes in extremes and contribution by human influences. Note that observed changes in marine extremes are assessed in the cross-chapter box 9.1 in Chapter 9. [PLACEHOLDER: TO BE UPDATED FOR FGD]

Phenomenon and direction of trend	**Observed/detected trends since 1950 (for +0.5°C global warming or higher)**	**Human contribution to the observed trends since 1950 (for +0.5°C global warming or higher)**
Warmer and/or more frequent hot days and nights over most land areas	***Virtually certain* on global scale** North America, Europe, Australia, Asia, South America:*Extremely likely* Central America, Southern Africa: *Medium confidence* Africa, except southern Africa: *Low confidence* because of lack of observations	***Extremely likely* main contributoron global scale; *very likely*main contributor on continental scale for North America, South America, Europe, Australia, Asia** Central America, Southern Africa: *Medium confidence* Africa (except southern Africa): *Low confidence* in generalbecause of lack of observations
Warmer and/or fewer cold days and nights over most land areas	***Virtually certain* on global scale** *Australasia: Very likely* *Asia: Very likely* *South America: Low evidence*	***Extremely likely* on global scale**
Warm spells/heatwaves; Increases in frequency or intensity over most land areas	***Virtually certain* on global scale** *Australasia: Very likely* *Asia: Very likely* *South America: Low evidence*	***Very likely* on global scale**
Cold spells/cold waves: Decreases in frequency or intensity over most land areas	***Virtually certain* on global scale** *South America: Low evidence, medium agreement*	***Very likely* on global scale**
Heavy precipitation events: increase in the frequency, intensity, and/or amount of heavy precipitation	***Likely* more regions with positive than negative trends**	***Likely* main contributor to the observed intensification of heavy precipitation in land regions**

Drought events: Increases in frequency, intensity and/or duration	Observed trends in drought measures are highly regional, with increases in some regions and decreases in others. Atmospheric evaporative demand displays a global drying tendency over continents, and there is an observed tendency towards increased drying in the dry season since the beginning of the 20th century, when aggregated on global scale.	There is *high confidence* that human influence has increased the potential for worsening of drought conditions and increased the tendency towards drying in the dry season since the beginning of the 20th century, when aggregated on the global scale. The drying tendency is dominated by warming- and radiation-induced increase in evaporative demand rather than by changes in precipitation.
Floods and water logging: Increases in intensity and/or frequency	*Low confidence* in the majority of the world regions with the exception of increases in the Amazon (*high confidence*), Northwest US and UK (*medium confidence*). *High confidence* in changes of flood seasonality, mostly in snow dominated regions.	*Low confidence* due to little evidence and high seasonality.
Increase in precipitation associated with tropical cyclones	*Low confidence* for detectable global trend in tropical cyclone (TC) rain rates, due to data limitations. *Low confidence* for detectable global change in TC translation speed.	*Low confidence* for global TC rain rates and changes in translation speed. *Low to medium confidence* for contribution of TCs to detectable anthropogenic contribution to extreme rainfall events. *Medium confidence* for detectable anthropogenic contribution to global near-surface water vapor increases, which is expected to increase TC rainfall, all other things equal. *Medium confidence* for anthropogenic contribution to extreme rainfall events, which TCs contribute to, over the United States and other regions with sufficient data coverage.
Increase in tropical cyclone intensity (maximum surface wind speed)	Generally *low confidence* in detection of trends in historical tropical cyclone intensity in any basin or globally due to lack of confidence resulting from data inhomogeneities.	Generally *low confidence* in attribution of any anthropogenic influence on historical changes in tropical cyclone intensity in any basin or globally due to lack of confidence resulting from data inhomogeneities, with exception of North Atlantic. North Atlantic: *Medium confidence* that a reduction in aerosol forcing has contributed at least in part to the observed increase in tropical cyclone intensity since the 1970s.*Low confidence* for direct role of greenhouse gas forcing.
Changes in frequency of tropical cyclones	*Low confidence* in detection of trends in historical tropical cyclone frequency in any basin or globally due to lack of confidence resulting	*Low confidence* in attribution of any anthropogenic influence on historical changes in tropical cyclone frequency in any basin or globally due to lack of confidence resulting

	from data inhomogeneities. Furthermore, physical process understanding is still unclear and there is no clear expectation for an increase in overall frequency with increasing greenhouse gas concentration.	from data inhomogeneities, with exception of North Atlantic. North Atlantic: *Medium confidence* that a reduction in aerosol forcing has contributed at least in part to the observed increase in tropical cyclone frequency since the 1970s. *Low confidence* for direct role of greenhouse gas forcing.
Poleward migration of tropical cyclones	*Low confidence* for a detectable global signal. *Medium confidence* for a detectable migration rate in the western North Pacific.	*Low confidence* for global migration. *Medium confidence* for migration in the western North Pacific.
Slowdown of tropical cyclone translation speed	*Low confidence* due to a present limited literature and lack of consensus on model results.	*Low confidence.*
Severe convective storms (tornadoes, hail, rainfall, wind, lightning)	*Low confidence* in past trends in hail and winds and tornado activity due to short length of high quality data records.	*Low confidence*.
Increase in compound events	*Medium confidence* that compound flooding risk has increased along the US coastline. *High confidence* that co-occurrent heatwaves and droughts are becoming more frequent under enhanced greenhouse gas forcing at global scale. *Medium confidence* wildfires have become more intense and that their frequency has increased in some fire-prone regions.	*Low confidence that human influences has contributed to changes in compound events leading to flooding.* *High confidence that human influence has increased the frequency of co-occurent heatwaves and droughts.* *Medium confidence that human influence has increased wildfire occurrence in some regions.*

[END TABLE 11.1 HERE]

[START TABLE 11.2 HERE]

Table 11.2: Synthesis table on projected changes in extremes. Note that projected changes in marine extremes are assessed in Chapter 9 and the Cross-chapter box 9.1 (marine heatwaves). [PLACEHOLDER: TO BE UPDATED FOR FINAL FGD, INCLUDING FOR PROJECTIONS AT +4°C]

Phenomenon and direction of trend	Projected changes at +1.5°C global warming	Projected changes at +2°C global warming	Projected changes at +3°C global warming
Warmer and/or more frequent hot days and	*Virtually certain* compared to pre-industrial on global	*Virtually certain* compared to pre-industrial on global	*Virtually certain*compared to pre-industrial on global

nights over most land areas	scale; *extremely likely* on all continents Warming of hottest days of up to +3°C in mid-latitudes (*medium confidence*)	scale; *extremely likely* on all continents Warming of hottest days of up to +4°C in mid-latitudes (*medium confidence*)	scale; *extremely likely* on all continents Warming of hottest days of up to +6°C in mid-latitudes (*medium confidence*)
Warmer and/or fewer cold days and nights over most land areas	*Virtually certain* compared to pre-industrial on global scale; *extremely likely* on all continents Warming of coldest nights of up to +4.5°C in Arctic, several northern high-latitude regions, and some northern mid-latitude regions (*medium confidence*)	*Virtually certain* compared to pre-industrial on global scale; *extremely likely* on all continents Warming of coldest nights of up to +6°C in Arctic, several northern high-latitude regions, and some northern mid-latitude regions (*medium confidence*)	*Virtually certain* compared to pre-industrial on global scale; *extremely likely* on all continents Warming of coldest nights of up to +9°C or larger in Arctic, several northern high-latitude regions, and some northern mid-latitude regions (*medium confidence*)
Warm spells/heatwaves; frequency and/or duration increases over most land areas	*Virtually certain* compared to pre-industrial on global scale; *extremely likely* on all continents	*Virtually certain* compared to pre-industrial on global scale; *extremely likely* on all continents	*Virtually certain* compared to pre-industrial on global scale; *extremely likely* on all continents
Cold spells/cold waves: Decreases in frequency, intensity and/or duration over most land areas	*Very likely*compared to pre-industrial on global scale	*Very likely*compared to pre-industrial on global scale	*Very likely*compared to pre-industrial on global scale
Heavy precipitation events: increase in the frequency, intensity, and/or amount of heavy precipitation	*High confidence* in most continents but *low confidence* in Australasia, Central and South America [PLACEHOLDER: TO BE UPDATED WITH MORE CMIP6 SIMULATIONS FOR FGD]	*Likely* in most continents but *low confidence* in Australasia, Central and South America [PLACEHOLDER: TO BE UPDATED WITH MORE CMIP6 SIMULATIONS FOR FGD]	*Very likely* in most continents but *low confidence* in Australasia, Central and South America [PLACEHOLDER: TO BE UPDATED WITH MORE CMIP6 SIMULATIONS FOR FGD]
Increases in intensity and/or duration of drought events	*High confidence* that atmospheric evaporative demand will continue to increase compared to pre-industrial conditions and lead to further drying tendencies in some regions *Medium confidence* in increase in drought probability in subtropical	*High confidence* that atmospheric evaporative demand will continue to increase compared to pre-industrial conditions and lead to further drying tendencies in some regions *Medium confidence* in increase in drought probability in subtropical	*High confidence* that atmospheric evaporative demand will continue to increase compared to pre-industrial conditions and lead to further drying tendencies in some regions *Medium confidence* in increase in drought probability in subtropical

	regions: Mediterranean, Southern Africa, Northeast Brazil, Southern North America and Central America *High confidence* in higher probability of atmospheric aridity, i.e. drier atmosphere, in subtropical and mid-latitude regions	regions (Mediterranean, Southern Africa, Northeast Brazil, Southern North America and Central America), with higher probability of intense/frequent droughts than at 1.5°C global warming *Medium confidence* in expansion of drought probability outside these regions given increased radiative forcing (e.g., central Europe and Central North America, the Amazon) *High confidence* in higher probability of atmospheric aridity, i.e. drier atmosphere, in subtropical and mid-latitude regions	regions (Mediterranean, South Africa, Northeast Brazil, Southern North America and Central America), with higher probability of intense/frequent droughts than at 2°C of global warming *Medium confidence* in expansion of drought probability outside these regions given increased radiative forcing (e.g., central Europe and Central North America, the Amazon), with probability of intense droughts being higher than at 2°C of global warming *High confidence* in higher probability of atmospheric aridity, i.e. drier atmosphere, in subtropical and mid-latitude regions
Increases in floods and water logging	*Medium confidence* that an increase in global warming to 1.5°C would lead to alarger fraction of land area affected by flood hazard at global scale compared to present	*Medium confidence* that an increase in global warming to 2°C compared to 1.5°C or present-day conditions would lead to a larger fraction of land area affected by flood hazard at global scale.	*High confidence* that flood hazard would be even more widespread at +3°C compared to +2°C given projected changes in heavy precipitation; in part lack of literature to quantitatively assess projected changes.
Increase in precipitation associated with tropical cyclones (TC)	*High confidence* in a projected increase of TC rain rates at the global scale; the median projected rate of increase is about 11%. *Medium confidence* that rainrates will increase in every basin.	*High confidence* in a projected increase of TC rain rates at the global scale; the median projected rate of increase is about 14%. *Medium confidence* that rainrates will increase in every basin.	*High confidence* in a projected increase of TC rain rates at the global scale; the median projected rate of increase is about 21%. *Medium confidence* that rainrates will increase in every basin.
Increase in mean tropical cyclone lifetime-maximum wind speed (intensity)	*Medium-to-high confidence* for a 3.75% increase.	*Medium-to-high confidence* for 5% increase.	*Medium-to-high confidence* for a 7.5% increase.

Changes in frequency of tropical cyclones	*Medium-to-high* confidence for an increase in the proportion of TCs that reach the strongest (Category 4-5) levels. The median projected increase in this proportion is about 10%..	*Medium-to-high* confidence for an increase in the proportion of TCs that reach the strongest (Category 4-5) levels. The median projected increase in this proportion is about 13%.	*Medium-to-high confidence* for an increase in the proportion of TCs that reach the strongest (Category 4-5) levels. The median projected increase in this proportion is about 20%.
Severe convective storms	There is *medium confidence* that the frequency of severe convective storms increases in the spring with enhancement of CAPE, leading extension of seasons of occurrence of severe convective storms. There is *high confidence* of future intensification of precipitation associated with severe convective storms.	Same as the left cell.	Same as the left cell.
Increase in compound events (frequency, intensity)	*High confidence* that co-occurrent heatwaves and droughts will continue to increase under higher levels of global warming, with higher frequency/intensity with every additional 0.5°C of global warming. *Medium confidence* that humid heatwaves will continue to increase under higher levels of global warming, with higher frequency/intensity with every additional 0.5°C of global warming. *Medium confidence* that compound flooding at the coastal zone will increase under higher levels of global warming, with higher frequency/intensity with every additional 0.5°C of global warming.		

[END TABLE 11.2 HERE]

11.2 Data and Methods

This section provides an assesment of data and challenges to study extreme events, of methodological aspects of the research on climate extremes, and of the modeling of extreme events. Key points and new developments in detection and attribution methods are briefly assessed as well. The main focus is on extreme events over land, as extremes in the ocean are assessed in Chapter 9 of this report.

11.2.1 Observations for extremes

Extremes are rare events, which means that the extremal portions of the distribution in the available observations are most relevant when analysing long-term changes in extremes. Compared with mean climate, there are unique challenges and special data requirements when characterizing long-term changes in extremes. The SREX and AR5 WGI reports (SREX Chapter 3, AR5 Chapter 2) discussed critical issues regarding the quality and availability of observed data and their relevance for the assessment of changes in extremes. The different types of observations (e.g., station-based, satellite, reanalysis), quality and quantity (e.g., homogeneity, record length), and the consistency of data for overall climate monitoring are assessed in Chapter 10 (Section 10.2.1). We provide here more background on aspects specifically related to observations of extremes.

11.2.1.1 Ground-based instrumental record

Several relevant extreme weather and climate events happen on time scales of hours to weeks, such as land and marine heatwaves, cold spells, flooding, tropical cyclones, and extra-tropical cyclones. The analysis of these events may require daily or sub-daily (one- to six-hourly) instrumental observations. However, such observational records are too short (less than 10 years) in many regions, and stations may not have been uniformly maintained or their data may not be openly available. On the other side of the spectrum, longer events such as droughts, which can last from a few weeks to several years ("mega-droughts", e.g., Ault et al. 2014) are necessarily rare and thus require even longer records to detect trends and distinguish human-induced signals from internal climate variability. Hence, the observational analysis of weather and climate extremes poses very unique data challenges.

The density of networks with available station data (at daily and monthly time scales) has decreased in recent years. The spatial coverage of observed data of relevance for extremes is uneven, and there are large data gaps for various regions such as Africa and South America (Donat et al., 2013a; Funk et al., 2015b). While spatial coverage of daily data can be improved by integrating data sources, such as the International Surface Temperature Initiative (ISTI) databank that combines the Global Historical Climatology Network (GHCN)–Daily data sets with other historical data sources (Karl et al., 2015), the level of improvement is still limited by the availability of underlying station observations (see also Chapters 1 and 10: Section 1.5.1.2, Section 10.2.2.3). Sub-daily observations of precipitation and temperature are more widely available than for humidity (Willett et al., 2014), which is necessary to calculate heat indices and other measures of human discomfort during heat waves. In-situ observations of soil moisture (Seneviratne et al., 2010; Dorigo et al., 2011), and to a lesser extent streamflow and runoff (Do et al., 2018), are limited as well, complicating the characterization of changes in drought and water logging statistics (Sections 11.5 and 11.6). Data inhomogeneity (Chapter 10, Section 10.2.2.2) due to changes in siting, instruments, or observation practices, is not always addressed, especially for precipitation data. In addition, different quality control schemes may have been used (Dunn et al., 2014). These introduce various sources of uncertainty, making trend analysis more uncertain.

Station data have been used to generate climate extreme products available in regular grid meshes (i.e., gridded datasets) to be used for different purposes, including infilling data gaps and climate model evaluation. However, when producing gridded datasets (Chapter 10, Section 10.2.2.4), the order in which the extremes' calculation and the interpolation are performed is important for evaluation. In some instances, daily values of station observations are first gridded and various indices representing different aspects of extremes are then computed. In regions with high station density, the gridded values are closer to extremes of area mean and thus more appropriate for comparisons with extremes estimated from climate model output, which is often considered to represent areal means (Chen and Knutson, 2008; Gervais et al., 2014; Avila et al., 2015; Di Luca et al., submitted). In regions with very limited station density, the gridded values are closer to point estimates of extremes. It follows that it can be difficult to interpret the extremes computed from gridded values due to different station densities in different regions. In other instances, the extreme indices are computed first and then gridded. These gridded values are more representative of point estimates of extremes, subject to some spatial smoothing due to gridding, making these products less suitable for climate model evaluation. Because of the spatial variability of the climate and varying station densities in different regions, these two types of data products are not always comparable.

Agreement between different global and regional datasets varies, with better agreement for extreme temperatures than for extreme precipitation (Donat et al. 2014). While index-based data products provide a broader spatial coverage than raw variables, deterioration of networks over time is also reported, particularly for Africa and parts of South and Central America (Donat et al., 2013). These differences can be substantial enough to lead to very different conclusions about whether a specific precipitation event is actually extreme (Angélil et al., 2017).

11.2.1.2 Satellite-based instrumental record

Satellite remote sensing offers complementary data to in-situ measurements and the opportunity for more spatially homogeneous, albeit shorter temporal coverage (see Chapter 10, Section 10.2.11). In some regions with sparse data coverage, they provide the main source of information on observed changes. In addition, a key advantage of satellite data for extremes is the temporal resolution of some products providing subdaily data for precipitation (e.g., TRMM; Maggioni et al. 2016), clouds (e.g., HIMAWARI; BESSHO et al. 2016; Chen et al. 2019), or winds (e.g., QuikSCAT; Lee et al. 2008; Chan and Chan 2012, 2015). However, satellites do not observe the primary atmospheric state variables directly and polar orbiting satellites do not observe any given place at all times. Hence, their utility as a substitute for high-frequency (i.e. daily) ground-based observations is limited. For instance, Timmermans et al. (2019) analysed extreme daily and pentad precipitation and found little relationship between the timing of observed extreme precipitation in satellite and gridded station data products over the United States.

Despite these limitations, some satellite records are now becoming long enough to assess longer-term changes in precipitation extremes (Alexander et al., 2019, submitted); Bador et al., submitted). A limited number of global land-based precipitation products date back to the early 1980s (Ashouri et al., 2015; Funk et al., 2015; Roca et al., 2019), while many others have data going back to at least the early 2000s (Huffman et al., 2001, 2007; Kubota et al., 2007; Roca et al., 2019; Xie et al., 2017). However, problems with homogeneity (e.g., instrumentation change, satellite drift, merging techniques), issues with how very dry and very wet precipitation is calculated, and problems with the orographic precipitation calculation have limited the usefulness of satellite products in climate assessments. Often datasets are not developed with extremes in mind and can show idiosyncrasies in the extremes but not in the mean (Bador et al., submitted;Masunaga et al., submitted). There is a lack of data outside of 50°S to 50°N except in northern Europe, where data sparsity is less of an issue because of the many other observational sources available. It is becoming recognised though that satellite products might offer a useful complement to existing global products which are primarily in situ-based (Alexander et al., 2019) but caution is required in the interpretation of long-term trends especially in regions with low station density, prohibiting calibration of the satellite observations(Harrison et al., 2019; Timmermans et al., 2019). Generally, the spread across products is larger for satellite-based products than those that are solely in situ-based. The mean of the current range of available products is closest to the mean of the majority of in situ-based products. Caution is recommended for all products dependent on their intended application (Alexander et al., 2019; Bador et al., 2020).

Shorter satellite products can still provide useful insights on the interannual variability of extremes, on potential emerging trends, and on mechanistic aspects leading to the occurrence of extreme events or relating them to potential impacts. For instance, the records of the Gravity Recovery and Climate Experiment (GRACE) that provided 15 years of data on water storage variability, provided useful insights on some emerging drying or wettening trends (e.g., Rodell et al., 2018). Several mechanistic studies on droughts (either on processes leading to droughts or on effects of droughts on other climate processes) have used satellite data products given the lack of large-scale ground observations for soil moisture (e.g., Otkin et al., 2016; Miralles et al., 2014; Dorigo et al., 2017; Stocker et al., 2019; Liu et al., submitted), or have provided insights on the performance of climate models (e.g., Scanlon et al., 2018; Humphrey et al., 2018). Recently also satellite datasets of land surface temperature have been used to assess processes related to hot extremes (e.g., Folwell et al., 2016).

11.2.1.3 Reanalysis data as observational proxy for extremes.

As analyses of past changes in climate extremes are restrained by the limited availability of suitable observational data (Section 11.2.1.1), studies have also used atmospheric reanalyses to investigate changes in climate extremes. Reanalyses are produced by assimilating certain types of observational data into atmospheric models, which are mostly frozen versions of operational forecast models (Dee et al., 2011; Onogi et al., 2007; Saha et al., 2010). If sufficiently constrained by observational data, reanalyses therefore represent the observed evolution of large-scale weather conditions. Reanalyses provide spatially and temporally complete coverage and physically consistent data (consistent both across different variables and in the representation of specific variable fields), which makes them a popular data basis for studies of past climate conditions. Similar to purely observational datasets, reanalyses are, however, also affected by inhomogeneities. These come primarily from issues with the observational input data used for assimilation (in particular specific inhomoheneities in local observations but also variability in the available network), imperfections in data assimilation schemes, and model uncertainty (Bengtsson et al., 2004; Thorne and Vose, 2010). These observations potentially confine the applicability of reanalyses to study long-term climatic changes. While reanalyses have been reported to represent high-quality and the most homogeneous observation-based datasets for the last approximately 30 years (Dee et al., 2011a), they are affected by distinct structural break points common to all reanalyses due to the introduction of certain types of data sources (such as the introduction of radio sondes in 1958 and the introduction of satellite data in 1979). In addition to the operational reanalyses, also two century-long reanalyses have been developed, which assimilate fewer observed variables but provide data throughout the entire 20th century, partly back to the mid-19th century (Compo et al., 2011; Poli et al., 2016).

Evaluating a selection of indicators representing temperature and precipitation extremes in a set of commonly-used reanalyses including ERA-Interim, ERA40, NCEP1, NCEP2, and JRA-25 (Dee et al., 2011b; Kalnay et al., 1996; Kanamitsu et al., 2002; ONOGI et al., 2007; Uppala et al., 2005), Donat et al. (2014) showed that changes in temperature extremes from reanalyses were most consistent with gridded observations after about 1980, but larger differences between reanalyses and gridded observations were found during the pre-satellite era. Generally lower agreement across datasets is found for extreme precipitation changes, although temporal and spatial correlations against observations were found to be still significant. Temperature and precipitation extremes from the century-long reanalyses (20CR and ERA-20C, Compo et al., 2011; Poli et al., 2016) were shown to reasonably agree with observations after about 1950, in particular in regions with good observational coverage, but often indicated different changes during the first half of the twentieth century (Donat et al., 2016a). In particular in regions with sparse observations, there is generally less agreement between different reanalyses products. For example, for extreme precipitation in Africa and parts of South America, different reanalyses indicate long-term changes of opposing signs (Donat et al., 2014b, 2016a). Timmermans et al. (2019) found little relationship (as measured by tail dependence) for extreme pentadal precipitation (five-day rainfall) between ERA-Interim and the gridded station data products over the United States. However, as the North American Regional Reanalysis (NARR) directly assimilates station precipitation data, they found this measure of agreement to be high for that product. For extra-tropical cyclones (ETCs, Section 11.7), several studies identified inconsistencies in reanalyses data (Krueger et al., 2013; Tilinina et al., 2013; Befort et al., 2016; Chang and Yau, 2016; Wang et al., 2016b).

[START BOX 11.2 HERE]

BOX 11.2: Extremes in palaeoclimate archives compared to instrumental records

Examining extremes in pre-instrumental information can help to put events occurring in the instrumental record (called ‘observed’ here) in a longer-term context. This box focuses on extremes in the Common Era (CE, the last 2000 years) and discusses evidence of extreme events in palaeoreconstructions, documentary evidence (such as grape harvest data, ecclesiastical documents, newspapers and logbooks) and model-based analyses. This discussion includes evidence of whether observed extremes have or have not been exceeded in the Common Era. This focus is because there is generally higher confidence in pre-instrumental information gathered from the more recent archives from the Common Era, than from earlier evidence. This box provides overviews of i) the AR5 assessments and ii) types of evidence assessed here, evidence of iii) droughts, iv) temperature extremes, v) palaeofloods and vi) palaeotempests, and vii) summary of remaining challenges.

Based on studies of palaeoclimate reconstructions, documentary evidence and early instrumental data, AR5 (and SREX) concluded with *high confidence* that droughts of greater magnitude and of longer duration than those observed in the instrumental period occurred in many regions during the last millennium. Evdidence assessed of past floods provided *high confidence* that floods during the past five centuries in northern and central Europe, western Mediterranean region and eastern Asia were of greater magnitude than those observed (Masson-Delmotte et al., 2013). The AR5 report *medium confidence* in evidence that floods in the near East, India and central North America are comparable to modern observed floods. The AR5 assessed 20th Century summer temperatures compared to those reconstructed in the Common Era but not shorter duration temperature extremes (Masson-Delmotte et al., 2013).

Given the rarity of extreme events and limited data samples available, even with literature published since the AR5, it remains difficult to quantify systematically the likelihood of such an event occurring in the past and whether the likelihood has changed in the instrumental period. Many factors affect confidence in information on pre-instrumental extremes. First, the geographical coverage of palaeoclimate reconstructions of extremes is not spatially uniform (Smerdon and Pollack, 2016) and depends on both the availability of archives and records, which are environmentally dependent, and also the differing attention and focus from the scientific community. In Australia, for example, the palaeoclimate network is sparser than for other regions, such as Asia, Europe and North America, and synthesised products rely on remote proxies and assumptions about the relationship of remote climates spatial coherence of precipitation (Cook et al., 2016c; Freund et al., 2017). Second, pre-instrumental evidence of extremes may be focused on understanding archetypal extreme events, such as the climatic impact of the 1815 eruption of Mount Tambora, Indonesia (Brohan et al., 2016; Veale and Endfield, 2016). These studies provide narrow evidence of extremes in response to specific forcings (Li, 2017) in particular locations, for specific epochs. Third, natural archives may provide information about extremes in one season only (e.g., some dendrochronlogical archives provide temperature but not precipitation data). Finally, the probability of finding an unprecedented extreme event increases with an increase of length of past record-keeping, in the absence of trends. Thus, there is also a comparatively higher chance for very rare extreme events to have occurred at some prior time in the combined palaeoclimate and historical records which provided extended records length.

Evidence of shorter duration extreme event types, such as floods and tropical storms, is further restricted by the comparatively low chronological controls and temporal resolution (e.g., monthly, seasonal, yearly, multiple years) of most archives compared to events (e.g., minutes to hours or days). Natural archives may be sensitive only to intense environmental disturbances, and so only sporadically record short duration or small spatial scale extremes. Interpreting sedimentary records as evidence of past short-duration extremes is also complex and requires clear understandings of natural processes. For example, palaeoflood reconstructions of flood recurrence and intensity produced from geological (eg. river and lake sediments, speleothems (Denniston and Luetscher, 2017), botanical (e.g., flood damage to trees, or tree ring reconstructions) and faunal (e.g., diatom fossil assemblages) require understandings of sediment sources and flood mechanisms. Pre-instrumental records of tropical storm intensity and frequency (also called palaeotempest records) derived overwash deposits of coastal lake and marsh sediments are difficult to interpret, with many factors affecting whether disturbances are deposited in archives (Muller et al., 2017) and deposits providing sporadic and incomplete preservation histories (e.g., Tamura et al., 2018).

Overall, the most complete pre-instrumental evidence of extremes occurs for high-duration, large spatial-scale extremes, such as for multi-year meteorological droughts or seasonal- and regional- scale temperature extremes. Additionally, more precise insights into recent extremes emerge where multiple studies have been undertaken, compared to confidence in extremes reported at single sites or in single studies which may not necessarily be representative of large-scale changes, or for reconstructions that synthesise multiple proxies over large areas (e.g., drought atlases). Such products combine palaeoclimate temperatures reconstructions and cover sub-continental- to hemispheric-scale regions to provide continuous records of the Common Era (e.g., Ahmed et al., 2013; Neukom et al., 2014 for temperature).

There is ***high confidence*** in the occurrence of high-duration and severe drought events during the Common

Era for many locations, although their severity compared to recent drought events differs for locations and length of reconstruction provided. In some regions (the Levant (Cook et al., 2016a), California in the United States (Cook et al., 2014b; Griffin and Anchukaitis, 2014) and the Andes (Domínguez-Castro et al., 2018)), recent observed drought extremes do not have precedents within the multi-century periods reconstructed in these studies in terms of duration and/or severity. In some regions (in Southwest North America (Asmerom et al., 2013; Cook et al., 2015a) and the Great Plains region (Cook et al., 2004), the Middle East (Kaniewski et al., 2012) and China (Gou et al., 2015)), recent drought extremes may have been exceed in the Common Era. In further locations, there is conflicting evidence for the severity of pre-instrumental droughts compared to observed extremes, depending on the length of reconstruction and seasonal perspective provided (see Cook et al., 2016b; Freund et al., 2017 for Australia). There can also be differing conclusions for the severity or even the occurrence of specific individual pre-instrumental droughts when different evidence is compared (e.g., Büntgen et al., 2015; Wetter et al., 2014).

There is ***medium confidence*** that the magnitude of large-scale, seasonal-scale extreme temperatures in observed records exceed those reconstructed over the Common Era in some locations such as Central Europe. In one example, multiple studies have examined the unusualness of present-day European summer temperature records in a long-term context, particularly in comparison to exceptionally warm 1540 CE in Central Europe. Several studies indicate that the recent extreme summers (2003 and 2010) in Europe have been unusually warm in the context over the last 500 years (Barriopedro et al., 2011; Wetter and Pfister, 2013; Wetter et al., 2014; Orth et al., 2016a), or longer (Luterbacher et al., 2016). Others studies show summer temperatures in Central Europe in 1540 were warmer than the present-day (1966–2015) mean, although note it is difficult to assess whether or not the 1540 summer was warmer than observed record extreme temperatures(Orth et al., 2016a).

There is ***high confidence*** that the magnitude of floods over the Common Era has exceeded observed records in some locations, including central Europe and eastern Asia. Recent literature supports previous AR5 assessments of floods (Wilhelm et al., 2018). High temporally resolved records provide evidence, for example, of Common Era floods exceeding probable maximum flood levels in the Upper Colorado River, USA (Greenbaum et al., 2014) and peak discharges that are double gauge levels along the middle Yellow River, China (Liu et al., 2014). Further studies demonstrate pre-instrumental or early instrumental differences in flood frequency compared to the instrumental period, including reconstructions of high and low flood frequency in the Alps (Swierczynski et al., 2013; Amann et al., 2015) and Himalayas (Ballesteros Cánovas et al., 2017). The combination of extreme historical flood episodes determined from documentary evidence also increases the confidence in flood frequency and magnitude determination, compared to using geomorphological archives alone (Kjeldsen et al., 2014). In regions such as Europe and China that have rich historical flood documents (Wilhelm et al., 2019), there is strong evidence of high magnitude flood events over historical periods (Benito et al., 2015; Kjeldsen et al., 2014; Macdonald and Sangster, 2017). A key feature of palaeoflood records is variability in flood recurrence at centennial timescales (Wilhelm et al., 2019), although constraining climate-flood relationships remains challenging. Pre-instrumental floods often occurred in considerably different contexts in terms of land use, irrigation and infrastructure and may not be directly insightful into modern river systems, which further prevents long term assessments of flood changes being made based on these sources.

There is ***medium confidence*** that periods of both more and less tropical cyclone activity than observed occurred over the Common Era in many regions. Palaeotempest studies cover a limited number of locations, and provide information on specific locations that cannot be extrapolated basin-wide (see Muller et al., 2017). In some locations, such as the Gulf of Mexico and New England coast, similarly intense storms to those observed recently have occurred multiple times over centennial timescales (Donnelly et al., 2001; Bregy et al., 2018). Further research focused on the frequency of tropical storm activity. Extreme storms occur considerably more frequently in particular periods of the Common Era compared to the instrumental period in northeast Queensland, Australia (Nott et al., 2009; Haig et al., 2014), and the Gulf Coast (e.g., Brandon et al., 2013), although the associated risk of surges or flooding may have increased (Lin et al., 2014).

Given the data limitations, dating uncertainities, and spatial and temporal inhomogeneities outlined here, it is not typically possible to assess potential observed changes in the characteristics of most extremes from a systematic long-term (palaeoclimatic) perspective in many locations. In one study, extended evidence of the last millennium from observational data and palaeoclimate reconstructions using tree rings indicate a detectable signal in the worldwide risk of droughts in the beginning of the early 20th Century (Marvel et al., 2019). However, it is also generally difficult to determine whether human or natural external forcing is having an influence on the likelihood of observed extreme events from these Common Era data.

In summary, there is *low confidence* in overall changes in extremes derived from palaeo-archives. The most robust evidence is *high confidence* that high-duration and severe drought events occurred at many locations during the last 2000 years. There is also *high confidence* that high-magnitude flood events occurred at some locations during the last 2000 years, but overall changes in infrastructure and human water management make comparison with present-day records difficult. There are remaining data limitations, dating uncertainities, and spatial and temporal inhomogeneities that limit a systematic long-term perspective on extremes being gained from palaeo-archives.

[END BOX 11.2 HERE]

11.2.2 Statistical methods for change detection

To detect a trend or likelihood/intensity change in extremes, the data set has to be of sufficient temporal and spatial coverage. Since the analysis of extremes often involves the examination of the tails of the statistical distributions, a parametric or non-parametric approach can be used to define extremes. The non-parametric approach is largely adopted in most of the literature to characterize moderate temperature and precipitation extremes with shorter return periods. The Expert Team on Climate Change Detection and Indices (ETCCDI - https://www.wcrp-climate.org/etccdi) defined 27 indices to characterize different aspects of moderate temperature and precipitation extremes, which are described by Frich et al. (2002), Alexander et al. (2006) and Donat et al. (2013), and were also extensively used in previous IPCC reports. In this chapter, a subset of these indices is assessed in detail (Section 11.3 and Section 11.4). For events with longer return periods (e.g., events that occur once in 20 years or even rarer), the parametric approach based on Extreme Value Theory (EVT) (Coles, 2001) is used and adopted in the literature (e.g., Kharin and Zwiers 2000; Brown et al. 2008; Kharin et al. 2013). These events are also assessed throughout this chapter. These two approaches are complementary as some of the ETCCDI indices can be used to derive estimates of rarer events (e.g., Wehner, submitted). While significant progress has been made since the AR5 in developing and applying advanced statistical methods to extreme weather and climate, it is clear that a stronger involvement of the statistics community could further enhance confidence in estimating the magnitude, changes, and uncertainties in extreme events.

11.2.3 Modelling and model evaluation for extremes

Chapter 10 (Section 10.3.3) provides an overall performance assessment of different model types in simulating and projecting regional climate. The ability of the various modelling approaches to simulate weather and climate extremes varies greatly, depending on the complexity and spatiotemporal scales of the events. Some extremes are also affected by local or regional feedbacks, which can increase spread in resulting projections because of discrepancies in the representation of the underlying processes. Abnormally hot or cold seasons are often large enough in scale that the appropriate large-scale meteorological patterns can be simulated well (Angélil et al., 2016, 2017;Stegall and Kunkel, 2017) at standard CMIP5/6 horizontal resolutions (~100km). On the other hand, limitations of current state-of-the-art models have been reported in representing floods (11.5) or droughts (11.6), implying overall *medium confidence* in the representation of the relevant processes for these types of extremes. AOGCMs and ESMs are usually able to represent some, although not all, aspects of synoptic scale phenomena such as heatwaves, cold snaps, extratropical cyclones, and atmospheric blocking (Mitchell et al., 2017; Rohrer et al., 2018). However, depending on the phenomena and the specific region, biases can be important, and are generally larger for the magnitude/intensity of events than for their frequency of occurrence (e.g., Zappa et al., 2013a). For short-duration events, AOGCMs and ESMs fail to reproduce some key features of the observed distribution. This is the case even for high temperature extremes in European regions densely covered by observations (Kew et al., 2018; Min, et al. 2013; Sippel, et al., 2016) and in Asia. In particular, minimum temperature extremes are less well represented (Seo et al., 2018). In some cases, observations-based emerging constraints can provide a selection of climate projections based on model performance (e.g., Stegehuis et al., 2013; Vogel et al., 2018; Donat et al., 2018). ESMs also display systematic biases in the representation of very persistent events, with an underestimation of multi-year drought events (Ault et al., 2014; Moon et al., 2018).

Statistical and dynamical downscaling (see Chapter 10, Section 10.3.1) of time slices of AOGCM simulations allows a better representation of some phenomena and more realistic surface forcings (e.g., topography and land-sea contrasts) often leading to a more realistic simulation of extreme temperatures and precipitation (Massey et al., 2015; Di Luca et al., 2016a; Guillod et al., 2017; Mizuta et al., 2017). A more detailed assessment of added value in downscaling is given in Section 10.3.3. Higher-resolution model simulations systematically show a more realistic representation of phenomena leading to extreme events including extratropical cyclones (Schaaf and Feser, 2018), tropical cyclones (Xue et al., 2013), atmospheric rivers (Whan and Zwiers, 2016), and precipitation in complex orography areas (Poschlod et al., 2018; Prein et al. 2013). Continental and regional-scale atmospheric modelling at 4km or finer (Chapter 10, Section 10.3.3.5.1) can resolve certain classes of short-term extreme events including convective storms (Ban et al., 2014; Kendon et al., 2017; Prein et al., 2017c, 2017a). However, multi-decadal convection-permitting simulations are not currently computationally feasible at global scales, limiting their usefulness in evaluating changes in extremes. And the limited ensemble sizes available for such very-hich resolution simulations reduce confidence in assessing the structural uncertainty in projected changes. In addition, regional climate model ensembles used for dynamical downscaling also have limitations compared to global-scale ESMs. For instance, in the European CORDEX ensemble, aerosol concentrations were prescribed as constant in projections (Bartók et al., 2017) and the land surface models used in the regional climate models do not account for physiological CO_2 effects (Section 11.6, Box 11.1) on photosynthesis (Schwingshackl et al., 2019). Both features are *likely* to explain an identified discrepancy in the projections of hot extremes in the CORDEX ensemble compared to the CMIP5 ESMs, whereby the CORDEX ensemble displays much smaller increases (Schwingshackl et al., 2019).

11.2.4 Storylines, assessing potential surprises, and low-probability high-impact extremes

The SREX assigned *low confidence* to potential surprises and low-probability high-impact events (SREX Chapter 3). Such surprises are also discussed in Chapter 4 and can either result from tipping points of the climate system (Section 1.4.5), such as the shutdown of the Atlantic thermohaline circulation or the drydown of the Amazonian rainforest (e.g., SR15 Chapter 3; Drijfhout et al. 2015), or from poor understanding of climate processes including climate feedbacks that may enhance or damp extremes either related to global or regional climate responses (Seneviratne et al., 2018;Sutton 2018). The l*ow confidence* does not by itself exclude the possibility of such surprises or affirm that abrupt and thus surprising changes in climate extremes will occur; it is instead an indication of the poor state of knowledge. Such outcomes, while unlikely, could be associated with very high impacts, and are thus highly relevant from a risk perspective, considering that risk is equal to the probability of an outcome times the impact of that outcome (see Chapter 1, Section 1.4.3, Box 11.4; Sutton 2018, 2019). Alternatively high impacts can occur when different extremes occur at the same time or in short succession at the same location or in several regions with shared vulnerability (e.g., food-basket regions Gaupp et al., 2019). These “compound events” are assessed in Section 11.8 and Box 11.3 provides a case-study example.

The difficulties in determining the likelihood of occurrence and time frame of potential tipping points and surprises persist. However, new literature has emerged on surprises and low-probability high-impact events. There are events that are sufficiently rare that they have not been observed in meteorological records, but whose occurrence is nonetheless plausible within the current state of the climate system. The rare nature of such events and the limited availability of relevant data makes it difficult to estimate their occurrence probability and thus gives little evidence on whether to include such hypothetical events in planning decisions and risk assessments. The estimation of such potential surprises is often limited to events that have historical analogues, albeit the magnitude of the event may differ. Additionally, there is also a limitation of available resources to exhaust all plausible trajectories of the climate system. As a result, there will still be events that cannot be anticipated. These events (also called 'grey or black swans') can be surprises to many in that the events have not been experienced, although their occurrence could be inferred by statistical means or physical modelling approaches (Chen et al., 2017; van Oldenborgh et al., 2017; Harrington and Otto, 2018a). Another approach focusing on the estimation of low-probability events and of events whose likelihood of occurrence is unknown consists in nudging physical climate models into an extreme atmospheric state and thus creating a non-probabilistic, physically self-consistent storyline of plausible extreme events and assessing their impacts and driving factors in past (Section 11.2.5) or future conditions (11.2.6) (Shepherd 2016; Zappa and Shepherd 2017; Shepherd et al. 2018; Sutton 2018;Wehrli et al., submitted;Hazeleger et al., 2015).

In many parts of the world, observational data are limited to 50-60 years. This means that the chance to observe an extreme event that occurs once in several hundred or more years is small. Thus when a very extreme event occurs, it becomes a surprise to many (Bao et al., 2017), and very rare events are often associated with high impact (van Oldenborgh et al., 2017; Philip et al., 2018a; Tozer et al., 2020). Such events do occur somewhere on the Earth from time to time, however. Attributing and projecting very rare events in a particular location by assessing their likelihood of occurrence within the same larger region and climate thus provides another way to make quantitative assessments regarding events that can locally be considered grey-swans. Some examples of such grey-swan events include for instance:

- Hurricane Harvey, that made landfall in Houston, TX in August 2017 (Section 11.7.1.4.)
- The 2010-2011 extreme floods in Queensland, Australia (Christidis et al., 2013a)
- The 2018 concurrent heatwaves across the northern Hemisphere (Box 11.3)
- Tropical cyclone Idai in Mozambique
- The California fires in 2018 and 2019
- The heat extremes in France in June and July 2019 (Vautard et al., submitted)
- The 2019-2020 Australia fires

One factor of surprise is the fact that we now live in a non-stationary climate, and that the framework of reference for adaptation is continuously moving (e.g., Schleussner et al., submitted). As an example, the concurrent heatwaves that occurred across the Northern Hemisphere in the summer of 2018 were considered very unusal and were indeed unprecedented given the total area that was concurrently affected (Toreti et al., 2019; Vogel et al., 2019; Drouard et al., 2019; Kornhuber et al., 2019); however, the probability of this event under 1°C global warming was found to be about 16% (Vogel et al., 2019), which is not extremely low. Furthermore, when other aspects of the risk, vulnerability, and exposure are historically high or have recently increased (see WG2, Chapter 16, Section 16.4), relatively moderate extremes can have very high impacts (Otto et al., 2015b; Philip et al., 2018a). As warming continues, the climate moves further away from its historical state with which we are familiar, resulting in an increased likelihood of unprecedented events and surprises. This is particularly the case under high warming levels such as the climate of the late 21st century under the RCP8.5 scenario.

11.2.5 Attribution of extremes

Attribution science concerns the identification of causes for given features of the climate system (e.g., trends, single extreme events). A general background and methods of attribution science is provided in the Cross-Chapter Box 1.4 and a different use of the term in regional contexts is assessed in Chapter 10 (Section 10.4.2). Trend detection using optimal fingerprinting methods is a well-established field, and has been assessed in the IPCC SREX (SREX Chapter 3) and IPCC AR5 (AR5 Chapter 10). The method is detailed in

Chapter 3 (Section 3.2.1). There are specific challenges when applying optimal fingerprinting to the detection and attribution of trends in extremes. In particular, the method generally requires the data to follow a Normal (Gaussian) distribution, which is often not the case for extremes. Recent studies showed that extremes can, however, be transferred to a Gaussian distribution, for example by averaging over space, so that optimal fingerprinting techniques can still be used (Zhang et al., 2013; Wen et al., 2013; and Wan et al., 2019). More recent studies have used non-stationary extreme value distributions which are more appropriate statistical descriptions and thus allow for detailed detection and attribution of regional trends in temperature extremes (Wang et al., 2017d).

Apart from the detection and attribution of trends in extremes, new approaches have been developed to answer the question whether and to what extent external drivers (in most studies, human-induced climate change) have altered the likelihood and intensity of an individual extreme event (National Academies of Sciences, Engineering, 2016). In the AR5 there was an emerging consensus that the role of external drivers of climate change in specific extreme weather events could be estimated and quantified in principle (AR5 Chapter 10, 10.6.2), but related assessments were still confined to particular case studies, often using a single model, and typically focussing on high-impact events with a clear attributable signal.

However, since AR5, the attribution of extreme weather events has emerged as a growing sub-field of climate research with an increasing body of literature (see series of supplements to the annual State of the Climate report (Peterson et al., 2012, 2013b; Herring et al., 2014, 2015, 2016, 2018), including the number of approaches to examining extreme events (described in Easterling et al., 2016; Otto, 2017; Stott et al., 2016)). Two distinct but complementary approaches have been used to examine the role of external drivers of climate change in specific extreme weather events: the likelihood- or magnitude-based approaches. These so-called risk-based approaches produce statements such as ‘anthropogenic climate change made this event type twice as likely’ or ‘anthropogenic climate change made this event 15% more intense’. Jézéquel et al. (2018) and Otto et al. (2016) identified that the framing of, and conditions imposed on, the attribution question can affect the sensitivity of an attribution statement. There is no single methodology to answer the question of whether and to what extent anthropogenic climate change altered the likelihood and intensity of an extreme event to occur, but recently key methodologies have emerged (van Oldenborgh et al., submitted; Philip et al., submitted)as well as efforts to calibrate the language used in different studies (Lewis et al., 2019b). There are a number of different analytical methods encompassed in the so-called risk-based approach based on observations and statistical analysis (e.g., van Oldenborgh et al., 2012), optimal fingerprint methods (Sun et al., 2014), regional climate and weather forecast models (e.g. Schaller et al., 2016), GCMs (Lewis and Karoly, 2013), and large ensembles of atmosphere-only GCMs (e.g., Lott et al., 2013). The magnitude-based approach similarly compares the magnitude and/or duration and spatial extent of an event of a fixed probability. While these two framing approaches were developed independently, many recent analyses assess both effects on the frequency and magnitude in a single framework.

A key component in any event attribution analysis is the level of conditioning on the state of the climate system. In the least conditional approach, the combined effect of the overall warming and changes in the large-scale atmospheric circulation are considered and often utilize fully-coupled climate models (Sun et al., 2014). More conditional approaches involve prescribing certain aspects of the climate system. These range from prescribing the pattern of the surface ocean change at the time of the event (e.g., Hoerling et al., 2013, 2014), often using AMIP-style global models, where the choice of sea surface temperature and ice patterns influences the attribution results (Sparrow et al., 2018), to prescribing the large-scale circulation of the atmosphere and using weather forecasting models or methods (e.g., (Pall et al., 2017; Patricola and Wehner, 2018; Wehner et al., 2018a). These highly conditional approaches have also been called “storylines” (Shepherd, 2016) and can be useful when applied to extreme events that are too rare to otherwise analyse or where the specific atmospheric conditions were central to the impact. However, the imposed conditions limit an overall assessment of the anthropogenic influence on an event as the fixed aspects of the analysis may also have been affected by climate change. For instance, the specified initial conditions in the highly conditional hindcast attribution approach often applied to tropical cyclones (e.g., Patricola and Wehner, 2018; Takayabu et al., 2015) permit only a conditional statement about the magnitude of the storm if similar large-scale meteorological patterns could have occurred in a world without climate change, thus precluding any attribution statement about the change in frequency.

The key sources of uncertainty in event attribution are the definition of the event and the uncertainty resulting from the framing and modelling approach. Observational uncertainties arise both in estimating the magnitude of an event as well as its rarity (Angélil et al., 2017). Results of attribution studies can also be very sensitive to the choice of climate variables (Sippel and Otto, 2014; Wehner et al., 2016). Attribution statements are also dependent on the spatial (Uhe et al. 2016; Cattiaux and Ribes 2018; Kirchmeier-Young et al. 2019) and temporal (Harrington, 2017; Leach et al., 2020) extent of event definitions, with large-scale averages generally yielding higher attributable changes in magnitude or probability due to the smoothing out of the noise. In general, confidence in attribution statements for large-scale heat and lengthy extreme precipitation events have higher confidence than shorter and more localized events such as extreme storms.

The reliability of the representation of the event in question in the climate models used in the study is of utmost importance (Angélil et al., 2016; Herger et al., 2018). Very extreme events stretch the capabilities of current-generation models, which is a factor in choosing a framing approach when GCMs are not able to simulate the underlying dynamics well, implying that the risk-based approach cannot be applied. The limited number of multi-model assessments of events and the lack of model evaluation have led to criticism of the emerging field of attribution science as a whole (Trenberth et al., 2015) and of individual studies (Angélil et al., 2017). It is overall well-established that multi-model and multi-approaches (e.g., combining observational analyses and model experiments) are necessary to derive robust estimates regarding the attribution of single events, in particular for extremes for which there is a less strong effect of human-induced climate change compared to natural climate variability, e.g., droughts: Hauser et al. 2017;Philip et al. 2018; Otto et al. 2018a, floods: Philip et al. 2019, and, more generally, in all cases where climate models are less robust in simulating the analysed events (van Oldenborgh et al., 2018; Kew et al., 2019b). While an overarching model evaluation framework for event attribution, applicable to all types of events, is currently not available, several ways of quantifying statistical uncertainty (Paciorek et al., 2018) and model evaluation (Lott and Stott, 2016; Philip et al., 2018, van Oldenborgh et al. in review, Philip et al., in review) have been employed. Paciorek et al. (2018) assessed a variety of advanced statistical methods to estimate standard error, making several recommendations for estimating risk ratio uncertainty (Section 11.2.4). The ability to confidently attribute the human influence on extreme events depends on these uncertainties and limits the confidence in the attribution of different types of events (National Academies of Sciences, Engineering, 2016). It should be noted that under present climate change (+1°C) some events can occur that would have had a (near) zero probability of occurrence under pre-industrial climate conditions (e.g., Imada et al., 2019; Vogel et al., 2019). This poses particular challenges for attribution science as the calculated probability ratios become infinite.

Event attribution studies provide now important evidence for the effects of climate change on a specific type of event and region. Given that for the relatively new field of event attribution, no best-practice methodologies exist yet, it is particularly important to clarify the assessment process and make steps transparent

[START FIGURE 11.4 HERE]

Figure 11.4: Flowchart, adapted from (Otto et al., submitted, a), depicting the assessment process to identify the quality of evidence in attribution studies and illustrating the different decision steps when assing the quality of evidence.

[END FIGURE 11.4 HERE]

(Fig. 11.4). In its most simple definition, evidence is simply the number of independent studies available in the literature (Mastrandrea et al., 2010). However, the available evidence for a certain type of extreme in a specific region can be low, medium, or high depending on how the study is conducted. Together with an assessment of the agreement of the studies, the quality of evidence will allow for a confidence level to be assigned to the assessment of how a type of event has changed or will change at a certain warming level. Figure 11.4 illustrates the different aspects that determine the quality of the evidence. High quality of evidence is given when independent models and methodologies are used, thorough model evaluation is conducted, and the observational data analysed is of high quality (Section 11.2.4). Low quality of evidence is assigned when either the observational data is poor, or the model(s) and methodologies employed do not allow for an assessment of the dependency of the result on the exact choices made.

11.2.6 Projecting changes in extremes as a function of global warming levels

The most important quantity used to characterize past and future climate change is the globally-averaged mean surface temperature (GMST) relative to its pre-industrial level. On the one hand, changes in GMST are linked quasi-linearly to global cumulative CO_2 emissions (IPCC, 2013). On the other hand, changes in regional climate, including many types of extremes, scale quasi-linearly with changes in GMST, often independently of the underlying emissions scenarios (SR15 Chapter 3; Seneviratne et al., 2016; Wartenburger et al., 2017; Matthews et al., 2017; Tebaldi and Knutti 2018, Sun et al., 2018a, Kharin et al., 2018, Beusch et al., 2019). Finally, the use of global temperature goals in the context of global policy documents (in particular the 2015 Paris Agreement, UNFCCC 2015), implies that information on changes in the climate system, and in particular extremes, as a function of GMST are of particular policy relevance.

Projections of future changes in extremes in relation to global warming levels have an important advantage in separating uncertainty associated with the global climate response (Chapter 4) from that resulting from the regional climate response associated with the given global warming levels (Seneviratne and Hauser, submitted). If the interest is in the projection of regional changes at certain global warming levels, such as those defined by the Paris Agreement, projections based on time periods and emission scenarios would have unnecessarily larger uncertainty due to differences in model global transient climate responses. To take advantage of this feature and to provide easy comparison with the SR15 assessment, assessments of projected changes in this chapter are largely provided in relation to future global warming levels, with a focus on changes at +1.5°C, +2°C, and +4°C of global warming above pre-industrial levels (Table 1.6). These correspond to a scenario compatible with the aim of the Paris Agreement (+1.5°C), a scenario slightly overshooting the aims of the Paris Agreement (+2°C), and a "worst-case" scenario with failed mitigation (+4°C). One limitation of this methodology is the path dependency found in a few cases (James et al., 2017), as some emission scenarios pathways (e.g., RCP2.6) do not sample higher warming levels and thus are more subject to noise (Wartenburger et al., 2017). The second concern is that this method is not suitable for impacts that have a temporal dependency such as sea-level rise (James et al., 2017). These are, however, limited in the case of climate extremes.

While regional changes in many types of extremes respond linearly with global mean temperature, generally irrespective of emission scenarios (see above), effects of local forcing can distort this relation. In particular, emission scenarios with the same radiative forcing can have different regional extreme precipitation responses under different aerosol forcing (Wang et al., 2017e). Another example is related to forcing from land use and land cover changes. Climate models are known to either overestimate or underestimate observed changes in annual maximum daily maximum temperature depending on the region and considered models (Donat et al., 2017; Vautard et al., submitted). Part of the discrepancies may be due to the lack of representation of some land forcings, in particular crop intensification and irrigation (Mueller et al., 2016b; Thiery et al., 2017; Findell et al., 2017; Thiery et al., in press). As these local forcings are not represented and as their future changes are difficult to project, these can be important caveats when using global warming scaling to project future changes for these regions.

The SR1.5 (SR1.5 Chapter 3) assessed different climate responses at 1.5°C of global warming, including transient climate responses, short-term stabilization responses, and long-term equilibrium stabilization responses, and their implications for future projections of different extremes. Indeed the temporal dimension, i.e. when the given global warming level occurs, also matters for projections, in particular beyond the 21st century and for some climate variables with large inertia (e.g., sea level rise and associated extremes). Nonetheless, for assessments focussed on conditions within the next decades and for the main extremes considered in this chapter, derived projections are relatively insensitive to details of climate scenarios and can be well estimated based on transient simulations (SR1.5 Chapter 3).

An important question is the global temperature at which a given change in a climate extreme can begin to emerge from climate noise. For this type of assessment, a "global temperature of emergence" (Kirchmeier-Young et al., 2019) can be determined, similarly to the well-established concept of "time of emergence" (Hawkins and Sutton, 2012). Figure 11.5 displays the global temperature of emergence for two types of climate extremes (Kirchmeier-Young et al., 2019), the 20-year return value of the the annual maximum of daily temperature (TXx_20yr) and of the annual maximum of the 1-day precipitation accumulation (Rx1day_20yr), based on the CanESM2 model (Arora et al., 2011) large ensemble when aggregated over 1 grid cell (2.8 degrees) or 25 grid cells (about 14 degrees). Results for another ESM are found to be qualitatively similar (Kirchmeier-Young et al., 2019), and similar analyses for the whole CMIP5 and CMIP6 ensembles for the IPCC AR6 large regions are also found to be consistent (Fig. 11.6). Overall, it is interesting to see that signals for extremes emerge very early for TXx_20yr, already below 0.2°C in many regions (Fig 11.5a,b), and at around 0.5°C in most regions. This is consistent with conclusions from the SR15 Chapter 3 for less-rare temperature extremes (TXx on yearly time scale), which shows that a difference as small as 0.5°C of global warming, e.g., between +1.5°C and +2°C of global warming, leads to detectable differences in temperature extremes in TXx in most IPCC-type large regions in CMIP5 projections (e.g,Wartenburger et al., 2017; Seneviratne et al., 2018b). For precipitation extremes (Rx1day_20year), the signals tend to emerge with larger changes in global warming, and tend to be stronger when aggregated on a larger scale than when analysed on the grid-cell level. This is also largely consistent with analyses for less-extreme heavy precipitation events (Rx5day on yearly time scale) in the SR15 Chapter 3. These results are consistent as well with the assessment of the SR15 Chapter 3 regarding the detectability of changes in extremes for a 0.5°C difference in global warming in the observational record (SR15 Chapter 3; (Schleussner et al., 2017)). It should be noted that detectable changes for a 0.5°C increment in global warming are also found for regional changes in other types of extremes (e.g., droughts in the Mediterranean and Southern Africa), as highlighted in the SR15 Chapter 3, Wartenburger et al. (2017) and Seneviratne et al. (2018b). Figure 11.6 also provides complementary analyses on a regional-scale of the global temperature of emergence for temperature and precipitation extremes in the full CMIP5 and CMIP6 ensembles. The results are found to be consistent with those in Figure 11.5.

To some extent, the analyses as functions of global warming replace the time axis with a global temperature axis. Nonetheless, information on the timing of given changes in extremes is obviously also relevant. Regading this information, i.e. the time frame at which given global warming levels are reached, the readers are referred to Chapter 4 (Section 4.6).

[START FIGURE 11.5 HERE]

Figure 11.5: Global warming level (°C) for the emergence of a robust increase in the probability of extremes attributable to anthropogenic forcing. The temperature displayed is from the 10-year period when the lower bound (5th percentile) of the risk ratio for 20-year TXx (a,b) and Rx1day (c,d) events first exceeds 1.0 and remains above 1.0 for all subsequent periods. The first column calculates extremes from each grid box, while the second column first calculates the mean of the surrounding 25 grid boxes (5 x 5) to represent larger-scale extremes. A perfect-model approach was used with the CanESM2 large ensemble and areas in grey indicate emergence did not occur before +4.7 °C. Adapted from Kirchmeier-Young et al. (2019).

[END FIGURE 11.5 HERE]

[START FIGURE 11.6 HERE]

Figure 11.6: Regional-scale analysis of the global mean temperature of emergence for temperature extremes and precipitation extremes based on the CMIP5 and CMIP6 ensembles. For definition of regions, see Atlas [adapted from Seneviratne and Hauser (submitted)], for a detection compared to pre-industrial time rather than late 20th century conditions].

[END FIGURE 11.6 HERE]

11.3 Temperature extremes

This section provides an assessment of changes in temperature extremes at global and regional scales, with the main focus on observed trends, the climate models' performance in simulating temperature extremes, as well as the detection and attribution and long-term projections of changes in temperature extremes. The metrics assessed for temperature extremes are mainly based on the definitions of the expert group on Climate Change Detection and Indices (ETCCDI) (Karl et al., 1999; Peterson et al., 2001), whereby the changes in temperature extremes are examined from three perspectives, i.e., frequency, magnitude, and duration. In this section, we refer to percentile-based indices (e.g., TX90p, the frequency of warm days) as frequency indicators and absolute measures (e.g., TXx, the maximum of daily maximum temperature) as magnitude indicators (see also Table 1 in Sillmann et al. 2013 for the definition). In addition, changes in the probability (e.g., once-in-20-year) of extreme temperatures are also assessed, in particular from model projections.

11.3.1 Mechanisms and drivers

The SREX Chapter 3 and AR5 WGI Chapter 10 concluded that greenhouse gas forcing is the dominant factor for the increases in intensity, frequency, and duration of warm extremes and the decrease in those of cold extremes, although many other factors also contribute to changes in temperature extremes. The general warming due to the increase of anthropogenic greenhouse gases in the atmosphere is the background of the changes in temperature extremes, and they are also modulated by variabilities at different time scales from shorter-term including intra-seasonal and inter-seasonal to inter-annual, decadal, and multi-decadal scales. The spatial scales of changes in extreme temperatures range from local and regional to larger scales such as continental or planetary. Changes might also be related to soil moisture-evapotranspiration-temperature and snow/ice-albedo-temperature feedbacks, land use change, or changes in aerosol concentrations (Sections 11.1.5, 11.1.6). Though the anthropogenic effect on large-scale circulation changes is not robustly detected in many cases (Chapter 3), drivers of extreme temperature due to large-scale atmospheric circulation patterns are affected by ocean-atmosphere interactions, land-atmosphere feedbacks, and local and regional forcings.

Changes in regional temperature extremes are observed over all land surfaces in the historical data record (Sections 11.3.2, 11.9), consistent with the observed global warming during that time period (Section 2.3.1.1). The changes in the intensity of temperature extremes, e.g., the temperature of the hottest days or coldest nights, are shown to increase more than GMST in several regions (e.g., Seneviratne et al., 2016, Wartenburger et al., 2017; IPCC SR15 Chapter 3). There are several reasons for this (Sections 11.1.4, 11.1.6, Box 11.1): 1) the mean differential warming between land and ocean with higher warming on land (Section 7.6.6.2); 2) snow/ice-albedo-temperature feedbacks in high latitudes and mountainous regions, which lead to a larger warming in regions/seasons with decreased snow/ice cover; and 3) soil moisture-evapotranspiration-temperature feedbacks leading to an additional warming in dry seasons/locations on land (see also hereafter). In addition, the decrease of plant transpiration under enhanced CO_2 concentrations is a direct CO_2 forcing of land temperatures (warming due to lack of cooling), which contributes to higher warming on land (Lemordant et al., 2016). At the regional scale, changes in temperature extremes, in observations and CMIP5 models, tend to follow changes in local mean temperature, although most regions display changes in skewness towards the hotter part of the distribution with some exceptions (Tamarin-Brodsky et al. 2019). Although the snow/ice-albedo feedback plays an important role in amplifying temperature variability in high-latitudes (Diro et al. 2018), the effect on temperature extremes is still unclear (Pithan and Mauritsen 2014; Gobiet et al. 2014; Section 11.6).

Warming at the global or regional scales may have a secondary impact on temperature-related extremes through large-scale circulation changes (Section 11.1.5). Extreme temperature events are associated with regional air mass excursions induced by circulation anomalies that are part of large-scale meteorological patterns (Grotjahn et al., 2016). This occurs directly through large-scale circulations that facilitates air mass excursions or alternatively the indirect modulation of variability, such as the interaction of storm track behaviour with blocking patterns. Quasi-stationary anticyclonic circulation anomalies or atmospheric blocking events are linked to temperature extremes in many regions in the mid-latitudes. Such large-scale circulation anomalies are also associated with temperature extremes in Australia (Parker et al., 2014; Perkins-Kirkpatrick et al., 2016), Europe (Brunner et al., 2017, 2018; Schaller et al., 2018), and Asia (Chen et al., 2016; Ratnam et al., 2016; Rohini et al., 2016). Mid-latitude planetary wave modulations affect short-duration temperature extremes such as heatwaves (Perkins, 2015; Kornhuber et al., 2020). Therefore, if the circulation changes in response to warming, these changes would affect temperature extremes (Clark and Brown, 2013; Tamarin-Brodsky et al., 2019). As highlighted in Chapters 2-4, it is *likely* that there have been observational changes in the extratropical jets and the mid-latitude jet meandering (Section 2.3.1.3.3); there is *high confidence* in human influence on the observed poleward shift of the jet in austral summer, but there is *low confidence* in the human influence on storm tracks and blocking activity (Section 3.3.3.3); and there is *high confidence* in the projections of the storm tracks in the southern hemisphere, but substantial uncertainty remains with *low confidence* in the northern hemispheric storm tracks and blocking (Section 4.5.1.6). There is also *low confidence* in possible effects of the Arctic warming on mid-latitude temperature extremes (Cross-chapter box 10.1). Hence, there is *low confidence* at the moment regarding greenhouse gas effects on temperature extremes that would be mediated through large-scale circulation changes.

Since the AR5, the effect of climate variability on extremes over various time scales from short-term intra-seasonal to longer multi-decadal has been examined. The modes of variability such as the North Atlantic Oscillation (NAO), the Arctic oscillation (AO), the Southern Annular Mode (SAM), the El Niño-Southern Oscillation (ENSO), and the Pacific Decadal Oscillation (PDO) (Section 11.1.5) can affect temperature extremes. Yet, large portion of changes in extreme temperature remains after the removal of the effect of those modes of variability at the multi-decadal scale and can be attributed to human influence (Wan et al., 2019)(Kamae et al., 2017b). An increase in temperature extremes is detected during the hiatus period, that is the “slower surface global warming” from the late 1990s to early 2010s (Box 3.1) (Kamae et al., 2014; Seneviratne et al., 2014; Imada et al., 2017). It is suggested that cold and warm extremes in mid-latitudes are associated with atmospheric circulation patterns including atmosphere-ocean coupled modes such as the Pacific Decadal Oscillation (PDO) and the Atlantic Multidecadal Oscillation (AMO) (Kamae et al., 2014; Johnson et al., 2018; Ruprich-Robert et al., 2018; Yu et al., 2019).

Feedback mechanisms including land-atmosphere feedbacks strongly modulate regional- and local-scale changes in temperature extremes (*high confidence*; Section 11.1.6; Seneviratne et al., 2013;Vogel et al., 2017; Donat et al., 2017; Sillmann et al. 2017; Hirsch et al. 2019; Lemordant et al., 2016). This effect is particularly notable in the mid-latitude regions where drying of soil moisture amplifies high temperatures (Whan et al., 2015; Douville et al., 2016). The soil moisture-temperature feedback was shown to be relevant for past and present-day heatwaves based on observations and model simulations (Miralles et al. 2014; Hauser et al. 2016; Meehl et al. 2016;Wehrli et al., 2019;Cowan et al., 2016). The uncertainty due to the land modelling is a cause of the discrepancy between observations and simulations (Clark et al., 2006; Mueller and Seneviratne, 2014; Meehl et al., 2016). The soil moisture-temperature feedback also has non-local effects (Vautard et al., 2007; Stéfanon et al., 2014).

Regional external forcings, such as land-use changes or anthropogenic aerosols, play an important role in the changes of temperature extremes at the regional scale in several regions (*high confidence*), as highlighted in Section 11.1.6. Deforestation has been shown to have contributed about one third of the warming of hot extremes at local scales in some mid-latitude regions since the pre-industrial time (Lejeune et al., 2018). There is *medium confidence* in the changes in temperature extremes due to land cover change given the large spread of Earth System Models in representing the underlying processes (Li et al. 2018b), which requires model weighting based on observational evidence. Some aspects of agricultural management, including no-till farming, irrigation, and overall crop intensification are *likely* to cool hot temperature extremes, but these processes are generally not represented in the CMIP5 and on-going CMIP6 simulations (Section 11.1.6). On the other hand, it has been suggested that double cropping could have led to increased hot extremes in the inter-cropping season in part of China (Jeong et al., 2014). Rapid increases in summertime warming in western Europe and northeast Asia since the 1990s are also linked to a reduction in anthropogenic aerosol precursor emissions over Europe, which was a key factor in increases in temperature extremes in both regions (Dong et al., 2016, 2017), in addition to the effect of increased greenhouse gas forcing (Section 10.4.2.2.6). This effect of aerosols on temperature-related extremes is also noted for declines in short-lived anthropogenic aerosol emissions over North America (Mascioli et al., 2016). These regional scale effects of global warming on temperature are extensively described in Chapter 10 (Europe: Section 10.4.3.2.6).

On the local scale, the urban heat island (UHI) effect also contributes to warming in cities, in addition to greenhouse gas forcing (e.g., Phelan et al., 2015; Chapman et al., 2017; Sun et al., 2019) . The UHI refers to the higher temperatures experienced in urban areas compared to the surrounding countryside and results from a reduction of vegetation in urban areas, reduced evapotranspiration, a higher occurrence of dark land surfaces with low albedo, and increased anthropogenic heat production. Studies note that the specific intensity of the UHI in individual cities depends on geographic features, climatic conditions, and seasonal variations of a city's particular location (Mohajerani et al., 2017). In addition, city population levels impact the degree of urban-rural surface temperature anomalies (Manoli et al., 2019). The UHI exacerbates the heat stress experienced during heatwaves for urban residents (Zhao et al., 2018b). The interaction between the UHI and heatwaves is sensitive to multiple considerations. The relationship between the UHI and future heatwaves depends on the scenarios considered and the degree of local warming (Zhao et al., 2018b). In terms of the impacts of heat, vulnerability to heat stress from the interaction of the UHI with heatwaves in Europe cities depends on city climatology and urban green space, with cooler cities more affected by additional heat (Ward et al., 2016). These effects may be partially mitigated through the implementation of reflective surfaces or increased vegetation cover in cities, which could potentially reduce mean warming and hot extremes (Li et al., 2014a; Seneviratne et al., 2018a).

Summary: There are multiple mechanisms underlying changes in extreme temperatures, with the greenhouse gases forcing being the dominant driver. At the regional scales, changes in circulation patterns and soil moisture-evapotranspiration-temperature or snow/ice-albedo-temperature feedbacks can play an important role in modulating long-term changes in temperature extremes. The short-term behaviour of extremes are also affected by decadal and multi-decadal natural variability and shorter-lived anthropogenic forcers. Land use, including land cover change and agricultural management, can affect trends and short-term variations. There is *low confidence* in projected changes in storm tracks, jets, and blocking and thus their influence in extreme temperatures in mid-latitudes.

11.3.2 Observed trends

The SREX Chapter 3 reported a *very likely* decrease in the number of cold days and nights and increase in the number of warm days and nights at the global scale. Confidence in trends was assessed as regionally variable (*low to medium confidence*) due to either a lack of observations or varying signals in sub-regions.

Since the SREX and AR5, many regional-scale studies have examined trends in extremes of shorter-duration measures such as daily temperatures and ETCCDI indices in many locations, providing strengthened evidence for increased heat-related extremes. The magnitude of trends in temperature-related observed extremes varies depending on the region, spatial and temporal scales, and metric assessed. In particular, we note the importance of distinguishing trends in frequency and magnitude measures of temperature. Furthermore, as noted in 11.2, in most locations observational data is of a length that restricts the assessment of long-term trends in daily temperature extremes. The frequency of warm days (TX90p) has increased, with larger decreases in the frequency of cold nights (TN10p) (from 12% of nights in 1951 to about 6% of nights in 2014) globally over the period of 1951-2014 (Alexander, 2016). Nearly all land regions showed statistically significant decreases in TN10p (Alexander, 2016), though trends in TX90p are variable with some decreases in the number of warm days in southern South America, mainly during austral summer (Rusticucci et al., 2017). A decrease in the number of five-day duration cold spells is also reported over nearly all land surface areas (Easterling et al., 2016). These global land-based changes in temperature extremes are also observed in a new global land surface daily air temperature dataset (Zhang et al., 2019c). Consistent warming trends in temperature extremes globally and in most land areas over the past century are also found in a range of largely independent observations-based data sets (Donat et al. 2016; Dunn et al. submitted). Analysis demonstrated seasonal variations in trends in temperature-related extremes. Over the recent 1997-2010 period, a further increase in warm-season temperature extremes was determined over most land areas, despite only slight warming of or constant global annual mean temperature (Seneviratne et al., 2014). Over that period, warm extreme trends were strongest in the warm season, with some cooling of warm extremes in the boreal winter recorded over a large fraction of the northern hemisphere mid and high latitudes (see also Section 11.3.1).

[INSERT FIGURE 11.7 HERE]

Figure 11.7: Linear trends over 1950-2018 in the annual maximum daily maximum temperature (TXx, top), the annual number of days when daily maximum temperature exceeds its 90th percentile during a base period 1961-1990 (TX90p, middle), and the annual minimum daily minimum temperature (TNn, bottom) based on the HadEX3 data set. Units are °C/decade for TXx and TNn and days/decade fir TX90p. HadEX3 is gridded product at 2.5° latitude x 3.75 ° longitude resolution. Linear trends are calculated only for grids with at least 66% annual values over the period. Areas without sufficient data are shown in grey. (adapted from Dunn et al. submitted)

[END FIGURE 11.7 HERE]

Various studies report trends in particular regions or countries, with many regions displaying trends in temperature-related extremes consistent with global averages. These are summarized in Tables 11.4-11.9 in Section 11.9. Figure 11.7 also shows the observed linear trend over 1951 to 2018 in TXx and TNn (the minimum of daily minimum temperature) from the HadEX3 dataset (Dunn et al. submitted).

In Africa (Table 11.4), recent observational studies show a considerable warming trend over most of the continent, accompanied by an increase in high temperature extremes. These include an increase in the frequency of warm days and nights and a decrease in the frequency of cold days and nights with *high confidence* over almost all the continent, where data are available (Donat et al., 2013b, 2014b; Kruger and Sekele, 2013; Chaney et al., 2014; Filahi et al., 2016; Ringard et al., 2016; Barry et al., 2018; Gebrechorkos et al., 2019). The increase in TNn is more significant than in TXx (Figure 11.1). Additionally, there is *medium confidence* that heatwaves, regardless of definition, have been becoming longer-lasting, hotter, and more spatially extensive in the last decades (Ceccherini et al., 2016; Moron et al., 2016; Russo et al., 2016).

In Asia (Table 11.5), there is *high confidence* in the increase of daily temperature extremes during the last decades over most of the Asian continent. Changes in temperature extremes in China are consistent with warming in the last decades (Zhou et al., 2016a; Yin et al., 2017; Qian et al., 2019), including decreases in cold extremes and increases in warm extremes, larger warming in the coldest day (night) than in the warmest day (night), and larger warming in the coldest (warmest) night than in the coldest (warmest) day (Zhou et al., 2016a). Over the south Asian region (Bangladesh, northern India, Nepal, Pakistan and Sri Lanka), warm extremes have similarly become more common and cold extremes less common, although the magnitude of warming varies (AlSarmi and Washington, 2014; Sheikh et al., 2015; Zahid et al., 2017; Roy, 2019). The warming trends in daily temperature extreme indices have also been observed in central Asia (Hu et al., 2016; Feng et al., 2018), the Himalaya and Tibetan Plateau (Sun et al., 2017), and southeast Asia (Supari et al., 2017).

In Australasia (Table 11.6), there is *high confidence* in increases in the number of warm days and warm nights and decreases in the number of cold days and cold nights since 1950 (Lewis and King, 2015; Jakob and Walland, 2016; Alexander and Arblaster, 2017). The increase in extreme minimum temperatures occurs in all seasons over most of Australia and typically exceeds the increase in extreme maximum temperature (Wang et al., 2013b; Jakob and Walland, 2016). Similar positive trends in extreme minimum and maximum temperatures have been observed in New Zealand, in particular in the autumn-winter seasons, although generally showing higher spatial variability (Caloiero, 2017). In the tropical western Pacific region, spatially coherent warming trends in maximum and minimum temperature extremes have been reported for the period of 1951–2011 (Whan et al., 2014).

In Europe (Table 11.8), there is *high confidence* in the increase in maximum temperatures and the frequency of heatwaves. The increase in the magnitude and frequency of high maximum temperatures has been observed consistently across regions including in central (Twardosz and Kossowska-Cezak, 2013; Christidis et al., 2015) and southern Europe (Croitoru and Piticar, 2013; El Kenawy et al., 2013; Christidis et al., 2015; Nastos and Kapsomenakis, 2015; Fioravanti et al., 2016; Ruml et al., 2017). In northern Europe, a strong increase in extreme winter warming events has been observed (Matthes et al., 2015; Vikhamar-Schuler et al., 2016).

In Central and South America (Table 11.7), there is *high confidence* that observed hot extremes (TN90p, TX90p) have increased and that cold extremes (TN10p, TX10p) have decreased over recent years, with trends varying among different extremes types, datasets, and regions (Skansi et al., 2013; Donat et al., 2016a; Rusticucci et al., 2017). There is *medium confidence* that TNn extremes are increasing faster than TXx extremes, with the largest warming rates observed over Northeast Brazil (NEB) and North South America (NSA) for cold nights (Skansi et al., 2013). However, there is *high confidence* that warm extremes (TXx and TX90p) have decreased in the last decades over most of South Eastern South America (SES) during austral summer (Rusticucci et al., 2017; Skansi et al., 2013;Wu and Polvani, 2017). According to Wu and Polvani (2017), a decrease in TXx by about 0.3°C/decade is reported over southeastern South America in HadEX2 over 1955–2005.

In North America (Table 11.9), there is substantial spatial and seasonal variation in trends in temperature extremes. Minimum temperatures display substantial warming across the continent, while there are more contrasted trends in the annual maximum temperatures (Fig 11.7). In the US, some stations show a cooling in monthly maximum temperatures, although minimum temperatures show significant warming (Lee et al., 2014; van Oldenborgh et al., 2019). The western United States, northern Midwest, and New England have experienced the largest increases in monthly temperatures. There is *medium confidence* that the lack of warming of the hottest extremes is due to crop intensification, based on an analysis of Mueller et al., (2016b) (see also Sections 11.1.6 and 11.3.1). In addition, it is possible that irrigation also played a role in masking the warming of hot extremes in this region (Thiery et al., 2017). The spatial variation in trends across the US varies depending on the dataset, time period, and temperature metric examined. For example, trends in daily maximum temperature values greater than the 95th percentile over 1979–2014 in NLDAS-2 show that warm anomalies have generally increased, except for parts of the Intermountain West and the western Northern Plains in winter where a decreasing trend has occurred (Yu et al., 2018). In Canada, changes in temperature-related extremes, for instance, increases in summer days and the number of hot days, are consistent with warming during the period of 1948-2014 (Vincent et al., 2018). In Mexico, a clear warming trend in TNn was found, particularly in the northern arid region (Montero-Martínez et al., 2018). The number of warm days has increased and the cold days have decreased (García-Cueto et al., 2019).

Trends in some measures of heatwaves are also observed at the global scale. Globally-averaged heatwave intensity, duration, and the number of heatwave days have increased from 1950-2011 (Perkins 2015). There are some regional differences in trends in characteristics of heatwaves with significant increases reported in Europe, Australia, Brazil (Bitencourt et al., 2016), and most of Argentina (Barros et al., 2015), although decreases in Excess Heat Factor (EHF), which is a metric for heatwave intensity, are observed in South America in data derived from HadGHCND (Cavanaugh and Shen, 2015).

Trends in some locations are also sensitive to the time period examined, or the heatwave metric analysed. The majority of heatwave characteristics examined in China between 1961-2014 show negative/positive trends in heatwave days before/after 1990, which reflects rapid warming since 1990 (You et al., 2017). The increases in frequency and duration of heatwaves since the 1990s are also observed in Mongolia (Erdenebat and Sato, 2016) and India (Ratnam et al., 2016; Rohini et al., 2016). In the UK, the lengths of short heatwaves have increased since the 1970s, while the lengths of long heatwaves (over 10 days) have decreased over some stations in the southeast of England (Sanderson et al., 2017b). In Africa, heatwaves, regardless of definition, have been becoming more frequent, longer-lasting, and hotter over more than three decades (Moron et al., 2016; Russo et al., 2016).

Summary: It is *virtually certain* that there has been an increase in the number of warm days and nights and a decrease in the number of cold days and nights on global scale since 1950. Both the coldest extremes and hottest extremes display increasing temperatures. It is *very likely*that these are also the cases at the regional scale in Europe, Australasia, Africa, and Asia, where data are available. Trends in temperature extremes are generally larger (by ca. 50% to 200%) than those in global mean temperature, due to larger warming on land and additional feedback effects (*high confidence*). It is *very likely* that there has been an increase in the intensity and duration of heatwaves and in the number of heatwave days at the global scale. These trends occur in Europe, Asia, and Australia. There is *medium confidence* in similar changes in temperature extremes in South America, the lower confidence is due to reduced data availability and fewer studies.

11.3.3 Model evaluation

The AR5 assessed that CMIP5 models generally capture observed spatial distributions of the mean state during 1986-2005, and trends in the second half of the 20th century for indices of extreme temperature (AR5 WG1 9.5.4.1). The CMIP5 modelled trends were consistent with both reanalyses and station-based estimates, with ensemble simulations outperforming individual model realisations. CMIP5 multi-model ensembles also simulate present-day warm extremes (in terms of 20-year return values), reasonably well, with errors typically within a few degrees Celsius over most of the globe (AR5 WGI 9.5.4.1).

Since the AR5, an increasing number of studies have been performed to evaluate the performance of CMIP5 models in simulating temperature extremes at regional and local scales. Validation of models depends on the metric assessed (e.g., change in mean or variability of extremes, spatial distribution, trends of past change), and no single metric is universally insightful about model performance.

Overall, the characteristics of changes in global-scale temperature extremes are captured by CMIP5 models, but with varying performance on the regional scale, in some regions displaying a good representation of specific features but in others also showing some quantitative biases (though good overall qualitative representation), either in terms of spatial features or trends over certain time periods. For example, over east Asia, the CMIP5 GCMs are able to simulate the climatological spatial distribution of the observed extreme temperature indices over China during 1986-2005, with the ensemble performing better than individual models and the ensemble simulateing intensity indices better than percentile indices (Zhou et al., 2014; Dong et al., 2015). Over North America, CMIP5 model skill in capturing observed ETCCDI metrics over the period 1979-2005 was higher in spring, compared to winter, summer, and autumn (Sillmann et al., 2013a; Grotjahn et al., 2016).

Initial analyses of CMIP6 simulations (Li et al. submitted; Kim et al. submitted, Wehner et al. submitted) indicate that the CMIP6 models generally capture the observed global and regional patterns of temperature extremes, with limited improvements over the CMIP5 models. But in-depth analyses of CMIP6 models' performance in simulating long-term changes in temperature extremes are still to emerge, limiting the scope of the assessment of CMIP6 models' performance here. The top panel of Figure 11.8 shows relative error estimates in simulating various indices of temperature extremes in the available CMIP6 models. Overall, no single model performs the best on all indices and the multi-model ensemble seems to out-perform any individual model due to its reduction in systematic bias. The middle and bottom panels of Figure 11.8 show errors in the 1979-2014 average annual TXx and annual TNn simulated by available CMIP6 models in comparison with HadEX3 and ERA5 (Li et al. submitted; Kim et al. submitted, Wehner et al. submitted). While the magnitude of the model error depends on the reference data set, the model evaluation drawn from them are quite similar. In general, models reproduce the spatial patterns and magnitudes of both cold and hot temperature extremes quite well. There are also systematic biases. Hot extremes tend to be too cool in mountainous and high latitude regions but too warm in the eastern United States and south America. For cold extremes, CMIP6 models are too cool except in northeastern Eurasia and the southern mid-latitudes. Errors in seasonal mean temperatures are uncorrelated to errors in extreme temperatures and often of opposite sign (Wehner et al. submitted). The errors between CMIP5 and CMIP6 are very similar and the pattern correlations between them are high. In general, CMIP5 and CMIP6 historical simulations are interchangeable in their performance in simulating the observed climatology of extreme temperature *(high confidence).*

[START FIGURE 11.8 HERE]

Figure 11.8: Top panel: A portrait diagram of relative spatially averaged root mean square errors (RMSEs) in the 1981–2000 climatologies of temperature indices simulated by the CMIP6 models with respect to the ERA-5 reanalysis (upper triangle), and HadEX3 (right triangle). The RMSEs are spatially averaged over global land 531 grid points. The top row indicates the mean relative RMSE across all indices for a particular model. The grey-shaded columns and blue-red columns on the right side indicates the standardized median RMSEmedian,std for CMIP6 and CMIP5 and their differences. Adapted from Kim et al., (submitted). Middle panel: Difference between CMIP6 multi-model average and ERA5 in their respective averages over 1979-2014. Bottom panel: Difference between CMIP6 multi-model average and HadEX3 in their respective averages over 1979-2014. The left in both middle and bottom panels is for TXx and the right for TNn. Unit is °C. Adapted from Kim et al., (submitted), Li et al., (submitted) and Wehner et al., (submitted).

[END FIGURE 11.8 HERE]

In terms of historical trends, the models' ability in capturing observed trends in temperature-related extremes depends on the metric evaluated, the time period considered, and how indices are calculated within models. Observed trends in global temperature extremes lie within the spread of simulated trends in CMIP5, with better consistency for the longer period considered (Sillmann et al., 2014). However, a systematic overestimation of the warming of hot extremes compared to local mean warming is identified for many land regions, in particular over Europe, North America, South America, and parts of western and southern Africa, for a comparison between the late 20th/early 21st century vs the mid-20th century (Ringard et al., 2016; Donat et al., 2017). This systematic bias is also consistent with an identification of overestimated mean June-July-August temperatures in many mid-latitude land regions in the CMIP5 GCMs, which also present a concomitant overestimation of dryness conditions (underestimated precipitation and evapotranspiration) in these regions (Mueller and Seneviratne, 2014). For the period from the late-1990s to the early-2000s, there is a discrepancy between observed and ensemble-simulated trends in global mean surface temperature due to the so-called hiatus (Karl et al., 2015; Fyfe et al., 2016; Santer et al., 2017), but this observation-model discrepancy does not generally extend to temperature extremes (Sillmann et al., 2014). The observed warming trends in TXx during this time period are well represented in CMIP5 simulations (Sillmann et al., 2014). Trends in TNn are less well represented in CMIP5 simulations, but the simulated trends are nevertheless consistent with observed trends globally and in many regions (Sillmann et al., 2014). Although the multi-model mean trend averaged over regions may be relatively small, the range of model differences in trends is large. The largest discrepancy between observed and simulated trends in cold extremes is found in the northern mid-latitudes, where observed cold extremes indicate a coherent zonal band of cooling trends over the period from the late-1990s and early-2000s (Sillmann et al., 2014). This discrepancy may suggest the influence of interannual variability and spatial and temporal scale (Marotzke and Forster, 2015; Hedemann et al., 2017). Some external forcing components not fully represented in current climate models may also have contributed to the observed local cooling trends in cold extremes (Meehl, Gerald A et al., 2013; England et al., 2014; Fyfe and Gillett, 2014; Sillmann et al., 2014).

Regionally, over east Asia, the CMIP5 ensemble performs well in reproducing the observational trend in temperature extremes averaged over China (Dong et al., 2015). Over Australia, the multi-model mean performs better than individual models in capturing observed trends in ETCCDI temperature measures in gridded observational datasets, with some individual models showing stronger or weaker than observed trends in temperature indices (Alexander and Arblaster, 2017). Over Europe, North America, South America, and parts of southern Africa, as mentioned, CMIP5 models simulate accelerated warming rates in TXx relative to annual average warming rates, which appears inconsistent with observations except over Europe, which may be due to relevant terrestrial processes (Meehl et al., 2016; Donat et al., 2017). In west and central Africa, Diedhiou et al., (2018) compared the scaling relationship of changes of ETCCDI temperature indices as a function of global temperature values for the period 1920–2010 (compared to the reference period 1961–1990) from CMIP5 models (historical) and observation-based data (GSWP3). Both models and observations show an increase in temperature, but the warming is around 1°C in CMIP5 models and 2°C in GSWP3, confirming that the models likely underestimate the temperature rise (Sherwood et al., 2014).

AMIP or SST-forced simulations are also used to assess the characteristics of temperature-related extremes (e.g., trends, heatwaves etc.). The observed trends in temperature extremes are generally well-captured by the SST-forced simulations although some regional features such as the lack of warming in daytime warm temperature extremes over South America are not reproduced in the model simulations (Dittus et al., 2018). The dynamics of heatwave events over central-eastern China are well reproduced by the AMIP models. However, the AMIP models assessed tend to produce too-persistent heatwave events (lasting more than 20 days). The bias in the duration of the events does not impact the reliability of the models' positive trends, which is mainly controlled by the changes in mean temperatures (Freychet et al., 2018).

Several regional climate models (RCMs) have also been evaluated in terms of their performances in simulating the climatology of extremes in various regions of the Coordinated Regional Downscaling Experiment (CORDEX) (Giorgi et al., 2009), especially in East Asia (Ji and Kang, 2015; Yu et al., 2015; Park et al., 2016; Bucchignani et al., 2017; Gao et al., 2017a; Shi et al., 2017; Hui et al., 2018; Niu et al., 2018; Wang et al., 2018a), Europe (Vautard et al., 2013; Cardoso et al., 2019), and Africa (Diallo et al., 2015). Compared to global climate models, RCM simulations show an added value in simulating temperature-related extremes, though this depends on topographical complexity and the parameters employed. The improvement with resolution is noted in east Asia (Park et al., 2016; Zhou et al., 2016b; Shi et al., 2017; Hui et al., 2018). However, in the European CORDEX ensemble, aerosol concentrations were prescribed as constant in projections (Bartók et al., 2017) and the land surface models used in the regional climate models do not account for physiological CO_2 effects on photosynthesis (Schwingshackl et al., 2019), which could lead to biases in the representation of temperature extremes in these projections (See Section 11.2.3). In addition, there are key cold deficiencies in temperature extremes over areas with complex topography (Niu et al., 2018). Over North America, 12 RCMs were evaluated over the ARCTIC-CORDEX region (Diaconescu et al., 2018). Models were able to simulate well climate indices related to mean air temperature and hot extremes over most of the Canadian Arctic, with the exception of the Yukon region where models displayed the largest biases related to topographic effects. Two RCMs were evaluated against observed extremes indices over North America over the period 1989–2009, with a cool bias in minimum temperature extremes in both RCMs shown (Whan and Zwiers, 2016). The most significant biases are found in TXx and TNn, with fewer differences in the simulation of the minimum of daily maximum tempertaure (TXn) and the maximum of daily minimum temperature (TNx) in central and western North America. Over Central and South America, maximum temperatures from the Eta RCM are generally underestimated, although hot days, warm nights, and heatwaves are increasing in the period 1961-1990, in agreement with observations (Chou et al., 2014b).

Summary: There is *high confidence* that climate models can reproduce the climatology and the overall warming in temperature extremes observed globally and, in most regions, although the magnitude of the trends may differ. The ability of models to capture observed trends in temperature-related

extremes depends on the metric evaluated, the way indices calculated, and the time periods and spatial scales considered.

11.3.4 Detection and attribution, event attribution

The SREX Chapter 3 assessed that it is *likely* that anthropogenic influences have led to warming of extreme daily minimum and maximum temperatures at the global scale. The AR5 concluded that human influence has *very likely* contributed to the observed changes in the frequency and intensity of daily temperature extremes on the global scale in the second half of the 20th century. These assessments are largely based on the analysis of changes in extreme daily temperatures, as studies on changes in temperature extremes of longer time scales such as extreme monthly or seasonal temperatures were limited at the time of assessments. With regard to individual, or regionally- or locally-specific events, the AR5 concluded that it is *likely* that human influence has substantially increased the probability of occurrence of heatwaves in some locations, in addition to natural weather variability contributing to the overall magnitude of heatwave events.

There is more recent literature on human influence on long-term changes in frequency or intensity of global-scale, continental-scale, and sometimes regional-scale extreme temperatures of shorter duration. Focusing on TXx, TNx, TXn, and TNn, Kim et al. (2016) compared changes in the HadEX2 datasets with those simulated by the CMIP5 models for 1951-2010 using the optimal fingerprinting method. Results confirm previous HadEX/CMIP3-based results, where an anthropogenic signal is detected through optimal fingerprinting at global and continental scales. Wang et al. (2017) fitted the observed daily extreme temperatures to a generalized extreme value distribution with model-simulated responses as predictors, and their results are similar to those of Kim et al. (2016). Seong et al. (submitted) compared changes in these extreme daily tempertaures in the HadEX3 observations and in simulations by the CMIP6 models for 1951-2015; they not only confirmed earlier results, but also found the new results to be more robust due to the extended period that improves the signal-to-noise ratio. Fischer and Knutti (2015) quantified that as much as 75% of the moderate daily hot extremes (above 99.9th percentile) over land are about five times higher than in pre-industrial conditions due to anthropogenic warming. Wan et al. (2019) and Wen et al. (2013) attributed observed increases in extreme hot temperatures to anthropogenic influence in Canada and China, respectively. More generally, anthropogenic signals are robustly detected in the changes in the mean of extreme daily temperatures at global and continental scales. The detected anthropogenic signals are clearly separable from the response to natural forcing, and results are generally insensitive to the use of different model samples as well as different data availability.

Long-term changes in various other temperature-related indices, including the percentage of days when daily temperature is above its 90th percentile or below its 10th percentile over the globe and in various regions have also been attributed to anthropogenic influence. Hu et al. (submitted) compared the changes in the number of warm nights, warm days, cold nights, and cold days in the HadEX3 observations and CMIP6 simulations for 1951-2015 over the globe and five continents including Asia, Europe, North and South America, and Austraila. They attributed observed changes in these indices over the globe and the five continents to the influence of anthropogenic forcing, dominated by greenhouse gases. Regional studies, including for Asia (Dong et al., 2018), Australia (Alexander and Arblaster, 2017), and Europe (Christidis and Stott, 2016) found similar results. Studies also found attributable trends in multi-day heat indices such as the Warm Spell Duration Index (WSDI). For example, Christidis and Stott (2016) found a detectable increase in WSDI in Europe over the previous two decades. At the continental scale, anthropogenic increases in WSDI are detectable (Lu et al., 2018). Using an index that combines multiple ETCCDI indices (Combined Extreme Index, CEI), a clear anthropogenic signal is found in the trends in the maximum and minimum temperature index components for North America, Asia, Australia, and Europe (Dittus et al., 2016). While various studies have described increasing trends in several heatwave metrics (HWD, HWA, EHF, etc.) in different global regions (e.g., Bandyopadhyay et al., 2016; Cowan et al., 2014; Sanderson et al., 2017), few recent studies have explicitly attributed these changes to causes and rather stated that observed trends are consistent with anthropogenic warming.

There are also studies examining the rate at which new high-temperature records are observed. Studies of monthly, seasonal, and annual records in various regions (Kendon, 2014; Lewis and King, 2015; Bador et al., 2016; Meehl et al., 2016) and globally (King, 2017) show an increase in hot record breaking. For global-scale records, an anthropogenic influence on the rate of record-breaking was detected in CMIP5 simulations as far back as the 1930s (King, 2017). Changes in anthropogenically-attributable record-breaking rates are noted to be largest over the Northern Hemisphere land surfaces (Shiogama et al., 2016).

Long-term changes in cold extremes on various timescales have also been examined. King (2017) found a decreased likelihood of the occurrence of cold extremes due to anthropogenic forcings. Focusing on the rate of cold record-breaking, this study showed that it was harder to attribute cold extremes to a particular cause due to the rarity of the occurrence of new records. Christidis and Stott (2016) found that a human influence could be detected in cold nights on a global scale, but changes in the cold extremes were not detected in Europe, providing different results to SREX where *likely* decreases in cold nights were reported (Table 3-2). Furthermore, no attributable signal was detected for the cold indices FD and ID (frost and icing days). This study was based on simulations by two climate models, however Yin and Sun (2018) found clear evidence of an anthropogenic signal when multiple model simulations were used. In some key wheat-producing regions of southern Australia, increases in frost days or frost season length have been reported (Crimp et al., 2016; Dittus, Karoly, Lewis, & Alexander, 2014). The increase in frost days or season-length in southern (east and west) Australia is linked to decreases in rainfall, cloud-cover, and subtropical ridge strength, despite an overall increase in regional mean temperatures (Dittus et al., 2014; Pepler et al., 2018).

There are a large number of studies focusing on extreme temperature events at monthly and seasonal scales, using various extreme event attribution methods. Using a combination of observations and 30 realisations of a single model, Diffenbaugh et al. (2017) examined the anthropogenic contribution to observed changes in the hottest day and hottest month. Anthropogenic warming was found to have increased the severity and probability of the hottest month over >80% of the available observational area. Similarly, Christidis and Stott (2014) examined how anthropogenic forcings changed the odds of warm years, summers, or winters in a number of regions using an attribution framework where two different types of ensembles of simulations were generated with an atmospheric model to represent the actual climate and what the climate would have been in the absence of human influences. In all cases, warm events become more probable because of anthropogenic forcings. Sun et al. (2014) found that changes in summer mean temperature over eastern China can be attributed to human influence and this influence has caused a more than 60-fold increase in the likelihood of the extreme warm 2013 summer since the 1950s. Extensions of this study to other regions and variables show similar results. Mueller et al. (2016a) found anthropogenic influence in most of the land regions they analysed and inferred large increases in the probability of the historically hottest summers over many regions. Li et al. (2017) focused on the change in wet-bulb globe temperature (WBGT) that measures environmental conditions related to heat stress in northern hemispheric land areas. They estimated that the probability of summer mean WGBT exceeding the highest recorded value in the observational history has increased by a factor of at least 70 at regional scales due to anthropogenic influence. In most regions of the Northern Hemisphere, changes in the likelihood of extreme summer average WBGT were found to be about an order of magnitude larger than changes in the likelihood of extreme hot summers estimated by surface air temperature. In addition to these generalised, global-scale approaches, extreme event studies have found an attributable increase in the likelihood of hot annual and seasonal temperatures in many locations, including Australia (Knutson et al., 2014a; Lewis and Karoly, 2014), China (Li et al. submitted;Sparrow et al. 2018), and Europe (King et al., 2015).

There have also been many extreme event attribution studies that have examined short duration temperature extremes (daily temperatures, temperature indices, heatwave metrics). Examples of these events from different regions are summarised in various annual Explaining Extreme Events supplements of the Bulletin of the American Meteorological Society (Peterson et al. 2012, 2013, Herring et al. 2014, 2015, 2016, 2018), including a number of approaches to examine extreme events (described in Easterling et al., 2016; Otto, 2017; Stott et al., 2016). Several studies of recent events from 2016 onwards have determined an infinite risk ratio (FAR of 1), indicating that the occurrence probability for such events is close to zero in model simulations without anthropogenic influences (see Herring et al., 2018). However, caution should be exercised in this interpretation if rigorous uncertainty quantification techniques have not been applied (Paciorek et al. 2018). In addition, the interpretation of infinite risk ratios should also consider that risk ratios can depend on the details of the event definition (including thresholds and spatial and temporal scales; see discussion below).

Further studies have focused on the attributable signal in observed cold extreme events, producing complex results. Individual attribution studies on the extremely cold winter of 2011 in Europe find a decreasing likelihood (BAMS EEE 2012). On small spatial scales, the role of natural variability and dynamical responses to anthropogenic warming have been identified as important and have been examined in event attribution studies. Several studies of extreme cold conditions occurring in the eastern US during 2014 and 2015 demonstrate that winter climate variability is decreasing due to anthropogenic influences and observed extreme cold spells are less probable due to climate change (Trenary et al., 2015, 2016; Wolter et al., 2015; Bellprat et al., 2016). These studies determined that extreme cold was caused largely by natural internal variability. A similar attributable reduction in the likelihood of a cold extreme was found in the cold spring of 2013 in the United Kingdom (Christidis et al., 2014) and of 2016 in eastern China (Qian et al., 2018; Sun et al., 2018b). Grose et al (2018) focused on the severe western Australian frost of 2016 and found an increase in risk due to anthropogenically-driven changes in circulation patterns that drive cold outbreaks and frost risk. However, larger thermodynamic changes may have still made severe frost events less probable.

The interpretation of differences in results from temperature event attribution analyses needs to be placed in the proper context, as different framing may lead to different results. The temperature event definition itself plays a crucial role in the attributable signal (Fischer and Knutti 2015; Kirchmeier-Young et al. 2019). Large-scale, longer-duration events tend to have notably larger attributable risk ratios (Angélil et al. 2014, 2018; Uhe et al. 2016; Harrington 2017; Kirchmeier-Young et al. 2019), as the anthropogenic signal is large in comparison to natural variability. While uncertainty in the best estimates of the risk ratios may be significant, the lower bounds can be quite insensitive to uncertainties in observations or model descriptions, thus increasing confidence in conservative attribution statements (Jeon et al, 2016). The relative strength of anthropogenic influences on temperature extremes is regionally variable, in part due to differences in changes in atmospheric circulation, land surface feedbacks, and other external drivers like aerosols. For example, in the Mediterranean, risk ratios of the order of a 100 have been found (Kew et al., accepted, BAMS 2018), whereas in the US changes are much less pronounced. This is probably an artefact of the land-surface feedback enhanced extreme 1930s temperatures that reduce the rarity of recent extremes, in addition to the definition of the events and framing of attribution analyses (e.g., spatial and temporal scales considered). In India, heatwave likelihoods are not changing (van Oldenborgh et al., 2018) or even decreasing in some parts while increasing in others (Wehner et al., 2016). In this region, short-lived aerosols or an increase in irrigation may be masking the warming effect of greenhouse gases (Wehner et al., 2018c). More generally, irrigation and crop intensification have been shown to lead to a cooling in some regions, in particular in North America, Europe, and India (Mueller et al., 2016b; Thiery et al., 2017; see also Section 11.1.6, 11.3.2) (*high confidence*), although these effects are not represented in the CMIP5 or CMIP6 GCMs. There is also evidence that several CMIP5 models represent the effects of deforestation on temperature extremes with the wrong sign (producing cooling instead of warming with deforestation, Lejeune et al., 2017), although there is *medium confidence* that deforestation has contributed about 1/3 of the total warming of hot extremes in some mid-latitude regions since pre-industrial times (Lejeune et al., 2018). Despite all of these differences, and larger uncertainties at the regional scale, nearly all studies demonstrated that human influence has contributed to an increase in the frequency or magnitude of hot extremes and to a decrease in the frequency or severity of cold extremes.

***Summary:* Since the AR5, there has been new evidence of human influences on various temperature extremes. Long-term changes in various aspects of long- and short-duration extreme temperatures, including intensity, frequency, duration, and other relevant characteristics have been detected in observations and attributed to human influence at the global and continental scales. Event attribution studies on temperature extremes point to human influence on recent extreme heat-related events, regardless of framing, methods, definitions of events, and regions. It is *extremely likely* that human influence is the main contributor to the observed increase in the likelihood and severity of hot**

extremes and the observed decrease in the likelihood and severity of cold extremes on global scales. It is *very likely* that this applies on continental scale. Some specific recent hot extreme events would have been *extremely unlikely* to occur without human influence on the climate system. Urbanization has exacerbated the effects of global warming in cities (*high confidence*). Changes in aerosol concentrations have affected trends in hot extremes in some regions, with the presence of aerosols leading to attenuated warming, in particular from 1950-1980. Irrigation and crop expansion have attenuated increases in summer hot extremes in some regions, such as the central North America (*medium confidence*).

11.3.5 Projections

The AR5 concluded that it is *virtually certain* that there will be more frequent hot extremes and fewer cold extremes at the global scale and over most land areas in a future warmer climate and it is *very likely* that heatwaves will occur with a higher frequency and longer duration. More recently, the SR15 Chapter 3 provided a more specific assessment regarding projected changes in hot extremes at 1.5°C vs 2°C global warming. It came to consistent conclusions, assessing that it is *very likely* that a global warming of 2°C versus 1.5°C would lead to more frequent and more intense hot extremes on land, as well as to longer warm spells, affecting many densely-inhabited regions. SR15 Chapter 3 also assessed that it is *very likely* that the strongest increases in the frequency of hot extremes are projected for the rarest events, while cold extremes will become less intense and less frequent and cold spells will be shorter.

The available studies since the AR5 and SR15 using either Global Climate Model (GCM) or Regional Climate Model (RCM) simulations provide more specific information on future projections of extreme temperatures and generally confirm the conclusions of the AR5 and SR15. Compared to the AR5, important literature updates include projections of temperature-related extremes relative to mean changes in global warming, analyses of CMIP6 projections, analyses of existing projections based on global mean stabilization goals, and the examination of new metrics. For the CMIP5 projections, the forced response pattern of hot extremes in RCP8.5 simulations over the period 2006-2100 shows the greatest intensification over mid-latitude land regions and an overall warming of the hottest days that substantially exceeds the global mean temperature change (Fischer et al., 2014; Seneviratne et al., 2016). Changes in spatiotemporal heatwaves strongly depend on the thresholds used to define them (i.e., based on historical or future climatologies, the latter being of possible relevance in case of adaptation); based on historical thresholds there are projected strong increases in heatwave area, duration, and magnitude (Vogel et al. submitted).

Over Africa (Table 11.4), future projections show an increase in extreme temperatures. Increases are also projected, with *high confidence*, in the frequency of hot extremes such as warm days, warm nights, and heatwaves over the continent, with the exception of Central Africa (Giorgi et al., 2014; Engelbrecht et al., 2015; Lelieveld et al., 2016; Russo et al., 2016; Dosio, 2017; Mba et al., 2018; Nangombe et al., 2018; Kruger et al., 2019).

In Asia (Table 11.5), increases in hot events and decreases in cold events are projected with *high confidence* over most of the continent (Zhou et al., 2014; Zhang et al., 2015c; Singh and Goyal, 2016; Xu et al., 2017; Gao et al., 2018; Han et al., 2018). Particularly, in southern Asia, more intense heatwaves of longer durations and occurring at a higher frequency are projected with *medium confidence* over India (Murari et al., 2015) and Pakistan (Nasim et al., 2018).

Over Australia (Table 11.6), there is *high confidence* in future increases in hot temperature extremes and decreases in cold temperature extremes (Alexander and Arblaster, 2017; Lewis et al., 2017; Herold et al., 2018). Over most of Australia, increases in extremes are projected to be predominantly driven by increases in long-term mean temperatures (Di Luca et al. submitted). Future projections indicate a decrease in the number of frost days regardless of the region and season considered.

In Europe (Table 11.8), there is *high confidence*of a projected increase in summer heatwaves, similar to 2003 and 2010, and in an increase in hot temperature extremes over the whole continent (Lau and Nath, 2014; Ozturk et al., 2015; Russo et al., 2015; Schoetter et al., 2015; Vogel et al., 2017; Winter et al., 2017; Lhotka et al., 2018; Rasmijn et al., 2018; Cardoso et al., 2019). An increase in ice-free arctic summers is projected even under moderate warming scenarios, with *medium confidence*(Laliberté et al., 2015; Sigmond et al., 2018). In the Alps, there is *high confidence* in a projected increase in temperature extremes in all seasons (Gobiet et al., 2014).

In Central and South America (Table 11.7), projections show an increase in TN and TX and in the frequency of warm nights (TN90p) and warm days (TX90p) and a decrease in the frequency of TN10p and TX10p (López-Franca et al., 2016; Stennett-Brown et al., 2017). Over SES, during the austral summer, the increase in the frequency of TN90p is larger than that projected for TX90p, consistent with observed past changes (López-Franca et al., 2016).

In North America (Table 11.9), projections of temperature extremes for the end of the 21st century show that warm (cold) days and warm (cold) nights are *very likely* to increase (decrease) in all regions. There is *medium confidence* in large increases in warm days and warm nights in summer, particularly over the United States and in large decreases in cold days in Canada in fall and winter (Grotjahn et al., 2016; Vose et al., 2017; Alexandru, 2018; Li et al., 2018a; Yang et al., 2018a; Zhang et al., 2019d).

Following the approach used in the SR15 report, which is based on the sampling of responses from transient simulations at given global warming levels (see also Section 11.2 for details), we also provide here projections of changes in temperature extremes at different global warming levels, based on the CMIP5 simulations (Figs. 11.9 and 11.10). Figures 11.9 and 11.10 confirm that 1) there are already substantial increases in the temperatures of hot and cold extremes at 1.5°C global warming, 2) that projected changes at 2°C are substantially larger than at 1.5°C in several regions, and 3) that a warming of temperature extremes of 5°C or more is already reached at 3°C global warming in several regions. As identified in previous analyses, hot spots of warming include the mid-latitude and subtropical regions for hot extremes, and the Arctic for cold extremes.

[START FIGURE 11.9 HERE]

Figure 11.9: Projected changes (°C) in annual maximum daily maximum temperature (TXx) at 1.5°C, 2°C, 3°C, and 4°C of global warming compared to the early-industrial baseline (1851-1900), based on simulations by 21 CMIP5 and 11 CMIP6 models. Stippling indicates where the multi-model average change is larger than the across-model standard deviation (Note to reviewers: stippling scheme will be changed in the FGD to be consistent with other chapters, maps will be updated if additional simulations from CMIP6 models become available).

[END FIGURE 11.9 HERE]

[START FIGURE 11.10 HERE]

Figure 11.10: Projected changes (°C) in annual minimum daily minimum temperature (TNn) at 1.5°C, 2°C, 3°C, and 4°C of global warming compared to the early-industrial baseline (1851-1900), based on simulations by 21 CMIP5 and 11 CMIP6 models. Stippling indicates where the multi-model average change is larger than the across-model standard deviation (Note to reviewers: stippling scheme will be changed in the FGD to be consistent with other chapters, maps will be updated if additional simulations from CMIP6 models become available).

[END FIGURE 11.10 HERE]

Figures 11.9 and 11.10 show projected changes in annual maximum daily maximum temperature (TXx) and annual minimum daily minimum temperature (TNn) when the global mean temperature warms by 1.5, 2.0, 3.0, and 4.0°C above its pre-industrial level. Projected warming is larger for TNn and exhibits strong equator-to-pole amplification similar to the warming of boreal winter mean temperatures. The warming of TXx is more uniform over land and does not exhibit this behaviour. Overall, the warming of temperature extremes tends to scale linearly with global warming (Seneviratne et al., 2016, Wartenburger et al., 2017; Li et al. submitted; see also IPCC SR15, Chapter 3), but with a stronger warming on land. Regions and seasons of strongest warming include – as highlighted above and in the SR15 Chapter 3 – the mid-latitude summer and the Arctic winter. In the mid-latitudes, warming in hot extremes is up to double that of GMST (Fig. 11.11), i.e. about +3°C at +1.5°C of global warming and about +8°C at +4°C of global warming. In the Arctic winter, the warming of the temperature of the coldest nights is up to 3 times the warming of GMSTi.e. about +4.5°C at +1.5°C global warming, and about +12°C at +4°C global warming(Appendix Figure11.A.1). There is *medium confidence* in these quantitative assessments of projected changes in the temperature of extremes because of inter-model spread. Figure 11.11 provides the scaling of the regional changes in TXx as a function of global warming. From this figure as well as two similar figures on regional changes in TNn and TMean in the Appendix (Figs. 11.A.1 and 11.A.2), it can be seen that projected changes in temperature extremes can deviate substantially from projected changes in mean warming in the same regions. As discussed in Section 11.1.6, additional processes that control the response of regional extremes include, in particular, soil moisture-evapotranspiration-temperature feedbacks for hot extremes in mid-latitude and subtropical regions, and snow/ice-albedo-temperature feedbacks in high-latitude regions.

Despite the quasi-linear scaling of changes in the magnitude of temperature extremes as a function of global warming, projections of the probability of exceeding a certain hot extreme threshold tend to show an exponential increase as a function of global warming (e.g., Fischer and Knutti, 2015, Kharin et al., 2018). For example, the frequency for present-day climate 20-year hot extremes is projected to increase by 80% at 1.5°C global warming level and by 180% at 2.0°C global warming level, while the increase in the frequency for present-day climate 100-year hot extremes is projected to increase by 200% and more than 700% at the 1.5°C and 2.0°C warming levels, respectively (Kharin et al., 2018).Such nonlinearities in the characteristics of future regional extremes are shown, for instance, for Europe (Seneviratne et al., 2018; Dosio and Fischer, 2018), Asia (Guo et al., 2017; Harrington and Otto, 2018b; King et al., 2018), and Australia (Lewis et al., 2017a) under various global mean warming thresholds. The non-linear increase of fixed-threshold indices (e.g., percentile-based for a given reference period or based on an absolute threshold) as a function of global warming is consistent with a linear warming of the absolute temperature of the temperature extremes (e.g., Whan et al., 2015).

Several studies of future projections of the hottest summer temperatures demonstrate decreases in the return times, i.e. a higher frequency, of such events (Mueller et al., 2016a; Lewis et al., 2017b). Tebaldi and Wehner (2018) analysed RCP4.5 and RCP8.5 projections from the CESM large ensemble (Kay et al., 2015) of 20-year return values of both TXx and the running 3-day average of the daily maximum temperature (or TX3x). At the middle of the 21st century, 66% of the land surface area would experience present-day 20-year return values every other year on average under the RCP8.5 scenario, as opposed to only 34% under RCP4.5. By the end of the century, these area fractions increase to 92% and 62%, respectively. While long-period return values of TX3x are slightly lower than for TXx, the relative changes are larger and more robust. These results further demonstrate that projections of temperature extremes are dependent on the metrics analysed and the details of the definition of extreme temperatures.

Projections of temperature-related extremes in RCMs in CORDEX regions demonstrate robust increases in future scenarios and can provide information on finer spatial scales than GCMs. Five RCMs in the CORDEX-East Asia region show projected decreases in the 20-year return values of temperature extremes (summer maxima), with models exhibiting warm biases projecting stronger warming (Park and Min, 2018). Similarly, in the African domain, future increases in warm days (TX90p) and nights (TN90p) are projected (Dosio, 2017; Mostafa et al., 2019). This regional-scale analysis provides fine scale information, such as distinguishing the increase in TX90p over sub-equatorial Africa (Democratic Republic of Congo, Angola and Zambia) with values over the Gulf of Guinea, Central African Republic, South Sudan, and Ethiopia.

As for the projected changes of extremes in 20-year return values under stabilization goals, Wehner et al. (2018a) analysed five of the HAPPI atmosphere-only models and Sanderson et al. (2017a) analysed an extension of the CESM large ensemble at these goals. Combining the results of these two studies, the global land average of the 20-year return values of TX3x increases about the same as the global land average warm season (summer) temperatures. These amounts are about 0.3-0.4°C larger than the targeted global average stabilized warming, reflecting that land warms more than oceans as greenhouse gas concentrations are increased. There are significant differences in the occurrence and intensity of heat extremes under warming of 1.5°C and 2°C above pre-industrial values. Changes in nearly all heat extremes have a strong correlation to global mean temperature, so that scenarios and times with greater temperature change experience greater index changes for many regions (Aerenson et al., 2018).

[START FIGURE 11.11 HERE]

Figure 11.11: Regional mean changes in annual maximum daily temperature (TXx) for land regions, the global land and global ocean, against changes in global mean surface temperature (Tglob) as simulated by CMIP5 models for historical conditions (black) and under different forcing scenarios including RCP2.6 (light blue), RCP4.5 (blue), RCP6.0 (light red), and (red) RCP8.5. The black line indicates the 1:1 reference scaling. The grey shading indicates the range over all RCPs. [Note to reviewers: the plot will be updated to include CMIP6 simulations for the FGD, as well as the final selected AR6 regions].

[END FIGURE 11.11 HERE]

Summary: Given the *virtually certain* increase in global mean temperature and the link between global mean temperature and local temperature extremes, it is *virtually certain* that further increases in the likelihood and severity of hot extremes and decreases in the likelihood and severity of cold extremes will occur throughout the 21st century and around the world. It is *virtually certain* that the number of hot days and hot nights and the length, frequency, and/or intensity of warm spells or heat waves (defined with respect to late 20th century conditions) will increase over most land areas. In most regions, changes in the magnitude of temperature extremes are proportional to global warming levels (*high confidence*). The likelihood of temperature extremes generally increases exponentially with increasing global warming levels (*high confidence*). Confidence in assessments depends on the spatial and temporal scale of the extreme in question, with *high confidence* inprojections of temperature-related extremes at global and continental scales for daily to seasonal scales. There is *high confidence* that the magnitude of temperature extremes increases more strongly on land than global mean temperature. This includes a projected warming of extreme hot daytime temperatures of up to twice that of the global warming in mid-latitudes, i.e. about +3°C at +1.5°C global warming and about +8°C at +4°C global warming (*medium confidence*). The warming of extreme cold night-time temperatures in the Arctic, in several northern high-latituderegions, and some mid-latitude regionsis additionally projected to be about three times larger than the warming of global mean temperature, i.e. about +4.5°C at +1.5°C global warming, and about +12°C at +4°C global warming (*medium confidence*).

11.4 Heavy precipitation

This section assesses changes in heavy precipitation at global and regional scales. The main focus of this section is on extreme precipitation at a daily scale due to data and literature availability; however, extreme precipitation of shorter durations at sub-daily scales and of a longer durations of five days or more are also assessed. A majority of studies have focused on long-term changes (trends) in the annual maximum one-day or five-day precipitation, while some studies have also used peaks-over-threshold methods, where peaks were defined based on selecting a specific percentile (e.g., 95th percentile or 99th percentile). Percentile-based definitions also vary depending on the selection of the sample, whether they are from the entire year or from only wet days (Schär et al., 2016). Many of the studies have also examined changes in rarer events such as those that occur once in 20 years, in particular in model projections.

11.4.1 Mechanisms and drivers

Extreme precipitation is controlled by two main drivers: the amount of moisture and the atmospheric uplift. SREX Chapter 3 assessed changes in heavy precipitation that are governed by thermodynamic and/or dynamic changes depending on the regions (see also Box 11.1). The thermodynamic contribution mostly follows the Clausius-Clapeyron (C-C) relationship and is generally responsible for an increase in heavy precipitation where the changes in atmospheric circulation are small. However, this C-C relationship does not hold in regions with significant changes in circulation patterns, where the dynamics of moisture supply from remote sources dominate. Further background on these processes is provided in Section 8.2.3.2, Box 11.1, and Section 11.7, which assesses extreme storms including tropical/extratropical cyclones and severe convective storms, which act as parent storms for heavy precipitation. Latent heating can invigorate parent storms (Nie et al., 2018; Zhang et al., 2019g), which can increase precipitation intensity above that expected from the Clausius-Clapeyron equation (super C-C). Changes in large-scale modes of circulation patterns that modulate precipitation extremes are difficult to isolate from internal variability based on the historical record (Chapter 2) and future projections (Chapter 4). For example, future changes in El Niño-Southern Oscillation (ENSO) and its associated effects on precipitation extremes are uncertain (Section 4.4.3.2).

Thermodynamic and dynamic processes are important in driving heavy precipitation changes associated with monsoon circulations. The observed and projected changes in the monsoon system are assessed in Sections 2.3.1.3.2, 4.4.1.4, and 8.2.2.2. The associated precipitation may be amplified under future global warming in some regions, including East and South Asia (KITOH, 2017), but our understanding of monsoon circulations remain limited because of the complexity of these systems (Seth et al., 2019). Projected changes in the Asian monsoon generally include an increase in precipitation in the coastal regions of East and South Asia (Freychet et al., 2015; KITOH, 2017; Lee et al., 2018;Li et al., 2019). It is projected that SSTs will increase more near the coasts of the continents, and that this pattern of changes in SST can result in heavier rainfalls near the coastal areas in East Asia via tropical cyclones (Mei and Xie, 2016) or the torrential areas over western Japan (Manda et al., 2014). Low-level monsoon westerlies with moisture surge towards the Indian subcontinent are associated with the warming of the Western Indian Ocean and this may lead to an increase in the occurrence of precipitation extremes over central India (Krishnan et al., 2016; Roxy et al., 2017).

There is evidence that a decline in atmospheric aerosols causes additional warming leading to an increase in extreme precipitation. Hence, aerosol forcing plays an important role in the 21st century projections of heavy precipitation (Lin et al., 2016). An explicit treatment of aersol-cloud interactions further improves the simulation of extreme precipitation in the CMIP5 suite of models, specifically over India and China (Lin et al., 2018b). Possible effects of aerosols on extreme precipitation are detected via changes in tropical cyclones, which were modulated by changes in large-circulation patterns due to aerosol forcing (Takahashi et al., 2017; Strong et al., 2018).

Since SREX, the number of studies on the impacts of local land cover and land use change on heavy precipitation has increased. For example, there is a growing literature that indicates increases in heavy precipitation in urban centres due to urbanization (Zhang et al., 2019e). There are four possible mechanisms: a) increase in atmospheric moisture due to horizontal convergence of air associated with the urban heat island effect (Shastri et al., 2015); b) increase in condensation due to urban aerosol emissions (Han et al., 2011; Sarangi et al., 2017); c) aerosol pollution that impacts cloud microphysics (Schmid and Niyogi, 2017) (Box 8.1), and d) urban structures and resulting impediments to atmospheric motion and additional diffusion (Ganeshan and Murtugudde, 2015; Paul et al., 2018; Shepherd, 2013). Other local factors may also have the potential to impact heavy precipitation, such as reservoir that enhanced local evaporation (Woldemichael et al., 2012), irrigation (Devanand et al., 2019), or large-scale land use and land cover change (Odoulami et al., 2019).

Summary: Extreme precipitation is controlled by both thermodynamic and dynamic processes.

Warming induced thermodynamic change results in an increase in extreme precipitation, at a rate that closely follows the Clausius-Clapeyron relationship. The effects of warming-induced dynamic change on extreme precipitation are more complicated and difficult to quantify. This is because of the involvement of a widerange of processes from large-scale circulation to small-scale processes such as storms. This is also due to the high uncertainty in projecting circulation changes. The large uncertainty in projecting changes in the dynamic processes results in large uncertainty in projected changes in extreme precipitation, in regions where circulation is expected to change.

11.4.2 Observed Trends

Both the SREX Chapter 3 and the AR5 Chapter 2 concluded that it is *likely* that the number of heavy precipitation events over land has increased in more regions than it has decreased, though there are wide regional and seasonal variations, and trends in many locations are not statistically significant. This assessment is continuously supported by post-AR5 studies. (Du et al., 2019) found a significant increase in the global average of the annual maximum precipitation amount falling in a day and in precipitation events that last more than one day. Recent development of the new data set HadEX3 (Dunn et al., submitted) reveals more regions with increases than with decreases in the annual maxima (Rx1day) and an increase in the contribution of rainfall from very extreme days to total precipitaton (R95pTOT). A global and continental analysis (Sun et al., submitted) of station data showed that the percentage of stations with statistically significant increasins in Rx1day is larger than expected by chance, while the percentage of stations with statistically significant decreases is smaller than expected by chance, over global lands as a whole and over North America, Europe, and Asia where data coverage is relatively good (Figure 11.12). Stations with significant increases or decreases are not concentrated in any particular region. There are more regions with significant increases than with significant decreases. They also indicate significant intensification of Rx1day at the global and continental scales and that a decrease is not significant. There is a higher percentage of stations showing significant increases over 1951-2018 than over 1951-2010, but the percentages of stations with significant decreases over the two periods are similar (Sun et al., submitted), indicating enhanced evidence of an intensification of Rx1day with an additional eight years of observations. Extreme precipitation in the 20th Century has increased close to the C-C scaling in most of the land stations where data is available (Sun et al., submitted). Donat et al. (2019) have found a robust increase in extreme precipitation over humid regions around the globe. In dry regions, the trend is not robust, but shows an increase and this is partly due to high variability of precipitation and sparse observational coverage over dry regions.

Daily precipitation extremes show spatially non-homogenous trends for the 20th Century over Africa, where data are available (Donat et al., 2014a; Mathbout et al., 2018b). In North Africa, there is *medium confidence* of an increase in precipitation extremes (Donat et al., 2014b; Sun et al., submitted). Over sub-Saharan Africa, increases in the frequency and intensity of extreme precipitation have been observed over the well-gauged areas during 1950-2013; however this covers only 15% of the total area of sub-Saharan Africa (Harrison et al., 2019). Significant increases for extreme precipitation-related indices are identified: in R10mm over Western Sahara and Sudan, in R20mm, SDII and R95p over the western Sahel and in SDII, RX5day, and consecutive wet day (CWD) counts over western and southern Africa. For West Africa, observational evicence has pointed, with *high confidence*, to a substantial increase in precipitation extremes and intensity in recent years (Mouhamed et al., 2013; Panthou et al., 2014, 2018; Evan et al., 2015; Barry et al., 2018). Over central Africa, there is *low confidence* in observed changes in extreme precipitation due to a severe lack of station data (Alexander et al., 2019). There is an increase in extreme precipitation events in Southern Africa (Weldon and Reason, 2014). There *is medium confidence* in the increase in extreme daily precipitation over most of the continent (Barry et al., 2018; Chaney et al., 2014, Sun etal 2019).

There is an overall increase in extreme daily precipitation over Asia; however this is dominated by high spatial variability. There is *high confidence* in the observed increase in daily precipitation extremes over central Asia (Hu et al., 2016), most of south Asia (Roxy et al., 2017; Sheikh et al., 2015; Rohini et al., 2016; Roxy et al., 2017; Sheikh et al., 2015; Zahid and Rasul, 2012; Adnan et al., 2016; Dimri et al., 2017; Sheikh et al., 2015; Krishnan et al, 2019a; Priya et al, 2017; Hunt et al., 2018); the northwest Himalaya (Malik et al., 2016), and parts of east Asia ((Nayak et al., 2017; Baek et al., 2017), whereas, no trend is observed over the eastern Himalayas or contrasting evidence exists (Sheikh et al., 2015; Talchabhadel et al., 2018). There is high spatial variability in the trends in extreme precipitation over China, with a mixture of regions with increases and decreases (Fu et al., 2013a; Jiang et al., 2013; Ma et al., 2015; Yin et al., 2015). Over China as a whole, the trend is not significant (Li et al., 2018e). There is also an increase in the spatial variability of extremes in India (Ghosh et al. 2012, Shashikanth et al. 2018). Increases have been observed in precipitation extremes associated with an increase in western disturbances over the western Himalayas since the 1950s (Ridley et al., 2013; Dimri et al., 2015; Madhura et al., 2015). The monsoon extremes over the western Himalayas also show increases associated with declining southwest monsoon circulation and increased activities of westerly upper-air troughs (Priya et al., 2017). Increases have been observed over Jakarta (Siswanto et al., 2015), but Rx1day over most parts of the Maritime Continent has decreased (Villafuerte and Matsumoto, 2015). In Iran, 50% of the stations show increases in extreme precipitation with an overall decline in the frequency (Najafi and Moazami, 2016).

Over the whole of Australia, trends (1911-2010) in extreme daily precipitation indices are usually positive but their magnitude depends strongly on the dataset (HadEX2 or WAP) and on the specific index being considered (Alexander and Arblaster, 2017). There have been increases in heavy precipitation in northwest Australia (Dey et al., 2019) and decreases in many areas of southern Australia. There is a significant increase in PRCPTOT, R10mm, R20mm, R95p, CWD in northwest Australia over the period 1951-2015, and a significant decrease in SDII in coastal eastern Australia. A significant decrease in CWD, PRCTOT, R10mm, R20mm, SDII is reported in southeast Australia. Over southeast Australia, gridded observations show an overall increase in rainfall extremes (e.g., Rx1day) for the period 1911-2014 although trends vary spatially and seasonally (Evans et al., 2017). Over southeastern Australia, positive and sometimes significant trends in CWD, PRCTOT, R10mm, R20mm and Rx1d are observed when considering AWAP gridded data while HadEX2 usually show less positive trends and even a different sign for SDII (Alexander and Arblaster, 2017; Evans et al., 2017). There is *low confidence* that the number of heavy snowfall events has remain unchanged in the last 25 years over the Snowy Mountains (Fiddes et al., 2015). Over New Zealand, decreases are observed for moderate-heavy precipitation events, but no significant trends for very heavy events (more than 64 mm in a day) for the period 1951-2012. There is *low confidence* in the changes in frequency of heavy rain days with mostly decreases (Caloiero, 2015; Harrington and Renwick, 2014;Li et al., 2017).

Since SREX, there has been a growing number of studies on regional trends of daily extreme precipitation in Europe. There is *medium confidence* in an observed increase in the intensity and frequency of daily extreme precipitation events (van den Besselaar et al., 2013; Cioffi et al., 2015). Dominant decreases in extreme precipitation are observed in the western Mediterranean and some increases in the eastern Mediterranean (Rajczak et al., 2013; Casanueva et al., 2014; de Lima et al., 2015; Gajić-Čapka et al., 2015; Sunyer et al., 2015; Ribes et al., 2019). There are regions such as Portugal, where a mixed trend is observed (Pedron et al., 2017). In the Netherlands, the total precipitation contributed from extremes doubles per degree C increase in warming and this primarily comes from an increase in frequency (Myhre et al., 2019). In Romania, decreases are observed for the total number of precipitation days (R0.1mm) and increases are found for the frequency of moderate and heavy precipitation (R5mm, R10mm) (Croitoru et al., 2016). An increase in extreme precipitation is observed in central Europe, which is associated with the warming of the Mediterranean Sea (Volosciuk et al., 2016); though there are large discrepancies among studies and regions and strong seasonal differences (Croitoru et al., 2013; Willems, 2013; Casanueva et al., 2014; Roth et al., 2014; Fischer et al., 2015). In north Europe, extreme rainfall trends are different depending on the season (Irannezhad et al., 2017). Evidence for increasing extreme precipitation is observed during summer and winter, but not in other seasons (Yiou and Cattiaux 2013, BAMS, Dong et al. 2013 BAMS, (Held and Soden, 2006; Grams et al., 2014; Madsen et al., 2014; Helama et al., 2018) .

In North America, specifically in the United States, there is *medium to high confidence* in an overall increase in heavy precipitation at the daily scale, both in terms of intensity and frequency (Sun et al., submitted;Donat et al., 2013; Huang et al., 2017; Villarini et al., 2012; Easterling et al., 2017; Wu, 2015;Howarth et al., 2019), except for the southern part of the US (Hoerling et al., 2016). In Canada, there is a lack of detectable trend in observed annual maximum daily (or shorter duration) precipitation (Shephard et al. 2014, Mekis et al. 2015, Vincent et al. 2018). In Mexico, increases are observed in R10mm and R95p (Donat et al., 2016a) and in PRCPTOT and RX1day (Donat et al., 2016b).

For South America, the dominant signal is a wetting trend with high spatial variability. There is *low confidence* in the change (decrease) in daily extreme precipitation in northeastern Brazil (Skansi et al., 2013; Luiz Silva et al., 2018) with decreases in Rx1day, R50mm, R95p, R99p in Custódia and Sta Maria da Boa Vista (PE) (Bezerra et al., 2018). The annual maximum one-day (RX1day), and the heavy rainfall (R99p) exhibit increases when spatially averaged over large regions of South America, including NWS, SWS, SAM and SSA, but with *low confidence* (Skansi et al., 2013). An increase in extreme rainfall in observed in AMZ with *medium confidence* (Skansi et al., 2013) and in SES with *high confidence* (Wu and Polvani, 2017; Barros et al., 2015). Among all sub-regions, SES shows the highest rate of increase for rainfall extremes, followed by AMZ. SES shows the highest rate for Rx1day and Rx5day, but not for R99p (Skansi et al., 2013). According to (Skansi et al., 2013), moderate and non-statistically significant decreases are also observed over northeast Brazil, southern Peru and southern Chile. In Central America, trends in annual precipitation are generally non-significant, although small (but significant) increases are found in Guatemala, El Salvador, and Panama (Hidalgo et al., 2017).

Analyses of long-term changes in extreme sub-daily precipitation have been conducted only in a few regions. (Sen Roy and Rouault, 2013) showed an increase in extreme sub-daily rainfall over South Africa during summer in the last two decades. Ali and Mishra (2018) found an increase in sub-daily extreme precipitation over urban regions of India and showed the role of warming on such observed changes through dynamic and thermodynamic scaling. More increases than decreases in hourly extreme precipitation are observed over China (Westra et al., 2014). In eastern China, the southern part shows an increasing trend with no trend over the northern part (Yu and Li, 2012). Hourly data of Peninsular Malaysia show an increase in heavy precipitation (Syafrina et al., 2015). In Australia, Chen et al. (2013) found that the changes in rainfall intensity at the hourly scale positively correlate with changes in the mean maximum temperature. Guerreiro et al. (2018) analysed long-term changes in the magnitude and frequency of extreme hourly precipitation in Australia between 1966-1989 and 1990-2013. They showed a detectable increase in hourly extreme precipitation, spatially averaged over 107 guage stations. The highest magnitudes of hourly precipitation increase at about 20% per 1 degree increase in global mean temperature, which is about 10% per one degree increase in Australia temperature. The rate of increase of daily precipitation extremes is about one-third of that for hourly extremes. But uncertainty in the result is large as the station network used in the study is sparse. In Europe, studies on sub-daily extreme precipitation events are available for a limited number of regions. An increase in hourly extreme precipitation was observed in Sicily (Arnone et al., 2013). Sub-hourly rainfall data over the UK for the period 1996-2009 shows an increase in intensity and a decrease in the duration of extreme precipitation (Chan et al., 2016). For North America, the hourly precipitation data from 13 stations in the US show a large increase in extreme precipitation (Muschinski and Katz, 2013). Barbero et al. (2017) selected 733 stations with good quality long-term hourly observations from over 6000 US stations, and analysed trends of annual maximum one-hour precipitation. They found that about 5% of stations showed a significant increase, which is a rate higher than what would be expected by chance and the percentage of stations with a significant decrease was lower than expected by chance. This indicates a detectable increase in hourly extreme precipitation. The rate of increase in relation to mean temperature across the United States is about 4% per one degree temperature increase, smaller than the C-C rate. When compared with changes in annual extreme daily precipitation, the rate of increase in hourly extremes is smaller than for daily extremes and it is also more difficult to detect changes in hourly extremes.

A well constrained quantification of changes in short duration extreme precipitation can require records with lengths that are several times the length of available observations (Li et al., 2018b). This makes it difficult to quantify long-term trends in hourly extreme precipitation in many places of the world due to limited data availability. The connection between saturation vapour pressure and temperature governed by the Clausius-Clapeyron relation and the fact that extreme short-duration precipitation occurs at a time of ample moisture availability have motivated a large number of studies that attempt to establish a relation between extreme precipitation and temperature. This relation is based on day-to-day temperature variations and a robust estimation of such a relation, sometimes called apparent scaling, is more attainable. The estimation of these scaling relationships typically involves binning hourly precipitation according to some temperature measure (e.g., near-surface or aloft, daily or hourly, or directly including a moisture component by using dew point temperature) and then estimating the scaling of high percentile (i.e. 95, 99th) precipitation as a function of the bin temperature. Various methods have been explored, but a consensus is forming on the importance of including moisture in the estimation (see e.g., Lenderink and Fowler, 2017).

A unique and very large-scale data collection effort for sub-daily precipitation across multiple continents (Lewis et al., 2019) has enabled a comprehensive analysis of the relation between sub-daily precipitation extremes and day-to-day temperature variations on the global scale. There is a super-C-C scaling of hourly peak intensities at continental scales for the majority of observed gauges when using dew point temperature as the scaling variable. This apparent scaling seems to be robust across methodologies and regions and ranges between C-C and two times C-C (e.g., Burdanowitz et al., 2019; Formayer and Fritz, 2017; Lenderink et al., 2017). Yet evidence that there is a correspondence between this apparent scaling of daily temperature and precipitation intensities and the response of precipitation extremes to climate changes, called ‘climate scaling’, still needs to be established. In fact, studies suggest apparent scaling may not be representative of climate scaling. Bao et al. (2017) showed ensemble simulations by regional climate model were able to reproduce the spatial distribution of apparent scaling over Australia including large rates in midlatitude locations but weak or negative rates in the tropics. Yet, the same simulation projects a consistent increase in extreme precipitation across the Australian continent. Sun et al. (2019) compared apparent scaling and climate scaling over North America in a large ensemble of simulations of the Canadian regional climate model. They found that apparent scaling of the current climate is a good predictor for apparent scaling of the future climate. However, the magnitude and spatial pattern of apparent and climate scaling rates are quantitatively different, with little spatial correlation between them, regardless of precipitation duration or choice of temperature variable.

Overall, there is lack of systematic analysis of long-term trends in sub-daily extreme precipitation over the globe, but the available studies limited to some regions show an increase in general. It is difficult to infer how sub-daily extreme precipitation may have changed based on the observed changes in daily extreme precipitation because sub-daily extreme precipitation may involve different processes and/or occur in different seasons in many parts of the world (Barbero et al., 2019). The relevance of the present day apparent scalings to the past or future changes in sub-daily extreme precipitation remains questionable. Given these considerations, there is *medium confidence* in the increase in sub-daily extreme precipitation in parts of the world land areas.

Studies on past changes in extreme precipitation of durations longer than a day are more limited, though there are some studies examining long-term trends in annual maximum five-day (Rx5day) precipitation. An analysis of long-term trends in Rx5day shows that at the global and continental scales, Rx5day has increased in a way similar to that of Rx1day. The percentage of stations with significant increases in Rx5day is slightly larger than that in Rx1day, but the percent increase in Rx5day is slightly smaller than that in Rx1day (Sun et al. 2019 JCLI-0892). There are also some regional studies indicating an increase. Zhang et al. (2018) showed an increase in the global monsoon region with a rate of 5.17% per degree C. In west Africa, an increase in Rx5day is also observed (Chaney et al., 2014; Barry et al., 2018). An increase is observed in spatially-averaged Rx5day over large regions of South America, including NWS, SWS, SAM and SSA, but with *low confidence* (Skansi et al., 2013). A significant increase in Rx5day is also observed in northwest Australia over the period 1951-2015 (Dey et al., 2019). It should be noted that heavy precipitation events are often studied for a fixed duration, though these events can persist beyond the durations being studied. Hence, there is a need to consider a metric to address the complexity of changing extreme precipitation of varying durations in an warming environment (Du et al., 2019).

[START FIGURE 11.12 HERE]

Figure 11.12:(a) Trends in annual maximum amount of one-day precipitation (Rx1day) during 1950–2018 at 8345 stations with sufficient data for the calculate data to estimate. Light blue dots indicate increases and light red dots mark decreases. Solid blue and red dots indicate statistically significant increases and decreases, respectively, as determined by a two-tailed test conducted at the 5% level. (b) Summary statistics of the percentage of stations with statistically significant trends in Rx1day in the observations during the same period and in 1000 bootstrap samples. The blue and red colors indicate significant positive and negative trends, respectively, in the observations. Box-and-whisker plots summarize the breadth of the distribution from 1000 bootstrap realizations under the no-trend null hypothesis. In the plots, the upper and lower edges of the boxes mark the 25th and the 75th percentiles and the red lines indicate the median values. The upper and lower whiskers show the 97.5th and the 2.5th percentiles, respectively. Adapted from (Sun et al., submitted).

[END FIGURE 11.12 HERE]

Summary

There is high confidence that heavy precipitation has intensified on global scale over land regions. It is likely that, since 1950, the annual maximum amount of precipitation falling in a day or over five consecutive days has increased in more regions than it has decreased, over land regions with sufficient observational coverage for assessment. The percentage of stations showing statistically significant increase is higher than that can be expected by chance while the percentage of stations with significant decrease trend is not different from the expectation by chance. This is also the case at the continental scale over three continents, including North America, Europe, and Asia. Larger percentage increases in heavy precipitation have been observed in the northern high-latitudes in all seasons, as well as in the mid-latitudes in the cold season (high confidence). Regional increases in the frequency and/or in the intensity of heavy rainfall have also been observed in i) most parts of Asia, northwest Australia, northern Europe, southeast South America, north South America and most of the United States (high confidence), and ii) west and south Africa, central Europe, eastern Mediterranean region, Mexico (medium confidence). Elsewhere, there is generally low confidence in observed trends in heavy precipitation due to data limitations.

11.4.3 Model evaluation

Since the AR5, the simulation of large-scale patterns of precipitation has improved. The uncertainty in observed rainfall is large and model evaluation of simulated short-term heavy precipitation is challenging. A common issue when evaluating model output is the scale mismatch between simulated and observed data (Avila et al., 2015, Alexander et al., 2019) as daily and subdaily precipitation are not spatially-continuous fields. Furthermore, simulations represent average conditions over grid cells but station-based observations are conducted at point locations and are often sparse. As a result, extreme precipitation is expected to be smaller in the spatially-coarse CMIP5 and CMIP6 model simulations than in gridded station observations. Gervais et al. (2014) estimated that the reduction in precipitation extremes can be as large as 30% when comparing areal-mean values representative of current GCM grid boxes (~100km) to point estimations. However, Risser and Wehner (2020) reversed the order of operations by performing gridding to 25km after fitting extreme value distributions and found that winter long-period return values are larger than from an extreme value analysis of available gridded station precipitation products and that model skill in evaluation of the CMIP6 HighResMIP models is affected. Some model evaluation studies have utilized output from reanalysis products as a globally-complete proxy for observations ((Sillmann et al., 2013a); Kim et al., submitted; Li et al., submitted). However, while uncertainties related to large-scale circulation are reduced and the scale mismatch problem eliminated, local processes share similar parameterizations to the models themselves, reducing the objectivity of the comparison.

Studies evaluating the overall skill of the different generations of the Coupled Model Intercomparison Project (CMIP) models (Flato et al., 2013; Watterson et al., 2014) have found quite modest, although steady, improvements. Improvements in the representation of the magnitude of the Expert Team on Climate Change Detection and Indices (ETCCDI) indices in CMIP5 over CMIP3 (Sillmann et al., 2013a; Chen and Sun, 2015a) have been attributed to higher resolution. And growing evidence suggests that high-resolution models (CMIP5 median resolution ~ 180 ×96) reproduce extreme rainfall comparable with observations (Sillmann et al., 2013b; Kusunoki, 2017, 2018b). The simulation of extreme precipitation in some models is improved by refining horizontal resolution alone (Wehner et al., 2014; Kusunoki, 2017, 2018), but this is insufficient in other models (Bador et al., submitted) as model parameterization also plays a significant role (Wu et al., 2019a). Models generally underestimate extreme precipitation (Borodina et al., 2017) and this is partially due to the parameterization of convection (Kendon et al., 2019, Kendon et al., 2017). It should be noted that these overall assessments are often based on relatively simple scores and might not reflect much of the improvements in new generations of models with a more comprehensive and better formulation of processes in model components (Di Luca et al., 2015a).

Adopting a spatial perspective, Dittus et al. (2016) utilized the areal extent of daily precipitation extremes to evaluate eight CMIP5 models in comparison with the observations over the period 1951-2005. They found that many CMIP5 models can reproduce the observed increase in the difference between areas experiencing an extreme high (90%) and an extreme low (10%) proportion of the annual total precipitation from heavy precipitation (R95p/PRCTOT) for the Northern Hemisphere regions. Regarding precipitation intensity, models have also been shown to reproduce the compensation between precipitation extremes and the rest of the distribution (Thackeray et al., 2018), a characteristic found in the observational record (Gu and Adler, 2018).

Extreme precipitation simulated by CMIP5 and CMIP6 models has been compared with various observational products. As horizontal resolutions of the CMIP6 models are not substantially different from those in CMIP5, the multimodel performance is not significantly different and the error patterns are highly correlated (Wehner et al., submitted). Kim et al. (submitted) compared simulated Rx1day and Rx5day with HadEX3 data (Dunn et al., submitted) and found the wetter CMIP6 to be closer to HadEX3 than the drier CMIP5. Figure 11.13 shows the multi-model ensemble bias in mean Rx1day over the period 1979-2014 from 21 available CMIP6 models, as measured by three independent reference data sets. It illustrates the principal difficulty in evaluating extreme precipitation from climate models. As expected from the scale mismatch problem described above, extreme precipitation in the CMIP6 models is significantly drier than HadEX3, a product constructed by gridding annual Rx1day at individual stations to a 1.25° x1.875° mesh. Model performance is much more mixed when compared to the 0.25° ERA5 reanalysis or REGEN, a daily precipitation product constructed by Kriging interpolation of a merger of a variety of daily station data sets to a 1° mesh (Contractor et al., 2019). However, the inconsistency of these bias estimates, even in regions with a relatively dense observing network, undermines confidence in both the sign and magnitude of model errors in the simulation of extreme precipitation.

The performance portrait in the upper right of Figure 11.13 shows that individual model performance is generally consistent across a number of different extreme precipitation metrics, as measured by global land root mean square error. Taylor plot based performance metrics reveal strong similarities in the patterns of extreme precipitation errors over land regions between CMIP5 and CMIP6 (Srivastava et al., submitted; Wehner et al., submitted) and between annual mean precipitation errors and Rx1day errors for both generations of models (Wehner et al., submitted). While it is difficult to evaluate models' performance in simulating the magnitude of extreme precipitation, models seem to perform well in capturing large-scale features of precipitation extremes, including intense precipitation extremes in the intertropical convergence zone (ITCZ), and weak precipitation extremes in dry areas in the tropical regions (Li et al., submitted). In general, CMIP5 and CMIP6 historical simulations are interchangeable in their performance in simulating the observed climatology of extreme precipitation *(high confidence).*

[START FIGURE 11.13 HERE]

Figure 11.13: Top panel (matrix): A portrait diagram of relative spatially averaged root mean square errors (RMSEs) in the 1981–2000 climatologies of precipitation indices simulated by the CMIP6 models with respect to the ERA-5 reanalysis (upper triangle), and HadEX3 (right triangle). The RMSEs are spatially averaged over global land 531 grid points. The top row indicates the mean relative RMSE across all indices for a particular model. The grey-shaded columns and blue-red columns on the right side indicates the standardized median RMSEmedian,std for CMIP6 and CMIP5 and their differences. Adapted from Kim et al., (submitted). Other panels (maps): Percent errors in the CMIP6 multimodel mean Rx1day (1979-2014) relative to HadEX3 (top), ERA5 (middle) and REGEN (bottom). Brown indicate that models are too dry, while blue indicates that they are too wet. Adapted from Kim et al., (submitted), Li et al., (submitted) and Wehner et al., (submitted).

[END FIGURE 11.13 HERE]

Studies using regional climate models (RCMs), for example, the Coordinated Regional Downscaling Experiment (CORDEX; (Giorgi et al., 2009)) over Africa (Gbobaniyi et al., 2014; Dosio et al., 2015; Klutse et al., 2016; Pinto et al., 2016), Australia, East Asia (Park et al., 2016), Europe (Prein et al., 2016a), and parts of North America (Diaconescu et al., 2018) suggest that extreme rainfall events are better captured in RCMs compared to their host GCMs due to their ability to address regional characteristics, e.g., topography and coastlines. However, CORDEX simulations do not show good skill over south Asia for heavy precipitation and do not add value with respect to their parent CMIP5 GCMs (Mishra et al., 2014a; Singh et al., 2017)

Model evaluation of HighResMIP-class (resolution minimum 50 km in the atmosphere and 0.25° in the ocean) simulations (Haarsma et al., 2016) is incomplete. Wehner et al. (2014) found that in a ~25km version of the Community Atmospheric Model (fvCAM5.1), long-period return values of seasonal RX5day were substantially increased over the same model at ~100km. While the high-resolution simulation of mid-latitude winter extreme precipitation over land is in reasonable agreement with observations, simulation of the summer extreme precipitation has a high bias. As simulated extreme precipitation in the tropics also appears to be too large, deficiencies in the parameterization of cumulus convection at this resolution are suspected. Indeed, precipitation distributions are much improved with a convection-permitting model over west Africa at both daily and sub daily time-scales (Berthou et al., 2019) and over Belgium in Europe (Vanden Broucke et al., 2019).

There is *high confidence* that the ability to simulate climate extremes has steadily increased since the SREX and the AR5, principally due to refinements in horizontal resolution of global and regional models. At about 25km, models begin to simulate tropical and other intense storms considerably better than at lower resolutions, leading to higher values of extreme precipitation closer to observations, especially in regions of highly variable topography (Section 10.5.3). However, representation of cumulus convection is a challenging issue and current parameterizations need improvements. Further progress in this regard awaits the computational advances necessary for explicit representation of convective processes in multi-decadal simulations. Despite these few exceptions, in general the ability of the models to simulate the extreme events in the present improves the confidence of projected changes.

Summary

There is *high confidence* in the ability of CMIP6 models to capture large-scale features of precipitation extremes. The overall performance of CMIP6 models in simulating precipitation intensity and frequency is similar to that of CMIP5 models (*high confidence*). Both CMIP5 and standard resolution CMIP6 models are drier when compared to HadEX3. Some CMIP6 HighResMIP models produce higher and somewhat more realistic values of extreme precipitation (*medium confidence*). As extreme precipitation at a point location should be larger than extremes in area-mean precipitation, the mismatch in spatial scales between HadEX3 that is based on station data and the climate models' grid

area mean makes it difficult to determine if the models truly underestimate extreme precipitation at the spatial scale they simulate.

11.4.4 Causes of the Observed Changes

Both the SREX and the AR5 concluded with *medium confidence* that anthropogenic forcing has contributed to a global scale intensification of heavy precipitation over the second half of the 20th century. These assessments were based on the evidence of anthropogenic influence on aspects of the global hydrological cycle, in particular, the human contribution to the warming-induced observed increase in atmospheric moisture that should lead to an increase in heavy precipitation, and limited evidence of anthropogenic influence on extreme precipitation of durations from one to five days.

New studies, including detection and attribution and event attribution studies, since the AR5 have significantly improved the understanding of human influence on extreme precipitation. In particular, detection and attribution analyses have provided consistent and robust evidence of human influence on extreme precipitation of one- and five-day durations at global to continental scales. Zhang et al. (2013) compared the observed and CMIP5 models simulated Rx1day and Rx5day over 1951-2005 and found that the intensification in these indices of extreme precipitation over the Northern Hemisphere land areas can be attributed to human influence. They found that the anthropogenic signal is detectable in the extreme precipitation observations while the natural forcing signal is not detectable. They further found that the intensification of extreme precipitation is about 5.2% per K (90% confidence interval 1.3% to 9.3%), consistent with the Clausius-Clapeyron scaling. Paik et al. (submitted) analysed observed and CMIP6-simulated Rx1day and Rx5day over 1951-2015, and found the influence of greenhouse gases to be the dominant contributor to the observed intensitification of Rx1day and Rx5day over global land areas, in the mid-to-high latitudes, western and eastern Eurasia, and the gobal dry regions. These findings are also corroborated by the results of the analysis of changes in the fraction of extreme precipitation in the total precipitation. Dong et al. (submitted) examined changes in the annual total precipitation falling into the top 5th or top 1st percent of daily precipitation in the observations and the CMIP6 simulations. They found essentially the same results as (Paik and et al. (submitted). Kirchmeier-Young and Zhang (submitted) used three large-ensemble simulations, including two by coupled models and one by a regional model, and both detection and attribution and event attribution approaches in their regional- and continental-scale analysis of changes in extreme precipitation in North America from 1961-2010. They concluded that human influence has contributed to the increase in frequency and intensity of regional precipitation extremes.

One study examined the volcanic impacts, showing detectable influence from natural forcing on extreme precipitation at the global scale. Paik and Min (2018) found substantial reductions in RX5day and SDII (simple daily intensity index) over the global summer monsoon regions after explosive volcanic eruptions, using the HadEX2 observations and CMIP5 multi-model ensemble for 1957-2000. From models, they found that the reduction in extreme precipitation is closely linked to the decrease in mean precipitation, for which both thermodynamic effects (moisture reduction due to surface cooling) and dynamic effects (monsoon circulation weakening) play important roles.

Comparing spatially aggregated changes in RX5day over the global land area for 1960-2010, Fischer et al., (2014) found a large fraction of land has experienced a strong intensification of heavy precipitation, which is generally captured by CMIP5 models including anthropogenic forcing but not by unforced simulations. CMIP5 models were, however, found to underestimate the observed trends in precipitation extremes. Shiogama et al., (2016) found human influence on the historical changes in record-breaking one-day precipitation to be statistically significant.

Attribution of long-term changes in extreme precipitation at regional scales is more limited and the results tend to be less robust. Li et al. (2017) detected anthropogenic influence on extreme precipitation in China using the optimal fingerprinting method, but anthropogenic influence is not detected when a different method is used (Li et al., 2018e), indicating the lack of robustness in the detection results. A weak signal-to-noise ratio seems to be the main cause for the lack of robustness as Li et al. (2018d) also showed that the signal would become robustly detectable 20 years in the future. Krishnan et al. (2016) attributed the observed decrease in low and moderate rain (intensity between 5 mm /day and 100 mm/day) occurrences and increase in heavy rain events (intensity > 100 mm/day) in the post-1950s over central India to the combined effects of GHG, aerosols, landuse and landcover changes, and rapid warming of the equatorial Indian Ocean SSTs.

Systematic studies on long-term changes in heavy precipitation of a duration longer than five days are lacking. Instead, the focus has been on individual events, i.e., the attribution of changes in the probability or the magnitude of a class of extreme precipitation events similar to those that occurred recently by comparing real-world and counterfactual-world simulations. Many of those studies are summarised in the annual supplement report on "Explaining Extreme Events from a Climate Perspective" (Herring et al., 2014, 2015, 2016, 2018; Peterson et al., 2012, 2013b). Some studies found an influence of anthropogenic activities on the probability or magnitude of observed extreme precipitation events, including European winters (Schaller et al., 2016; Otto et al., 2018b), parts of the US for individual events (Knutson et al., 2014c; Szeto et al., 2015; Eden et al., 2016; van Oldenborgh et al., 2017), or China (Burke et al., 2016; Zhou et al., 2017; Sun and Miao, 2018; Yuan et al., 2018b). Other studies, however, suggested a lack of evidence about anthropogenic influences (Imada et al., 2013; Schaller et al., 2014; Otto et al., 2015c; Siswanto et al., 2015). Yet, there are also studies whose results are inconclusive because of limited reliable simulations (Christidis et al., 2013b; Angélil et al., 2016). Overall, both the spatial and temporal scale on which extreme precipitation eventrs are defined are important for attribution, event with large spatial scale has larger signal to noise ratio and thus signal is more readily detectable. At the current level of global warming, there is strong enough signal to be detectable for large scale extreme precipitation events but the chance to detect such signal for smaller scale events becomes smaller (Kirchmeier-Young et al., 2019).

Anthropogenic influence may have affected the large scale meteorological processes necessary for extreme precipitation and the localized thermodynamic and dynamic processes, both contributing to changes in extreme precipitation events. There are differences between attributing the causes of seasonal (or longer) extreme precipitation events and individual extreme storms (see Section 11.6) as the relative roles of these two factors can vary greatly and appropriate attribution methods may also be different (see Section 11.2.5). Several new methods have been proposed to disentangle these effects by either conditioning on the circulation state or attributing analogues. In particular, the extremely wet winter of 2013/2014 in the UK can be attributed, approximately to the same degree, to both temperature-induced increases in saturation vapor pressure and changes in the large scale circulation (Vautard et al., 2016; Yiou et al., 2017). There are multiple cases indicating an increase in very extreme precipitation in relation to temperature above 6-7%/ °C, the Clausius-Clapeyron rate (Pall et al., 2017;Risser and Wehner, 2017; van der Wiel et al., 2017; van Oldenborgh et al., 2017;Wang et al., 2018). Overall, the events in question in these cases are exceedingly rare and the attribution statements are highly conditional on the observed large scale factors (Wehner et al., 2018d). Yet, it is not known if and to what extent the large scale properties have changed (see Section 11.4.1).

Almost all existing event attribution studies on extreme precipitation are motivated by the need to understand the causes of a recent event that caused flooding (Section 11.5) leading to loss and damages. As precipitation is only one of the multiple factors, albeit an important one, that affects floods and as floods are only one of multiple factors causing damages, attribution of human influence to the probability of a precipitation event does not by itself directly attribute human influence to the flood or to the related damages. For example, Teufel et al. (2017) showed that while human influence increased the odds of the flood-producing rainfall for the 2013 Alberta flood in Canada, it was not detected to have influenced the probability of the flood itself. Similarly, Schaller et al.(2016) showed human influence in the increase in the probability of heavy precipitation and its resulting flood of the river Thames in winter 2014, but its contribution to the additional properties at risk was inconclusive.

In summary, it is *likely* that anthropogenic influence is the main cause of the observed intensification of heavy precipitation in land regions. Multiple lines of new evidence since the AR5 have improved the confidence for human influence. The observed global increase in annual maximum one-day and five-

day precipitation can be attributed to human influence. A large fraction of land showed enhanced extreme precipitation and a larger probability of record-breaking one-day precipitation than expected by chance, both of which can only be explained when anthropogenic greenhouse gas forcing is considered. At continental and regional scales, human influence on extreme precipitation is less detectable because of higher variability, but evidence is emerging. There is evidence of human influence on intensification of extreme precipitation in North America. There is also new evidence of human contributions to the increase in the probability or magnitude for some individual events in different parts of the world.

11.4.5 Projections

The AR5 concluded that it is *very likely* that extreme precipitation events will be more frequent and more intense over most of the mid-latitude land masses and wet tropics in a warmer world (Collins et al., 2013a). Post-AR5 studies using either GCMs and/or RCMs provide more lines of evidence supporting previous assessments. Projections based on CMIP5 model simulations show that the rate of change of Rx1day with warming is independent of the forcing scenario (Pendergrass et al., 2015). This is confirmed by (Sillmann et al., 2017a). (Sillmann et al., 2019) further showed, based on Precipitation Driver and Response Model Intercomparison Project (PDRMIP) simulations, that the rate of change in extreme precipitation that occurs once a year or less frequently, in relation to surface warming, is similar across all forcing agents including CO_2, CHAPTER 4, SOL, and black carbon. Both Lin et al. (2016) and Lin et al. (2018) found that that the rate of change for annual extremes is independent of the forcing agent, but the rate of change for moderate extreme precipitation may depend on the forcing agent. The moderate extreme precipitation used in Lin et al. (2016) and Lin et al. (2018) includes maximum one-day precipitation in each of 12 calendar months. As precipitation can have a distinct annual cycle in many parts of the world, their results may also be compounded by the effect of this annual cycle, and it is thus unclear if the difference in the rate of change for that moderate extreme precipitation truly reflects the difference in the responses to greenhouse gases and aerosols. There is thus *high confidence* that extreme precipitation that occurs once a year or less frequently scales with surface warming and is independent of the forcing agents.

Changes in Rx1day during the historic period for half-a-degree warming are consistent with the difference in the projected changes for 1.5°C and 2°C warming scenarios, as simulated by global models (Fischer and Knutti, 2015). While the magnitudes of projected changes differ according to different levels of warming, with larger changes under higher levels of global warming, the spatial patterns of the projected changes are quite similar, as shown in Figure 11.14. Changes in extreme precipitation across land areas are nearly always positive and increase with global warming level. This is different from projected changes in mean precipitation, which show a decrease over land in low latitudes. Decreases in extreme precipitation are confined mostly to subtropical ocean areas and are highly correlated to decreases in mean precipitation due to storm track shifts. These subtropical decreases can propagate to nearby land areas in individual realizations. Projected long-period Rx1day return value changes are larger than changes in mean Rx1day and increase with increasing rarity (Li et al., submitted; (Wehner, submitted). These differences amongst mean and extreme precipitation projected changes illustrate that the complicated interaction of dynamic and thermodynamic mechanisms varies locally and with the rarity considered.

[START FIGURE 11.14 HERE]

Figure 11.14: Projected percentage changes (%) in annual maximum one-day precipitation at 1.5°C, 2°C, 3°C, and 4°C of global warming compared to the early-industrial baseline (1851-1900), based on simulations by 21 CMIP5 and 11 CMIP6 models. Stippling indicates where the multi-model average change is larger than the across-model standard deviation (Note to reviewers: stippling scheme will be changed in the FGD to be consistent with other chapters, maps will be updated if additional simulations from CMIP6 models become available)

[END FIGURE 11.14 HERE]

Changes in Rx1day during the historic period for half-a-degree warming are consistent with the difference in the projected changes for 1.5°C and 2°C warming scenarios as simulated by the global models (Fischer and Knutti, 2015). This appears to also be the case even for higher levels warming. As showed in Li et al., (submitted) and Seneviratne and Hauser (submitted) an increase in extreme precipitation seems to scale linearly with the level of global warming. Figure 11.15 shows changes in the 50-year return values of Rx1day and Rx5day in relation to global warming levels as simulated by the CMIP6 models. The scaling of extreme precipitation is independent of the forcing scenarios or climate sensitivities of the models. The median value of the scaling over the land, across all SSP scenarios and all models, is close to 7% per °C for the 50-year return value of Rx1day and it is just slightly smaller for the 50-yr return value of Rx5day (note to the reviewers: this part will be updated with additional CMIP6 simulations in FGD). These indicate that a small increment such as 0.5°C in global warming can result in an increase in extreme precipitation. This may even be the case at continental and regional scales (Seneviratne and Hauser, submitted). Similar to changes in the response of extreme temperature to warming, the changes in the magnitude of extreme precipitation scale with global warming level linearly but the changes in the probability of extreme precipitation of fixed magnitude are a rate faster than linear, with more rapid increase for more rare events. For example, the frequency for present-day climate 20-year extreme precipitation is projected to increase by 10% at 1.5°C global warming level and by 22% at 2.0°C global warming level, while the increase in the frequency for present-day climate 100-year extreme precipitation is projected to increase by 20% and more than 45% at the 1.5°C and 2.0°C warming levels, respectively (Kharin et al., 2018). Dosio and Fischer, (2018) have shown a marked projected change in extreme precipitation in comparison to mean precipitation in Europe. In a 3°C warmer world, there will be a robust increase in extreme rainfall over 80% of land areas in north Europe. An additional half degree of warming from 1.5°C to 2°C would result in an increase in regional extreme precipitation over China, irrespective of the return periods (Li et al., 2018f). Projections with the HAPPI project show that extreme precipitation will amplify in the Asian-Australian monsoon region with an additional half degree of warming, though there is uncertainty in the projections for Australia (Chevuturi et al., 2018). The frequency of extreme precipitation will increase in east Asia and India. Increased daily extreme precipitation is projected for Africa with an additional half degree of warming by the CORDEX regional models and these projections are similar to the simulations by coarse-resolution global climate models (Nikulin et al., 2018).

[START FIGURE 11.15 HERE]

Figure 11.15: Global land median changes in the 50-year return values of annual maximum 1-day precipitation (Rx1day; A-B) and 5-day precipitation (Rx5day; C-D) against changes in global annual mean surface air temperature (GMST) in the CMIP6 multi-model ensemble projections under different future forcing scenarios. At each land grid cell, the corresponding return values are first estimated in each of the six overlapping 30-year periods (i.e., 2021-2050, 2031-2060, …, 2071-2100) for each model and forcing scenario. Then the global land median relative changes in the estimated return values from one period to a later period and the corresponding GMST changes are plotted as scatter points, with these scatter points marked according to forcing scenarios (A and C) or climate models (B and C). The black solid lines mark the median regression lines of the scatter points, while the grey shading bounds the 5-95% regression lines of the scatter points. The black dashed lines show the 7% per °C (CC-scaling rate) reference line. Adapted from (Li et al., submitted).

[END FIGURE 11.15 HERE]

In north Africa and the Sahara, there is *low confidence* in the changes in extreme precipitation, either due to a lack of agreement among studies on the sign of changes (Sillmann et al., 2013a; Giorgi et al., 2014) or due to insufficient evidence. There is *high confidence* that heavy precipitation is *likely* projected to increase by the end of the century under RCP8.5 in west Africa (Diallo et al., 2016; Dosio, 2016; Sylla et al., 2016;

Abiodun et al., 2017; Akinsanola and Zhou, 2018; Dosio et al., 2019) and *medium confidence* for an increase in central Africa (Fotso-Nguemo et al., 2018, 2019; Sonkoué et al., 2019) and east Africa (Ongoma et al., 2018). Over southern Africa there is *high confidence* that heavy precipitation is *likely* projected to increase by the end of the century and RCP8 (Dosio, 2016; Pinto et al., 2016; Abiodun et al., 2017; Dosio et al., 2019). However, over western South Africa, heavy rainfall amounts are projected to decrease. This is mainly due to a decrease in the frequency of the prevailing westerly winds south of the continent, which translates into fewer cold fronts and closed mid-latitudes cyclones (Engelbrecht et al., 2009; Pinto et al., 2018). The pattern of change in heavy precipitation under RCP4.5 in the majority of African regions is very similar to the pattern of change under RCP8.5, however the magnitude is smaller. With increases in global warming levels, there is *high confidence* that extreme precipitation is *likely* projected to increase in the majority of land regions in Africa (Pfahl et al., 2017; Diedhiou et al., 2018; Akinyemi and Abiodun, 2019; Giorgi et al., 2019).

There is *high confidence* that extreme precipitation is projected to increase in most parts of Asia under both RCP4.5 and RCP8.5 scenarios. An increase in heavy rainfall is projected in most parts of Asia together with increases in rainfall intensity (Zhou et al., 2014; Guo et al., 2016, 2018; Xu et al., 2016; Endo et al., 2017; Han et al., 2018; Kim et al., 2018b; Fujita et al., submitted). The precipitation extreme indices, including RX5day, R95p, and days of heavy precipitation (i.e.,R10mm), are all projected to increase under RCP4.5 and RCP8.5 scenarios in central and northern Asia (Xu et al., 2017; Han et al., 2018). A general wetting across the whole Tibetan Plateau is projected, with increases in heavy precipitation in the 21st century (Zhou et al., 2014; Zhang et al., 2015c; Gao et al., 2018). There is *high confidence* that the future rainfall extremes will increase in the Himalaya under warming scenarios (Palazzi et al., 2013; Rajbhandari et al., 2015; Wu et al., 2017; Paltan et al., 2018) despite limited evidence of a future decreasing trend of WDs (Hunt et al., 2018). The extreme daily precipitation is also projected to increase in south Asia (Shashikanth et al., 2018Han et al., 2018; Xu et al., 2017). In east Asia, there is *medium confidence* in the projected intensification of extreme precipitation (Guo et al., 2018; Li et al., 2018a; Seo et al., 2014; Sui et al., 2018; Wang et al., 2017b, 2017c; Xu et al., 2016; Zhou et al., 2014, Nayak et al., 2017).

Over Australia, there is *low confidence* in the projected changes in extreme rainfall. This is due to a lack of consistency among climate models and no significant future changes in extreme rainfall (Alexander and Arblaster, 2017; Evans et al., 2017). Future projected changes in extreme precipitation over north Australia are uncertain and do not show agreement among models. (Perkins et al., 2014b; Alexander and Arblaster, 2017; Evans et al., 2017; Dey et al., 2018). In south Australia, extreme precipitation is projected to increase, but the agreement among models is quite low (Alexander and Arblaster, 2017; Evans et al., 2017).

There is *medium confidence* in increases in rainfall extremes in boreal winter and summer over Europe (Madsen et al., 2014; OB et al., 2015; Nissen and Ulbrich, 2017). Over central and southern Europe, there is *low to medium confidence* in the changes in extreme rainfall manly due to discrepancies among studies and strong seasonal differences (Argüeso et al., 2012; Croitoru et al., 2013; Rajczak et al., 2013; Casanueva et al., 2014; Patarčić et al., 2014; Paxian et al., 2014; Roth et al., 2014; Fischer and Knutti, 2015; Monjo et al., 2016). In the Alps region, the intensity of precipitation extremes is projected to increase in all seasons (Gobiet et al., 2014), particularly in winter (Fischer et al., 2015). Projected increases in sub-daily extreme precipitation are lower compared to the daily scale in northeastern Europe, whereas opposite intensification is projected for western Europe near the sea (Scoccimarro et al., 2015).

Over North America, likely increases in the frequency and intensity of heavy rainfall are projected (Easterling et al., 2017; Wu, 2015; Zhang et al. 2018f)(Innocenti et al., 2019) for most of the continent. Projections of extreme precipitation over Mexico and Central America are more uncertain, with decreases possible (Sillmann et al., 2013b; Alexandru, 2018)

Over South America, in general there is a decrease in heavy rainfall amount (Chou et al., 2014b) with increases in southeastern South America and the Amazon (Chou et al., 2014b; Giorgi et al., 2014).

The number of studies on the projections of heavy hourly precipitation are limited due to high computing requirements for long-term simulations of the climate at a very high temporal resolution. The hourly precipitation extremes over CONUS are projected to increase, as shown by Andreas F Prein et al. (2016). Model simulations at a scale permitting convection project increases in extreme sub-daily precipitation over Africa (Kendon et al., 2019). Studies on the projections of longer-term extremes are also few in number. Climate simulations with the CESM large ensemble show a 3-fold increase in the frequency of the 100-yr precipitation accumulation in the future under RCP 8.5 (Norris et al., 2019b). In Japan, monthly extreme precipitation is projected to increase under 4°C global warming for around 80% of stations in the summer (Hatsuzuka and Sato, 2019).

Summary: Over almost all land regions, it is *very likely* that extreme precipitation will be more intense and more frequent in a warmer world. The increase in the magnitude of extreme precipitation will be, in general, proportional to the global warming level, with an increase of 7% and a slightly smaller rate in the 50-yr event of annual maximum 1-day and 5-day precipitation per 1°C warming, respectively (*high confidence*). The increase in the likelihood of extreme precipitation will *very likely*accelerate with increased global warming, with larger incremental increases at higher global warming levels and for rarer events. There can be large differences in the increase regionally.

11.5 Floods

There are different flood types (e.g., flash floods, river floods, groundwater floods, surge floods, coastal floods) due to differences in major drivers and processes involved (Nied et al., 2014; Aerts et al., 2018). Floods can be influenced by one or multiple drivers. Rainfall intensity is an important driver, in particular for flash floods; other drivers such as antecedent soil moisture, snow depth, and groundwater level are also important for some types of floods (Sikorska et al., 2015). In the case of surge floods or coastal floods, flooding may be affected by both heavy precipitation and sea level rise (Wahl et al., 2015, 2017) (see also Section 11.8). Floods as natural hazards are difficult to measure or quantify and, for this reason, many of the existing studies on changes in floods focus on flood indicators that can be measured, such as runoff or streamflow. Thus, the assessment of changes in floods in this section considers literature on changes in flow.

11.5.1 Mechanisms and drivers

Since the AR5, the number of studies on understanding changes in flooding has substantially increased. Several studies have highlighted basin-scale, complex interactions between hydrology and climate, including snow processes; temperature that affects soil freezing, evapotranspiration and snowmelt; and characteristics of precipitation such as timing, intensity, duration, and total amount. In addition, basin characteristics (e.g., topography, soil types, basin size), antecedent moisture conditions (Berghuijs et al., 2016; Paschalis et al., 2014), and plant-physiological effects (Kooperman et al., 2018) have also been assessed. The role each of these drivers play can be quite different for different flood types.

The main drivers for river floods include precipitation, antecedent soil moisture (Paschalis et al., 2014; Berghuijs et al., 2016; Fitsum and Ashish, 2016; Grillakis et al., 2016), and snow cover (Berghuijs et al., 2019). Additionally, other factors also play an important role. These include physiographic characteristics (e.g., hydraulic structures, stream morphology) (Nakayama and Shankman, 2013; Borga et al., 2014), land-use and land-cover characteristics (Aich et al., 2016; Rogger et al., 2017), water management (Pisaniello et al., 2012; Kim and Sanders, 2016), feedbacks between climate, soil, snow, vegetation etc. (Hall et al., 2014; Ortega et al., 2014; Berghuijs et al., 2016; Buttle et al., 2016; Teufel et al., 2019). The complexity of the factors involved as well as their interplay means that an extreme precipitation event does not necessarily translate into a flood event and an increase in precipitation extremes may not result in an increase in river floods (Sharma et al., 2018). Nevertheless, at the regional scale, there seems to be some correspondence between long-term changes in flooding and precipitation in some regions such as the US (Berghuijs et al. 2016; Peterson et al. 2013), China (Zhang et al., 2015a), and the western Mediterranean (Llasat et al., 2016).

It has been speculated that the physiology of plants could influence river floods in the future because of CO_2 fertilizing effects that improve water-use efficiency by plants (Roderick et al., 2015; Milly and Dunne, 2016; Swann et al., 2016; Swann, 2018) thereby reducing evapotranspiration and contributing to the maintenance of soil moisture and streamflow levels (Yang et al., 2019). It has been suggested that this mechanism could increase the magnitude of floods driven by heavy precipitation (Kooperman et al., 2018). Yet, an increase in leaf area index and vegetation coverage could also limit the fertilizing effects, as larger vegetation coverage is also related to larger water consumption overall (Mátyás and Sun, 2014; Evaristo and McDonnell, 2019). Therefore, there is *low confidence* in the overall effects on future floods caused by the physiological responses of plants to an increase in CO_2 concentration in the atmosphere.

Flash floods can be caused by different factors, such as extreme precipitation (Cho et al., 2016; Archer and Fowler, 2018), glacier lake outbursts (Schneider et al., 2013; Schwanghart et al., 2016), or dam breaks (Biscarini et al., 2016). Urban flash floods are often caused by brief, but very intense rainfall, along with a high fraction of impervious surfaces (Hettiarachchi et al., 2018). Because of this direct connection, changes in very intense precipitation translate to changes in urban flood potential. Many factors, such as the overland flow rate and the design of urban (Falconer et al., 2009) and storm water drainage systems (Maksimović et al., 2009) affect flood generation. Therefore, there can be a spectrum of responses in flood intensities to a similar magnitude of change in rainfall extremes (Smith et al., 2013).

Mechanisms involved in coastal floods can be more complicated than those of inland floods, involving precipitation, winds, tides, tropical cyclones (Reed et al., 2015a), storm surges (Möller et al., 2014; Little et al., 2015; Muis et al., 2016), and sea level rise (Chapter 9) (Woodruff et al., 2013). In fact, coastal flood water during tropical cyclones can come from a mix of fresh water and salt water when large storm surges co-occur with heavy precipitation (Wahl et al., 2015) (Section 11.7). Additionally, coastal topography and physiography (Vousdoukas et al., 2016; Paprotny et al., 2019), protective infrastructures, and the economic development (Chakraborty et al., 2014; Felsenstein and Lichter, 2014; Hinkel et al., 2014; Muis et al., 2015; Vousdoukas et al., 2018a) are all relevant.

Summary: Heavy precipitation is an important factor causing flooding, but floods are affected by many other factors, including antecedent soil moisture, snow pack and snow-melting in cold regions, surge and tides in coastal regions, and human water management, depending on the type of floods. Because of the complex relationship between hydrology and climate, there is not always a one-to-one correspondence between an extreme precipitation event and a flood event, or between changes in extreme precipitation and changes in floods. However, flash floods are more directly related to extreme precipitation.

11.5.2 Observed trends

The SREX report (SREX Ch. 3) assessed *low confidence* for changes in the magnitude or frequency of floods at the global scale due to limited available records and confounding effects of changes in land use and engineering. This assessment was consistent with the AR5 report (AR5 Ch. 2), which stressed a lack of evidence and strong spatial heterogeneity. The recent SR15 report (SR15 Ch. 3) found increases in flood frequency and extreme streamflow in some regions, but decreases in other regions. The number of studies analysing flood trends has increased since the AR5 report, and there are also new analyses available since the SR15 (Berghuijs et al., 2017; Blöschl et al., 2019; Gudmundsson et al., 2019). The vast majority of studies focus on river floods, while studies on changes in urban or coastal floods are lacking. Streamflow measurements are not evenly distributed over space, and coverage in many regions of Africa, South America, and parts of Asia is poor (e.g., Do et al., 2017). Here we assess changes i) in the magnitude of peak flow, ii) in the frequency of high flows, and iii) in the seasonality of peak flows.

11.5.2.1 Changes in the magnitude of peak flow

Do et al. (2017) analysed trends in annual maximum peak flow in more than 3500 streamflow stations in the US, central and north Europe, Africa, Brazil, and Australia for 1961-2005. They found 7.1% of global stations with sufficient data showed a significant positive trend and 11.9% of stations showed a significant negative trend. They also found statistical evidence of decreasing trends in North and South America and in Australia, and statistical evidence of increasing trends in Europe and parts of South America. This suggests that there may be regionality in peak flow trends. As shown in Figure 11.16, Gudmundsson et al. (2019) have found that trends in the indicators of mean and extreme streamflow are regionally consistent, with drying in some regions (e.g., in the Mediterranean) and wetting in other regions (e.g., north Asia). Ishak et al. (2013) showed that in Australia, negative trends dominate in annual maximum flow (at 22% of stations) and that stations with significant negative trends were mostly located in the southeast and southwest. At continental and sub-continental scales, there can also be regional differences. Bai et al. (2016) showed a negative trend in annual maximum flow in central China that is linked to a decrease in precipitation intensity and an increase in the number of dams. Yet, Zhang et al. (2015) showed that there are no changes in peak flow in the Pearl river basin in southern China. In the Amazon basin, there is a significant increase in extreme flow associated with the strengthening of the Walker circulation (Barichivich et al., 2018), but no trends were found in annual maximum flow in west Africa (Nka et al. (2015)). Peterson et al., (2013a) documented strong spatial differences in the trends over North America, with an increase in the northwest US and a decrease in the southeast US. Their finding is consistent with other studies for North America (Armstrong et al., 2014; Archfield et al., 2016; Mallakpour and Villarini, 2015; Burn and Whitfield, 2016; Wehner *et al.,* 2018). In Europe, the long-term high flow data do not show clear trends (Hall et al., 2014; Mediero et al., 2015; Kundzewicz et al., 2018). Mangini et al. (2018) found strong spatial heterogeneity, with a similar percentage of stations showing significant positive (10%) and significant negative (8%) trends in the peak flow across central and north Europe for the period 1961-2015. Mudersbach et al. (2017) examined changes in a 138-year daily streamflow records for the Elbe River and did not find a long term trend in peak flow. Blöschl et al. (2019) suggested a spatial pattern of an increase in annual peak flow records over 1960 to 2000 in northwestern Europe and a decrease in south and eastern Europe.

[START FIGURE 11.16 HERE]

Figure 11.16: Trends in annual maximum daily streamflow during 1971-2010 for IPCC SREX regions with at least 50 streamflow gauge stations with sufficient data (from Gudmundsson et al. 2019).

[END FIGURE 11.16 HERE]

11.5.2.2 Trends in the frequency of high flows

Mallakpour and Villarini (2015) examined trends in the magnitude of annual maximum daily flow and in the frequency of high daily flow events that occurred twice-a-year on average over the central US. They found that while there is evidence of significance changes in the annual peak flow, strong evidence points to an increasing frequency of high flows. The apparent inconsistency between changes in the magnitude of annual peak flow and in the frequency of high flows should be interpreted in the proper context. The methods for trend detection for the magnitude and the frequency are different, and the analysis of changes in frequency also involves events less extreme than the annual peak flow. Analyses of European high flow using the same approach did not find coherent trends across Europe, except in the UK (Mangini et al., 2018; Mediero et al., 2015). There was a reduction in the frequency of high flows in the Segre basin of south Europe during 1950-2013 that seems to be related to water management practices, though extreme precipitation events also reduced during the period (Vicente-Serrano et al., 2017b). Increased water use was also suggested by Mallakpour and Villarini (2015) as a possible cause of the decrease in high flow frequency in Nebraska and Kansas, since the frequency of heavy rainfall days increased but the water table decreased as a consequence of a higher groundwater withdrawal. There is *low confidence* in the trends in peak flow frequency because there are only limited studies and because flows in many places are heavily affected by water management and thus excluded from analyses.

11.5.2.3 Changes in the seasonality of peak flows

Changes have been observed in the seasonality of peak flows in some regions, in particular in regions where snowmelt dominates. Burn and Whitfield (2016) analyzed spring peak flow timing in Canada. They showed that, because of warming, the spring peak flow has become earlier in catchments that are predominately fed by snowmelt. They also found that the timing of peak flow becomes more irregular in other catchments, suggesting a shift from a snowmelt flood regime to a more mixed flood regime, with an increasing importance of rainfall events in the generation of high flows. Blöschl et al. (2017) analysed changes in the timing of floods in Europe, using a dataset of more than 4000 gauging stations from 1960 to 2010. They found clear changes in the timing of winter and spring floods, including earlier snowmelt floods in northeastern Europe, earlier winter floods in western Europe, and later winter floods around the North Sea and parts of the Mediterranean coast. The earlier peak spring flood is due to warming-induced snowmelt, while changes in the flood timing in other European regions are related to changes in the timing of winter storms.

Summary: There is *high confidence* the seasonality of floods has changed in cold regions where snowmelt is involved. There is *high confidence* that significant trends in a flood proxy represented by peak streamflow have been observed in some regions over the past decades, including increases in parts of northern Asia, southern South America, the northeast US, the UK, and the Amazon and decreases in parts of the Mediterranean, northeast Brazil, south Australia, central China, and the southeast US. Estimation of past changes in floods is still challenging in many parts of the world because of gaps in observational data.

11.5.3 Model evaluation

Several studies have assessed the capability of hydrological and hydrodynamic models to reproduce flow peaks and flood area using observational meteorological data and terrain information. These studies mostly focus on river flow (Keller et al., 2019; Li et al., 2019b), river flooded area (Tehrany et al., 2014; Nyaupane et al., 2018; Gangrade et al., 2019), and, to lesser extent, urban (Gori et al., 2019) and coastal floods (Yin et al., 2019b). Studies that evaluate the performance of models in the simulation of urban and coastal floods are limited.

The quality of the flood simulations strongly depends on the spatial scale of the analysis, since flooding processes and interactions among them are different in small catchments compared to the large basins. The reproduction of the flood processes in large basins is more difficult, as larger basins involve more complex water management and water use. Regional-scale hydrological models perform better than global-scale hydrological models. However, over-fitting of complex hydrological models is an important source of uncertainty. A good statistic in hydrological model calibration does not guarantee a good reproduction of hydrological processes under forced climate conditions. Studies that use different regional hydrological models show wide spread in flood simulations (Dankers et al., 2014; Roudier et al., 2016; Trigg et al., 2016; Krysanova et al., 2017). Huang et al. (2017) investigated performance of nine hydrological models in different large basins of the world. They showed that the regional models reproduced moderate and high flows (0.02 – 0.1 flow exceedance probabilities) well, but for the most extreme flows (0-0.02 flow exceedance probability) there are large biases, independent of the climatic and physiographic characteristics of the basins. Global-scale hydrological models have even more challenges. The models struggle to reproduce the timing or magnitude of the seasonal cycle. Additionally, the ensemble mean of multiple models performs worse than any individual model (Zaherpour et al., 2018).

The use of hydrological models for assessing changes in floods, especially for future projections, adds another dimension of uncertainty. In addition to differences in hydrological models (Roudier et al., 2016; Thober et al., 2018), there is also a cascading of uncertainty from different sources, including emission scenarios, the driving climate models' (both RCMs and GCMs) structure and parameters (Hundecha et al., 2016; Krysanova et al., 2017), and natural climate variability, as well as the way climate model data is processed (or downscaled) as input for the hydrological models (Muerth et al., 2013). For example, (Maier et al., 2018) used a modeling framework, including outputs from two GCMs forced with three emission scenarios, a rainfall-runoff model, and a coupled surface water-groundwater model to study the impact of climate change on the inundation characteristics of a floodplain of the Rhine River in Hesse, Germany. They found large uncertainties in the simulated inundation characteristics that can be attributed mainly to the different GCMs. Overall, a shift in the inundation pattern, possibly in both directions, and an increase in inundation extent are simulated. Arnell and Gosling (2016) downscaled simulations by 21 GCMs under the CMIP3 A1B scenario to force a hydrological model at the global scale. They showed low consistency among projections in large parts of the world.

Summary: Regional hydrological models, using reliable atmospheric input variables, are able to reproduce moderate and high flows (0.02 – 0.1 flow exceedance probabilities) well, but their simulation for the most extreme flows (0-0.02 flow exceedance probability) can have large biases. Global-scale hydrological models still struggle with reproducing the timing or magnitude of the seasonal cycle of flow. Projections of future floods are hampered by these difficulties and cascading uncertainties from different sources, including emission scenarios and the reliability of climate models that generate inputs.

11.5.4 Attribution

There are very few studies focused on the attribution of flood events. It is difficult to assess the confidence in attribution from these studies since structural differences in hydrological models are very large compared to climate models. Thus, it is difficult to employ the same multi-method approach to individual event attribution studies (Section 11.2.5), but this does allow for an estimate of modeling uncertainty. Most of the studies focus on flash floods and urban floods, which are closely related to intense precipitation events (Hannaford, 2015). In other cases, event attribution focused on runoff using hydrological models, and examples include river basins in the UK (Schaller et al., 2016; Kay et al., 2018) (see Section 11.4.4), the Okavango river in Africa (Wolski et al., 2014), and the Brahmaputra in Bangladesh (Philip et al., 2019). The existing model uncertainties and the lack of studies overall suggest a *low confidence* in general statements to attribute flood events to anthropogenic climate change.

Furthermore, the anthropogenic signal is different in different regions and basins. For some flood events, the probability of high floods in the current climate is lower than in a climate without an anthropogenic influence (Wolski et al., 2014; Teufel et al., 2017), while in other cases the results are opposite and anthropogenic influence leads to more intense floods (Cho et al., 2016; Pall et al., 2017; van der Wiel et al., 2017; Philip et al., 2018b; Teufel et al., 2019). Drivers such as land cover change and river management can also increase the likelihood of high floods (Ji et al., 2020). Some individual regions have been well studied, which allows for *high confidence* in the attribution of increased flooding in these cases (Section 11.9 Table, and summary Figure Section 11.2). For example, flooding in the UK following increased winter precipitation (Schaller et al., 2016; Kay et al., 2018) can be attributed to anthropogenic climate change (Schaller et al., 2016; Vautard et al., 2016; Yiou et al., 2017; Otto et al., 2018b) (Section 11.4.4).

Gudmundsson et al. (2019) compared the spatial pattern of the observed regional trends in mean and high river flows over 1971-2010 with those simulated by global hydrological models driven by outputs of climate models under all historical forcing or by climate model pre-industrial simulations. They found complex spatial patterns of extreme river flow trends. They also found that the observed trend pattern can be reproduced only if anthropogenic climate change is considered. The simulated effects of water and land management cannot reproduce the observed trend pattern. This study provides evidence of human influence on extreme river flow trends on the global scale. As there is only one study and multiple caveats, including relatively poor observational data coverage, there is *low confidence* about human influence on the global scale.

Summary: Warming has affected spatial trend patterns of extreme river flow on the global scale (*low*

***confidence*). There is *low confidence* in attributing changes in the probability or magnitude of some studied flood events to human influence because of different results and important differences between models and methods used. For some recent flood events that are driven mainly by extreme precipitation, there is *high confidence* in human influence on the occurrence or intensity of these events.**

11.5.5 Future projections

The SREX report (SREX Ch. 3) stressed the low availability of studies on flood projections under different emission scenarios and concluded there was *low confidence* in projections of flood events given the complexity of the mechanisms driving floods at the regional scale. The AR5 report (WG II, Ch. 3) justified a *medium confidence* statement on the pattern of future flood changes, that includes flood hazards increasing over about half of the globe (parts of south and Southeast Asia, tropical Africa, northeast Eurasia, South America) and flood hazards decreasing in other parts of the world, despite uncertainties in GCMs and their coupling to hydrological models. SR15 (SR15 Ch. 3; IPCC 2018) assessed that there was *medium confidence* that a global warming of 2°C would lead to an expansion of the fraction of global area affected by flood hazards, compared to conditions at 1.5°C of global warming, as a consequence of changes in heavy precipitation.

The majority of new studies that produce future flood projections based on hydrological models driven with outputs of climate models focus on changes in a flood proxy, i.e., the magnitude of peak flow and the frequency of high flows in rivers. They do not typically consider aspects that are also important to actual flood severity or flood damage such as flood prevention measures (Neumann et al., 2015; Şen, 2018), flood control policies (Barraqué, 2017), and future changes in land cover. As a result, our assessment also focuses on these flood proxies. At the global scale, Alfieri et al., (2016) used downscaled projections from seven GCMs as input to drive a hydrodynamic model. They found successive increases in the frequency of high floods in all continents except Europe, associated with increasing levels of global warming (1.5°C, 2°C, 4°C). These results are supported by (Paltan et al., 2018), who applied a simplified runoff aggregation model forced by outputs from four GCMs. Huang et al. (2018) used three well-established hydrological models forced with bias-corrected outputs from four GCMs to produce projections for four river basins including the Rhine, Upper Mississippi, Upper Yellow, and Upper Niger under 1.5, 2.0, and 3.0°C global warming. These basins were chosen because they represent different geographic, land cover, and hydro-climatic characteristics and their flood characteristics can be well reproduced by the hydrological models. This study found diverse projections for different basins, including a shift towards earlier flooding for the Rhine and the Upper Mississippi, a substantial increase in flood frequency in the Rhine only under the 1.5 and 2.0°C scenarios, and a decrease in flood frequency in the Upper Mississippi under all scenarios.

The projected changes in floods are uneven in different parts of the world, although studies generally show a larger fraction of regions with an increase than with a decrease. Dankers et al. (2014) used nine hydrological models forced by GCMs. They found an increase in peak flow in more than half of the global land grids, with a consistent signal in central and eastern Siberia, southeast Asia, and India. Hirabayashi et al. (2013) used outputs from 11 climate models in combination with a global river routing model with an inundation scheme to investigate global flood risk under a changing climate. They found large increases in the flood frequency (defined as the exceedance probability of the 100-yr return levels from the late 20th century) in southeast Asia, peninsular India, eastern Africa, and the northern half of the Andes, and a decrease in Europe (except for the British Isles), southern South America, and the southern US by the end of the 21st century under the RCP8.5 scenario. The patterns of change are similar under other forcing scenarios though the magnitude of changes are smaller. Arnell and Gosling (2016) examined changes in river flood risk using a global hydrological model driven by outputs from 21 CMIP3 GCMs under the A1B scenario. Despite the use of earlier climate models and different emission scenarios, their findings are generally similar to those of Hirabayashi et al. (2013). In particular, they found an increase in flood magnitude across humid tropical Africa, south and east Asia, the majority of South America, and the high latitudes of Asia and North America, but a decrease in the 100-year peak flow in the Mediterranean and in large areas of central and eastern Europe, southwest Africa, and Central America. Based on seven-day flood magnitudes and using four GCMs, Döll *et al.* (2018) compared changes in mean and high flows under the 1.5°C and 2.0°C global warming worlds with the climate of 2006-2015. They showed an increase in high flow in some regions and a decrease in other regions. These changes include a decrease in flood frequency in east Europe and south Canada and an increase in southeast Asia, although the agreement between models was low, except in eastern Europe. These results suggest *medium confidence* in flood trends at the global scale, in agreement with projections of extreme precipitation, but *low confidenc*e in projected regional changes.

At regional and local scales, projected changes in river floods are characterized by high uncertainty. In Europe, two studies (Alfieri et al., 2015; Roudier et al., 2016) projected an increase in the frequency of high flows, consistent with the projected increase in extreme precipitation (Rajczak and Schär, 2017). Yet, agreement for the future projections among studies is poor. Roudier et al.(2016) and Alfieri et al. (2015) projected an increase in the magnitude of floods in South Europe, yet Giuntoli et al. (2015) projected no change and Dankers et al., (2014) and (Guerreiro et al., 2018a) projected a decrease. Inconsistencies in the future projections also exist for other regions, including the Alps (Köplin et al., 2014; Thober et al., 2018), Scandinavia (Alfieri et al., 2015; Arheimer and Lindström, 2015; Hall et al., 2014), central and eastern Europe (Hall et al., 2014; Roudier et al., 2016; Shkolnik et al., 2018), and the British Isles (Dankers et al., 2014; Hall et al., 2014; Thober et al., 2018; Guerreiro et al. 2018). Projected changes in the magnitude of annual peak flow for east Asia differ among studies, including an increase (Hirabayashi et al., 2013; Dankers et al., 2014; Gu et al., 2014; Liu et al., 2017) or no changes (Arnell and Gosling, 2016). Yet, there seems to be a consistent increase in the annual peak flow projected for northern Eurasia (Shkolnik et al., 2018).

Studies based on the use of regional hydrological models show a general increase in the magnitude of high flows in the United States. Naz et al. (2016) forced a hydrological model with dynamically downscaled and bias corrected outputs from 10 GCMs. They showed a general increase in the magnitude or frequency of high flows in the conterminous US, though the agreement among the models is low in the west and the east. Wobus et al (2017) examined the projected changes in the frequency of the 100-yr flow in more than 50,000 streams in the conterminous US, using a hydrological model driven by statistically downscaled and bias-corrected outputs from 29 GCMs under the RCP 8.5 scenario. They found a substantial increase in the frequency of high flows over the entire US. Results of these studies based on regional hydrological models can have large differences with those based on global hydrological models, which indicate a decrease in the magnitude or frequency of floods over a large portion of North America (e.g., Hirabayashi et al., 2013; Arnell and Gosling, 2016). Over South America, most studies based on global and regional hydrological models show an increase in the magnitude and frequency of high flows in the western Amazon (Sorribas et al., 2016; Langerwisch et al., 2013; Guimberteau et al., 2013; Zulkafli et al., 2016) and the Andes (Bozkurt et al., 2018).

Projected changes in the magnitude or frequency of high river flows on a regional scale show a wide spread. These diverse projections need to be placed in the proper context, considering the difficulty in obtaining a robust estimate of the future changes at such spatial scales. Several factors may have contributed to the apparent disagreement among projections for the same region or locality Kundzewicz et al. (2017). These include the use of hydrological models of differing scales (global or regional), different emission scenarios, outputs from different climate models, and different flood definitions. A large and quite coherent picture emerges from studies based on various global hydrological models forced with output from different GCMs. This includes high agreement that a larger fraction of the land will see an increase in the magnitude and frequency of high flows than will see a decrease. An increase in found in southeast and north Asia, North America, the Andes and western Amazonia. Yet, many small processes that are important at the regional and local scales are not well represented in global models, making it difficult to interpret projections of a global hydrological model at regional and local levels. Regional hydrological models, especially when used in combination with regional climate models, provide better representations of regional processes, including orography, land cover, and storms. They provide more a realistic simulation of river flow, but the added complexity predictably increases the level of uncertainty in the projections. The wide range of changes in the projections of river floods in Europe clearly illustrate this (Kundzewicz et al. (2017).

Studies on urban flood projections are limited, but available studies project an increase in urban flood potential, for example in cities of North America (Kermanshah et al., 2017; Hettiarachchi et al., 2018), in northern China (Zhou et al., 2018b), and in India (Vemula et al., 2019). Because of the direct connection between extreme precipitation and urban flood potential in developed urban areas, there is *high confidence* in an increase in flood potential in these areas where extreme precipitation is projected to increase, especially at high global warming levels. There are few direct projections for changes in coastal floods, but flood risk should increase in the coastal regions where sea level is projected to rise (Kulp and Strauss, 2017; Pellikka et al., 2018; Rojas et al., 2018; Yin et al., 2019b). At the global scale, unprecedented coastal flood risk is projected for the second half of the 21st century (Vousdoukas et al., 2018b). Jevrejeva et al. (2018) suggest an important increase in coastal floods, with a dramatic increase in the associated economic costs; the upper-middle income countries, and particularly China, would be the most affected. Thus, the projections needed in developing countries (Roberts et al., 2017; Ruckert et al., 2017). For example, Takagi et al. (2016) suggested that coastal flood extent from 2000 - 2050 could increase by 110.5 km^2 in Jakarta and the rate of increase in 2025-2050 would be 3.4 times faster than during the 2000-2025 period. Similar projections are suggested for Singapore (Cannaby et al., 2015). In northeast China, the coastal floods are projected to increase by 6.6% and 7.8% for the period 2050-2099 under RCP 4.5 and RCP 8.5 scenarios, respectively (Zhang et al., 2019f).

Summary: There is *high confidence* in an increase in flood potential in developed urban areas where extreme precipitation is projected to increase, especially at high global warming levels. Global hydrological models project a larger fraction of the land areas to be affected by an increase in river floods than by a decrease in river floods (*medium confidence)*. There is *medium confidence* that river floods will increase in the west Amazon, the Andes, and northern Eurasia. Regional changes in river floods are more uncertain because complex hydrological process are involved.

11.6 Droughts

Drought refers to a period of time with anomalies from average moisture conditions during which limitations in water availability result in negative impacts for various components of natural systems and economic sectors. Depending on the systems or sectors being impacted, drought may be classified in different types (e.g., Fig. 11.17 and Table 11.3) such as agricultural (e.g., crop yield reductions or failure, often related to soil moisture deficits), ecological (e.g., tree mortality), or hydrological (e.g., water shortage in streams or storages such as reservoirs, lakes, lagoons, and groundwater) droughts. Obviously, the distinction of drought types is not absolute as a drought can impact different sectors at the same time. Because of this, drought cannot be characterized using a single universal definition (Lloyd-Hughes, 2014) or directly measured based on a single variable (SREX Chapter 3, Wilhite and Pulwarty, 2017). Drought can happen on a wide range of timescales - from "flash droughts" on a scale of weeks (Hunt et al., 2014; Otkin et al., 2018) to multi-year or decadal rainfall deficits (Ault et al., 2014; Cook et al., 2016b; Garreaud et al., 2017). Droughts are often analysed using indices, which are measures of drought severity, duration and frequency, addressing different types of drought characteristics. There are several drought indices published in the scientific literature, as also highlighted in the IPCC SREX report (SREX Chapter 3). These can range from anomalies in single variables (e.g., precipitation, soil moisture, runoff, evapotranspiration) to complex indices combining different drought aspects. Table 11.3 provides a list of indices used to characterize different types of droughts.

[START FIGURE 11.17 HERE]

Figure 11.17: Sketch of processes and drivers related to different drought types. Note that all relationships are indicated under the dry range of the given variable and may not apply to humid conditions (e.g., impacts of soil moisture on evapotranspiration). The asterisk (*) denotes that under conditions of critical soil moisture deficits, plant water deficits are generally critically affected by high levels of atmospheric evaporative demand (only a + relationship); however the effects can be limited outside the growing season and under humid soil moisture but dry atmospheric conditions (see text for details). The double asterisk (**) denotes

that under critical soil moisture deficits CO_2 effects on plant water savings can be limited as evidenced by experimental studies in which water and CO_2 effects are controlled (see text for details).

[END FIGURE 11.17 HERE]

[START TABLE 11.3 HERE]

Table 11.3: Different types of droughts, associated metrics, general description and associated references

Drought type	Further information	Drought metric	Comments	Key references
Critical precipitation deficits	sometimes referred to as "meteorological drought"	Standardized Precipitation Index (SPI), Consecutive Dry Days (CDD)	SPI is defined for given time scales in order to identify precipitation deficits over different periods. CDD is usually based on daily precipitation records. Dry-spell length is another commonly used term.	(Donat et al., 2013a; Orlowsky and Seneviratne, 2013; Sillmann et al., 2013a; Spinoni et al., 2014; Kingston et al., 2015; Stagge et al., 2017)
Critical increase in atmospheric evaporative demand	high levels of potential evaporation; is related (but not only) to "atmospheric dryness"	Potential evaporation, Evaporative Demand Drought Index (EDDI), which is the standardization of the Potential evaporation (Hobbins et al., 2012, 2016; McEvoy et al., 2016) .	In most regions atmospheric water demand/potential evaporation is not measured, but there are few direct observations by means of evaporation pans. There is *low confidence* in estimates based on observations of temperature only for the estimation of trends (Sheffield et al., 2012; Vicente-Serrano et al., 2020). Nevertheless, there is *medium confidence* (because of the limited number of pan evaporation observations) that physically-based models (e.g., Penman-Monteith) using all aerodynamic and radiative drivers from observations can reproduce the observed magnitude and variability potential evaporation (Azorin-Molina et al., 2015; Stephens et al., 2018; Sun et al., 2018c; Vicente-Serrano et al., 2018a).	(Hobbins et al., 2012, 2016; Sheffield et al., 2012; Wang et al., 2012; McEvoy et al., 2016; Stephens et al., 2018)
Critical soil moisture deficits	sometimes referred to as "agricultural drought"	Soil moisture anomalies (SMA), Standardized Soil Moisture Index (SSMI)	Networks of ground-based soil moisture measurements are available in different regions, but sparse (Dorigo et al., 2011). Surface soil moisture can be monitored from satellite, but only since the 1980s at the earliest (Dorigo et al., 2017), and they are affected by important temporal inhomogeneities (Dorigo et al., 2015). There is *medium confidence* in soil moisture derived from physically-based land surface models using all relevant observations- or reanalysis-based meteorological variables (precipitation, radiation, wind, temperature, humidity) as input (Hanel et al., 2018; Moravec et al., 2019; Seager et al., 2019), although soil moisture simulations are affected by uncertainties when compared with the magnitude and temporal variability of	(Orlowsky and Seneviratne, 2013; Seneviratne et al., 2013; AghaKouchak, 2014; Sohrabi et al., 2015; Zhao and Dai, 2015; Berg and Sheffield, 2018; Samaniego et al., 2018)

			soil moisture measurements (Stillman et al., 2016; Yuan and Quiring, 2017; Ford and Quiring, 2019).	
Critical hydrological deficits	sometimes referred to as “hydro-logical drought”	SRI (Standardized Runoff Index), SSI (Standardized Streamflow Index), low flows	Usually based on monthly records (SRI and SSI) although daily streamflow is also used to quantify hydrological deficits (low flows). Observational data is available but not in all regions (e.g., missing in many parts of Africa)	(Van Lanen et al., 2013; Wada et al., 2013; Forzieri et al., 2014; Prudhomme et al., 2014; Schewe et al., 2014; Van Loon and Laaha, 2015; Gosling et al., 2017)
Combined synthetic measures of drought	Synthetic metrics of drought based on meteorological data	Precipitation Evapotranspiration Index (SPEI), Palmer Drought Severity Index (PDSI), Standardized	These drought indices are generated using precipitation and estimates of atmospheric evaporative demand. The quality of the outputs depend on the methods used to determine the atmospheric demand. These indices have limitations to be considered proxies of soil moisture deficits (in the case of the SPEI, because of the use of Epot instead of actual evapotranspiration; in the case of PDSI, because of its oversimplified form compared to state-of-the-art land surface models), whereby SPEI is easier to physically interpret. Given these limitations, the SPEI is not intended to be a soil moisture proxy but can allow to identify vegetation stress conditions in which atmospheric evaporative demand plays an important role.	(Dai, 2013; Beguería et al., 2014; Cook et al., 2014a; Vicente-Serrano et al., 2015; Dai et al., 2018)

[END TABLE 11.3 HERE]

11.6.1 Mechanisms and drivers

Similar to many other extreme events (see Box 11.1), droughts occur as a combination of thermodynamical and dynamical processes. Thermodynamical processes contributing to drought, which are mostly related to heat and moisture exchanges and also in part modulated by plant coverage and physiology, can be affected by greenhouse gas forcing both at global and regional scale. They affect for instance atmospheric humidity, temperature, radiation, which in turn lead to modified precipitation and/or evapotranspiration in some regions and time frames. On the other hand, dynamical processes are particularly important to explain drought variability on several time scales, from few weeks (flash droughts) to multiannual (decadal droughts). Nevertheless, there is limited evidence of circulation changes attributable to greenhouse gas forcing that are affecting long-term changes in drought.

11.6.1.1 Precipitation deficits

Overall, precipitation is generally the main driving factor controlling drought development. There is *high confidence* that atmospheric dynamic, which varies on interannual, decadal and longer time scales, is the main contributor to precipitation deficits in the majority of the world regions (Schubert et al., 2016), but anomalies in the moisture transport also contribute to trigger and intensify them (Drumond et al., 2019; Herrera-Estrada et al., 2019). In some regions and time frames, e.g., in the US Great Plains in summer (Koster et al., 2011) or the warm season in the greater Alpine region (Haslinger et al., 2019), soil moisture-precipitation feedbacks may also play a substantial role in affecting precipitation deficits, and possibly even a dominant role (Gimeno et al., 2012). Nevertheless, in the vast majority of the world regions precipitation deficits are driven by dynamic mechanisms recorded on different spatial scales (including synoptic – atmospheric rivers and extratropical cyclones, blocking and ridges- (Sousa et al., 2017), dominant hemispheric circulation patterns (Kingston et al., 2015) and global ocean-atmosphere coupled patterns like ENSO (Dai and Zhao, 2017).

El Niño-Southern Oscillation (ENSO) is an important driver of drought in large regions of the world (e.g., North and South America, South Africa, Australia) (Dai, 2013; Seager and Hoerling, 2014; Burgman and Jang, 2015; Schubert et al., 2016; Baek et al., 2019). In other areas, droughts are affected by the combination of ENSO and other mechanisms (e.g., the Indian Ocean Dipole in East Africa and Indonesia) (Funk et al., 2018b; Lestari et al., 2018). Precipitation in other regions such as Northern Eurasia, Europe and North Africa, central and eastern Canada and the middle East are not SST-driven and other circulation patterns affect precipitation deficits (Schubert et al., 2016; Kingston et al., 2015; Raymond et al., 2018). In tropical and subtropical regions precipitation deficits have been linked to expansions and contractions of the Hadley cell (Nguyen et al., 2015; Davis and Birner, 2016; Feldl and Bordoni, 2016). However, multi-decadal changes in the position of the Hadley cell are part of the natural climate variability (Bronnimann et al., 2015), and there is still *low confidence* in a climate change signal independent of the natural climate variability (Staten et al., 2018). Nonetheless, there is *low confidence* that changes in large scale circulation patterns drive trends in precipitation deficits (see Chapter 2). In future projections, there is a strong regional disagreement between models regarding teleconnections between ENSO and regional precipitation (Yeh et al., 2018). Similar uncertainties are recorded in continental circulation modes, as with the future role of the North Atlantic Oscillation on Europe's precipitation (Deser et al., 2017). There is *high confidence* that precipitation is also affected by soil moisture feedbacks in some regions (SREX Chapter 3, Koster et al. 2011; Taylor et al. 2012; Guillod et al. 2015; Tuttle and Salvucci 2016), whereby the sign of the feedbacks may be either positive or negative and either local or non-local (Taylor et al., 2012; Guillod et al., 2015; Tuttle and Salvucci, 2016). State-of-the-art Earth System Models tend to underestimate non-local negative feedbacks (Taylor et al. 2012). Positive soil moisture-precipitation feedbacks are shown to contribute to decreases in precipitation in some regions in climate model projections (Vogel et al., 2017, 2018).

11.6.1.2 Atmospheric evaporative demand

Potential evaporation (Epot), also known as atmospheric evaporative demand (AED), is the amount of evaporation that would occur from an open surface water given actual meteorological conditions; it is also close to potential evapotranspiration, which is the highest evapotranspiration that can occur from a given land surface if soil moisture is unlimited. Epot is affected by atmospheric dryness, often quantified with the vapor pressure deficit (VPD). But other drivers are also highly relevant, including solar radiation and wind speed (Hobbins et al., 2012; Mcvicar et al., 2012; Sheffield et al., 2012).

Epot can be estimated using different methods (McMahon et al., 2013) and those solely based on air temperature usually overestimate it in magnitude and time trends (Tomas-Burguera et al., 2017). Epot is by definition different to actual evapotranspiration (ET), which is the water flux from soil and vegetation to the atmosphere, and for which Epot represents an upper bound. ET is a key hydrological variable and it is often much smaller than Epot (in particular in arid environments). An increase in Epot does not necessarily lead to increased ET (Milly and Dunne, 2016), since if soil moisture is limited, soil evaporation and/or plant transpiration cannot supply the atmospheric demand (Box 11.1). Nevertheless, under low soil moisture conditions, it strongly contributes to agricultural/ecological drought impacts (Anderegg et al., 2013, 2016; Williams et al., 2013), and if it leads to ET changes, during periods of drought deficits, also to hydrological droughts (Seneviratne et al., 2012a; Teuling et al., 2013). The influence of Epot on drought depends on the drought type, the environmental conditions and the moisture availability (Vicente-Serrano et al., 2020). The dynamic of Epot is controlled by circulation variability (Park Williams et al., 2014; Chai et al., 2018; Martens et al., 2018). Thermodynamic processes also play a fundamental role. Increased atmospheric CO_2 concentrations have warmed the atmosphere and in the absence of other influences, this increases Epot by means of enhanced VPD. Land-atmosphere feedbacks are also important in affecting atmospheric moisture content (Seneviratne et al. 2010; Berg et al. 2016; Haslinger et al. 2019; Zhou et al. 2019; Box 11.1), including the differential warming between ocean and continental areas that affect the water vapor saturation of the oceanic air masses that bring moisture to the continents (Sherwood and Fu, 2014; Byrne and O'Gorman, 2018). Finally, given land-atmosphere coupling and actual ecosystem properties, in vegetated areas maximum evapotranspiration, or "potential evapotranspiration", is also affected by a vegetation resistance (Maes et al., 2019) and high CO_2 concentration may lead to increased evapotranspiration given its influences on plant stomatal conductance (Milly and Dunne, 2016), plant functional traits (Anderegg et al., 2019), and water use efficiency (Roderick et al. 2015; Berg et al. 2016; Swann et al. 2016; Box 1.1).

11.6.1.3 Soil moisture deficits

Soil moisture shows an important correlation with precipitation variability (Khong et al., 2015; Scaini et al., 2015; Seager et al., 2019), but ET also plays a substantial role in further depleting moisture from soils in particular in humid regions during droughts (Seneviratne et al., 2012a; Teuling et al., 2013). In addition, soil moisture may play a role in drought self-intensification under dry conditions in which ET is decreased and leads to higher atmospheric evaporative demand (see Section 11.1.1.3) , an effect that can also contribute to "flash droughts" (Otkin et al., 2016, 2018). If soil moisture becomes limited, ET is reduced, which on one hand may decrease the rate of soil drying, but on the other hand can lead to further atmospheric drying through various feedback loops (Seneviratne et al., 2010; Teuling, 2018; Vogel et al., 2018; Miralles et al., 2019). The process can be complex since vegetation coverage plays a role in modulating albedo and in providing access to deeper stores of water (both in the soil and groundwater), and land cover changes may alter ET (Sterling et al., 2013; Döll et al., 2016; Woodward et al., 2014). Thus, vegetation coverage can be critical to assess soil moisture variations. In the US Great Plains woodlands are characterised by lower soil moisture content in comparison to neighbouring pastures (Hao et al., 2019) and earlier spring greening contributes to summer soil drying in the Northern Hemisphere (Lian et al., 2020). In addition, boundary-layer feedbacks are also involved (Miralles et al., 2014). Soil moisture limitations is often more relevant than atmospheric dryness to explain gross primary production anomalies or vegetation stress, mostly in sub-humid and semi-arid regions (Stocker et al. 2018; Liu et al. submitted).

While CO_2 concentrations are shown to potentially affect plant evapotranspiration and increase plant water-use efficiency (see 11.1.1.2), there is evidence that under critical soil moisture deficits CO_2 effects on plant water savings are limited, given results of recent experimental studies in which water and CO_2 effects are controlled. The effect would be different to that observed under normal/humid conditions. For environmental/agricultural drought conditions under higher warming, the role of CO_2 effects on actual evapotranspiration could be different to that under humid or normal conditions (or even than for mild drought conditions) (Morgan et al. 2004; Xu, Jiang, Jia, & Zhou, 2016). Different experiments based on enriched CO_2 conditions have indeed shown that elevated CO_2 does not necessarily reduce nor delay tree mortality under drought (Bachofen et al. 2018; Duan et al., 2014, 2015), a response also shown in pastures and shrubs (Nackley et al., 2018) and in crops (Dikšaitytė, Viršilė, Žaltauskaitė, Januškaitienė, & Juozapaitienė, 2019). On the other hand, Morgan et al. (2011)report a substantial alleviation of drought conditions for crops under enhanced CO_2, but also highlight that these effects would be likely to be limited under very intense drought conditions. Hence we assess that there is *medium confidence* that CO_2 effects would reduce water needs by plants under non-extreme droughts but not under very extreme soil moisture drought conditions.

11.6.1.4 Hydrological deficits

Drivers of hydrological droughts are complex. On the one hand, there are soil hydrological processes, which control the propagation of meteorological droughts throughout different parts of the hydrological cycle (Van Loon and Van Lanen, 2012) that are spatially and temporally complex (Herrera-Estrada et al., 2017; Huang et al., 2017d) and difficult to quantify (Apurv et al., 2017; Konapala and Mishra, 2017; Hasan et al., 2019). On the other hand, hydrological droughts are affected by land cover, groundwater and soil characteristics

(Van Lanen et al., 2013; Van Loon and Laaha, 2015; Barker et al., 2016) as well as human activities (water management and demand, damming and land use changes (Van Loon et al., 2016; He et al., 2017; Veldkamp et al., 2017; Wu et al., 2018a; Xu et al., 2019b). Wada et al. (2013) estimate that human water consumption has intensified the magnitude of hydrological droughts by 20%-40% over the last 50 years. Thus, these authors suggesteded that in the Mediterranean, and the central US, as well as in parts of Brazil, the human water use contribution to hydrological droughts was more important than climatic factors (see also Martins et al., 2017; Otto et al., 2015; Vicente-Serrano et al., 2017, 2019c). On the other hand, a study from Gudmundsson et al. (submitted) based on the latest version of the ISIMIP multi-model experiment suggests that the contribution of human water use is smaller than that of anthropogenic climate change. Groundwater abstractions may also affect streamflow drought duration (Tijdeman et al., 2018).

11.6.1.5 Combined synthetic measures of drought

Given difficulties for drought quantification and data constrains for hydrological variables (e.g., soil moisture, streamflow, groundwater), but also environmental (e.g., forest growth and mortality, biomass production) and agricultural impacts (i.e., crop failure, yield reduction), simplified synthetic drought metrics that combine both precipitation and Epot have been developed. These indices have the advantage of being based on meteorological information, which is available worldwide. However, they have also some limitations in their suitability (e.g., usually they are poor estimation approaches of the soil moisture variability).

The PDSI has been widely used to monitor and quantify drought severity, but it is affected by several constrains, which questions its applicability (see further details in SREX Chapter 3 and in Berg and Sheffield 2018). Its main limitation is that it is not based on a robust water balance model as it oversimplifies soil surface hydrological processes (SREX Chapter 3). In addition, its calibration is targeted on present climate and can perform poorly under warmer climates (SREX Chapter 3). Even calculated using a self-calibration approach, the PDSI has strong problems of spatial comparability since it is an index that represents different drought frequencies among sites. Finally, it cannot be calculated on different time-scales (Ma et al., 2014; Peña-Gallardo et al., 2018b, 2018a; Tian et al., 2018), which is essential to evaluate drought impacts on a variety agricultural, environmental, hydrological and socioeconomic systems. Because of the numerous limitations of the PDSI, we only provide limited consideration to recent trends and projections based on this index.

The SPEI combines precipitation and Epot on different time scales, being equally sensitive to these two variables (Vicente-Serrano et al., 2015), although given statistical characteristics of precipitation series, SPEI variability is mostly driven by precipitation variability. SPEI is not intended to be a proxy of soil moisture, but rather a flexible metric of vegetation water stress. In the SPEI the soil moisture limitation does not exist, and increased AED always reduces SPEI, independently of ET. While this means that SPEI cannot provide an estimate of soil moisture condition, the resulting estimates are nonetheless of relevance for vegetation stress since during periods of low precipitation, although ET is limited, the AED enhances the evapotranspiration deficit (ET-AED), particularly in dry regions and in humid regions during periods of critical soil moisture deficits. This implies water stress for vegetation (i.e., the inability to photosynthesize because the atmosphere is too dry for stomata to open) that may lead to fatal ecosystem impacts (e.g., forest mortality, Williams et al. 2013; Allen et al. 2015; Anderegg et al. 2016). This explains why in dry climates and in humid regions during dry periods, the SPEI is well correlated with impacts on crop yields (Potopová et al., 2015; Wang et al., 2016a; Zipper et al., 2016; Parsons et al., 2019; Shekhar and Shapiro, 2019), vegetation activity (Huang et al., 2015; Bachmair et al., 2018) and forest growth (Peña-Gallardo et al., 2018b). Interestingly, even under these conditions, some studies report a correlation of SPEI with soil moisture deficits (Scaini et al., 2015; Wang et al., 2015; Tian et al., 2018; Zhang et al., 2018e). On the contrary, under humid conditions AED effects are negligible given sufficient soil water availability. This would imply overestimations of the drought stress caused by the AED in the SPEI (Cook et al., 2014a; Berg and Sheffield, 2018; Scheff, 2018; Vicente-Serrano et al., 2020).

Summary: There are several drought types that may affect assessments regarding their changes under increased greenhouse gas forcing (*high confidence*). It is important to distinguish precipitation deficits from soil moisture deficits, streamflow deficits, increased atmospheric evaporative demand, and other measures of drought conditions and land water deficits. Drought events are both the result of dynamical and thermodynamical processes.

11.6.2 Observed trends

The SREX report (SREX Chapter 3) and the AR5 (AR Chapter 2) assessed that there was *low to medium confidence* in trends in global droughts. Natural climate variability driven by large-scale mechanisms (e.g., ENSO, PDO) may mask drought trends (Trenberth et al., 2014; Dai et al., 2018). Estimating drought trends has limitations given large uncertainties in publicly available data products (Trenberth et al., 2014; Beguería et al., 2016; Dai and Zhao, 2017). Some key climate variables (e.g., relative humidity, wind speed) show high uncertainties (Trenberth et al., 2014), low spatial coverage (Willett et al., 2014), and temporal inhomogeneities (Azorin-Molina et al., 2014). Measurements of soil moisture are also limited. Ground-based soil moisture observations are available in some regions but still scarce (Dorigo et al., 2011; Quiring et al., 2016). Long-term satellite-based estimates are mostly available for surface soil moisture based on microwave remote sensing and only since the 1980s (Dorigo et al. 2017), and they are also affected by important uncertainties (Dorigo et al., 2015); in addition, surface soil moisture and root-zone soil moisture (which is more relevant to plants), are found to substantially differ in climate models (Berg et al., 2017) and show low temporal agreement with soil moisture observations (Ford and Quiring, 2019). There are, however, less limitations in the availability of streamflow observations for assessing hydrological drought trends. Global databases of streamflow observations have been recently compiled (Do et al., 2018; Gudmundsson et al., 2018), although large regions are not yet covered (Central and South America, Africa and Asia) and in others the time series are relatively short for assessments of trends.

11.6.2.1 Precipitation deficits

Strong precipitation deficits have been recorded in recent decades in the Amazon (2005, 2010), southwestern China (2009-2010), southwestern North America (2011-2014), Australia (2001-2009), California (2014), the middle East (2012-2016), Chile (2010-2015), among others (van Dijk et al., 2013; Mann and Gleick, 2015; Rowell et al., 2015; Marengo and Espinoza, 2016; Dai and Zhao, 2017; Garreaud et al., 2017, 2019; Marengo et al., 2017; Brito et al., 2018; Cook et al., 2018). Global studies show no significant trends in time series of the Standardized Precipitation Index (SPI) (Orlowsky and Seneviratne, 2013; Spinoni et al., 2014), and in derived drought frequency and severity data (Spinoni et al., 2019), with very few exceptions in West Africa consistent with studies based on trends in the CDD (Chaney et al. 2014; Donat et al. 2014; Barry et al. 2018; Dunn et al. submitted), and South America (Figure 11.19). Regional studies suggest an increase of precipitation deficits in East Africa (Funk et al., 2015a; Nicholson, 2017). An upward trend in CDD has been suggested in Northeastern Brazil, the South America Monsoon, Southeastern South America and Northwestern South America (Skansi et al., 2013; Donat et al., 2016a) and a more general drying trend in Chile (30-48°S) (Saurral et al., 2017; Boisier et al., 2018). Also an increase in CDD is suggested in northern China since 1990s (Zhang et al., 2019a) and in Southeastern Asia (Dunn et al., submitted). In North America, there are no long-term trends in precipitation deficits (Spinoni et al., 2019). In Australia, with the exceptions of southwest Western and south Australia, droughts have become less frequent, shorter and less intense (Gallant et al., 2013). In Nigeria there is a noticeable increase of the SPI, indicative of less drought conditions (Ogunrinde et al., 2019), and no changes in the SPI have been recorded in the mountain areas of Morocco (Zkhiri et al., 2019). In South Africa there is an increase in the CDD (Dunn et al., submitted). In central Europe there are no relevant changes in the frequency of dry spells (Zolina et al., 2013) and in the SPI (Hauser et al., 2017; Spinoni et al., 2017), although in the Alps there is a decrease in wet days (Gobiet et al., 2014). In Northern Europe there are no changes in drought severity (Spinoni et al., 2014, 2017; Kay et al., 2018). In Southern Europe, some studies suggest an increase of precipitation deficits (Hoerling et al., 2012; Gudmundsson and Seneviratne, 2016; Spinoni et al., 2017), but other studies suggest that at least in the western Mediterranean there are no significant trends in SPI drought duration and magnitude since 1960 (Domínguez-Castro et al. 2019). The characteristic pattern in the Mediterranean area is a high spatial diversity in the precipitation deficits and important temporal variability (Vicente-Serrano et al., submitted). While weak drying trends in precipitation are found over the whole Southern European regions since 1950, there are no identifiable trends when considering timeseries going back to 1850 (Vicente-Serrano et al., submitted), in agreement with precipitation reconstructions over the last 250 years (Hanel et al., 2018).

11.6.2.2 Atmospheric evaporative demand

Increases in Epot have intensified recent drought events (Park Williams et al., 2014; Seager et al., 2015; Basara et al., 2019; García-Herrera et al., 2019), enhanced vegetation stress (Allen et al., 2015; Panginés de Cárcer et al., 2018; Yuan et al., 2019), and contributed to the depletion of soil moisture promoting enhanced ET (Teuling et al., 2013). Studies suggest that atmospheric dryness records earlier than other metrics drought onset and flash droughts (Hobbins et al., 2016; McEvoy et al., 2016; Yao et al., 2018; Basara et al., 2019). Trends in Epot based on measurements (Evaporation pans) and physical models (i.e., the Penman-Monteith equation (Pereira et al., 2015)) provide indication of possible trends in the influence of atmospheric dryness on drought. Given the observed global temperature increases (see Chapter 2 and Section 11.3) and dominant decrease in relative humidity (Simmons et al., 2010; Willett et al., 2014; Vicente-Serrano et al., 2018b), VPD has increased globally (Barkhordarian et al., 2019; Yuan et al., 2019). In some world regions, pan evaporation (Epan) has increased as a consequence of VPD changes [e.g., in China (Li et al., 2013; Sun et al., 2018c; Yang et al., 2018b), the Western Mediterranean (Azorin-Molina et al., 2015) and Australia (Stephens et al., 2018)]. Nevertheless, there is an important regional variability and in other areas Epan has decreased [e.g., Mexico (Breña-Naranjo et al., 2016) or the Tibetean Plateau (Zhang et al., 2018a)] or it did not show substantial changes [e.g., in Uruguay, Vicente-Serrano et al., 2018a]. Physical models also show an important regional diversity, with an increase in New Zealand (Salinger, 2013) or the Mediterranean (Gocic and Trajkovic, 2014; Vicente-Serrano et al., 2014a; Piticar et al., 2016), a decrease in India (Jhajharia et al., 2015), and strong spatial variability in North America (Seager et al., 2015). This variability is driven by the role of other meteorological variables that affect Epot. Among them wind speed is very relevant (McVicar et al., 2012), and studies suggest a relevant reduction of the wind speed (Zhang et al., 2019h) that could compensate the role of the VPD increase. Nevertheless, VPD trends would dominate over wind speed trends to explain Epot changes (Wang et al., 2012), which are dominantly positive worldwide (Vicente-Serrano et al., 2020).

11.6.2.3 Soil moisture deficits

There are limited measurements of soil moisture from ground observations (Dorigo et al., 2011; Qiu et al., 2016; Quiring et al., 2016), which impedes their use in the analysis of trends. Among the few existing observational studies covering at least two decades, Liu et al. (2015) identified a general declining trend in North China between 1983 and 2012, but in central China trends are dominantly positive (Qiu et al., 2016). Alternatively, satellite measurements may be used. Dorigo et al. (2012) analysed global remote sensing soil moisture from 1988 to 2010, and suggested drying trends in the Southern US, central South America, central Eurasia, northern Africa and the Middle East, Mongolia and northeast China, northern Siberia, and Western Australia. Nevertheless, these trends must be considered very carefully since satellite soil moisture is affected by strong uncertainties when compared with in-situ soil moisture observations (Dorigo et al., 2015; Rodell et al., 2018). Reanalysis datasets have also been used to analyse soil moisture trends, although the different reanalysis products strongly differ and show important limitations in reproducing soil moisture variability (Liu et al., 2014). There are also several studies that have modelled long-term soil moisture deficits using meteorological data and land-atmosphere models (see uncertainties associated to these models in 11.6.3.3). In regions such as South-Eastern North America there are no long-term trends, with soil moisture deficits in the last decades comparable to those recorded in the 20th century (Park Williams et al., 2017). A similar temporal pattern characterised by no changes is found in central North America (Seager et al., 2019) and East Africa (Kew et al., 2019a). Nevertheless, the majority of studies suggest an increase in the frequency and areal extent of soil moisture deficits with examples in East Asia from 1948 to 2010 (Cheng et al., 2015), India between 1980 and 2008 (Mishra et al., 2014b), North China between 1960 and 2010 (Qin et al., 2015b; Jia et al., 2018), Northwest North America between 1950 and 2013 (Ahmadalipour and Moradkhani, 2017) and the Czech Republic between 1961 and 2012 (Trnka et al., 2015b). In Central Europe and the Mediterranean, soil moisture models suggest an increase in the frequency of soil-moisture deficits (Hanel et al., 2018; Moravec et al., 2019). Given that precipitation deficits do not show general trends in the last decades in these areas (See 11.6.2.1), the possible explanation of the dominant negative trends recorded in the modeled soil moisture could be related to the increase in Epot (See 11.6.2.2), which would enhance ET. This would contribute to deplete soil moisture during droughts (Seneviratne et al., 2012a; Teuling et al., 2013), as suggested by modeling approaches in China (Cheng et al., 2015; Li et al., 2019c) and central Europe (Trnka et al., 2015a; Van Der Linden et al., 2019).

11.6.2.4 Hydrological deficits

There are few studies analysing trends in hydrological drought but there is evidence of increased hydrological droughts in the Mediterranean (Giuntoli et al., 2013; Lorenzo-Lacruz et al., 2013; Gudmundsson et al. 2019), China (Zhang et al., 2018b) and southern Africa (Gudmundsson et al., 2019). In Northwestern Europe there is no evidence of changes in the severity of hydrological droughts during the 20th century (Barker et al., 2019). In the US, depending on the methods, datasets and study periods, there are differences between studies that suggest an increase (Shukla et al., 2015; Udall and Overpeck, 2017) vs a decrease in hydrological drought frequency (Mo and Lettenmaier, 2018), but in general there is strong spatial variability (Poshtiri and Pal, 2016). Shukla et al. (2015) suggested that the high temperatures observed in 2014 in California increased hydrological drought severity, and Udall and Overpeck (2017) estimated that between 1/6 and ½ of the flow reduction in the Colorado river between 2000-2014 was related to the unprecedented high temperatures (Xiao et al., 2018). In the Mediterranean region there is also hydrological drought intensification, which could be either explained by human uses and land cover changes (Vicente-Serrano et al., 2019b), or related to the influence of precipitation trends (Giuntoli et al., 2013; Gudmundsson et al., 2017) and increased Epot (Vicente-Serrano et al., 2014b). The Epot effects on hydrological droughts would be associated to increased ET in the humid headwaters due to large natural revegetation processes (García-Ruiz et al., 2011; Teuling et al., 2019), and the increase in the length of the vegetation active period (Frank et al., 2015), but also to the water evaporated from water bodies and from large irrigated lands (Martínez-Granados et al., 2011; Vicente-Serrano et al., 2017a).

11.6.2.5 Combined synthetic measures of drought

Drought trend analysis have often been based on drought indices that combine precipitation and Epot, such as the PDSI (Dai, 2013; Dai and Zhao, 2017; Dai et al., 2018) or the SPEI (Spinoni et al., 2019). Given the limitations of the PDSI stated above, we limit the assessment of drought trends based on this index in the report.

SPEI suggests slightly higher increases in the regions affected by drying over the last decades in comparison to the SPI (Spinoni et al., 2019), mainly in regions of West and South Africa, the Mediterranean and West China (Figure 11.18). A number of regional studies based on the SPEI have also showed SPEI-based drying trends in the Amazon (Marengo and Espinoza, 2016b; Fu et al., 2013), central America (Hidalgo et al., 2017), Iran (Tabari and Aghajanloo, 2013), South Asia (Niranjan Kumar et al., 2013), the Fertile Crescent (Kelley et al., 2015; Mathbout et al., 2018), regions of China (Yu et al., 2014; Chen and Sun, 2015b; Wu et al., 2019b) and Southern Europe (Cook et al., 2014a; Ozturk et al., 2015; Roudier et al., 2016; Gudmundsson et al., 2017; Stagge et al., 2017; González-Hidalgo et al., 2018).Nevertheless, it is necessary to carefully evaluate these SPEI-based drying trends, given that Epot effects on soil moisture (Manning et al., 2018) and on agricultural/ecological droughts (Yang et al., 2016), can be different under humid and dry conditions and between drought types (see further discussion in Section 11.6.1.1). Although SPEI in humid regions are not very sensitive to Epot variability (Vicente-Serrano et al., 2015), this metric could potentially overestimate

Epot effects in these regions. Nevertheless in water-limited regions, Epot has potentially contributed to increase the drought severity during low rainfall periods (Vicente-Serrano et al., 2020), given the sustained decrease of the SPEI in the Mediterranean region over the last decades (Stagge et al., 2017).

[START FIGURE 11.18 HERE]

Figure 11.18: Observed trends in drought severity and frequency obtained from 3-month SPEI and SPI based on Global Precipitation Climatology Centre (GPCC) precipitation using the Climate Research Unit (CRU) Epot datasets from 1981 to 2016. The threshold to identify drought episodes was set at -1 SPI/SPEI units, which represents 20% of probability (1 event in 5 years).Based on (Spinoni et al., 2019).

[END FIGURE 11.18 HERE]

[INSERT FIGURE 11.19 HERE]

Figure 11.19: Observed linear trend over 1951-2018 in the annual consecutive dry days (CDD) from the most recent HadEX3 data set. Units: days/decade. (from Dunn et al., submitted)

[END FIGURE 11.19 HERE]

Summary: There is *high confidence* that atmospheric evaporative demand has increased on average on continents, contributing to increase water stress during precipitation deficits. Trends in precipitation deficits are regionally variable and not significant when averaged at global scale (*high confidence)*. There is *high confidence* that precipitation deficits have increased since the mid 20^th^ century in West Africa and Southern Africa. There is *medium confidence* in trends in soil moisture deficits based on observations-driven land surface models, which suggest an increase in the frequency of soil moisture deficits in some regions (North China, Northwest North America and the Mediterranean). There is *medium confidence* that some regions show more frequent hydrological droughts (e.g., South Africa, South North America, the Mediterranean). There is *medium confidence* that trends in potential evapotranspiration have exceeded trends in precipitation in some regions and seasons.

11.6.3 Model evaluation

Assessment of model performance for drought is difficult given the different drought types, impacts and metrics used to assess drought. In addition, assessing the reliability of drought trends in model outputs is also difficult given observational constrains for most of modeled drought metrics. Finally, there are uncertainties associated to the internal climate variability, which is very large for droughts, and model divergences.

11.6.3.1 Precipitation deficits

Models show limited performance and large spread in identifying precipitation deficits and associated long-term trends in comparison with observations (Nasrollahi et al., 2015). Orlowsky and Seneviratne (2013) compared drought trends using three different observation precipitation datasets and simulations by 32 CMIP5 models from 1950 to 2009 and showed agreement only in high latitudes (i.e., > 55° degrees North from the equator). Knutson and Zeng (2018) found a strong tendency for CMIP5 historical runs to simulate a drying precipitation trend bias compared to observed trends (1901-2010), particularly in mid- to high latitudes, where the observed increasing precipitation trends were significantly undersimulated by models. Models generally underestimate the severity of the precipitation deficits in comparison to the observations

(Ukkola et al., 2018). In addition, future projections show an important spread among models in the projected frequency of precipitation deficits (Touma et al., 2015; Zhao et al., 2016; Engström and Keellings, 2018). There are important spatial differences in the spread, which is higher in the regions where an enhanced drought condition is projected and under high-emission scenarios (Orlowsky and Seneviratne, 2013). The spread among models is the lowest in East North America but very high in the Mediterranean or Central America (Touma et al., 2015). Nonetheless, some event attribution studies have concluded that very wet seasons and droughts at regional scales can be adequately simulated by some climate models (Schaller et al., 2016; Otto et al., 2018c).

11.6.3.2 Atmospheric evaporative demand

Scheff and Frierson (2015) analysed average Epot in 17 CMIP5 GCMs for the period 1981-1999 and although the spatial patterns of the model outputs resemble with the observations, the magnitude of Epot showed strong divergence among models globally and regionally. The most comprehensive evaluation study was by Liu and Sun (2016) that compared the atmospheric evaporative demand obtained from 12 CMIP5 GCMs in China with Epan observations for the period 1961-2000. They showed that although the GCMs captured well seasonal cycles, regional averages were underestimated given bias in air temperature and VPD. Sheffield et al. (2013) stressed the low capability of the models to provide realistic values of the latent heat. In addition Liu and Sun (2016) found strong bias among the different models, both in the agreement with the observations and in the physical drivers that control both aerodynamic and radiative Epot drivers. Although the bias recorded in the different variables tend to be compensated in the Penman-Monteith equation (Liu and Sun, 2017), the GCMs did not capture well the dominant Epan negative trends recorded by observations between 1961 and 2000, and most of the models showed a dominant positive trend. In summary, there is *low confidence* that models may identify anomalous atmospheric drying given the lack of studies and model limitations.

11.6.3.3 Soil moisture deficits

Modeling soil moisture deficits shows more uncertainty than modeling precipitation deficits since in addition to the uncertainties related to cloud and precipitation processes, there is uncertainty related to the soil hydrological processes (Lu et al., 2019). The spatial resolution of models is a limitation since representation of some land-atmosphere feedbacks and topographical effects requirest detailed resolution (Van Der Linden et al. 2019; Nicolai-Shaw et al. 2015).

Overall, there are contrasting results on the performance of land surface models in representing soil moisture. Anomalies are generally reasonably well captured by models driven with observations-based forcing (e.g., Dirmeyer et al. 2006; Albergel et al. 2013; Xia et al. 2014; Balsamo et al. 2015; Reichle et al. 2017), but there can be substantial intermodel spread, also for trends (Albergel et al. 2013). Some studies comparing modeled soil moisture and observations show that models with good skill can nonetheless display substantial biases in absolute soil moisture (Xia et al., 2014; Gu et al., 2019a), although this is to be expected given the nature of soil moisture and the fact that it is best assessed as water-balance anomalies (Koster et al., 2009). Other studies report limited agreement in the interannual variability of soil moisture representation (Stillman et al., 2016; Yuan and Quiring, 2017) and noticeable seasonal differences in the model skill (Xia et al., 2014, 2015). Ford and Quiring (2019) have compared the temporal variability of soil moisture observations and model outputs in different regions of North America showing very low shared variance in the series (< 30%), independently of the region, model and the depth at which the soil moisture is measured/modeled.

There are also varying results regarding the performance of climate models in representing soil moisture variability and properties. Stegehuis et al., (2013) used an ensemble of regional climate model simulations for Europe and showed that models dry the soil too much in early summer, resulting in an excessive decrease of the latent heat fluxes, with potential implications for more severe drought in dry environments (Teuling, 2018; Van Der Linden et al., 2019). Moreover, the spread of the soil moisture outputs among different models is more important than internal variability and scenario uncertainty (Ukkola et al., 2018; Lu et al., 2019) and the bias is strongly related to the sign of the projected change. Vogel et al., (2018) identified a trimodal distribution of hydrological and temperature projections in CMIP5 global climate models in Central Europe, whereby the driest climate models which project the most warming are found to have substantial bias in soil moisture-temperature coupling in present climate. Recently, Humphrey et al. (2018) identified a possible systematic bias in climate models in the representation of soil moisture drought effects on carbon uptake on land, which appears related to a too limited soil moisture range compared to observations.

Despite the mentioned limitations, the (land surface and climate) model representation of soil moisture processes is based on long-standing developments in the climate research community and uses physical and biological understanding of the underlying processes. Overall, we assess that there is *medium confidence* in the representation of soil moisture deficits in land surface and climate models.

11.6.3.4 Hydrological deficits

The simulation of hydrological deficits is much more problematic than simulating mean streamflow or peak flows (Fundel et al., 2013; Stoelzle et al., 2013; Velázquez et al., 2013; Staudinger et al., 2015) since models tend to be too responsive to the climate forcing and they do not satisfactory capture low flows (Tallaksen and Stahl, 2014). Simulations of hydrological drought metrics show uncertainties related to the contribution of both GCMs and hydrological models (Bosshard et al., 2013; Giuntoli et al., 2015; Samaniego et al., 2017; Vetter et al., 2017), but hydrological models forced by the same climate input data also show a large spread (Van Huijgevoort et al., 2013; Ukkola et al., 2018). In a very comprehensible study, Tallaksen and Stahl (2014) analysed the simulations of streamflow droughts in seven global (hydrological and land surface) models and compared the results with observations in near-natural catchments of Europe for the period 1963-2000. This study showed an important spread among models and a tendency to overestimate the number of drought events and to underestimate drought duration and drought-affected area.

11.6.3.5 Combined synthetic measures of drought

A number of studies have analysed the capacity of models to determine drought severity and trends based on synthetic drought indices. Logically, given the limitations to reproduce the dynamic of precipitation deficits and atmospheric dryness stated in 11.6.3.1 and 11.6.3.2, the modeled drought indices based on these two variables are also affected by uncertainties and biases. Zhao and Dai (2017) analysed trends in the PDSI using observations and CMIP3 and CMIP5 model ensembles between 1950 and 2014 and suggested a consistent signal between models and observations at the global scale, with a general increase of the PDSI. However, they showed low spatial agreement in the trends with the exception of some regions like the Mediterranean, South Asia and Northwest US (Abatzoglou and Rupp, 2017). There is an important spread in PDSI and SPEI projections among different models (Cook et al., 2014). With the exception of the Mediterranean, South North America and Central America, in which the majority of the models simulate a drying trend in the SPEI, in the rest of the world the models strongly differ, with the most important spread in the Sahel (Touma et al., 2015), one of the most critical regions for drought projections.

Summary: There is overall *medium confidence* in the ability of climate models to simulate trends and anomalies in precipitation deficits, atmospheric dryness, soil moisture deficits, streamflow deficits on global and regional scale. There is also overall *medium confidence* in the ability of land surface models and hydrological models to simulate trends and anomalies in soil moisture deficits or streamflow deficits on global and regional scale. However, the evaluation of climate, land surface and hydrological models for the simulation of droughts is complex, due to the regional scope of observed drought trends, the high interannual variability (and thus low signal-to-noise ratio) in trends of drought-related measures, and the lack of relevant measurements in several regions, in particular for soil moisture and streamflow.

11.6.4 Attribution

Anthropogenic influence on drought and water scarcity is complex. This includes both human influence to the climate and climate system that indirectly affect drought as well as other influences due to land use and other socio-economical activities (Van Loon et al., 2016). Studies attributing changes in drought are limited, and they typically fall into two main types. One type is concerned about human influence on the probability or magnitude of recent drought conducted in the event attribution framework. Many of this type of studies focus on human influence on the lack of precipitation that leads to drought condition. Another type studies focus on long-term trend, most often focusing on soil moisture. These studies may not analyse changes in drought per se, but changes in mean soil moisture that can be inferred to be related to the occurrence of events with high soil moisture deficits. These two type of studies are assessed in the following two subsections on precipitation deficits and soil moisture, respectively. In both cases, studies are limited by attribution techniques and observed data sources, both of them varying among studies. Many drought-focused attribution studies can be inconclusive due to lack of observational data (e.g., Philip et al., 2017) and a lack of sufficiently reliable model simulations to determine the reliability of the attributable signal (Uhe et al., 2017; Otto et al., 2018a; Philip et al., 2018a). Furthermore, the attributable signal varies depending on the region, event timescale considered and the attributable signal of large-scale modes of variability, such as ENSO.

11.6.4.1 Precipitation deficits

There have been a number of attribution studies of recent drought events in various regions with a focus on meteorological drought. Some studies have determined that human influence has increased the severity or likelihood of recent droughts but others find the results to be inconclusive (García-Herrera et al., 2019).

In Europe, human influence was found to have enhanced the magnitude of the 2011-2012 winter drought over the Iberian Peninsula where winter precipitation decreased between the 1960s and 2000s (Trigo et al., 2013; Angélil et al., 2017). A multi-method and multi-model attribution study on the 2015 Central European drought did not find conclusive evidence whether human-induced climate change was a driver of the rainfall deficit, as the results depended on model and method used (Hauser et al., 2017). While there is not a clear trend in precipitation records over Mediterranean region during 1850-2018 (Vicente-Serrano et al., submitted), there is evidence of drying, contributed by human emissions of greenhouse gases (Hoerling et al., 2012; Knutson and Zeng, 2018), mostly as a consequence of the enhanced Epot (Vicente-Serrano et al., 2014b; Stagge et al., 2017; González-Hidalgo et al., 2018).

Two studies showed that greenhouse gases forcing worsened the 2016 southern African drought. One study found that the likelihood of flash drought over southern Africa was tripled during the last 60 years mainly due to anthropogenic climate change (Yuan et al., 2018a). Another was a multi-step attribution study. It showed that climate change likely increased the intensity of the 2015/16 El Niño, contributing to further decreases in southern African precipitation, crop production and food availability (Funk et al., 2018a). However, there is only *low confidence* in the results, as the study was based on a single model. A study on the three-year 2015-2017 drought in the Western Cape region of South Africa also found a threefold increase in the likelihood of the lack of rainfall (Otto et al., 2018c). Several studies have focused on recent droughts in East Africa. An attributable signal in the lack of rainfall was not found in droughts occurred in different years with different spatial extents in the last decade over the region (Marthews et al., 2015; Uhe et al., 2017; Otto et al., 2018a; Philip et al., 2018a; Kew et al., 2019a). In terms of dependence on event timescales, Lott et al. (2013) examined East African drought and found no evidence for human influence on the 2010 short rain failure, but an attributable increase in 2011 long rain failure, although the magnitude of increase depended on the estimated pattern by which human influence changed observed SSTs. Further studies have provided attribution statements of African drought events to large-scale modes of variability, such as the strong 2015 El Niño (Philip et al., 2018a) and increased SSTs overall (Funk et al., 2015c, 2018b). In a single model study of the 2014 southern Levant drought (Bergaoui et al., 2015) found an anthropogenic influence on both magnitude of the event and its likelihood.

In addition to investigating drought in different locations and of varying duration, drought attribution studies in North America (Wehner et al., 2017) also explore different drought types (meteorological, agricultural and hydrological). This re-examination demonstrates that, in addition to the region and event definition, attribution statements are potentially dependent on the system examined, model treatment of human influence on observed SSTs and overall attribution framework used. Overall, the anthropogenic influence on US droughts is complex, with *limited evidence* for an attributable anthropogenic signal on observed precipitation deficits.

An attributable anthropogenic signal in observed droughts has not been found in regions of Asia and South America. No climate change signal was found in the record dry spell over Singapore-Malaysia in 2014 (Mcbride et al., 2015) or the drought in central southwest Asia in 2013/2014 (Barlow and Hoell, 2015). Similarly, in recent droughts occurring in South America, specifically in the southern Amazon region in 2010 (Shiogama et al., 2013) and in northeast Brazil in 2014 (Otto, et al. 2015) and 2016 (Martins, E.S.P.R., Coelho, C.A.S., Haarsma, R., Otto, F.E.L., King, A.D., van Oldenborgh, G.J., Kew, S., Philip, S., Vasconcelos Junior, F.C. and Cullen, 2017; Quan et al., 2018) anthropogenic climate change was not a dominant influence.

Results of drought event attribution studies in Australia show either an increase in drought likelihood or no change depending on methods, regions and season. While the meteorological conditions associated with the 2013 New Zealand drought were attributed by Harrington et al. (2014) using the fully coupled CMIP5 models to be more probable as a result of anthropogenic climate change, Angélil et al. (2017) did not find a corresponding change in the dry end of simulated precipitation from a stand-alone atmospheric model. Several studies of Australian droughts of varying length demonstrate no significant change in meteorological droughts in the region related to anthropogenic climate change based on analysis of precipitation deficits (Cai et al., 2014b; King et al., 2014). However, co-occurring hot and dry conditions, such as in 2006 across southeast Australia are *likely* to have increased due to climate change (King et al., 2017).

Studies also highlight a complex interplay of anthropogenic and non-anthropogenic climatological factors. For example, anthropogenic warming contributed to the 2014 east African drought by increasing east African and west Pacific temperatures, and increasing the gradient between standardized western and central Pacific SST causing reduced rainfall, evapotranspiration, and soil moisture (Funk et al., 2015c). Several events have been independently re-examined using a single analytical approach and climate model datasets (Angélil et al., 2017), identifying several instances of diverging claims of the anthropogenic attributable change.

11.6.4.2 Soil moisture deficits

Detection and attribution analyses of long-term changes on drought are limited, focusing mostly on soil moisture. Mueller and Zhang (2016) evaluated trends in reconstructed historical soil moisture for 1951-2005 and compared them with those in the CMIP5 simulations. They concluded that anthropogenic forcing contributed significantly to the observed drying and that the increases in the land surface area affected by drought (defined by soil moisture deficits) can be reproduced by CMIP5 models only if anthropogenic forcings are involved. Gu et al. (2019b) compared reconstructed soil moisture in the root zone layer during 1948-2005 with those simulated by CMIP5 models; they concludedthat observed global soil moisture drying can be explained by human influence and cannot be explained by the influence of natural external forcing. Padrón et al. (2019) analyzed reconstructed and CMIP5 simulated dry season water availability, defined as precipitation minus evapotranspiration (i.e. equivalent to soil moisture and runoff availability), over 1902-2014. They found consistent changes towards drying in the average water availability during the driest month of the year in the recent three decades when compared with that in the first half of the 20th century. Model simulations under anthropogenic forcing can explain such changes while those under natural external forcing cannot.The drying is mainly caused by increase in evaporation (induced by increased temperature and radiation) rather than by reduction in precipitation. Because of the lack of observed soil moisture or PDSI, a common feature of these studies is the use of reconstructed data partly based on observations either through dynamical assimilation or statistical means, making it difficult to quantify the amount of drying and lowering our confidence in the identified drying for the historical time. Yet, all studies point to warming induced drying in the soil moisture and warming has been attributed to human influence. While it is difficult to assess the quantitative contribution of human influence to the assessed soil moisture drying, the balance of evidence leads us to conclude that that is *high confidence* that human influence has contributed to a global-scale tendency towards soil moisture drying in the dry season, mostly related to increased evaporative demand rather than changes in precipitation.

11.6.4.3 Hydrological deficits

There is limited evidence on the attribution of trends in hydrological deficits, A recent study of Gudmundsson et al. (submitted) suggests that anthropogenic climate change has impacted the magnitude of low flows at the global scale in simulations of the ISIMIP ensemble. Human water use could play a role on local scale and Wada et al. (2013) estimate that human water consumption has intensified the magnitude of hydrological droughts by 20%-40% over the last 50 years.

11.6.4.4 Combined synthetic measures of drought

Marvel et al. (2019) compared tree ring based reconstruction of the Palmer drought severity index (PDSI) over the past millennium with PDSI estimates driven with CMIP5 models. Their results suggest that the signal of greenhouse gases forcing is present in the reconstruction in the recent decades (1980 to present) but cannot be robustly detected. Their findings also suggest that a signal of greenhouse gases forcing can be robustly detected in the first half of the 20th century. The results from this study need to be placed in context as PDSI has known limitations in representing drought response to warming, and the uncertainty in the use of proxy-based reconstructed PDSI also needs to be accounted for. Additionally, a robust detection of anthropogenic signal in the first half of the 21st century when warming was relatively weak does not seem to be consistent with a lack of robust detection of anthropogenic since 1980 for which warming is stronger.

Summary

With the exception of attribution studies assessing changes in precipitation deficits, a common feature of drought attribution studies is the use of reconstructed data partly based on observations either through dynamical assimilation or statistical means, making it difficult to quantify the amount of drying and lowering our confidence in the identified drying for the historical time. Yet, all available studies point to an evapotranspiration-driven drying in soil moisture (or water availability, which encompasses soil moisture) when aggregated on global scale, which is related to increased warming and radiation, both of which have been attributed to human influence. While it is difficult to assess the quantitative contribution of human influence to the assessed soil moisture drying, the balance of evidence leads us to conclude that there is *high confidence* that human influence has contributed to a global-scale tendency towards soil moisture drying in the dry season, mostly related to increased evaporative demand rather than changes in precipitation. The human contribution to trends in precipitation or runoff is more uncertain, as is the attribution of regional changes in drought.

Overall, there is *high confidence* that human influence has increased the potential for worsening of drought conditions and increased the tendency towards drying in the dry season since the beginning of the 20th century, when aggregated on the global scale. The drying tendency is dominated by warming- and radiation-induced increase in evaporative demand rather than by changes in precipitation. At local to regional scales, human influence on drought and water scarcity is complex, as it includes climate forcing, land use changes, water management, and socio-economical influences. There is *low confidence* in the contribution of greenhouse gas forcing to changes in atmospheric circulation processes affecting drought.

11.6.5 Projections

The SREX report (SREX Chapter 3) highlighted *medium confidence* in projections of increased drought severity in some regions, including southern Europe and the Mediterranean, central Europe, Central America and Mexico, northeast Brazil, and southern Africa. The report stressed *low confidence* elsewhere given large spread between models and scenarios. The AR5 (AR5 Chapter 11 and 12) also stressed large uncertainties in drought projections at the regional and global scales. The assessment of drought mechanisms under future climate change scenarios is hampered by the limited availability of reliable model simulations, which is both the result of a large climate model dependency of drought projections in some regions (Section 11.6.3). Moreover, uncertainties in drought projections are affected by statistical issues related to the way of calculating drought metrics for future scenarios given the use of different time scales and changes to distribution functions but also vegetation-CO_2 feedbacks (Vicente-Serrano et al., 2019). Overall, there are substantial increases in risks of drying from 1.5°C to 2°C global warming as well as for further additional increments of global warming (Figs. 11.20 and 11.21). These findings, which are based on CMIP6 analyses are consistent with CMIP5 analyses (see Appendix), the conclusions of the SR15 Chapter 3, Greve et al. (2018), and Xu et al. (2019).

11.6.5.1 Precipitation deficits

Studies based on CMIP5 projections show a consistent signal in the sign and spatial pattern of projections of precipitation deficits in some regions. Orlowsky and Seneviratne (2013) and Martin (2018) showed that the model ensemble displayed robust signal-to-noise ratio in the Mediterranean, South Africa, Southern North America, Central America and Northeast Brazil, regions in which more frequent and severe droughts are projected, although in South Africa recent studies also suggest a weak shift in the probability distribution functions of precipitations series both at 1.5 and 2°C warming levels (Nangombe et al., 2018). Projections for the number of CDDs in CMIP6 (Figure 11.20) for different levels of global warming relative to 1850-1900 show similar projected patterns. The robustness of the patterns in projected precipitation deficits identified in the global studies is also consistent with results from regional studies (Giorgi et al., 2014; Pinto et al., 2016; Maúre et al., 2018). In Africa, a strong increase in the length of dry spells (CDD) is projected by the end of the 21st century over most of the continent with the exception of central and eastern Africa (Sillmann et al., 2013a; Giorgi et al., 2014; Han et al., 2019) and in West Africa, where there is lack of agreement in sign of change between studies (Sillmann et al., 2013a; Akinsanola and Zhou, 2018; Han et al., 2019), although CDD would increase with stronger global warming levels (Klutse et al., 2018). In Asia there are expected large regional differences in the drought projections. In the middle East, an increase of the dry days and the drought duration is projected in about 80% of the region (Tabari and Willems, 2018). Whereas in central Asia there are projected small changes in CDD (Han et al., 2018), this metric is projected to increase in south China but to decrease in north China (Zhou et al., 2014; Han et al., 2018), in agreement with projections of the SPI (Huang et al., 2018a). In the Tibetan Plateau there is a general projected decrease in drought, but with large uncertainty (Zhou et al., 2014). Frequency and area extents of severe, extreme, and exceptional precipitation droughts based on the CDD are projected to increase in India in the near-term and until the mid 21st century (Salvi and Ghosh, 2016). In Southeast Asia, an increasing frequency of precipitation deficits is projected as a consequence of increasing frequency of extreme El Niño (Cai et al., 2014a, 2015, 2018). In central America, projections suggest an increase in mid-summer drought (Imbach et al., 2018) and increased CDD (Chou et al., 2014a; Giorgi et al., 2014). In the Amazon, there is also a projected increase in dryness (Marengo and Espinoza, 2016), which is however the combination of a projected increase in the frequency and geographic extent of meteorological drought in the eastern Amazon, and an opposite trend in the West (Duffy et al., 2015). In Southwestern South America, there is a projected increase of the CDD (Chou et al., 2014a; Giorgi et al., 2014) and in Chile drying is projected to prevail (Boisier et al., 2018). In the South America monsoon region, an increase in CDD is projected(Chou et al., 2014a; Giorgi et al., 2014), but a decrease is projected in South Eastern South America and Southern South America (Giorgi et al., 2014). In Central America, mid summer drought is expected to intensify during 2071-2095 for the RCP8.5 scenario (Corrales-Suastegui et al., 2019). In Canada and most of the US, and based on the SPI, Swain and Hayhoe (2015)identified drier summer conditions in projections over most of the region, and there is a consistent signal toward an increase in duration and intensity of droughtsin southern North America (Pascale et al., 2016; Escalante-Sandoval and Nuñez-Garcia, 2017). In California, more precipitation variability is projected, characterised by increased frequency of consecutive drought and humid periods (Swain et al., 2018). Finally, in Southern Europe model projections display a consistent drying among models (Hertig and Tramblay, 2017; Guerreiro et al., 2018a; Raymond et al., 2019), and in Central Europe there is substantial spread in projections, with some models projecting very strong drying and others close to no trend (Vogel et al., 2018). Vogel et al. (2018) identified that the driest (and wettest) models did not present land-atmosphere coupling features consistent with observations, and that an observationally-constrained ensemble displayed weaker drying. On the other hand, the driest models of the ensemble are the ones perfoming best in capturing the driest conditions in observations, despite a poorer performance for interannual variability(Orth et al., 2016b).

11.6.5.2 Atmospheric evaporative demand

Effects of atmospheric evaporative demand on droughts is a critical issue under future projections (Vicente-Serrano et al., 2020). Considering a purely atmospheric demand, the CMIP5 models project strong increase in Epot over the majority of the world under the RCP8.5 scenario (Scheff and Frierson, 2015). The role of the Epot on drought severity in future projections may vary considering physical and plant physiological processes, including the possible role of CO_2 fertilization on vegetation water use efficiency (Roderick et al., 2015; Milly and Dunne, 2016; Swann et al., 2016; Greve et al., 2017; Scheff et al., 2017; Lemordant et al., 2018; Swann, 2018). Soil moisture also contribute to these trends given effects on ET and land-atmosphere feedbacks (Berg et al., 2016; Teuling, 2018). Nonetheless, increases in ET could be limited compared to the increased Epot due to soil moisture limitation (Berg et al., 2016), with implications for hydrological drought projections. CO_2 fertilization could reduce Epot in vegetated areas, explaining why some studies suggest small runoff reduction in future climate scenarios (Roderick et al., 2015; Yang et al., 2019). Overall, there are some uncertainties since, on the one hand, fertilizing CO_2 effects will not enterely compensate atmospheric dryness associated to enhanced temperature and VPD (Liu and Sun, 2017); in large tropical and subtropical regions (e.g., South Africa, the Amazon, the Mediterranean and South North America), maximum evapotranspiration is projected to strongly increase even when considering CO_2 fertilization (Vicente-Serrano et al., 2020). On the other hand, Huang et al. (2017) showed that humid areas warmed at 60-80% of the rate of the dry regions, and stressed that this differential warming is not well represented in GCMs. This issue could imply underestimated warming in dry areas, reinforcing thermodynamic processes in water-limited environments and enhancing Epot (Dai et al., 2018). Moreover, there is a number of ecophysiological and anatomical processes that may reduce the role of the CO_2 fertilization on plant processes (Menezes-Silva et al., 2019) and the benefit of the CO_2 fertilization could be minimal during low precipitation periods given stomatal closure in response to low soil moisture (Allen et al., 2015).

11.6.5.3 Soil moisture deficits

Areas with projected soil moisture decreases do not fully coincide with areas with projected precipitation decreases, although there substantial consistency in the respective patterns (Dirmeyer et al., 2013; Berg and Sheffield, 2018). Moisture in the top soil layer (10 cm., surface soil moisture) is projected to decline more than precipitation at all warming levels (Lu et al., 2019), extending the regions affected by severe soil moisture deficits over most of South and Central Europe (Lehner et al., 2017; Ruosteenoja et al., 2018; Samaniego et al., 2018; Van Der Linden et al., 2019), South North America by 2050 (Cook et al., 2019), and South America (Orlowsky and Seneviratne, 2013), South Africa (Lu et al., 2019), East Africa (Rowell et al., 2015), India (Mishra et al., 2014b) and East Asia (Cheng et al., 2015) (Figure 11.21), possibly as a consequence of enhanced Epot and associated increased ET as highlighted by some studies (Orlowsky and Seneviratne, 2013; Dai et al., 2018). Projected changes in total soil moisture display less widespread drying than those for surface soil moisture (Berg et al., 2017), but still more than for precipitation (Fig. 11.20). The severity of droughts based on surface soil moisture in future projections is stronger than projections based on precipitation, runoff and the combined synthetic climate drought indices (Dai et al., 2018; Vicente-Serrano et al., 2019). In some areas the signal to noise ratio among models is low and only in the Mediterranean and Europe, the southwestern United States, and southern Africa the projections show a substantial signal to noise ratio in soil moisture projections (Lu et al., 2019).

11.6.5.4 Hydrological deficits

Some studies support wetting tendencies as a response to a warmer climate when considering globally-averaged changes in runoff over land (Roderick et al., 2015; Greve et al., 2017; Yang et al., 2018d), and streamflow projections respond to enhanced CO_2 concentrations in CMIP5 models (Yang et al., 2019). Nevertheless, when focusing on low-runoff periods the model projections also show a reinforcemet in large world regions (Dai et al., 2018; Vicente-Serrano et al., 2019). Global averages of hydrological drought are projected to display an increase in drought severity and duration (Wanders and Van Lanen, 2015). The regions that are more affected are the Mediterranean, the middle East, South Africa, South Australia and Southern South America (Prudhomme et al., 2014; Wanders and Van Lanen, 2015). Models have smaller spread in future projections for northern latitudes, the Horn of Africa and Indonesia where a reduction of drought severity is projected. In Northern China, although the drought frequency is expected to be reduced, hydrological drought severity would rise dramatically given increased variability in precipitation and evapotranspiration (Jiao and Yuan, 2019). Streamflow droughts are projected to become more severe in Europe, except for north and northeast Europe. Streamflow in southern Europe is projected to be reduced by 10-30% (Forzieri et al., 2014; Roudier et al., 2016).Based on high-resolution (5km) simulations for Europe with 3 hydrological models, driven by 5 global climate models, for 3 different scenarios, Marx et al., (2018) identify that low-flow signal in Europe amplifies with increasing warming levels. This includes a drying in the Mediterranean region (lower low flows) and a wetting in the Alpine and Northern region (higher low flows). In the Mediterranean, the level of warming amplifies the signal from −12 % under 1.5 °C, compared to the baseline period 1971–2000, to −35% under global warming of 3°C, largely due to the projected decreases in annual precipitation, while the signal is amplified from +22 (1.5 °C) to +45% (°C) in the Alpine region due to changes in snow accumulation. In Southern North America, an increase of hydrological drought severity is projected for 2050 as a consequence of reduced precipitation and enhanced evapotranspiration (Cook et al., 2019). There is, however, only *medium confidence* in these projections due to large uncertainties in the hydrological/impact model used (Prudhomme et al., 2014; Schewe et al., 2014; Gosling et al., 2017) and uncertainty in the projection of future human activities including water demands, land cover changes, etc., which may represent more than 50% of the projected changes in hydrological droughts (Wanders and Wada, 2015). In addition, regions dependent on mountainous snowpack as a temporary reservoir are at risk of severe hydrological droughts in a warmer world. For instance, in the western United States, a 22% reduction in winter snow water equivalent is projected under a high emissions scenario by 2050 relative to historical levels with a further decrease to a 70% reduction by 2100 (Rhoades et al. 2018). The exact magnitude of the influence of higher temperatures on snow-related droughts is, however, difficult to estimate (Mote et al., 2016) since the streamflow changes could affect the timing of peak streamflows but not necessarily their magnitude. In addition, projected changes in hydrological droughts downstream of declining glaciers can be very complex to assess (Chapter 9 and the SROCC).

11.6.5.5 Combined synthetic measures of drought

Global drying tendencies are identified in future projections when focusing on drought indices calculated from precipitation and Epot as the PDSI or the SPEI (Zhao and Dai, 2017; Dai et al., 2018). In general, the inclusion of a purely atmospheric evaporative demand in the drought indices expands the spatial extent of drought conditions based on precipitation deficits (expanded to regions in the Amazon, most of North America, Europe, central Asia and East China) (Cook et al., 2014a; Touma et al., 2015; Lehner et al., 2017; Dai et al., 2018; Naumann et al., 2018; Potopová et al., 2018; Spinoni et al., 2018b; Senatore et al., 2019; Vicente-Serrano et al., 2019b). A number of regional studies based on these drought indices also suggest a reinforcement of drought in East Asia (Rhee and Cho, 2016; Chen and Sun, 2017a, 2017b; Gao et al., 2017b; Wang et al., 2018c), South Australia (Olson et al., 2016; Herold et al., 2018), South Africa (Abiodun et al., 2019), South North America (Venkataraman et al., 2016) and Canada (Tam et al., 2019). There is, however, some uncertainty in these findings given the complex role of Epot on drought, which depends on the drought type, the environmental conditions and the anomalies in precipitation (Vicente-Serrano et al., 2020), so in humid regions or in those that show a projected increase in precipitation, these indices could overestimate the influence of Epot on drought trends (Vicente-Serrano et al., 2020). Also, in dry regions, since Epot is an overestimate for actual evapotranspiration these projected changes cannot be equated with soil moisture drought, but could still be relevant for vegetation stress (Table 11.3).Milly and Dunne (2016) show that a purely meteorological metric of atmospheric dryness overestimates the projections of soil moisture and streamflow deficits given the decoupling of ET and Epot when ET is reduced due to soil moisture limitation or/and possible CO_2 fertilizing effects (Berg et al., 2016). Nevertheless, in water-limited regions the effect of Epot on drought projections is coherent with an enhanced vegetation water stress. Thus the projections by these drought indices could be representative of some forms of vegetation stress despite a decoupling to soil moisture. In addition, depending on processing, projections in PDSI or SPEI can be consistent with projected soil moisture and runoff deficits globally (Dai et al., 2018; Lu et al., 2019; Vicente-Serrano et al., 2019). In addition, the the fertilizing CO_2 effects on vegetation processes under limited soil moisture are very uncertain (Allen et al., 2015; Menezes-Silva et al., 2019).

Summary

There is *high confidence* that atmospheric evaporative demand will continue to increase with increasing global warming and lead to further drying tendencies in some regions. There is *medium confidence* in projected increases in the frequency and severity of precipitation deficits in the Mediterranean region, Southern Africa, Southern North America, Central America and Northeastern Brazil. The *confidence* is assessed to be *medium* because while there is high agreement among climate models, there are uncertainties in drought representation in the climate models, the use of drought metrics in the projections, and lack of observations in several regions to evaluate models. In addition, there is *medium confidence* that soil moisture and streamflow droughts may also be affected by physiological CO_2 effects on plants' transpiration under enhanced CO_2 concentrations. Projections of soil moisture deficits show stronger increase in drought area and severity than projections of changes in precipitation deficits (*medium confidence*). There is *medium confidence for* an increase in hydrological droughts in the Mediterranean, Southern Africa, South Australia and Southern South America. Drought indices that consider the relative changes in precipitation vs Epot show a general increase in drought severity but there are uncertainties in these trends given the complex influence of Epot on drought severity depending on drought types and climate characteristics. These projections are strongly dependent on the warming scenario considered, with stronger drought trends for higher warming levels in some regions, even for changes as small as 0.5°C in global warming (*high confidence*). Some regions with humid or transitional climate characteristics in the 20th century are projected to become drier (*medium confidence*).

[INSERT FIGURE 11.20 HERE]

Figure 11.20: Projected changes in Consecutive Dry Days for projections at 1.5°C, 2°C, 3°C and 4°C of global warming compared to pre-industrial conditions (1850-1900), using empirical scaling relationship based on transient CMIP6 simulations.. [Stippling will be added for FGD]

[END FIGURE 11.20 HERE]

[INSERT FIGURE 11.21 HERE]

Figure 11.21: Projected changes in surface soil moisture for projections at 1.5°C, 2°C, 3°C and 4°C of global warming compared to pre-industrial conditions (1850-1900), using empirical scaling relationship based on transient CMIP6 simulations. [Stippling will be added for FGD]

[END FIGURE 11.21 HERE]

11.7 Extreme storms

Extreme storms, such as tropical and extratropical cyclones, severe convective storms, and atmospheric rivers often have substantial societal impacts. Quantifying the relationship between climate change and extreme storms is challenging, partly because extreme storms are rare, short-lived, and local, and individual events are largely influenced by stochastic variability. The high degree of random variability makes detection and attribution of extreme storm trends more uncertain than detection and attribution of trends of other aspects of the environment in which the storms evolve (e.g., larger-scale temperature trends). Projecting changes in extreme storms is also challenging because of constraints in the models' ability to accurately represent the small-scale physical processes that can drive these changes. Despite the challenges though, good progress has been since the AR5.

A capsule summary of the most relevant assessment and confidence statements from previous reports is provided here.

The SREX (chapter 3) stated:
1) There is *low confidence* in observed long-term (40 years or more) trends in tropical cyclone (TC) intensity, frequency, and duration, and any observed trends in phenomena such as tornadoes and hail.
2) It is *likely* that extratropical storm tracks have shifted poleward in both the Northern and Southern Hemispheres and that heavy rainfalls and mean maximum wind speeds associated with TCs will increase with continued greenhouse gas (GHG) warming.
3) It is *likely* that the global frequency of TCs will either decrease or remain essentially unchanged while it is *more likely than not* that the frequency of the most intense storms will increase substantially in some ocean basins.
4) There is *low confidence* in projections of small-scale phenomena such as tornadoes and hail storms.
5)There is *medium confidence* that there will be reduced frequency and a poleward shift of mid-latitude cyclones due to future anthropogenic climate change.

The AR5 maintained an assessment of *low confidence* in observed long-term trends in TC metrics but modified this statement from the SREX to state that it is *virtually certain* that there are increasing trends in North Atlantic TC activity since the 1970s with *medium confidence* that anthropogenic aerosol forcing has contributed to these trends. Unchanged from the SREX, the AR5 concluded that it is *likely* that TC precipitation and mean intensity will increase and *more likely than not* that the frequency of the strongest storms increase with continued GHG warming. *Confidence* in projected trends in overall TC frequency remained *low*. *Confidence* in observed and projected trends in hail storm and tornado events also remained *low*.

The SROCC assessment of past and projected tropical and extratropical cyclones essentially follows the conclusions of the AR5 with some additional detail. Literature subsequent to the AR5 adds support to the likelihood of increasing trends in TC intensity and precipitation and frequency of the most intense storms while some newer studies have added uncertainty to projected trends in overall frequency. A growing body of post-AR5 research on the poleward migration of TCs led to a new assessment in the SROCC of *low confidence* that the migration in the western North Pacific represents a detectable climate change contribution from anthropogenic forcing.

The conclusions of the SR1.5 essentially mirror the AR5 assessment of tropical and extratropical cyclones adding that heavy precipitation associated with TCs is projected to be higher at 2°C compared to 1.5°C global warming (*medium confidence*).

The SREX, AR5, SROCC, and SR1.5 do not provide assessments of the atmospheric river literature and the SROCC and SR1.5 do not assess severe convective storms and extreme winds. In this section, we assess the state of knowledge on the four phenomena of tropical cyclones, midlatitude storms, severe convective storms, and extreme winds. Extreme aspects of atmospheric rivers are also included in midlatitude storms. In this respect, our report will closely mirror the SROCC assessment of tropical and extratropical cyclones while updating the SREX and AR5 assessment of severe convective storms and extreme winds and introducing an assessment of atmospheric river literature.

11.7.1 Tropical cyclones

11.7.1.1 Mechanisms and drivers

Tropical cyclones (TCs) respond to their ambient environment in a number of ways. For example, latent and sensible surface heat fluxes provide moist enthalpy that can be converted to wind, upper-level atmospheric temperatures modulate the thermodynamic limit on the peak winds that can be achieved, mid-to-upper-level winds steer the TCs and largely determine their translation speed (which strongly affects local rainfall amounts), and vertical wind shear generally inhibits TC genesis and intensification. Changes in these and other environmental factors, whether as natural variability or by external forcing, are expected to manifest in changes in TC characteristics. This is true for both past and future changes.

The genesis, development, and tracks of TCs depend on conditions of the larger-scale circulations of the atmosphere and ocean (Christensen et al., 2013). Large-scale atmospheric circulations, such as the Hadley and Walker circulations and the monsoon circulations, and internal variability acting on various time-scales, from intra-seasonal (e.g., the Madden-Julian and Boreal Summer Intraseasonal oscillations, and equatorial waves) and inter-annual (e.g., the El Niño-Southern Oscillation and Pacific and Atlantic meridional modes), to inter-decadal (e.g., the Atlantic meridional overturning circulation and inter-decadal Pacific oscillation) can all significantly affect TCs. This broad range of natural variability makes detection of anthropogenic effects difficult, and it is uncertain how the projected changes of these various modes of variability will affect future changes in TC activity. Aerosol forcing also affects SST patterns and cloud microphysics, and it is *likely* that observed changes in TC activity are partly caused by changes in aerosol forcing (Evan et al., 2011; Sobel et al., 2016; Takahashi et al., 2017; Zhao et al., 2018a). Among possible changes from these drivers, there is *medium confidence* that the Hadley cell has widened and will continue to widen in the future (Chapter 3, 4, and 5). This *likely* causes latitudinal shifts of TC tracks (Sharmila and Walsh, 2018). Regional TC activity changes are also strongly affected by projected changes in SST warming patterns (Yoshida et al., 2017), which are highly uncertain (Chapter 4, 9).

11.7.1.2 Observed trends

Identifying past trends in TC metrics remains a challenge due to the heterogeneous character of the historical instrumental data, which are known as "best-track" data (Schreck et al., 2014), and there is *low confidence* that any reported long-term (multidecadal to centennial) trend in TC frequency- or intensity-based metrics are not affected by changes in technology used to collect the best-track data. This should not be interpreted as implying that no physical (real) trends exist, but rather as indicating that either the quality or the temporal length of the data is not adequate to provide robust trend detection statements, particularly in the presence of multidecadal variability. Further uncertainty is introduced by an incomplete understanding of the mechanisms driving the observed multidecadal variability (Knutson et al., 2019a). For example, the relative contributions of internal variability and external forcing to observed Atlantic multidecadal variability is still a question of heightened debate (Sobel et al., 2016; cross-ref chapter 3).

There are ongoing efforts to homogenize the best-track data (Elsner et al., 2008; Emanuel et al., 2018; Kossin, 2019; Kossin et al., 2013; Landsea, 2015; Kossin et al., 2020) and there is substantial literature that finds positive trends in intensity-related metrics in the best-track during the "satellite period", which is generally limited to the past 40 years or so (e.g., Kang and Elsner 2012; Kishtawal et al. 2012; Kossin et al. 2013; Mei and Xie 2016; Zhao et al. 2018; Tauvale and Tsuboki 2019). When best-track trends are tested using homogenized data, the trends generally remain positive but are smaller in amplitude, sometimes to the point of becoming statistically insignificant (Kossin et al., 2013; Holland and Bruyère, 2014). However, there is evidence that the ~40-year period of highest quality satellite era data is near the timescale required for TC intensity trends to emerge from the noise, given the observed changes in the environment (Bender et al., 2010; Kossin et al., 2013). Based on observed trends in the background environment, and our theoretical understanding of how these trends affect TC intensity, it is expected that a trend in TC intensity might become detectable over the past 40 years or so, but might also be sensitive to shortening the period of analysis. Consistent with this, Kossin et al. (2020) extended the homogenized TC intensity record to the period 1979–2017 and identified significant global increases in major TC exceedance probability of about 8% per decade, but the significance of the increase was marginal. This is consistent with numerical modeling simulations, which generally indicate an increase in mean TC peak intensity and the proportion of very intense TCs in a warming world (Knutson et al., 2015, 2019b; Walsh et al., 2015, 2016). In addition to trends in TC intensity, there is evidence that TC intensification rates have increased within the satellite era (Balaguru et al., 2018; Bhatia et al., 2018) and TC intensification rates simulated by a high-resolution coupled model provide support that natural variability alone is unlikely to explain the magnitude of the observed upward trend in the Atlantic basin since the early 1980s (Bhatia et al., 2019; Murakami, submitted).

A subset of the best-track data corresponding to hurricanes that have directly impacted the United States since 1900 is considered to be reliable, and shows no trend in the frequency of U.S. landfall events (Knutson et al., 2019a). However, in this period since 1900, an increasing trend in normalized U.S. hurricane damage (Grinsted et al., 2019) and a decreasing trend in TC translation speed over the U.S. (Kossin, 2019) has been identified. A similarly reliable subset of the data representing TC landfall frequency over Australia shows a decreasing trend since the late 1800s (Callaghan and Power, 2011; Knutson et al., 2019a) and a paleoclimate proxy reconstruction shows that recent levels of TC interactions along parts of the Australian coastline are the lowest in the past 550–1,500 years (Haig et al., 2014). As with all regional analyses of TC frequency, it is generally unclear whether any identified changes are due to a basin-wide change in TC frequency, or to systematic track shifts (or both). From an impacts perspective, however, these changes over land are highly relevant and emphasize that large-scale changes in TC behavior can have a broad spectrum of impacts on a regional scale.

Subsequent to the AR5, two metrics that are argued to be comparatively less sensitive to data issues than frequency- and intensity-based metrics have been analysed, and trends in these metrics have been identified over the past ~70 years or more (Knutson et al., 2019a). The first metric, the mean latitude where TCs reach their peak intensity, exhibits a global and regional poleward migration during the satellite period (Kossin et al., 2014). The poleward migration can influence TC hazard exposure and risk (Kossin et al., 2016a) and is consistent with the independently-observed expansion of the tropics (Lucas et al., 2014). The migration has been linked to changes in the Hadley circulation (Altman et al., 2018; Sharmila and Walsh, 2018; Studholme and Gulev, 2018). The migration is also apparent in the mean locations where TCs exhibit eyes (Knapp et al., 2018), which is when TCs are most intense. Part of the northern hemisphere poleward migration is due to interbasin changes in TC frequency (Kossin et al., 2014, 2016b; Moon et al., 2015, 2016) and the trends, as expected, can be sensitive to the time period chosen (Tennille and Ellis, 2017; Kossin, 2018; Song and Klotzbach, 2018) and to subsetting of the data by intensity (Zhan and Wang, 2017).

The poleward migration is particularly pronounced and well-documented in the western North Pacific basin (Kossin et al., 2016a; Oey and Chou, 2016; Liang et al., 2017; Nakamura et al., 2017; Altman et al., 2018; Daloz and Camargo, 2018; Sun et al., 2019a; Yamaguchi and Maeda, submitted) and a significant poleward trend remains after accounting for the known modes of dominant interannual to decadal variability in the region (Knutson et al., 2019a). A poleward trend in the western North Pacific is also found in CMIP5 model-simulated TCs (in the recent historical period 1980–2005) although it is weaker than observed and is not statistically significant (Kossin et al., 2016a). However, the trend is significant in 21st century CMIP5 projections under the Representative Concentration Pathway8.5 scenario, with a similar spatial pattern and magnitude to the past observed changes in that basin over the period 1945–2016, supporting a possible anthropogenic contribution to the observed trends (Kossin et al., 2016a; Knutson et al., 2019a). A pronounced poleward shift in the western North Pacific is also found in HighResMIP projected simulations (Roberts et al., 2019b).

[START FIGURE 11.22 HERE]

Figure 11.22: Summary schematic of past and projected changes in tropical cyclone (TC), extra-tropical cyclone (ETC), atmospheric river (AR), and severe convective storm (SCS) behaviour and their associated confidence levels. Changes are shown at the global scale (statements 1–5) and regional scale (statements 6, 7).

[END FIGURE 11.22 HERE]

A second metric that is argued to be comparatively less sensitive to data issues than frequency- and intensity-based metrics is TC translation speed (Kossin, 2018a), which exhibits a global slowdown in the best-track data over the period 1949-2016. TC translation speed is a measure of the speed at which TCs move across the Earth's surface and is very closely related to local rainfall amounts (i.e., slower translation speed causes greater local rainfall). TC translation speed also affects structural wind damage and coastal storm surge by changing hazard event duration. The slowdown is observed in the best-track data from all basins except the Northern Indian Ocean and is also found in a number of regions where TCs interact directly with land. The slowing trends identified in the best-track data by Kossin (2018) have been argued to be largely due to data heterogeneity. Moon et al. (2019) and Lanzante (2019) provide evidence that meridional TC track shifts project onto the slowing trends and argue that these shifts are due to the introduction of satellite data. Kossin (2019) provides evidence that the slowing trend is real by focusing on Atlantic TC track data over the coterminous United States in the 118-year period 1900–2017, which are generally considered reliable. In this period, TC translation speed has decreased by 17% and the slowing trend is robust and significant after removing multidecadal variability from the time series. Yamaguchi et al. (2019) use large ensemble simulations to argue that part of the slowdown is due to actual latitudinal shifts of TC tracks, rather than data artefacts, in addition to atmospheric circulation changes.

The slowing TC translation speed is expected to increase local rainfall amounts, which would increase coastal and inland flooding. In combination with slowing translation speed, abrupt TC track direction changes – that can be associated with track "meanders" or "stalls" – have become increasingly likely along the North American coast since the mid-20th century leading to more rainfall in the region (Hall and Kossin, 2019). It is not yet clear, however, what the cause of the observed slowdown is. It is consistent with the physical linkage between warming and slowing circulation (Held and Soden 2006, see also Sections 8.2.1.3 and 8.2.2.1.2), and with expectations of arctic amplification and weakening circulation patterns through weakening meridional temperature gradients (Coumou et al., 2018) or through changes in planetary wave dynamics (Mann et al., 2017). But slowing trends have not been unambiguously observed in circulation patterns that steer TCs such as the Walker and Hadley circulations (Chemke and Polvani, 2019), although these circulations generally slow down in numerical simulations under global warming (He and Soden, 2015;Vecchi and Soden, 2007;Vecchi et al., 2006).

In summary, there is mounting evidence that a variety of TC characteristics have changed over various time periods. It is *likely* that the proportion of stronger TCs has increased globally over the past 40 years. This is consistent with theoretical understanding and numerical simulations, which provides *medium confidence* that the increase has become detectable. It is *very likely* that the average location where tropical cyclones reach their peak wind-intensity has migrated poleward in the western North Pacific Ocean since the 1940s, and there is *medium confidence* that this migration lies outside the range of natural variability. There is *medium confidence* that TC translation speed has slowed detectably over the U.S. since 1900, but *low confidence* for a global signal because of the potential for data heterogeneity. There is *low confidence* in the cause of the slowdown in any region due to a lack of

robust agreement among models that simulate TCs, although the slowdown is consistent with theory and modelling studies that indicate a general slowing of atmospheric circulation with warming.

11.7.1.3 Model evaluation

Accurate projections of future TC activity have two principal requirements: accurate representation of changes in the relevant environmental factors (e.g., SST) that can affect TC activity, and accurate representation of actual TC activity in a given environmental condition. For evaluation of projections of TC-relevant environmental variables, the confidence statements of the AR5 were based on global temperature and moisture, but not on the detailed regional structure of SST and atmospheric circulation changes such as steering flows and vertical shear, which affect characteristics of TCs (genesis, intensity, tracks, etc). Various aspects of TC metrics are used to evaluate how models are capable at simulating present-day TC climatologies and variability (e.g., TC frequency, wind-intensity, precipitation, size, tracks, and their seasonal and interannual changes) (Walsh et al., 2015; Camargo and Wing, 2016; Knutson et al., 2019a, 2019b). Other examples of TC climatology/variability metrics are spatial distributions of TC occurrence and genesis (Walsh et al., 2015) and seasonal cycles and interannual variability of basin-wide activity (Zhao et al., 2009; Shaevitz et al., 2014; Kodama et al., 2015; Murakami et al., 2015b; Yamada et al., 2017) or landfalling activity (Lok and Chan, 2017).

CMIP5/6 class climate models (~100-200 km grid spacing) cannot simulate TCs of Category 4-5 intensity. They do simulate storms of relatively high vorticity that are at best described as “tropical cyclone-like” but metrics like storm counts are highly dependent on tracking algorithms (Wehner et al., 2015; Zarzycki and Ullrich, 2017; Roberts et al., submitted, b). HighResMIP-class global models (~10-60 km grid spacing) begin to capture some structures of TCs more realistically as well as produce intense TCs of Category 4-5 despite the effects of parameterized deep cumulus convection processes (Murakami et al., 2015b; Wehner et al., 2015; Yamada et al., 2017; Roberts et al., 2018). Convection-permitting models (~1-10 km grid-spacing) such as used in some dynamical downscaling studies provide further realism (Tsuboki et al., 2015). Model characteristics besides resolution, especially details of convective parameterization, can influence a model’s ability to simulate intense TCs (Reed and Jablonowski, 2011; Zhao et al., 2012; He and Posselt, 2015; Kim et al., 2018a; Zhang and Wang, 2018). However, models’ dynamical cores also affect simulated TC properties (Reed et al., 2015b). Both wide-area regional and global convection-permitting models without the need for parameterized convection are becoming more useful for TC projection studies [regional model projection studies (Tsuboki et al., 2015; Kanada et al., 2017a; Gutmann et al., 2018) and global model projection studies (Satoh et al., 2015, 2017; Yamada et al., 2017)], as they capture more realistic eye-wall structures of TCs (Kinter et al., 2013) and are becoming more useful for investigating changes in TC structures (Kanada et al., 2013; Yamada et al., 2017). Large ensemble simulations of global climate models with 60 km grid spacing provide TC statistics that allow more reliable detection of changes in the projections, which are not well captured in any single experiment (Yoshida et al., 2017).

Operational forecasting models are very good at simulating TCs, and their use for climate projection studies shows promise. However, there is limited application for future projections as they are highly tuned for operational purposes. Intercomparison of operational models indicates that enhancement of horizontal resolution can provide more credible projections of TCs (Nakano et al., 2017).

Atmosphere-ocean interaction is an important process in TC evolution, and atmosphere-ocean coupled models are generally better than atmosphere-only models at capturing realistic processes related to TCs (Murakami et al., 2015b; Kanada et al., 2017b). Higher resolution ocean models improve simulation of TCs by reducing SST climatology bias (Ogata et al., 2015, 2016; Roberts et al., 2019). For example, in a case study of Hurricane Harvey, Trenberth et al. (2018) suggested that the lack of realistic hurricane activity within coupled climate models hampers the models’ ability to simulate SST and ocean heat content and their changes.

Even with higher resolution atmosphere-ocean coupled models, TC projection studies still rely on assumptions in experimental design that introduce uncertainty. Computational constraints often limit the number of simulations, resulting in relatively small ensemble sizes and an incomplete analysis of possible future SST magnitude and pattern changes (Zhao and Held, 2011; Knutson et al., 2013). Uncertainties in aerosol forcing also are reflected in TC projection uncertainty (Wang et al., 2014).

11.7.1.4 Detection and attribution, event attribution

There is general agreement in the literature that anthropogenic greenhouse gases and aerosols have measurably affected observed oceanic and atmospheric variability in TC-prone regions (chapter 3). This led to the AR5 assessment of *medium confidence* that humans have contributed to the observed increase in Atlantic hurricane activity since the 1970s. Literature subsequent to the AR5 lends further support to this statement (Knutson et al., 2019a). However, there is still no consensus on the relative magnitude of human and natural influences on past changes in Atlantic hurricane activity, and particularly which factor has dominated the observed increase. A recent result using high-resolution dynamical model experiments showed that the observed spatial contrast in TC trends cannot be explained only by multi-decadal natural variability, and external forcing also played an important role (Murakami, submitted).

The recent active TC seasons in some basins, particularly in 2015, have been tested for an anthropogenic influence. Murakami et al., 2017 explored the unusually high TC frequency near Hawaii and in the eastern Pacific basin. Zhang et al. (2016) considered unusually high Accumulated Cyclone Energy (ACE) in the western North Pacific. Yang et al. (2017) and Yamada et al. (2019) looked at TC intensification in the western North Pacific. These studies suggest that the anomalous TC activity in 2015 was not solely explained by the effect of a super El Nino (see BOX 11.3), and that there was an anthropogenic contribution. Takahashi et al. (2017) suggested that a decrease in sulfate aerosol emissions caused about half of the observed decreasing trends in TC genesis frequency in the south-eastern region of the western North Pacific during 1992–2011. Murakami et al. (2018) concluded that the active 2017 Atlantic hurricane season was mainly caused by pronounced SSTs in the tropical North Atlantic and that these types of seasonal events will intensify with projected anthropogenic forcing.

In a case study of Hurricane Sandy (2012), Lackmann (2014) finds no statistically significant impact of anthropogenic climate change on intensity while projection in a warmer world showed significantly increased intensity. In typhoon Haiyan, which struck the Philippines on 8 November 2013, Takayabu et al. (2015) took an event attribution approach with cloud system-resolving (~1km) downscaling ensemble experiments to evaluate the anthropogenic effect on typhoons, and showed that the intensity of the simulated worst case storm in the actual conditions was stronger than that in a hypothetical condition without historical anthropogenic forcing. However, in a similar approach with two coarser parameterized convection models, Wehner et al. (2018) found conflicting human influences on Haiyan's intensity. Kanada et al. (2017) obtained robust anthropogenic intensification of a strong typhoon using 5-km mesh multi-models to simulate realistic rapid intensification of a TC (Kanada and Wada, 2016). In contrast to these convection permitting simulations, Patricola and Wehner (2018) found little evidence of an attributable change in intensity in 15 different TCs using a regional climate model configured between 3 and 4.5 km resolution. They did however find attributable increases in heavy precipitation totals for some of the 15 TCs that could be traced to changes in storm structure.

The dominant factor in the extreme rainfall amounts during Hurricane Harvey's passage onto the U.S. in 2017 was its slow translation speed. But studies published after the event have argued that anthropogenic climate change contributed to an increase in rain rate, which compounded the extreme local rainfall caused by the slow translation. Emanuel (2017) used a large set of synthetically-generated storms and showed that the occurrence of extreme rainfall as observed in Harvey was substantially enhanced by anthropogenic changes to the larger-scale ocean and atmosphere characteristics. Trenberth et al. (2018) linked Harvey's rainfall totals to the anomalously large ocean heat content from the Gulf of Mexico. van Oldenborgh et al. (2017) and Risser and Wehner (2017) applied extreme value analysis to extreme rainfall records in the

Houston, Texas region and both attributed large increases to climate change. Large precipitation increases during Harvey due to global warming were also found using climate models (van Oldenborgh et al., 2017; Wang et al., 2018b). Harvey precipitation totals were estimated in these papers to be 3 to 10 times more likely due to climate change. A best estimate from a regional climate and flood model is that urbanization increased the risk of the Harvey flooding by a factor of 21 (Zhang et al., 2018d). Precipitation increases greater than expected from Clausius-Clapeyron scaling were predicted in advance from a forecast model for Hurricane Florence in 2008 by Reed et al., (2019), and were linked to anthropogenic factors.

11.7.1.5 Projections

A summary of studies on TC projections for the late 21st century, particularly studies since the AR5, is given by (Knutson et al., 2019b), which represents an assessment report mandated by the World Meteorological Organization (WMO). Studies subsequent to Knutson et al. (2019b) are generally consistent and the confidence assessments here closely follow theirs, although there are some differences due to the different confidence calibrations between the IPCC and WMO reports.

There is not an established theory for the drivers of future changes in the frequency of TCs. Most but not all high resolution global simulations project significant reductions in the total number of tropical cyclones with the bulk of the reduction at the weaker end of the intensity spectrum as the climate warms (Knutson et al., 2019b). Recent exceptions based on high-resolution coupled model results are noted in Bhatia et al., 2018 and Vecchi et al., 2019). Vecchi et al. (2019) showed that the representation of synoptic-scale seeds for TC genesis in their high-resolution model causes different projection of global TC frequency, and there is evidence for a decrease in seeds in some projected TC simulations (Sugi et al., 2019). A Genesis Potential Index (GPI) derived from climate models is generally projected to increase as the climate warms (Zhang et al., 2010). However, while GPI well describes the observed interannual variability of current TC frequency (Camargo et al., 2007), it fails to predict the decreased TC frequency found in high resolution model simulations (Wehner et al., 2015), suggesting a limitation of the use of the empirical GPI for projections of TC genesis. In a different approach, a seeded downscaled multi-model projection (Emanuel, 2013) exhibits increases in TC frequency consistent with GPI-based projections. This disparity in the sign of the projected change in global TC frequency further emphasizes the lack of process understanding of tropical cyclogenesis (Walsh et al., 2015).

Changes in SST and atmospheric temperature and moisture play a role in tropical cyclogenesis (Walsh et al., 2015). Reductions in vertical convective mass flux due to increased tropical stability have been associated with a reduction in cyclogenesis (Held and Zhao, 2011; Sugi et al., 2012). Satoh et al. (2015a) further posits that the robust simulated increase in intense TCs, and hence increased vertical mass flux, must lead to a decrease in TC frequency because of this association. GPI can be modified to mimic the TC frequency decreases of a model by altering the treatment of humidity (Camargo et al., 2014) supporting the idea that increased mid-tropospheric saturation deficit (Emanuel et al., 2008) controls TC frequency, but the approach remains empirical. Other possible controlling factors, such as a decline in the number of seeds (held constant in Emanuel's downscaling approach) caused by increased atmospheric stability have been proposed, but questioned as an important factor (Patricola et al., 2018). The resolution of atmospheric models affects the number of seeds, hence TC genesis frequency (Vecchi et al., 2019; Sugi et al., submitted). The diverse and sometimes inconsistent projected changes in global TC frequency by high-resolution models indicate that better process understanding and improvement of the models are needed to raise confidence in these changes.

Most model simulations are consistent in their projection of increases in the proportion of intense TC (Category 4-5) as well as an increase in the intensity of the strongest TCs (Wehner et al., 2018a; Murakami et al., 2012; Tsuboki et al., 2015). The general reduction in the total number of TCs, which is concentrated in weaker storms (Category 0-1), contributes to this increase. The models are somewhat less consistent in projecting an increase in the frequency of Category 4-5 TCs (Wehner et al., 2018a). The projected increase in the intensity of the strongest TCs is consistent with theoretical understanding (e.g., Emanuel 1987) and observations (e.g., Kossin et al., 2020). A summary of projections of TC characteristics is shown in Fig. 5 of Knutson et al., 2019c, and in Roberts et al., 2019b). [Note to reviewers: HighResMIP results to be included in the FGD]. For a 2ºC global warming, the median proportion of Category 4–5 TCs increases by 13%, while the median global TC frequency decreases by 14%, which infers that the median of the global Category 4–5 TC frequency is slightly reduced by 1% or almost unchanged (Knutson et al., 2019b).

The increase in global TC maximum surface wind speeds is about 5% for a 2ºC global warming across a number of high resolution multi-decadal studies (Knutson et al., 2019b). TCs are also measured by quantities such as Accumulated Cyclone Energy (ACE) and power dissipation index (PDI), which conflate TC intensity, frequency, and duration (Murakami et al., 2014). Several TC modeling studies (Yamada et al., 2010; Kim et al., 2014; Knutson et al., 2015) project little change or decreases in global accumulated value of PDI or ACE, which is due to the decrease in the total number of TCs. These projections can vary substantially between ocean basins, possibly due to differences in regional SST warming and warming patterns (Sugi et al., 2017; Yoshida et al., 2017).

Existing studies generally agree on a projected increase in global average TC rainfall rates with a consensus increase of about 12% for a 2ºC global warming consistent with Clausius-Clapeyron scaling (Knutson et al., 2019b). Increases substantially greater than Clausius-Clapeyron scaling are projected in some regions, which has been shown to be caused by increased low-level moisture convergence due to projected intensity increases in those regions (Knutson et al., 2015;Liu et al., 2019;Phibbs and Toumi, 2016).Projections of TC precipitation using large-ensemble experiments (Kitoh and Endo, 2019) show that the annual maximum 1-day precipitation total is projected to increase, except for the western North Pacific where there is only a small change or even a reduction is projected, mainly due to a projected decrease of TC frequency in the western North Pacific. They also show that the 10-year return value of extreme Rx1day associated with TCs will greatly increase in a region extending from Hawaii to the south of Japan.

Projected changes in TC tracks or TC areas of occurrence vary considerably among available studies, although there is better agreement in the western North Pacific. Several studies project either poleward or eastward expansion of TC occurrence over the western North Pacific region, and more TC occurrence in the central North Pacific (Yamada et al., 2017; Yoshida et al., 2017; Wehner et al., 2018a). A poleward expansion of the latitude of maximum TC intensity in the western North Pacific is consistent with observations (Kossin et al., 2014, 2016a). In the North Atlantic, while the location of TC maximum intensity does not show clear poleward migration observationally (Kossin et al., 2014; Kossin 2018b), it tends to migrate poleward in projections (Garner et al., 2017). The poleward migration is less robust among models and observations in other regions (e.g., Tauvale and Tsuboki, 2019). There is presently no clear consensus in projected changes in TC translation speed (Knutson et al., 2019b), although recent studies suggest a slowdown outside of the tropics (Yamaguchi et al., 2019;Zhang et al., In review) .

The spatial extent, or "size", of the TC wind-field is an important determinant of storm surge and damage. No detectable anthropogenic influences on TC size have been identified to date. However, projections by high resolution models indicate future broadening of TC wind-fields when compared in TCs of similar intensity (Yamada et al., 2017) although the details may be basin dependent (Knutson et al., 2015). A plausible mechanism is that as the tropopause height becomes higher with global warming, the eye wall areas become wider because the eye walls are inclined outward with height to the tropopause. This effect is only reproduced in high resolution convection-permitting models capturing eye walls, and such modeling studies are not common. Moreover, the projected TC size changes are generally of the order of 10% or less, and these size changes are still highly variable between basins and studies. Thus, the projected change in TC size is uncertain.

The coastal effects of TCs depend on TC intensity, size, track, and translation speed. Projected increases in sea level, average TC intensity, and TC rainfall rates each generally act to further elevate future storm surge and fresh-water flooding risk. Changes in TC frequency could contribute toward increasing or decreasing future storm surge risk, depending on the net effects of changes in weaker vs stronger storms. Several studies (McInnes et al., 2014, 2016; Little et al., 2015; Garner et al., 2017; Timmermans et al., 2017, 2018) have explored future storm surge risk in the context of anthropogenic climate change with the influence of both sea level rise and the changes in future TC changes. Garner et al. (2017) investigated the near future changes in risks of New York City coastal flooding, and suggested a small change in storm-surge height because effects of TC intensification are compensated by the offshore shifts in TC tracks, but concluded that the overall effect due to the rising sea levels would likely increase of the flood risk. For the Pacific islands, McInnes et al. (2014) find that the future projected increase in storm surge risk in Fiji is dominated by sea level rise, and projected TC changes cause only a minor contribution. Among various storm surge risk factors, there is *high confidence* that sea level rise will lead to higher risk of extreme coastal water levels in most regions, of all other factors assumed equal.

In the North Atlantic, vertical wind shear – which inhibits TC genesis and intensification – varies in a quasi-dipole pattern with one center of action in the tropics and another along the U.S. southeast coast (Vimont and Kossin, 2007). This pattern of variability creates a protective barrier of high shear along the U.S. coast during periods of heightened TC activity in the tropics (Kossin, 2017), and appears to be a natural part of the Atlantic ocean-atmosphere climate system (Ting et al. 2019). Greenhouse gas forcing in CMIP-5 and Community Earth System Model Large Ensemble (CESM-LE; Kay et al., 2015) simulations, however, erodes the pattern and degradesthe natural shear barrier along the U.S. coast. Following the Representative Concentration Pathway 8.5 (RCP8.5) emission scenario, the magnitude of the erosion of the barrier equals the amplitude of past natural variability (time of emergence) by the mid-twenty-first century (Ting et al., 2019). The projected reduction of shear along the U.S. east coast with warming is consistent among studies (e.g., Vecchi and Soden, 2007b).

In summary, there is *high confidence* that average peak tropical cyclone wind speeds and the proportion of Category 4-5 tropical cyclones will increase globally with warming. There is *medium confidence* that the frequency of Category 4-5 TCs will increase. There is *high confidence* that average tropical cyclone rain-rates will increase with warming, and there is *medium confidence* that the peak rain-rates will increase at greater than the Clausius-Clapeyron scaling rate of 7% per °C of warming in some regions due to increased low-level moisture convergence caused by regional increases in wind-intensity. There is *medium confidence* that the average location where tropical cyclones reach their peak wind-intensity will migrate poleward in the western North Pacific Ocean as the tropics expand with warming. There is *medium confidence* that the global frequency of TCs over all categories will decrease or remain unchanged. There is *low confidence* that the spatial extent of the TC wind-field will increase within fixed intensity categories.

11.7.2 Midlatitude storms

This section assesses synoptic scale storms that affect midlatitude regions including extratropical cyclones (ETCs) and atmospheric rivers (ARs). The focus is on midlatitude storms that are either classified as extreme, based on some measure of their intensity, or are associated with the occurrence of extremes in weather variables such as precipitation or near-surface wind speeds (Seneviratne et al., 2012b). Since the the AR5, the high relevance of ETCs and ARs for extreme precipitation events has been well established (Pfahl and Wernli, 2012; Catto and Pfahl, 2013; Utsumi et al., 2017) with 80% or more of hourly and daily precipitation extremes being associated with either ETCs or fronts over oceanic midlatitude regions, and somewhat smaller but still very large proportions of events over midlatitude land regions (Utsumi et al., 2017). The emphasis in this section is on individual midlatitude storms that have been identified using some detection and tracking algorithm. The midlatitude storm tracks, referring to those regions where the main tracks of extratropical disturbances occur as sequences of low (cyclonic) and high (anticyclonic) pressure systems, are not directly assessed in this section. Detection and attribution of changes in storm tracks are assessed in Chapter 3 (Section 3.3.3.3), observed trends in Chapter 2 (Section 2.3.1.4.3) and projected changes in Chapter 4 (Section 4.5.1.6). More on storm tracks and ETCs can be found in Section 8.3.2.8.

11.7.2.1 Definitions, mechanisms and drivers

ETCs are usually defined as synoptic-scale (~1000 km) low pressure systems with cyclonic rotation that develop over middle and high latitudes (Seneviratne et al., 2012b; Hartmann et al., 2013). ETCs exhibit a variety of sizes, shapes, durations, vertical structures and translation speeds which translates into substantial ambiguity when designing algorithms to detect and track ETCs (Neu et al., 2013). Detection and tracking methods can differ in a number of aspects including, but not limited to, the choice of the variable used for detection (e.g., mean sea level pressure, lower-tropospheric vorticity, etc), thresholds used to decide when a cyclone is present (detection) and hypotheses about how to group cyclones as part of the same event (tracking). In addition, contrary to tropical cyclones for which the Saffir-Simpson scale is commonly used to classify their intensity, there is no consensus on a single scale to define the intensity of ETCs. Weak, moderate and strong ETCs are instead defined using some dynamical aspect of the storm based on the specific variable (mean sea level pressure, winds, vorticity, etc) employed by detection and tracking method (Neu et al., 2013). Uncertainties across methods have been shown to decrease as stronger ETCs are considered, as most methods are able to capture the strongest and longer duration ETCs (Neu et al., 2013; Pepler et al., 2015).

The frequency and intensity of ETCs vary spatially and on monthly, interannual and interdecadal time scales due to several large-scale drivers, including the strength of horizontal temperature gradients at different altitudes, static stability, and amount of water vapour. Changes in these environmental factors, whether associated with natural variations or with changes in external forcings, are expected to influence the local intensity and frequency of ETCs and associated precipitation. Modes of variability such as El Niño-Southern Oscillation (ENSO), the Pacific Decadal Oscillation (PDO), and the North Atlantic oscillation (NAO) induce substantial interannual and interdecadal variability, complicating the identification of trends over 20 or 30 year periods (Reboita et al., 2015; Varino et al., 2018).

11.7.2.2 Observed trends

The SREX stated that “it is *likely* that there has been a poleward shift in the main Northern and Southern Hemisphere extratropical storm tracks during the last 50 years” (Seneviratne et al., 2012b) although there was *low confidence* “due to inconsistencies between studies or lack of long-term data in some parts of the world (particularly in the Southern Hemisphere (SH))”. Since the AR5 and SREX, new reanalysis products have been made available including the European Centre for Medium-Range Weather Forecasts 20th century reanalysis (ERA20C, Poli et al., 2013) but the study of trends in midlatitude storms remains difficult due to the large interannual and decadal variability (Reboita et al., 2015; Varino et al., 2018)and due to temporal and spatial heterogeneities in the number and type of assimilated reanalysis data, particularly before the satellite era (Krueger et al., 2013; Tilinina et al., 2013; Befort et al., 2016; Chang and Yau, 2016; Wang et al., 2016b).

There is *low confidence* that the total number of deep ETCs (systems with central pressure <980 hPa) has increased over the Southern Hemisphere during the satellite era (since 1979) with 8 reanalyses showing positive trends and 5 of them showing statistically significant trends (Reboita et al., 2015; Wang et al., 2016b). However, characterising ETC’s intensity using the absolute central pressure can be problematic to identify historical trends or changes because of its dependence on the background mean sea level pressure which varies in time (seasonal and decadal) and space (Chang, 2014). For example, positive trends in the number of very deep cyclones (central pressure <960 hPa) were identified in both the ERA-20C and the NOAA-20CR reanalyses since 1960 in the Southern Hemisphere but only the ERA-20C reanalysis showed an increase in the number of systems with strong near-surface wind speeds (windstorms; defined using the local 98th percentile) over the same period (Befort et al., 2016). There is *low confidence* in decadal trends of the number of very deep cyclones (<960 hPa) over the North Atlantic and North Pacific. In 5 reanalysis products including the some of the latest high-resolution reanalyses (ERA-Interim, MERRA, NCEP-CFSR), Tilinina et al. (2013) showed that the number of very deep cyclones (<960 hPa) increased from 1979 to 1990 and then declined until 2010 in the North Atlantic while the number reached a peak in about 2000 and then decreased until 2010 over the North Pacific.

In summary, there is *low confidence* in past changes in the frequency and intensity of extratropical cyclones due to heterogeneities in the data and inconsistent results between studies.

11.7.2.3 Model evaluation

The AR5 stated that CMIP5 climate models "are able to capture the general characteristics of storm tracks and extratropical cyclones, and there is some evidence of improvement since the AR4" (Flato et al., 2013). Since the AR5, a large number of studies have evaluated the ability of climate models to simulate several characteristics of midlatitude storms including the frequency and intensity of ETCs (Colle et al., 2013; Zappa et al., 2013a; Pithan et al., 2016), ARs (Placeholder: to be completed for the FGD) and fronts (Catto et al., 2013, 2015). In addition, an increasing number of studies have evaluated fields associated with midlatitude storms including precipitation, clouds and near-surface winds (Catto, 2016; Hawcroft et al., 2016, 2017, 2018; Trzeciak et al., 2016).

The evaluation of the frequency and intensity of ETCs commonly employs reanalyses data because the identification and tracking of ETCs require evenly distributed data in time and space. The comparison between ETC characteristics obtained from different datasets (simulations or reanalyses) is complicated because they depend not only on the "quality" of the model but also on their horizontal resolution, with higher horizontal resolution data usually leading to more and stronger ETCs (Blender and Schubert, 2000; Shkolnik and Efimov, 2013; Di Luca et al., 2015b). To assess common spatial scales in both reanalysis and simulated datasets, data are either preprocessed (e.g., Di Luca et al., 2015b; Neu et al., 2013; Zappa et al., 2013b) or tracking algorithms are tuned (e.g., Nissen et al., 2014). For example, Zappa et al. (2013a) and Seiler and Zwiers (2016) identified and tracked ETCs in 850-hPa vorticity fields derived from CMIP5 models and reanalysis data after removing fine-scale spatial variability from the vorticity field.

There is *high confidence* that CMIP-class models underestimate the dynamical intensity of ETCs as measured using a variety of metrics (mean pressure gradient, mean vorticity, near-surface winds, etc) over several regions (Colle et al., 2013; Zappa et al., 2013a; Di Luca et al., 2016b; Trzeciak et al., 2016; Seiler et al., 2018). Over the Northern Hemisphere, Seiler and Zwiers (2016) evaluated the performance of CMIP5 models to simulate ETCs undergoing explosive development (i.e., showing a decrease in mean sea level pressure of at least 24 hPa in 24 hours) against three reanalyses products. They found that models well-simulate the spatial distribution of explosive systems over the North Atlantic and North Pacific but showed that three quarters of the models underestimate their frequency. The general underestimation of the intensity of ETCs has been linked with the horizontal resolution of CMIP-type models, with the models' performance improving as horizontal resolution increases (Colle et al., 2013; Zappa et al., 2013a; Di Luca et al., 2016b; Trzeciak et al., 2016; Seiler et al., 2018). The systematic bias in the intensity of ETCs has also been associated with the inability of coarse resolution models to well-resolve diabatic processes particularly those related to the release of latent heat (Willison et al., 2013; Trzeciak et al., 2016). While Trzeciak et al. (2016) argued that horizontal resolution of about 100 km might be sufficient to remove most of biases, Willison et al. (2013) showed that the positive diabatic feedback is significantly enhanced when simulated with 20-km relative to 120-km grid spacing.

Since the AR5, several studies have evaluated ETC's associated precipitation by compositing the precipitation field around the detected ETCs. Hawcroft et al. (2018) showed that CMIP5 models well-simulate the spatial distribution of precipitation related with an average ETC over the Northern Hemisphere together with some of the main features of ETC life cycle. These include the peak in precipitation occurring just before the maximum in dynamical intensity (e.g., vorticity) as observed in reanalysis and observations. There is, however, large observational uncertainty in ETC's associated precipitation (Hawcroft et al., 2018). Hawcroft et al. (2016) evaluated the ETC's associated precipitation using a high-resolution climate model (HiGEM; about 1° latitude by 1° longitude) against the ERA-Interim reanalysis and Global Precipitation Climatology Project (GPCP) observations, and found that HiGEM overestimates the proportion of the total precipitation falling from the most intensely precipitating ETCs. Catto et al (2015) evaluated the contribution of frontal precipitation to the total precipitation in winter and found that CMIP5 models systematically produce too many fronts with too low precipitation intensity over midlatitude oceanic areas in both hemispheres.

In summary, there is evidence that CMIP-class models are able to well-simulate some aspects of ETCs and the associated fronts, but their coarse horizontal resolution together with their limited ability to resolve diabatic processes such as latent heat release leads to a systematic underestimation of the intensity of the strongest ETCs (*high confidence*). This limits our confidence in CMIP models to predict future changes in the intensity of ETCs because the contribution from diabatic processes is expected to increase in the future due to the increase in water vapour. In addition, there is substantial evidence that the response of extreme precipitation water vapour increases differs between climate models with parameterized and with explicit convection (Section 11.4).

11.7.2.4 Projections

The frequency of ETCs is expected to change following changes in the storms tracks as discussed in sections 4.5.1.6 and 8.3.2.8. In agreement with earlier reports (Christensen et al., 2013), recent studies project that changes in the dynamical intensity of ETCs (e.g., wind speeds) will be small showing increases or decreases that follow changes in the storm tracks. Yettella and Kay (2017) detected and tracked ETCs in an ensemble of 30 CESM-LE simulations, differing only in their initial conditions, and found that the averaged wind speeds around ETC centres (i.e., dynamical intensity) changes little between present (1986-2005) and future (2081-2100) periods. Using historical reanalysis data, Li et al. (2014) evaluated changes in a cold and warm period of the Atlantic Multidecadal Variability and found no robust change in the intensity of cyclones as measured by quantities such as vorticity or wind speed over the North Atlantic. Using CMIP5 models, Zappa et al. (2013b) found an overall reduction in the number of cyclones associated with 850-hPa wind speed larger than 25 m/s over the North Atlantic and Europe with the number of the 10% strongest cyclones decreasing by about 8 and 6% in DJF and JJA. Over the North Pacific, Chang (2014) showed that CMIP5 models project a decrease of the frequency of the strongest ECTs by the end of the century according to simulations using the RCP8.5 scenario. Strong ETCs were defined using the central pressure perturbation (i.e., depth, largely related with low-level wind speeds). Using projections from CMIP5 GCMs under the RCP85 scenario (1981-2000 to 2081-2100), Seiler and Zwiers (2016b) projected a northward shift of the number of explosive ETCs in the northern Pacific, with fewer and weaker events south, and more frequent and stronger events north of 45°N. In the Atlantic, the total number of explosive cyclones is projected to decrease by about 17% with the largest changes over the North America's east coast. The decrease of the frequency of explosive North America's east coast ETCs was also found using a higher-resolution RCM driven by a single GCM (Seiler et al., 2018)while maximum wind speeds showed slight increases or no changes depending on the model considered.

Over the Southern Hemisphere, future changes (RCP8.5 scenario; 1980-1999 to 2081-2100) in extreme ETCs were studied by Chang (2017) using 26 CMIP5 models and a variety of intensity metrics (850-hPa vorticity, 850-hPa wind speed, mean sea level pressure and near-surface wind speed). They showed an overall decrease of about 6% in the total number of ETCs over the 30-60°S latitude-band between historical and future periods. However, they found that the number of extreme cyclones is projected to increase by at least 20% but as much as 50% depending on the specific metric used defined extreme ETCs. Increases in the number of strong cyclones appear to be robust across models and for most seasons although they show strong regional variations with increases occurring mostly over the southern flank of the storms track, consistent with a shift and intensification of the storm track.Using a high-resolution regional climate model ensemble, Pepler et al. (2016)small changes or decreases of the number of ETCs with strong winds over the eastern coast of Australia.

As reported in the AR5, despite small or negligible changes in the dynamical intensity of ETCs, there is *high confidence* that the precipitation associated with ETCs will increase in the future (Zappa et al., 2013b; Marciano et al., 2015; Pepler et al., 2016; Michaelis et al., 2017; Yettella and Kay, 2017; Zhang and Colle, 2017; Hawcroft et al., 2018; Kodama et al., 2019). Based on a large ensemble of GCM simulations, Yettella and Kay (2017) found that the mean precipitation associated with ETCs will increase in the future following the increase in water vapour (i.e., due to thermodynamic effects; See Box 11.1) with the exception of the Mediterranean and some areas in North America in winter. Using 16 CMIP5 models, Hawcroft et al. (2018) showed substantial increases in the number of heavy precipitating extratropical cyclones over most regions of the Northern Hemisphere with a tripling in the frequency of events above the present day 99th percentile of 6-hourly accumulated precipitation. Studies performed using higher resolution models also showed systematic increases in precipitation rates around ETC centres (Marciano et al., 2015; Pepler et al., 2016; Michaelis et al., 2017; Kodama et al., 2019). Using a single global high-resolution climate model with an explicit representation of convection, Kodama et al. (2019) showed that, in both hemispheres, the precipitation associated with strong (10% deepest MSLP anomalies) oceanic ETCs increases in simulations following the increase in water vapour (i.e., about 7% per degree of surface warming) while the average ETC only increases by about 3% per degree of near-surface warming. The strong relation found between changes in precipitation associated with ETCs and the increase in water vapour suggests that changes in precipitation are dominated by changes in thermodynamic processes with little influence from changes in the dynamical structure (Kodama et al., 2019).

The intensification of precipitation is likely to show regional and seasonal differences due to distinct changes in atmospheric humidity and dynamical conditions (Zappa et al., 2015; Hawcroft et al., 2018) with even some decreases in specific regions such as the Mediterranean (Zappa et al., 2015). There is some evidence that changes in the dynamical intensity of ETCs might be dependent on the horizontal resolution of climate models with some studies showing different projections for weak, moderate and strong ETCs (Booth et al., 2013; Michaelis et al., 2017). In the North Atlantic region, Michaelis et al. (2017) used a 20-km resolution model to show that the increased precipitation around moderate and strong ETCs results in enhanced latent heat release leading to a strengthening of low-tropospheric wind speeds, and for strong ECTs, also increases in near-surface wind speeds. A modelling study by Booth et al. (2013) showed that the higher availability of moisture in the future led to a more rapid development of ETCs and a higher frequency of extreme winds.

Recent advances in the science of atmospheric rivers are discussed in detail in Section 8.3.2.8. These midlatitude storms can produce extreme winds and precipitation with significant impacts but also are primary sources of water in some regions. Very large ARs or sequential occurrences of multiple but less severe ARs in the same region may trigger landslides and/or floods and are an example of a compound extreme event (Section 11.8). While a qualitative AR definition has been accepted (AMS2018), quantitative definitions vary considerably and are currently being compared in the Atmospheric River Intercomparison Project (Rutz et al., 2020). An AR category scale based on vertically integrated water vapor transport and storm duration describes their intensity and impacts with 5 levels ranging from beneficial to hazardous (Ralph et al., 2019). However, application of this scale at the time of the AR6 is still limited.

In summary, there is *high confidence* that average and maximum ETC rain-rates will increase with warming, mostly due to increases in atmospheric water vapour. There is *medium confidence* that wind speeds associated with ETCs will change following changes in the storm tracks, with increases/decreases depending on the region being considered. There is *medium confidence* that changes in the intensity of ETCs, including wind speeds and precipitation, depend on the horizontal resolution of climate models and whether they include an explicit representation of convective processes.

11.7.3 Severe convective storms

Severe convective storms are convective systems that are associated with extreme phenomena such as tornadoes, hail, heavy precipitation (rain or snow), strong winds, and lightning. The assessment of changes in severe convective storms in the SREX and AR5 is limited and focused mainly on tornadoes and hail storms. In Chapter 3 of SREX (Seneviratne et al., 2012b), it is assessed as low confidence in observed trends in tornadoes and hail because of data inhomogeneities and inadequacies in monitoring systems. Subsequent works assessed in the Climate Science Special Report (Kossin et al., 2017) led to the assessment on the observed tornado activity over the 2000s in the United States with a decrease in the number of days per year with tornadoes and an increase in the number of tornadoes on these days (*medium confidence*). However, there is *low confidence* in past trends for hail and severe thunderstorm winds. Climate models consistently project environmental changes that would support an increase in the frequency and intensity of severe thunderstorms that combines tornadoes, hail, and winds (*high confidence*), but there is *low confidence* in the details of the projected increase. Regional aspects of severe convective storms are also assessed in Chapter 12 (Section 12.3.3.2 for climatic impact drivers, Section 12.4.5.3 for Europe, Section 12.4.6.3 for North America, and Section 12.7.2 for regional gaps and uncertainties).

11.7.3.1 Mechanisms and drivers

Severe convective storms are sometimes embedded in synoptic-scale weather systems such as tropical and extratropical cyclones and fronts (Kunkel et al., 2013). They are also generated as individual events as meso-scale convective systems (MCSs) and mesoscale convective complex (MCC) (a special type of a large-organized and long-lived MCS) without clearly embedded within larger-scale weather systems. In addition to general vigorousness of precipitation, hails, and winds associated with MCSs, characteristics of MCSs are viewed in new perspectives in recent years, probably because of both development of dense meso-scale observing networks and advances in high-resolution meso-scale modelling (Sections 11.7.3.2 and 11.7.3.3). The horizontal scale of MCSs is discussed with their organization of the convective structure and it is examined with a concept of "convective aggregation" in recent years (Holloway et al., 2017). MCSs sometimes take a linear shape and stay almost stationary with successive production of cumulonimbus on the upstream side (back-building type convection), and cause heavy rainfall (Schumacher and Johnson, 2005). Many of recent severe rainfall events in Japan are associated with line-shaped precipitation systems (Kunii et al., 2016; Oizumi et al., 2018; Tsuguti et al., 2018), suggesting common characteristics of severe precipitation at least in the Eastern Asia. The convective modes of severe storms in the United States can be classified into rotating or linear modes and preferable environmental conditions such as vertical shear for these modes are identified (Trapp et al., 2005; Smith et al., 2013; Allen, 2018). Cloud microphysics characteristics of MCSs are examined and roles of warm rain processes on extreme precipitations are also stressed recently (Hamada et al., 2015; Sohn et al., 2013). Idealized studies also suggests importance of ice and mixed phase processes of cloud microphysics on extreme precipitation (Sandvik et al., 2018; Bao and Sherwood, 2019). However, it is unknown whether these types of MCSs are becoming more frequent in recent periods nor observed ubiquitously all over the world.

Severe convective storms occur under conditions preferable for deep convection, that is, conditionally unstable stratification, sufficient moisture both in lower and middle levels of the atmosphere, and a strong vertical shear. These large-scale environmental conditions are viewed as necessary conditions for the occurrence of severe convective systems, or the resulting tornadoes and lightning, and relative relevance of these factors strongly depends on regions (e.g., Allen, 2018; Tochimoto and Niino, 2018). Frequently used metrics are atmospheric static stability, moisture content, convection available potential energy (CAPE) and convective inhibition (CIN), wind shears or helicity including storm-relative environmental helicity (SREH) (Tochimoto and Niino, 2018; Elsner et al., 2019). These metrics, largely controlled by large-scale atmospheric circulations or synoptic weather systems such as TCs and ETCs, are then generally used to examine severe convective systems. The uncertainty however arises from the balance between factors affecting severe storm occurrence; for example, the warming of mid-tropospheric temperatures *likely* leads to an increase in the freezing level, which leads to increased melting of smaller hailstones, while there may be some offset by stronger updrafts driven by increasing CAPE which would favour the growth of larger hailstones, leading to less melting when falling (Allen, 2018).

In early June of the Eastern Asia, associated with the Baiu/Changma/Mei-yu, severe precipitations are frequently caused with MCSs. Severe precipitations are also caused by remote effects of TCs known as predecessor rain events (PREs) (Galarneau et al., 2010). Atmospheric rivers and other coherent types of enhanced water vapor flux also have the potential to induce severe convective systems (Kamae et al., 2017a; Waliser and Guan, 2017; Ralph et al., 2018). Combined with the above drivers, topographical effects also enhances intensity and duration of severe convective systems and associated precipitation (Ducrocq et al., 2008; Piaget et al., 2015).

11.7.3.2 Observed trends

Observed trends of severe convective storms or MCSs are not so much documented, but climatology of MCSs are analysed in specific regions (North America, South America, Europe, Asia). As definition of severe convective storms varies depending on literatures, it is not straightforward to make a synthetic view of observed trends of severe convective storms in different regions. However, analysis using satellite observations provides global view of MCSs (Kossin et al., 2017). Global distribution of thunderstorms are captured (Zipser et al., 2006; Liu and Zipser, 2015) by using the satellite precipitation measurements by the Tropical Rainfall Measuring Mission (TRMM) and Global Precipitation Mission (GPM) (Hou et al., 2014). The climatological characteristics of MCSs are provided by using satellite analysis in South America (Durkee and Mote, 2010; Rasmussen and Houze, 2011; Rehbein et al., 2018) and those of MCC in marine time continent by Trismidianto and Satyawardhana (2018). Analysis of the environmental condition favourable for severe convective events indirectly indicates climatology and trends of severe convective events (Allen et al., 2018), though favourable conditions depends on locations, such as the difference for tornadoes associated with extratropical cyclones between the United States and Japan (Tochimoto and Niino, 2018).

The observed trends of severe convective storms in the United States indicate that there is no significant increase of convective storms, and hails and severe thunderstorms (Kossin et al., 2017; Kunkel et al., 2013). It is *likely* that tornado activity has increased in the United States particularly over the 2000s, with a decrease in the number of days per year where tornadoes are observed but an increase in the number of tornadoes on days when they occur (Elsner et al., 2015, 2019; Kossin et al., 2017; Allen, 2018). Trends of MCSs are relatively more visible for particular aspects of MCSs such as activities in seasons and dependency on duration. MCSs have increased in occurrence and precipitation amounts since 1979 (Easterling et al., 2017).Feng et al. (2016) analysed that the observed increases in springtime total and extreme rainfall in the central United States are dominated by MCSs, with increased frequency and intensity of long-lasting MCSs.

Studies on trends of severe convective storms and their ingredients out of the United States are limited. Westra et al. (2014) found that there is an increase in the intensity of short-duration convective events (minutes to hours) over the whole world. In Europe, climatology of tornadoes shows increase of detected tornadoes between 1800 to 2014, but this trend might be affected by density of observations (Antonescu et al., 2016b, 2016a). Increase in trend of extreme daily rainfall in south eastern France, where MCSs play a key role in this type of event(Blanchet et al., 2018; Ribes et al., 2019). Thunderstorm climatology in the Mediterranean analysed for the period from 2005 to 2014 did not show a clear trend (Galanaki et al. 2018). In Sahelian region, Taylor et al. (2017) analysed MCSs using satellite observations since 1982 and showed increase in frequency of extreme storms. In Bangladesh, the annual number of propagating MCSs decreases significantly during 1998-2015 based on TRMM precipitation data (Habib et al., 2019). Prein and Holland (2018) estimated hail hazard from large-scale environmental conditions using a statistical approach and showed increase trends in the United States, Europe, and Australia. However, trends of hail on regional scales are difficult to validate because of insufficient length of observations and inhomogeneous record (Allen, 2018). The high spatial variability of hail suggests it is reasonable that there would be local signals of both positive and negative trends and the trends that are occurring in hail globally is uncertain.

In summary, it is *likely* that tornado activity has increased in the United States over the 2000s with a decrease in the number of days per year where tornadoes are observed. Detected tornadoes are also increased in Europe, but its trend depends on density of observation. It is *very likely* that extreme precipitation associated with severe convective storms has increased.

11.7.3.3 Model evaluation

The explicit representation of severe convective storms requires non-hydrostatic models with horizontal grid spacings below 5 km denoted as convection-permitting models or storm resolving models (Section 10.3.3). Convection-permitting models are becoming available to run over a wide domain such as a continental scale or even over the global area and show realistic climatological characteristics of MCSs (Prein et al., 2015; Satoh et al., 2019). Such high-resolution simulations are computationally too expensive to perform at the larger domain and for long periods and alternative methods by using a regional climate model with dynamical downscaling are generally used (Section 10.3.1). Convection-permitting models are used as the flagship project of CORDEX to particularly study projections of thunderstorms (Section 10.3.3). North American MCSs simulations by a convection-permitting model conducted by Prein et al. (2017a) shows that the simulation is able to capture the main characteristics of the observed MCSs such as their size, precipitation rate, propagation speed, and lifetime.Cloud-permitting model simulations in Europe also show sub-daily precipitation realistically (Ban et al., 2014; Kendon et al., 2014). Evaluation of precipitation conducted using convection-permitting simulations around Japan shows that finer resolution improves intense precipitation (Murata et al., 2017).MCSs over the African region simulated using convection-permitting models shows better extreme rainfall (Kendon et al., 2019) and diurnal cycle and convective rainfall over land than the coarser resolution RCMs or GCMs (Stratton et al., 2018; Crook et al., 2019).

11.7.3.4 Detection and attribution, event attribution

It is extremely difficult to detect differences in time and space of severe convective storms (Kunkel et al., 2013). Although some ingredients that are favourable for severe thunderstorms have increased over the years, others have not; thus, overall, changes in the frequency of environments favourable for severe thunderstorms have not been statistically significant. Event attribution studies on severe convection events are now undertaken for some of cases, such as the case of the July 2018 heavy rainfall event in Japan (BOX 11.3) and the December 2015 extreme rainfall event in Chennai, India (van Oldenborgh et al., 2016; Boyaj et al., 2018).

11.7.3.5 Projections

Future projections of severe convective storms are usually studied using a time slice approach by comparing simulations performed using historical conditions with those using future hypothesized conditions (Kendon et al., 2017). Up to now, individual studies using convection-permitting models gives projection of extreme events associated with severe convective storms. Prein et al. (2017b) investigated future projection of North American MCSs simulations and show increase in MCS frequency and increase in total MCS precipitation volume by the combined effect of increases in maximum precipitation rates associated with MCSs and increases in their size. Rasmussen et al. (2017) investigated future changes in the diurnal cycle of precipitation by capturing organized and propagating convection and showed that weak to moderate convection will decrease and strong convection will increase in frequency in the future. Ban et al. (2015) found the day-long and hour-long precipitation events in summer intensify in the European region covering the Alps. Kendon et al. (2019) showed future increases in extreme 3-hourly precipitation in the Africa. Murata et al. (2015) investigated future projection of precipitation around Japan and showed a decrease of monthly mean precipitation in the eastern Japan Sea side region in December, suggesting convective clouds become shallower in the future in the winter of the Japan Sea.

The other approach is projection of environmental conditions which control characteristics of severe convective storms. Severe convective storms are generally formed in environments with large CAPE and tornadic storms are in particular formed with a combination of large CAPE and strong vertical wind shear. There are large differences within the CMIP5 ensemble for these environmental conditions, which contributes to some degree of uncertainty (Allen, 2018). Despite this limitation, projected change of the environmental conditions in the United States shows an increase in CAPE and no changes or decreases in the vertical wind shear, suggesting favourable conditions for an increase in tornadoes and hails in the future (Brooks, 2013). It is *medium confidence* that the frequency of severe convective storms increases in the spring, accompanied by a less significant increase in the summer months (Diffenbaugh et al., 2013; Gensini and Mote, 2015; Hoogewind et al., 2017). Future changes in severe convection environments *likely* shows enhancement of instability with less robust change in frequency of strong vertical wind shear in Europe (Púčik et al. 2017)and in Japan (Muramatsu et al. 2016). In Japan, the frequency of conditions favourable for strong tornadoes *likely* increase in spring and partly in summer.

Summary

Severe convective storms are convective systems that associate with severe weather events such as tornadoes, hail, heavy precipitation (rain or snow), strong winds, and lightning. Because definition of severe convective storms varies depending on literatures and regions, it is not straightforward to make a synthetic view over the world. However, characteristics of severe convective storms and their changes are being analysed by satellite observation and dense and wide ground observation networks. They are also analysed by new viewpoints such as convective aggregation, convective modes including line-shaped convective systems, or cloud microphysics like warm rain processes. Observation shows that there is *medium confidence* that tornado activity has increased in the United States over the 2000s with a decrease in the number of days per year when tornadoes are observed. Detected tornadoes are also increased in Europe, but its trend depends on density of observation. It is *very likely* that extreme precipitation associated with severe convective storms has increased. For projections, there is *medium confidence* that the frequency of severe convective storms increases in the spring with enhancement of CAPE, leading extension of seasons of occurrence of severe convective storms. There is *high confidence* of future intensification of precipitation associated with severe convective storms.

11.7.4 Extreme Winds

In previous IPCC reports, near-surface wind (including extremes), has not been assessed as a variable in its own right but rather in the context of other extreme atmospheric or oceanic phenomena. The exception was the SREX report (Seneviratne et al., 2012b), which specifically examined past changes and projections of mean and extreme near-surface wind speeds . For observed wind trends, several studies reported declining trends in mean 10-m anemometer wind speeds over the continental northern mid-latitudes and Australia and increasing trends in Alaska, the Canadian Arctic and Antarctica. A stronger decline in extreme winds compared to mean winds was also reported for the continental northern mid-latitudes. Due to the small number of studies and uncertainties in terrestrial-based surface wind measurements, the findings were assigned *low confidence* in the SREX. Projections of mean and 99th percentile wind speed in the CMIP3 multi-model ensemble indicated an increase in mean winds over Europe, parts of Central and North America, the tropical South Pacific, and the Southern Ocean. Mean wind speed declines were found along the equator and the subtropical ridge in both hemispheres and positive trends in winds further poleward but with low confidence. the AR5 similarly reported a weakening of mean and maximum winds from the 1960's or 1970's to the early 2000's in the tropics and midlatitudes and increases in high latitudes but with low confidence in changes in observed surface winds over land noting that upper air winds were less studied (Hartmann et al., 2013). In terms of future climate, the mid-latitude jets were projected with medium confidence to move polewards in both hemispheres by 1 to 2 degrees under high emissions scenarios with stronger shifts in the SH (Collins et al., 2013a). IPCC SROCC concluded that extreme winds in some tropical cyclones had increased as a result of climate change based on event attribution methodologies and that there was emerging evidence for an increase in the annual global proportion of Category 4 or 5 tropical cyclones with *low confidence*.

A contributing factor to the *low confidence* in observed wind speed changes is the changes in observing systems over time and the different observing systems that are typically used for marine winds (e.g., satellite-derived winds over the oceans, (Hartmann et al., 2013; Zieger et al., 2014) compared to anemometer winds over land. Inhomogeneity in terrestrial wind measurements (e.g., anemometer heights (Troccoli et al., 2012) and type of measurement (e.g., the average of four daily measurements or 24-hour wind runs (Azorin-Molina et al., 2017) contribute to the *low confidence* in wind trends. An additional source of uncertainty is the sensitivity of anemometer data to changes in site characteristics such as surrounding vegetation or buildings, instrument elevation and instrument age (e.g., Troccoli et al. 2012)). Also, length of record determines the extent to which long term trends can be determined from natural climate variability (McVicar et al., 2012).

Although not specifically addressing extreme wind speed changes, a review of 148 studies examining terrestrial surface wind change found negative wind speed trends (stilling) in the tropics and mid-latitudes of both hemispheres across the globe of -0.014 m s-1 a-1, while positive trends were reported at high-latitudes poleward of 70 (McVicar et al., 2012). An earlier study attributed the stilling to both changes in atmospheric circulation and an increase in surface roughness due to an overall increase in vegetation cover [Vautard et al., 2010]. Since then, a number of additional studies have mostly confirmed these general negative mean-wind trends based on anemometer data for Spain (Azorin-Molina et al., 2017); Turkey, (Dadaser-Celik and Cengiz, 2014); Netherlands, (Wever, 2012); Saudi Arabia, (Rehman, 2013); Romania, [Marin et al., 2014] and China, (Chen et al., 2013a). [Lin et al., 2012] note that wind speed variability over China is greater at high elevation locations compared to those closer to mean sea level. (Hande et al., 2012) using radiosonde data found an increase in surface wind speed on Macquarie Island.

A number of new studies have examined surface wind speeds over the ocean based on satellite observations from altimeters or Special Sensor Microwave/Imagers (SSM/I) (Tokinaga and Xie, 2010). It has been noted that wind speed trends tend to be stronger in the altimeters although the spatial patterns of change by both instruments are qualitatively similar (Zieger et al., 2014). Liu et al. (2016) found positive trends in surface wind speeds over the Arctic in 20 years of satellite observations. Small positive trends in mean wind speed were found in 33 years of satellite data together with larger trends in 90th percentile values over global oceans (Ribal and Young, 2019). These results were consistent with an earlier study that found a positive trend in 1-in-100 year wind speeds (Young et al., 2012). A positive wind change was found for the Arabian Sea and Bay of Bengal (Shanas and Kumar, 2015) and (Zheng et al., 2017) found the positive wind speed trends over the ocean were larger during winter seasons than summer seasons.

Extreme cyclonic windstorms that share some characteristics with both tropical and extra-tropical cyclones occur regularly over the Mediterranean Sea and are often referred to as “Medicanes” (Emanuel, 2018; Ragone et al., 2018). Medicanes pose substantial threat to regional islands and coastal zones. A growing body of literature consistently finds that the frequency of medicanes decreases under warming while the strongest medicanes become stronger (González-Alemán et al., 2019; Tous et al., 2016; Romero and Emanuel, 2017; Romera et al., 2017; Cavicchia et al., 2014; Romero and Emanuel, 2013; Gaertner et al., 2007). This is also consistent with expected global changes in tropical cyclones under warming (11.7.1). Based on the consistency of these studies, it is *likely* that medicanes will decrease in frequency while the strongest medicanes become stronger under warming scenario projections (*medium confidence*).

11.8 Compound events

The IPCC SREX first defined compound events as “(1) two or more extreme events occurring simultaneously or successively, (2) combinations of extreme events with underlying conditions that amplify the impact of the events, or (3) combinations of events that are not themselves extremes but lead to an extreme event or impact when combined (Seneviratne et al., 2012b). Further definitions of compound events have emerged since SREX. Zscheischler et al. (2018) define compound events broadly as “the combination of multiple drivers and/or hazards that contributes to societal or environmental risk”. We use this definition in the present assessment, because of its clear focus on the risk framework established by the IPCC, and also highlighting that compound events may not necessarily result from dependent drivers. This definition of compound events includes concurrent climate extremes, but also includes events with extreme impacts associated with climate drivers that might not be extremes themselves. Drivers include processes, variables, and phenomena in the climate and weather domain that may span over multiple spatial and temporal scales. Hazards (such as floods, heatwaves, wildfire) are usually the immediate physical precursors to negative impacts, but can occasionally have positive outcomes (Flach et al., 2018).

The combination of two or more – not necessarily extreme – weather or climate events that occur i) at the same time, ii) in close succession, or iii) concurrently in different regions, can lead to extreme impacts that are much larger than the sum of the impacts due to the occurrence of individual extremes alone. This is because multiple stressors can exceed the coping capacity of a system more quickly. The contributing events can be of similar types (clustered multiple events) or of different types. Many major weather- and climate-related catastrophes are inherently of a compound nature (Zscheischler et al., 2018). This has been highlighted for a broad range of hazards such as droughts, heatwaves, wildfires, coastal extremes, and floods (Westra et al., 2016). Co-occurring extreme precipitation and extreme winds can result in infrastructural damage (Martius et al., 2016); the compounding of storm surge and precipitation extremes can cause coastal floods (Wahl et al., 2015); and the combination of drought and heat can lead to tree mortality (Allen et al., 2015). Extremes may occur at different locations but affect the same system, for instance, spatially-concurrent climate extremes affecting crop yields and food prices (Anderson et al., 2019; Singh et al., 2018).

Finally, impacts may occur because of large multivariate anomalies in the climate drivers, if systems are adapted to historical multivariate climate variability (Flach et al., 2017). For instance, ecosystems are typically adapted to the local covariability of temperature and precipitation such that a bivariate anomaly may have a large impact even though neither temperature nor precipitation may be extreme based on a univariate assessment (Mahony and Cannon, 2018). Given that almost all systems are affected by weather and climate phenomena at multiple space-time scales, it is natural to consider extremes in a compound event framework. Despite this recognition, the literature on past and future changes in compound events is limited. This section assesses examples of types of compound events in available literature.

11.8.1 Concurrent extremes at coastal and estuarine regions

Coastal and estuarine zones are prone to a number of meteorological extreme events and also to concurrent extremes. A major hazard in coastal regions around the world is floods, and flood risk may be influenced by the dependence between storm surge, extreme rainfall, and river flow. Floods with multiple drivers are often referred to as “compound floods” (Moftakhari et al., 2017; Wahl et al., 2015).

At US coasts, the likelihood of co-occurring storm surge and heavy precipitation is higher for the Atlantic/Gulf coast relative to the Pacific coast (Wahl et al., 2015). Furthermore, all 6 studied locations at the US coast with long overlapping time series show an increase in the dependence between heavy precipitation and storm surge over the last century, leading to more frequent co-occurring storm surge and heavy precipitation events at the present day (Wahl et al., 2015). Storm surge and extreme rainfall are also dependent in most locations at the Australian coasts (Zheng et al., 2013) and in Europe along the Dutch coasts (Ridder et al., 2018), along the Mediterranean Sea, the Atlantic coast and the North Sea (Bevacqua et al., 2019). Flood risk can be assessed via the dependence between storm surge and river flow. For instance, the occurrence of a North Sea storm surge in close succession with an extreme Rhine or Meuse river discharge is much more likely due to their dependence compared to if both events would be independent (Kew et al., 2013; Klerk et al., 2015). Significant dependence between high sea levels and high river discharge are found for more than half of the available station observations, which are mostly located around the coasts of North America, Europe, Australia, and Japan (Ward et al., 2018). Combining global river discharge with a global storm surge model, hotspots of compound flooding have been discovered that are not well covered by observations, including Madagascar, Northern Morocco, Vietnam, and Taiwan (Couasnon et al., 2019, in review). In the Dutch Noorderzijlvest area, there is more than a two-fold increase in frequency of exceeding the highest warning level compared to the case if storm surge and heavy precipitation were independent (van den Hurk et al., 2015). In other regions and seasons, the dependence can be insignificant (Wu et al., 2018b) and there can be significant seasonal and regional differences in the storm surge-heavy precipitation relationship. Flood risk may also be influenced by the dependence between storm surge and river flow. Assessments of flood likelihoods are often not based on actual flood measurements and instead flood risk is estimated from its main drivers including astronomical tides, storm surge, heavy precipitation, and high streamflow. Such single driver analyses might underestimate flood risk if multiple correlated drivers contribute to the risk (e.g., van den Hurk et al., 2015).

Many coastal areas are also prone to the occurrence of compound precipitation and wind extremes, which can cause damage, including to infrastructure and natural environments. A high percentage of co-occurring wind and precipitation extremes are found in coastal regions and in areas with frequent tropical cyclones. Finally, the combination of extreme wave height and duration is also shown to influence coastal erosion processes (Corbella and Stretch, 2012).

Aspects of concurrent extremes in coastal and estuarine environments have increased in frequency and/or magnitude over the last century in some regions. These include an increase in the dependence between heavy precipitation and storm surge over the last century, leading to more frequent co-occurring storm surge and heavy precipitation events in the present day along US coastlines (Wahl et al., 2015). In Europe, the risk of compound flooding increases most strongly along the Atlantic coast and the North Sea under strong warming. The increasing risk of compound flooding is mostly driven by an intensification of precipitation extremes and aggravated flooding risk due to sea level rise (Bevacqua et al., 2019). Sea level extremes and their physical impacts in the coastal zone arise from a complex set of atmospheric, oceanic, and terrestrial processes that interact on a range of spatial and temporal scales and will be modified by a changing climate, including sea level rise (McInnes et al., 2016). Interactions between sea level rise and storm surges (Little et al., 2015), and sea level and fluvial flooding (Moftakhari et al., 2017) are projected to lead to more frequent and more intense compound coastal flooding events as sea levels continue to rise.

Summary

There is *medium confidence* that the probability of compound flooding has increased in some locations, including along the US coastline, over the last century. There is *medium confidence* that the risk of compound flooding in coastal regions will increase due to both sea level rise and increases in heavy precipitation.

11.8.2 Concurrent droughts and heatwaves

Concurrent droughts and heatwaves have a number of negative impacts on human society and natural ecosystems. Studies since the SREX and AR5 show several occurrences of observed combinations of drought and heatwaves in various regions.

Over most land regions, temperature and precipitation are strongly negatively correlated during summer (Zscheischler and Seneviratne, 2017), mostly due to land-atmosphere feedbacks (Seneviratne et al., 2010) but also because synoptic-scale weather systems favourable for extreme heat are also unfavourable for rain (Berg et al., 2015). This leads to a strong correlation between droughts and heatwaves (Zscheischler and Seneviratne, 2017), which is amplified by drought conditions (including low antecedent rainfall and soil moisture) enhancing summer temperature extremes (Mueller and Seneviratne, 2012, Whan et al., 2015) as well as an amplification of heatwave conditions through upwind drought (Schumacher et al., 2019). Drought events characterized by low precipitation and extreme high temperatures have occurred, for example, in California (AghaKouchak et al., 2014), inland eastern Australia (King et al., 2014), and large parts of Europe (Orth et al., 2016b). Concurrent droughts and heat can lead to crop failure (Barnabas et al., 2007), a reduction of carbon uptake potential of ecosystems (Ciais et al., 2005; Zscheischler et al., 2014; von Buttlar et al., 2018; Sippel et al., 2018b), tree mortality (Allen et al., 2010, 2015), increased wildfire risk (Brando et al., 2014; Ruffault et al., 2018), and higher risk of failure of electric power plants (Bartos and Chester, 2015; Cook et al., 2015).

The likelihood of co-occurring meteorological droughts and heatwaves has increased in the observational period in many regions and will continue to do so under unabated warming (Hao et al., 2013; Herrera-Estrada and Sheffield, 2017; Zscheischler and Seneviratne, 2017). Overall, projections of increases in co-occurring drought and heatwaves are reported in northern Eurasia (Schubert et al., 2014), Europe (Manning et al., 2019; Sedlmeier et al., 2018), and multiple regions of the United States (Diffenbaugh et al., 2015; Herrera-Estrada and Sheffield 2017), northwest China (Li et al., 2019c; Kong et al., 2019, submitted) and India (Sharma and Mujumdar, 2017).The dominant signal is related to the increase in heatwave occurrence, which means that even if drought occurrence is unaffected, compound hot and dry events will be more frequent.

Drought and heatwaves are also associated with wildfires, related through high temperatures, low soil moisture, and low humidity. Concurrent hot and dry conditions amplify wildfire risks in southern Europe (Russo et al., 2017), northern Eurasia (Schubert et al., 2014), the US (Littell et al., 2016), and Australia (Hope et al., 2019). Wildfire occurrence in California has been linked to anthropogenic climate change via a significant increase in vapour pressure deficit, a primary driver of wildfires (Williams et al., 2019). A study of the western US examined the correlation between historical water-balance deficits and annual area burned, across a range of vegetation types from temperate rainforest to desert (McKenzie and Littell, 2017). The relationship between temperature and dryness, and wildfire, varied with ecosystem, and the fire-climate relationship was both nonstationary and vegetation-dependent.
In many fire-prone regions, such as the Mediterranean and China's Daxing'anling region, projections for increased severity of future drought and heatwaves may lead to an increased frequency of wildfires relative to observed (Ruffault et al., 2018;Tian et al., 2017). However, at the global scale, the total burned area has been decreasing over the last 18 years due to human activities mostly related to changes in land use (Andela et al., 2017).

Summary

There is *high confidence* that concurrent heatwaves and droughts have increased in frequency over the last century at a global scale due to human influence. There is *medium confidence* that wildfire risk has increased in some regions over the last century. There is *high confidence* that compound hot and dry conditions become more likely in nearly all land regions as global mean temperature increases.

11.8.3 Other types of compound events

Humans are very susceptible to extremely hot and humid conditions, which can induce hyperthermia in humans and other mammals, as dissipation of metabolic heat becomes impossible. The effect of extremely hot and dry conditions on humans is often measured with combined indicators such as the Wet Bulb Globe Temperature (WBGT) or variants thereof, which integrate temperature and relative humidity. WBGT has had a detectable anthropogenic increase over many land regions since the 1970s, driven by anthropogenic increases in temperature (Knutson and Ploshay, 2016; Li et al., 2017a). By 2080, the relative frequency of present-day extreme WBGT events could rise by a factor of 100–250 in the tropics and parts of the mid-latitudes, areas which are projected to contain approximately half the world's population (Coffel et al., 2018). This is approximately double the frequency change projected for temperature alone.

High temperatures and droughts are also often strongly correlated with high ozone concentrations (Tai and Val Martin, 2017; Tai et al., 2014; Wang et al., 2017c; Zhang et al., 2018b). Ozone can negatively affect ecosystem carbon uptake (Oliver et al., 2018c; Franz et al., 2018). As future heat waves become more intense, in regions where ozone precursors are going down, such as North America and Europe, future heat waves are projected to have lower surface ozone; however, in areas of Asia and Africa where ozone precursors are not projected to decrease, future more intense heat waves produce even more severe surface ozone events (Meehl et al., 2018).

Heavy rainfall on saturated soil during the summer months (SES) and concurrent heavy rainfall and snowmelt, also called rain-on-snow events (ROS), are often the main flood-generating process in high latitudes (Cohen et al., 2015) and mountainous areas (Merz and Blöschl 2003; McCabe et al., 2007). In southern Norway, the probability of occurrence of SES events during the summer is projected to increase by 38% until 2070-2099 under a high emission scenario (Poschlod et al., 2019, submitted). In contrast, the frequency of ROS is projected to decrease by 48% on average, which is largely driven by decreases in snowfall. In mid-latitude regions, the interaction between antecedent moisture conditions (e.g., soil moisture stores and/or reservoir levels) and flood-producing rainfall is often a key determinant of flood hazards (e.g., (Bennett et al., 2018)), with the interaction between these multiple drivers potentially explaining the observed decrease in flood hazards (Do et al., 2017) in many regions globally despite observed increases in precipitation extremes (Sharma et al., 2018).

Climate change can affect the clustering of some hazards and will lead to the emergence of new types of compound events. For instance, climate models suggest that the serial clustering of extratropical cyclones may decrease in the North Atlantic and parts of western Europe while increasing near Newfoundland (Pinto et al., 2013). Furthermore, successive heatwaves can compound the impacts of a tropical cyclone and pose a serious threat to humans. Climate change could increase the number of people that may experience at least one such event in a 30-year period from currently 0.4 million to 2 million at 2 °C global warming and 11.8 million at 4 °C (Matthews et al., 2019).

[START BOX 11.3 HERE]

BOX 11.3: Case study: Global-scale concurrent climate anomalies at the example of the 2015/2016 Super El Niño and the 2018 boreal spring/summer extremes

Occurrence of concurrent or near-concurrent extremes in different parts of a region, or in different places of the world challenges adaptation and risk management capacity (Box 11.4). This can occur as a result of natural climate variability, as climates in different parts of the world are inter-connected through teleconnections. In addition, in a warming climate, the probability of having several locations being affected simultaneously by e.g., temperature hot extremes and heatwaves increases strongly as a function of global warming, with detectable changes even for changes as small as 0.5°C of additional global warming (Sections 11.2.6 and 11.3; Box 11.3, Figure 1). Recent articles have highlighted the risks associated with concurrent extremes over large spatial scales (e.g., Boers et al., 2019; Lehner and Stocker, 2015;Gaupp et al., 2019). There is evidence that such global-scale extremes associated with hot temperature extremes are increasing in occurrence (Sippel et al., 2015; Vogel et al., 2019). Hereafter, we focus on two recent global-scale events that featured concurrent extremes in several regions across the world The first focuses on concurrent extremes driven by variability in tropical Pacific SSTs associated with the 2015/2016 Super El Niño, while the second is a case study of the impacts of global warming combined with abnormal atmospheric circulation patterns in the 2018 boreal spring/summer.

[START BOX 11.3, FIGURE 1 HERE]

Box 11.3, Figure 1: Analysis of the percentage of land area affected by temperature extremes larger than a) two or b) three standard deviations in June-July-August (JJA) between 30°N and 80°N using an approach using a standard normalization (orange) and a corrected normalization (grey). The more appropriate estimate is the corrected normalization. These panels show for both estimates a substantial increase in the overal land area affected by very high hot extremes since 1990 onward. From Sippel et al. 2015.

[END BOX 11.3, FIGURE 1 HERE]

2015/2016 El Niño or "Super El Niño"

El Niño-Southern Oscillation (ENSO) is one of the phenomena that have the ability to bring multitudes of extremes in different parts of the world, especially in the extreme cases of El Niño. Additionally, the background climate warming associated with greenhouse gas forcing can significantly exacerbate extremes in parts of the world even under normal El Niño conditions. According to some measures, the 2015/2016 El Niño was the strongest El Niño over the past 145 years (Barnard et al., 2017), with Sea Surface Temperatures (SST) warmer than 29°C at Niño 3.4 (Funk et al., 2016). Newman et al. (2018) found that the 2015/2016 warmth was unprecedented at the central equatorial Pacific (Niño4: 5°N–5°S, 150°E–150°W) and that this exceptional warmth was unlikely to have occurred entirely naturally, appearing to reflect an anthropogenically-forced trend. There is *medium confidence* that both the ENSO amplitude and the frequency of high-magnitude events since 1950 is higher than over the pre-industrial period (Chapter 2; Section 11.1.5), suggesting that global extremes similar to those associated with the 2015/2016 El Niño would occur more frequently under further increases in global warming. A brief summary of what happened that year is provided hereafter. We provide some highlights illustrating extremes that occurred in different parts of the world during the 2015/2016 El Niño event, hereafter referred to as "Super El Niño".

The state of the climate in 2015 reviewed by Blunden and Arndt (2016) and World Meteorological Organization (2016) summarized extreme aspects due to the super El Niño: in combination with modified hydrological conditions induced by global warming (enhanced moistening or drying of the air depending on the region; Chapter 8 and Box 11.1), the strong El Niño enhanced precipitation variability around the world and drought conditions prevailed across many areas for most of the year. Emissions from tropical Asian biomass burning in 2015 were also severely enhanced (Cross-Chapter Box 11.3, Figure 2).

Several regions were strongly affected by droughts in 2015, including Indonesia, the Amazon region, Ethiopia, Southern Africa, and Europe. As a result, global measurements of land water anomalies were particularly low in that year (Humphrey et al., 2018). In 2015, Indonesia experienced a severe drought and forest fire causing pronounced impact on economy, ecology and human health due to haze crisis (Hartmann et al., 2018). The extent of the drought season in Indonesia during 2015 has intensified the flammability of forest and peatlands leading to a severe fire season (Field et al., 2016). During 2015, forest and peatland fires have released 227 ± 67 Tg C (Huijnen et al., 2016; Patra et al., 2017), which was in between the 2013 CO_2 emission from fossil fuel in Japan and India (Field et al., 2016). The Amazon region experienced the most intense droughts of this century in 2015/2016. This drought was more severe than the previous major droughts that occurred in the Amazon in 2005 and 2010 (Erfanian et al., 2017; Panisset et al., 2018), which had been both assessed as 1-in-100 year types of events (Lewis et al., 2011). The 2015/2016 Amazon drought impacted the entirety of South America north of 20°S during the austral spring and summer (Erfanian et al., 2017). According to Panisset et al. (2018), 80% of the Amazon Basin area was stricken by precipitation deficits during this drought, which spanned from September 2015 to May 2016 (Ribeiro et al., 2018). Jiménez-Muñoz et al. (2016), using the self-calibrating Palmer Drought Severity Index (van der Schrier et al., 2013; note, however, some limitations with this index, Section 11.6), showed that the 2015/2016 El Niño event, combined with the regional warming trend, was associated with unprecedented warming and a larger extent of extreme drought in Amazonia compared to the earlier strong El Niño events in 1982/1983 and 1997/1998. The 2015/2016 anomalous dryness increased the forest fire incidence by 36% compared to the preceding 12 years (Aragão et al., 2018). The active fires occurred over an area of 799,293 km^2, impacting areas in central Amazonia barely affected by fires in the past (Aragão et al., 2018). As a consequence, forest fires increased the biomass burning outbreaks and the carbon monoxide (CO) concentration in the area, affecting air quality (Ribeiro et al., 2018). This out-of-season drought affected the water availability for human consumption and agricultural irrigation and it also left rivers with very low water levels, without conditions of ship transportation, due to large sandbanks, preventing the arrival of food, medicines, and fuels. Eastern African countries were impacted by drought in 2015. The drought in Ethiopia was the worst in several decades. It was found that the Ethiopian drought was associated with the super El Niño in 2015/2016 that developed early in the year (Blunden and Arndt, 2016; Philip et al., 2018a). Because the Ethiopian drought is well correlated with ENSO in the observations, it is suggested that the strong 2015/2016 El Niño did increase the severity of the drought in Ethiopia (Philip et al., 2018a). Extremely dry conditions were experienced across most of southern Africa during October 2015–March of 2016(Funk et al., 2016), associated with one of the super El Niño (Blamey et al., 2018). It was suggested that anthropogenic warming contributed to the 2015 Ethiopian and southern African droughts by increasing SSTs associated with the super El Niño and local air temperatures (Funk et al., 2016, 2018b). According to Yuan et al. (2018) flash drought over Southern Africa increased by 220% from 1961 to 2016, mainly due to anthropogenic climate change and it was intensified during the super El Niño in the midst of heat waves. The 2015/2016 super El Niño also induced drying in western, eastern and even southern Europe (King et al., 2020). It should be noted that 2015 was a year that displayed a particularly high CO_2 growth rate, possibly related to some of the mentioned droughts, in particular in Indonesia and the Amazon region, leading to higher CO_2 release in combination with less CO_2 uptake from land areas (Humphrey et al. 2018). The impact of the super El Niño on vegetation systems via drought was also shown from satellite data (Kogan and Guo, 2017).

In 2015, the activity of tropical cyclones was notably high in the North Pacific (Blunden and Arndt, 2016). Over the western North Pacific, the number of category 4 and 5 Tropical Cyclones (TCs) was 13, which is more than twice its typical annual value of 6.3 (Zhang et al., 2016a). Similarly, a record-breaking number of TCs was observed in the eastern North Pacific, particularly in the western part of that domain (Collins et al., 2016; Murakami et al., 2017). These extraordinary TC activities were related to the average SST anomaly during that year, which were associated with the super El Niño event in 2015 and the positive phase of the Pacific Meridional Mode (PMM) (Murakami et al., 2017). However, it has been suggested that the intense TC activities in both the western and the eastern North Pacific in 2015 were not only due to the El Niño, but also to a contribution of anthropogenic forcing (Murakami et al., 2017; Yang et al., 2018c). In the 2015/2016 super El Niño years, the TC activities were similarly strong in the western Pacific as in the 1997/1998 strong El Niño. However, differences in possible TC characteristics between the two super El Niño years in 1997 and 2015 were suggested to be due to the additional effect of PMM (Hong et al., 2018; Yamada et al., 2019). It was suggested that the impact of the Indian Ocean SST also contributes to the extreme TC activity in 2015 (Zhan et al., 2018).

[START BOX 11.3, FIGURE 2 HERE]

Box 11.3, Figure 2: Geographical distribution of notable climate anomalies and events occurring around the world in 2015. The warm/cold/dry/wet categories are defined according to precipitation and temperature anomalies for the period DJF 2015/2016 which coincides with the highest magnitude of ENSO.

[END BOX 11.3, FIGURE 2 HERE]

[START BOX 11.3, TABLE 1 HERE]

Box 11.3, Table 1: List of events related to the 2015/2016 Super El Niño in the literature.

Region	Period	Events	References
Indonesia	July 2015 to June 2016	droughts, forest fire	(Field et al., 2016; Huijnen et al., 2016; Patra et al., 2017; Hartmann et al., 2018)
Amazon	September 2015 to May 2016	droughts, forest fire	(Jiménez-Muñoz et al., 2016; Erfanian et al., 2017; Aragão et al., 2018; Panisset et al., 2018; Ribeiro et al., 2018)
The entirety of South America north of 20°S	the austral spring and summer 2015/2016	droughts	(Erfanian et al., 2017)

Ethiopia	February-September 2015	droughts	(Blunden and Arndt, 2016; Philip et al., 2018a)
Southern Africa	November 2015–April 2016	droughts	(Funk et al., 2016, 2018a; Blamey et al., 2018; Yuan et al., 2018a)
Eastern North Pacific	Boreal summer 2015	a record-breaking number of tropical cyclones	(Collins et al., 2016; Murakami et al., 2017)
Western North Pacific	Boreal summer 2015	the large number (13) of category 4 and 5 tropical cyclones	(Blunden and Arndt, 2016; Mueller et al., 2016a; Zhang et al., 2016b; Hong et al., 2018; Yamada et al., 2019)

Global-scale temperature extremes in boreal 2018 spring and summer

In the 2018 boreal spring-summer season (May-August), wide areas of the mid-latitudes in the Northern Hemisphere experienced heat extremes and in part enhanced drought (Kornhuber et al., 2019; Vogel et al., 2019; Box 11.3, Figure 3). Between May and August 2018, the reported impacts included the following (Vogel et al., 2019): 90 deaths from heat strokes in Quebec (Canada), 1469 deaths from heat strokes in Japan (Shimpo et al., 2019), 48 heat-related deaths in South Korea (Min et al., 2020), heat warning affecting 90’000 students in the USA, fires in numerous countries (Canada (British Columbia), USA (California), Lapland, Latvia), crop losses in the UK, Germany and Switzerland (Vogel et al., 2019) and overall in central and northern Europe (leading to yield reductions of up to 50% for the main crops, (Toreti et al., 2019), fish deaths in Switzerland, and melting of roads in the Netherlands and the UK, among others. In addition to the numerous hot and dry extremes, an extremely heavy rainfall event occurred over wide areas of Japan from 28 June to 8 July 2018 (Tsuguti et al., 2018), which was followed by a heatwave (Japan Meteorological Agency, 2018). The heavy precipitation event caused more than 230 deaths in Japan, and was named as “the Heavy Rain Event of July 2018”. The heavy precipitation event was characterized by unusually widespread and persistent rainfall and locally anomalous total precipitation led by line-shaped precipitation systems, which are frequently associated with heavy precipitation events in East Asia (Kunii et al., 2016; Oizumi et al., 2018; Tsuguti et al., 2018; Section 11.7.3). This precipitation event and the subsequent heatwave are related to abnormal condition of the jet and North Pacific Subtropical High in this month (Shimpo et al., 2019), which caused extreme conditions from Europe, Eurasia, and North America (Kornhuber et al., 2019; Cross-Chapter Box 11.3, Figure 3). An event attribution study showed that the anomalous North Pacific Subtropical High could not be simulated without greenhouse gas forcing in an ESM, suggesting that it would have been *extremely unlikely* (i.e, less than 1% chance) to happen without human-induced global warming (Imada et al., 2019). A role of Atlantic SST anomaly on the meandering jets and the subtropical high have been suggested (Liu et al., 2019a). The extreme rainfall in Japan was caused by anomalous moisture transport with a combination of abnormal jet condition (Takemi and Unuma, 2019; Takemura et al., 2019; Tsuji et al., 2019; YOKOYAMA et al., 2020), which can be viewed as an atmospheric river (Yatagai et al., 2019; Sections 8.2.2.8, 11.7.2). This moisture flux was caused by intensified inflow velocity and high SST around Japan (Kawase et al., 2019; Sekizawa et al., 2019). Kawase et al. (2019) showed that the extreme rainfall in Japan during this event was increased by approximately 7% due to recent rapid warming around Japan. These dynamic and thermodynamic components generally have substantial influence on extreme rainfall in East Asia (Oh et al., 2018), but it is under investigation whether these factors were due to anthropogenic forcing.

[START BOX 11.3, FIGURE 3 HERE]

Box 11.3, Figure 3: Global extreme climate events in July 2018 (Japan Meteorological Agency, 2018). This figure shows overlaid climate extremes (warm, cold, wet and dry) from weekly reports for July 2018. [FGD PLACEHOLDER: WILL INCLUDE AN UPDATED FIGURE PROVIDING ANOMALIES OVER THE WHOLE DURATION OF THE EVENT, I.E. AT LEAST MAY-AUGUST 2018]

[END BOX 11.3, FIGURE 3 HERE]

Regarding the hot extremes that occurred across the Northern Hemisphere in the 2018 boreal May-July time period, Vogel et al. (2019) found that the event was unprecedented in terms of the total area affected by hot extremes (on average about 22% of populated and agricultural areas in the Northern Hemisphere) for that period, but was consistent with a +1°C climate which is the estimated present-day global mean temperature anomaly (SR15). Indeed, the probability of such an event was about 16% under a 1°C global warming (Box 11.3, Figure 4). This study also found that events similar to the 2018 May-July temperature extremes would approximately occur 2 out of 3 years under +1.5°C global warming, and every year under +2°C of global warming (Box 11.3, Figure 4). Imada et al. (2019) also suggests that the mean annual occurrence of extremely hot days in Japan will be expected to increase by 1.8 times under a global warming level of 2°C above pre-industrial levels. Hence, while the 2018 event had a strong circulation component (Box 11.3, Figure 3), the widespread temperatures anomalies that occurred in that year should not have been unexpected given climate simulations for present-day warming, and it is *virtually certain* that these concurrent events would not have occurred without human-induced global warming (Vogel et al., 2019). Concurrent events of this type are also projected to happen more frequently under higher levels of global warming (Box 11.3, Figure 4). On the other hand, there is currently *low confidence* in projected changes in the frequency or strength of the anomalous circulation patterns leading to concurrent extremes (e.g., Cross-Chapter Box 10.1).

[START BOX 11.3, FIGURE 4 HERE]

Box 11.3, Figure 4: (left) Probabilities for exceeding concurrent hot day areas in the reference period 1958–1988 (p_0) for the multimodel ensemble (gray range) and observations (black line). The 2018 area is highlighted by a purple vertical dashed line in each subpanel. (right) CMIP5-based multi-model range of probabilities for exceeding concurrent hot days areas experienced in May-July 2018 for global warming of +1°C (orange), +1.5°C (red) and +2°C (dark red) with respect to 1870-1900. From Vogel et al. (2019).

[END BOX 11.3, FIGURE 4 HERE]

The case studies presented in this Box 11.3 illustrate the current state of knowledge regarding the contribution of human-induced climate change to recent concurrent extremes in the global domain. Recent years have seen a more frequent occurrence of such events. The heatwave in Europe in the 2019 boreal summer and its coverage in the global domain is an additional example (Vautard et al., submitted). However, there are still very few studies investigating which types of concurrent extreme events could occur under increasing global warming. It has been noted that such events could also be of particular risk for concurrent impacts in the world's breadbaskets (Zampieri et al., 2017;(Kornhuber et al., 2020).

[END BOX 11.3 HERE]

11.9 Regional information on extremes

This section complements and expands the regional assessments provided for specific extremes in Sections 11.3, 11.4, 11.5, 11.6 and 11.7. The regional assessment is presented here using a separate table for Africa (Table 11.4), Asia (Table 11.5), Australasia (Table 11.6), Central and South America (Table 11.7), Europe (Table 11.8), and North America (Table 11.9). Tables contain regional information for observed trends, detection and attribution and event attribution and future projections for all types of extremes based on the AR6 reference set of regions (see Section 1.5.2.2 for a description).

[START TABLE 11.4 HERE]

Table 11.4: Regional assessments for Africa.

	Temperature extremes			Precipitation extremes and flooding (including effects of TC, ETC and atmospheric rivers)			Droughts, dryness and aridity		
	Observed trends	Detection and attribution; event attribution	Projections	Observed trends	Detection and attribution; event attribution	Projections	Observed trends	Detection and attribution; event attribution	Projections
North Africa (S.MED)	*High confidence:* Increase in frequency of warm extremes(TX90P, TN90P) and decrease in frequency of cold extremes (TX10P,TN10P) since 1981 (Donat et al., 2013a, 2014a, 2016a; Filahi et al., 2016; Driouech et al., submitted) *Low confidence:* Insufficient evidence to assess trends on heat and cold waves	*Low confidence*: High temperature extremes in context of dry events are attributable to anthropogenic climate change (Bergaoui et al., 2015)	*High confidence:* Increase of heat waves by end of the 21st century) (Giorgi et al., 2014) Increase in frequency of warm extremes(TX90P, TN90P) (Lelieveld et al., 2016)	*Low confidence:* Increase in heavy precipitationin the West (Donat et al., 2014a) Decrease in heavy precipitation in the East (Donat et al., 2014a; Mathbout et al., 2018b)	*Low confidence:* Insufficient evidence to attribute observed trends and events.	*Low confidence:* Lack of agreement in sign of change of R95p (Sillmann et al., 2013a; Giorgi et al., 2014).	*Low confidence:* Increase in dryness (CDD) in the East (Donat et al., 2014a; Mathbout et al., 2018b) and decrease in the West (Donat et al., 2014a) Increase in dryness (SPEI) over NW Africa (Morocco) (Driouech et al., submitted)	*Low confidence:* Drying attributable to climate change (Bergaoui et al., 2015)	*Medium confidence:* Increase in dryness (CDD) (Sillmann et al., 2013a; Giorgi et al., 2014; Han et al., 2019)

Sahara (SAH)	*Medium confidence:* Increase in frequency of warm extremes (TX90P,TN90P, WSDI) and decrease in cold extremes (TX10P, TN10P, CSDI), since 1981. (Donat et al., 2014a; Moron et al., 2016).	*Low confidence:* Insufficient evidence to attribute observed trends and events.	*High confidence:* Increase of heat waves by end of the 21st century) (Giorgi et al., 2014) Increase in frequency of warm extremes (TX90P, TN90P). (Dosio, 2017).	*Low confidence:* Increase in heavy precipitation in west Sahara and Sudan (Donat et al., 2014a).	*Low confidence:* Insufficient evidence to attribute observed trends and events.	*Low confidence:* insufficient evidence to assess trends.	*Low confidence:* insufficient evidence to assess trends	*Low confidence:* Insufficient evidence to attribute observed trends and events.	*Low confidence:* Lack of agreement in sign of change of CDD (Sillmann et al., 2013a; Giorgi et al., 2014; Han et al., 2019)
West Africa (WAF)	*Medium confidence:* Increase in frequency of warm extremes(TX90P, TN90P ,WSDI) decrease in cold extremes (TX10P, TN10P) (Mouhamed et al., 2013; Chaney et al., 2014; Barry et al., 2018).	*Low confidence:* Insufficient evidence to attribute observed trends and events.	*High confidence:* Increase in heat waves by end of the 21st century) (Giorgi et al., 2014). Increase in frequency of warm extremes (TX90P,TN90) in boreal summer and winter (Dosio, 2017).	*Medium confidence:* Increase in heavy precipitation but varies spatially (Mouhamed et al., 2013; Chaney et al., 2014; Sanogo et al., 2015; Zittis, 2017; Barry et al., 2018) Increased frequency of storms over western Sahel since 1982 causing torrential precipitation (Taylor et al., 2017).	*Low confidence:* No attributable change in extreme rainfall (Parker et al., 2017).	*High confidence:* Increase in intensity of heavy precipitation by the by end of the 21st century (Sillmann et al., 2013a; Giorgi et al., 2014; Sylla et al., 2016; Akinsanola and Zhou, 2018; Dosio et al., 2019).	*Medium confidence:* Decrease of CDD since 1980 (Chaney et al., 2014; Barry et al., 2018).	*Low confidence* that late onset of the rainy season is not attributable to climate change (Lawal et al., 2016)	*Low confidence:* Lack of agreement in sign of change of CDD (Sillmann et al., 2013a; Akinsanola and Zhou, 2018; Han et al., 2019) *High confidence:* Increase in dryness CDD over Guinea coast under 1.5C and 2C of global warming (Klutse et al., 2018)

Central Africa (CAF)	*Low confidence:* Insufficient evidence to assess trends because the ground-based datasets are sporadic and sparse	*Low confidence:* Insufficient evidence to attribute observed trends and events.	*High confidence*(Mba et al., 2018) for local change in RCMs	*Low confidence:* Insufficient evidence to assess trends because the ground-based datasets are sporadic and sparse	*Low confidence:* There is no attributable signal to changes in extreme precipitation (Otto et al., 2013)	*High confidence:* Increase in heavy precipitation (Diedhiou et al. 2018; Fotso-Nguemo et al. 2018; Sonkoué et al. 2019), particularly RCMs	*High confidence* Decrease in mean rainfall. More evidence to assess the trends and its variability (Aguilar et al., 2009; Hua et al., 2016)	*Low confidence:* There is no attributable signal to changes in low precipitation (Otto et al., 2013) Long-term (1979-2014) drought over Central Africa can be explained by the large-scale response of the atmosphere to tropical sea surface temperature variations(Hua et al., 2016)	*High confidence:* Decrease in CWD (Fotso-Nguemo et al., 2018; Kendon et al., 2019; Sonkoué et al., 2019)
North East Africa (NEAF) and Central East Africa (CEAF)	*Medium confidence:* Increases in frequency of warm days (TX90P)	*Medium confidence:* Increased temperature attributable to climate change (Otto et al., 2015a; Philip et al., submitted)	*High confidence:* Likely increases in frequency of warm days (TX90P) and decreases in frequency of cold days (TX10P)	*Low confidence:* Insufficient evidence to assess trends	*Low confidence:* Insufficient evidence to attribute observed trends and events.	*Low confidence:* insufficient evidence to assess trends	*Medium confidence:* Increase in frequency of meteorological droughts (Funk et al., 2015a; Nicholson, 2017)	*Low confidence* high evidence that observed drying is not attributable to anthropogenic climate change(Uhe et al., 2017; Funk et al., 2018b; Otto et al., 2018a; Philip et al., 2018a)	*Low confidence:* lack of agreement in the sign of change (SREX suggest decreases in CDD but (Osima et al., 2018, Dosio el al 2019) suggest in increases)

South WestAfrica (SWAF)	*High confidence :* likely increases in frequency of warm days (TX90P), and decreases in cold days (TX10P) (Donat et al., 2013a) *Medium confidence:* Increases in heatwaves frequency (Russo et al., 2016)	*Low confidence:* Insufficient evidence to attribute observed trends and events.	*High confidence:* likely increases in frequency of warm days (TX90P) and decreases in frequency of cold days (TX10P) (Donat et al., 2013a) *High confidence:* very likely increases in the frequency of heat waves (Engelbrecht et al., 2015; Russo et al., 2016; Dosio, 2017)	*Medium confidence:* increases in heavy precipitation but with spatially varying trends. Increases in precipitation intensity (SDII) (Donat et al., 2013a)	*Low confidence:* Insufficient evidence to attribute observed trends and events.	*Medium confidence:* increases in the frequency of heavy precipitation but varying spatially (Pinto et al., 2016) *High confidence:* increases in precipitation intensity (Pinto et al., 2016, Dosio el al 2019)	*Medium confidence:* increase in dryness (CDD)	*Medium confidence:* Recent meteorological drought attributable to anthropogenic climate change (Otto et al., 2018c)Ch. 17,18: (Herring et al., 2018)	*High confidence:* Likely increases in dryness (Giorgi et al. 2014; Pinto et al. 2016;Maúre et al., 2018, Dosio el al 2019) (CDD and SPEI, SPI*)
South East Africa (SEAF)	*High confidence :* likely increases in frequency of warm days (TX90P), and decreases in cold days (TX10P) (Donat et al., 2013a) *Medium confidence:* Increases in the frequency of heat waves (Russo et al., 2016)	*Low confidence:* Insufficient evidence to attribute observed trends and events.	*High confidence*: likely increases in warm days and decreases in cold days very likely increases in the frequency of heat waves (Engelbrecht et al., 2015; Russo et al., 2016; Dosio, 2017)	*Medium confidence:* increases in heavy precipitation but with spatially varying trends. Increases in precipitation intensity (SDII) (Donat et al., 2013a)	*Low confidence:* Insufficient evidence to attribute observed trends and events.	*Medium confidence:* increases in heavy precipitation but varying spatially (Pinto et al., 2016) *High confidence:* likely increases in precipitation intensity (Pinto et al., 2016, Dosio el al 2019)	*Medium confidence:* increase in dryness (CDD)	*Medium confidence:* Recent meteorological drought attributable to anthropogenic climate change (Bellprat et al., 2015)	*High confidence:* Likely increases in dryness (Giorgi et al. 2014; Pinto et al. 2016; Maúre et al., 2018, Dosio el al 2019) (CDD and SPEI, SPI*)

[END TABLE 11.4 HERE]

[START TABLE 11.5 HERE]

Table 11.5: Regional assessments for Asia

	Temperature extremes			Precipitation extremes and flooding			Droughts, dryness and aridity		
	Observed trends	Detection and attribution;event attribution	Projections	Observed trends	Detection and attribution;event attribution	Projections	Observed trends	Detection and attribution;event attribution	Projections
Arabian Peninsula (ARP)	*High confidence:*Increase in frequency and magnitude of warm extremes, decrease in frequency and severity of cold extremes (Almazroui et al., 2014; Donat et al., 2014a; Nazrul Islam et al., 2015; Dunn et al., submitted)		*High confidence:* Increase in the frequency and magnitude of warm extremes and decrease in frequency and severity of cold exremes (Xu et al., 2017; Han et al., 2018; Almazroui, 2019)	*Low confidence:* Decreases in the frequency of extreme precipitation (Donat et al., 2014a)	*Low confidence:* Surface heating and topography intensified 2009 Jeddah extreme precipitation event (Almazroui et al., 2018).	*Low confidence* : Changes in extreme precipitation are uncertain for much of the region, though an increase in precipitation extremes is projected for the south (Sillmann et al., 2013b; Han et al., 2018; Kharin et al., 2018)(Almazroui and Saeed, 2020)	*Low confidence :* Increase in drought conditions due to decreased rainfall and increased dry days (Donat et al., 2014a; Amin et al., 2016; Rajsekhar and Gorelick, 2017)		*Low confidence* : Increase in drought conditions, especially in the north (Barlow et al., 2016; Rajsekhar and Gorelick, 2017; Tabari and Willems, 2018).
West Central Asia (WCA)	*High confidence*: Increase in frequency and magnitude of warm extremes, decrease in frequency and severity of cold extremes (Soltani et al., 2016; Alizadeh-Choobari and		*High confidence*: Increase in the frequency and magnitude of warm extremes and decrease in frequency and severity of cold exremes (Xu et al., 2017; Han et al.,	*Low confidence*: Trends in extreme precipitation vary by index and location (Soltani et al., 2016; Alizadeh-Choobari and Najafi, 2018; Rahimi and Fatemi,		*Low confidence:* Increase in extreme precipitation (Sillmann et al., 2013b; Han et al., 2018; Kharin et al., 2018).	*Low confidence*: Decrease in CDD (Soltani et al., 2016), decrease in soil moisture (Li et al., 2017c) and increase in drought severity and frequency in some regions	*Low confidence:* No attribution found for the winter 2013/14 drought (Barlow and Hoell, 2015)	*Low confidence:* Increase in dry days (Han et al., 2018; Tabari and Willems, 2018)

	Najafi, 2018; Feng et al., 2018; Rahimi and Hejabi, 2018; Fallah-Ghalhari et al., 2019; Zhang et al., 2019c).		2018; AshrafVaghefi et al., 2019)	2019; Dunn et al., submitted).			(Modarres et al., 2016; Hameed et al., 2018)		
Russian-Far-East (RFE)	*High confidence*: Increase in frequency and magnitude of warm extremes, decrease in frequency and severity of cold extremes (Donat et al., 2016a; Zhang et al., 2019c; Dunn et al., submitted)		*High confidence*: Increase in the frequency and magnitude of warm extremes and decrease in frequency and severity of cold exremes (Xu et al., 2017; Han et al., 2018; Khlebnikova et al., 2019a)			*Low confidence:* Increase in precipitation extremes (Sillmann et al., 2013b; Xu et al., 2017; Han et al., 2018; Kharin et al., 2018)	*Low confidence:* Increase in dry days (Khlebnikova et al., 2019b)		*Low confidence:* Decreases in CDD are projected in most regions (Han et al., 2018)
E. Siberia (ESB)	*High confidence:* Increase in frequency and magnitude of warm extremes, decrease in frequency and severity of cold extremes (Dashkhuu et al., 2015; Donat et al., 2016a; Zhang et al., 2019c; Dunn et al., submitted)	*Low confidence:* Attribution of changes in temperatures extremes for a broader region of Asia mid-to-high latitudes (Dong et al., 2018)	*High confidence*: Increase in the frequency and magnitude of warm extremes and decrease in frequency and severity of cold exremes (Xu et al., 2017; Han et al., 2018; Khlebnikova et al., 2019a)			*Medium confidence:* Increase in precipitation extremes (Sillmann et al., 2013b; Xu et al., 2017; Han et al., 2018; Kharin et al., 2018; Khlebnikova et al., 2019b)	*Low confidence:* Decrease in dry days for much of the region, but parts of the south show increases (Khlebnikova et al., 2019b)		
W. Siberia (WSB)	*High confidence:* Increase in warm extremes and decrease in cold extremes (Degefie et	*Low confidence:* Attribution of changes in temperatures extremes for a	*High confidence:* Increase in the frequency and magnitude of warm extremes and	*Low confidence:* No siginifcant trends in precipitation extremes found in the north (Degefie et		*Medium confidence:* Increase in precipitation extremes	*Low confidence:* Decrease in CDD for much of the region (Zhang et al., 2017, 2019b;		

	al., 2014; Salnikov et al., 2015; Donat et al., 2016a; Zhang et al., 2019c, 2019b; Dunn et al., submitted)	broader region of Asia mid-to-high latitudes (Dong et al., 2018)	decrease in frequency and severity of cold exremes (Xu et al., 2017; Han et al., 2018; Khlebnikova et al., 2019a)	al., 2014), but an increase in extreme precipitation in the south (Zhang et al., 2017)		(Sillmann et al., 2013b; Xu et al., 2017; Han et al., 2018; Kharin et al., 2018; Khlebnikova et al., 2019b)	Khlebnikova et al., 2019b) and soil moisture in the south (Li et al., 2017c)		
Russian-Arctic (RAR)	*High confidence:* Decrease in the frequency and severity of cold extremes (Donat et al., 2016a; Sui et al., 2017; Dunn et al., submitted)		*High confidence* Increase in the frequency and magnitude of warm extremes and decrease in frequency and severity of cold exremes (Xu et al. 2017; Han et al. 2018;Khlebnikova et al. 2019a)			*Medium confidence:* Increase in precipitation extremes (Sillmann et al., 2013b; Han et al., 2018; Kharin et al., 2018; Khlebnikova et al., 2019b)			*Low confidence:* Decrease in dry spells (Khlebnikova et al., 2019b)
Tibetan Plateau (TIB)	*High confidence*: Increase in the frequency and magnitude of warm extremes and decrease in the frequency and severity of cold extremes. (Donat et al., 2016a; Hu et al., 2016; Sun et al., 2017; Yin et al., 2019a; Zhang et al., 2019c; Dunn et al., submitted)	*Medium confidence:* Most of the observed changes in temperature extremes are attributable to anthropogenic forcing (Yin et al., 2019a)	*High confidence*: Increase in the frequency and magnitude of warm extremes and decrease in frequency and severity of cold exremes (Zhou et al., 2014; Singh and Goyal, 2016; Zhang et al., 2016a; Xu et al., 2017; Han et al., 2018; Li et al., 2018a)	*Low confidence*: Increase in extreme precipitation over most of the region, (Jiang et al., 2013; Hu et al., 2016; Ge et al., 2017; Zhan et al., 2017; Liu et al., 2019b)but decreases at some locations in the east/southeast (Ge et al., 2017)		*Medium confidence*: Increase in heavy precipitation (Zhou et al., 2014; Zhang et al., 2015c; Gao et al., 2018; Han et al., 2018)	*Low confidence*: Decrease in CDD (Jiang et al., 2013; Donat et al., 2016a; Hu et al., 2016), Decrease in drought occurrence and severity based on other metrics (Chen and Sun, 2015b; Liu et al., 2019b; Wu et al., 2019b) but drought frequency increased in more		*Low confidence*: A general decrease is projected but with large uncertainty (Zhou et al., 2014)

							recent decades (Wu et al., 2019b)		
South Asia (SAS)	*Medium confidence*: Some increases in the frequency and severity warm extremes and decreases in the frequency and severity of cold extremes, but trends vary seasonally, regionally, and by index. (Sheikh et al., 2015; Donat et al., 2016a; Chakraborty et al., 2018; Dimri, 2019; Roy, 2019; Dunn et al., submitted) Increase in the intensity and frequency of heatwaves (Zahid and Rasul, 2012; Rohini et al., 2016)	*Medium confidence*: Observed changes in minimum temperature over Mahandi river basin during the pre-monsoon and monsoon season can be attributed to an anthropogenic effect (Kumar, 2017).	*High confidence*: Increase in the frequency and magnitude of warm extremes and decrease in frequency and severity of cold exremes (Sillmann et al., 2013b; Xu et al., 2017; Han et al., 2018; Kharin et al., 2018; Ali et al., 2019) More intense heatwaves of longer duration at a higher frequency in India (Murari et al., 2015) and in Pakistan (Nasim et al., 2018) .	*High confidence*: Increasing trends in extreme precipitation over most of South Asia (Pai et al., 2015; Sheikh et al., 2015; Malik et al., 2016; Rohini et al., 2016; Roxy et al., 2017; Kim et al., 2019), but some northern regions show decreases (Hussain and Lee, 2013; Malik et al., 2016; Kim et al., 2019)	*Low confidence*: Broadly, anthropogenic forcing has increased the frequency of extreme precipitation(Mukherjee et al., 2018), but no robust attribution found for individual events (Singh et al., 2014; van Oldenborgh et al., 2016)	*Medium confidence*: Increase in extreme precipitation (Sillmann et al., 2013b; Xu et al., 2017; Han et al., 2018; Mukherjee et al., 2018; Ali et al., 2019; Rai et al., 2019)	*Low confidence:* Increase in drought conditions for many regions (Niranjan Kumar et al., 2013; Malik et al., 2016; Guhathakurta et al., 2017).	Low confidence: Aerosol loadings contribute to an increase the severity of droughts (Fadnavis et al., 2019)	*Medium confidence*: Increase in the frequency of dry spells and droughts (Mishra et al., 2014b; Salvi and Ghosh, 2016), though increases are weaker at the end of the century (Mishra et al., 2014b)
East Asia (EAS)	*High confidence:* Increase in the frequency and magnitude of warm extremes and decrease in the frequency and severity of cold extremes. (Wang et al., 2013a; Lu et al.,	*High confidence*: Anthropogenic influences on extreme temperature including their magnitude, frequency, and duration (Lu et al., 2016, 2018; Takahashi et al.,	*High confidence*: Increase in the frequency and magnitude of warm extremes and decrease in frequency and severity of cold exremes (Seo et al., 2014; Zhou et al.,	*High confidence*: Strong regional differences of annual total precipitation amount, average daily precipitation rate, and the proportion of heavy precipitation;	*Low confidence*: Human influence has increased daily precipitation extremes over China in recent decades (Chen and Sun, 2017c; Li et al., 2017b), and contribution to the	*Medium confidence*: Intensification in extreme precipitation (Kusunoki and Mizuta, 2013; Zhou et al., 2014; Seo et al., 2014; Xu et al., 2016;	*Medium confidence:* Since the 1950s some regions of China have experienced a trend to more intense and longer droughts, although the nortwestern	*Medium confidence*: There is evidence that the droughts have changed as a result of anthropogenic influences, including the drought	*Medium confidence*: CDD is projected to increase in south China and decrease in north China (Zhou et al., 2014; Kusunoki, 2018a) The occurrence probability of hot

	2016, 2018; Zhou et al., 2016a; Lin et al., 2017; Yin et al., 2017)	2016; Zhou et al., 2016a; Yin et al., 2017; Imada et al., 2019)	2014; Xu et al., 2016; Wang et al., 2017a, 2017c; Guo et al., 2018; Li et al., 2018c; Sui et al., 2018)	negative trends in a southwest–northeast belt, while positive trends in eastern and northwestern China (Zhou et al., 2016a). Observed increase in extreme precipitation intensity (Baek et al., 2017; Nayak et al., 2017; Ye and Li, 2017) .	shift from light to heavy precipitation over eastern China (Ma et al., 2017).	Nayak et al., 2017; Wang et al., 2017c, 2017a; Guo et al., 2018; Kusunoki, 2018a; Li et al., 2018c; Sui et al., 2018; Ohba and Sugimoto, 2019) The heavy snowfall is projected to increase in northern China (Zhou et al., 2018a) and central Janpa (Kawase et al., 2016)	part of China experienced less frequent, less intense, or shorter drought (Yu et al., 2014; Chen and Sun, 2015b; Qin et al., 2015a)	occurrences, severity, and the drought regimes (Chen and Sun, 2017a, 2017b). Less precipitation combined with high temperature during boreal winter is one of major contributor for drought in southwest China (Qin et al., 2015a)	drought events (SPEI < -1.0) will increase to nearly 100% by the year 2050 (Chen and Sun, 2017a, 2017b)
Southeast Asia (SEA)	*High confidence:* Increase in the frequency and magnitude of warm extremes and decrease in the frequency and severity of cold extremes.(Donat et al., 2016a; Supari et al., 2017; Cheong et al., 2018; Zhang et al., 2019c; Dunn et al., submitted).	*Low confidence*: Increase in the likelihood of hot conditions attributable (King et al., 2016b)	*High confidence:* Increase in the frequency and magnitude of warm extremes and decrease in frequency and severity of cold exremes (Sillmann et al., 2013b; Xu et al., 2017; Han et al., 2018; Kharin et al., 2018).	*Low confidence*: Increase in extreme precipitation for much of the region (Siswanto et al., 2015; Villafuerte and Matsumoto, 2015; Supari et al., 2017; Cheong et al., 2018; Li et al., 2018g), but decrease in the southeast (Villafuerte and Matsumoto, 2015; Cheong et al., 2018)	*Low confidence:* Trends in extreme precipitation are linked to the increasing global mean temperature (Villafuerte and Matsumoto, 2015).	*Medium confidence:* Increase in extreme precipitation (Basconcillo et al., 2016; Xu et al., 2017; Han et al., 2018; Tangang et al., 2018; Ge et al., 2019).		*Low confidence:* Increase in drought conditions attributable (King et al., 2016b) Drought in Indonesia was found to be made more likely by El Niño and climate change (King et al., 2016c; Hariadi, 2017) but no link to climate change could be made for the 2015	*Medium confidence:* Increase in CDD and drought risk for much of the region, but decrease in the northwest (Tangang et al., 2018) Changes in ENSO and IOD patterns favourable for increased drought (Cai et al., 2014a, 2015, 2018)

								drought in Singapore/Malaysia (Mcbride et al., 2015).	

[END TABLE 11.5 HERE]

[START TABLE 11.6 HERE]

Table 11.6: Regional assessments for Australasia

	Temperature extremes			Precipitation extremes and flooding (including effects of TC, ETC and atmospheric rivers)			Droughts, dryness and aridity		
	Observed trends	Detection and attribution; event attribution	Projections	Observed trends	Detection and attribution; event attribution	Projections	Observed trends	Detection and attribution; event attribution	Projections
Northern Australia (NAU)	*High confidence*: Increase in the frequency of warm days (TX90p) and warms nights (TN90p) and decrease in the frequency of cold days (TN10p) and cold nights (TX10p) (Alexander and Arblaster, 2017; Wang et al., 2013b; Jakob and Walland, 2016; Lewis and King, 2015).	*High confidence*: Increase in trends of temperature extremes, and in the likelihood of extremes events on daily to annual timescales due to anthropogenic warming (Lewis and Karoly, 2013; Perkins et al., 2014a; Lewis and King, 2015).	*High confidence*: Increase in the frequency of warm temperature extremes and decrease in the frequency of cold temperature extremes (Alexander and Arblaster, 2017; Lewis et al., 2017; Herold et al., 2018).	*Low- to-medium confidence*: Positive trends are observed over the northwest for various rainfall extreme indices (Dey et al., 2019) for daily and hourly data (Guerreiro et al., 2018b). Negative trends observed in the number of TCs over North Australia (Dowdy, 2014).	*Low confidence*: Trends in northwest Australia rainfall attributable to anthropogenic aerosols, but large spread in models (Dey et al., 2019)	*Medium confidence*: Extreme precipitation is projected to increase mainly over the northern part of NAU (Perkins et al., 2014b; Alexander and Arblaster, 2017; Evans et al., 2017; Dey et al., 2018).	*Low confidence*: Decrease in the number, duration and intensity of droughts over northwest Australia (Gallant et al., 2013).	*Low confidence*: No evidence has been found.	*Low confidence*: Projections do not show significant trends in this region (Herold et al., 2018).

Central Australia (CAU)	*High confidence.* Increase in the frequency of warm days (TX90p) and warms nights (TN90p) and decrease in the number of cold days (TX10p) and cold nights (TN10p) (Alexander and Arblaster, 2017; Wang et al., 2013b; Jakob and Walland, 2016).	*High confidence*: Increase in trends of temperature extremes, and in the likelihood of extreme events on daily to annual timescales due to anthropogenic warming (Lewis and Karoly, 2013; Perkins et al., 2014a; Lewis and King, 2015).	*High confidence*: Increase in the frequency of warm temperature extremes and decrease in the frequency of cold temperature extremes (Alexander and Arblaster, 2017; Lewis et al., 2017; Herold et al., 2018).	*Low confidence:* Over the central Australia trends in extreme precipitation indices are usually positive (Alexander and Arblaster, 2017).		*Low confidence*: Extreme precipitation is projected to increase but the agreement among models is low (Alexander and Arblaster, 2017; Evans et al., 2017).	*Low confidence*: Decrease in the frequency of CDD (Alexander and Arblaster, 2017).		*Low confidence*: Increase in CDD (Alexander and Arblaster, 2017; Herold et al., 2018).
Eastern Australia (EAU)	*High confidence*: Increase in the number of warm days (TX90p) and warms nights (TN90p) and decrease in the number of cold days (TX10p) and cold nights (TX10p) (Alexander and Arblaster, 2017; Wang et al., 2013b; Jakob and Walland, 2016; Lewis and King, 2015).	*High confidence*: Increase in trends of temperature extremes, and in the likelihood of extreme events on daily to annual timescales due to anthropogenic warming (Lewis and Karoly, 2013; Perkins et al., 2014a; Lewis and King, 2015).	*High confidence*: Increase in the frequency of warm temperature extremes and decrease in the frequency of cold temperature extremes (Alexander and Arblaster, 2017; Lewis et al., 2017; Herold et al., 2018).	*Low confidence*: Increase in the magnitude of extreme precipitation over most of the region with more significant trends during summer (Evans et al., 2017).	*Low confidence*: Anthropogenic greenhouse gas influence on extreme rainfall events in eastern Australia is highly uncertain (Christidis et al., 2013a; King et al., 2013; Lewis and Karoly, 2014a)	*Low confidence*: Extreme precipitation is projected to increase but the agreement among models is low (Alexander and Arblaster, 2017; Evans et al., 2017).		*Low confidence*: Single study shows probability of drought conditions in 2013 in Queensland were not significantly altered by anthropogenic forcings (King et al., 2014)	*Medium confidence*: Increase in the frequency of CDD (Alexander and Arblaster, 2017). Increase in SPEI in summer/autumn over eastern Australia and decrease in winter/spring, though significance of trends is variable (Herold et al. 2018).
Southern Australia (SAU)	*High confidence*: Increase in the number of warm days	*High confidence*: Increase in trends of temperature extremes, and in the likelihood of	*High confidence*: Increase in warm temperature extremes and decreases in cold	*Low confidence:* Increase over southeast Australia, although trends are generally not significant for several	*Low confidence*: Anthropogenic greenhouse gas influence on extreme rainfall events in southern and	*Low confidence*: Extreme precipitation is projected to increase but the agreement among models is low	*Low confidence*: Across much of south Australia, droughts became less frequent,		*Medium confidence*: Robust decrease in precipitation, soil moisture and SPEI

	(TX90p) and warms nights (TN90p) and decrease in the number of cold days and cold nights (Alexander and Arblaster, 2017; Wang et al., 2013b; Jakob and Walland, 2016; Lewis and King, 2015). *Medium confidence*: Increase in the number of frost days in early spring over southeast Australia and in winter over southwest Australia (Crimp et al., 2016; Dittus et al., 2014;Pepler et al. 2018).	extreme events on daily to annual timescales due to anthropogenic warming (Lewis and Karoly, 2013; Perkins et al., 2014a; Lewis and King, 2015).	temperature extremes (Alexander and Arblaster, 2017; Lewis et al., 2017; Herold et al., 2018). Decrease in the number of frost days in southeast and southwest Australia regardless of the region and season considered (Gobbett et al., 2018; Herold et al., 2018)	extreme rainfall indices including RX1day (Evans et al., 2017) As many positive as negative significant trends (Westra et al., 2013). Extreme precipitation increases are larger and more robust in hourly compared to daily data (Guerreiro et al., 2018b). The number of heavy snowfall events has remain unchanged over the Snowy Mountains (Fiddes et al., 2015).	eastern Australia is highly uncertain (Christidis et al., 2013a; King et al., 2013; Lewis and Karoly, 2014a)**.**	(Alexander and Arblaster, 2017; Evans et al., 2017). Robust decrease in ETCs in winter in the Australian east coast based on GCMs and RCMs (Dowdy et al., 2013b, 2013a; Ji et al., 2015; Pepler et al., 2016)	shorter and less intense. Exceptions include far southwest Western Australia, which has had statistically significant increases in drought intensity and southeast Australia which has shown a significant increase in the average length of droughts (Gallant et al., 2013).		in spring over all southern Australia and in winter/summer mainly over the southwest (Olson et al., 2016; Zhao and Dai, 2017; Herold et al., 2018). Southwest Australia identified as a hot spot for drought risks in the future (Prudhomme et al., 2014).
New Zealand (NZE)	*High confidence*: Most stations show positive and generally significant trends for monthly minimum and maximum temperatures. All daily temperature extremes show warming trends with cold			*Low confidence*: Some evidence of changes in the frequency of heavy rain days with mostly decreases (Harrington and Renwick, 2014; Caloiero, 2015)	*Low confidence*: Single study of extreme 2011 rainfall in northern South Island indicates that amount was higher as a result of the emission of anthropogenic greenhouse gases (Dean et al., 2013)	*Medium confidence*: Extreme rainfall is likely to increase everywhere with larger increases for higher warming scenarios and more pronounced for shorter duration events (NIWA, 2018).	*Low confidence*: Some evidence of a trend towards more drought in most areas of NZ (Salinger, 2013)	*Low confidence*: Single study of 2013 North Island drought found dry conditions more favourable as a result of anthropogenic climate change (Harrington et al., 2014)	*Low confidence*: Drought severity (measured using potential evapotranspiration deficit, PED) is projected to increase in most areas of the country, except for Taranaki-Manawatu, West Coast and Southland (NIWA, 2018)

	extremes (TN10 and TX10) increasing faster than warm extremes (TN90 and TX90) (Caloiero, 2017).								
Western Pacific Islands	*High confidence*: Western Pacific islands show warming trends, mostly significant, for all temperature extreme indices including TN10, TX10, TN90 and TX90 (Whan et al., 2014; McGree et al., 2019). Largest warming trends are found in the hottest day (night) of the year with weaker warming trends in the coolest day (night) of the year (Whan et al., 2014)			*Low Confidence:* Western Pacific Islands show decreases in both total and extreme precipitation (southwestern French Polynesia and the southern subtropics). There was a decrease in moderate- to high-intensity precipitation events (southwestern French Polynesia from December to February). Strong drying trends have also been identified in the low- to moderate-extreme indices in the June–August and September–November periods (McGree et al., 2019)					

[END TABLE 11.6 HERE]

[START TABLE 11.7 HERE]

Table 11.7: Regional assessments for Central and South America

	Temperature extremes			Precipitation extremes and flooding (including effects of TC, ETC and atmospheric rivers)			Droughts, dryness and aridity		
	Observed trends	Detection and attribution; event attribution	Projections	Observed trends	Detection and attribution; event attribution	Projections	Observed trends	Detection and attribution; event attribution	Projections
South Central America (SCA)	*High confidence*: Increase in surface air temperature in most of SCA, bu decrease in parts of Honduras and northern Panama (Hidalgo et al., 2017). Increase in the frequency of warm extremes (TX90p, and TN90p) and decrease in the frequency of cold extremes (TX10p, and TN10p) (Donat et al., 2016a).		*High confidence*: Increase in the frequency warm extremes (TX90p, and TN90p) and decrease in the frequency of cold extremes (TX10p, and TN10p) (Stennett-Brown et al., 2017; Yang et al., 2018a). Massive heat waves events projected at the end of the 21st century (Angeles-Malaspina et al., 2018).	*Low confidence*: Increase in the frequency (R10mm), and magnitude (R95p) of precipitation extremes (Donat et al., 2016a).		*Low confidence*: General decrease in the magnitude of precipitation extremes (Chou et al., 2014a; Giorgi et al., 2014), especially in the north (Stennett-Brown et al., 2017; Imbach et al., 2018) but increase in the frequency of extreme precipitation (R50mm) in the eastern coast (Imbach et al., 2018) Strong declines in mean daily rainfall are projected for July in Belize (Stennett-Brown et al., 2017).	*Low confidence*: Mostly decrease in the frequency of CDD (Donat et al., 2016a).		*Low confidence*: Mostly increase in the frequency of CDD (Kitoh et al., 2011; Chou et al., 2014a; Giorgi et al., 2014; Stennett-Brown et al., 2017).
Caribbean (CAR)	*Medium confidence:* Warmer conditions over the north and cooler conditions over the eastern Caribbean (McLean et al., 2015).		*High confidence*: Increase in the frequency of warm extremes (TX90p, and TN90p) and	*Medium confidence:* Negative trends in R95p over the northern and eastern Caribbean (McLean et al., 2015).		*Low confidence:* Declines in R10mm, RX1day and R95p over central Caribbean with increases for	*Medium confidence:* Positive trends in CDD over some locations in the northern and eastern Caribbean (McLean et al., 2015).		*Low confidence:* Increases in CDD over most stations, with decreases over eastern Caribbean and Bahamas (Stennett-

			decrease in the frequency of cold extremes (TX10p, and TN10p) (Jones et al., 2016; Stennett-Brown et al., 2017). Massive heat waves events projected at the end of the 21st century (Angeles-Malaspina et al., 2018).			northern Caribbean (Stennett-Brown et al., 2017; Yang et al., 2018a).			Brown et al., 2017; Yang et al., 2018a).
North South America (NSA)	*High confidence*: Increase in the frequency of warm extremes (TX90p, TN90p, and WSDI) and decrease in the frequency of cold extremes (TX10p, and TN10p). Increase in the magnitude of temperature extremes (TXx, TXn, TNn and TNx) (Skansi et al., 2013). Increase in the magnitude of maximum and minimum temperatures (Almeida et al., 2017). Increase in the frequency and length of heat waves (Bitencourt et al., 2016; Geirinhas et al., 2018).		*High confidence*: Increase in the frequency of warm extremes (TX90p, and TN90p) and decrease in the frequency of cold extremes (TX10p, and TN10p) (López-Franca et al., 2016).	*High confidence*: Increase in the frequency (R20mm) and magnitude (RX1day, RX5day, and R95p) of precipitation extremes (Skansi et al., 2013; Valverde and Marengo, 2014). Increase in the frequency of anomalous severe floods (Gloor et al., 2015).	Increase in extreme precipitation with warming (Li et al.,2019)	*Low confidence*: Decrease in the frequency of CWD (Seiler et al., 2013; Chou et al., 2014a) Inconsistent trends in the magnitude of precipitation extremes (R95p) with both decreases (Seiler et al., 2013; Chou et al., 2014a) and increases (Giorgi et al. 2014).	*Low confidence*: Decrease in the frequency of CDD (Skansi et al., 2013) over NSA while (Valverde and Marengo, 2014) show increase over southeastern Amazon. No evidence of significant trend in drought frequency, intensity, and duration, although the areal-extent show increasing trends (Awange et al., 2016). Increase in the frequency of anomalous severe droughts (Gloor et al., 2015).		*Medium confidence*: Increase in dryness (Marengo and Espinoza, 2016; Menéndez et al., 2016; Zaninelli et al., 2019) Increase in the frequency and geographic extent of meteorological drought in the eastern Amazon, and the opposite in the West (Duffy et al., 2015).
North Eastern South America (NES)	*High confidence*: Increase in the frequency of warm extremes: TX90p, TN90p, and		*High confidence*: Increasein the frequency of warm extremes: TX90p, and	*Medium confidence*: Decrease in the frequency (R50mm) and magnitude (RX1day, RX5day,	*Medium confidence:* Increase in extreme precipitation	*Low confidence*: Decrease in the magnitude of precipitation extremes (R95p)	*Medium confidence*: Mostly increases in the frequency of CDD (Skansi et al., 2013).		*Medium confidence*: Increase in dryness, (Marengo and Bernasconi, 2015; Zaninelli et al., 2019)

	WSDI and decrease in the frequency of cold extremes: TX10p, and TN10p). Increase in the magnitude of temperature extremes (TXx, TXn, TNn and TNx) (Skansi et al., 2013). Increase in the frequency and length of heat waves (Bitencourt et al., 2016; Geirinhas et al., 2018).		TN90p and decrease in the frequency of cold extremes: TX10p, and TN10p (López-Franca et al., 2016).	R95p and R99p) of precipitation extremes (Skansi et al., 2013; Bezerra et al., 2018; Luiz Silva et al., 2018).	with warming (Li et al., 2019)	(Chou et al., 2014a; Giorgi et al., 2014).	The percentage of area affected by drought exhibits an increasing trend for SPI (Brito et al., 2018).		Increase in the frequency of CDD (Sillmann et al., 2013a; Chou et al., 2014a; Giorgi et al., 2014).
North Western South America (NWS)	*High confidence*: Increase in the frequency of warm extremes: TX90p, TN90p, and WSDI and decrease in the frequency of cold extremes: TX10p, and TN10p. Increase in the magnitude of temperature extremes (TXx, TXn, TNn and TNx)(Skansi et al., 2013).		*High confidence*: Increase in the frequency of warm extremes: TX90p, and TN90p and decrease in the frequency of cold extremes: TX10p, and TN10p (López-Franca et al., 2016).	*Low confidence*: Increase in the magnitude of precipitation extremes (RX1day, R95p and R99p) (Skansi et al., 2013).	*Medium confidence:* Increase in extreme precipitation with warming (Li et al., 2019)	*Low confidence*: Decrease in the frequency of CWD (Chou et al., 2014a) Inconsistent trends in the magnitude of precipitation extremes (R95p) with both decreases () and increases (Giorgi et al. 2014 and Seiler et al. 2013) found	*Low confidence*: Mostly increases in the frequency of CDD (Skansi et al., 2013; Donat et al., 2016a).		*Low confidence*: Increase in the frequency of CDD (Chou et al., 2014a; Giorgi et al., 2014)
South Western South America (SWS)	*High confidence*: Increase in the frequency of warm extremes: TX90p, TN90p, and WSDI and decrease in the frequency of cold extremes: TX10p, and TN10p. Increase in the magnitude of temperature extremes (TXx, TXn, TNn and TNx) (Skansi et al., 2013; Meseguer-Ruiz et al., 2018).		*High confidence*: Increase in the frequency of warm extremes: TX90p, and TN90p and decrease in the frequency of cold extremes: TX10p, and TN10p (López-Franca et al., 2016).	*Low confidence*: Increase in extreme rainfall (Skansi et al., 2013).	*Medium confidence:* Increase in extreme precipitation with warming (Li et al., 2019)	*Low confidence*: Inconsistent trends in the magnitude of precipitation extremes (R95p) with both decreases (Chou et al., 2014a). And increases (Giorgi et al., 2014) found.	*Medium confidence*: Robust drying trend in Chile (30-48°S) (Saurral et al., 2017; Boisier et al., 2018)	*Low confidence*: Anthropogenic forcing responsible for drying signal in Chile (Boisier et al., 2018).	*Low confidence*: Increase in CDD (Chou et al., 2014a; Giorgi et al., 2014).

South America Monsoon (SAM)	*Medium confidence*: Decrease in the frequency of cold extremes - TN10p (Donat et al., 2016a). Increase in the frequency and length of heat waves (Bitencourt et al., 2016).		*High confidence*: Increase in the frequency of warm extremes: TX90p, and TN90p and decrease in the frequency of cold extremes: TX10p, and TN10p (López-Franca et al., 2016).	*Low confidence*: Mostly increases in extreme precipitation (RX1day, R95p, R99p) (Skansi et al., 2013).	*Medium confidence:* Increase in extreme precipitation with warming (Li et al., 2019)	*Low confidence*: Inconsistent trends in the magnitude of precipitation extremes (R95p) with both decreases (Chou et al., 2014a). and increases (Giorgi et al., 2014) found.	*Low confidence*: Mostly increases in the frequency of CDD (Skansi et al., 2013).		*Medium confidence*: Mostly increase in the frequency of CDD (Chou et al., 2014a; Giorgi et al., 2014). Drier conditions related to a decrease in water availability (Zaninelli et al., 2019).
South Eastern South America (SES)	*High confidence*: Increase in the frequency of warm extremes and decrease in the frequency of cold extremes over most of SES (Skansi et al., 2013), especially in October and November (Rusticucci et al., 2017). Decrease in warm extremes (TXx) over south western SES (Skansi et al., 2013; Donat et al., 2016a; Wu and Polvani, 2017), mainly during summer (Rusticucci et al., 2017). Increase in intensity and in frequency of heat waves (Barros et al., 2015; Bitencourt et al., 2016; Ceccherini et al., 2016).	*Low confidence*: Anthropogenic forcings increased the risk of the Argentinian heat wave of Dec/2013 (Hannart et al., 2015). Over Southeast Brazil, the observed warming trend is mostly attributed to greenhouse gases (Abreu et al., 2019).	*High confidence*: Increase in the frequency of warm extremes: TX90p, and TN90p and decrease in the frequency of cold extremes: TX10p, and TN10p (López-Franca et al., 2016).	*High confidence*: Increase in the magnitude (Wu and Polvani, 2017)(Barros et al., 2015)(Lovino et al., 2018)and frequency (Zandonadi et al. 2016;Valverde and Marengo 2014)of extreme precipitation in many regions	*Medium confidence*: Anthropogenic climate change has increased the risk of the April-May 2017 extreme rainfall in the Uruguay River basin (de Abreu et al., 2019). Increase in extreme precipitation with warming (Li et al., 2019)	*Medium confidence*: Increase in the magnitude (R95p) (Chou et al., 2014a; Giorgi et al., 2014) and frequency (RX5day) (Kitoh et al., 2011) of precipitation extremes	*Low confidence*: Inconsistent trends in annual CDD with both decreases (Rivera et al., 2013). and increases noted (Skansi et al. 2013;Valverde and Marengo 2014).		*Medium confidence*: Mostly decreases in CDD (Chou et al., 2014a; Giorgi et al., 2014). Tendency toward wetting in SES(Zaninelli et al. 2019;Menéndez et al. 2016; Mourão et al. 2016).
Southern South America (SSA)	*Medium confidence*: Increase in the frequency of warm extremes: TX90p, TN90p, and WSDI and decrease in the frequency of cold		*High confidence*: Increase in the frequency of warm extremes: TX90p, and TN90p and decrease in the	*Low confidence*: Increase in maximum precipitation extremes (Skansi et al., 2013).	*Low confidence*: Antropogenic forcing partially explains the precipitation	*Low confidence*: Increase in the magnitude of precipitation extremes (R95p) (Giorgi et al., 2014).	*Low confidence*: Decrease in CDD (Skansi et al., 2013).		*Low confidence*: Projected decreasing in CDD (Giorgi et al., 2014). Drier conditions related to a decrease in

	extremes: TX10p, and TN10p. Increase in the magnitude of temperature extremes (TXx, TXn, TNn and TNx) (Skansi et al., 2013).		frequency of cold extremes: TX10p, and TN10p (López-Franca et al., 2016).		changes observed in southern Andes (Vera and Díaz 2015;Li et al., 2019)				water availability (Zaninelli et al., 2019).

[END TABLE 11.7 HERE]

[START TABLE 11.8 HERE]

Table 11.8: Regional assessments for Europe

	Temperature extremes			Precipitation extremes and flooding			Droughts		
	Observed trends	Detection and attribution; event attribution	Projections	Observed trends	Detection and attribution; event attribution	Projections	Observed trends	Detection and attribution; event attribution	Projections
Greenland/Iceland (GIC)	*Medium confidence:* Increase in frequency and magnitude of warm extremes, decrease in frequency and severity of cold extremes (Mernild et al., 2014; Donat et al., 2016a; Sui et al., 2017)		*High confidence* Increase in the frequency and magnitude of warm extremes and decrease in frequency and severity of cold exremes (Sillmann et al., 2013b; Kharin et al., 2018; Wehner et al., 2018b)			*Medium confidence:* Increase in precipitation extremes (Sillmann et al., 2013b; Kharin et al., 2018)			
North Europe (NEU)	*High confidence*: Strong increase in extreme winter warming events	*High confidence*: Attribution studies of	*High confidence*: strong decrease in heating degree days (Spinoni et	*High confidence*: Change in flood seasonality in Scandinavia (Matti et	*High confidence*: Wet summer of 2012 not	*High confidence*: Reduction of flows from snow melt but increase river flow	*High confidence*: No important changes in drought severity	*Medium confidence*: Decrease of dry years in	*Low confidence*: Increase in droughts in

	(Matthes et al., 2015; Vikhamar-Schuler et al., 2016).	temperature extremes in Central England (King et al., 2015; Roth et al., 2018). *High confidence*: Cold winter of 2009/2010 has become less likely due to anthropegenic climate change(Otto et al., 2012)(Massey et al., BAMS 2012, (Christiansen et al., 2018)). *Low confidence*: evidence of detectable circulation change attributable to climate change (Nilsen et al., 2017).	al., 2018a). *Medium confidence:* Frequent ice-free arctic summers projected even under moderate warming scenarios (Laliberté et al., 2015; Sigmond et al., 2018).	al., 2017). Extreme rainfall trends are different depending on season(Irannezhad et al., 2017). Evidence for more extreme precipitation in summer and winter but not other seasons (Yiou and Cattiaux 2013, BAMS, Dong et al. 2013 BAMS, (Held and Soden, 2006; Grams et al., 2014; Madsen et al., 2014; Helama et al., 2018). *Medium confidence*: Snow cover is declining but by how much and how it effects large scale teleconnections not straightforward (Cohen et al., 2014; Bokhorst et al., 2016). High confidence: Increased extreme snow-melt events (Hansen et al., 2014; Pedersen et al., 2015)	attributable to climate change (Schaller et al., 2014; Otto et al., 2015c; Wilcox et al., 2018). *High confidence:* Recent extreme wet winters are attributable to climate change (Schaller et al., 2016; Vautard et al., 2016; Otto et al., 2018b).	through increased precip(Madsen et al., 2014; Donnelly et al., 2017; Thober et al., 2018). *High confidence:* Shift of strong ETCs and ARs closer to Scandinavia (Ramos et al., 2016; Romero and Emanuel, 2017).	based on different metrics (Orlowsky and Seneviratne, 2013; Spinoni et al., 2014, 2017; Dai et al., 2018). *High confidence*: Small changes in drought frequency (Kay et al., 2018)	Scandinavia (Gudmundsson and Seneviratne, 2016).	Northern Scandinavia (Spinoni et al., 2018b) *Medium confidence:* decrease in droughts in NEU (Spinoni et al., 2015).
Central Europe (CEU) (without Alps)	*High confidence*: Increase in the maximum temperatures and the frequency of heat waves. Consistent signal among studies and regions (Twardosz	*High confidence*: Human-induced climate change has contributed to the increase in the frequency and intensity of short-term heat	*High confidence*: Increase of extreme temperatures and increased frequency of heat waves similar to 2003 and 2010 (Lau and Nath,	*Medium confidence*: Increase of extreme precipitation events. Large discrepancies among studies and regions and strong seasonal differences (Croitoru et al., 2013; Willems, 2013;	*Low confidence*: Attribution of extreme wet events to human climate signal (Wilcox et al., 2018).	*Medium confidence*: Increase in extreme precipitation events, although important seasonal differences (Rajczak et al., 2013; Rajczak and Schär,	*High confidence*: No relevant changes in the frequency of dry spells (Zolina et al., 2013) and in drought severity (Orlowsky and Seneviratne,	*Medium confidence*: Attribution of the 2017 drought event to climate change (García-Herrera et al., 2018).	*Low confidence*: Drought projections in central Europe based on precipitation (Orlowsky and Seneviratne, 2013). *High confidence:* drought projections

	and Kossowska-Cezak, 2013; Shevchenko et al., 2014; Christidis et al., 2015; Scherrer et al., 2016).	waves and heat stress (Sippel et al., 2017, 2018a).	2014; Russo et al., 2015; Vogel et al., 2017; Lhotka et al., 2018; Rasmijn et al., 2018).	Casanueva et al., 2014; Roth et al., 2014; Fischer et al., 2015).		2017; Tölle et al., 2018)	2013; Cook et al., 2014a; Spinoni et al., 2017).		based on soil moisture and drought indices (Lehner et al., 2017; Zhao and Dai, 2017; Dai et al., 2018; Samaniego et al., 2018).
Alps	*High confidence*: Increase in temperature extremes (Gobiet et al., 2014; Stoffel and Corona, 2018). *High confidence:* Strong increase in heatwave duration and intensity and decrease in cold spells (Brugnara et al., 2016)		*High confidence*: Projected increase in temperature extremes in all seasons (Gobiet et al., 2014).	*High confidence*: Negative trends in snow cover below 2000m (Beniston et al., 2018) and glaciers (Gardent et al., 2014; Fischer et al., 2015; Roudier et al., 2016; Beniston et al., 2018). *Medium confidence:* increase in Rain on snow events that lead to flood (Beniston and Stoffel, 2016). *Low confidence:*floods increase (Roudier et al., 2016).		*High confidence*: Intensity of precipitation extremes increase in all seasons (Gobiet et al., 2014) particularly winter (Fischer et al., 2015). *Medium confidence:* flood increase(Roudier et al., 2016) despite declining snow amounts (Frei et al., 2018; Hanzer et al., 2018). *High confidence:*Elevation increase of the snow lines (Beniston et al., 2018)(Marty et al., 2017). *Medium confidence:* decrease in snowfall extremes (Vries et al., 2014). *Medium confidence:* Changes in rainfall seasonality (Brönnimann et al., 2018)	*Medium confidence*: Wet days decrease in summer, (Gobiet et al., 2014). Runoff decreases in particular in summer (Hanzer et al., 2018).		*Medium confidence*: Decrease in wet days in summer projected to continue (Fischer et al., 2015). *Mediumconfidence*: Drought probabilities increase in summer (Haslinger et al., 2016)
Mediterranean (MED)	*High confidence*: Increase of heat waves, tropical nights with few	*High confidence*: Human attribution of	*High confidence*: Projected increase in summer heat	*Medium confidence*: Evolution of precipitation events, with strong regional	*Medium confidence*: Extreme events	*Low confidence*: Increase of extreme precipitation events. High spread between	*High confidence*: Increased dryness caused by an increase in	*Medium confidence*: Attribution of the 2014 eastern	*High confidence*: Increase of climatic and hydrological droughts based on

*See Africa table for portions of this region in Africa	differences among studies and regions, No important differences between West and East Mediterranean (Croitoru and Piticar, 2013; El Kenawy et al., 2013; Christidis et al., 2015; Nastos and Kapsomenakis, 2015; Fioravanti et al., 2016; Kawase et al., 2016; Ruml et al., 2017; Türkeş and Erlat, 2018)	extreme temperature events (Sippel and Otto, 2014; Wilcox et al., 2018).	waves and maximum temperature extremes (Nastos and Kapsomenakis, 2015; Ozturk et al., 2015; Schoetter et al., 2015; Cardoso et al., 2019).	differences even at the local scale. Dominant decrease in the Western Mediterranean and some increase in Eastern Mediterranean (Rajczak et al., 2013; Casanueva et al., 2014; de Lima et al., 2015; Gajić-Čapka et al., 2015; Sunyer et al., 2015; Pakalidou and Karacosta, 2018; Ribes et al., 2019).	associated to natural variability (Añel et al., 2014; U.S. Department of Agriculture Economic Research Service, 2016).	studies and regions (Argüeso et al., 2012; Rajczak et al., 2013; Patarčić et al., 2014; Paxian et al., 2014; Monjo et al., 2016; Zollo et al., 2016; Samuels et al., 2018)	atmospheric evaporative demand and increase of hydrological droughts (Cook et al., 2014a; Ozturk et al., 2015; Roudier et al., 2016; Gudmundsson et al., 2017; Stagge et al., 2017; González-Hidalgo et al., 2018).	Mediterranean drought events to climate change (Bergaoui et al., 2015).	precipitation, soil moisture, runoff and drought indices (Orlowsky and Seneviratne, 2013; Cook et al., 2014a; Prudhomme et al., 2014; Schewe et al., 2014; Ozturk et al., 2015; Dai et al., 2018; Samaniego et al., 2018).
EEU (move to Europe table)	*High confidence:* Increase in frequency and magnitude of warm extremes, decrease in frequency and severity of cold extremes (Donat et al., 2016a; Zhang et al., 2019c; Dunn et al., submitted)		*High confidence:* Increase in the frequency and magnitude of warm extremes and decrease in frequency and severity of cold exremes (Sillmann et al., 2013b; Kharin et al., 2018; Wehner et al., 2018b; Khlebnikova et al., 2019a)	*Low confidence:* Increase in extreme precipitation (Donat et al., 2016a; Dunn et al., submitted) but can vary spatially (Ashabokov et al., 2017)		*Medium confidence:* Increase in precipitation extremes (Sillmann et al., 2013b; Kharin et al., 2018; Khlebnikova et al., 2019b)	*Low confidence:* Increase in CDD and number of dry days (Khlebnikova et al., 2019b)		*Low confidence:* Increase in CDD (Khlebnikova et al., 2019b)

[END TABLE 11.8 HERE]

[START TABLE 11.9 HERE]

Table 11.9: Regional assessments for North America

	Temperature extremes			Precipitation extremes and flooding (including effects of TC, ETC and atmospheric rivers)			Droughts, dryness and aridity		
	Observed trends	Detection and attribution; event attribution	Projections	Observed trends	Detection and attribution; event attribution	Projections	Observed trends	Detection and attribution; event attribution	Projections
North Central America (NCA)	*High confidence*: Increase in the frequency and magnitude of hot extremes and decrease in the severity of cold extremes (Martinez-Austria and Bandala, 2017; Montero-Martínez et al., 2018; García-Cueto et al., 2019), particularly in the northern arid region		*High confidence*: Increase in temperature extremes and the length of warm spells (Kharin et al., 2013; Sillmann et al., 2013b; Alexandru, 2018; Wehner et al., 2018b)	*Low confidence*: Increase in the frequency and the magnitude of precipitation extremes (Donat et al., 2016a; García-Cueto et al., 2019).		*Low confidence*: Possible decrease in extreme precipitation but uncertainty is high(Sillmann et al., 2013b; Alexandru, 2018).	*Low confidence*: Mostly decrease in the frequency of CDD (Donat et al., 2016a).		*Low confidence:* Increase in duration and intensity of droughts over northern and northwestern Mexico (Feng and Fu, 2013; Escalante-Sandoval and Nuñez-Garcia, 2017).
N. W. North America (NWN)	*High confidence*: Increases in extreme hot temperatures and larger increases in extreme cold temperatures (Vincent et al., 2018; Zhang et al., 2019d).	*Medium confidence*: Most of the observed warming attributed to anthropogenic forcing (Wan et al., 2019).	*High confidence*: Increases in the magnitude and frequency of hot extremes and decreases in the frequency and severity of cold extremes (Bennett and Walsh, 2015; Li et al., 2018d; Zhang et al., 2019d).	*Medium confidence*: No detectable trend in observed annual maximum daily (or shorter duration) precipitation (Shephard et al., 2014; Mekis et al., 2015; Vincent et al., 2018).	*Low confidence*: Anthropogenic climate change increased the likelihood of extreme rainfall like that contributing to the 2013 Alberta flood (Teufel et al., 2017) and other extremes (Kirchmeier-Young and	*High confidence*: Increase in the frequency and magnitude of precipitation extremes (Bennett and Walsh, 2015; Zhang et al., 2019d).	*Low confidence*: Periodic droughts have occurred across much of Canada, but no long-term changes are evident (Bonsal et al., 2019).		*Medium confidence*: Increased drought risk during summer, especially in the south(Swain and Hayhoe, 2015; Bonsal et al., 2019; Tam et al., 2019)

					Zhang, submitted).				
N. E. Canada (NEC)	*High confidence*: Increases in extreme hot temperatures and larger increases in extreme cold temperatures (Vincent et al., 2018; Zhang et al., 2019d)	*Medium confidence*: Most of the observed warming attributed to anthropogenic influence (Wan et al., 2019).	*High confidence*: Increases in the magnitude and frequency of hot extremes and decreases in the frequency and severity of cold extremes(Li et al., 2018d; Zhang et al., 2019d)	*Medium confidence*: No detectable trend in observed annual maximum daily (or shorter duration) precipitation (Shephard et al., 2014; Mekis et al., 2015; Vincent et al., 2018).		*High confidence*: Increase in the frequency and magnitude of precipitation extremes (Zhang et al., 2019d).	*Low confidence*: No long-term changes in drought are evident (Bonsal et al., 2019).		*Medium confidence*: Wetter during spring but drier in summer for much of the region based on SPI (Swain and Hayhoe, 2015) and SPEI (Tam et al., 2019).
C. North America (CNA)	*High confidence*: Increase in the frequency of heat waves and hot extremes and decrease in the frequency of cold waves and cold extremes. Increase in the coldest daily temperature of the year (TNn)(Vose et al., 2017)	*Medium confidence*: Anthropogenic warming detectable over northern regions (Vose et al., 2017) Anthropogenic forcing has increased the risk of many hot events (Vose et al., 2017).	*High confidence*: Increase in temperatures of both extremely warm and extremely cold days. More severe heat waves and less severe cold waves. (Vose et al., 2017; Wehner et al., 2018b).	*High confidence*: Increase in precipitation extremes(Wu, 2015; Easterling et al., 2017). Increase in extreme hurricane rainfall events (Emanuel, 2017; Risser and Wehner, 2017; van Oldenborgh et al., 2017; Trenberth et al., 2018; Wang et al., 2018b).	*Medium confidence*: The probability of extreme precipitation events has increased due to anthropogenic forcing (Easterling et al., 2017; Kirchmeier-Young and Zhang, submitted). The influence of external forcing is detected in the intensification of precipitation extremes over North America (Kirchmeier-Young and	*High confidence*: Increase in precipitation extremes (Easterling et al., 2017) Increase in hurricane rain rates (medium to high confidence) (Knutson et al., 2015; Kossin et al., 2017)	*High confidence*: Drought has decreased over much of the continental United States (Easterling et al., 2017).	*Medium confidence*: Little evidence is found for a human influence on observed precipitation deficits, but much evidence is found for a human influence on surface soil moisture deficits due to increased evapotranspiration caused by higher temperatures. (Easterling et al., 2017)	*High confidence*: Under higher scenarios and assuming no change to current water-resources management, chronic, long-duration hydrological drought is increasingly possible by the end of this century (Easterling et al., 2017). Drier conditions (SPI) over most of U.S. during spring and summer (Swain and Hayhoe, 2015).

					Zhang, submitted) Hurricane Harvey increased rate of occurrence associated with anthropogenic warming (Emanuel, 2017; Risser and Wehner, 2017; van Oldenborgh et al., 2017; Trenberth et al., 2018; Wang et al., 2018b)				
E. North America (ENA)	*High confidence*: Increase in the frequency of heat waves and hot extremes and decrease in the frequency of cold waves and cold extremes. Increase in the coldest daily temperature of the year (TNn)(Vose et al., 2017; Vincent et al., 2018; Zhang et al., 2019d).	*Medium confidence*: Anthropogenic warming detectable over northern regions(Vose et al., 2017; Wan et al., 2019). Anthropogenic forcing has increased the risk of many hot events (Vose et al., 2017)	*High confidence*: Increase in temperatures of both extremely warm and extremely cold days. More severe heat waves and less severe cold waves. (Vose et al., 2017; Wehner et al., 2018b; Zhang et al., 2019d).	*Medium confidence*: Increase in precipitation extremes across the United States (Wu, 2015; Easterling et al., 2017), but no detectable trend in observed annual maximum daily (or shorter duration) precipitation in Canada (Shephard et al., 2014; Mekis et al., 2015; Vincent et al., 2018). *High confidence*: Increase in extreme hurricane rainfall events (Emanuel, 2017; Risser and Wehner, 2017; van Oldenborgh et al., 2017; Trenberth et al., 2018; Wang et al., 2018b).	*Medium confidence*: The probability of extreme precipitation events has increased due to anthropogenic forcing (Easterling et al., 2017; Teufel et al., 2019; Kirchmeier-Young and Zhang, submitted). The influence of external forcing is detected in the intensification of precipitation extremes (Kirchmeier-	*High confidence*: Increase in precipitation extremes (Easterling et al. 2017, Zhang et al. 2018f) Increase in hurricane rain rates (medium to high confidence) (Knutson et al., 2015; Kossin et al., 2017)	*High confidence*: Drought has decreased over much of the continental United States (Easterling et al., 2017).	*Medium confidence*: Little evidence is found for a human influence on observed precipitation deficits, but much evidence is found for a human influence on surface soil moisture deficits due to increased evapotranspiration caused by higher temperatures. (Easterling et al., 2017)	*High confidence*: Under higher scenarios and assuming no change to current water-resources management, chronic, long-duration hydrological drought is increasingly possible by the end of this century (Easterling et al., 2017). Drier conditions (SPI) over most of U.S. during spring and summer (Swain and Hayhoe, 2015).

					Young and Zhang, submitted)				
W. North America (WNA)	*High confidence*: Increase in the frequency of heat waves and decrease in the frequency of cold waves. Increase in the coldest daily temperature of the year (TNn) (Vose et al., 2017).	*Medium confidence*: Anthropogenic warming detectable (Vose et al., 2017).	*High confidence*: Increase in temperatures of both extremely warm and extremely cold days. More severe heat waves and less severe cold waves. (Vose et al., 2017; Palipane and Grotjahn, 2018; Wehner et al., 2018b).	*High confidence*: Increase in precipitation extremes (Easterling et al. 2017; Wu 2015).	*Medium confidence*: The probability of extreme precipitation events has increased due to anthropogenic forcing (Easterling et al., 2017; Kirchmeier-Young and Zhang, submitted) The influence of external forcing is detected in the intensification of precipitation extremes over North America (Kirchmeier-Young and Zhang, submitted)	*High confidence*: Increase in precipitation extremes (Easterling et al., 2017)	*High confidence*: Drought has decreased over much of the continental United States (Easterling et al., 2017).	*Medium confidence*: Little evidence is found for a human influence on observed precipitation deficits, but much evidence is found for a human influence on surface soil moisture deficits due to increased evapotranspiration caused by higher temperatures. (Easterling et al., 2017)	*High confidence*: Under higher scenarios and assuming no change to current water-resources management, chronic, long-duration hydrological drought is increasingly possible by the end of this century (Easterling et al., 2017). Drier conditions (SPI) over most of U.S. during spring and summer (Swain and Hayhoe, 2015).

[END TABLE 11.9 HERE]

[START BOX 11.4 HERE]

BOX 11.4: Reasons for concern related to weather and climate extremes: Informing on changes in extremes supporting related adaptation assessments

The AR5 WG2 chapter 19 (Oppenheimer et al., 2014, IPCC AR5 WG2) included an assessment of risk as function of global warming for five identified “Reasons For Concern” (RFCs). The risk assessment was subdivided in four categories (Box 11.4, Fig. 1): undetectable (white), moderate (yellow), high (red), very high (purple). Very high risk indicates a level of risk at which limits to adaptability may be reached (O’Neill et al., 2017). One of the five RFCs are Risks associated with extreme weather events (RFC2; Box 11.4, Fig.1).

[START BOX 11.4, FIGURE 1 HERE]

Box 11.4, Figure 1:“Reasons for concerns” (RFCs), highlighting RFC2 on “Risks associated with extreme weather events. From Oppenheimer, M. et al (2014), IPCC AR5 WG2).

[END BOX 11.4, FIGURE 1 HERE]

The RFCs have been further developed in the SR1.5, where it has been recognized that even an apparently small increase of +0.5°C of global warming compared to +1.5°C would substantially increase the frequency and severity of extremes (also consistent with more recent analyses, see e.g., Section 11.2.6). In the SROCC two alternative versions of the RFCs have additionally been presented, one under a high adaptation scenario, the other one with current adaptation levels, highlighting the fact that limits to adaptation strongly depend on other factors than just the hazard. Research published since has demonstrated that a key indicator for adaptation and thus limits to it is the governance of a country (Andrijevic et al., 2019). This is very relevant to the Reason For Concern #2 on climate extremes in several respects. For RFC2, “high risk” for global warming at 1.5°C and above was assessed in the IPCC AR5 WG2 (Oppenheimer et al., 2014, IPCC AR5 WG2), but no assessment was provided for a possible transition to “very high risk” at higher warming levels which would correspond to conditions at which societies could no longer adapt. The reason for not assigning this transition was because there was not enough literature at the time to determine the global warming level at which the limits of adaption were reached (Oppenheimer et al., 2014, IPCC AR5 WG2).

While still limited, there is now new literature available to better estimate the reasons for concerns arising from extremes, building on the assessment conducted in this chapter and providing new physical evidence on changes in extremes at different global warming levels. These show large incremental increases in extremes that should inform the assessment of limits to adaptation in the upcoming IPCC AR6 Working Group 2 report (synthesized in Chapter 16 of that report). In particular, there is an emerging body of research on the attribution of extreme weather events occurring today, at 1°C of global warming, highlighting an emerging occurrence of unprecedented events to which societies were not well prepared (Section 11.2.5; see also Box 11.3). Furthermore, new literature on compound events shows the potential risks associated with increased probabilities of multi-variate extremes, e.g., cluster of events and/or extremes happening at the same time/location or affecting similar sectors in different regions simultaneously and that can lead to more impacts than if they had happened in isolation (Section 11.8, Box 11.3). This means that in many regions societies are not adapted to today’s climate (also called “adaptation deficit”) or would be already very challenged. Thus the rate of change poses a crucial barrier to adaptation in particular when the potential to adaptation depends strongly on socio-economic factors such as governance that improve slowly. We note that the adaptation deficit can be expected to be stronger for extreme events, which are rarer and which society has less opportunity to adapt to.

Concretely, this means that even in the most optimistic scenario for socio-economic development, SSP1, many countries would in 2050 live under a government struggling to provide disaster preparedness and thus face difficulties to adapt to changing hazards (Schleussner et al., submitted). At the same time, it is in particular in these countries that extreme events and foremostly heat extremes are strongly emerging already (Harrington and Otto, 2018b), demonstrating that only in SSP1 and with slowly increasing temperatures, necessary adaptation cannot be reached for billions of people. For higher warming levels, e.g., at ca 4°C (RCP8.5), near 75% of the world population could be affected by extreme hot days of up to 5 standard deviations (Lehner and Stocker, 2015). At 4°C of global warming, countries representing more than 70% of the global population and global gross domestic product could also face increases in flood risk in excess of 500% (Alfieri et al., 2017).

These assessments only focus on one type of extreme events occurring. As highlighted in Section 11.8 and Box 11.3, further research shows that several locations under moderate warming levels could be affected simultaneously, or very repeatedly by different types of extremes (Mora et al., 2018, Gaupp et al., 2019; Vogel et al. 2019)Box 11.3 shows that concurrent events at different locations, which can lead to major impacts across the world, can also result from the combination of anomalous circulation or natural variability (ENSO) patterns with amplification of resulting responses by human-induced global warming. Also multi-variate extremes at single locations pose specific challenges to adaptation (Section 11,8), whereby the probability of occurrence of such compound events strongly increases with increasing global warming levels (Vogel et al., submitted, a). Therefore, in order to estimate whether and at what level of global warming very high risks arising from extremes would occur that could challenges limits to adaptation, the spatial extent of extremes and the potential of compounding extremes need to be assessed. Sections 11.3, 11.7 and 11.8 highlight increasing evidence that temperature extremes, higher intensity precipitation accompanying tropical cyclones, and compound events such as dry/hot conditions conducive to fire or storm surges resulting from sea level rise and heavy precipitation events, pose widespread threats to societies already at relatively low warming levels. Studies have already shown that the probability for some recent extreme events is so small in the undisturbed world such that such that these event may not have been possible without human influence (Section 11.2.6). With additional warming, such events would become more frequent and wide spread. Some recent extreme heat events that are historical have become once in 5 years event in the current climate and will become annual event with an additional 1°C of global warming (Sun et al., 2018a). There is robust evidence that the magnitude of extreme temperature and precipitation increases proportionally to the level of global warming (Section 11.2.6; Section 11.3, 11.4).

Recent literature also provides a better understanding of impacts of extremes on different sectors. This includes impacts on :

- health (Ayeb-Karlsson et al., 2019)
- food security, for instance through the concomitant impacts of extremes on several breadbaskets (Gaupp et al., 2019; Zampieri et al. 2017)
- unique and threatened systems, e.g., through the strong increase in marine heatwaves (Frölicher, et al., 2018)

This new evidence shows that changes in extremes lead to high risks for a large number of people, even at low levels of global warming. It remains however the case, that the evidence of changing hazards is highly uncertain in particular in those areas where vulnerability and exposure are high (Otto et al. submitted). While the identification of the exact thresholds at which extremes could exceed the limits of adaptation will be addressed in the IPCC AR6 Working Group 2 report, it is important that this assessment considers the new dimensions of risks associated with climate extremes assessed in the most recent literature, as well as the available evidence regarding how extremes are changing at different global warming levels (Box 11.4, Table1; see also Section 11.2.6 and Table 1.1).

[START BOX 11.4, TABLE 1 HERE]

Box 11.4, Table 1: Examples of changes in extreme conditions (single extremes, compound events) potentially challenging adaptation at different global warming levels

	+1°C (present-day)	+1.5°C	+2°C	+3°C	+4°C
Risk ratio for annual hottest daytime temperature (TXx) with 1% of probability under present-day warming (+1°C) (Kharin et al., 2018): Global land	1	3.3 (i.e. 230% higher probability)	8.2 (i.e. 720% higher probability)	Not assessed	Not assessed
Risk ratio for heavy precipitation events (Rx1day) with 1% of probability under present-day warming (+1°C) (Kharin et al., 2018): Global land	1	1.2 (i.e. 20% higher probability)	1.5 (i.e. 50% higher probability)	Not assessed	Not assessed
Probability of "extremes extremes" hot days with 1/1000 probability at the end of 20th century (Vogel et al., submitted, a): Global land	~20 days over 20 years in most locations	about ~50 days in 20 years in most locations	about ~150 days in 20 years in most locations	about ~500 days in 20 years in most locations	Not assessed
Probability of co-occurrence in the same week of hot days with 1/1000 probability and dry days with 1/1000 probability at the end of 20th century (Vogel et al., submitted, a): Amazon	0% probability	~1 week within 20 years	~4-5 weeks within 20 years	>9 weeks within 20 years	Not assessed
Projected soil moisture drought duration per year (Samaniego et al., 2018): Mediterranean region	41 days (+46% compared to late 20th century)	58 days (+107% compared to late 20th century)	71 days (+154% compared to late 20th century)	125 days (+346% compared to late 20th century)	Not assessed

[END BOX 11.4, TABLE 1 HERE]

[END BOX 11.4 HERE]

[START BOX 11.5 HERE]

BOX 11.5: Climate extremes in small islands territories

(James Kossin, Sergio Vicente-Serrano, and other authors)

In general, paleoclimatic reconstructions show that small island territories have been substantially affected by floods and droughts (De Boer et al., 2014; Lane et al., 2014; Margalef et al., 2014; de Boer et al., 2015) and human communities have developed strategies to cope with extreme climate events that have been passed on over generations (McNamara and Prasad, 2014; Weir et al., 2017). Climate change could dramatically reduce the capacity of the current adaptive measures and force large migrations (Weir et al., 2017). This is already observed in some small islands that experience recurrent freshwater crises (Pearce et al., 2018).

In the small islands of the Pacific, drought is a major natural hazard given their precarious water resources. In these islands, groundwater is the main freshwater source, which strongly depends on rainfall variability (Post et al., 2018). Pumping of groundwater plays an additional role by increasing the salinity of the aquifer and reinforcing the negative effects of droughts. In 54% of the Marshall Islands, Barkey and Bailey (2017) showed a high vulnerability of groundwater to drought episodes. Bailey *et al.* (2016) projected a 20% in groundwater availability by 2050 in Coral Atoll islands of the Federal States of Micronesia, but stressed that under high sea level rise the decrease can be higher than 50% because the intrusion of marine water in the aquifer, as well as drought events, increases the salinity of the freshwater sources. Groundwater resources are expected to be substantially reduced in other small island territories such as the Maldives, in which Bailey *et al.* (2015) projected by 2030 a reduction of 34% as a consequence of more severe drought events. This is consistent with global models that project a dramatic increase of dry conditions in the small islands of the central Indian Ocean, associated with increased frequency of extreme Indian Ocean dipole events. The frequency of dry events could change from one event every 17.3 years to one event every 6.3 years at the end of the twenty-first century (Cai et al., 2014c).

Other studies have analysed recent drought trends in small island territories worldwide based on meteorological observations. McGree *et al.* (2016) analysed a vast territory in the West Pacific region covering a large number of archipelagos using the Standardized Precipitation Index (SPI) and other meteorological metrics from 1951 to 2010. The main finding was the strong spatial variability between the different archipelagos, with strong decadal variability of droughts controlled by the Interdecadal Pacific Oscillation and interannual variability largely determined by ENSO, but no significant trends (Ludert et al., 2018). McGree *et al.* (2016) found a robust strong positive trend in the drought frequency and severity in the Hawaiian islands, in agreement with studies that have analysed precipitation trends. In Hawaii, Frazier and Giambelluca (2017) showed that between 1920 and 2012, over the 90% of the islands showed a rainfall reduction, which has caused a clear decrease in the canopy greenness (Barbosa and Asner, 2017), and a streamflow decrease and increase in the frequency of zero flow days (Strauch et al., 2015). In the Caribbean Islands, Herrera and Ault (2017) developed a Palmer Drought Severity Index (PDSI) dataset from 1950 to 2016 and showed a clear drying trend in the region. The 2013-2016 period showed the most severe drought during the period and it is suggested that this event was strongly related to anthropogenic warming, which would have increased the severity of the event by 17% and the spatial extent by 7% (Herrera et al., 2018). These trends in the Caribbean are consistent with future projections. Karmalkar *et al.* (2013) analysed drought projections in the Caribbean islands using CMIP3 models and found evidence for an increase in drought severity at the end of the century, mainly due to precipitation decrease during the early wet season. Trends are also observed in Atlantic Islands, as in Madeira, where there have been changes in drought severity with a trend toward more frequent and severe drought episodes since 2001 (Espinosa et al., 2019). The drought that affected this island in 2012 was the most extreme in the last 150 years (Liberato et al., 2017). Studies have also found drought trends in Mauritius (Dhurmea et al., 2019), and the Fiji islands (Kumar et al., 2014).

There are limited studies of coastal flooding trends in small island territories, although the existing studies suggest an increased risk as a consequence of sea level rise. This would increase the flood intensity associated with wind-waves and tropical and extra-tropical storms. Examples of this increased risk are found in the Maldives (Wadey et al., 2017), the Solomon (Albert et al., 2016) and the Pacific islands in general (Hoeke et al., 2013). Recent unprecedented coastal floods were recorded in December 2008 in the Marshall islands (Merrifield et al., 2014; Gingerich et al., 2017). Future projections show robust increases in hazard probability of extreme wave events and related floods in small islands. For example, Shope *et al.* (2016) suggested that islands of the Western Tropical Pacific will experience a noticeable increase of coastal flooding events at the end of the twentieth century under the RCP 8.5 scenario.

River flood trends in small island territories are much more difficult to assess due to limited data in these island sub-regions, and there are very few studies on this topic. McAneney *et al.* (2017) analysed 122-year flood depths in the Ba river on Viti Levu Island (Fiji) using data from a colonial sugar refining company and although they found high interannual variability with strong control by ENSO, they did not find significant trends in the frequency and magnitude of floods. Nevertheless, unprecedented flash flood events have been observed in small island territories. A representative example was the flood recorded on 20 October 2011 in the Sumiyo river basin in the Amami Oshina Island (Subtropical Japan), when 130 mm of rain was reported over two hours, which caused unprecedented flood inundation accompanied by landslides and debris flows (Hashimoto et al., 2013).

Many small island territories experience tropical cyclone (TC) impacts (Gould et al. 2018; Keener et al. 2018). These impacts can be beneficial (as important contributions to freshwater supplies) or deleterious (e.g., damage and mortality from extreme wind and storm surge). Sea level rise is expected to compound the effects of TC surge events impacting small island territories. In general, TCs are expected to become stronger and produce more flooding rain with warming, both of which will increase TC risk, but the detailed effects of climate change on TCs vary by region (Knutson et al. 2019 and Section 11.7.1). For example, projected warming of sea surface temperature (SST) in the tropical North Atlantic (tNA), which intensifies TC wind and rainfall, is expected to be accompanied by increased vertical atmospheric wind shear (Vecchi and Soden 2007; Ting et al. 2019) in the tNA, which offsets the effects of warming SST. Additionally, the mean position where TCs reach peak intensity migrates poleward as the tropics expand due to warming (Kossin et al. 2014; section 11.7.1), which may decrease TC exposure in small island territories in the tropics. In summary, the effects of climate change on TCs is expected to increase impacts on small island territories, but these increases are expected to vary by region.

[SUMMARY TO BE ADDED FOR FGD]

[END BOX 11.5 HERE]

11.10 Limits to the assessment

There are some remaining areas associated with knowledge gaps in extremes research at present. Some topics are still unsufficiently investigated such as hail. Also, possible changes associated with global and regional tipping points (high-risks low-probability events) are associated with *low confidence*, but cannot be excluded, especially at high global warming levels (>3°C). Finally, there are still remaining important observational gaps in several world’s regions, in particular in Africa.

Frequently Asked Questions

FAQ 11.1: How do changes in climate extremes compare with changes in climate averages?

Climate extremes, such as heat waves and extreme precipitation events, can significantly impact ecosystems and societies, so it is important to understand how global warming may alter the frequency and severity of such events. For near-surface temperature, increases in extreme heat events are expected to be larger in magnitude extremes will occur on the backdrop of global mean warming.

One way to illustrate both averages and extremes for a given aspect of climate or weather (e.g., extreme heat relative to average temperature) is by showing a probability density function (PDF), which approximates the relative frequency of occurrence of the full range of possible values for a given variable, such as daily maximum temperatures. The extreme values at either end of the PDF may have much lower probabilities, and would thus be rare events. In the case of near-surface temperature, the distribution of observed temperatures is commonly approximated by the familiar bell curve, or Gaussian PDF—this is a symmetric distribution where both low and high extreme values are equally likely (FAQ 11.1, Figure 1.a). Precipitation, however, is usually better approximated by a distribution with a skewed shape—one that is asymmetrical, where extremes with low precipitation amounts occur with a greater probability than high-precipitation extremes (FAQ 11.1, Figure 1.b).

In this context, changes can be viewed in terms of how the shape and average values of a PDF for a given aspect of climate change as a result of global warming. For example, Figure 1 illustrates hypothetical PDFs for temperature and rainfall and how those distributions might change in the future compared to historical conditions. As shown in the figure, the probability of a historical extreme may change as a result of a simple shift in the average, but it is also possible that the variability or shape of the distribution may change in more complex ways

Climate model simulations show that, at local scales, changes in the daily temperature PDF are dominated by a shift in which all values, including the mean and the extremes, are displaced towards warmer temperatures. In most places, land regions warm more than global average. These changes arise due to both the increase of greenhouse gases and local processes that can either amplify or offset the overall warming influence of increasing greenhouse gase concentrations. As a result, changes in local mean temperatures can vary greatly across regions and throughout the year, though most land regions warm more than the global average. In some cases, local processes may have little effect on changes in average conditions but can influence extreme events when they are moderated or exacerbated by specific weather conditions. For example, daily hot extremes can be more likely or more severe in situations where there is limited availability of soil moisture. Also changes in surface albedo (the fraction of incoming solar energy reflected by the surface) have been shown to have more effect on hot extremes than on average temperatures. This is because there tends to be more incident shortwave radiation on hot days, so an increased surface reflectivity associated with higher albedo will result in a stronger net cooling.

Likewise, the absence of increases in the maximum temperatures observed on hot days may be explained by processes affecting extremes rather than averages. Notably, the absence of warming in India has been ascribed to cooling from increased concentrations of aerosols (small particles in the atmosphere) as a result of burning fossil fuels and in the U.S. Midwest to local land management practices, including irrigation and cropland intensification.

Rainfall changes are generally more complicated than a simple shift in the distribution and also result from the combined effects of various processes occurring at different temporal and spatial scales. FAQ 11.1, Figure 1.b illustrates a case where the future PDF is more skewed (that is, more asymmetrical) than the historical PDF, with a larger mean value together with a higher probability of heavy precipitation events and a lower probability of light precipitation events. Heavy precipitation events are expected to increase in severity and frequency in a warming climate because water vapour increases 7% for every degree Celsius increase in surface temperature, meaning there is more water available to fall as precipitation.

However, at regional scales, changes in the dynamics of the climate system, including atmospheric circulation, can modulate, or even reverse the increases in extreme precipitation. Annual average precipitation amounts will only increase at rates of about 2–3% per degree Celsius of warming due to limitations from the rate at which the associated energy dissipates in the atmosphere, mostly at global scales.

[START FAQ 11.1, FIGURE 1 HERE]

FAQ 11.1, Figure 1: *Schematic representations of the probability density function of (a) daily temperature, which tends to be approximately Gaussian, and (b) daily precipitation, which has a skewed distribution. Solid lines represent a previous (historical) distribution and dashed lines a changed (future) distribution. The probability of occurrence, or frequency, of extremes is denoted by the shaded areas. In the case of temperature (red and blue shade), changes in the frequencies of extremes can be affected either by changes only in the mean, or average (shift) or in both the mean and the variance, or shape (shift+var). For example, the wider distribution of the shift+var case means that both cold and warm extremes are more common relative to the average than in the historical or future (shift) cases. But combined with the increase in average, this increase in variability means a higher probability of extremely warm temperatures compared to the future (shift) case, where the variability does not increase. Similarly, in a skewed distribution such as that of precipitation (green shaded), a change in the mean of the distribution generally affects its variability or spread, and thus an increase in mean precipitation would also imply an increase in heavy precipitation extremes, and vice-versa. In addition, the shape of the right-hand tail could also change, affecting extremes. Furthermore, climate change may alter the frequency of precipitation and the duration of dry spells between precipitation events. (Parts a–c modified from Folland et al., 2001, and modified from Peterson et al., 2008, as in Zhang and Zwiers, 2012.)*

[END FAQ 11.1, FIGURE 1 HERE]

FAQ 11.2: Could unprecedented extremes occur as a result of human-induced climate change?

As the climate changes, associated unusual or extreme events will also change. Future extreme events will be similar to those experienced in the past, but some will occur with much larger magnitudes than before and some events will occur much more frequently, possibly resulting in events or impacts that are unprecendented. Some locations may experience events (such as wildfires) not previously observed in those areas, with possible concerns for impacts on human and natural systems. The occurrence of multiple extreme events simultaneously or in close succession may also change the severity of events and impacts relative to what has been experienced in the past.

Human and natural systems have generally adapated to the climate of the last few decades and centuries, where extreme and rare events occured. As human-induced changes shift the climates of the future, the climate moves away from the state to which local human and natural systems are currently adapated. Extreme events already test, and sometimes exceed, the limits of those human and natural systems, so changes in the frequency or severity of some types of extreme events may result in different impacts than in the past.

In a warmer climate, extreme events may occur with differing characteristics to what we have experienced in the past. Characteristics of the same events types (e.g., heatwaves, floods or droughts) may change: future extremes may be more severe, may occur more frequently or may occur for differing durations.
We have experienced heatwaves in the past and we will experience heatwaves in the future, but in a warmer climate, the heatwaves will generally have hotter temperatures and last longer than past heatwaves. For example, the 2013 severe heatwave event in China today is projected to occur, of be exceeded, in 50% of future summers in even the moderate RCP4.5 scenario.

Human-induced changes could result in extreme events that have unprecedented impacts. However, the impact of an event depends not just on its physical attributes but also on the exposure and vulnerability of systems, and these may also change. Changes in heat extremes in the future, for example, could lead to unprecedented severity or duration of heat events and coral reef bleaching in novel locations. Coral reef heat stress depends on the magnitude and duration of temperatures above a certain threshold. Either a short-duration, high-magnitude event or a long-duration, lower-magnitude event can cause bleaching. Such impact thresholds also exist for human and animal physiologies, suggesting that some new climates may lead to serious health concerns. While these extreme events types (e.g., heatwaves) are similar to those already experienced, future extreme events may be considered a new type of event because of their unprecedented impacts.

Compound events – where multiple hazards combine to elevate risks and impacts – are also an important consideration for future extremes and unprecedented impacts (FAQ 11.2, Figure 1). For example, the occurrence of drought combined with extreme heat will increase the risk of wildfires and agriculture losses. Another example is a drought followed by extreme rainfall, which exacerbates the runoff as well as introducing multiple impacts. A changing climate may alter the interaction between hazards or result in the combination of multiple unprecedented events. It is possible that compound events will exceed the adaptive capacity or resilience of the human and natural systems more quickly than individual events. The result could include types or levels of impacts (societal, economic, ecological, etc.) not seen at all previously.

There is also the possibility of the future occurrence of extreme events that have not been anticipated. In many regions, observational data are limited to 50–60 years, which means that we may not have a complete understanding of what sort of extremes (such as the hottest maximum temperatures or the maximum amount of rainfall) are possible for some areas, even in a stable climate. The shortness of the observational record may mean that events that are very rare, but not impossible, are difficult to anticipate or plan for. When such rare or unprecedented extreme events occur, they may be suprising and have particularly large impacts. As warming continues, the climate moves further away from the historical state that we are familiar with, and unprecedented or suprising events, become more likely. Additionally, landscapes that are changing rapidly or at risk of crossing important thresholds, such as areas currently covered by perennial ice or permafrost, may be at higher risk of unique or locally unprecedented events.

[START FAQ 11.2, FIGURE 1 HERE]

FAQ 11.2, Figure 1: Illustration of enhanced risks associated with compound events (from Zscheischler et al., 2018b), The hypothetical present-day distribution of two climatic drivers and their potential future distribution, together with a critical region in which impacts are induced. Continuous lines depict the 50th and 80th percentiles, dashed lines denote the 95th percentiles. The coloured points denote different possibilities to generate potentially critical events. The critical region is shown in orange with a blurred border to illustrate uncertainty in the estimation of its extent. The critical region can only be known if enough critical events have occurred (or can be simulated) to characterize it. This figure illustrates that climate change is modifying the envelope of the distribution of climate extremes we have at the moment, which possibly could yield new unprecedented extremes which are within some "critical region" in which new impacts could happen.

[END FAQ 11.2, FIGURE 1 HERE]

FAQ 11.3: Did climate change cause that recent extreme event in my country?

The climate and weather we experience varies from day to day and from year to year. As a result, we have always experienced extreme weather and climate events. However, there is strong evidence that characteristics of many individual extreme events have already changed because of human driven changes to the climate system. Some types of highly impactful extreme weather events have occurred more often and have become more severe due to these human influences. As the climate continues to warm, the frequency or severity of some extreme weather events will continue to change as the human influences on these events increase.

Many factors contribute to the occurrence of complex, rare events. Attributing the causal influence of climate change on current extreme weather events requires considering both natural and human influences. Recent developments have allowed scientists to quantify the human influence on the magnitude or frequency of specific extreme weather events. For a wide variety of recent extreme weather events, an influence from global warming has been demonstrated. Borrowing methods from epidemiology, this influence is often expressed as a change in the likelihood of an extreme event of the observed magnitude and/or as a change in the magnitude of the event for a fixed estimated probability of occurrence.

[START FAQ 11.3, FIGURE 1 HERE]

FAQ 11.3, Figure 1: Examples of how temperature extremes differ in cooler and warmer climates. Changes in extreme events can be thought of as either changes in the frequency of events of a given magnitude or as changes in the magnitude of events that occur at the same frequency. These two concepts are closely related, as illustrated in this example for (a) hot extremes and (b) cold extremes. The vertical axis shows the range of extreme temperatures on a logarithmic scale, while the horizontal axis shows the estimated average time between events, referred to as the return period of an event. In a warmer climate, extreme hot events of the same magnitude occur more frequently (that is, the return period for a given temperature decreases) and cooler events occur less frequently (return period increases) as indicated by the horizontal arrows between curves. If we look at events of a fixed rarity (constant return period), we see that in a warmer climate, both hot and cold extreme temperature events of a given return period are warmer (vertical arrows), although not necessarily by the same amount.

[END FAQ 11.3, Figure 1 HERE]

The change in temperature extremes as the climate warms is illustrated in FAQ 11.3, Figure 1: a depiction of the magnitude of extreme temperature events versus their frequency. Both cooler and warmer worlds experience hot and cold temperature extremes, but with different frequencies and magnitudes. In a warmer climate, the cold events of a given temperature occur less often than in the cooler climate, while hot events of a given temperature occur more frequently. For example, a "once every 50 years" cold event in the cooler climate is more rare in the warmer climate, while the "once every 50 years" hot event is less rare. Similarly, when comparing the magnitude of events of a constant rarity between these two worlds, both hot and cold temperature events are warmer in the warmer world.

Many individual heat waves and extreme precipitation events have been intensified by human changes to the composition of the atmosphere. The causes of any specific extreme climate or weather event are complex mix of human and natural factors. The science of extreme event attribution quantifies the relative contributions of human and natural influences on these events. Hence, on a case by case basis, scientists can produce a quantitative estimate of the contribution of human influences to the severity or likelihood of an extreme event. However, other human activities also contribute to changes in some types of extreme weather events. For instance, urbanization can also lead to increased flood and heat wave risks, while high levels of air pollution can reduce observed high temperatures. In some cases, large natural variability in the climate system prevents making a conclusive attribution statement about the human influence on an extreme event.

Additionally, attribution of certain classes of extreme weather (e.g., tornadoes) is beyond our current modelling and theoretical capabilities.

A related question is whether some recent extreme events would have actually been impossible had humans not altered the climate system. While we have seen climate and weather events that are unprecedented in the historical record, we do not yet have convincing evidence that any of these events would have actually been impossible in the absence of climate change. However, some events that would have been very rare are now relatively common place. As the climate continues to warm, high temperatures and precipitation accumulations that were impossible prior to human intervention in the climate system are expected to occur.

References

Abatzoglou, J. T., and Rupp, D. E. (2017). Evaluating climate model simulations of drought for the northwestern United States. *Int. J. Climatol.* 37, 910–920. doi:10.1002/joc.5046.

Abatzoglou, J. T., and Williams, A. P. (2016). Impact of anthropogenic climate change on wildfire across western US forests. *Proc. Natl. Acad. Sci.*, 201607171. doi:10.1073/pnas.1607171113.

Abiodun, B. J., Adegoke, J., Abatan, A. A., Ibe, C. A., Egbebiyi, T. S., Engelbrecht, F., et al. (2017). Potential impacts of climate change on extreme precipitation over four African coastal cities. *Clim. Change* 143. doi:10.1007/s10584-017-2001-5.

Abiodun, B. J., Makhanya, N., Petja, B., Abatan, A. A., and Oguntunde, P. G. (2019). Future projection of droughts over major river basins in Southern Africa at specific global warming levels. *Theor. Appl. Climatol.* 137, 1785–1799. doi:10.1007/s00704-018-2693-0.

Abreu, R. C., Tett, S. F. B., Schurer, A., and Rocha, H. R. (2019). Attribution of Detected Temperature Trends in Southeast Brazil. *Geophys. Res. Lett.*, 2019GL083003. doi:10.1029/2019GL083003.

Adnan, M., Rehman, N., and Shahbir, J. (2016). Predicting the Frequency and Intensity of Climate Extremes by Regression Models. *J. Climatol. Weather Forecast.* 04. doi:10.4172/2332-2594.1000185.

Aerenson, T., Tebaldi, C., Sanderson, B., and Lamarque, J.-F. (2018). Changes in a suite of indicators of extreme temperature and precipitation under 1.5 and 2 degrees warming. *Environ. Res. Lett.* 13, 035009. doi:10.1088/1748-9326/aaafd6.

Aerts, J. C. J. H., Botzen, W. J., Clarke, K. C., Cutter, S. L., Hall, J. W., Merz, B., et al. (2018). Integrating human behaviour dynamics into flood disaster risk assessment /704/242 /706/689/2788 /706/2805 perspective. *Nat. Clim. Chang.* 8, 193–199. doi:10.1038/s41558-018-0085-1.

AghaKouchak, A. (2014). A baseline probabilistic drought forecasting framework using standardized soil moisture index: Application to the 2012 United States drought. *Hydrol. Earth Syst. Sci.* 18, 2485–2492. doi:10.5194/hess-18-2485-2014.

AghaKouchak, A., Cheng, L., Mazdiyasni, O., and Farahmand, A. (2014). Global warming and changes in risk of concurrent climate extremes: Insights from the 2014 California drought. *Geophys. Res. Lett.* 41, 8847–8852. doi:10.1002/2014GL062308.

Aguilar, E., Barry, A. A., Brunet, M., Ekang, L., Fernandes, A., Massoukina, M., et al. (2009). Changes in temperature and precipitation extremes in western central Africa, Guinea Conakry, and Zimbabwe, 1955-2006. *J. Geophys. Res. Atmos.* 114. doi:10.1029/2008JD011010.

Ahmadalipour, A., and Moradkhani, H. (2017). Analyzing the uncertainty of ensemble-based gridded observations in land surface simulations and drought assessment. *J. Hydrol.* 555, 557–568. Available at: https://www.scopus.com/inward/record.uri?eid=2-s2.0-85032588691&doi=10.1016%2Fj.jhydrol.2017.10.059&partnerID=40&md5=714ab65d1f4412aaf0ac8b93c9c19cc2.

Ahmed, M., Anchukaitis, K. J., Asrat, A., Borgaonkar, H. P., Braida, M., Buckley, B. M., et al. (2013). Continental-scale temperature variability during the past two millennia. *Nat. Geosci.* 6, 339–346. doi:10.1038/ngeo1797.

Aich, V., Liersch, S., Vetter, T., Fournet, S., Andersson, J. C. M., Calmanti, S., et al. (2016). Flood projections within the Niger River Basin under future land use and climate change. *Sci. Total Environ.* 562, 666–677. doi:10.1016/j.scitotenv.2016.04.021.

Akinsanola, A. A., and Zhou, W. (2018). Projections of West African summer monsoon rainfall extremes from two CORDEX models. *Clim. Dyn.* doi:10.1007/s00382-018-4238-8.

Akinyemi, F. O., and Abiodun, B. J. (2019). Potential impacts of global warming levels 1.5° C and above on climate extremes in Botswana. *Clim. Change*, 1–14.

Albergel, C., Dorigo, W., Reichle, R. H., Balsamo, G., de Rosnay, P., Muñoz-Sabater, J., et al. (2013). Skill and Global Trend Analysis of Soil Moisture from Reanalyses and Microwave Remote Sensing. *J. Hydrometeorol.* 14, 1259–1277. doi:10.1175/JHM-D-12-0161.1.

Albert, S., Leon, J. X., Grinham, A. R., Church, J. A., Gibbes, B. R., and Woodroffe, C. D. (2016). Interactions between sea-level rise and wave exposure on reef island dynamics in the Solomon Islands. *Environ. Res. Lett.* 11. Available at: https://www.scopus.com/inward/record.uri?eid=2-s2.0-84975473957&doi=10.1088%2F1748-9326%2F11%2F5%2F054011&partnerID=40&md5=f9b17441abb8407d4436140e5bd5ecda.

Alexander, L., Bador, M., Roca, R., Steefan Contractor, Donat, M. G., and Phuong Loan, N. (submitted). Intercomparison of annual precipitation indices and extremes over global land areas from in situ, space-based and reanalysis products. *Environ. Res. Lett.*(submitted).

Alexander, L. V. (2016). Global observed long-term changes in temperature and precipitation extremes: A review of progress and limitations in IPCC assessments and beyond. *Weather Clim. Extrem.* 11, 4–16. doi:10.1016/J.WACE.2015.10.007.

Alexander, L. V., Zhang, X., Peterson, T. C., Caesar, J., Gleason, B., Klein Tank, A. M. G., et al. (2006). Global observed changes in daily climate extremes of temperature and precipitation. *J. Geophys. Res.* 111, D05109. doi:10.1029/2005JD006290.

Alexander, L. V, and Arblaster, J. M. (2017). Historical and projected trends in temperature and precipitation extremes in Australia in observations and CMIP5. *Weather Clim. Extrem.* 15, 34–56.

Alexander, L. V, Fowler, H. J., Bador, M., Behrangi, A., Donat, M. G., Dunn, R., et al. (2019). On the use of indices to study extreme precipitation on sub-daily and daily timescales. *Environ. Res. Lett.* 14, 125008. doi:10.1088/1748-9326/ab51b6.

Alexandru, A. (2018). Consideration of land-use and land-cover changes in the projection of climate extremes over North America by the end of the twenty-first century. *Clim. Dyn.* 50, 1949–1973. doi:10.1007/s00382-017-3730-x.

Alfieri, L., Bisselink, B., Dottori, F., Naumann, G., de Roo, A., Salamon, P., et al. (2017). Global projections of river flood risk in a warmer world. *Earth's Futur.* 5, 171–182. doi:10.1002/2016EF000485.

Alfieri, L., Burek, P., Feyen, L., and Forzieri, G. (2015). Global warming increases the frequency of river floods in Europe. *Hydrol. Earth Syst. Sci.* 19, 2247–2260. doi:10.5194/hess-19-2247-2015.

Ali, H., and Mishra, V. (2018). Contributions of Dynamic and Thermodynamic Scaling in Subdaily Precipitation Extremes in India. *Geophys. Res. Lett.* 45, 2352–2361. doi:10.1002/2018GL077065.

Ali, S., Eum, H.-I., Cho, J., Dan, L., Khan, F., Dairaku, K., et al. (2019). Assessment of climate extremes in future projections downscaled by multiple statistical downscaling methods over Pakistan. *Atmos. Res.* 222, 114–133. doi:10.1016/j.atmosres.2019.02.009.

Alizadeh-Choobari, O., and Najafi, M. S. (2018). Extreme weather events in Iran under a changing climate. *Clim. Dyn.* 50. doi:10.1007/s00382-017-3602-4.

Alkama, R., and Cescatti, A. (2016). Biophysical climate impacts of recent changes in global forest cover. *Science* 351, 600–604. doi:10.1126/science.aac8083.

Allen, C. D., Breshears, D. D., and McDowell, N. G. (2015). On underestimation of global vulnerability to tree mortality and forest die-off from hotter drought in the Anthropocene. *Ecosphere* 6, art129. doi:10.1890/ES15-00203.1.

Allen, C. D., Macalady, A. K., Chenchouni, H., Bachelet, D., McDowell, N., Vennetier, M., et al. (2010). A global overview of drought and heat-induced tree mortality reveals emerging climate change risks for forests. *For. Ecol. Manage.* 259, 660–684. doi:10.1016/j.foreco.2009.09.001.

Allen, J. T. (2018). *Climate Change and Severe Thunderstorms*. doi:10.1093/acrefore/9780190228620.013.62.

Allen, M. R., Dube, O. P., Solecki, W., Aragón-Durand, F., Cramer, W., Humphreys, S., et al. (2018). "Framing and Context," in *Global Warming of 1.5°C. An IPCC Special Report on the impacts of global warming of 1.5°C above pre-industrial levels and related global greenhouse gas emission pathways, in the context of strengthening the global response to the threat of climate change,* eds. V. Masson-Delmotte, P. Zhai, H.-O. Pörtner, D. Roberts, J. Skea, P. R. Shukla, et al. (In Press).

Almazroui, M. (2019). Temperature Changes over the CORDEX-MENA Domain in the 21st Century Using CMIP5 Data Downscaled with RegCM4: A Focus on the Arabian Peninsula. *Adv. Meteorol.* 2019. doi:10.1155/2019/5395676.

Almazroui, M., Islam, M. N., Dambul, R., and Jones, P. D. (2014). Trends of temperature extremes in Saudi Arabia. *Int. J. Climatol.* 34, 808–826. doi:10.1002/joc.3722.

Almazroui, M., Raju, P. V. S., Yusef, A., Hussein, M. A. A., and Omar, M. (2018). Simulation of extreme rainfall event of November 2009 over Jeddah, Saudi Arabia: the explicit role of topography and surface heating. *Theor. Appl. Climatol.* 132, 89–101. doi:10.1007/s00704-017-2080-2.

Almazroui, M., and Saeed, S. (2020). Contribution of extreme daily precipitation to total rainfall over the Arabian Peninsula. *Atmos. Res.* 231, 104672. doi:https://doi.org/10.1016/j.atmosres.2019.104672.

Almeida, C. T., Oliveira-Júnior, J. F., Delgado, R. C., Cubo, P., and Ramos, M. C. (2017). Spatiotemporal rainfall and temperature trends throughout the Brazilian Legal Amazon, 1973-2013. *Int. J. Climatol.* 37, 2013–2026. doi:10.1002/joc.4831.

AlSarmi, S. H., and Washington, R. (2014). Changes in climate extremes in the Arabian Peninsula: analysis of daily data. *Int. J. Climatol.* 34, 1329–1345. doi:10.1002/joc.3772.

Altman, J., Ukhvatkina, O. N., Omelko, A. M., Macek, M., Plener, T., Pejcha, V., et al. (2018). Poleward migration of the destructive effects of tropical cyclones during the 20th century. *Proc. Natl. Acad. Sci.* 115, 11543 LP – 11548. doi:10.1073/pnas.1808979115.

Amann, B., Szidat, S., and Grosjean, M. (2015). A millennial-long record of warm season precipitation and flood frequency for the North-western Alps inferred from varved lake sediments: implications for the future. *Quat. Sci. Rev.* 115, 89–100. doi:10.1016/j.quascirev.2015.03.002.

Amin, M. T., Mahmoud, S. H., and Alazba, A. A. (2016). Observations, projections and impacts of climate change on water resources in Arabian Peninsula: current and future scenarios. *Environ. Earth Sci.* 75, 864. doi:10.1007/s12665-016-5684-4.

AMS2018 AMS2018. Available at: http://glossary.ametsoc.org/wiki/Atmospheric_river.
Andela, N., Morton, D. C., Giglio, L., Chen, Y., van der Werf, G. R., Kasibhatla, P. S., et al. (2017). A human-driven decline in global burned area. *Science* 356, 1356–1362. doi:10.1126/science.aal4108.
Anderegg, W. R. L., Kane, J. M., and Anderegg, L. D. L. (2013). Consequences of widespread tree mortality triggered by drought and temperature stress. *Nat. Clim. Chang.* 3, 30–36. doi:10.1038/nclimate1635.
Anderegg, W. R. L., Klein, T., Bartlett, M., Sack, L., Pellegrini, A. F. A., Choat, B., et al. (2016). Meta-analysis reveals that hydraulic traits explain cross-species patterns of drought-induced tree mortality across the globe. *Proc. Natl. Acad. Sci. U. S. A.* 113, 5024–5029. doi:10.1073/pnas.1525678113.
Anderegg, W. R. L., Trugman, A. T., Bowling, D. R., Salvucci, G., and Tuttle, S. E. (2019). Plant functional traits and climate influence drought intensification and land–atmosphere feedbacks. *Proc. Natl. Acad. Sci. U. S. A.* 116, 14071–14076. doi:10.1073/pnas.1904747116.
Anderson, W. B., Seager, R., Baethgen, W., Cane, M., and You, L. (2019). Synchronous crop failures and climate-forced production variability. *Sci. Adv.* 5, eaaw1976. doi:10.1126/sciadv.aaw1976.
Andrijevic, M., Crespo Cuaresma, J., Muttarak, R., and Schleussner, C.-F. (2019). Governance in socioeconomic pathways and its role for future adaptive capacity. *Nat. Sustain.* doi:10.1038/s41893-019-0405-0.
Añel, J. A., López-Moreno, J. I., Otto, F. E. L., Vicente-Serrano, S. M., Schaller, N., Massey, N., et al. (2014). The extreme snow accumulation in the Western Spanish Pyrenees during winter and spring 2013. *Bull. Am. Meteorol. Soc.* 95, S73–S74.
Angeles-Malaspina, M., González-Cruz, J. E., and Ramírez-Beltran, N. (2018). Projections of Heat Waves Events in the Intra-Americas Region Using Multimodel Ensemble. *Adv. Meteorol.* 2018, 1–16. doi:10.1155/2018/7827984.
Angélil, O., Perkins-Kirkpatrick, S., Alexander, L. V, Stone, D., Donat, M. G., Wehner, M., et al. (2016). Comparing regional precipitation and temperature extremes in climate model and reanalysis products. *Weather Clim. Extrem.* 13, 35–43. doi:https://doi.org/10.1016/j.wace.2016.07.001.
Angélil, O., Stone, D. A., Tadross, M., Tummon, F., Wehner, M., and Knutti, R. (2014). Attribution of extreme weather to anthropogenic greenhouse gas emissions: Sensitivity to spatial and temporal scales. *Geophys. Res. Lett.* 41, 2150–2155. doi:10.1002/2014GL059234.
Angélil, O., Stone, D., Perkins-Kirkpatrick, S., Alexander, L. V., Wehner, M., Shiogama, H., et al. (2018). On the nonlinearity of spatial scales in extreme weather attribution statements. *Clim. Dyn.* 50, 2739–2752. doi:10.1007/s00382-017-3768-9.
Angélil, O., Stone, D., Wehner, M., Paciorek, C. J., Krishnan, H., and Collins, W. (2017). An Independent Assessment of Anthropogenic Attribution Statements for Recent Extreme Temperature and Rainfall Events. *J. Clim.* 30, 5–16. doi:10.1175/JCLI-D-16-0077.1.
Antonescu, B., Schultz, D. M., Holzer, A., and Groenemeijer, P. (2016a). Tornadoes in Europe: An Underestimated Threat. *Bull. Am. Meteorol. Soc.* 98, 713–728. doi:10.1175/BAMS-D-16-0171.1.
Antonescu, B., Schultz, D. M., Lomas, F., and Kühne, T. (2016b). Tornadoes in Europe: Synthesis of the Observational Datasets. *Mon. Weather Rev.* 144, 2445–2480. doi:10.1175/MWR-D-15-0298.1.
Apurv, T., Sivapalan, M., and Cai, X. (2017). Understanding the Role of Climate Characteristics in Drought Propagation. *Water Resour. Res.* 53, 9304–9329. Available at: https://www.scopus.com/inward/record.uri?eid=2-s2.0-85038925893&doi=10.1002%2F2017WR021445&partnerID=40&md5=e74a67da8eff15f35f4c6e8b28d9822c.
Aragão, L. E. O. C., Anderson, L. O., Fonseca, M. G., Rosan, T. M., Vedovato, L. B., Wagner, F. H., et al. (2018). 21st Century drought-related fires counteract the decline of Amazon deforestation carbon emissions. *Nat. Commun.* 9, 536. doi:10.1038/s41467-017-02771-y.
Archer, D. R., and Fowler, H. J. (2018). Characterising flash flood response to intense rainfall and impacts using historical information and gauged data in Britain. *J. Flood Risk Manag.* 11, S121–S133. doi:10.1111/jfr3.12187.
Archfield, S. A., Hirsch, R. M., Viglione, A., and Blöschl, G. (2016). Fragmented patterns of flood change across the United States. *Geophys. Res. Lett.* 43, 10,232-10,239. doi:10.1002/2016GL070590.
Argüeso, D., Hidalgo-Muñoz, J. M., Ga ́ Miz-Fortis, S. R., Esteban-Parra, M. J., and Castro-Díez, Y. (2012). Evaluation of WRF Mean and Extreme Precipitation over Spain: Present Climate (1970-99). *J. Clim.* 25, 4883–4895. doi:10.1175/JCLI-D-11-00276.1.
Arheimer, B., and Lindström, G. (2015). Climate impact on floods: Changes in high flows in Sweden in the past and the future (1911-2100). *Hydrol. Earth Syst. Sci.* 19, 771–784. doi:10.5194/hess-19-771-2015.
Armstrong, W. H., Collins, M. J., and Snyder, N. P. (2014). Hydroclimatic flood trends in the northeastern United States and linkages with large-scale atmospheric circulation patterns. *Hydrol. Sci. J.* 59, 1636–1655. doi:10.1080/02626667.2013.862339.
Arnell, N. W., and Gosling, S. N. (2016). The impacts of climate change on river flood risk at the global scale. *Clim. Change* 134, 387–401. doi:10.1007/s10584-014-1084-5.
Arnone, E., Pumo, D., Viola, F., Noto, L. V., and La Loggia, G. (2013). Rainfall statistics changes in Sicily. *Hydrol. Earth Syst. Sci.* 17, 2449–2458. doi:10.5194/hess-17-2449-2013.

Arora, V. K., Scinocca, J. F., Boer, G. J., Christian, J. R., Denman, K. L., Flato, G. M., et al. (2011). Carbon emission limits required to satisfy future representative concentration pathways of greenhouse gases. *Geophys. Res. Lett.* 38. doi:10.1029/2010GL046270.
Ashabokov, B. A., Tashilova, A. A., Kesheva, L. A., and Taubekova, Z. A. (2017). Trends in precipitation parameters in the climate zones of southern Russia (1961-2011). *Russ. Meteorol. Hydrol.* 42, 150–158. doi:10.3103/S1068373917030025.
Ashouri, H., Hsu, K.-L., Sorooshian, S., Braithwaite, D. K., Knapp, K. R., Cecil, L. D., et al. (2015). PERSIANN-CDR: Daily Precipitation Climate Data Record from Multisatellite Observations for Hydrological and Climate Studies. *Bull. Am. Meteorol. Soc.* 96, 69–83. doi:10.1175/BAMS-D-13-00068.1.
AshrafVaghefi, S., Keykhai, M., Jahanbakhshi, F., Sheikholeslami, J., Ahmadi, A., Yang, H., et al. (2019). The future of extreme climate in Iran. *Sci. Rep.* 9, 1464. doi:10.1038/s41598-018-38071-8.
Asmerom, Y., Polyak, V. J., Rasmussen, J. B. T., Burns, S. J., and Lachniet, M. (2013). Multidecadal to multicentury scale collapses of Northern Hemisphere monsoons over the past millennium. *Proc. Natl. Acad. Sci. U. S. A.* 110, 9651–9656. doi:10.1073/pnas.1214870110.
Ault, T. R., Cole, J. E., Overpeck, J. T., Pederson, G. T., and Meko, D. M. (2014). Assessing the Risk of Persistent Drought Using Climate Model Simulations and Paleoclimate Data. *J. Clim.* 27, 7529–7549. doi:10.1175/JCLI-D-12-00282.1.
Avila, F. B., Dong, S., Menang, K. P., Rajczak, J., Renom, M., Donat, M. G., et al. (2015). Systematic investigation of gridding-related scaling effects on annual statistics of daily temperature and precipitation maxima: A case study for south-east Australia. *Weather Clim. Extrem.* 9, 6–16. doi:10.1016/j.wace.2015.06.003.
Avila, F. B., Pitman, A. J., Donat, M. G., Alexander, L. V, and Abramowitz, G. (2012). Climate model simulated changes in temperature extremes due to land cover change. *J. Geophys. Res. Atmos.* 117. doi:10.1029/2011JD016382.
Awange, J. L., Mpelasoka, F., and Goncalves, R. M. (2016). When every drop counts: Analysis of Droughts in Brazil for the 1901-2013 period. *Sci. Total Environ.* 566–567, 1472–1488. doi:10.1016/j.scitotenv.2016.06.031.
Ayeb-Karlsson, S., Kniveton, D., Cannon, T., van der Geest, K., Ahmed, I., Derrington, E. M., et al. (2019). I will not go, I cannot go: cultural and social limitations of disaster preparedness in Asia, Africa, and Oceania. *Disasters* 43, 752–770. doi:10.1111/disa.12404.
Azorin-Molina, C., Vicente-Serrano, S. M., Mcvicar, T. R., Jerez, S., Sanchez-Lorenzo, A., López-Moreno, J.-I., et al. (2014). Homogenization and assessment of observed near-surface wind speed trends over Spain and Portugal, 1961-2011. *J. Clim.* 27. doi:10.1175/JCLI-D-13-00652.1.
Azorin-Molina, C., Vicente-Serrano, S. M., McVicar, T. R., Revuelto, J., Jerez, S., and López-Moreno, J. I. (2017). Assessing the impact of measurement time interval when calculating wind speed means and trends under the stilling phenomenon. *Int. J. Climatol.* 37, 480–492. doi:10.1002/joc.4720.
Azorin-Molina, C., Vicente-Serrano, S. M., Sanchez-Lorenzo, A., McVicar, T. R., Morán-Tejeda, E., Revuelto, J., et al. (2015). Atmospheric evaporative demand observations, estimates and driving factors in Spain (1961-2011). *J. Hydrol.* 523, 262–277. doi:10.1016/j.jhydrol.2015.01.046.
Bachmair, S., Tanguy, M., Hannaford, J., and Stahl, K. (2018). How well do meteorological indicators represent agricultural and forest drought across Europe? *Environ. Res. Lett.* 13. doi:10.1088/1748-9326/aaafda.
Bachofen, C., Moser, B., Hoch, G., Ghazoul, J., and Wohlgemuth, T. (2018). No carbon "bet hedging" in pine seedlings under prolonged summer drought and elevated CO 2. *J. Ecol.* 106, 31–46. doi:10.1111/1365-2745.12822.
Bador, M., Alexander, L., Contractor, S., and Roca, R. (2020). Diverse estimates of annual maxima daily precipitation in 22 state-of-the-art quasi-global land observation datasets. *Environ. Res. Lett.*
Bador, M., Boe, J., Terray, L., Alexander, L. V., Bellucci, A., Haarsma, R. J., et al. (submitted). Impact of higher spatial atmospheric resolution on precipitation extremes over land in global climate models. *J. Geophys. Res. Atmos.*(submitted).
Bador, M., Terray, L., and Boé, J. (2016). Detection of anthropogenic influence on the evolution of record-breaking temperatures over Europe. *Clim. Dyn.* 46, 2717–2735. doi:10.1007/s00382-015-2725-8.
Baek, H.-J., Kim, M.-K., and Kwon, W.-T. (2017). Observed short- and long-term changes in summer precipitation over South Korea and their links to large-scale circulation anomalies. *Int. J. Climatol.* 37, 972–986. doi:10.1002/joc.4753.
Baek, S. H., Steiger, N. J., Smerdon, J. E., and Seager, R. (2019). Oceanic Drivers of Widespread Summer Droughts in the United States Over the Common Era. *Geophys. Res. Lett.* 46, 8271–8280. doi:10.1029/2019GL082838.
Bai, P., Liu, X., Liang, K., and Liu, C. (2016). Investigation of changes in the annual maximum flood in the Yellow River basin, China. *Quat. Int.* 392, 168–177. doi:10.1016/j.quaint.2015.04.053.
Bailey, R. T., Barnes, K., and Wallace, C. D. (2016). Predicting Future Groundwater Resources of Coral Atoll Islands. *Hydrol. Process.* 30, 2092–2105. Available at: https://www.scopus.com/inward/record.uri?eid=2-s2.0-84959066219&doi=10.1002%2Fhyp.10781&partnerID=40&md5=43bf97efedaebab086292d590a674176.
Bailey, R. T., Khalil, A., and Chatikavanij, V. (2015). Estimating current and future groundwater resources of the

maldives. *J. Am. Water Resour. Assoc.* 51, 112–122. Available at: https://www.scopus.com/inward/record.uri?eid=2-s2.0-84922793830&doi=10.1111%2Fjawr.12236&partnerID=40&md5=84f0dff645787e41b9e7c002767098ea.

Balaguru, K., Foltz, G. R., and Leung, L. R. (2018). Increasing Magnitude of Hurricane Rapid Intensification in the Central and Eastern Tropical Atlantic. *Geophys. Res. Lett.* 45, 4238–4247. doi:10.1029/2018GL077597.

Ballesteros Cánovas, J. A., Trappmann, D., Shekhar, M., Bhattacharyya, A., and Stoffel, M. (2017). Regional flood-frequency reconstruction for Kullu district, Western Indian Himalayas. *J. Hydrol.* 546, 140–149. doi:10.1016/j.jhydrol.2016.12.059.

Balsamo, G., Albergel, C., Beljaars, A., Boussetta, S., Brun, E., Cloke, H., et al. (2015). ERA-Interim/Land: a global land surface reanalysis data set. *Hydrol. Earth Syst. Sci.* 19, 389–407. doi:10.5194/hess-19-389-2015.

Ban, N., Schmidli, J., and Schär, C. (2014). Evaluation of the new convective-resolving regional climate modeling approach in decade-long simulations. *J. Geophys. Res. Atmos.* 119, 7889–7907. doi:10.1002/2014JD021478.

Ban, N., Schmidli, J., and Schär, C. (2015). Heavy precipitation in a changing climate: Does short-term summer precipitation increase faster? *Geophys. Res. Lett.* 42, 1165–1172. doi:10.1002/2014GL062588.

Bandyopadhyay, N., Bhuiyan, C., and Saha, A. K. (2016). Heat waves, temperature extremes and their impacts on monsoon rainfall and meteorological drought in Gujarat, India. *Nat. Hazards* 82, 367–388. doi:10.1007/s11069-016-2205-4.

Bao, J., and Sherwood, S. C. (2019). The Role of Convective Self-Aggregation in Extreme Instantaneous Versus Daily Precipitation. *J. Adv. Model. Earth Syst.* 11, 19–33. doi:10.1029/2018MS001503.

Bao, J., Sherwood, S. C., Alexander, L. V, and Evans, J. P. (2017). Future increases in extreme precipitation exceed observed scaling rates. *Nat. Clim. Chang.* 7, 128–132. doi:10.1038/nclimate3201.

Barbero, R., Fowler, H. J., Blenkinsop, S., Westra, S., Moron, V., Lewis, E., et al. (2019). A synthesis of hourly and daily precipitation extremes in different climatic regions. *Weather Clim. Extrem.* 26, 100219. doi:10.1016/j.wace.2019.100219.

Barbero, R., Fowler, H. J., Lenderink, G., Blenkinsop, S., R., B., J., F. H., et al. (2017). Is the intensification of precipitation extremes with global warming better detected at hourly than daily resolutions? *Geophys. Res. Lett.* 44, 974–983. doi:10.1002/2016GL071917.

Barbosa, J. M., and Asner, G. P. (2017). Effects of long-term rainfall decline on the structure and functioning of Hawaiian forests. *Environ. Res. Lett.* 12. Available at: https://www.scopus.com/inward/record.uri?eid=2-s2.0-85030764097&doi=10.1088%2F1748-9326%2Faa7ee4&partnerID=40&md5=ffbc9c56596a36be3f6f5d6fef02c176.

Barichivich, J., Gloor, E., Peylin, P., Brienen, R. J. W., Schöngart, J., Espinoza, J. C., et al. (2018). Recent intensification of Amazon flooding extremes driven by strengthened Walker circulation. *Sci. Adv.* 4. doi:10.1126/sciadv.aat8785.

Barker, L. J., Hannaford, J., Chiverton, A., and Svensson, C. (2016). From meteorological to hydrological drought using standardised indicators. *Hydrol. Earth Syst. Sci.* 20, 2483–2505. doi:10.5194/hess-20-2483-2016.

Barker, L. J., Hannaford, J., Parry, S., Smith, K. A., Tanguy, M., and Prudhomme, C. (2019). Historic hydrological droughts 1891-2015: Systematic characterisation for a diverse set of catchments across the UK. *Hydrol. Earth Syst. Sci.* 23, 4583–4602. doi:10.5194/hess-23-4583-2019.

Barkey, B. L., and Bailey, R. T. (2017). Estimating the impact of drought on groundwater resources of the Marshall Islands. *Water (Switzerland)* 9. Available at: https://www.scopus.com/inward/record.uri?eid=2-s2.0-85011300226&doi=10.3390%2Fw9010041&partnerID=40&md5=c29590f1f14535ed108a5985d7effde0.

Barkhordarian, A., Saatchi, S. S., Behrangi, A., Loikith, P. C., and Mechoso, C. R. (2019). A Recent Systematic Increase in Vapor Pressure Deficit over Tropical South America. *Sci. Rep.* 9, 15331. doi:10.1038/s41598-019-51857-8.

Barlow, M., and Hoell, A. (2015). Drought in the Middle East and Central–Southwest Asia During Winter 2013/14. *Bull. Am. Meteorol. Soc.* 96, S71–S76. doi:10.1175/BAMS-D-15-00127.1.

Barlow, M., Zaitchik, B., Paz, S., Black, E., Evans, J., and Hoell, A. (2016). A review of drought in the Middle East and southwest Asia. *J. Clim.* 29, 8547–8574. doi:10.1175/JCLI-D-13-00692.1.

Barnabas, B., Jager, K., and Feher, A. (2007). The effect of drought and heat stress on reproductive processes in cereals. *Plant. Cell Environ.*, 11–38. doi:10.1111/j.1365-3040.2007.01727.x.

Barnard, P. L., Hoover, D., Hubbard, D. M., Snyder, A., Ludka, B. C., Allan, J., et al. (2017). Extreme oceanographic forcing and coastal response due to the 2015–2016 El Niño. *Nat. Commun.* 8, 14365. doi:10.1038/ncomms14365.

Barraqué, B. (2017). The common property issue in flood control through land use in France. *J. Flood Risk Manag.* 10, 182–194. doi:10.1111/jfr3.12092.

Barriopedro, D., Fischer, E. M., Luterbacher, J., Trigo, R. M., and Garcia-Herrera, R. (2011). The Hot Summer of 2010: Redrawing the Temperature Record Map of Europe. *Science* 332, 220–224. doi:10.1126/science.1201224.

Barros, V. R., Boninsegna, J. A., Camilloni, I. A., Chidiak, M., Magrín, G. O., and Rusticucci, M. (2015). Climate change in Argentina: trends, projections, impacts and adaptation. *Wiley Interdiscip. Rev. Clim. Chang.* 6, 151–

169. doi:10.1002/wcc.316.
Barry, A. A., Caesar, J., Klein Tank, A. M. G., Aguilar, E., McSweeney, C., Cyrille, A. M., et al. (2018). West Africa climate extremes and climate change indices. *Int. J. Climatol.* 38, e921–e938. doi:10.1002/joc.5420.
Bartók, B., Wild, M., Folini, D., Lüthi, D., Kotlarski, S., Schär, C., et al. (2017). Projected changes in surface solar radiation in CMIP5 global climate models and in EURO-CORDEX regional climate models for Europe. *Clim. Dyn.* 49, 2665–2683. doi:10.1007/s00382-016-3471-2.
Bartos, M. D., and Chester, M. V. (2015). Impacts of climate change on electric power supply in the Western United States. *Nat. Clim. Chang.* 5, 748–752. doi:10.1038/nclimate2648.
Basara, J. B., Christian, J. I., Wakefield, R. A., Otkin, J. A., Hunt, E. H., and Brown, D. P. (2019). The evolution, propagation, and spread of flash drought in the Central United States during 2012. *Environ. Res. Lett.* 14. Available at: https://www.scopus.com/inward/record.uri?eid=2-s2.0-85072698642&doi=10.1088%2F1748-9326%2Fab2cc0&partnerID=40&md5=66f27b5e781714efc714031fc489f20d.
Basconcillo, J., Lucero, A., Solis, A., Sandoval Jr, R., Bautista, E., Koizumi, T., et al. (2016). Statistically downscaled projected changes in seasonal mean temperature and rainfall in Cagayan Valley, Philippines. *J. Meteorol. Soc. Japan. Ser. II* 94, 151–164.
Befort, D. J., Wild, S., Kruschke, T., Ulbrich, U., and Leckebusch, G. C. (2016). Different long-term trends of extra-tropical cyclones and windstorms in ERA-20C and NOAA-20CR reanalyses. *Atmos. Sci. Lett.* 17, 586–595. doi:10.1002/asl.694.
Beguería, S., Vicente-Serrano, S. M., Reig, F., and Latorre, B. (2014). Standardized precipitation evapotranspiration index (SPEI) revisited: Parameter fitting, evapotranspiration models, tools, datasets and drought monitoring. *Int. J. Climatol.* 34. doi:10.1002/joc.3887.
Beguería, S., Vicente-Serrano, S. M., Tomás-Burguera, M., and Maneta, M. (2016). Bias in the variance of gridded data sets leads to misleading conclusions about changes in climate variability. *Int. J. Climatol.* 36. doi:10.1002/joc.4561.
Bellprat, O., García-Serrano, J., Fučkar, N. S., Massonnet, F., Guemas, V., and Doblas-Reyes, F. J. (2016). The Role of Arctic Sea Ice and Sea Surface Temperatures on the Cold 2015 February Over North America. *Bull. Am. Meteorol. Soc.* 97, S36–S41. doi:10.1175/BAMS-D-16-0159.1.
Bellprat, O., Lott, F. C., Gulizia, C., Parker, H. R., Pampuch, L. A., Pinto, I., et al. (2015). Unusual past dry and wet rainy seasons over Southern Africa and South America from a climate perspective. *Weather Clim. Extrem.* 9, 36–46. doi:10.1016/J.WACE.2015.07.001.
Bender, M. A., Knutson, T. R., Tuleya, R. E., Sirutis, J. J., Vecchi, G. A., Garner, S. T., et al. (2010). Modeled Impact of Anthropogenic Atlantic Hurricanes. *Science* 327, 454–458.
Bengtsson, L., Semenov, V. A., and Johannessen, O. M. (2004). The Early Twentieth-Century Warming in the Arctic—A Possible Mechanism. *J. Clim.* 17, 4045–4057. doi:10.1175/1520-0442(2004)017<4045:TETWIT>2.0.CO;2.
Beniston, M., Farinotti, D., Stoffel, M., Andreassen, L. M., Coppola, E., Eckert, N., et al. (2018). The European mountain cryosphere: a review of its current state, trends, and future challenges. *Cryosph.* 12, 759–794. doi:10.5194/tc-12-759-2018.
Beniston, M., and Stoffel, M. (2016). Rain-on-snow events, floods and climate change in the Alps: Events may increase with warming up to 4°C and decrease thereafter. *Sci. Total Environ.* 571, 228–236. doi:https://doi.org/10.1016/j.scitotenv.2016.07.146.
Bennett, B., Leonard, M., Deng, Y., and Westra, S. (2018). An empirical investigation into the effect of antecedent precipitation on flood volume. *J. Hydrol.* 567, 435–445. doi:10.1016/j.jhydrol.2018.10.025.
Bennett, K. E., and Walsh, J. E. (2015). Spatial and temporal changes in indices of extreme precipitation and temperature for Alaska. *Int. J. Climatol.* 35, 1434–1452. doi:10.1002/joc.4067.
Berg, A., Findell, K., Lintner, B., Giannini, A., Seneviratne, S. I., van den Hurk, B., et al. (2016). Land–atmosphere feedbacks amplify aridity increase over land under global warming. *Nat. Clim. Chang.* 6, 869–874. doi:10.1038/nclimate3029.
Berg, A., Lintner, B. R., Findell, K., Seneviratne, S. I., van den Hurk, B., Ducharne, A., et al. (2015). Interannual Coupling between Summertime Surface Temperature and Precipitation over Land: Processes and Implications for Climate Change*. *J. Clim.* 28, 1308–1328. doi:10.1175/JCLI-D-14-00324.1.
Berg, A., and Sheffield, J. (2018). Climate Change and Drought: the Soil Moisture Perspective. *Curr. Clim. Chang. Reports* 4, 180–191. doi:10.1007/s40641-018-0095-0.
Berg, A., Sheffield, J., and Milly, P. C. D. (2017). Divergent surface and total soil moisture projections under global warming. *Geophys. Res. Lett.* 44, 236–244. doi:10.1002/2016GL071921.
Bergaoui, K., Mitchell, D., Otto, F., Allen, M., Zaaboul, R., McDonnell, R., et al. (2015). The Contribution of Human-Induced Climate Change to the Drought of 2014 in the Southern Levant Region. *Bull. Am. Meteorol. Soc.* 96, S66–S70. doi:10.1175/BAMS-D-15-00129.1.
Berghuijs, W. R., Aalbers, E. E., Larsen, J. R., Trancoso, R., and Woods, R. A. (2017). Recent changes in extreme floods across multiple continents. *Environ. Res. Lett.* 12. Available at:

https://www.scopus.com/inward/record.uri?eid=2-s2.0-85036470234&doi=10.1088%2F1748-9326%2Faa8847&partnerID=40&md5=b047d343920ef6afa81450dce7249ca0.

Berghuijs, W. R., Harrigan, S., Molnar, P., Slater, L. J., and Kirchner, J. W. (2019). The Relative Importance of Different Flood-Generating Mechanisms Across Europe. *Water Resour. Res.* 55, 4582–4593. Available at: https://www.scopus.com/inward/record.uri?eid=2-s2.0-85067466087&doi=10.1029%2F2019WR024841&partnerID=40&md5=ee47a8836fe71557c9e1ecff372fcb0f.

Berghuijs, W. R., Woods, R. A., Hutton, C. J., and Sivapalan, M. (2016). Dominant flood generating mechanisms across the United States. *Geophys. Res. Lett.* 43, 4382–4390. doi:10.1002/2016GL068070.

Berthou, S., Rowell, D. P., Kendon, E. J., Roberts, M. J., Stratton, R. A., Crook, J. A., et al. (2019). Improved climatological precipitation characteristics over West Africa at convection-permitting scales. *Clim. Dyn.* 53, 1991–2011. doi:10.1007/s00382-019-04759-4.

BESSHO, K., DATE, K., HAYASHI, M., IKEDA, A., IMAI, T., INOUE, H., et al. (2016). An Introduction to Himawari-8/9— Japan’s New-Generation Geostationary Meteorological Satellites. *J. Meteorol. Soc. Japan. Ser. II* 94, 151–183. doi:10.2151/jmsj.2016-009.

Beusch, L., Gudmundsson, L., and Seneviratne, S. I. (2019). Emulating Earth System Model temperatures: from global mean temperature trajectories to grid-point level realizations on land. *Earth Syst. Dyn. Discuss.*, 1–28. doi:10.5194/esd-2019-34.

Bevacqua, E., Maraun, D., Vousdoukas, M. I., Voukouvalas, E., Vrac, M., Mentaschi, L., et al. (2019). Higher probability of compound flooding from precipitation and storm surge in Europe under anthropogenic climate change. *Sci. Adv.* 5, eaaw5531. doi:10.1126/sciadv.aaw5531.

Bezerra, B. G., Silva, L. L., Santos e Silva, C. M., and de Carvalho, G. G. (2018). Changes of precipitation extremes indices in São Francisco River Basin, Brazil from 1947 to 2012. *Theor. Appl. Climatol.* doi:10.1007/s00704-018-2396-6.

Bhatia, K. T., Vecchi, G. A., Knutson, T. R., Murakami, H., Kossin, J., Dixon, K. W., et al. (2019). Recent increases in tropical cyclone intensification rates. *Nat. Commun.* 10, 1–9. doi:10.1038/s41467-019-08471-z.

Bhatia, K., Vecchi, G., Murakami, H., Underwood, S., and Kossin, J. (2018). Projected response of tropical cyclone intensity and intensification in a global climate model. *J. Clim.* 31, 8281–8303. doi:10.1175/JCLI-D-17-0898.1.

Biasutti, M., Voigt, A., Boos, W. R., Braconnot, P., Hargreaves, J. C., Harrison, S. P., et al. (2018). Global energetics and local physics as drivers of past, present and future monsoons. *Nat. Geosci.* 11, 392–400. doi:10.1038/s41561-018-0137-1.

Bindoff, N. L., Stott, P. A., AchutaRao, K., Allen, M. R., Gillett, N., Gutzler, D., et al. (2013). "Detection and Attribution of Climate Change: from Global to Regional," in *Climate Change 2013 - The Physical Science Basis*, ed. Intergovernmental Panel on Climate Change (Cambridge: Cambridge University Press), 867–952. doi:10.1017/CBO9781107415324.022.

Biscarini, C., Francesco, S. D., Ridolfi, E., and Manciola, P. (2016). On the simulation of floods in a narrow bending valley: The malpasset dam break case study. *Water (Switzerland)* 8. doi:10.3390/w8110545.

Bitencourt, D. P., Fuentes, M. V., Maia, P. A., and Amorim, F. T. (2016). Frequência, Duração, Abrangência Espacial e Intensidadedas Ondas de Calor no Brasil. *Rev. Bras. Meteorol.* 31, 506–517. doi:10.1590/0102-778631231420150077.

Blamey, R. C., Kolusu, S. R., Mahlalela, P., Todd, M. C., and Reason, C. J. C. (2018). The role of regional circulation features in regulating El Niño climate impacts over southern Africa: A comparison of the 2015/2016 drought with previous events. *Int. J. Climatol.* 38, 4276–4295. doi:10.1002/joc.5668.

Blanchet, J., Molinié, G., and Touati, J. (2018). Spatial analysis of trend in extreme daily rainfall in southern France. *Clim. Dyn.* 51, 799–812. doi:10.1007/s00382-016-3122-7.

Blender, R., and Schubert, M. (2000). Cyclone Tracking in Different Spatial and Temporal Resolutions. *Mon. Weather Rev.* 128, 377. doi:10.1175/1520-0493(2000)128<0377:CTIDSA>2.0.CO;2.

Blöschl, G., Hall, J., Parajka, J., Perdigão, R. A. P., Merz, B., Arheimer, B., et al. (2017). Changing climate shifts timing of European floods. *Science* 357, 588–590. doi:10.1126/science.aan2506.

Blöschl, G., Hall, J., Viglione, A., Perdigão, R. A. P., Parajka, J., Merz, B., et al. (2019). Changing climate both increases and decreases European river floods. *Nature* 573, 108–111. doi:10.1038/s41586-019-1495-6.

Blunden, J., and Arndt, D. S. (2016). State of the Climate in 2015. *Bull. Am. Meteorol. Soc.* 97, Si-S275. doi:10.1175/2016BAMSStateoftheClimate.1.

Boers, N., Goswami, B., Rheinwalt, A., Bookhagen, B., Hoskins, B., and Kurths, J. (2019). Complex networks reveal global pattern of extreme-rainfall teleconnections. *Nature* 566, 373–377. doi:10.1038/s41586-018-0872-x.

Boisier, J. P., Alvarez-Garretón, C., Cordero, R. R., Damiani, A., Gallardo, L., Garreaud, R. D., et al. (2018). Anthropogenic drying in central-southern Chile evidenced by long-term observations and climate model simulations. *Elem Sci Anth* 6, 74. doi:10.1525/elementa.328.

Bokhorst, S., Pedersen, S. H., Brucker, L., Anisimov, O., Bjerke, J. W., Brown, R. D., et al. (2016). Changing Arctic snow cover: A review of recent developments and assessment of future needs for observations, modelling, and

impacts. *Ambio* 45, 516–537. doi:10.1007/s13280-016-0770-0.
Bonsal, B. R., Peters, D. L., Seglenieks, F., Rivera, A., and Berg, A. (2019). "Changes in freshwater availability across Canada," in *Canada's Changing Climate Report*, eds. E. J. Bush and D. S. Lemmen (Ottawa), 261–342.
Booth, J. F., Wang, S., and Polvani, L. (2013). Midlatitude storms in a moister world: lessons from idealized baroclinic life cycle experiments. *Clim. Dyn.* 41, 787–802. doi:10.1007/s00382-012-1472-3.
Borga, M., Stoffel, M., Marchi, L., Marra, F., and Jakob, M. (2014). Hydrogeomorphic response to extreme rainfall in headwater systems: Flash floods and debris flows. *J. Hydrol.* 518, 194–205. doi:10.1016/j.jhydrol.2014.05.022.
Borodina, A., Fischer, E. M., and Knutti, R. (2017). Models are likely to underestimate increase in heavy rainfall in the extratropical regions with high rainfall intensity. *Geophys. Res. Lett.* 44, 7401–7409. doi:10.1002/2017GL074530.
Bosshard, T., Carambia, M., Goergen, K., Kotlarski, S., Krahe, P., Zappa, M., et al. (2013). Quantifying uncertainty sources in an ensemble of hydrological climate-impact projections. *Water Resour. Res.* 49, 1523–1536. doi:10.1029/2011WR011533.
Boyaj, A., Ashok, K., Ghosh, S., Devanand, A., and Dandu, G. (2018). The Chennai extreme rainfall event in 2015: The Bay of Bengal connection. *Clim. Dyn.* 50, 2867–2879. doi:10.1007/s00382-017-3778-7.
Bozkurt, D., Rojas, M., Boisier, J. P., and Valdivieso, J. (2018). Projected hydroclimate changes over Andean basins in central Chile from downscaled CMIP5 models under the low and high emission scenarios. *Clim. Change* 150, 131–147. doi:10.1007/s10584-018-2246-7.
Brando, P. M., Balch, J. K., Nepstad, D. C., Morton, D. C., Putz, F. E., Coe, M. T., et al. (2014). Abrupt increases in Amazonian tree mortality due to drought-fire interactions. *Proc. Natl. Acad. Sci.* 111, 6347–6352. doi:10.1073/pnas.1305499111.
Brandon, C. M., Woodruff, J. D., Lane, D. P., and Donnelly, J. P. (2013). Tropical cyclone wind speed constraints from resultant storm surge deposition: A 2500 year reconstruction of hurricane activity from St. Marks, FL. *Geochemistry, Geophys. Geosystems* 14, 2993–3008. doi:10.1002/ggge.20217.
Bregy, J. C., Wallace, D. J., Minzoni, R. T., and Cruz, V. J. (2018). 2500-year paleotempestological record of intense storms for the northern Gulf of Mexico, United States. *Mar. Geol.* 396, 26–42. doi:10.1016/j.margeo.2017.09.009.
Breña-Naranjo, J., Laverde B., M., and Pedrozo-Acuña, A. (2016). Changes in pan evaporation in Mexico from 1961 to 2010. *Int. J. Climatol.* 37. doi:10.1002/joc.4698.
Brito, S. S. B., Cunha, A. P. M. A., Cunningham, C. C., Alvalá, R. C., Marengo, J. A., and Carvalho, M. A. (2018). Frequency, duration and severity of drought in the Semiarid Northeast Brazil region. *Int. J. Climatol.* 38, 517–529. doi:10.1002/joc.5225.
Brogli, R., Kröner, N., Sørland, S. L., Lüthi, D., and Schär, C. (2018). The Role of Hadley Circulation and Lapse-Rate Changes for the Future European Summer Climate. *J. Clim.* 32, 385–404. doi:10.1175/JCLI-D-18-0431.1.
Brohan, P., Compo, G. P., Brönnimann, S., Allan, R. J., Auchmann, R., Brugnara, Y., et al. (2016). The 1816 'year without a summer' in an atmospheric reanalysis. *Clim. Past Discuss.*, 1–11. doi:10.5194/cp-2016-78.
Bronnimann, S., Fischer, A. M., Rozanov, E., Poli, P., Compo, G. P., and Sardeshmukh, P. D. (2015). Southward shift of the northern tropical belt from 1945 to 1980. *Nat. Geosci.* 8, 969–974. doi:10.1038/ngeo2568.
Brönnimann, S., Rajczak, J., Fischer, E. M., Raible, C. C., Rohrer, M., and Schär, C. (2018). Changing seasonality of moderate and extreme precipitation events in the Alps. *Nat. Hazards Earth Syst. Sci.* 18, 2047–2056. doi:10.5194/nhess-18-2047-2018.
Brooks, H. E. (2013). Severe thunderstorms and climate change. *Atmos. Res.* 123, 129–138. doi:10.1016/j.atmosres.2012.04.002.
Brown, S. J., Caesar, J., and Ferro, C. A. T. (2008). Global changes in extreme daily temperature since 1950. *J. Geophys. Res. Atmos.* 113, n/a-n/a. doi:10.1029/2006JD008091.
Brown, T., Leach, S., Wachter, A., and Guarduno, A. (2020). THE NORTHERN CALIFORNIA 2018 EXTREME FIRE SEASON. *Bull. Am. Meteorol. Soc.* doi:10.1175/BAMS-D-19-0275.1.
Brugnara, Y., Auchmann, R., Brönnimann, S., Bozzo, A., Berro, D. C., and Mercalli, L. (2016). Trends of mean and extreme temperature indices since 1874 at low-elevation sites in the southern Alps. *J. Geophys. Res. Atmos.* 121, 3304–3325. doi:10.1002/2015JD024582.
Brunner, L., Hegerl, G. C., and Steiner, A. K. (2017). Connecting atmospheric blocking to European temperature extremes in spring. *J. Clim.* 30, 585–594. doi:10.1175/JCLI-D-16-0518.1.
Brunner, L., Schaller, N., Anstey, J., Sillmann, J., and Steiner, A. K. (2018). Dependence of Present and Future European Temperature Extremes on the Location of Atmospheric Blocking. *Geophys. Res. Lett.* 45, 6311–6320. doi:10.1029/2018GL077837.
Bucchignani, E., Zollo, A. L., Cattaneo, L., Montesarchio, M., and Mercogliano, P. (2017). Extreme weather events over China: assessment of COSMO-CLM simulations and future scenarios. *Int. J. Climatol.* 37, 1578–1594. doi:10.1002/joc.4798.
Büntgen, U., Tegel, W., Carrer, M., Krusic, P. J., Hayes, M., and Esper, J. (2015). Commentary to Wetter et al. (2014):

Limited tree-ring evidence for a 1540 European 'Megadrought.' *Clim. Change* 131, 183–190. doi:10.1007/s10584-015-1423-1.
Burdanowitz, J., Buehler, S. A., Bakan, S., and Klepp, C. (2019). The sensitivity of oceanic precipitation to sea surface temperature. *Atmos. Chem. Phys.* 19, 9241–9252. doi:10.5194/acp-19-9241-2019.
Burgman, R. J., and Jang, Y. (2015). Simulated U.S. drought response to interannual and decadal pacific SST variability. *J. Clim.* 28, 4688–4705. doi:10.1175/JCLI-D-14-00247.1.
Burke, C., Stott, P., Ciavarella, A., and Sun, Y. (2016). Attribution of Extreme Rainfall in Southeast China During May 2015. *Bull. Am. Meteorol. Soc.* 97, S92–S96. doi:10.1175/BAMS-D-16-0144.1.
Burn, D. H., and Whitfield, P. H. (2016). Changes in floods and flood regimes in Canada. *Can. Water Resour. J.* 41, 139–150. doi:10.1080/07011784.2015.1026844.
Buttle, J. M., Allen, D. M., Caissie, D., Davison, B., Hayashi, M., Peters, D. L., et al. (2016). Flood processes in Canada: Regional and special aspects. *Can. Water Resour. J.* 41, 7–30. doi:10.1080/07011784.2015.1131629.
Byrne, M. P., and O'Gorman, P. A. (2015). The response of precipitation minus evapotranspiration to climate warming: Why the "Wet-get-wetter, dry-get-drier" scaling does not hold over land. *J. Clim.* 28, 8078–8092. doi:10.1175/JCLI-D-15-0369.1.
Byrne, M. P., and O'Gorman, P. A. (2018). Trends in continental temperature and humidity directly linked to ocean warming. *Proc. Natl. Acad. Sci. U. S. A.* 115, 4863–4868. doi:10.1073/pnas.1722312115.
Cai, W., Borlace, S., Lengaigne, M., Van Rensch, P., Collins, M., Vecchi, G., et al. (2014a). Increasing frequency of extreme El Niño events due to greenhouse warming. *Nat. Clim. Chang.* 4, 111–116. doi:10.1038/nclimate2100.
Cai, W., Purich, A., Cowan, T., Van Rensch, P., and Weller, E. (2014b). Did climate change-induced rainfall trends contribute to the australian millennium drought? *J. Clim.* 27, 3145–3168. doi:10.1175/JCLI-D-13-00322.1.
Cai, W., Santoso, A., Wang, G., Weller, E., Wu, L., Ashok, K., et al. (2014c). Increased frequency of extreme Indian ocean dipole events due to greenhouse warming. *Nature* 510, 254–258. doi:10.1038/nature13327.
Cai, W., Santoso, A., Wang, G., Yeh, S. W., An, S. Il, Cobb, K. M., et al. (2015). ENSO and greenhouse warming. *Nat. Clim. Chang.* 5, 849–859. doi:10.1038/nclimate2743.
Cai, W., Wang, G., Gan, B., Wu, L., Santoso, A., Lin, X., et al. (2018). Stabilised frequency of extreme positive Indian Ocean Dipole under 1.5°C warming. *Nat. Commun.* 9, 4–11. doi:10.1038/s41467-018-03789-6.
Callaghan, J., and Power, S. B. (2011). Variability and decline in the number of severe tropical cyclones making land-fall over eastern Australia since the late nineteenth century. *Clim. Dyn.* 37, 647–662. doi:10.1007/s00382-010-0883-2.
Caloiero, T. (2015). Analysis of rainfall trend in New Zealand. *Environ. Earth Sci.* 73, 6297–6310. doi:10.1007/s12665-014-3852-y.
Caloiero, T. (2017). Trend of monthly temperature and daily extreme temperature during 1951–2012 in New Zealand. *Theor. Appl. Climatol.* 129, 111–127. doi:10.1007/s00704-016-1764-3.
Camargo, S. J., Emanuel, K. A., and Sobel, A. H. (2007). Use of a Genesis Potential Index to Diagnose ENSO Effects on Tropical Cyclone Genesis. *J. Clim.* 20, 4819–4834. doi:10.1175/JCLI4282.1.
Camargo, S. J., Tippett, M. K., Sobel, A. H., Vecchi, G. A., and Zhao, M. (2014). Testing the performance of tropical cyclone genesis indices in future climates using the HiRAM model. *J. Clim.* 27, 9171–9196. doi:10.1175/JCLI-D-13-00505.1.
Camargo, S. J., and Wing, A. A. (2016). Tropical cyclones in climate models. *Wiley Interdiscip. Rev. Clim. Chang.* 7, 211–237. doi:10.1002/wcc.373.
Cannaby, H., Palmer, M. D., Howard, T., Bricheno, L., Calvert, D., Krijnen, J., et al. (2015). Projected sea level rise and changes in extreme storm surge and wave events during the 21st century in the region of Singapore. *Ocean Sci. Discuss.* 12, 2955–3001. Available at: https://www.scopus.com/inward/record.uri?eid=2-s2.0-85042575028&doi=10.5194%2Fosd-12-2955-2015&partnerID=40&md5=42c9a3bd47148171c95681366f68a08a.
Cardoso, R. M., Soares, P. M. M., Lima, D. C. A., and Miranda, P. M. A. (2019). Mean and extreme temperatures in a warming climate: EURO CORDEX and WRF regional climate high-resolution projections for Portugal. *Clim. Dyn.* 52, 129–157. doi:10.1007/s00382-018-4124-4.
Casanueva, A., Rodríguez-Puebla, C., Frías, M. D., and González-Reviriego, N. (2014). Variability of extreme precipitation over Europe and its relationships with teleconnection patterns. *Hydrol. Earth Syst. Sci.* 18, 709–725. doi:10.5194/hess-18-709-2014.
Cattiaux, J., and Ribes, A. (2018). Defining Single Extreme Weather Events in a Climate Perspective. *Bull. Am. Meteorol. Soc.* 99, 1557–1568. doi:10.1175/BAMS-D-17-0281.1.
Catto, J. L. (2016). Extratropical cyclone classification and its use in climate studies. *Rev. Geophys.*, 486–520. doi:10.1002/2016RG000519.Extratropical.
Catto, J. L., Jakob, C., and Nicholls, N. (2013). A global evaluation of fronts and precipitation in the ACCESS model. *Aust. Meteorol. Oceanogr. J.* 63, 191–203. doi:10.22499/2.6301.012.
Catto, J. L., Jakob, C., and Nicholls, N. (2015). Can the CMIP5 models represent winter frontal precipitation? *Geophys.*

Res. Lett. doi:10.1002/2015GL066015.
Catto, J. L., and Pfahl, S. (2013). The importance of fronts for extreme precipitation. *J. Geophys. Res. Atmos.* 118, 10791–10801. doi:10.1002/jgrd.50852.
Cavanaugh, N. R., and Shen, S. S. P. (2015). The Effects of Gridding Algorithms on the Statistical Moments and Their Trends of Daily Surface Air Temperature. *J. Clim.* 28, 9188–9205. doi:10.1175/JCLI-D-14-00668.1.
Cavicchia, L., von Storch, H., and Gualdi, S. (2014). Mediterranean Tropical-Like Cyclones in Present and Future Climate. *J. Clim.* 27, 7493–7501. doi:10.1175/JCLI-D-14-00339.1.
Ceccherini, G., Russo, S., Ameztoy, I., Romero, C. P., and Carmona-Moreno, C. (2016). Magnitude and frequency of heat and cold waves in recent decades: the case of South America. *Nat. Hazards Earth Syst. Sci.* 16, 821–831. doi:10.5194/nhess-16-821-2016.
Chadwick, R., Boutle, I., and Martin, G. (2013). Spatial patterns of precipitation change in CMIP5: Why the rich do not get richer in the tropics. *J. Clim.* 26, 3803–3822. doi:10.1175/JCLI-D-12-00543.1.
Chai, R., Sun, S., Chen, H., and Zhou, S. (2018). Changes in reference evapotranspiration over China during 1960–2012: Attributions and relationships with atmospheric circulation. *Hydrol. Process.* 32, 3032–3048. doi:10.1002/hyp.13252.
Chakraborty, D., Sehgal, V. K., Dhakar, R., Varghese, E., Das, D. K., and Ray, M. (2018). Changes in daily maximum temperature extremes across India over 1951-2014 and their relation with cereal crop productivity. *Stoch. Environ. Res. Risk Assess.* 32. doi:https://doi.org/10.1007/s00477-018-1604-3.
Chakraborty, J., Collins, T. W., Montgomery, M. C., and Grineski, S. E. (2014). Social and spatial inequities in exposure to flood risk in Miami, Florida. *Nat. Hazards Rev.* 15. Available at: https://www.scopus.com/inward/record.uri?eid=2-s2.0-84904497484&doi=10.1061%2F%28ASCE%29NH.1527-6996.0000140&partnerID=40&md5=e016664fde653fa44fc256f6dce587a1.
Chan, K. T. F., and Chan, J. C. L. (2012). Size and Strength of Tropical Cyclones as Inferred from QuikSCAT Data. *Mon. Weather Rev.* 140, 811–824. doi:10.1175/MWR-D-10-05062.1.
Chan, K. T. F., and Chan, J. C. L. (2015). Global climatology of tropical cyclone size as inferred from QuikSCAT data. *Int. J. Climatol.* 35, 4843–4848. doi:10.1002/joc.4307.
Chan, S. C., Kendon, E. J., Roberts, N. M., Fowler, H. J., and Blenkinsop, S. (2016). The characteristics of summer sub-hourly rainfall over the southern UK in a high-resolution convective permitting model. *Environ. Res. Lett.* 11, 094024. doi:10.1088/1748-9326/11/9/094024.
Chaney, N. W., Sheffield, J., Villarini, G., and Wood, E. F. (2014). Development of a high-resolution gridded daily meteorological dataset over sub-Saharan Africa: Spatial analysis of trends in climate extremes. *J. Clim.* doi:10.1175/JCLI-D-13-00423.1.
Chang, E. K. M. (2014). Impacts of background field removal on CMIP5 projected changes in Pacific winter cyclone activity. *J. Geophys. Res. Atmos.* 119, 4626–4639. doi:10.1038/175238c0.
Chang, E. K. M. (2017). Projected Significant Increase in the Number of Extreme Extratropical Cyclones in the Southern Hemisphere. *J. Clim.* 30, 4915–4935. doi:10.1175/JCLI-D-16-0553.1.
Chang, E. K. M., and Yau, A. M. W. (2016). Northern Hemisphere winter storm track trends since 1959 derived from multiple reanalysis datasets. *Clim. Dyn.* 47, 1435–1454. doi:10.1007/s00382-015-2911-8.
Chapman, S., Watson, J. E. M., Salazar, A., Thatcher, M., and McAlpine, C. A. (2017). The impact of urbanization and climate change on urban temperatures: a systematic review. *Landsc. Ecol.* 32, 1921–1935. doi:10.1007/s10980-017-0561-4.
Chemke, R., and Polvani, L. M. (2019). Opposite tropical circulation trends in climate models and in reanalyses. *Nat. Geosci.* 12, 528–532. doi:10.1038/s41561-019-0383-x.
Chen, C.-T., and Knutson, T. (2008). On the Verification and Comparison of Extreme Rainfall Indices from Climate Models. *J. Clim.* 21, 1605–1621. doi:10.1175/2007JCLI1494.1.
Chen, D., Guo, J., Yao, D., Lin, Y., Zhao, C., Min, M., et al. (2019). Mesoscale Convective Systems in the Asian Monsoon Region From Advanced Himawari Imager: Algorithms and Preliminary Results. *J. Geophys. Res. Atmos.* 124, 2210–2234. doi:10.1029/2018JD029707.
Chen, H., and Sun, J. (2015a). Assessing model performance of climate extremes in China: an intercomparison between CMIP5 and CMIP3. *Clim. Change* 129, 197–211. doi:10.1007/s10584-014-1319-5.
Chen, H., and Sun, J. (2015b). Changes in Drought Characteristics over China Using the Standardized Precipitation Evapotranspiration Index. *J. Clim.* 28, 5430–5447. doi:10.1175/JCLI-D-14-00707.1.
Chen, H., and Sun, J. (2017a). Anthropogenic warming has caused hot droughts more frequently in China. *J. Hydrol.* 544, 306–318.
Chen, H., and Sun, J. (2017b). Characterizing present and future drought changes over eastern China. *Int. J. Climatol.* 37, 138–156. doi:10.1002/joc.4987.
Chen, H., and Sun, J. (2017c). Contribution of human influence to increased daily precipitation extremes over China. *Geophys. Res. Lett.* doi:10.1002/2016GL072439.
Chen, L., Li, D., and Pryor, S. C. (2013a). Wind speed trends over China: Quantifying the magnitude and assessing

causality. *Int. J. Climatol.* 33, 2579–2590. doi:10.1002/joc.3613.
Chen, R., Wen, Z., and Lu, R. (2016). Evolution of the circulation anomalies and the quasi-biweekly oscillations associated with extreme heat events in Southern China. *J. Clim.* 29, 6909–6921. doi:10.1175/JCLI-D-16-0160.1.
Chen, S., Li, Y., Kim, J., and Kim, S. W. (2017). Bayesian change point analysis for extreme daily precipitation. *Int. J. Climatol.* 37, 3123–3137. doi:10.1002/joc.4904.
Chen, Y.-R., Yu, B., and Jenkins, G. (2013b). Secular Variation in Rainfall Intensity and Temperature in Eastern Australia. *J. Hydrometeorol.* 14, 1356–1363. doi:10.1175/JHM-D-12-0110.1.
Cheng, L., Hoerling, M., Smith, L., and Eischeid, J. (2018). Diagnosing Human-Induced Dynamic and Thermodynamic Drivers of Extreme Rainfall. *J. Clim.* 31, 1029–1051. doi:10.1175/JCLI-D-16-0919.1.
Cheng, S., Guan, X., Huang, J., Ji, F., and Guo, R. (2015). Long-term trend and variability of soil moisture over East Asia. *J. Geophys. Res.* 120, 8658–8670. Available at: https://www.scopus.com/inward/record.uri?eid=2-s2.0-84943450279&doi=10.1002%2F2015JD023206&partnerID=40&md5=d1bdb74834f4e4c05f225a72fd7135e3.
Cheong, W. K., Timbal, B., Golding, N., Sirabaha, S., Kwan, K. F., Cinco, T. A., et al. (2018). Observed and modelled temperature and precipitation extremes over Southeast Asia from 1972 to 2010. *Int. J. Climatol.* 38, 3013–3027. doi:10.1002/joc.5479.
Chevuturi, A., Klingaman, N. P., Turner, A. G., and Hannah, S. (2018). Projected Changes in the Asian-Australian Monsoon Region in 1.5°C and 2.0°C Global-Warming Scenarios. *Earth's Futur.* 6, 339–358. doi:10.1002/2017EF000734.
Cho, C., Li, R., Wang, S.-Y., Yoon, J.-H., and Gillies, R. R. (2016). Anthropogenic footprint of climate change in the June 2013 northern India flood. *Clim. Dyn.* 46, 797–805. doi:10.1007/s00382-015-2613-2.
Chou, S. C., Lyra, A., Mourão, C., Dereczynski, C., Pilotto, I., Gomes, J., et al. (2014a). Assessment of Climate Change over South America under RCP 4.5 and 8.5 Downscaling Scenarios. *Am. J. Clim. Chang.* 03, 512–527. doi:10.4236/ajcc.2014.35043.
Chou, S. C., Lyra, A., Mourão, C., Dereczynski, C., Pilotto, I., Gomes, J., et al. (2014b). Evaluation of the Eta Simulations Nested in Three Global Climate Models. *Am. J. Clim. Chang.* 03, 438–454. doi:10.4236/ajcc.2014.35039.
Christensen, J. H., Kumar Krishna, K., Aldrian, E., An, S.-I., Cavalcanti, I. F. A., Castro, M. de, et al. (2013). "Climate Phenomena and their Relevance for Future Regional Climate Change," in *Climate Change 2013 - The Physical Science Basis*, ed. Intergovernmental Panel on Climate Change (Cambridge, United Kingdom and New York, NY, USA: Cambridge University Press), 1217–1308. doi:10.1017/CBO9781107415324.028.
Christiansen, B., Alvarez-Castro, C., Christidis, N., Ciavarella, A., Colfescu, I., Cowan, T., et al. (2018). Was the Cold European Winter of 2009/10 Modified by Anthropogenic Climate Change? An Attribution Study. *J. Clim.* 31, 3387–3410. doi:10.1175/JCLI-D-17-0589.1.
Christidis, N., Jones, G. S., and Stott, P. A. (2015). Dramatically increasing chance of extremely hot summers since the 2003 European heatwave. *Nat. Clim. Chang.* 5, 46–50. doi:10.1038/nclimate2468.
Christidis, N., and Stott, P. A. (2014). Change in the Odds of Warm Years and Seasons Due to Anthropogenic Influence on the Climate. *J. Clim.* 27, 2607–2621.
Christidis, N., and Stott, P. A. (2016). Attribution analyses of temperature extremes using a set of 16 indices. *Weather Clim. Extrem.* 14, 24–35. doi:10.1016/j.wace.2016.10.003.
Christidis, N., Stott, P. A., and Ciavarella, A. (2014). The effect of anthropogenic climate change on the cold spring of 2013 in the United Kingdom. *Bull. Am. Meteorol. Soc.* 95, S15–S18. doi:10.1175/1520-0477-95.9.S1.1.
Christidis, N., Stott, P. A., Karoly, D. J., and Ciavarella, A. (2013a). An Attribution Study of the Heavy Rainfall Over Eastern Australia in March 2012. *Bull. Am. Meteorol. Soc.* 94, S58-61.
Christidis, N., Stott, P. A., Scaife, A. A., Arribas, A., Jones, G. S., Copsey, D., et al. (2013b). A New HadGEM3-A-Based System for Attribution of Weather- and Climate-Related Extreme Events. *J. Clim.* 26, 2756–2783. doi:10.1175/JCLI-D-12-00169.1.
Ciais, P., Reichstein, M., Viovy, N., Granier, A., Ogée, J., Allard, V., et al. (2005). Europe-wide reduction in primary productivity caused by the heat and drought in 2003. *Nature* 437, 529–533. doi:10.1038/nature03972.
Cioffi, F., Lall, U., Rus, E., and Krishnamurthy, C. K. B. (2015). Space-time structure of extreme precipitation in Europe over the last century. *Int. J. Climatol.* 35, 1749–1760. doi:10.1002/joc.4116.
Clark, R. T., and Brown, S. J. (2013). Influences of Circulation and Climate Change on European Summer Heat Extremes. *J. Clim.* 26, 9621–9632. doi:10.1175/JCLI-D-12-00740.1.
Clark, R. T., Brown, S. J., and Murphy, J. M. (2006). Modeling Northern Hemisphere Summer Heat Extreme Changes and Their Uncertainties Using a Physics Ensemble of Climate Sensitivity Experiments. *J. Clim.* 19, 4418–4435. doi:10.1175/JCLI3877.1.
Coffel, E. D., Horton, R. M., and de Sherbinin, A. (2018). Temperature and humidity based projections of a rapid rise in global heat stress exposure during the 21st century. *Environ. Res. Lett.* 13, 014001. doi:10.1088/1748-9326/aaa00e.
Cohen, J., Furtado, J. C., Jones, J., Barlow, M., Whittleston, D., and Entekhabi, D. (2014). Linking Siberian Snow

Cover to Precursors of Stratospheric Variability. *J. Clim.* 27, 5422–5432. doi:10.1175/JCLI-D-13-00779.1.
Cohen, J., Ye, H., and Jones, J. (2015). Trends and variability in rain-on-snow events. *Geophys. Res. Lett.* 42, 7115–7122. doi:10.1002/2015GL065320.
Coles, S. (2001). *An Introduction to Statistical Modeling of Extreme Values*. London, UK: Springer Series in Statistics.
Colle, B. A., Zhang, Z., Lombardo, K. A., Chang, E., Liu, P., and Zhang, M. (2013). Historical evaluation and future prediction of eastern North American and Western Atlantic extratropical cyclones in the CMIP5 models during the cool season. *J. Clim.* doi:10.1175/JCLI-D-12-00498.1.
Collins, J. M., Klotzbach, P. J., Maue, R. N., Roache, D. R., Blake, E. S., Paxton, C. H., et al. (2016). The record-breaking 2015 hurricane season in the eastern North Pacific: An analysis of environmental conditions. *Geophys. Res. Lett.* 43, 9217–9224. doi:10.1002/2016GL070597.
Collins, M., Knutti, R., Arblaster, J., Dufresne, J.-L., Fichefet, T., Friedlingstein, P., et al. (2013a). "Long-term Climate Change: Projections, Commitments and Irreversibility," in *Climate Change 2013 - The Physical Science Basis*, ed. Intergovernmental Panel on Climate Change (Cambridge, United Kingdom and New York, NY, USA: Cambridge University Press), 1029–1136. doi:10.1017/CBO9781107415324.024.
Collins, M., Knutti, R., Arblaster, J., Dufresne, J.-L., Fichefet, T., Friedlingstein, P., et al. (2013b). "Long-term Climate Change: Projections, Commitments and Irreversibility Pages 1029 to 1076," in *Climate Change 2013 - The Physical Science Basis*, ed. Intergovernmental Panel on Climate Change (Cambridge, United Kingdom and New York, NY, USA: Cambridge University Press), 1029–1136. doi:10.1017/CBO9781107415324.024.
Compo, G. P., Whitaker, J. S., Sardeshmukh, P. D., Matsui, N., Allan, R. J., Yin, X., et al. (2011). The Twentieth Century Reanalysis Project. *Q. J. R. Meteorol. Soc.* 137, 1–28. doi:10.1002/qj.776.
Contractor, S., Donat, M. G., Alexander, L. V, Ziese, M., Meyer-Christoffer, A., Schneider, U., et al. (2019). Rainfall Estimates on a Gridded Network (REGEN) -- A global land-based gridded dataset of daily precipitation from 1950--2013. *Hydrol. Earth Syst. Sci. Discuss.* 2019, 1–30. doi:10.5194/hess-2018-595.
Cook, B. I., Anchukaitis, K. J., Touchan, R., Meko, D. M., and Cook, E. R. (2016a). Spatiotemporal drought variability in the Mediterranean over the last 900 years. *J. Geophys. Res. Atmos.* 121, 2060–2074. doi:10.1002/2015JD023929.
Cook, B. I., Ault, T. R., and Smerdon, J. E. (2015a). Unprecedented 21st century drought risk in the American Southwest and Central Plains. *Sci. Adv.* 1. doi:10.1126/sciadv.1400082.
Cook, B. I., Cook, E. R., Smerdon, J. E., Seager, R., Williams, A. P., Coats, S., et al. (2016b). North American megadroughts in the Common Era: Reconstructions and simulations. *Wiley Interdiscip. Rev. Clim. Chang.* 7, 411–432. doi:10.1002/wcc.394.
Cook, B. I., Mankin, J. S., and Anchukaitis, K. J. (2018). Climate Change and Drought: From Past to Future. *Curr. Clim. Chang. Reports* 4, 164–179. doi:10.1007/s40641-018-0093-2.
Cook, B. I., Palmer, J. G., Cook, E. R., Turney, C. S. M., Allen, K., Fenwick, P., et al. (2016c). The paleoclimate context and future trajectory of extreme summer hydroclimate in eastern Australia. *J. Geophys. Res.* 121, 12,812-820,838.
Cook, B. I., Seager, R., Park Williams, A., Puma, M. J., McDermid, S., Kelley, M., et al. (2019). Climate change amplification of natural drought variability: The historic mid-twentieth-century North American drought in a warmer world. *J. Clim.* 32, 5417–5436. doi:10.1175/JCLI-D-18-0832.1.
Cook, B. I., Smerdon, J. E., Seager, R., and Coats, S. (2014a). Global warming and 21st century drying. *Clim. Dyn.* 43, 2607–2627. doi:10.1007/s00382-014-2075-y.
Cook, B. I., Smerdon, J. E., Seager, R., and Cook, E. R. (2014b). Pan-Continental Droughts in North America over the Last Millennium. *J. Clim.* 27, 383–397. doi:10.1175/JCLI-D-13-00100.1.
Cook, E. R., Woodhouse, C. A., Mark Eakin, C., Meko, D. M., and Stahle, D. W. (2004). Long-Term Aridity Changes in the Western United States. *Science* 306, 1015–1018. doi:10.1126/science.1102586.
Cook, M. A., King, C. W., Davidson, F. T., and Webber, M. E. (2015b). Assessing the impacts of droughts and heat waves at thermoelectric power plants in the United States using integrated regression, thermodynamic, and climate models. *Energy Reports* 1, 193–203. doi:10.1016/j.egyr.2015.10.002.
Corbella, S., and Stretch, D. D. (2012). Multivariate return periods of sea storms for coastal erosion risk assessment. *Nat. Hazards Earth Syst. Sci.* 12, 2699–2708. doi:10.5194/nhess-12-2699-2012.
Corrales-Suastegui, A., Fuentes-Franco, R., and Pavia, E. G. (2019). The mid-summer drought over Mexico and Central America in the 21st century. *Int. J. Climatol.* doi:10.1002/joc.6296.
Couasnon, A., Eilander, D., Muis, S., Veldkamp, T. I. E., Haigh, I. D., Wahl, T., et al. (submitted). Measuring compound flood potential from river discharge and storm surge extremes at the global scale and its implications for flood hazard. *Nat. Hazards Earth Syst. Sci.*(submitted). doi:https://doi.org/10.5194/nhess-2019-205.
Coumou, D., Di Capua, G., Vavrus, S., Wang, L., and Wang, S. (2018). The influence of Arctic amplification on mid-latitude summer circulation. *Nat. Commun.* 9, 2959. doi:10.1038/s41467-018-05256-8.
Coumou, D., Lehmann, J., and Beckmann, J. (2015). The weakening summer circulation in the Northern Hemisphere mid-latitudes. *Science* 348, 324–327. doi:10.1126/science.1261768.

Cowan, T., Hegerl, G. C., Colfescu, I., Bollasina, M., Purich, A., and Boschat, G. (2016). Factors Contributing to Record-Breaking Heat Waves over the Great Plains during the 1930s Dust Bowl. *J. Clim.* 30, 2437–2461. doi:10.1175/JCLI-D-16-0436.1.

Cowan, T., Purich, A., Perkins, S., Pezza, A., Boschat, G., and Sadler, K. (2014). More frequent, longer, and hotter heat waves for Australia in the Twenty-First Century. *J. Clim.* 27, 5851–5871. doi:10.1175/JCLI-D-14-00092.1.

Crimp, S. J., Zheng, B., Khimashia, N., Gobbett, D. L., Chapman, S., Howden, M., et al. (2016). Recent changes in southern Australian frost occurrence: Implications for wheat production risk. *Crop Pasture Sci.* 67, 801–811. doi:10.1071/CP16056.

Croitoru, A.-E., Chiotoroiu, B.-C., Ivanova Todorova, V., and Torică, V. (2013). Changes in precipitation extremes on the Black Sea Western Coast. *Glob. Planet. Change* 102, 10–19. doi:10.1016/j.gloplacha.2013.01.004.

Croitoru, A.-E., and Piticar, A. (2013). Changes in daily extreme temperatures in the extra-Carpathians regions of Romania. *Int. J. Climatol.* 33, 1987–2001. doi:10.1002/joc.3567.

Croitoru, A.-E., Piticar, A., and Burada, D. C. (2016). Changes in precipitation extremes in Romania. *Quat. Int.* 415, 325–335. doi:10.1016/J.QUAINT.2015.07.028.

Crook, J., Klein, C., Folwell, S., Taylor, C. M., Parker, D. J., Stratton, R., et al. (2019). Assessment of the Representation of West African Storm Lifecycles in Convection-Permitting Simulations. *Earth Sp. Sci.* 6, 818–835. doi:10.1029/2018EA000491.

Dadaser-Celik, F., and Cengiz, E. (2014). Wind speed trends over Turkey from 1975 to 2006. *Int. J. Climatol.* 34, 1913–1927. doi:10.1002/joc.3810.

Dai, A. (2013). Increasing drought under global warming in observations and models. *Nat. Clim. Chang.* 3, 52. Available at: http://dx.doi.org/10.1038/nclimate1633.

Dai, A., and Zhao, T. (2017). Uncertainties in historical changes and future projections of drought. Part I: estimates of historical drought changes. *Clim. Change* 144, 519–533. doi:10.1007/s10584-016-1705-2.

Dai, A., Zhao, T., and Chen, J. (2018). Climate Change and Drought: a Precipitation and Evaporation Perspective. *Curr. Clim. Chang. Reports* 4, 301–312. doi:10.1007/s40641-018-0101-6.

Daloz, A. S., and Camargo, S. J. (2018). Is the poleward migration of tropical cyclone maximum intensity associated with a poleward migration of tropical cyclone genesis? *Clim. Dyn.* 50, 705–715. doi:10.1007/s00382-017-3636-7.

Dankers, R., Arnell, N. W., Clark, D. B., Falloon, P. D., Fekete, B. M., Gosling, S. N., et al. (2014). First look at changes in flood hazard in the Inter-Sectoral Impact Model Intercomparison Project ensemble. *Proc. Natl. Acad. Sci.* 111, 3257–3261. doi:10.1073/pnas.1302078110.

Dashkhuu, D., Kim, J. P., Chun, J. A., and Lee, W.-S. (2015). Long-term trends in daily temperature extremes over Mongolia. *Weather Clim. Extrem.* 8, 26–33. doi:10.1016/j.wace.2014.11.003.

Davin, E. L., Seneviratne, S. I., Ciais, P., Olioso, A., and Wang, T. (2014). Preferential cooling of hot extremes from cropland albedo management. *Proc. Natl. Acad. Sci.* 111, 9757–9761. doi:10.1073/pnas.1317323111.

Davis, N., and Birner, T. (2016). Climate model biases in the width of the tropical belt. *J. Clim.* 29, 1935–1954. doi:10.1175/JCLI-D-15-0336.1.

de Abreu, R. C., Cunningham, C., Rudorff, C. M., Rudorff, N., Abatan, A. A., Tett, S. F. B., et al. (2019). Contribution of Anthropogenic Climate Change to April–May 2017 Heavy Precipitation over the Uruguay River Basin. *Bull. Am. Meteorol. Soc.* 100, S37–S41. doi:10.1175/BAMS-D-18-0102.1.

De Boer, E. J., Tjallingii, R., Vélez, M. I., Rijsdijk, K. F., Vlug, A., Reichart, G.-J., et al. (2014). Climate variability in the SW Indian Ocean from an 8000-yr long multi-proxy record in the Mauritian lowlands shows a middle to late Holocene shift from negative IOD-state to ENSO-state. *Quat. Sci. Rev.* 86, 175–189. Available at: https://www.scopus.com/inward/record.uri?eid=2-s2.0-84892855256&doi=10.1016%2Fj.quascirev.2013.12.026&partnerID=40&md5=afcb5a7c7b024b2eedc82ab5b15ceb12.

de Boer, E. J., Vélez, M. I., Rijsdijk, K. F., de Louw, P. G. B., Vernimmen, T. J. J., Visser, P. M., et al. (2015). A deadly cocktail: How a drought around 4200 cal. yr BP caused mass mortality events at the infamous 'dodo swamp' in Mauritius. *Holocene* 25, 758–771. Available at: https://www.scopus.com/inward/record.uri?eid=2-s2.0-84926468755&doi=10.1177%2F0959683614567886&partnerID=40&md5=88e165c2c8e167ffd7ed21875660f5fe.

de Lima, M. I. P., Santo, F. E., Ramos, A. M., and Trigo, R. M. (2015). Trends and correlations in annual extreme precipitation indices for mainland Portugal, 1941–2007. *Theor. Appl. Climatol.* 119, 55–75. doi:10.1007/s00704-013-1079-6.

Dean, S. M., Rosier, S., Carey-Smith, T., and Stott, P. A. (2013). The role of climate change in the two-day extreme rainfall in Golden Bay, New Zealand, December 2011. *Bull. Am. Meteorol. Soc.* 94, S61–S63.

Dee, D. P., Källén, E., Simmons, A. J., and Haimberger, L. (2011a). Comments on "Reanalyses Suitable for Characterizing Long-Term Trends." *Bull. Am. Meteorol. Soc.* 92, 65–70. doi:10.1175/2010BAMS3070.1.

Dee, D. P., Uppala, S. M., Simmons, A. J., Berrisford, P., Poli, P., Kobayashi, S., et al. (2011b). The ERA-Interim

reanalysis: configuration and performance of the data assimilation system. *Q. J. R. Meteorol. Soc.* 137, 553–597. doi:10.1002/qj.828.
Degefie, D. T., Fleischer, E., Klemm, O., Soromotin, A. V., Soromotina, O. V., Tolstikov, A. V., et al. (2014). Climate extremes in South Western Siberia: past and future. *Stoch. Environ. Res. Risk Assess.* 28, 2161–2173. doi:10.1007/s00477-014-0872-9.
Denniston, R. F., and Luetscher, M. (2017). Speleothems as high-resolution paleo fl ood archives. 170, 1–13. doi:10.1016/j.quascirev.2017.05.006.
Deser, C., Hurrell, J. W., and Phillips, A. S. (2017). The role of the North Atlantic Oscillation in European climate projections. *Clim. Dyn.* 49, 3141–3157. doi:10.1007/s00382-016-3502-z.
Devanand, A., Huang, M., Ashfaq, M., Barik, B., and Ghosh, S. (2019). Choice of Irrigation Water Management Practice Affects Indian Summer Monsoon Rainfall and Its Extremes. *Geophys. Res. Lett.* 46, 9126–9135. doi:10.1029/2019GL083875.
Dey, R., Lewis, S., Arblaster, J., and Abram, N. (2018). A Review of Past and Projected Changes in Australia's Rainfall. *Wiley Interdiscip. Rev. Clim. Chang.*
Dey, R., Lewis, S. C., and Abram, N. J. (2019). Investigating observed northwest Australian rainfall trends in Coupled Model Intercomparison Project phase 5 detection and attribution experiments. *Int. J. Climatol.* 39, 112–127. doi:10.1002/joc.5788.
Dhurmea, K. R., Boojhawon, R., and Rughooputh, S. D. D. V. (2019). A drought climatology for Mauritius using the standardized precipitation index. *Hydrol. Sci. J.* 64, 227–240. Available at: https://www.scopus.com/inward/record.uri?eid=2-s2.0-85062462477&doi=10.1080%2F02626667.2019.1570209&partnerID=40&md5=d2af24491d0962b14998e5611249bbd9.
Di Luca, A., Argüeso, D., Evans, J. P. J. P., De Elía, R., Laprise, R., Elía, R., et al. (2016a). Quantifying the overall added value of dynamical downscaling and the contribution from different spatial scales. *J. Geophys. Res. Atmos.* 121, 1575–1590. doi:10.1002/2015JD024009.Received.
Di Luca, A., de Elia, R., Bador, M., and Argueso, D. (submitted). Contribution of mean climate to hot temperature extremes for present and future climates. *Weather Clim. Extrem.*(submitted).
Di Luca, A., de Elía, R., and Laprise, R. (2015a). Challenges in the Quest for Added Value of Regional Climate Dynamical Downscaling. *Curr. Clim. Chang. Reports* 1, 10–21. doi:10.1007/s40641-015-0003-9.
Di Luca, A., Evans, J. J. P., Pepler, A. S. A., Alexander, L. V. L., and Argüeso, D. (2016b). Evaluating the representation of Australian East Coast Lows in a regional climate model ensemble. *J. South. Hemisph. Earth Syst. Sci.* 66, 108–124. doi:10.22499/3.6602.003.
Di Luca, A., Evans, J. P. J. P., Pepler, A., Alexander, L., and Argüeso, D. (2015b). Resolution sensitivity of cyclone climatology over Eastern Australia using six reanalysis products. *J. Clim.* 28, 9530–9549. doi:10.1175/JCLI-D-14-00645.1.
Diaconescu, E. P., Mailhot, A., Brown, R., and Chaumont, D. (2018). Evaluation of CORDEX-Arctic daily precipitation and temperature-based climate indices over Canadian Arctic land areas. *Clim. Dyn.* 50, 2061–2085. doi:10.1007/s00382-017-3736-4.
Diallo, I., Giorgi, F., Deme, A., Tall, M., Mariotti, L., and Gaye, A. T. (2016). Projected changes of summer monsoon extremes and hydroclimatic regimes over West Africa for the twenty-first century. *Clim. Dyn.* doi:10.1007/s00382-016-3052-4.
Diallo, I., Giorgi, F., Sukumaran, S., Stordal, F., and Giuliani, G. (2015). Evaluation of RegCM4 driven by CAM4 over Southern Africa: mean climatology, interannual variability and daily extremes of wet season temperature and precipitation. *Theor. Appl. Climatol.* 121, 749–766. doi:10.1007/s00704-014-1260-6.
Díaz, L. B., and Vera, C. S. (2018). South American precipitation changes simulated by PMIP3/CMIP5 models during the Little Ice Age and the recent global warming period. *Int. J. Climatol.* 38, 2638–2650. doi:10.1002/joc.5449.
Diedhiou, A., Bichet, A., Wartenburger, R., Seneviratne, S. I., Rowell, D. P., Sylla, M. B., et al. (2018). Changes in climate extremes over West and Central Africa at 1.5 °C and 2 °C global warming. *Environ. Res. Lett.* 13, 065020. doi:10.1088/1748-9326/aac3e5.
Diffenbaugh, N. S., Scherer, M., and Trapp, R. J. (2013). Robust increases in severe thunderstorm environments in response to greenhouse forcing. *Proc. Natl. Acad. Sci.* 110, 16361 LP – 16366. doi:10.1073/pnas.1307758110.
Diffenbaugh, N. S., Singh, D., Mankin, J. S., Horton, D. E., Swain, D. L., Touma, D., et al. (2017). Quantifying the influence of global warming on unprecedented extreme climate events. *Proc. Natl. Acad. Sci.* 114, 4881–4886.
Diffenbaugh, N. S., Swain, D. L., and Touma, D. (2015). Anthropogenic warming has increased drought risk in California. *Proc. Natl. Acad. Sci.* 112, 3931 LP – 3936. doi:10.1073/pnas.1422385112.
Dimri, A. P. (2019). Comparison of regional and seasonal changes and trends in daily surface temperature extremes over India and its subregions. *Theor. Appl. Climatol.* 136. doi:10.1007/s00704-018-2486-5.
Dimri, A. P., Niyogi, D., Barros, A. P., Ridley, J., Mohanty, U. C., Yasunari, T., et al. (2015). Western Disturbances: A review. *Rev. Geophys.* 53, 225–246. doi:10.1002/2014RG000460.

Dirmeyer, P. A., Gao, X., Zhao, M., Guo, Z., Oki, T., and Hanasaki, N. (2006). GSWP-2: Multimodel Analysis and Implications for Our Perception of the Land Surface. *Bull. Am. Meteorol. Soc.* 87, 1381–1398. doi:10.1175/BAMS-87-10-1381.
Dirmeyer, P. A., Jin, Y., Singh, B., and Yan, X. (2013). Trends in land-atmosphere interactions from CMIP5 simulations. *J. Hydrometeorol.* 14, 829–849. doi:10.1175/JHM-D-12-0107.1.
Diro, G. T., Sushama, L., and Huziy, O. (2018). Snow-atmosphere coupling and its impact on temperature variability and extremes over North America. *Clim. Dyn.* 50, 2993–3007. doi:10.1007/s00382-017-3788-5.
Dittus, A. J., Karoly, D. J., Donat, M. G., Lewis, S. C., and Alexander, L. V (2018). Understanding the role of sea surface temperature-forcing for variability in global temperature and precipitation extremes. *Weather Clim. Extrem.*, 0–1.
Dittus, A. J., Karoly, D. J., Lewis, S. C., and Alexander, L. V. (2014). An investigation of some unexpected frost day increases in southern Australia. *Aust. Meteorol. Oceanogr. J.* 64, 261–271. doi:10.22499/2.6404.002.
Dittus, A. J., Karoly, D. J., Lewis, S. C., Alexander, L. V., and Donat, M. G. (2016). A multiregion model evaluation and attribution study of historical changes in the area affected by temperature and precipitation extremes. *J. Clim.* 29, 8285–8299. doi:10.1175/JCLI-D-16-0164.1.
Do, H. X., Gudmundsson, L., Leonard, M., and Westra, S. (2018). The Global Streamflow Indices and Metadata Archive (GSIM) – Part 1: The production of a daily streamflow archive and metadata. *Earth Syst. Sci. Data* 10, 765–785. doi:10.5194/essd-10-765-2018.
Do, H. X., Westra, S., and Leonard, M. (2017). A global-scale investigation of trends in annual maximum streamflow. *J. Hydrol.* 552, 28–43. doi:10.1016/j.jhydrol.2017.06.015.
Döll, P., Douville, H., Güntner, A., Müller Schmied, H., and Wada, Y. (2016). Modelling Freshwater Resources at the Global Scale: Challenges and Prospects. *Surv. Geophys.* 37, 195–221. doi:10.1007/s10712-015-9343-1.
Döll, P., Trautmann, T., Gerten, D., Schmied, H. M., Ostberg, S., Saaed, F., et al. (2018). Risks for the global freshwater system at 1.5 °c and 2 °c global warming. *Environ. Res. Lett.* 13. doi:10.1088/1748-9326/aab792.
Domínguez-Castro, F., García-Herrera, R., and Vicente-Serrano, S. M. (2018). Wet and dry extremes in Quito (Ecuador) since the 17th century. *Int. J. Climatol.* 38. doi:10.1002/joc.5312.
Domínguez-Castro, F., Vicente-Serrano, S. M., Tomás-Burguera, M., Peña-Gallardo, M., Beguería, S., El Kenawy, A., et al. (2019). High spatial resolution climatology of drought events for Spain: 1961–2014. *Int. J. Climatol.* 39, 5046–5062. doi:10.1002/joc.6126.
Donat, M. G., and Alexander, L. V. (2012). The shifting probability distribution of global daytime and night-time temperatures. *Geophys. Res. Lett.* 39, n/a-n/a. doi:10.1029/2012GL052459.
Donat, M. G., Alexander, L. V., Herold, N., and Dittus, A. J. (2016a). Temperature and precipitation extremes in century-long gridded observations, reanalyses, and atmospheric model simulations. *J. Geophys. Res. Atmos.* 121, 11,174-11,189. doi:10.1002/2016JD025480.
Donat, M. G., Alexander, L. V., Yang, H., Durre, I., Vose, R., Dunn, R. J. H. H., et al. (2013a). Updated analyses of temperature and precipitation extreme indices since the beginning of the twentieth century: The HadEX2 dataset. *J. Geophys. Res. Atmos.* 118, 2098–2118. doi:10.1002/jgrd.50150.
Donat, M. G., Alexander, L. V, Yang, H., Durre, I., Vose, R., and Caesar, J. (2013b). Global Land-Based Datasets for Monitoring Climatic Extremes. *Bull. Am. Meteorol. Soc.* 94, 997–1006.
Donat, M. G., Angélil, O., and Ukkola, A. M. (2019). Intensification of precipitation extremes in the world's humid and water-limited regions. *Environ. Res. Lett.* 14, 065003. doi:10.1088/1748-9326/ab1c8e.
Donat, M. G. G., Peterson, T. C. C., Brunet, M., King, A. D. D., Almazroui, M., Kolli, R. K. K., et al. (2014a). Changes in extreme temperature and precipitation in the Arab region: long-term trends and variability related to ENSO and NAO. *Int. J. Climatol.* 34, 581–592. doi:10.1002/joc.3707.
Donat, M. G., Lowry, A. L., Alexander, L. V., O'Gorman, P. A., and Maher, N. (2016b). More extreme precipitation in the world's dry and wet regions. *Nat. Clim. Chang.* 6, 508–513. doi:10.1038/nclimate2941.
Donat, M. G., Pitman, A. J., and Angélil, O. (2018). Understanding and Reducing Future Uncertainty in Midlatitude Daily Heat Extremes Via Land Surface Feedback Constraints. *Geophys. Res. Lett.* 45, 10,627-10,636. doi:10.1029/2018GL079128.
Donat, M. G., Pitman, A. J., and Seneviratne, S. I. (2017). Regional warming of hot extremes accelerated by surface energy fluxes. *Geophys. Res. Lett.* 44, 7011–7019.
Donat, M. G., Sillmann, J., Wild, S., Alexander, L. V., Lippmann, T., and Zwiers, F. W. (2014b). Consistency of Temperature and Precipitation Extremes across Various Global Gridded In Situ and Reanalysis Datasets. *J. Clim.* 27, 5019–5035. doi:10.1175/JCLI-D-13-00405.1.
Dong, B., Sutton, R. T., Chen, W., Liu, X., Lu, R., and Sun, Y. (2016). Abrupt summer warming and changes in temperature extremes over Northeast Asia since the mid-1990s: Drivers and physical processes. *Adv. Atmos. Sci.* 33, 1005–1023. doi:10.1007/s00376-016-5247-3.
Dong, B., Sutton, R. T., and Shaffrey, L. (2017). Understanding the rapid summer warming and changes in temperature extremes since the mid-1990s over Western Europe. *Clim. Dyn.* 48, 1537–1554. doi:10.1007/s00382-016-3158-8.

Dong, S., Sun, Y., Aguilar, E., Zhang, X., Peterson, T. C., Song, L., et al. (2018). Observed changes in temperature extremes over Asia and their attribution. *Clim. Dyn.* 51, 339–353. doi:10.1007/s00382-017-3927-z.

Dong, S., Sun, Y., Li, C., Zhang, X., Min, S. K., and Kim, Y. H. (submitted). Attribution of precipitation extremes with updated observations and CMIP6 simulations. *J. Clim.*(submitted).

Dong, S., Xu, Y., Zhou, B., and Shi, Y. (2015). Assessment of indices of temperature extremes simulated by multiple CMIP5 models over China. *Adv. Atmos. Sci.* 32, 1077–1091. doi:10.1007/s00376-015-4152-5.

Donnelly, C., Greuell, W., Andersson, J., Gerten, D., Pisacane, G., Roudier, P., et al. (2017). Impacts of climate change on European hydrology at 1.5, 2 and 3 degrees mean global warming above preindustrial level. *Clim. Change* 143, 13–26. doi:10.1007/s10584-017-1971-7.

Donnelly, J. P., Smith Bryant, S., Butler, J., Dowling, J., Fan, L., Hausmann, N., et al. (2001). 700 yr sedimentary record of intense hurricane landfalls in southern New England. *Geol. Soc. Am. Bull.* 113, 714–727. doi:10.1130/0016-7606(2001)113<0714:YSROIH>2.0.CO;2.

Dorigo, W. A., Gruber, A., De Jeu, R. A. M., Wagner, W., Stacke, T., Loew, A., et al. (2015). Evaluation of the ESA CCI soil moisture product using ground-based observations. *Remote Sens. Environ.* 162, 380–395. Available at: https://www.scopus.com/inward/record.uri?eid=2-s2.0-84929061651&doi=10.1016%2Fj.rse.2014.07.023&partnerID=40&md5=93a1ce532e804c18a5616f8fe286da5b.

Dorigo, W. A., Wagner, W., Hohensinn, R., Hahn, S., Paulik, C., Xaver, A., et al. (2011). The International Soil Moisture Network: a data hosting facility for global in situ soil moisture measurements. *Hydrol. Earth Syst. Sci.* 15, 1675–1698. doi:10.5194/hess-15-1675-2011.

Dorigo, W., de Jeu, R., Chung, D., Parinussa, R., Liu, Y., Wagner, W., et al. (2012). Evaluating global trends (1988-2010) in harmonized multi-satellite surface soil moisture. *Geophys. Res. Lett.* 39. doi:10.1029/2012GL052988.

Dorigo, W., Wagner, W., Albergel, C., Albrecht, F., Balsamo, G., Brocca, L., et al. (2017). ESA CCI Soil Moisture for improved Earth system understanding: State-of-the art and future directions. *Remote Sens. Environ.* 203, 185–215. doi:10.1016/j.rse.2017.07.001.

Dosio, A. (2016). Projections of climate change indices of temperature and precipitation from an ensemble of bias-adjusted high-resolution EURO-CORDEX regional climate models. *J. Geophys. Res. Atmos.* 121, 5488–5511. doi:10.1002/2015JD024411.

Dosio, A. (2017). Projection of temperature and heat waves for Africa with an ensemble of CORDEX Regional Climate Models. *Clim. Dyn.* 49, 493–519. doi:10.1007/s00382-016-3355-5.

Dosio, A., and Fischer, E. M. (2018). Will Half a Degree Make a Difference? Robust Projections of Indices of Mean and Extreme Climate in Europe Under 1.5°C, 2°C, and 3°C Global Warming. *Geophys. Res. Lett.* 45, 935–944. doi:10.1002/2017GL076222.

Dosio, A., Jones, R. G., Jack, C., Lennard, C., Nikulin, G., and Hewitson, B. (2019). What can we know about future precipitation in Africa? Robustness, significance and added value of projections from a large ensemble of regional climate models. *Clim. Dyn.*, 1–26. doi:10.1007/s00382-019-04900-3.

Dosio, A., Panitz, H.-J., Schubert-Frisius, M., and Lüthi, D. (2015). Dynamical downscaling of CMIP5 global circulation models over CORDEX-Africa with COSMO-CLM: evaluation over the present climate and analysis of the added value. *Clim. Dyn.* 44, 2637–2661.

Douville, H., Colin, J., Krug, E., Cattiaux, J., and Thao, S. (2016). Midlatitude daily summer temperatures reshaped by soil moisture under climate change. *Geophys. Res. Lett.* 43, 812–818. doi:10.1002/2015GL066222.

Douville, H., and Plazzotta, M. (2017). Midlatitude Summer Drying: An Underestimated Threat in CMIP5 Models? *Geophys. Res. Lett.* 44, 9967–9975. doi:10.1002/2017GL075353.

Dowdy, A. J. (2014). Long-term changes in Australian tropical cyclone numbers. *Atmos. Sci. Lett.* 15, 292–298. doi:10.1002/asl2.502.

Dowdy, A. J., Mills, G. A., and Timbal, B. (2013a). Large-scale diagnostics of extratropical cyclogenesis in eastern Australia. *Int. J. Climatol.*, n/a--n/a. doi:10.1002/joc.3599.

Dowdy, A. J., Mills, G. A., Timbal, B., and Wang, Y. (2013b). Changes in the risk of extratropical cyclones in eastern Australia. *J. Clim.* 26, 1403–1417. doi:10.1175/JCLI-D-12-00192.1.

Drijfhout, S., Bathiany, S., Beaulieu, C., Brovkin, V., Claussen, M., Huntingford, C., et al. (2015). Catalogue of abrupt shifts in Intergovernmental Panel on Climate Change climate models. *Proc. Natl. Acad. Sci.* 112, E5777–E5786. doi:10.1073/pnas.1511451112.

Driouech, F., Khouakhi, A., Moutia, S., Badi, W., ElRhaz, K., and Chehbouni, A. (submitted). Recent observed country-wide climate trends in Morocco. *Int. J. Climatol.*(submitted).

Drouard, M., Kornhuber, K., and Woollings, T. (2019). Disentangling Dynamic Contributions to Summer 2018 Anomalous Weather Over Europe. *Geophys. Res. Lett.* 46, 12537–12546. doi:10.1029/2019GL084601.

Drumond, A., Stojanovic, M., Nieto, R., Vicente-Serrano, S. M., and Gimeno, L. (2019). Linking Anomalous Moisture Transport And Drought Episodes in the IPCC Reference Regions. *Bull. Am. Meteorol. Soc.* 100, 1481–1498. doi:10.1175/BAMS-D-18-0111.1.

Du, H., Alexander, L. V, Donat, M. G., Lippmann, T., Srivastava, A., Salinger, J., et al. (2019). Precipitation From

Persistent Extremes is Increasing in Most Regions and Globally. *Geophys. Res. Lett.* 46, 6041–6049. doi:10.1029/2019GL081898.

Ducrocq, V., Nuissier, O., Ricard, D., Lebeaupin, C., and Thouvenin, T. (2008). A numerical study of three catastrophic precipitating events over southern France. II: Mesoscale triggering and stationarity factors. *Q. J. R. Meteorol. Soc.* 134, 131–145. doi:10.1002/qj.199.

Duffy, P. B., Brando, P., Asner, G. P., and Field, C. B. (2015). Projections of future meteorological drought and wet periods in the Amazon. *Proc. Natl. Acad. Sci.* 112, 13172–13177. doi:10.1073/pnas.1421010112.

Dunn, R., Alexander, L., Donat, M., Zhang, X., and Al., E. (submitted). Development of an updated Global land in-situ based dataset of temperature and precipitation extremes: HadEX3. *J. Geophys. Res. Atmos.*(submitted).

Dunn, R. J. H., Donat, M. G., and Alexander, L. V (2014). Investigating uncertainties in global gridded datasets of climate extremes. *Clim. Past Discuss.* 10, 2105–2161.

Durkee, J. D., and Mote, T. L. (2010). A climatology of warm-season mesoscale convective complexes in subtropical South America. *Int. J. Climatol.* 30, 418–431. doi:10.1002/joc.1893.

Easterling, D. R., Arnold, J. R., Knutson, T., Kunkel, K. E., LeGrande, A. N., Leung, L. R., et al. (2017). Ch. 7: Precipitation Change in the United States. Climate Science Special Report: Fourth National Climate Assessment, Volume I. , eds. D. J. Wuebbles, D. W. Fahey, K. A. Hibbard, D. J. Dokken, B. C. Stewart, and T. K. Maycock Washington, DC, DC, USA: U.S. Global Change Research Program doi:10.7930/J0H993CC.

Easterling, D. R., Kunkel, K. E., Wehner, M. F., and Sun, L. (2016). Detection and attribution of climate extremes in the observed record. *Weather Clim. Extrem.* 11, 17–27. doi:https://doi.org/10.1016/j.wace.2016.01.001.

Eden, J., Wolter, K., Otto, F. E. L. O., and van Oldenborgh, G. J. (2016). Multi-method attribution analysis of extreme precipitation in Boulder, Colorado. *Environ. Res. Lett.* 11, 124009. Available at: http://stacks.iop.org/1748-9326/11/i=12/a=124009.

El Kenawy, A., López-Moreno, J. I., and Vicente-Serrano, S. M. (2013). Summer temperature extremes in northeastern Spain: Spatial regionalization and links to atmospheric circulation (1960-2006). *Theor. Appl. Climatol.* 113, 387–405. doi:10.1007/s00704-012-0797-5.

Elsner, J. B., Elsner, S. C., and Jagger, T. H. (2015). The increasing efficiency of tornado days in the United States. *Clim. Dyn.* 45, 651–659. doi:10.1007/s00382-014-2277-3.

Elsner, J. B., Fricker, T., and Schroder, Z. (2019). Increasingly powerful tornadoes in the United States. *Geophys. Res. Lett.*, 1–10. doi:10.1029/2018GL080819.

Elsner, J. B., Kossin, J. P., and Jagger, T. H. (2008). The increasing intensity of the strongest tropical cyclones. *Nature* 455, 92–95. doi:10.1038/nature07234.

Emanuel, K. (2017). Assessing the present and future probability of Hurricane Harveys rainfall. *Proc. Natl. Acad. Sci.* 114, 12681–12684. doi:10.1073/pnas.1716222114.

Emanuel, K. (2018). 100 Years of Progress in Tropical Cyclone Research. *Meteorol. Monogr.* 59, 15.1-15.68. doi:10.1175/AMSMONOGRAPHS-D-18-0016.1.

Emanuel, K. A. (1987). The dependence of hurricane intensity on climate. *Nature* 326, 483.

Emanuel, K. A. (2013). Downscaling CMIP5 climate models shows increased tropical cyclone activity over the 21st century. doi:10.1073/pnas.1301293110.

Emanuel, K., Caroff, P., Delgado, S., Guard, C. "Chip," Guishard, M., Hennon, C., et al. (2018). On the Desirability and Feasibility of a Global Reanalysis of Tropical Cyclones. *Bull. Am. Meteorol. Soc.* 99, 427–429. doi:10.1175/BAMS-D-17-0226.1.

Emanuel, K., Sundararajan, R., and Williams, J. (2008). Hurricanes and Global Warming: Results from Downscaling IPCC AR4 Simulations. *Bull. Am. Meteorol. Soc.* 89, 347–368. doi:10.1175/BAMS-89-3-347.

Endo, H., Kitoh, A., Mizuta, R., and Ishii, M. (2017). Future Changes in Precipitation Extremes in East Asia and Their Uncertainty Based on Large Ensemble Simulations with a High-Resolution AGCM. 13, 0–5. doi:10.2151/sola.2017-002.

Engelbrecht, F. A., McGregor, J. L., and Engelbrecht, C. J. (2009). Dynamics of the Conformal-Cubic Atmospheric Model projected climate-change signal over southern Africa. *Int. J. Climatol.* 29, 1013–1033.

Engelbrecht, F., Adegoke, J., Bopape, M.-J., Naidoo, M., Garland, R., Thatcher, M., et al. (2015). Projections of rapidly rising surface temperatures over Africa under low mitigation. *Environ. Res. Lett.* 10, 085004. doi:10.1088/1748-9326/10/8/085004.

England, M. H., Mcgregor, S., Spence, P., Meehl, G. A., Timmermann, A., Cai, W., et al. (2014). Recent intensification of wind-driven circulation in the Pacific and the ongoing warming hiatus. *Nat. Clim. Chang.* 4, 222–227. doi:10.1038/nclimate2106.

Engström, J., and Keellings, D. (2018). Drought in the Southeastern USA: an assessment of downscaled CMIP5 models . *Clim. Res.* 74, 251–262. Available at: https://www.int-res.com/abstracts/cr/v74/n3/p251-262/.

Erdenebat, E., and Sato, T. (2016). Recent increase in heat wave frequency around Mongolia: role of atmospheric forcing and possible influence of soil moisture deficit. *Atmos. Sci. Lett.* 17, 135–140. doi:10.1002/asl.616.

Erfanian, A., Wang, G., and Fomenko, L. (2017). Unprecedented drought over tropical South America in 2016:

significantly under-predicted by tropical SST. *Sci. Rep.* 7, 5811. doi:10.1038/s41598-017-05373-2.
Escalante-Sandoval, C., and Nuñez-Garcia, P. (2017). Meteorological drought features in northern and northwestern parts of Mexico under different climate change scenarios. *J. Arid Land* 9, 65–75. doi:10.1007/s40333-016-0022-y.
Espinosa, L. A., Portela, M. M., and Rodrigues, R. (2019). Spatio-temporal variability of droughts over past 80 years in Madeira Island. *J. Hydrol. Reg. Stud.* 25. Available at: https://www.scopus.com/inward/record.uri?eid=2-s2.0-85070761818&doi=10.1016%2Fj.ejrh.2019.100623&partnerID=40&md5=d88a3c179fd813d332a51af945414f0a.
Evan, A. T., Flamant, C., Lavaysse, C., Kocha, C., and Saci, A. (2015). Water Vapor–Forced Greenhouse Warming over the Sahara Desert and the Recent Recovery from the Sahelian Drought. *J. Clim.* 28, 108–123. doi:10.1175/JCLI-D-14-00039.1.
Evan, A. T., Kossin, J. P., Chung, C. E., and Ramanathan, V. (2011). Arabian Sea tropical cyclones intensified by emissions of black carbon and other aerosols. *Nature* 479, 94–97. doi:10.1038/nature10552.
Evans, J. P., Argueso, D., Olson, R., and Di Luca, A. (2017). Bias-corrected regional climate projections of extreme rainfall in south-east Australia. *Theor. Appl. Climatol.* 130, 1085–1098. doi:10.1007/s00704-016-1949-9.
Evaristo, J., and McDonnell, J. J. (2019). Global analysis of streamflow response to forest management. *Nature* 570, 455–461. doi:10.1038/s41586-019-1306-0.
Fadnavis, S., Sabin, T. P., Roy, C., Rowlinson, M., Rap, A., Vernier, J.-P., et al. (2019). Elevated aerosol layer over South Asia worsens the Indian droughts. *Sci. Rep.* 9, 10268. doi:10.1038/s41598-019-46704-9.
Falconer, R. H., Cobby, D., Smyth, P., Astle, G., Dent, J., and Golding, B. (2009). Pluvial flooding: new approaches in flood warning, mapping and risk management. *J. Flood Risk Manag.* 2, 198–208. doi:10.1111/j.1753-318X.2009.01034.x.
Fallah-Ghalhari, G., Shakeri, F., and Dadashi-Roudbari, A. (2019). Impacts of climate changes on the maximum and minimum temperature in Iran. *Theor. Appl. Climatol.* 138. doi:10.1007/s00704-019-02906-9.
Feldl, N., and Bordoni, S. (2016). Characterizing the Hadley circulation response through regional climate feedbacks. *J. Clim.* 29, 613–622. doi:10.1175/JCLI-D-15-0424.1.
Felsenstein, D., and Lichter, M. (2014). Social and economic vulnerability of coastal communities to sea-level rise and extreme flooding. *Nat. Hazards* 71, 463–491. Available at: https://www.scopus.com/inward/record.uri?eid=2-s2.0-84893930146&doi=10.1007%2Fs11069-013-0929-y&partnerID=40&md5=80a3b474eedc6e57ad28f10a552227de.
Feng, R., Yu, R., Zheng, H., and Gan, M. (2018). Spatial and temporal variations in extreme temperature in Central Asia. *Int. J. Climatol.* 38, e388–e400. doi:10.1002/joc.5379.
Feng, S., and Fu, Q. (2013). Expansion of global drylands under a warming climate. *Atmos. Chem. Phys.* 13, 10081–10094. doi:10.5194/acp-13-10081-2013.
Feng, Z., Leung, L. R., Hagos, S., Houze, R. A., Burleyson, C. D., and Balaguru, K. (2016). More frequent intense and long-lived storms dominate the springtime trend in central US rainfall. *Nat. Commun.* 7, 13429. doi:10.1038/ncomms13429.
Fiddes, S. L., Pezza, A. B., and Barras, V. (2015). A new perspective on Australian snow. *Atmos. Sci. Lett.* 16, 246–252. doi:10.1002/asl2.549.
Field, R. D., van der Werf, G. R., Fanin, T., Fetzer, E. J., Fuller, R., Jethva, H., et al. (2016). Indonesian fire activity and smoke pollution in 2015 show persistent nonlinear sensitivity to El Niño-induced drought. *Proc. Natl. Acad. Sci.* 113, 9204–9209. doi:10.1073/pnas.1524888113.
Filahi, S., Tanarhte, M., Mouhir, L., El Morhit, M., and Tramblay, Y. (2016). Trends in indices of daily temperature and precipitations extremes in Morocco. *Theor. Appl. Climatol.* 124, 959–972. doi:10.1007/s00704-015-1472-4.
Findell, K. L., Berg, A., Gentine, P., Krasting, J. P., Lintner, B. R., Malyshev, S., et al. (2017). The impact of anthropogenic land use and land cover change on regional climate extremes. *Nat. Commun.* 8, 989. doi:10.1038/s41467-017-01038-w.
Fioravanti, G., Piervitali, E., and Desiato, F. (2016). Recent changes of temperature extremes over Italy: an index-based analysis. *Theor. Appl. Climatol.* 123, 473–486. doi:10.1007/s00704-014-1362-1.
Fischer, A. M., Keller, D. E., Liniger, M. A., Rajczak, J., Schär, C., and Appenzeller, C. (2015). Projected changes in precipitation intensity and frequency in Switzerland: a multi-model perspective. *Int. J. Climatol.* 35, 3204–3219. doi:10.1002/joc.4162.
Fischer, E. M., and Knutti, R. (2015). Anthropogenic contribution to global occurrence of heavy-precipitation and high-temperature extremes. *Nat. Clim. Chang.* 5, 560–564. doi:10.1038/nclimate2617.
Fischer, E. M., and Knutti, R. (2016). Observed heavy precipitation increase confirms theory and early models. *Nat. Clim. Chang.* 6, 986–991. doi:10.1038/nclimate3110.
Fischer, E. M., Sedláček, J., Hawkins, E., and Knutti, R. (2014). Models agree on forced response pattern of precipitation and temperature extremes. *Geophys. Res. Lett.* 41, 8554–8562. doi:10.1002/2014GL062018.
Fitsum, W., and Ashish, S. (2016). Should flood regimes change in a warming climate? The role of antecedent moisture conditions. *Geophys. Res. Lett.* 43, 7556–7563. doi:10.1002/2016GL069448.

Flach, M., Gans, F., Brenning, A., Denzler, J., Reichstein, M., Rodner, E., et al. (2017). Multivariate anomaly detection for Earth observations: a comparison of algorithms and feature extraction techniques. *Earth Syst. Dyn.* 8, 677–696. doi:10.5194/esd-8-677-2017.
Flach, M., Sippel, S., Gans, F., Bastos, A., Brenning, A., Reichstein, M., et al. (2018). Contrasting biosphere responses to hydrometeorological extremes: revisiting the 2010 western Russian heatwave. *Biogeosciences* 15, 6067–6085. doi:10.5194/bg-15-6067-2018.
Flato, G., Marotzke, J., Abiodun, B., Braconnot, P., Chou, S. C., Collins, W., et al. (2013). Evaluation of Climate Models. *Clim. Chang. 2013 Phys. Sci. Basis. Contrib. Work. Gr. I to Fifth Assess. Rep. Intergov. Panel Clim. Chang.*, 741–866. doi:10.1017/CBO9781107415324.020.
Folwell, S. S., Harris, P. P., and Taylor, C. M. (2016). Large-Scale Surface Responses during European Dry Spells Diagnosed from Land Surface Temperature. *J. Hydrometeorol.* 17, 975–993. doi:10.1175/JHM-D-15-0064.1.
Ford, T. W., and Quiring, S. M. (2019). Comparison of Contemporary In Situ, Model, and Satellite Remote Sensing Soil Moisture With a Focus on Drought Monitoring. *Water Resour. Res.* Available at: https://www.scopus.com/inward/record.uri?eid=2-s2.0-85062331732&doi=10.1029%2F2018WR024039&partnerID=40&md5=db3e33e53648f77f20113b8a6529e756.
Formayer, H., and Fritz, A. (2017). Temperature dependency of hourly precipitation intensities - surface versus cloud layer temperature. *Int. J. Climatol.* 37, 1–10. doi:10.1002/joc.4678.
Forzieri, G., Feyen, L., Rojas, R., Flörke, M., Wimmer, F., and Bianchi, A. (2014). Ensemble projections of future streamflow droughts in Europe. *Hydrol. Earth Syst. Sci.* 18, 85–108. doi:10.5194/hess-18-85-2014.
Fotso-Nguemo, T. C., Chamani, R., Yepdo, Z. D., Sonkoué, D., Matsaguim, C. N., Vondou, D. A., et al. (2018). Projected trends of extreme rainfall events from CMIP5 models over Central Africa. *Atmos. Sci. Lett.* 19, e803. doi:10.1002/asl.803.
Fotso-Nguemo, T. C., Diallo, I., Diakhaté, M., Vondou, D. A., Mbaye, M. L., Haensler, A., et al. (2019). Projected changes in the seasonal cycle of extreme rainfall events from CORDEX simulations over Central Africa. *Clim. Change* 155, 339–357.
Frank, D. C., Poulter, B., Saurer, M., Esper, J., Huntingford, C., Helle, G., et al. (2015). Water-use efficiency and transpiration across European forests during the Anthropocene. *Nat. Clim. Chang.* 5, 579–583. doi:10.1038/nclimate2614.
Franz, M., Alonso, R., Arneth, A., Büker, P., Elvira, S., Gerosa, G., et al. (2018). Evaluation of simulated biomass damage in forest ecosystems induced by ozone against observation-based estimates. *Biogeosciences*. doi:10.5194/bg-2018-358.
Frazier, A. G., and Giambelluca, T. W. (2017). Spatial trend analysis of Hawaiian rainfall from 1920 to 2012. *Int. J. Climatol.* 37, 2522–2531. Available at: https://www.scopus.com/inward/record.uri?eid=2-s2.0-84982204086&doi=10.1002%2Fjoc.4862&partnerID=40&md5=ebde0c65e4fd403272394cff50661b9b.
Frei, P., Kotlarski, S., Liniger, M. A., and Schär, C. (2018). Future snowfall in the Alps: projections based on the EURO-CORDEX regional climate models. *Cryosph.* 12, 1–24. doi:10.5194/tc-12-1-2018.
Freund, M., Henley, B. J., Karoly, D. J., Allen, K. J., and Baker, P. J. (2017). Multi-century cool- and warm-season rainfall reconstructions for Australia's major climatic regions. *Clim. Past* 13, 1751–1770. doi:10.5194/cp-13-1751-2017.
Freychet, N., Hsu, H.-H., Chou, C., and Wu, C.-H. (2015). Asian Summer Monsoon in CMIP5 Projections: A Link between the Change in Extreme Precipitation and Monsoon Dynamics. *J. Clim.* 28, 1477–1493. doi:10.1175/JCLI-D-14-00449.1.
Freychet, N., Tett, S. F. B., Hegerl, G. C., and Wang, J. (2018). Central-Eastern China Persistent Heat Waves: Evaluation of the AMIP Models. *J. Clim.* 31, 3609–3624. doi:10.1175/JCLI-D-17-0480.1.
Frich, P., Alexander, L., Della-Marta, P., Gleason, B., Haylock, M., Klein Tank, A., et al. (2002). Observed coherent changes in climatic extremes during the second half of the twentieth century. *Clim. Res.* 19, 193–212. doi:10.3354/cr019193.
Frölicher, T. L., Fischer, E. M., and Gruber, N. (2018). Marine heatwaves under global warming. *Nature* 560, 360–364. doi:10.1038/s41586-018-0383-9.
Fu, G., Yu, J., Yu, X., Ouyang, R., Zhang, Y., Wang, P., et al. (2013a). Temporal variation of extreme rainfall events in China, 1961–2009. *J. Hydrol.* 487, 48–59. doi:10.1016/J.JHYDROL.2013.02.021.
Fu, R., Yin, L., Li, W., Arias, P. A., Dickinson, R. E., Huang, L., et al. (2013b). Increased dry-season length over southern Amazonia in recent decades and its implication for future climate projection. *Proc. Natl. Acad. Sci. U. S. A.* 110, 18110–18115. doi:10.1073/pnas.1302584110.
Fuckar, N., Otto, F. E. L., Lehner, F., Pinto, I., Howard, E., Sparrow, S. N., et al. (2020). On High Precipitation in Mozambique, Zimbabwe, and Zambia in February 2018. *Bull. Am. Meteorol. Soc.* doi:10.1175/BAMS-D-19-0162.1.
Fujita, M., Kodama, C., Yamada, Y., Noda, A. T., Nakano, M., Nasuno, T., et al. (submitted). Projecting the Impact of Tropical Cyclones on Precipitation Patterns Around Japan Under a Warmer Climate Using NICAM AMIP-Type

25-Year Simulations. *J. Meteorol. Soc. Japan*(submitted). Available at: https://www.dropbox.com/s/b7vmfqvxc3wsyqj/Fujita_etal2018JMSJ_submitted20180617.pdf?dl=0.

Fundel, F., Jörg-Hess, S., and Zappa, M. (2013). Monthly hydrometeorological ensemble prediction of streamflow droughts and corresponding drought indices. *Hydrol. Earth Syst. Sci.* 17, 395–407. doi:10.5194/hess-17-395-2013.

Funk, C., Davenport, F., Harrison, L., Magadzire, T., Galu, G., Artan, G. A., et al. (2018a). Anthropogenic Enhancement of Moderate-to-Strong El Niño Events Likely Contributed to Drought and Poor Harvests in Southern Africa During 2016. *Bull. Am. Meteorol. Soc.* 99, S91–S96. doi:10.1175/BAMS-D-17-0112.1.

Funk, C., Harrison, L., Shukla, S., Korecha, D., Magadzire, T., Husak, G., et al. (2016). Assessing the Contributions of Local and East Pacific Warming to the 2015 Droughts in Ethiopia and Southern Africa. *Bull. Am. Meteorol. Soc.* 97, S75–S80. doi:10.1175/BAMS-D-16-0167.1.

Funk, C., Harrison, L., Shukla, S., Pomposi, C., Galu, G., Korecha, D., et al. (2018b). Examining the role of unusually warm Indo-Pacific sea surface temperatures in recent African droughts. *Q. J. R. Meteorol. Soc.*, 1–20. doi:10.1002/acr.

Funk, C., Husak, G., Michaelsen, J., Shukla, S., Hoell, A., Fieldbrad, L., et al. (2013). 15 . ATTRIBUTION OF 2012 AND 2003 – 12 RAINFALL DEFICITS IN EASTERN KENYA AND SOUTHERN SOMALIA. *Bull. Amer. Meteor. Soc.* 94, S45–S48.

Funk, C., Nicholson, S. E., Landsfeld, M., Klotter, D., Peterson, P., and Harrison, L. (2015a). The Centennial Trends Greater Horn of Africa precipitation dataset. *Sci. Data* 2, 150050. Available at: http://dx.doi.org/10.1038/sdata.2015.50.

Funk, C., Peterson, P., Landsfeld, M., Pedreros, D., Verdin, J., Shukla, S., et al. (2015b). The climate hazards infrared precipitation with stations—a new environmental record for monitoring extremes. *Sci. Data* 2, 150066. doi:10.1038/sdata.2015.66.

Funk, C., Shukla, S., Hoell, A., and Livneh, B. (2015c). Assessing the contributions of east African and west pacific warming to the 2014 boreal spring east African drought. *Bull. Am. Meteorol. Soc.* 96, S77–S82. doi:10.1175/BAMS-D-15-00106.1.

Fyfe, J. C., and Gillett, N. P. (2014). Recent observed and simulated warming. *Nat. Clim. Chang.* 4, 150–151.

Fyfe, J. C., Meehl, G. A., England, M. H., Mann, M. E., Santer, B. D., Flato, G. M., et al. (2016). Making sense of the early-2000s warming slowdown. *Nat. Clim. Chang.* 6, 224.

Gaertner, M. A., Jacob, D., Gil, V., Domínguez, M., Padorno, E., Sánchez, E., et al. (2007). Tropical cyclones over the Mediterranean Sea in climate change simulations. *Geophys. Res. Lett.* 34, L14711. doi:10.1029/2007GL029977.

Gajić-Čapka, M., Cindrić, K., and Pasarić, Z. (2015). Trends in precipitation indices in Croatia, 1961–2010. *Theor. Appl. Climatol.* 121, 167–177. doi:10.1007/s00704-014-1217-9.

Galanaki, E., Lagouvardos, K., Kotroni, V., Flaounas, E., and Argiriou, A. (2018). Thunderstorm climatology in the Mediterranean using cloud-to-ground lightning observations. *Atmos. Res.* 207, 136–144. doi:https://doi.org/10.1016/j.atmosres.2018.03.004.

Galarneau, T. J., Bosart, L. F., and Schumacher, R. S. (2010). Predecessor rain events ahead of tropical cyclones. *Mon. Weather Rev.* 138, 3272–3297. doi:10.1175/2010MWR3243.1.

Gallant, A. J. E., Reeder, M. J., Risbey, J. S., and Hennessy, K. J. (2013). The characteristics of seasonal-scale droughts in Australia, 1911-2009. *Int. J. Climatol.* 33, 1658–1672. doi:10.1002/joc.3540.

Gangrade, S., Kao, S.-C., Dullo, T. T., Kalyanapu, A. J., and Preston, B. L. (2019). Ensemble-based flood vulnerability assessment for probable maximum flood in a changing environment. *J. Hydrol.* 576, 342–355. Available at: https://www.scopus.com/inward/record.uri?eid=2-s2.0-85067869457&doi=10.1016%2Fj.jhydrol.2019.06.027&partnerID=40&md5=72972344f3ebfb2125b85c5f16c1be2d.

Gao, X., Shi, Y., Han, Z., Wang, M., Wu, J., Zhang, D., et al. (2017a). Performance of RegCM4 over major river basins in China. *Adv. Atmos. Sci.* 34, 441–455. doi:10.1007/s00376-016-6179-7.

Gao, X., Zhao, Q., Zhao, X., Wu, P., Pan, W., Gao, X., et al. (2017b). Temporal and spatial evolution of the standardized precipitation evapotranspiration index (SPEI) in the Loess Plateau under climate change from 2001 to 2050. *Sci. Total Environ.* 595, 191–200. Available at: https://www.scopus.com/inward/record.uri?eid=2-s2.0-85016777118&doi=10.1016%2Fj.scitotenv.2017.03.226&partnerID=40&md5=cc5aaa1a02c23aea4ae0374ad171ce4f.

Gao, Y., Xiao, L., Chen, D., Xu, J., and Zhang, H. (2018). Comparison between past and future extreme precipitations simulated by global and regional climate models over the Tibetan Plateau. *Int. J. Climatol.* 38, 1285–1297. doi:10.1002/joc.5243.

García-Cueto, O. R., Santillán-Soto, N., López-Velázquez, E., Reyes-López, J., Cruz-Sotelo, S., and Ojeda-Benítez, S. (2019). Trends of climate change indices in some Mexican cities from 1980 to 2010. *Theor. Appl. Climatol.* 137, 775–790. doi:10.1007/s00704-018-2620-4.

García-Herrera, R., Garrido-Pérez, J.M. Barriopedro, D., Ordóñez, C., Vicente-Serrano, S.M. Nieto, R., Gimeno, L.,

Sorí, R., et al. (2019). The European 2016/2017 drought. *J. Clim.* 32, 3169–3187.
García-Ruiz, J. M., López-Moreno, J. I., Vicente-Serrano, S. M., Lasanta-Martínez, T., and Beguería, S. (2011). Mediterranean water resources in a global change scenario. *Earth-Science Rev.* 105. doi:10.1016/j.earscirev.2011.01.006.
Gardent, M., Rabatel, A., Dedieu, J.-P., and Deline, P. (2014). Multitemporal glacier inventory of the French Alps from the late 1960s to the late 2000s. *Glob. Planet. Change* 120, 24–37. doi:https://doi.org/10.1016/j.gloplacha.2014.05.004.
Garner, A. J., Mann, M. E., Emanuel, K. A., Kopp, R. E., Lin, N., Alley, R. B., et al. (2017). Impact of climate change on New York City's coastal flood hazard: Increasing flood heights from the preindustrial to 2300 CE. *Proc. Natl. Acad. Sci.* 114, 11861 LP – 11866. Available at: http://www.pnas.org/content/114/45/11861.abstract.
Garreaud, R. D., Alvarez-Garreton, C., Barichivich, J., Boisier, J. P., Christie, D., Galleguillos, M., et al. (2017). The 2010–2015 megadrought in central Chile: impacts on regional hydroclimate and vegetation. *Hydrol. Earth Syst. Sci.* 21, 6307–6327. doi:10.5194/hess-21-6307-2017.
Garreaud, R. D., Boisier, J. P., Rondanelli, R., Montecinos, A., Sepúlveda, H. H., and Veloso-Aguila, D. (2019). The Central Chile Mega Drought (2010–2018): A climate dynamics perspective. *Int. J. Climatol.* Available at: https://www.scopus.com/inward/record.uri?eid=2-s2.0-85069917630&doi=10.1002%2Fjoc.6219&partnerID=40&md5=564b212c08bf17036516e40e6f86e209.
Gaupp, F., Hall, J., Mitchell, D., and Dadson, S. (2019). Increasing risks of multiple breadbasket failure under 1.5 and 2 °C global warming. *Agric. Syst.* 175, 34–45. doi:https://doi.org/10.1016/j.agsy.2019.05.010.
Gbobaniyi, E., Sarr, A., Sylla, M. B., Diallo, I., Lennard, C., Dosio, A., et al. (2014). Climatology, annual cycle and interannual variability of precipitation and temperature in CORDEX simulations over West Africa. *Int. J. Climatol.* 34, 2241–2257.
Ge, F., Zhu, S., Peng, T., Zhao, Y., Sielmann, F., Fraedrich, K., et al. (2019). Risks of precipitation extremes over Southeast Asia: does 1.5 C or 2 C global warming make a difference? *Environ. Res. Lett.* 14, 044015. doi:https://doi.org/10.1088/1748-9326/aaff7e.
Ge, G., Shi, Z., Yang, X., Hao, Y., Guo, H., Kossi, F., et al. (2017). Analysis of precipitation extremes in the Qinghai-Tibetan plateau, China: Spatio-temporal characteristics and topography effects. *Atmosphere (Basel).* 8, 1–16. doi:10.3390/atmos8070127.
Gebrechorkos, S. H., Hülsmann, S., and Bernhofer, C. (2019). Changes in temperature and precipitation extremes in Ethiopia, Kenya, and Tanzania. *Int. J. Climatol.* 39, 18–30.
Geirinhas, J. L., Trigo, R. M., Libonati, R., Coelho, C. A. S., and Palmeira, A. C. (2018). Climatic and synoptic characterization of heat waves in Brazil. *Int. J. Climatol.* 38, 1760–1776. doi:10.1002/joc.5294.
Gensini, V. A., and Mote, T. L. (2015). Downscaled estimates of late 21st century severe weather from CCSM3. *Clim. Change* 129, 307–321. doi:10.1007/s10584-014-1320-z.
Gervais, M., Tremblay, L. B., Gyakum, J. R., and Atallah, E. (2014). Representing Extremes in a Daily Gridded Precipitation Analysis over the United States: Impacts of Station Density, Resolution, and Gridding Methods. *J. Clim.* 27, 5201–5218. doi:10.1175/JCLI-D-13-00319.1.
Ghosh, S., Das, D., Kao, S.-C., and Ganguly, A. R. (2012). Lack of uniform trends but increasing spatial variability in observed Indian rainfall extremes. *Nat. Clim. Chang.* 2. doi:10.1038/nclimate1327.
Gimeno, L., Stohl, A., Trigo, R. M., Dominguez, F., Yoshimura, K., Yu, L., et al. (2012). Oceanic and terrestrial sources of continental precipitation. *Rev. Geophys.* 50. doi:10.1029/2012RG000389.
Gingerich, S. B., Voss, C. I., and Johnson, A. G. (2017). Seawater-flooding events and impact on freshwater lenses of low-lying islands: Controlling factors, basic management and mitigation. *J. Hydrol.* 551, 676–688. Available at: https://www.scopus.com/inward/record.uri?eid=2-s2.0-85015295439&doi=10.1016%2Fj.jhydrol.2017.03.001&partnerID=40&md5=5ea297ba37bc974ec3e61d1c29c33b82.
Giorgi, F., Coppola, E., Raffaele, F., Diro, G. T., Fuentes-Franco, R., Giuliani, G., et al. (2014). Changes in extremes and hydroclimatic regimes in the CREMA ensemble projections. *Clim. Change* 125, 39–51. doi:10.1007/s10584-014-1117-0.
Giorgi, F., Jones, C., and Asrar, G. (2009). Addressing climate information needs at the regional level: the CORDEX framework. *WMO Bull.* 58, 175.
Giorgi, F., Raffaele, F., and Coppola, E. (2019). The response of precipitation characteristics to global warming from climate projections. *Earth Syst. Dyn.* 10, 73–89. doi:10.5194/esd-10-73-2019.
Giuntoli, I., Renard, B., Vidal, J.-P., and Bard, A. (2013). Low flows in France and their relationship to large-scale climate indices. *J. Hydrol.* 482, 105–118. doi:10.1016/j.jhydrol.2012.12.038.
Giuntoli, I., Vidal, J.-P., Prudhomme, C., and Hannah, D. M. (2015). Future hydrological extremes: The uncertainty from multiple global climate and global hydrological models. *Earth Syst. Dyn.* 6, 267–285. doi:10.5194/esd-6-267-2015.
Gloor, M., Barichivich, J., Ziv, G., Brienen, R., Schöngart, J., Peylin, P., et al. (2015). Recent Amazon climate as

background for possible ongoing and future changes of Amazon humid forests. *Global Biogeochem. Cycles* 29, 1384–1399. doi:10.1002/2014GB005080.

Gobbett, D. L., Nidumolu, U., and Crimp, S. (2018). Modelling frost generates insights for managing risk of minimum temperature extremes. *Weather Clim. Extrem.*, 1–9. doi:10.1016/j.wace.2018.06.003.

Gobiet, A., Kotlarski, S., Beniston, M., Heinrich, G., Rajczak, J., and Stoffel, M. (2014). 21st century climate change in the European Alps—A review. *Sci. Total Environ.* 493, 1138–1151. doi:10.1016/j.scitotenv.2013.07.050.

Gocic, M., and Trajkovic, S. (2014). Analysis of trends in reference evapotranspiration data in a humid climate. *Hydrol. Sci. J.* 59, 165–180. doi:10.1080/02626667.2013.798659.

González-Alemán, J. J., Pascale, S., Gutierrez-Fernandez, J., Murakami, H., Gaertner, M. A., and Vecchi, G. A. (2019). Potential Increase in Hazard From Mediterranean Hurricane Activity With Global Warming. *Geophys. Res. Lett.* 46, 1754–1764. doi:10.1029/2018GL081253.

González-Hidalgo, J. C., Vicente-Serrano, S. M., Peña-Angulo, D., Salinas, C., Tomas-Burguera, M., and Beguería, S. (2018). High-resolution spatio-temporal analyses of drought episodes in the western Mediterranean basin (Spanish mainland, Iberian Peninsula). *Acta Geophys.* 66, 381–392. doi:10.1007/s11600-018-0138-x.

Gori, A., Blessing, R., Juan, A., Brody, S., and Bedient, P. (2019). Characterizing urbanization impacts on floodplain through integrated land use, hydrologic, and hydraulic modeling. *J. Hydrol.* 568, 82–95. Available at: https://www.scopus.com/inward/record.uri?eid=2-s2.0-85055743682&doi=10.1016%2Fj.jhydrol.2018.10.053&partnerID=40&md5=69960772a661d8a328b278015d623bf8.

Gosling, S. N., Zaherpour, J., Mount, N. J., Hattermann, F. F., Dankers, R., Arheimer, B., et al. (2017). A comparison of changes in river runoff from multiple global and catchment-scale hydrological models under global warming scenarios of 1 °C, 2 °C and 3 °C. *Clim. Change* 141, 577–595. doi:10.1007/s10584-016-1773-3.

Gou, X., Deng, Y., Gao, L., Chen, F., Cook, E., Yang, M., et al. (2015). Millennium tree-ring reconstruction of drought variability in the eastern Qilian Mountains, northwest China. *Clim. Dyn.* 45, 1761–1770. doi:10.1007/s00382-014-2431-y.

Grams, C. M., Binder, H., Pfahl, S., Piaget, N., and Wernli, H. (2014). Atmospheric processes triggering the central European floods in June 2013. *Nat. Hazards Earth Syst. Sci.* 14, 1691–1702. doi:10.5194/nhess-14-1691-2014.

Greve, P., Gudmundsson, L., and Seneviratne, S. I. (2018). Regional scaling of annual mean precipitation and water availability with global temperature change. *Earth Syst. Dyn.* 9, 227–240. doi:10.3929/ethz-b-000251688.

Greve, P., Orlowsky, B., Mueller, B., Sheffield, J., Reichstein, M., and Seneviratne, S. I. (2014). Global assessment of trends in wetting and drying over land. *Nat. Geosci.* 7, 716–721. doi:10.1038/NGEO2247.

Greve, P., Roderick, M. L., and Seneviratne, S. I. (2017). Simulated changes in aridity from the last glacial maximum to 4xCO2. *Environ. Res. Lett.* 12, 114021. doi:10.1088/1748-9326/aa89a3.

Griffin, D., and Anchukaitis, K. J. (2014). How unusual is the 2012-2014 California drought? *Geophys. Res. Lett.* 41, 9017–9023. doi:10.1002/2014GL062433.

Grillakis, M. G., Koutroulis, A. G., Komma, J., Tsanis, I. K., Wagner, W., and Blöschl, G. (2016). Initial soil moisture effects on flash flood generation – A comparison between basins of contrasting hydro-climatic conditions. *J. Hydrol.* 541, 206–217. doi:10.1016/J.JHYDROL.2016.03.007.

Grinsted, A., Ditlevsen, P., and Christensen, J. H. (2019). Normalized US hurricane damage estimates using area of total destruction, 1900‒2018. *Proc. Natl. Acad. Sci.* 116, 23942 LP – 23946. doi:10.1073/pnas.1912277116.

Grose, M. R., Black, M., Risbey, J. S., Uhe, P., Hope, P. K., Haustein, K., et al. (2018). Severe Frosts in Western Australia in September 2016. *Bull. Am. Meteorol. Soc.* 99, S150–S154. doi:10.1175/BAMS-D-17-0088.1.

Grose, M. R., Risbey, J. S., Black, M. T., and Karoly, D. J. (2015). Attribution of Exceptional Mean Sea Level Pressure Anomalies South of Australia in August 2014. *Bull. Am. Meteorol. Soc.* 96, S158–S162. doi:10.1175/BAMS-D-15-00116.1.

Grotjahn, R., Black, R., Leung, R., Wehner, M. F., Barlow, M., Bosilovich, M., et al. (2016). North American extreme temperature events and related large scale meteorological patterns: a review of statistical methods, dynamics, modeling, and trends. *Clim. Dyn.* 46, 1151–1184. doi:10.1007/s00382-015-2638-6.

Gu, G., and Adler, R. F. (2018). Precipitation Intensity Changes in the Tropics from Observations and Models. *J. Clim.* 31, 4775–4790. doi:10.1175/JCLI-D-17-0550.1.

Gu, H., Yu, Z., Wang, G., Wang, J., Ju, Q., Yang, C., et al. (2014). Impact of climate change on hydrological extremes in the Yangtze River Basin, China. *Stoch. Environ. Res. Risk Assess.* 29, 693–707. doi:10.1007/s00477-014-0957-5.

Gu, X., Li, J., Chen, Y. D., Kong, D., and Liu, J. (2019a). Consistency and Discrepancy of Global Surface Soil Moisture Changes From Multiple Model-Based Data Sets Against Satellite Observations. *J. Geophys. Res. Atmos.* 124, 1474–1495. doi:10.1029/2018JD029304.

Gu, X., Zhang, Q., Li, J., Singh, V. P., Liu, J., Sun, P., et al. (2019b). Attribution of Global Soil Moisture Drying to Human Activities: A Quantitative Viewpoint. *Geophys. Res. Lett.* 46, 2573–2582. doi:10.1029/2018GL080768.

Gudmundsson, L., Boulange, J., Do, H. X., Gosling, S. N., Grillakis, M. G., Koutroulis, A. G., et al. (submitted).

Globally observed trends in mean and extreme river flow attribution to man-made climate change. *Science*(submitted).
Gudmundsson, L., Do, H. X., Leonard, M., and Westra, S. (2018). The Global Streamflow Indices and Metadata Archive (GSIM) -- Part 2: Quality control, time-series indices and homogeneity assessment. *Earth Syst. Sci. Data* 10, 787–804. doi:10.5194/essd-10-787-2018.
Gudmundsson, L., Leonard, M., Do, H. X., Westra, S., and Seneviratne, S. I. (2019). Observed Trends in Global Indicators of Mean and Extreme Streamflow. *Geophys. Res. Lett.* 46, 756–766. doi:10.1029/2018GL079725.
Gudmundsson, L., and Seneviratne, S. I. (2016). Anthropogenic climate change affects meteorological drought risk in Europe. *Environ. Res. Lett.* 11. doi:10.1088/1748-9326/11/4/044005.
Gudmundsson, L., Seneviratne, S. I., and Zhang, X. (2017). Anthropogenic climate change detected in European renewable freshwater resources. *Nat. Clim. Chang.* 7, 813–816. doi:10.1038/nclimate3416.
Guerreiro, S. B., Dawson, R. J., Kilsby, C., Lewis, E., and Ford, A. (2018a). Future heat-waves, droughts and floods in 571 European cities. *Environ. Res. Lett.* 13. Available at: https://www.scopus.com/inward/record.uri?eid=2-s2.0-85048079035&doi=10.1088%2F1748-9326%2Faaaad3&partnerID=40&md5=cf82f8157d9162eeded65183eb566743.
Guerreiro, S. B., Fowler, H. J., Barbero, R., Westra, S., Lenderink, G., Blenkinsop, S., et al. (2018b). Detection of continental-scale intensification of hourly rainfall extremes. *Nat. Clim. Chang.* 8, 803–807. doi:10.1038/s41558-018-0245-3.
Guhathakurta, P., Menon, P., Inkane, P. M., Krishnan, U., and Sable, S. T. (2017). Trends and variability of meteorological drought over the districts of India using standardized precipitation index. *J. Earth Syst. Sci.* 126, 120. doi:https://doi.org/10.1007/s12040-017-0896-x.
Guillod, B. P., Jones, R. G., Bowery, A., Haustein, K., Massey, N. R., Mitchell, D. M., et al. (2017). weather@home 2: validation of an improved global--regional climate modelling system. *Geosci. Model Dev.* 10, 1849–1872. doi:10.5194/gmd-10-1849-2017.
Guillod, B. P., Orlowsky, B., Miralles, D. G., Teuling, A. J., and Seneviratne, S. I. (2015). Reconciling spatial and temporal soil moisture effects on afternoon rainfall. *Nat. Commun.* 6, 6443. doi:10.1038/ncomms7443.
Guimberteau, M., Ronchail, J., Espinoza, J. C. C., Lengaigne, M., Sultan, B., Polcher, J., et al. (2013). Future changes in precipitation and impacts on extreme streamflow over Amazonian sub-basins. *Environ. Res. Lett.* 8, 014035. doi:10.1088/1748-9326/8/1/014035.
Guo, J., Huang, G., Wang, X., Li, Y., and Lin, Q. (2018). Dynamically-downscaled projections of changes in temperature extremes over China. *Clim. Dyn.* 50, 1045–1066. doi:10.1007/s00382-017-3660-7.
Guo, X., Huang, J., Luo, Y., Zhao, Z., and Xu, Y. (2016). Projection of precipitation extremes for eight global warming targets by 17 CMIP5 models. *Nat. Hazards* 84, 2299–2319. doi:10.1007/s11069-016-2553-0.
Guo, X., Huang, J., Luo, Y., Zhao, Z., and Xu, Y. (2017). Projection of heat waves over China for eight different global warming targets using 12 CMIP5 models. *Theor. Appl. Climatol.* 128, 507–522. doi:10.1007/s00704-015-1718-1.
Gutmann, E. D., Rasmussen, R. M., Liu, C., Ikeda, K., Bruyere, C. L., Done, J. M., et al. (2018). Changes in hurricanes from a 13-Yr convection-permitting pseudo- global warming simulation. *J. Clim.* 31, 3643–3657. doi:10.1175/JCLI-D-17-0391.1.
Haarsma, R. J., Roberts, M. J., Vidale, P. L., Senior, C. A., Bellucci, A., Bao, Q., et al. (2016). High Resolution Model Intercomparison Project (HighResMIP~v1.0) for CMIP6. *Geosci. Model Dev.* 9, 4185–4208. doi:10.5194/gmd-9-4185-2016.
Habib, S. M. A., Sato, T., and Hatsuzuka, D. (2019). Decreasing number of propagating mesoscale convective systems in Bangladesh and surrounding area during 1998–2015. *Atmos. Sci. Lett.* 20, e879. doi:10.1002/asl.879.
Haig, J., Nott, J., and Reichart, G.-J. (2014). Australian tropical cyclone activity lower than at any time over the past 550–1,500 years. *Nature* 505, 667–671. doi:10.1038/nature12882.
Hall, A., and Qu, X. (2006). Using the current seasonal cycle to constrain snow albedo feedback in future climate change. *Geophys. Res. Lett.* 33, L03502. doi:10.1029/2005GL025127.
Hall, J., Arheimer, B., Borga, M., Brázdil, R., Claps, P., Kiss, A., et al. (2014). Understanding flood regime changes in Europe: A state-of-the-art assessment. *Hydrol. Earth Syst. Sci.* 18, 2735–2772. doi:10.5194/hess-18-2735-2014.
Hall, T. M., and Kossin, J. P. (2019). Hurricane stalling along the North American coast and implications for rainfall. *npj Clim. Atmos. Sci.* 2, 1–9. doi:10.1038/s41612-019-0074-8.
Hamada, A., Takayabu, Y. N., Liu, C., and Zipser, E. J. (2015). Weak linkage between the heaviest rainfall and tallest storms. *Nat. Commun.* 6, 1–6. doi:10.1038/ncomms7213.
Hameed, M., Ahmadalipour, A., and Moradkhani, H. (2018). Apprehensive drought characteristics over Iraq: Results of a multidecadal spatiotemporal assessment. *Geosci.* 8, 1–16. doi:10.3390/geosciences8020058.
Han, F., Cook, K. H., and Vizy, E. K. (2019). Changes in intense rainfall events and dry periods across Africa in the twenty-first century. *Clim. Dyn.*, 1–21. doi:10.1007/s00382-019-04653-z.
Han, J.-Y., Baik, J.-J., and Khain, A. P. (2011). A Numerical Study of Urban Aerosol Impacts on Clouds and Precipitation. *J. Atmos. Sci.* 69, 504–520. doi:10.1175/JAS-D-11-071.1.

Han, T., Chen, H., Hao, X., and Wang, H. (2018). Projected changes in temperature and precipitation extremes over the Silk Road Economic Belt regions by the Coupled Model Intercomparison Project Phase 5 multi-model ensembles. *Int. J. Climatol.* 38, 4077–4091. doi:10.1002/joc.5553.
Hande, L. B., Siems, S. T., and Manton, M. J. (2012). Observed Trends in Wind Speed over the Southern Ocean. *Geophys. Res. Lett.* 39, 1–5. doi:10.1029/2012GL051734.
Hanel, M., Rakovec, O., Markonis, Y., Máca, P., Samaniego, L., Kyselý, J., et al. (2018). Revisiting the recent European droughts from a long-term perspective. *Sci. Rep.* 8. doi:10.1038/s41598-018-27464-4.
Hannaford, J. (2015). Climate-driven changes in UK river flows: A review of the evidence. *Prog. Phys. Geogr.* 39, 29–48.
Hannart, A., Vera, C., Otto, F. E. L., and Cerne, B. (2015). Causal influence of anthropogenic forcings on the argentinian heat wave of December 2013. *Bull. Am. Meteorol. Soc.* 96, S41–S45. doi:10.1175/BAMS-D-15-00137.1.
Hansen, B. B., Isaksen, K., Benestad, R. E., Kohler, J., Pedersen, Å. Ø., Loe, L. E., et al. (2014). Warmer and wetter winters: characteristics and implications of an extreme weather event in the High Arctic. *Environ. Res. Lett.* 9, 114021. doi:10.1088/1748-9326/9/11/114021.
Hanzer, F., Förster, K., Nemec, J., and Strasser, U. (2018). Projected cryospheric and hydrological impacts of 21st century climate change in the Ötztal Alps (Austria) simulated using a physically based approach. *Hydrol. Earth Syst. Sci.* 22, 1593–1614. doi:10.5194/hess-22-1593-2018.
Hao, Y., Liu, Q., Li, C., Kharel, G., An, L., Stebler, E., et al. (2019). Interactive effect of meteorological drought and vegetation types on root zone soil moisture and runoff in Rangeland Watersheds. *Water (Switzerland)* 11. doi:10.3390/w11112357.
Hariadi, M. H. (2017). Projected drought severity changes in Southeast Asia under medium and extreme climate change. 53. Available at: http://edepot.wur.nl/420042%0Ahttp://publicaties.minienm.nl/documenten/projected-drought-severity-changes-in-southeast-asia-under-medium-and-extreme-climate-change.
Harrington, L. J. (2017). Investigating differences between event-as-class and probability density-based attribution statements with emerging climate change. *Clim. Change* 141, 641–654. doi:10.1007/s10584-017-1906-3.
Harrington, L. J., Gibson, P. B., Dean, S. M., Mitchell, D., Rosier, S. M., and Frame, D. J. (2016). Investigating event-specific drought attribution using self-organizing maps. *J. Geophys. Res. Atmos.* 121, 12,712-766,780. doi:10.1002/2016JD025602.
Harrington, L. J., and Otto, F. E. L. (2018a). Adapting attribution science to the climate extremes of tomorrow. *Environ. Res. Lett.* 13, 123006. doi:10.1088/1748-9326/aaf4cc.
Harrington, L. J., and Otto, F. E. L. (2018b). Changing population dynamics and uneven temperature emergence combine to exacerbate regional exposure to heat extremes under 1.5 °C and 2 °C of warming. *Environ. Res. Lett.* 13, 034011. doi:10.1088/1748-9326/aaaa99.
Harrington, L., and Renwick, J. (2014). Secular changes in New Zealand rainfall characteristics 1950-2009. *Weather Clim.* 34, 50–59.
Harrington, L., Rosier, S., Dean, S. M., Stuart, S., and Scahill, A. (2014). the Role of Anthropogenic Climate Change in the 2013 Drought Over North Island, New Zealand [in "Explaining Extremes of 2013 from a climate perspective"]. *Bull. Am. Meteorol. Soc.* 95, S45–S48. Available at: https://apps.webofknowledge.com/full_record.do?product=WOS&search_mode=GeneralSearch&qid=11&SID=S17wXqJSlJ1xTKbLqQv&page=1&doc=14.
Harrison, L., Funk, C., and Peterson, P. (2019). Identifying changing precipitation extremes in Sub-Saharan Africa with gauge and satellite products. *Environ. Res. Lett.* 14, 085007. doi:10.1088/1748-9326/ab2cae.
Hartmann, D. J., Klein Tank, A. M. G., Rusticucci, M., Alexander, L. V, Brönnimann, S., Charabi, Y. A.-R., et al. (2013). Observations: Atmosphere and Surface. *Clim. Chang. 2013 Phys. Sci. Basis. Contrib. Work. Gr. I to Fifth Assess. Rep. Intergov. Panel Clim. Chang.*, 159–254. doi:10.1017/CBO9781107415324.008.
Hartmann, F., Merten, J., Fink, M., and Faust, H. (2018). Indonesia's Fire Crisis 2015 A Twofold Perturbation on the Ground. *Pacific Geogr.* 49, 4–11. doi:10.23791/490411.
Hasan, H. H., Mohd Razali, S. F., Muhammad, N. S., and Ahmad, A. (2019). Research Trends of Hydrological Drought: A Systematic Review. *Water* 11. doi:10.3390/w11112252.
Hashimoto, A., Tai, A., Oshikawa, H., and Komatsu, T. (2013). Characteristics of flood disaster and evacuation activities of residents at Amami Oshima Island, Japan. 357, 48–56. Available at: https://www.scopus.com/inward/record.uri?eid=2-s2.0-84883370425&partnerID=40&md5=e926821e7d548eb82472a62860e4991b.
Haslinger, K., Hofstätter, M., Kroisleitner, C., Schöner, W., Laaha, G., Holawe, F., et al. (2019). Disentangling Drivers of Meteorological Droughts in the European Greater Alpine Region During the Last Two Centuries. *J. Geophys. Res. Atmos.* doi:10.1029/2018JD029527.
Haslinger, K., Schöner, W., and Anders, I. (2016). Future drought probabilities in the Greater Alpine Region based on COSMO-CLM experiments – spatial patterns and driving forces. *Meteorol. Zeitschrift* 25, 137–148.

doi:10.1127/metz/2015/0604.
Hatsuzuka, D., and Sato, T. (2019). Future Changes in Monthly Extreme Precipitation in Japan Using Large-Ensemble Regional Climate Simulations. *J. Hydrometeorol.* 20, 563–574. doi:10.1175/JHM-D-18-0095.1.
Hauser, M., Gudmundsson, L., Orth, R., Jézéquel, A., Haustein, K., Vautard, R., et al. (2017). Methods and Model Dependency of Extreme Event Attribution: The 2015 European Drought. *Earth's Futur.* 5, 1034–1043. doi:10.1002/2017EF000612.
Hauser, M., Orth, R., and Seneviratne, S. I. (2016). Role of soil moisture versus recent climate change for the 2010 heat wave in western Russia. *Geophys. Res. Lett.* 43, 2819–2826. doi:10.1002/2016GL068036.
Hawcroft, M., Dacre, H., Forbes, R., Hodges, K., Shaffrey, L., and Stein, T. (2017). Using satellite and reanalysis data to evaluate the representation of latent heating in extratropical cyclones in a climate model. *Clim. Dyn.* doi:10.1007/s00382-016-3204-6.
Hawcroft, M. K., Shaffrey, L. C., Hodges, K. I., and Dacre, H. F. (2016). Can climate models represent the precipitation associated with extratropical cyclones? *Clim. Dyn.* doi:10.1007/s00382-015-2863-z.
Hawcroft, M., Walsh, E., Hodges, K., and Zappa, G. (2018). Significantly increased extreme precipitation expected in Europe and North America from extratropical cyclones. *Environ. Res. Lett.* 13. doi:10.1088/1748-9326/aaed59.
Hawkins, E., and Sutton, R. (2012). Time of emergence of climate signals. *Geophys. Res. Lett.* 39, n/a-n/a. doi:10.1029/2011GL050087.
Hazeleger, W., van den Hurk, B. J. J. M., Min, E., van Oldenborgh, G. J., Petersen, A. C., Stainforth, D. A., et al. (2015). Tales of future weather. *Nat. Clim. Chang.* 5, 107–113. doi:10.1038/nclimate2450.
He, F., and Posselt, D. J. (2015). Impact of Parameterized Physical Processes on Simulated Tropical Cyclone Characteristics in the Community Atmosphere Model. *J. Clim.* 28, 9857–9872.
He, J., and Soden, B. J. (2015). Anthropogenic Weakening of the Tropical Circulation: The Relative Roles of Direct CO2 Forcing and Sea Surface Temperature Change. *J. Clim.* 28, 8728–8742. doi:10.1175/JCLI-D-15-0205.1.
He, X., Wada, Y., Wanders, N., and Sheffield, J. (2017). Intensification of hydrological drought in California by human water management. *Geophys. Res. Lett.* 44, 1777–1785. doi:10.1002/2016GL071665.
Hedemann, C., Mauritsen, T., Jungclaus, J., and Marotzke, J. (2017). The subtle origins of surface-warming hiatuses. *Nat. Clim. Chang.* 7, 336–339. doi:10.1038/nclimate3274.
Helama, S., Sohar, K., Läänelaid, A., Bijak, S., and Jaagus, J. (2018). Reconstruction of precipitation variability in Estonia since the eighteenth century, inferred from oak and spruce tree rings. *Clim. Dyn.* 50, 4083–4101. doi:10.1007/s00382-017-3862-z.
Held, I. M., and Soden, B. J. (2006). Robust responses of the hydrological cycle to global warming. *J. Clim.* 19, 5686–5699. doi:10.1175/JCLI3990.1.
Held, I. M., and Zhao, M. (2011). The Response of Tropical Cyclone Statistics to an Increase in CO2 with Fixed Sea Surface Temperatures. *J. Clim.* 24, 5353–5364. doi:10.1175/JCLI-D-11-00050.1.
Herger, N., Angélil, O., Abramowitz, G., Donat, M., Stone, D., and Lehmann, K. (2018). Calibrating Climate Model Ensembles for Assessing Extremes in a Changing Climate. *J. Geophys. Res. Atmos.* 123, 5988–6004. doi:10.1029/2018JD028549.
Herold, N., Ekström, M., Kala, J., Goldie, J., and Evans, J. P. (2018). Australian climate extremes in the 21st century according to a regional climate model ensemble: Implications for health and agriculture. *Weather Clim. Extrem.* 20, 54–68. doi:10.1016/j.wace.2018.01.001.
Herrera-Estrada, J. E., Martinez, J. A., Dominguez, F., Findell, K. L., Wood, E. F., and Sheffield, J. (2019). Reduced Moisture Transport Linked to Drought Propagation Across North America. *Geophys. Res. Lett.* 46, 5243–5253. doi:10.1029/2019GL082475.
Herrera-Estrada, J. E., Satoh, Y., and Sheffield, J. (2017). Spatiotemporal dynamics of global drought. *Geophys. Res. Lett.* 44, 2254–2263. Available at: https://www.scopus.com/inward/record.uri?eid=2-s2.0-85014520720&doi=10.1002%2F2016GL071768&partnerID=40&md5=d154f7c365186aae3b1e47a13f29052f.
Herrera-Estrada, J. E., and Sheffield, J. (2017). Uncertainties in future projections of summer droughts and heat waves over the contiguous United States. *J. Clim.* 30, 6225–6246. doi:10.1175/JCLI-D-16-0491.1.
Herrera, D. A., Ault, T. R., Fasullo, J. T., Coats, S. J., Carrillo, C. M., Cook, B. I., et al. (2018). Exacerbation of the 2013–2016 Pan-Caribbean Drought by Anthropogenic Warming. *Geophys. Res. Lett.* 45, 10,619-10,626. doi:10.1029/2018GL079408.
Herrera, D., and Ault, T. (2017). Insights from a new high-resolution drought Atlas for the Caribbean spanning 1950-2016. *J. Clim.* 30, 7801–7825. Available at: https://www.scopus.com/inward/record.uri?eid=2-s2.0-85029009389&doi=10.1175%2FJCLI-D-16-0838.1&partnerID=40&md5=9b969ffa38c1cbb15ffc1606691f8c91.
Herring, S. C., Christidis, N., Hoell, A., Kossin, J. P., Schreck, C. J., and Stott, P. A. (2018). Explaining Extreme Events of 2016 from a Climate Perspective. *Bull. Am. Meteorol. Soc.* 99, S1–S157. doi:10.1175/BAMS-ExplainingExtremeEvents2016.1.
Herring, S. C., Hoell, A., Hoerling, M. P., Kossin, J. P., Schreck, C. J., and Stott, P. A. (2016). Explaining Extreme Events of 2015 from a Climate Perspective. *Bull. Am. Meteorol. Soc.* 97, S1–S145. doi:10.1175/BAMS-

ExplainingExtremeEvents2015.1.
Herring, S. C., Hoerling, M. P., Kossin, J. P., Peterson, T. C., and Stott, P. A. (2015). Explaining Extreme Events of 2014 from a Climate Perspective. *Bull. Am. Meteorol. Soc.* 96, S1–S172. doi:10.1175/BAMS-ExplainingExtremeEvents2014.1.
Herring, S. C., Hoerling, M. P., Peterson, T. C., and Stott, P. a. (2014). Explaining Extreme Events of 2013 from a Climate Perspective. *Bull. Am. Meteorol. Soc.* 95, S1–S104. doi:10.1175/1520-0477-95.9.S1.1.
Hertig, E., and Tramblay, Y. (2017). Regional downscaling of Mediterranean droughts under past and future climatic conditions. *Glob. Planet. Change* 151, 36–48. Available at: https://www2.scopus.com/inward/record.uri?eid=2-s2.0-85006105559&doi=10.1016%2Fj.gloplacha.2016.10.015&partnerID=40&md5=671e1e3fef7ef93958b6dbc3e63e0ec4.
Hettiarachchi, S., Wasko, C., and Sharma, A. (2018). Increase in flood risk resulting from climate change in a developed urban watershed - The role of storm temporal patterns. *Hydrol. Earth Syst. Sci.* 22, 2041–2056. doi:10.5194/hess-22-2041-2018.
Hidalgo, H. G., Alfaro, E. J., and Quesada-Montano, B. (2017). Observed (1970–1999) climate variability in Central America using a high-resolution meteorological dataset with implication to climate change studies. *Clim. Change* 141, 13–28. doi:10.1007/s10584-016-1786-y.
Hinkel, J., Lincke, D., Vafeidis, A. T., Perrette, M., Nicholls, R. J., Tol, R. S. J., et al. (2014). Coastal flood damage and adaptation costs under 21st century sea-level rise. *Proc. Natl. Acad. Sci. U. S. A.* 111, 3292–3297. Available at: https://www.scopus.com/inward/record.uri?eid=2-s2.0-84895835798&doi=10.1073%2Fpnas.1222469111&partnerID=40&md5=427854124748c3c7d662f35aff65e1ae.
Hirabayashi, Y., Mahendran, R., Koirala, S., Konoshima, L., Yamazaki, D., Watanabe, S., et al. (2013). Global flood risk under climate change. *Nat. Clim. Chang.* 3, 816–821. doi:10.1038/nclimate1911.
Hirsch, A. L., Evans, J. P., Di Virgillio, G., Perkins-Kirkpatrick, S. E., Argüeso, D., Pitman, A. J., et al. (2019). Amplification of Australian heatwaves via local land-atmosphere coupling. *J. Geophys. Res. Atmos.*, 2019JD030665. doi:10.1029/2019JD030665.
Hirsch, A. L., Guillod, B. P., Seneviratne, S. I., Beyerle, U., Boysen, L. R., Brovkin, V., et al. (2018). Biogeophysical Impacts of Land-Use Change on Climate Extremes in Low-Emission Scenarios: Results From HAPPI-Land. *Earth's Futur.* 6, 396–409. doi:10.1002/2017EF000744.
Hirsch, A. L., Pitman, A. J., Seneviratne, S. I., Evans, J. P., and Haverd, V. (2014). Summertime maximum and minimum temperature coupling asymmetry over Australia determined using WRF. *Geophys. Res. Lett.* 41, 1546–1552. doi:10.1002/2013GL059055.
Hirsch, A. L., Wilhelm, M., Davin, E. L., Thiery, W., and Seneviratne, S. I. (2017). Can climate-effective land management reduce regional warming? *J. Geophys. Res. Atmos.* 122, 2269–2288. doi:10.1002/2016JD026125.
Hirschi, M., Seneviratne, S. I., Alexandrov, V., Boberg, F., Boroneant, C., Christensen, O. B., et al. (2011). Observational evidence for soil-moisture impact on hot extremes in southeastern Europe. *Nat. Geosci.* 4, 17–21. doi:10.1038/ngeo1032.
Hobbins, M. T., Wood, A., McEvoy, D. J., Huntington, J. L., Morton, C., Anderson, M., et al. (2016). The evaporative demand drought index. Part I: Linking drought evolution to variations in evaporative demand. *J. Hydrometeorol.* 17, 1745–1761. doi:10.1175/JHM-D-15-0121.1.
Hobbins, M., Wood, A., Streubel, D., and Werner, K. (2012). What drives the variability of evaporative demand across the conterminous United States? *J. Hydrometeorol.* 13, 1195–1214. doi:10.1175/JHM-D-11-0101.1.
Hoegh-Guldberg, O., Jacob, D., Taylor, M., Bindi, M., Brown, S., Camilloni, I., et al. (2018). "Impacts of 1.5°C Global Warming on Natural and Human Systems," in *Global Warming of 1.5°C. An IPCC Special Report on the impacts of global warming of 1.5°C above pre-industrial levels and related global greenhouse gas emission pathways, in the context of strengthening the global response to the threat of climate change,* eds. V. Masson-Delmotte, P. Zhai, H. O. Pörtner, D. Roberts, J. Skea, P. R. Shukla, et al. (Geneva, Switzerland: In Press). Available at: https://www.ipcc.ch/sr15.
Hoeke, R. K., McInnes, K. L., Kruger, J. C., McNaught, R. J., Hunter, J. R., and Smithers, S. G. (2013). Widespread inundation of Pacific islands triggered by distant-source wind-waves. *Glob. Planet. Change* 108, 128–138. Available at: https://www.scopus.com/inward/record.uri?eid=2-s2.0-84880595114&doi=10.1016%2Fj.gloplacha.2013.06.006&partnerID=40&md5=5a40f4c585950f6e90da9c0b8fcc801f.
Hoerling, M., Eischeid, J., Kumar, A., Leung, R., Mariotti, A., Mo, K., et al. (2014). Causes and predictability of the 2012 great plains drought. *Bull. Am. Meteorol. Soc.* 95, 269–282. doi:10.1175/BAMS-D-13-00055.1.
Hoerling, M., Eischeid, J., Perlwitz, J., Quan, X.-W., Wolter, K., and Cheng, L. (2016). Characterizing Recent Trends in U.S. Heavy Precipitation. *J. Clim.* 29, 2313–2332. doi:10.1175/JCLI-D-15-0441.1.
Hoerling, M., Eischeid, J., Perlwitz, J., Quan, X., Zhang, T., Pegion, P., et al. (2012). On the Increased Frequency of Mediterranean Drought. *J. Clim.* 25, 2146–2161. doi:10.1175/JCLI-D-11-00296.1.

Hoerling, M., Kumar, A., Dole, R., Nielsen-Gammon, J. W., Eischeid, J., Perlwitz, J., et al. (2013). Anatomy of an extreme event. *J. Clim.* 26, 2811–2832. doi:10.1175/JCLI-D-12-00270.1.

Holland, G., and Bruyère, C. L. (2014). Recent intense hurricane response to global climate change. *Clim. Dyn.* 42, 617–627. doi:10.1007/s00382-013-1713-0.

Holloway, C. E., Wing, A. A., Bony, S., Muller, C., Masunaga, H., L'Ecuyer, T. S., et al. (2017). Observing Convective Aggregation. *Surv. Geophys.* 38, 1199–1236. doi:10.1007/s10712-017-9419-1.

Hong, C.-C., Lee, M.-Y., Hsu, H.-H., and Tseng, W.-L. (2018). Distinct Influences of the ENSO-Like and PMM-Like SST Anomalies on the Mean TC Genesis Location in the Western North Pacific: The 2015 Summer as an Extreme Example. *J. Clim.* 31, 3049–3059. doi:10.1175/JCLI-D-17-0504.1.

Hoogewind, K. A., Baldwin, M. E., and Trapp, R. J. (2017). The Impact of Climate Change on Hazardous Convective Weather in the United States: Insight from High-Resolution Dynamical Downscaling. *J. Clim.* 30, 10081–10100. doi:10.1175/JCLI-D-16-0885.1.

Hope, P., Black, M. T., Lim, E.-P., Dowdy, A., Wang, G., Fawcett, R. J. B., et al. (2019). On Determining the Impact of Increasing Atmospheric CO_2 on the Record Fire Weather in Eastern Australia in February 2017. *Bull. Am. Meteorol. Soc.* 100, S111–S117. doi:10.1175/BAMS-D-18-0135.1.

Hou, A. Y., Kakar, R. K., Neeck, S., Azarbarzin, A. A., Kummerow, C. D., Kojima, M., et al. (2014). The Global Precipitation Measurement Mission. *Bull. Am. Meteorol. Soc.* 95, 701–722. doi:10.1175/BAMS-D-13-00164.1.

Howarth, M. E., Thorncroft, C. D., and Bosart, L. F. (2019). Changes in Extreme Precipitation in the Northeast United States: 1979–2014. *J. Hydrometeorol.* 20, 673–689. doi:10.1175/JHM-D-18-0155.1.

Hu, T., Sun, Y., Zhang, X., Min, S.-K., and Kim, Y.-H. (submitted). Human influnece on frequency of tempertaure extremes. *Environ. Res. Lett.*(submitted).

Hu, Z., Li, Q., Chen, X., Teng, Z., Chen, C., Yin, G., et al. (2016). Climate changes in temperature and precipitation extremes in an alpine grassland of Central Asia. *Theor. Appl. Climatol.* 126, 519–531. doi:10.1007/s00704-015-1568-x.

Hua, W., Zhou, L., Chen, H., Nicholson, S. E., Raghavendra, A., and Jiang, Y. (2016). Possible causes of the Central Equatorial African long-term drought. *Environ. Res. Lett.* 11. doi:10.1088/1748-9326/11/12/124002.

Huang, H., Winter, J. M., Osterberg, E. C., Horton, R. M., and Beckage, B. (2017a). Total and Extreme Precipitation Changes over the Northeastern United States. *J. Hydrometeorol.* 18, 1783–1798. doi:10.1175/JHM-D-16-0195.1.

Huang, J., Yu, H., Dai, A., Wei, Y., and Kang, L. (2017b). Drylands face potential threat under 2 °C global warming target. *Nat. Clim. Chang.* 7, 417–422. doi:10.1038/nclimate3275.

Huang, J., Zhai, J., Jiang, T., Wang, Y., Li, X., Wang, R., et al. (2018a). Analysis of future drought characteristics in China using the regional climate model CCLM. *Clim. Dyn.* 50, 507–525. Available at: https://www.scopus.com/inward/record.uri?eid=2-s2.0-85015819727&doi=10.1007%2Fs00382-017-3623-z&partnerID=40&md5=2674dff633a462e1da7fbd3e785703d6.

Huang, K., Yi, C., Wu, D., Zhou, T., Zhao, X., Blanford, W. J., et al. (2015). Tipping point of a conifer forest ecosystem under severe drought. *Environ. Res. Lett.* 10. doi:10.1088/1748-9326/10/2/024011.

Huang, S., Kumar, R., Flörke, M., Yang, T., Hundecha, Y., Kraft, P., et al. (2017c). Evaluation of an ensemble of regional hydrological models in 12 large-scale river basins worldwide. *Clim. Change* 141, 381–397. doi:10.1007/s10584-016-1841-8.

Huang, S., Kumar, R., Rakovec, O., Aich, V., Wang, X., Samaniego, L., et al. (2018b). Multimodel assessment of flood characteristics in four large river basins at global warming of 1.5, 2.0 and 3.0 K above the pre-industrial level. *Environ. Res. Lett.* 13. Available at: https://www.scopus.com/inward/record.uri?eid=2-s2.0-85060181123&doi=10.1088%2F1748-9326%2Faae94b&partnerID=40&md5=4a45bec0a2f1aeb66951075a0e82b06d.

Huang, S., Li, P., Huang, Q., Leng, G., Hou, B., and Ma, L. (2017d). The propagation from meteorological to hydrological drought and its potential influence factors. *J. Hydrol.* 547, 184–195. doi:10.1016/J.JHYDROL.2017.01.041.

Huang, X., Hall, A. D., and Berg, N. (2018c). Anthropogenic Warming Impacts on Today's Sierra Nevada Snowpack and Flood Risk. *Geophys. Res. Lett.* 45, 6215–6222. doi:10.1029/2018GL077432.

Huffman, G. J., Adler, R. F., Morrissey, M. M., Bolvin, D. T., Curtis, S., Joyce, R., et al. (2001). Global Precipitation at One-Degree Daily Resolution from Multisatellite Observations. *J. Hydrometeorol.* 2, 36–50. doi:10.1175/1525-7541(2001)002<0036:GPAODD>2.0.CO;2.

Huffman, G. J., Bolvin, D. T., Nelkin, E. J., Wolff, D. B., Adler, R. F., Gu, G., et al. (2007). The TRMM Multisatellite Precipitation Analysis (TMPA): Quasi-Global, Multiyear, Combined-Sensor Precipitation Estimates at Fine Scales. *J. Hydrometeorol.* 8, 38–55. doi:10.1175/JHM560.1.

Hui, P., Tang, J., Wang, S., Niu, X., Zong, P., and Dong, X. (2018). Climate change projections over China using regional climate models forced by two CMIP5 global models. Part I: evaluation of historical simulations. *Int. J. Climatol.* 38, e57–e77. doi:10.1002/joc.5351.

Huijnen, V., Wooster, M. J., Kaiser, J. W., Gaveau, D. L. A., Flemming, J., Parrington, M., et al. (2016). Fire carbon

emissions over maritime southeast Asia in 2015 largest since 1997. *Sci. Rep.* 6, 1–8. doi:10.1038/srep26886.
Humphrey, V., Zscheischler, J., Ciais, P., Gudmundsson, L., Sitch, S., and Seneviratne, S. I. (2018). Sensitivity of atmospheric CO2 growth rate to observed changes in terrestrial water storage. *Nature* 560, 628–631. doi:10.1038/s41586-018-0424-4.
Hundecha, Y., Sunyer, M. A., Lawrence, D., Madsen, H., Willems, P., Bürger, G., et al. (2016). Inter-comparison of statistical downscaling methods for projection of extreme flow indices across Europe. *J. Hydrol.* 541, 1273–1286. doi:10.1016/j.jhydrol.2016.08.033.
Hunt, E. D., Svoboda, M., Wardlow, B., Hubbard, K., Hayes, M., and Arkebauer, T. (2014). Monitoring the effects of rapid onset of drought on non-irrigated maize with agronomic data and climate-based drought indices. *Agric. For. Meteorol.* 191, 1–11. doi:10.1016/j.agrformet.2014.02.001.
Hunt, K. M. R., Turner, A., and Shaffrey, L. C. (2018). Falling trend of western disturbances in future climate simulations. *J. Clim.* Under Revi.
Hussain, M. S., and Lee, S. (2013). The regional and the seasonal variability of extreme precipitation trends in Pakistan. *Asia-Pacific J. Atmos. Sci.* 49, 421–441. doi:10.1007/s13143-013-0039-5.
Imada, Y., Maeda, S., Watanabe, M., Shiogama, H., Mizuta, R., Ishii, M., et al. (2017). Recent enhanced seasonal temperature contrast in Japan from large ensemble high-resolution climate simulations. *Atmosphere (Basel).* 8. doi:10.3390/atmos8030057.
Imada, Y., Watanabe, M., Kawase, H., Shiogama, H., and Arai, M. (2019). The July 2018 High Temperature Event in Japan Could Not Have Happened without Human-Induced Global Warming. *SOLA* 15A, 8–12. doi:10.2151/sola.15A-002.
Imada, Y., Watanabe, M., Mori, M., Kimoto, M., Shiogama, H., and Ishii, M. (2013). Contribution of Atmospheric Circulation Change to the 2012 Heavy Rainfall in Southwestern Japan. *Bull. Am. Meteorol. Soc.* 96, 52–54.
Imbach, P., Chou, S. C., Lyra, A., Rodrigues, D., Rodriguez, D., Latinovic, D., et al. (2018). Future climate change scenarios in Central America at high spatial resolution. *PLoS One* 13, e0193570. doi:10.1371/journal.pone.0193570.
Innocenti, S., Mailhot, A., Leduc, M., Cannon, A. J., and Frigon, A. (2019). Projected Changes in the Probability Distributions, Seasonality, and Spatiotemporal Scaling of Daily and Subdaily Extreme Precipitation Simulated by a 50-Member Ensemble Over Northeastern North America. *J. Geophys. Res. Atmos.* 124, 10427–10449. doi:10.1029/2019JD031210.
IPCC (2012). *Managing the Risks of Extreme Events and Disasters to Advance Climate Change Adaptation. A Special Report of Working Groups I and II of the Intergovernmental Panel on Climate Change*. Cambridge University Press.
IPCC (2013). *Climate Change 2013 - The Physical Science Basis. Contribution of Working Group I to the Fifth Assessment Report of the Intergovernmental Panel on Climate Change*. , ed. Intergovernmental Panel on Climate Change Cambridge: Cambridge University Press doi:10.1017/CBO9781107415324.
IPCC (2018). "Summary for Policymakers. In: Global warming of 1.5°C," in *An IPCC Special Report on the impacts of global warming of 1.5°C above pre-industrial levels and related global greenhouse gas emission pathways, in the context of strengthening the global response to*, eds. V. Masson-Delmotte, P. Zhai, H.-O. Pörtner, D. Roberts, J. Skea, P. R. Shukla, et al. (In Press), 32.
IPCC (2019a). "Climate Change and Land: an IPCC special report on climate change, desertification, land degradation, sustainable land management, food security, and greenhouse gas fluxes in terrestrial ecosystems," in, eds. P. R. Shukla, J. Skea, E. C. Buendia, V. Masson-Delmotte, H.-O. Pörtner, D. C. Roberts, et al. (In Press).
IPCC (2019b). IPCC Special Report on the Ocean and Cryosphere in a Changing Climate. , eds. H.-O. Pörtner, D. C. Roberts, V. Masson-Delmotte, P. Zhai, M. Tignor, E. Poloczanska, et al. In Press.
Irannezhad, M., Chen, D., Kløve, B., and Moradkhani, H. (2017). Analysing the variability and trends of precipitation extremes in Finland and their connection to atmospheric circulation patterns. *Int. J. Climatol.* 37, 1053–1066. doi:10.1002/joc.5059.
Ishak, E. H., Rahman, A., Westra, S., Sharma, A., and Kuczera, G. (2013). Evaluating the non-stationarity of australian annual maximum flood. *J. Hydrol.* 494, 134–145. doi:10.1016/j.jhydrol.2013.04.021.
Ishiyama, T., Satoh, M., and Yamada, Y. (2018). Potential differences in North Pacific tropical cyclone activity between the super El Niño years of 1997 and 2015. *J. Meteorol. Soc. Japan*.
Jakob, D., and Walland, D. (2016). Variability and long-term change in Australian temperature and precipitation extremes. *Weather Clim. Extrem.* 14, 36–55. doi:10.1016/j.wace.2016.11.001.
James, R., Washington, R., Schleussner, C.-F., Rogelj, J., and Conway, D. (2017). Characterizing half-a-degree difference: a review of methods for identifying regional climate responses to global warming targets. *Wiley Interdiscip. Rev. Clim. Chang.* 8, e457.
Japan Meteorological Agency (2018). Primary Factors behind the Heavy Rain Event of July 2018 and the Subsequent Heatwave in Japan from Mid-July Onward. Available at: http://ds.data.jma.go.jp/tcc/tcc/news/press_20180822.pdf.

Jeon, S., Paciorek, C. J., and Wehner, M. F. (2016). Quantile-based bias correction and uncertainty quantification of extreme event attribution statements. *Weather Clim. Extrem.* 12, 24–32. doi:https://doi.org/10.1016/j.wace.2016.02.001.

Jeong, S.-J., Ho, C.-H., Piao, S., Kim, J., Ciais, P., Lee, Y.-B., et al. (2014). Effects of double cropping on summer climate of the North China Plain and neighbouring regions. *Nat. Clim. Chang.* 4, 615–619. doi:10.1038/nclimate2266.

Jevrejeva, S., Jackson, L. P., Grinsted, A., Lincke, D., and Marzeion, B. (2018). Flood damage costs under the sea level rise with warming of 1.5◦C and 2◦C. *Environ. Res. Lett.* 13. Available at: https://www.scopus.com/inward/record.uri?eid=2-s2.0-85056530720&doi=10.1088%2F1748-9326%2Faacc76&partnerID=40&md5=69d08c624a714ff97950a7af8e9b07ec.

Jézéquel, A., Dépoues, V., Guillemot, H., Trolliet, M., Vanderlinden, J.-P., and Yiou, P. (2018). Behind the veil of extreme event attribution. *Clim. Change*. doi:10.1007/s10584-018-2252-9.

Jhajharia, D., Kumar, R., Dabral, P. P., Singh, V. P., Choudhary, R. R., and Dinpashoh, Y. (2015). Reference evapotranspiration under changing climate over the Thar Desert in India. *Meteorol. Appl.* 22, 425–435. doi:10.1002/met.1471.

Ji, F., Evans, J. P. J. P., Argueso, D., Fita, L., and Di Luca, A. (2015). Using large-scale diagnostic quantities to investigate change in East Coast Lows. *Clim. Dyn.* 45, 2443–2453. doi:10.1007/s00382-015-2481-9.

Ji, P., Yuan, X., Jiao, Y., Wang, C., Han, S., and Shi, C. (2020). Anthropogenic contributions to the 2018 extreme flooding over upper Yellow River basin in China. *Bull. Am. Meteorol. Soc.* doi:10.1175/BAMS-D-19-0105.1.

Ji, Z., and Kang, S. (2015). Evaluation of extreme climate events using a regional climate model for China. *Int. J. Climatol.* 35, 888–902. doi:10.1002/joc.4024.

Jia, B., Liu, J., Xie, Z., and Shi, C. (2018). Interannual variations and trends in remotely sensed and modeled soil moisture in China. *J. Hydrometeorol.* 19, 831–847. Available at: https://www.scopus.com/inward/record.uri?eid=2-s2.0-85047910255&doi=10.1175%2FJHM-D-18-0003.1&partnerID=40&md5=19be83c528672b248a3000d3bb5bd4f4.

Jiang, F., Hu, R.-J., Wang, S.-P., Zhang, Y.-W., and Tong, L. (2013). Trends of precipitation extremes during 1960–2008 in Xinjiang, the Northwest China. *Theor. Appl. Climatol.* 111, 133–148. doi:10.1007/s00704-012-0657-3.

Jiao, Y., and Yuan, X. (2019). More severe hydrological drought events emerge at different warming levels over the Wudinghe watershed in northern China. *Hydrol. Earth Syst. Sci.* 23, 621–635. doi:10.5194/hess-23-621-2019.

Jiménez-Muñoz, J. C., Mattar, C., Barichivich, J., Santamaría-Artigas, A., Takahashi, K., Malhi, Y., et al. (2016). Record-breaking warming and extreme drought in the Amazon rainforest during the course of El Niño 2015–2016. *Sci. Rep.* 6, 33130. doi:10.1038/srep33130.

Johnson, N. C., Xie, S. P., Kosaka, Y., and Li, X. (2018). Increasing occurrence of cold and warm extremes during the recent global warming slowdown. *Nat. Commun.* 9, 4–6. doi:10.1038/s41467-018-04040-y.

Jones, P. D., Harpham, C., Burton, A., and Goodess, C. M. (2016). Downscaling regional climate model outputs for the Caribbean using a weather generator. *Int. J. Climatol.* 36, 4141–4163. doi:10.1002/joc.4624.

Kalnay, E., Kanamitsu, M., Kistler, R., Collins, W., Deaven, D., Gandin, L., et al. (1996). The NCEP/NCAR 40-Year Reanalysis Project. *Bull. Am. Meteorol. Soc.* 77, 437–471. doi:10.1175/1520-0477(1996)077<0437:TNYRP>2.0.CO;2.

Kamae, Y., Mei, W., Xie, S. P., Naoi, M., and Ueda, H. (2017a). Atmospheric rivers over the Northwestern Pacific: Climatology and interannual variability. *J. Clim.* 30, 5605–5619. doi:10.1175/JCLI-D-16-0875.1.

Kamae, Y., Shiogama, H., Imada, Y., Mori, M., Arakawa, O., Mizuta, R., et al. (2017b). Forced response and internal variability of summer climate over western North America. *Clim. Dyn.* 49, 403–417. doi:10.1007/s00382-016-3350-x.

Kamae, Y., Shiogama, H., Watanabe, M., and Kimoto, M. (2014). Attributing the increase in Northern Hemisphere hot summers since the late 20th century. *Geophys. Res. Lett.* 41, 5192–5199. doi:10.1002/2014GL061062.

Kanada, S., Takemi, T., Kato, M., Yamasaki, S., Fudeyasu, H., Tsuboki, K., et al. (2017a). A multimodel intercomparison of an intense typhoon in future, warmer climates by Four 5-km-Mesh models. *J. Clim.* 30, 6017–6036. doi:10.1175/JCLI-D-16-0715.1.

Kanada, S., Tsujino, S., Aiki, H., Yoshioka, M. K., Miyazawa, Y., Tsuboki, K., et al. (2017b). Impacts of SST Patterns on Rapid Intensification of Typhoon Megi (2010). *J. Geophys. Res. Atmos.* 122, 13,213-245,262. doi:10.1002/2017JD027252.

Kanada, S., and Wada, A. (2016). Sensitivity to Horizontal Resolution of the Simulated Intensifying Rate and Inner-Core Structure of Typhoon Ida, an Extremely Intense Typhoon. *J. Meteorol. Soc. Japan. Ser. II* 94A, 181–190. doi:10.2151/jmsj.2015-037.

Kanada, S., Wada, A., and Sugi, M. (2013). Future changes in structures of extremely intense tropical cyclones using a 2-km mesh nonhydrostatic model. *J. Clim.* 26, 9986–10005. doi:10.1175/JCLI-D-12-00477.1.

Kanamitsu, M., Ebisuzaki, W., Woollen, J., Yang, S.-K., Hnilo, J. J., Fiorino, M., et al. (2002). NCEP–DOE AMIP-II Reanalysis (R-2). *Bull. Am. Meteorol. Soc.* 83, 1631–1644. doi:10.1175/BAMS-83-11-1631.

Kang, N. Y., and Elsner, J. B. (2012). Consensus on climate trends in Western North pacific tropical cyclones. *J. Clim.* 25, 7564–7573. doi:10.1175/JCLI-D-11-00735.1.
Kaniewski, D., Van Campo, E., and Weiss, H. (2012). Drought is a recurring challenge in the Middle East. *Proc. Natl. Acad. Sci. U. S. A.* 109, 3862–3867. doi:10.1073/pnas.1116304109.
Karl, T. R., Arguez, A., Huang, B., Lawrimore, J. H., McMahon, J. R., Menne, M. J., et al. (2015). Possible artifacts of data biases in the recent global surface warming hiatus. *Science* 348, 1469 LP – 1472. Available at: http://science.sciencemag.org/content/348/6242/1469.abstract.
Karl, T. R., Nicholls, N., and Ghazi, A. (1999). CLIVAR/GCOS/WMO Workshop on Indices and Indicators for Climate Extremes - Workshop summary. in *Climatic Change* doi:10.1023/A:1005491526870.
Karmalkar, A. V, Taylor, M. A., Campbell, J., Stephenson, T., New, M., Centella, A., et al. (2013). A review of observed and projected changes in climate for the islands in the Caribbean. *Atmosfera* 26, 283–309. Available at: https://www.scopus.com/inward/record.uri?eid=2-s2.0-84875527745&doi=10.1016%2FS0187-6236%2813%2971076-2&partnerID=40&md5=5436cae941f3c0c3323adba9858732c8.
Kawase, H., Imada, Y., Tsuguti, H., Nakaegawa, T., Seinino, N., Murata, A., et al. (2019). The heavy rain event of July 2019 in Japan enhanced by historical warming. *Bull Am Meteorol Soc*. doi:10.1175/BAMS-D-19-0173.1.
Kawase, H., Murata, A., Mizuta, R., Sasaki, H., Nosaka, M., Ishii, M., et al. (2016). Enhancement of heavy daily snowfall in central Japan due to global warming as projected by large ensemble of regional climate simulations. *Clim. Change* 139, 265–278. doi:10.1007/s10584-016-1781-3.
Kay, A. L., Bell, V. A., Guillod, B. P., Jones, R. G., and Rudd, A. C. (2018). National-scale analysis of low flow frequency: historical trends and potential future changes. *Clim. Change* 147, 585–599. doi:10.1007/s10584-018-2145-y.
Kay, J. E., Deser, C., Phillips, A., Mai, A., Hannay, C., Strand, G., et al. (2015). The Community Earth System Model (CESM) Large Ensemble Project: A Community Resource for Studying Climate Change in the Presence of Internal Climate Variability. *Bull. Am. Meteorol. Soc.* 96, 1333–1349. doi:10.1175/BAMS-D-13-00255.1.
Keller, L., Rössler, O., Martius, O., and Weingartner, R. (2019). Comparison of scenario-neutral approaches for estimation of climate change impacts on flood characteristics. *Hydrol. Process.* 33, 535–550. Available at: https://www.scopus.com/inward/record.uri?eid=2-s2.0-85058947911&doi=10.1002%2Fhyp.13341&partnerID=40&md5=4f3c00ec07e0ec0609c9643363614b5b.
Kelley, C. P., Mohtadi, S., Cane, M. A., Seager, R., and Kushnir, Y. (2015). Climate change in the Fertile Crescent and implications of the recent Syrian drought. *Proc. Natl. Acad. Sci. U. S. A.* 112, 3241–3246. doi:10.1073/pnas.1421533112.
Kendon, E. J., Ban, N., Roberts, N. M., Fowler, H. J., Roberts, M. J., Chan, S. C., et al. (2017). Do Convection-Permitting Regional Climate Models Improve Projections of Future Precipitation Change? *Bull. Am. Meteorol. Soc.* 98, 79–93. doi:10.1175/BAMS-D-15-0004.1.
Kendon, E. J., Roberts, N. M., Fowler, H. J., Roberts, M. J., Chan, S. C., and Senior, C. A. (2014). Heavier summer downpours with climate change revealed by weather forecast resolution model. *Nat. Clim. Chang.* 4, 570–576. doi:10.1038/nclimate2258.
Kendon, E. J., Stratton, R. A., Tucker, S., Marsham, J. H., Berthou, S., Rowell, D. P., et al. (2019). Enhanced future changes in wet and dry extremes over Africa at convection-permitting scale. *Nat. Commun.* 10, 1794. doi:10.1038/s41467-019-09776-9.
Kendon, M. (2014). Has there been a recent increase in UK weather records? *Weather* 69, 327–332. doi:10.1002/wea.2439.
Kermanshah, A., Derrible, S., and Berkelhammer, M. (2017). Using climate models to estimate urban vulnerability to flash floods. *J. Appl. Meteorol. Climatol.* 56, 2637–2650. Available at: https://www.scopus.com/inward/record.uri?eid=2-s2.0-85030331550&doi=10.1175%2FJAMC-D-17-0083.1&partnerID=40&md5=f6f2cbf0aee8326d783a025339f5aaa9.
Kew, S. F., Philip, S. Y., Hauser, M., Hobbins, M., Wanders, N., van Oldenborgh, G. J., et al. (2019a). Impact of precipitation and increasing temperatures on drought in eastern Africa. *Earth Syst. Dyn. Discuss.* 2019, 1–29. doi:10.5194/esd-2019-20.
Kew, S. F., Philip, S. Y., Jan van Oldenborgh, G., van der Schrier, G., Otto, F. E. L., and Vautard, R. (2019b). The Exceptional Summer Heat Wave in Southern Europe 2017. *Bull. Am. Meteorol. Soc.* 100, S49–S53. doi:10.1175/BAMS-D-18-0109.1.
Kew, S. F., Selten, F. M., Lenderink, G., and Hazeleger, W. (2013). The simultaneous occurrence of surge and discharge extremes for the Rhine delta. *Nat. Hazards Earth Syst. Sci.* 13, 2017–2029. doi:10.5194/nhess-13-2017-2013.
Kharin, V. V., Flato, G. M., Zhang, X., Gillett, N. P., Zwiers, F., and Anderson, K. J. (2018). Risks from Climate Extremes Change Differently from 1.5°C to 2.0°C Depending on Rarity. *Earth's Futur.* 6, 704–715. doi:10.1002/2018EF000813.
Kharin, V. V., Zwiers, F. W., Zhang, X., and Wehner, M. (2013). Changes in temperature and precipitation extremes in

the CMIP5 ensemble. *Clim. Change* 119, 345–357. doi:10.1007/s10584-013-0705-8.
Kharin, V. V, and Zwiers, F. W. (2000). Changes in the Extremes in an Ensemble of Transient Climate Simulations with a Coupled Atmosphere–Ocean GCM. *J. Clim.* 13, 3760–3788. doi:10.1175/1520-0442(2000)013<3760:CITEIA>2.0.CO;2.
Khlebnikova, E. I., Rudakova, Y. L., Sall', I. A., Efimov, S. V., and Shkolnik, I. M. (2019a). Changes in indicators of temperature extremes in the 21st century: ensemble projections for the territory of Russia. *Russ. Meteorol. Hydrol.* 44, 159–168. doi:10.3103/S1068373919030014.
Khlebnikova, E. I., Rudakova, Y. L., and Shkolnik, I. M. (2019b). Changes in precipitation regime over the territory of Russia: Data of regional climate modeling and observations. *Russ. Meteorol. Hydrol.* 44, 431–439. doi:10.3103/S106837391907001X.
Khong, A., Wang, J. K., Quiring, S. M., and Ford, T. W. (2015). Soil moisture variability in Iowa. *Int. J. Climatol.* 35, 2837–2848. doi:10.1002/joc.4176.
Kim, B., and Sanders, B. F. (2016). Dam-Break Flood Model Uncertainty Assessment: Case Study of Extreme Flooding with Multiple Dam Failures in Gangneung, South Korea. *J. Hydraul. Eng.* 142, 05016002. doi:10.1061/(ASCE)HY.1943-7900.0001097.
Kim, D., Moon, Y., Camargo, S. J., Wing, A. A., Sobel, A. H., Murakami, H., et al. (2018a). Process-Oriented Diagnosis of Tropical Cyclones in High-Resolution GCMs. *J. Clim.* 31, 1685–1702. doi:10.1175/JCLI-D-17-0269.1.
Kim, G., Cha, D.-H., Park, C., Lee, G., Jin, C.-S., Lee, D.-K., et al. (2018b). Future changes in extreme precipitation indices over Korea. *Int. J. Climatol.* 38, e862–e874. doi:10.1002/joc.5414.
Kim, H. S., Vecchi, G. A., Knutson, T. R., Anderson, W. G., Delworth, T. L., Rosati, A., et al. (2014). Tropical cyclone simulation and response to CO2 doubling in the GFDL CM2.5 high-resolution coupled climate model. *J. Clim.* 27, 8034–8054. doi:10.1175/JCLI-D-13-00475.1.
Kim, I. W., Oh, J., Woo, S., and Kripalani, R. H. (2019). Evaluation of precipitation extremes over the Asian domain: observation and modelling studies. *Clim. Dyn.* 52, 1317–1342. doi:10.1007/s00382-018-4193-4.
Kim, Y.-H., Min, S.-K., Zhang, X., Sillmann, J., and Sandstad, M. (submitted). Evaluation of the CMIP6 multi-model ensemble for climate extreme indices. *Weather Clim. Extrem.*(submitted).
Kim, Y. H., Min, S. K., Zhang, X., Zwiers, F., Alexander, L. V., Donat, M. G., et al. (2016). Attribution of extreme temperature changes during 1951–2010. *Clim. Dyn.* 46, 1769–1782. doi:10.1007/s00382-015-2674-2.
King, A. D. (2017). Attributing changing rates of temperature record-breaking to anthropogenic influences: Climate change and record-breaking. 1–13.
King, A. D., Black, M. T., Min, S.-K., Fischer, E. M., Mitchell, D. M., Harrington, L. J., et al. (2016a). Emergence of heat extremes attributable to anthropogenic influences. *Geophys. Res. Lett.* 43, 3438–3443. doi:10.1002/2015GL067448.
King, A. D., Jan van Oldenborgh, G., Karoly, D. J., Lewis, S. C., and Cullen, H. (2015). Attribution of the record high Central England temperature of 2014 to anthropogenic influences. *Environ. Res. Lett.* 10, 054002. doi:10.1088/1748-9326/10/5/054002.
King, A. D., Karoly, D. J., Donat, M. G., and Alexander, L. V. (2014). Climate change turns Australia's 2013 big dry into a year of record-breaking heat. [In "Explaining Extreme Events of 2013 from a Climate Perspective"]. *Bull. Am. Meteorol. Soc.* 95, S41–S45. doi:10.1175/1520-0477-95.9.S41.
King, A. D., Karoly, D. J., and Henley, B. J. (2017). Australian climate extremes at 1.5 °C and 2 °C of global warming. *Nat. Clim. Chang.* 7, 412–416. doi:10.1038/nclimate3296.
King, A. D., Karoly, D. J., and van Oldenborgh, G. J. (2016b). Climate Change and El Niño Increase Likelihood of Indonesian Heat and Drought. *Bull. Am. Meteorol. Soc.* 97, S113–S117. doi:10.1175/BAMS-D-16-0164.1.
King, A. D., Knutti, R., Uhe, P., Mitchell, D. M., Lewis, S. C., Arblaster, J. M., et al. (2018). On the linearity of local and regional temperature changes from 1.5°C to 2°C of global warming. *J. Clim.*, JCLI-D-17-0649.1. doi:10.1175/JCLI-D-17-0649.1.
King, A. D., Lewis, S. C., Perkins, S. E., Alexander, L. V, Donat, M. G., Karoly, D. J., et al. (2013). Limited evidence of anthropogenic influence on the 2011 - 12 extreme rainfall over Southeast Australia. *Bull. Amer. Meteor. Soc.* 94, 55–58.
King, A. D., Oldenborgh, G. J. van, and Karoly, D. J. (2016c). Climate Change and El NiÑo Increase Likelihood of Indonesain Heat and Drought. *Bull. Am. Meteorol. Soc.* 97, S113–S117. Available at: http://www.ametsoc.net/eee/2015/22_indonesia_heat.pdf.
King, M. P., Yu, E., and Sillmann, J. (2020). Impact of strong and extreme El Niños on European hydroclimate. *Tellus A Dyn. Meteorol. Oceanogr.* 72, 1–10. doi:10.1080/16000870.2019.1704342.
Kingston, D. G., Stagge, J. H., Tallaksen, L. M., and Hannah, D. M. (2015). European-scale drought: Understanding connections between atmospheric circulation and meteorological drought indices. *J. Clim.* 28, 505–516. doi:10.1175/JCLI-D-14-00001.1.
Kinter, J. L., Cash, B., Achuthavarier, D., Adams, J., Altshuler, E., Dirmeyer, P., et al. (2013). Revolutionizing climate

modeling with project athena: A multi-institutional, international collaboration. *Bull. Am. Meteorol. Soc.* 94, 231–245. doi:10.1175/BAMS-D-11-00043.1.
Kirchmeier-Young, M. C., and Zhang, X. (submitted). Human influence has intensified extreme precipitation in North America. *Proc. Natl. Acad. Sci.*(submitted).
Kirchmeier-Young, M. C., Zwiers, F. W., Gillett, N. P., and Cannon, A. J. (2017). Attributing extreme fire risk in Western Canada to human emissions. *Clim. Change* 144, 365–379. doi:10.1007/s10584-017-2030-0.
Kirchmeier-Young, M. C., Wan, H., Zhang, X., and Seneviratne, S. I. (2019). Importance of Framing for Extreme Event Attribution: The Role of Spatial and Temporal Scales. *Earth's Futur.* 7, 1192–1204. doi:10.1029/2019EF001253.
Kirshbaum, D. J., Merlis, T. M., Gyakum, J. R., and McTaggart-Cowan, R. (2017). Sensitivity of Idealized Moist Baroclinic Waves to Environmental Temperature and Moisture Content. *J. Atmos. Sci.* 75, 337–360. doi:10.1175/jas-d-17-0188.1.
Kishtawal, C. M., Jaiswal, N., Singh, R., and Niyogi, D. (2012). Tropical cyclone intensification trends during satellite era (1986-2010). *Geophys. Res. Lett.* 39, 1–6. doi:10.1029/2012GL051700.
KITOH, A. (2017). The Asian Monsoon and its Future Change in Climate Models: A Review. *J. Meteorol. Soc. Japan. Ser. II* 95, 7–33. doi:10.2151/jmsj.2017-002.
Kitoh, A., and Endo, H. (2019). Future Changes in Precipitation Extremes Associated with Tropical Cyclones Projected by Large-Ensemble Simulations. *J. Meteorol. Soc. Japan. Ser. II* 97, 141–152. doi:10.2151/jmsj.2019-007.
Kitoh, A., Kusunoki, S., and Nakaegawa, T. (2011). Climate change projections over South America in the late 21st century with the 20 and 60 km mesh Meteorological Research Institute atmospheric general circulation model (MRI-AGCM). *J. Geophys. Res.* 116, D06105. doi:10.1029/2010JD014920.
Klerk, W. J., Winsemius, H. C., van Verseveld, W. J., Bakker, A. M. R., and Diermanse, F. L. M. (2015). The co-incidence of storm surges and extreme discharges within the Rhine–Meuse Delta. *Environ. Res. Lett.* 10, 035005. doi:10.1088/1748-9326/10/3/035005.
Klutse, N. A. B., Ajayi, V. O., Gbobaniyi, E. O., Egbebiyi, T. S., Kouadio, K., Nkrumah, F., et al. (2018). Potential impact of 1.5 °C and 2 °C global warming on consecutive dry and wet days over West Africa. *Environ. Res. Lett.* 13, 055013. doi:10.1088/1748-9326/aab37b.
Klutse, N. A. B., Sylla, M. B., Diallo, I., Sarr, A., Dosio, A., Diedhiou, A., et al. (2016). Daily characteristics of West African summer monsoon precipitation in CORDEX simulations. *Theor. Appl. Climatol.* 123, 369–386.
Knapp, K. R., Velden, C. S., Wimmers, A. J., Knapp, K. R., Velden, C. S., and Wimmers, A. J. (2018). A Global Climatology of Tropical Cyclone Eyes. *Mon. Weather Rev.* 146, 2089–2101. doi:10.1175/MWR-D-17-0343.1.
Knutson, T., Camargo, S. J., Chan, J. C. L., Emanuel, K., Ho, C.-H., Kossin, J., et al. (2019a). Tropical Cyclones and Climate Change Assessment: Part I: Detection and Attribution. *Bull. Am. Meteorol. Soc.* 100, 1987–2007. doi:10.1175/BAMS-D-18-0189.1.
Knutson, T., Camargo, S. J., Chan, J. C. L., Emanuel, K., Ho, C.-H., Kossin, J., et al. (2019b). Tropical Cyclones and Climate Change Assessment: Part II. Projected Response to Anthropogenic Warming. *Bull. Am. Meteorol. Soc.*, BAMS-D-18-0194.1. doi:10.1175/BAMS-D-18-0194.1.
Knutson, T. R., and Ploshay, J. J. (2016). Detection of anthropogenic influence on a summertime heat stress index. *Clim. Change* 138, 25–39. doi:10.1007/s10584-016-1708-z.
Knutson, T. R., Sirutis, J. J., Vecchi, G. A., Garner, S., Zhao, M., Kim, H.-S., et al. (2013). Dynamical Downscaling Projections of Twenty-First-Century Atlantic Hurricane Activity: CMIP3 and CMIP5 Model-Based Scenarios. *J. Clim.* 26, 6591–6617. doi:10.1175/JCLI-D-12-00539.1.
Knutson, T. R., Sirutis, J. J., Zhao, M., Tuleya, R. E., Bender, M., Vecchi, G. A., et al. (2015). Global Projections of Intense Tropical Cyclone Activity for the Late Twenty-First Century from Dynamical Downscaling of CMIP5/RCP4.5 Scenarios. *J. Clim.* 28, 7203–7224. doi:10.1175/JCLI-D-15-0129.1.
Knutson, T. R., and Zeng, F. (2018). Model Assessment of Observed Precipitation Trends over Land Regions: Detectable Human Influences and Possible Low Bias in Model Trends. *J. Clim.* 31, 4617–4637. doi:10.1175/JCLI-D-17-0672.1.
Knutson, T. R., Zeng, F., and Wittenberg, A. T. (2014a). MULTIMODEL ASSESSMENT OF EXTREME ANNUAL-MEAN WARM ANOMALIES DURING 2013 OVER REGIONS OF AUSTRALIA AND THE WESTERN TROPICAL PACIFIC. 95.
Knutson, T. R., Zeng, F., and Wittenberg, A. T. (2014b). Multimodel assessment of extreme annual-mean warm anomalies during 2013 over regions of Australia and the western tropical Pacific [in "Explaining Extremes of 2013 from a Climate Perspective"]. *Bull Am Meteorol Soc* 95, S26–S30. Available at: http://www2.ametsoc.org/ams/assets/File/publications/BAMS_EEE_2013_Full_Report.pdf.
Knutson, T., Zeng, F., and Wittenberg, A. (2014c). Seasonal and annual mean precipitation extremes during during 2013: A U.S. focused analysis. *Bull. Amer. Meteor. Soc.* 95, S19–S23.
Kodama, C., Stevens, B., Mauritsen, T., Seiki, T., and Satoh, M. (2019). A New Perspective for Future Precipitation Change from Intense Extratropical Cyclones. *Geophys. Res. Lett.* 46. doi:10.1029/2019GL084001.

Kodama, C., Yamada, Y., Noda, A. T., Kikuchi, K., Kajikawa, Y., Nasuno, T., et al. (2015). A 20-year climatology of a NICAM AMIP-type simulation. *J. Meteorol. Soc. Japan* 93, 393–424. doi:10.2151/jmsj.2015-024.

Kogan, F., and Guo, W. (2017). Strong 2015–2016 El Niño and implication to global ecosystems from space data. *Int. J. Remote Sens.* 38, 161–178. doi:10.1080/01431161.2016.1259679.

Konapala, G., and Mishra, A. (2017). Review of complex networks application in hydroclimatic extremes with an implementation to characterize spatio-temporal drought propagation in continental USA. *J. Hydrol.* 555, 600–620. Available at: https://www.scopus.com/inward/record.uri?eid=2-s2.0-85032658690&doi=10.1016%2Fj.jhydrol.2017.10.033&partnerID=40&md5=2095ffe9b6a218e3e79e331506c682dd.

Kong, Q., Guerreiro, S. B., Blenkinsop, S., Li, X.-F., and Fowler, H. J. (2020). Increases in summertime concurrent drought and heatwave in Eastern China. *Weather Clim. Extrem.* 28, 100242. doi:10.1016/j.wace.2019.100242.

Kooperman, G. J., Fowler, M. D., Hoffman, F. M., Koven, C. D., Lindsay, K., Pritchard, M. S., et al. (2018). Plant Physiological Responses to Rising CO2 Modify Simulated Daily Runoff Intensity With Implications for Global-Scale Flood Risk Assessment. *Geophys. Res. Lett.* 45, 12,412-457,466. doi:10.1029/2018GL079901.

Köplin, N., Schädler, B., Viviroli, D., and Weingartner, R. (2014). Seasonality and magnitude of floods in Switzerland under future climate change. *Hydrol. Process.* 28, 2567–2578. doi:10.1002/hyp.9757.

Kornhuber, K., Coumou, D., Vogel, E., Lesk, C., Donges, J. F., Lehmann, J., et al. (2020). Amplified Rossby waves enhance risk of concurrent heatwaves in major breadbasket regions. *Nat. Clim. Chang.* 10, 48–53. doi:10.1038/s41558-019-0637-z.

Kornhuber, K., Osprey, S., Coumou, D., Petri, S., Petoukhov, V., Rahmstorf, S., et al. (2019). Extreme weather events in early summer 2018 connected by a recurrent hemispheric wave-7 pattern. *Environ. Res. Lett.* 14, 54002. doi:10.1088/1748-9326/ab13bf.

Kossin, J. P. (2017). Hurricane intensification along United States coast suppressed during active hurricane periods. *Nature* 541, 390–393. doi:10.1038/nature20783.

Kossin, J. P. (2018). A global slowdown of tropical-cyclone translation speed. *Nature* 558, 104–107. doi:10.1038/s41586-018-0158-3.

Kossin, J. P. (2019). Reply to: Moon, I.-J. et al.; Lanzante, J. R. *Nature* 570, E16–E22. doi:10.1038/s41586-019-1224-1.

Kossin, J. P., Emanuel, K. A., and Camargo, S. J. (2016a). Past and Projected Changes in Western North Pacific Tropical Cyclone Exposure. *J. Clim.* 29, 5725–5739. doi:10.1175/JCLI-D-16-0076.1.

Kossin, J. P., Emanuel, K. A., and Vecchi, G. A. (2014). The poleward migration of the location of tropical cyclone maximum intensity. *Nature*, 4–7. doi:10.1038/nature13278.

Kossin, J. P., Emanuel, K. A., and Vecchi, G. A. (2016b). Comment on 'Roles of interbasin frequency changes in the poleward shifts of the maximum intensity location of tropical cyclones.' *Environ. Res. Lett.* 11, 068001. doi:10.1088/1748-9326/11/6/068001.

Kossin, J. P., Hall, T., Knutson, T., Kunkel, K. E., Trapp, R. J., Waliser, D. E., et al. (2017). Ch. 9: Extreme Storms. Climate Science Special Report: Fourth National Climate Assessment, Volume I. , eds. D. J. Wuebbles, D. W. Fahey, K. A. Hibbard, D. J. Dokken, B. C. Stewart, and T. K. Maycock Washington, DC doi:10.7930/J07S7KXX.

Kossin, J. P., Knapp, K. R., Olander, T. L., and Velden, C. S. (submitted). Global increase in major tropical cyclone exceedance probability over the past 40 years. *Proc. Natl. Acad. Sci.*(submitted).

Kossin, J. P., Olander, T. L., and Knapp, K. R. (2013). Trend analysis with a new global record of tropical cyclone intensity. *J. Clim.* 26, 9960–9976. doi:10.1175/JCLI-D-13-00262.1.

Koster, R. D., Guo, Z., Yang, R., Dirmeyer, P. A., Mitchell, K., and Puma, M. J. (2009). On the Nature of Soil Moisture in Land Surface Models. *J. Clim.* 22, 4322–4335. doi:10.1175/2009JCLI2832.1.

Koster, R. D., Mahanama, S. P. P., Yamada, T. J., Balsamo, G., Berg, A. A., Boisserie, M., et al. (2011). The second phase of the global land-atmosphere coupling experiment: Soil moisture contributions to subseasonal forecast skill. *J. Hydrometeorol.* 12, 805–822. doi:10.1175/2011JHM1365.1.

Krishnan, R., Sabin, T. P., Vellore, R., Mujumdar, M., Sanjay, J., Goswami, B. N., et al. (2016). Deciphering the desiccation trend of the South Asian monsoon hydroclimate in a warming world. *Clim. Dyn.* 47, 1007–1027. doi:10.1007/s00382-015-2886-5.

Kröner, N., Zubler, E., Schär, C., Kotlarski, S., Fischer, E., and Lüthi, D. (2016). Separating climate change signals into thermodynamic, lapse-rate and circulation effects: theory and application to the European summer climate. *Clim. Dyn.* 48, 3425–3440. doi:10.1007/s00382-016-3276-3.

Krueger, O., Schenk, F., Feser, F., and Weisse, R. (2013). Inconsistencies between long-term trends in storminess derived from the 20CR reanalysis and observations. *J. Clim.* 26, 868–874. doi:10.1175/JCLI-D-12-00309.1.

Kruger, A. C., Rautenbach, H., Mbatha, S., Ngwenya, S., and Makgoale, T. E. (2019). Historical and projected trends in near-surface temperature indices for 22 locations in South Africa. *S. Afr. J. Sci.* 115. doi:10.17159/sajs.2019/4846.

Kruger, A. C., and Sekele, S. S. (2013). Trends in extreme temperature indices in South Africa: 1962-2009. *Int. J.*

Climatol. 33, 661–676. doi:10.1002/joc.3455.
Krysanova, V., Vetter, T., Eisner, S., Huang, S., Pechlivanidis, I., Strauch, M., et al. (2017). Intercomparison of regional-scale hydrological models and climate change impacts projected for 12 large river basins worldwide - A synthesis. *Environ. Res. Lett.* 12. doi:10.1088/1748-9326/aa8359.
Kubota, T., Shige, S., Hashizume, H., Aonashi, K., Takahashi, N., Seto, S., et al. (2007). Global Precipitation Map Using Satellite-Borne Microwave Radiometers by the GSMaP Project: Production and Validation. *IEEE Trans. Geosci. Remote Sens.* 45, 2259–2275. doi:10.1109/TGRS.2007.895337.
Kulp, S., and Strauss, B. H. (2017). Rapid escalation of coastal flood exposure in US municipalities from sea level rise. *Clim. Change* 142, 477–489. Available at: https://www.scopus.com/inward/record.uri?eid=2-s2.0-85019146893&doi=10.1007%2Fs10584-017-1963-7&partnerID=40&md5=c7ba0df89c42c21a27b2195a58e4aad9.
Kumar, R., Stephens, M., and Weir, T. (2014). Rainfall trends in Fiji. *Int. J. Climatol.* 34, 1501–1510. Available at: https://www.scopus.com/inward/record.uri?eid=2-s2.0-84897916226&doi=10.1002%2Fjoc.3779&partnerID=40&md5=b040899ceea1c4a3967f508aed79d9ba.
Kumar, S., Allan, R. P., Zwiers, F., Lawrence, D. M., and Dirmeyer, P. A. (2015). Revisiting trends in wetness and dryness in the presence of internal climate variability and water limitations over land. *Geophys. Res. Lett.* 42, 10,867-10,875. doi:10.1002/2015GL066858.
Kumar, S., and Kumar, S. (2017). Climatic variability and extreme weather events in Bihar. *J. Agrometeorol.* 19.
Kumar, S. P. and R. S. N. and D. N. (2017). Linkage between global sea surface temperature and hydroclimatology of a major river basin of India before and after 1980. *Environ. Res. Lett.* 12, 124002. Available at: http://stacks.iop.org/1748-9326/12/i=12/a=124002.
Kundzewicz, Z. W., Krysanova, V., Dankers, R., Hirabayashi, Y., Kanae, S., Hattermann, F. F., et al. (2017). Differences in flood hazard projections in Europe–their causes and consequences for decision making. *Hydrol. Sci. J.* 62, 1–14. doi:10.1080/02626667.2016.1241398.
Kundzewicz, Z. W., Pin'skwar, I., and Brakenridge, G. R. (2018). Changes in river flood hazard in Europe: A review. *Hydrol. Res.* 49, 294–302. doi:10.2166/nh.2017.016.
Kunii, M., Otsuka, M., Shimoji, K., and Seko, H. (2016). Ensemble Data Assimilation and Forecast Experiments for the September 2015 Heavy Rainfall Event in Kanto and Tohoku Regions with Atmospheric Motion Vectors from Himawari-8. *Sola* 12, 209–214. doi:10.2151/sola.2016-042.
Kunkel, K. E., Karl, T. R., Brooks, H., Kossin, J., Lawrimore, J. H., Arndt, D., et al. (2013). Monitoring and understanding trends in extreme storms: State of knowledge. *Bull. Am. Meteorol. Soc.* 94, 499–514. doi:10.1175/BAMS-D-11-00262.1.
Kusunoki, S. (2017). Future Changes in Global Precipitation Projected by the Atmospheric Model MRI-AGCM3.2H with a 60-km Size. *Atmos.* 8. doi:10.3390/atmos8050093.
Kusunoki, S. (2018a). Future changes in precipitation over East Asia projected by the global atmospheric model MRI-AGCM3.2. *Clim. Dyn.* 51, 4601–4617. doi:10.1007/s00382-016-3499-3.
Kusunoki, S. (2018b). Is the global atmospheric model MRI-AGCM3.2 better than the CMIP5 atmospheric models in simulating precipitation over East Asia? *Clim. Dyn.* 51, 4489–4510. doi:10.1007/s00382-016-3335-9.
Kusunoki, S., and Mizuta, R. (2013). Changes in precipitation intensity over East Asia during the 20th and 21st centuries simulated by a global atmospheric model with a 60 km grid size. *J. Geophys. Res. Atmos.* 118, 11,007-11,016. doi:10.1002/jgrd.50877.
Lackmann, G. M. (2013). The south-central U.S. flood of may 2010: Present and future. *J. Clim.* 26, 4688–4709. doi:10.1175/JCLI-D-12-00392.1.
Lackmann, G. M. (2014). Hurricane Sandy before 1900 and after 2100. *Bull. Am. Meteorol. Soc.* 96, 547–560. doi:10.1175/BAMS-D-14-00123.1.
Laliberté, F., Howell, S. E. L., and Kushner, P. J. (2015). Regional variability of a projected sea ice-free Arctic during the summer months. *Geophys. Res. Lett.* 43, 256–263. doi:10.1002/2015GL066855.
Landsea, C. W. (2015). Comments on "Monitoring and understanding trends in extreme storms: state of knowledge.". *Bull. Am. Meteorol. Soc.* 96, 1175–1182. doi:10.1175/1520-0477-96.7.1175.
Lane, C. S., Horn, S. P., and Kerr, M. T. (2014). Beyond the Mayan Lowlands: Impacts of the Terminal Classic Drought in the Caribbean Antilles. *Quat. Sci. Rev.* 86, 89–98. Available at: https://www.scopus.com/inward/record.uri?eid=2-s2.0-84892846141&doi=10.1016%2Fj.quascirev.2013.12.017&partnerID=40&md5=e401cd788eba3c383edcf5268c975e63.
Langerwisch, F., Rost, S., Gerten, D., Poulter, B., Rammig, A., and Cramer, W. (2013). Potential effects of climate change on inundation patterns in the Amazon Basin. *Hydrol. Earth Syst. Sci.* 17, 2247–2262. doi:10.5194/hess-17-2247-2013.
Lanzante, J. R. (2019). Uncertainties in tropical-cyclone translation speed. *Nature* 570, E6–E15. doi:10.1038/s41586-019-1223-2.

Lau, N.-C., and Nath, M. J. (2014). Model simulation and projection of European heat waves in present-day and future climates. *J. Clim.* 27, 3713–3730. doi:10.1175/JCLI-D-13-00284.1.
Lawal, K. A., Abatan, A. A., Angélil, O., Olaniyan, E., Olusoji, V. H., Oguntunde, P. G., et al. (2016). The Late Onset of the 2015 Wet Season in Nigeria. *Bull. Am. Meteorol. Soc.* 97, S63–S69. doi:10.1175/BAMS-D-16-0131.1.
Leach, N., Li, S., Sparrow, S., van Oldenborgh, G. J., Lott, F. C., Weisheimer, A., et al. (2020). Anthropogenic influence on the 2018 summer warm spell in Europe: the impact of different spatio-temporal scales. *Bull. Am. Meteorol. Soc.* Available at: http://ametsoc.net/eee/2018/8_Leach0201_w.pdf.
Lee, C.-S., Cheung, K. K. W., Hui, J. S. N., and Elsberry, R. L. (2008). Mesoscale Features Associated with Tropical Cyclone Formations in the Western North Pacific. *Mon. Weather Rev.* 136, 2006–2022. doi:10.1175/2007MWR2267.1.
Lee, D., Min, S., Fischer, E., Shiogama, H., and Bethke, I. (2018). Impacts of half a degree additional warming on the Asian summer monsoon rainfall characteristics. *Environ. Res. Lett.* 13. doi:10.1088/1748-9326/aab55d.
Lee, J., Li, S., Lund, R., Lee, J., Li, S., and Lund, R. (2014). Trends in Extreme U.S. Temperatures. *J. Clim.* 27, 4209–4225. doi:10.1175/JCLI-D-13-00283.1.
Lehner, F., Coats, S., Stocker, T. F., Pendergrass, A. G., Sanderson, B. M., Raible, C. C., et al. (2017). Projected drought risk in 1.5°C and 2°C warmer climates. *Geophys. Res. Lett.* 44, 7419–7428. doi:10.1002/2017GL074117.
Lehner, F., and Stocker, T. F. (2015). From local perception to global perspective. *Nat. Clim. Chang.* 5, 731–734. doi:10.1038/nclimate2660.
Lejeune, Q., Davin, E. L., Gudmundsson, L., Winckler, J., and Seneviratne, S. I. (2018). Historical deforestation locally increased the intensity of hot days in northern mid-latitudes. *Nat. Clim. Chang.* 8, 386–390. doi:10.1038/s41558-018-0131-z.
Lejeune, Q., Seneviratne, S. I., and Davin, E. L. (2017). Historical Land-Cover Change Impacts on Climate: Comparative Assessment of LUCID and CMIP5 Multimodel Experiments. *J. Clim.* 30, 1439–1459. doi:10.1175/JCLI-D-16-0213.1.
Lelieveld, J., Proestos, Y., Hadjinicolaou, P., Tanarhte, M., Tyrlis, E., and Zittis, G. (2016). Strongly increasing heat extremes in the Middle East and North Africa (MENA) in the 21st century. *Clim. Change* 137, 245–260. doi:10.1007/s10584-016-1665-6.
Lemordant, L., Gentine, P., Stéfanon, M., Drobinski, P., and Fatichi, S. (2016). Modification of land-atmosphere interactions by CO2 effects: Implications for summer dryness and heat wave amplitude. *Geophys. Res. Lett.* 43, 10,240-10,248. doi:10.1002/2016GL069896.
Lemordant, L., Gentine, P., Swann, A. S., Cook, B. I., and Scheff, J. (2018). Critical impact of vegetation physiology on the continental hydrologic cycle in response to increasing CO 2. *Proc. Natl. Acad. Sci.* 115, 4093–4098. doi:10.1073/pnas.1720712115.
Lenderink, G., Barbero, R., Loriaux, J. M., and Fowler, H. J. (2017). Super-Clausius–Clapeyron Scaling of Extreme Hourly Convective Precipitation and Its Relation to Large-Scale Atmospheric Conditions. *J. Clim.* 30, 6037–6052. doi:10.1175/JCLI-D-16-0808.1.
Lenderink, G., and Fowler, H. J. (2017). Understanding rainfall extremes. *Nat. Clim. Chang.* 7, 391. Available at: https://doi.org/10.1038/nclimate3305.
Lestari, D. O., Sutriyono, E., Sabaruddin, S., and Iskandar, I. (2018). Respective Influences of Indian Ocean Dipole and El Niño-Southern Oscillation on Indonesian Precipitation. *J. Math. Fundam. Sci.* 50, 257–272. doi:10.5614/j.math.fund.sci.2018.50.3.3.
Lewis, S. C., Blake, S. A. P., Trewin, B., Black, M. T., Dowdy, A. J., Perkins-Kirkpatrick, S. E., et al. (2019a). Deconstructing factors contributing to the 2018 fire weather in Queensland, Australia. *Bull. Am. Meteorol. Soc.*, BAMS-D-19-0144.1. doi:10.1175/BAMS-D-19-0144.1.
Lewis, S. C., and Karoly, D. J. (2013). Anthropogenic contributions to Australia's record summer temperatures of 2013. *Geophys. Res. Lett.* 40, 3705–3709. doi:10.1002/grl.50673.
Lewis, S. C., and Karoly, D. J. (2014a). Are estimates of anthropogenic and natural influences on Australia's extreme 2010–2012 rainfall model-dependent? *Clim. Dyn.* 45, 679–695. doi:10.1007/s00382-014-2283-5.
Lewis, S. C., and Karoly, D. J. (2014b). The Role of Anthropogenic Forcing in the Record 2013 Australia-Wide Annual and Spring Temperatures [in "Explaining Extremes of 2013 from a Climate Perspective"]. *Bull. Am. Meteorol. Soc.* 95, S31--S34.
Lewis, S. C., and King, A. D. (2015). Dramatically increased rate of observed hot record breaking in recent Australian temperatures. *Geophys. Res. Lett.* 42, 7776–7784. doi:10.1002/2015GL065793.
Lewis, S. C., King, A. D., and Mitchell, D. M. (2017a). Australia's Unprecedented Future Temperature Extremes Under Paris Limits to Warming. *Geophys. Res. Lett.* 44, 9947–9956.
Lewis, S. C., King, A. D., and Perkins-Kirkpatrick, S. E. (2017b). Defining a New Normal for Extremes in a Warming World. *Bull. Am. Meteorol. Soc.* 98, 1139–1151. doi:10.1175/BAMS-D-16-0183.1.
Lewis, S. C., King, A. D., Perkins-Kirkpatrick, S. E., and Wehner, M. F. (2019b). Toward Calibrated Language for Effectively Communicating the Results of Extreme Event Attribution Studies. *Earth's Futur.* 7, 1020–1026.

doi:10.1029/2019EF001273.
Lewis, S. L., Brando, P. M., Phillips, O. L., van der Heijden, G. M. F., and Nepstad, D. (2011). The 2010 Amazon Drought. *Science* 331, 554–554. doi:10.1126/science.1200807.
Lhotka, O., Kyselý, J., and Farda, A. (2018). Climate change scenarios of heat waves in Central Europe and their uncertainties. *Theor. Appl. Climatol.* 131, 1043–1054. doi:10.1007/s00704-016-2031-3.
Li, C., Fang, Y., Caldeira, K., Zhang, X., Diffenbaugh, N. S., and Michalak, A. M. (2018a). Widespread persistent changes to temperature extremes occurred earlier than predicted. *Sci. Rep.* 8, 1007. doi:10.1038/s41598-018-19288-z.
Li, C., Zhang, X., Zwiers, F., Fang, Y., and Michalak, A. M. (2017a). Recent Very Hot Summers in Northern Hemispheric Land Areas Measured by Wet Bulb Globe Temperature Will Be the Norm Within 20 Years. *Earth's Futur.* 5, 1203–1216. doi:10.1002/2017EF000639.
Li, C., Zwiers, F. W., Zhang, X., Li, G., Sun, Y., and Wehner, M. (submitted). Changes in temperature and precipitation extremes in the new-generation CMIP6 models. *J. Clim.*(submitted).
Li, C., Zwiers, F., Zhang, X., and Li, G. (2018b). How much information is required to well-constrain local estimates of future precipitation extremes? *Earth's Futur.*, 2018EF001001. doi:10.1029/2018EF001001.
Li, D., Bou-Zeid, E., and Oppenheimer, M. (2014a). The effectiveness of cool and green roofs as urban heat island mitigation strategies. *Environ. Res. Lett.* 9, 055002. doi:10.1088/1748-9326/9/5/055002.
Li, D., Zhou, T., Zou, L., Zhang, W., and Zhang, L. (2018c). Extreme High-Temperature Events Over East Asia in 1.5°C and 2°C Warmer Futures: Analysis of NCAR CESM Low-Warming Experiments. *Geophys. Res. Lett.* 45, 1541–1550. doi:10.1002/2017GL076753.
Li, G., Zhang, X., Cannon, A. J., Murdock, T., Sobie, S., Zwiers, F., et al. (2018d). Indices of Canada's future climate for general and agricultural adaptation applications. *Clim. Change* 148, 249–263. doi:10.1007/s10584-018-2199-x.
Li, H., Chen, H., and Wang, H. (2017b). Effects of anthropogenic activity emerging as intensified extreme precipitation over China. *J. Geophys. Res. Atmos.* 122, 6899–6914. doi:10.1002/2016JD026251.
Li, M. (2017). Temperature reconstruction and volcanic eruption signal from tree-ring width and maximum latewood density over the past 304 years in the southeastern Tibetan Plateau. 2021–2032. doi:10.1007/s00484-017-1395-0.
Li, M., Woollings, T., Hodges, K., and Masato, G. (2014b). Extratropical cyclones in a warmer, moister climate: A recent Atlantic analogue. *Geophys. Res. Lett.* 41, 8594–8601. doi:10.1002/2014GL062186.
Li, S., Otto, F. E. L., Harrington, L. J., Sparrow, S. N., and Wallom, D. (2019a). A pan-South-America assessment of avoided exposure to dangerous extreme precipitation by limiting to 1.5 °C warming. *Environ. Res. Lett.* doi:10.1088/1748-9326/ab50a2.
Li, W., Jiang, Z., Zhang, X., and Li, L. (2018e). On the Emergence of Anthropogenic Signal in Extreme Precipitation Change Over China. *Geophys. Res. Lett.* doi:10.1029/2018GL079133.
Li, W., Jiang, Z., Zhang, X., Li, L., and Sun, Y. (2018f). Additional risk in extreme precipitation in China from 1.5 °C to 2.0 °C global warming levels. *Sci. Bull.* 63, 228–234. doi:10.1016/J.SCIB.2017.12.021.
Li, W., Lin, K., Zhao, T., Lan, T., Chen, X., Du, H., et al. (2019b). Risk assessment and sensitivity analysis of flash floods in ungauged basins using coupled hydrologic and hydrodynamic models. *J. Hydrol.* 572, 108–120. Available at: https://www.scopus.com/inward/record.uri?eid=2-s2.0-85062342916&doi=10.1016%2Fj.jhydrol.2019.03.002&partnerID=40&md5=46ad0260d0d3cd615944aacd5e8f833b.
Li, X., Liu, L., Li, H., Wang, S., and Heng, J. (2019c). Spatiotemporal soil moisture variations associated with hydro-meteorological factors over the Yarlung Zangbo River basin in Southeast Tibetan Plateau. *Int. J. Climatol.* Available at: https://www.scopus.com/inward/record.uri?eid=2-s2.0-85068500165&doi=10.1002%2Fjoc.6202&partnerID=40&md5=5aefae9bea65c424b00b74b087373a95.
Li, X., Wang, X., and Babovic, V. (2018g). Analysis of variability and trends of precipitation extremes in Singapore during 1980–2013. *Int. J. Climatol.* 38, 125–141. doi:10.1002/joc.5165.
Li, X. X., Chen, H., Wei, J., Hua, W., Sun, S., Ma, H., et al. (2018h). Inconsistent Responses of Hot Extremes to Historical Land Use and Cover Change Among the Selected CMIP5 Models. *J. Geophys. Res. Atmos.* 123, 3497–3512. doi:10.1002/2017JD028161.
Li, X., You, Q., Ren, G., Wang, S., Zhang, Y., Yang, J., et al. (2019d). Concurrent droughts and hot extremes in northwest China from 1961 to 2017. *Int. J. Climatol.* 39, 2186–2196. doi:10.1002/joc.5944.
Li, Y., Zhao, M., Motesharrei, S., Mu, Q., Kalnay, E., and Li, S. (2015). Local cooling and warming effects of forests based on satellite observations. *Nat. Commun.* 6, 6603. doi:10.1038/ncomms7603.
Li, Z., Chen, Y., Fang, G., and Li, Y. (2017c). Multivariate assessment and attribution of droughts in Central Asia. *Sci. Rep.* 7, 1–12. doi:10.1038/s41598-017-01473-1.
Li, Z., Chen, Y., Shen, Y., Liu, Y., and Zhang, S. (2013). Analysis of changing pan evaporation in the arid region of Northwest China. *Water Resour. Res.* 49, 2205–2212. Available at: https://www.scopus.com/inward/record.uri?eid=2-s2.0-

84877984528&doi=10.1002%2Fwrcr.20202&partnerID=40&md5=d47b3789c3abeb5aa9434dc27e9738aa.
Li, Z., Sun, Y., Li, T., Ding, Y., and Hu, T. (2019e). Future Changes in East Asian Summer Monsoon Circulation and Precipitation Under 1.5 to 5 °C of Warming. *Earth's Futur.*, 2019EF001276. doi:10.1029/2019EF001276.
Lian, X., Piao, S., Li, L. Z. X., Li, Y., Huntingford, C., Ciais, P., et al. (2020). Summer soil drying exacerbated by earlier spring greening of northern vegetation. *Sci. Adv.* 6, eaax0255. doi:10.1126/sciadv.aax0255.
Liang, J., Wang, C., and Hodges, K. I. (2017). Evaluation of tropical cyclones over the South China Sea simulated by the 12 km MetUM regional climate model. *Q. J. R. Meteorol. Soc.* 143, 1641–1656. doi:10.1002/qj.3035.
Liberato, M. L. R., Ramos, A. M., Gouveia, C. M., Sousa, P., Russo, A., Trigo, R. M., et al. (2017). Exceptionally extreme drought in Madeira Archipelago in 2012: Vegetation impacts and driving conditions. *Agric. For. Meteorol.* 232, 195–209. Available at: https://www.scopus.com/inward/record.uri?eid=2-s2.0-84983527028&doi=10.1016%2Fj.agrformet.2016.08.010&partnerID=40&md5=c344f5463ec61ddf4994d2798c9ab277.
Lin, L., Wang, Z., Xu, Y., and Fu, Q. (2016). Sensitivity of precipitation extremes to radiative forcing of greenhouse gases and aerosols. *Geophys. Res. Lett.* 43, 9860–9868. doi:10.1002/2016GL070869.
Lin, L., Wang, Z., Xu, Y., Fu, Q., and Dong, W. (2018a). Larger Sensitivity of Precipitation Extremes to Aerosol Than Greenhouse Gas Forcing in CMIP5 Models. *J. Geophys. Res. Atmos.* doi:10.1029/2018JD028821.
Lin, L., Xu, Y., Wang, Z., Diao, C., Dong, W., and Xie, S.-P. (2018b). Changes in Extreme Rainfall Over India and China Attributed to Regional Aerosol-Cloud Interaction During the Late 20th Century Rapid Industrialization. *Geophys. Res. Lett.* 45, 7857–7865. doi:10.1029/2018GL078308.
Lin, N., Lane, P., Emanuel, K. A., Sullivan, R. M., and Donnelly, J. P. (2014). Heightened hurricane surge risk in northwest Florida revealed from climatological-hydrodynamic modeling and paleorecord reconstruction. *J. Geophys. Res. Atmos.* 119, 8606–8623. doi:10.1002/2014JD021584.
Lin, P., He, Z., Du, J., Chen, L., Zhu, X., and Li, J. (2017). Recent changes in daily climate extremes in an arid mountain region, a case study in northwestern China's Qilian Mountains. *Sci. Rep.* 7, 1–15. doi:10.1038/s41598-017-02345-4.
Littell, J. S., Peterson, D. L., Riley, K. L., Liu, Y., and Luce, C. H. (2016). A review of the relationships between drought and forest fire in the United States. *Glob. Chang. Biol.* 22, 2353–2369. doi:10.1111/gcb.13275.
Little, C. M., Horton, R. M., Kopp, R. E., Oppenheimer, M., Vecchi, G. A., and Villarini, G. (2015). Joint projections of US East Coast sea level and storm surge. *Nat. Clim. Chang.* 5, 1114. doi:10.1038/nclimate2801.
Liu, B., Zhu, C., Su, J., Ma, S., and Xu, K. (2019a). Record-Breaking Northward Shift of the Western North Pacific Subtropical High in July 2018. *J. Meteorol. Soc. Japan. Ser. II* 97, 913–925. doi:10.2151/jmsj.2019-047.
Liu, C., and Zipser, E. J. (2015). The global distribution of largest, deepest, and most intense precipitation systems. *Geophys. Res. Lett.* 42, 3591–3595. doi:10.1002/2015GL063776.
Liu, L., Gudmundsson, L., Hauser, M., Qin, D., Li, S., and Seneviratne, S. I. (submitted). Soil moisture dominates dryness stress on ecosystem production in global observations. *Nat. Commun.*(submitted).
Liu, L., Xu, H., Wang, Y., and Jiang, T. (2017). Impacts of 1.5 and 2 °C global warming on water availability and extreme hydrological events in Yiluo and Beijiang River catchments in China. *Clim. Change* 145, 145–158. doi:10.1007/s10584-017-2072-3.
Liu, L., Zhang, R., and Zuo, Z. (2014). Intercomparison of spring soil moisture among multiple reanalysis data sets over eastern China. *J. Geophys. Res.* 119, 54–64. Available at: https://www.scopus.com/inward/record.uri?eid=2-s2.0-84893974446&doi=10.1002%2F2013JD020940&partnerID=40&md5=8c2750d6469c1a15d8b949fd32100ead.
Liu, M., Shen, Y., Qi, Y., Wang, Y., and Geng, X. (2019b). Changes in precipitation and drought extremes over the past half century in China. *Atmosphere (Basel).* 10. doi:10.3390/atmos10040203.
Liu, M., Vecchi, G. A., Smith, J. A., and Knutson, T. R. (2019c). Causes of large projected increases in hurricane precipitation rates with global warming. *npj Clim. Atmos. Sci.* 2, 1–5. doi:10.1038/s41612-019-0095-3.
Liu, Q., Babanin, A. V., Zieger, S., Young, I. R., and Guan, C. (2016). Wind and wave climate in the Arctic Ocean as observed by altimeters. *J. Clim.* 29, 7957–7975. doi:10.1175/JCLI-D-16-0219.1.
Liu, W., and Sun, F. (2016). Assessing estimates of evaporative demand in climate models using observed pan evaporation over China. *J. Geophys. Res.* 121, 8329–8349. doi:10.1002/2016JD025166.
Liu, W., and Sun, F. (2017). Projecting and attributing future changes of evaporative demand over china in CMIP5 climate models. *J. Hydrometeorol.* 18, 977–991. doi:10.1175/JHM-D-16-0204.1.
Liu, Y., Pan, Z., Zhuang, Q., Miralles, D. G., Teuling, A. J., Zhang, T., et al. (2015). Agriculture intensifies soil moisture decline in Northern China. *Sci. Rep.* 5. Available at: https://www.scopus.com/inward/record.uri?eid=2-s2.0-84953867186&doi=10.1038%2Fsrep11261&partnerID=40&md5=2364376cd4dbd466d08463b4688dbdda.
Llasat, M. C., Marcos, R., Turco, M., Gilabert, J., and Llasat-Botija, M. (2016). Trends in flash flood events versus convective precipitation in the Mediterranean region: The case of Catalonia. *J. Hydrol.* 541, 24–37. doi:10.1016/j.jhydrol.2016.05.040.
Lloyd-Hughes, B. (2014). The impracticality of a universal drought definition. *Theor. Appl. Climatol.* 117, 607–611. doi:10.1007/s00704-013-1025-7.

Lok, C. C. F., and Chan, J. C. L. (2017). Changes of tropical cyclone landfalls in South China throughout the twenty-first century. *Clim. Dyn.* 0, 0. doi:10.1007/s00382-017-4023-0.
López-Franca, N., Zaninelli, P., Carril, A., Menéndez, C., and Sánchez, E. (2016). Changes in temperature extremes for 21st century scenarios over South America derived from a multi-model ensemble of regional climate models. *Clim. Res.* 68, 151–167. doi:10.3354/cr01393.
Lorenz, R., Argüeso, D., Donat, M. G., Pitman, A. J., Hurk, B. Van Den, Berg, A., et al. (2016). Influence of land-atmosphere feedbacks on temperature and precipitation extremes in the GLACE-CMIP5 ensemble. *J. Geophys. Res.* 121, 607–623. doi:10.1002/2015JD024053.
Lorenzo-Lacruz, J., Mor̗an-Tejeda, E., Vicente-Serrano, S. M., and Ĺopez-Moreno, J. I. (2013). Streamflow droughts in the Iberian Peninsula between 1945 and 2005: Spatial and temporal patterns. *Hydrol. Earth Syst. Sci.* 17. doi:10.5194/hess-17-119-2013.
Lott, F. C., Christidis, N., and Stott, P. A. (2013). Can the 2011 East African drought be attributed to human-induced climate change? *Geophys. Res. Lett.* 40, 1177–1181. doi:10.1002/grl.50235.
Lott, F. C., and Stott, P. A. (2016). Evaluating Simulated Fraction of Attributable Risk Using Climate Observations. *J. Clim.* 29, 4565–4575. doi:10.1175/JCLI-D-15-0566.1.
Lovino, M. A., Müller, O. V., Berbery, E. H., and Müller, G. V. (2018). How have daily climate extremes changed in the recent past over northeastern Argentina? *Glob. Planet. Change* 168, 78–97. doi:10.1016/J.GLOPLACHA.2018.06.008.
Lu, C., Sun, Y., Wan, H., Zhang, X., and Yin, H. (2016). Anthropogenic influence on the frequency of extreme temperatures in China. *Geophys. Res. Lett.* 43, 6511–6518. doi:10.1002/2016GL069296.
Lu, C., Sun, Y., and Zhang, X. (2018). Multimodel detection and attribution of changes in warm and cold spell durations. *Environ. Res. Lett.* 13, 074013. doi:10.1088/1748-9326/aacb3e.
Lu, J., Carbone, G. J., and Grego, J. M. (2019). Uncertainty and hotspots in 21st century projections of agricultural drought from CMIP5 models. *Sci. Rep.* 9. Available at: https://www.scopus.com/inward/record.uri?eid=2-s2.0-85063318884&doi=10.1038%2Fs41598-019-41196-z&partnerID=40&md5=87978465e442678df337a600d7095deb.
Lucas, C., Timbal, B., and Nguyen, H. (2014). The expanding tropics: a critical assessment of the observational and modeling studies. *Wiley Interdiscip. Rev. Clim. Chang.* 5, 89–112. doi:10.1002/wcc.251.
Luiz Silva, W., Xavier, L. N. R., Maceira, M. E. P., and Rotunno, O. C. (2018). Climatological and hydrological patterns and verified trends in precipitation and streamflow in the basins of Brazilian hydroelectric plants. *Theor. Appl. Climatol.* doi:10.1007/s00704-018-2600-8.
Luterbacher, J., Werner, J. P., Smerdon, J. E., Fernández-Donado, L., González-Rouco, F. J., Barriopedro, D., et al. (2016). European summer temperatures since Roman times. *Environ. Res. Lett.* 11, 024001. doi:10.1088/1748-9326/11/2/024001.
Ma, M., Ren, L., Yuan, F., Jiang, S., Liu, Y., Kong, H., et al. (2014). A new standardized Palmer drought index for hydro-meteorological use. *Hydrol. Process.* 28, 5645–5661. doi:10.1002/hyp.10063.
Ma, S., Zhou, T., Dai, A., and Han, Z. (2015). Observed Changes in the Distributions of Daily Precipitation Frequency and Amount over China from 1960 to 2013. *J. Clim.* 28, 6960–6978. doi:10.1175/JCLI-D-15-0011.1.
Ma, S., Zhou, T., Stone, D. A., Polson, D., Dai, A., Stott, P. A., et al. (2017). Detectable Anthropogenic Shift toward Heavy Precipitation over Eastern China. *J. Clim.* 30, 1381–1396. doi:10.1175/JCLI-D-16-0311.1.
Madhura, R. K., Krishnan, R., Revadekar, J. V, Mujumdar, M., and Goswami, B. N. (2015). Changes in western disturbances over the Western Himalayas in a warming environment. *Clim. Dyn.* 44, 1157–1168. doi:10.1007/s00382-014-2166-9.
Madsen, H., Lawrence, D., Lang, M., Martinkova, M., and Kjeldsen, T. R. (2014). Review of trend analysis and climate change projections of extreme precipitation and floods in Europe. *J. Hydrol.* 519, 3634–3650. doi:10.1016/j.jhydrol.2014.11.003.
Maes, W. H., Gentine, P., Verhoest, N. E. C., and Miralles, D. G. (2019). Potential evaporation at eddy-covariance sites across the globe. *Hydrol. Earth Syst. Sci.* 2019, 925–948. doi:10.5194/hess-2017-682.
Maggioni, V., Meyers, P. C., and Robinson, M. D. (2016). A Review of Merged High-Resolution Satellite Precipitation Product Accuracy during the Tropical Rainfall Measuring Mission (TRMM) Era. *J. Hydrometeorol.* 17, 1101–1117. doi:10.1175/JHM-D-15-0190.1.
Mahony, C. R., and Cannon, A. J. (2018). Wetter summers can intensify departures from natural variability in a warming climate. *Nat. Commun.* 9, 783. doi:10.1038/s41467-018-03132-z.
Maier, N., Breuer, L., Chamorro, A., Kraft, P., and Houska, T. (2018). Multi-source uncertainty analysis in simulating floodplain inundation under climate change. *Water (Switzerland)* 10. Available at: https://www.scopus.com/inward/record.uri?eid=2-s2.0-85048930216&doi=10.3390%2Fw10060809&partnerID=40&md5=772688a5bd8ac6678f78279bf00211ff.
Maksimović, Č., Prodanović, D., Boonya-Aroonnet, S., Leitão, J. P., Djordjević, S., and Allitt, R. (2009). Overland flow and pathway analysis for modelling of urban pluvial flooding. *J. Hydraul. Res.* 47, 512–523.

doi:10.1080/00221686.2009.9522027.
Malik, N., Bookhagen, B., and Mucha, P. J. (2016). Spatiotemporal patterns and trends of Indian monsoonal rainfall extremes. *Geophys. Res. Lett.* 43, 1710–1717. doi:10.1002/2016GL067841.
Mallakpour, I., and Villarini, G. (2015). The changing nature of flooding across the central United States. *Nat. Clim. Chang.* 5, 250. Available at: http://dx.doi.org/10.1038/nclimate2516.
Manda, A., Nakamura, H., Asano, N., Iizuka, S., Miyama, T., Moteki, Q., et al. (2014). Impacts of a warming marginal sea on torrential rainfall organized under the Asian summer monsoon. *Sci. Rep.* 4, 1–6. doi:10.1038/srep05741.
Mangini, W., Viglione, A., Hall, J., Hundecha, Y., Ceola, S., Montanari, A., et al. (2018). Detection of trends in magnitude and frequency of flood peaks across Europe. *Hydrol. Sci. J.* 63, 493–512. doi:10.1080/02626667.2018.1444766.
Mann, M. E., and Gleick, P. H. (2015). Climate change and California drought in the 21st century. *Proc. Natl. Acad. Sci. U. S. A.* 112, 3858–3859. doi:10.1073/pnas.1503667112.
Mann, M. E., Rahmstorf, S., Kornhuber, K., Steinman, B. A., Miller, S. K., and Coumou, D. (2017). Influence of Anthropogenic Climate Change on Planetary Wave Resonance and Extreme Weather Events. *Sci. Rep.* 7, 45242. Available at: http://dx.doi.org/10.1038/srep45242.
Manning, C., Widmann, M., Bevacqua, E., Van Loon, A. F., Maraun, D., and Vrac, M. (2018). Soil moisture drought in Europe: A compound event of precipitation and potential evapotranspiration on multiple time scales. *J. Hydrometeorol.* 19, 1255–1271. doi:10.1175/JHM-D-18-0017.1.
Manning, C., Widmann, M., Bevacqua, E., Van Loon, A. F., Maraun, D., and Vrac, M. (2019). Increased probability of compound long-duration dry and hot events in Europe during summer (1950–2013). *Environ. Res. Lett.* 14, 094006. doi:10.1088/1748-9326/ab23bf.
Manoli, G., Fatichi, S., Schläpfer, M., Yu, K., Crowther, T. W., Meili, N., et al. (2019). Magnitude of urban heat islands largely explained by climate and population. *Nature* 573, 55–60. doi:10.1038/s41586-019-1512-9.
Marciano, C. G., Lackmann, G. M., and Robinson, W. A. (2015). Changes in U.S. East Coast cyclone dynamics with climate change. *J. Clim.* 28, 468–484. doi:10.1175/JCLI-D-14-00418.1.
Marengo, J. A., and Bernasconi, M. (2015). Regional differences in aridity/drought conditions over Northeast Brazil: present state and future projections. *Clim. Change* 129, 103–115. doi:10.1007/s10584-014-1310-1.
Marengo, J. A., and Espinoza, J. C. (2016). Extreme seasonal droughts and floods in Amazonia: causes, trends and impacts. *Int. J. Climatol.* 36, 1033–1050. doi:10.1002/joc.4420.
Marengo, J. A., Torres, R. R., and Alves, L. M. (2017). Drought in Northeast Brazil—past, present, and future. *Theor. Appl. Climatol.* 129, 1189–1200. doi:10.1007/s00704-016-1840-8.
Margalef, O., Martínez Cortizas, A., Kylander, M., Pla-Rabes, S., Cañellas-Boltà, N., Pueyo, J. J., et al. (2014). Environmental processes in Rano Aroi (Easter Island) peat geochemistry forced by climate variability during the last 70kyr. *Palaeogeogr. Palaeoclimatol. Palaeoecol.* 414, 438–450. Available at: https://www.scopus.com/inward/record.uri?eid=2-s2.0-84908635346&doi=10.1016%2Fj.palaeo.2014.09.025&partnerID=40&md5=a8556c17d0e187de3f91c301d7e2ed5f.
Marlier, M. E., Defries, R. S., Voulgarakis, A., Kinney, P. L., Randerson, J. T., Shindell, D. T., et al. (2013). El Niño and health risks from landscape fire emissions in southeast Asia. *Nat. Clim. Chang.* 3, 131–136. doi:10.1038/nclimate1658.
Marotzke, J., and Forster, P. M. (2015). Forcing, feedback and internal variability in global temperature trends. *Nature* 517, 565–570. doi:10.1038/nature14117.
Martens, B., Waegeman, W., Dorigo, W. A., Verhoest, N. E. C., and Miralles, D. G. (2018). Terrestrial evaporation response to modes of climate variability. *npj Clim. Atmos. Sci.* 1, 43. doi:10.1038/s41612-018-0053-5.
Marthews, T. R., Otto, F. E. L., Mitchell, D., Dadson, S. J., and Jones, R. G. (2015). The 2014 Drought in the Horn of Africa: Attribution of Meteorological Drivers. *Bull. Am. Meteorol. Soc.* 96, S83–S88. doi:10.1175/BAMS-D-15-00115.1.
Martin, E. R. (2018). Future Projections of Global Pluvial and Drought Event Characteristics. *Geophys. Res. Lett.* doi:10.1029/2018GL079807.
Martinez-Austria, P., and Bandala, E. (2017). Temperature and Heat-Related Mortality Trends in the Sonoran and Mojave Desert Region. *Atmosphere (Basel).* 8, 53. doi:10.3390/atmos8030053.
Martínez-Granados, D., Maestre-Valero, J. F., Calatrava, J., and Martínez-Alvarez, V. (2011). The Economic Impact of Water Evaporation Losses from Water Reservoirs in the Segura Basin, SE Spain. *Water Resour. Manag.* 25, 3153–3175. doi:10.1007/s11269-011-9850-x.
Martins, E.S.P.R., Coelho, C.A.S., Haarsma, R., Otto, F.E.L., King, A.D., van Oldenborgh, G.J., Kew, S., Philip, S., Vasconcelos Junior, F.C. and Cullen, H. (2017). A multimethod attribution analysis of the prolonged Northeast Brazil hydrometeorological drought (2012-16). *Bull. Am. Meteorol. Soc.* 98, 65–68. Available at: http://www.ametsoc.net/eee/2016/ Chapter 13.pdf.
Martius, O., Pfahl, S., and Chevalier, C. (2016). A global quantification of compound precipitation and wind extremes.

Geophys. Res. Lett. 43, 7709–7717. doi:10.1002/2016GL070017.
Marty, C., Schlögl, S., Bavay, M., and Lehning, M. (2017). How much can we save? Impact of different emission scenarios on future snow cover in the Alps. *Cryosph.* 11, 517–529. doi:10.5194/tc-11-517-2017.
Marvel, K., Cook, B. I., Bonfils, C. J. W., Durack, P. J., Smerdon, J. E., and Williams, A. P. (2019). Twentieth-century hydroclimate changes consistent with human influence. *Nature* 569, 59–65. doi:10.1038/s41586-019-1149-8.
Marx, A., Kumar, R., Thober, S., Rakovec, O., Wanders, N., Zink, M., et al. (2018). Climate change alters low flows in Europe under global warming of 1.5, 2, and 3 °C. *Hydrol. Earth Syst. Sci.* 22, 1017–1032. doi:10.5194/hess-22-1017-2018.
Mascioli, N. R., Fiore, A. M., Previdi, M., and Correa, G. (2016). Temperature and Precipitation Extremes in the United States: Quantifying the Responses to Anthropogenic Aerosols and Greenhouse Gases. *J. Clim.* 29, 2689–2701. doi:10.1175/JCLI-D-15-0478.1.
Massey, N., Jones, R., Otto, F. E. L., Aina, T., Wilson, S., Murphy, J. M., et al. (2015). weather@home-development and validation of a very large ensemble modelling system for probabilistic event attribution. *Q. J. R. Meteorol. Soc.* 141, 1528–1545. doi:10.1002/qj.2455.
Masson-Delmotte, V., M, S., Abe-Ouchi, A., Beer, J., Ganopolski, A., Rouco, J. F. G., et al. (2013). "Information from Paleoclimate Archives. In: Climate Change 2013: The Physical Science Basis. Contribution of Working Group I to the Fifth Assessment Report of the Intergovernmental Panel on Climate Change," in, 383–464. doi:10.1017/CBO9781107415324.013.
Mastrandrea, M., Field, C. B., Stocker, T. F., Edenhofer, O., Ebi, K. L., Frame, D. J., et al. (2010). Guidance Note for Lead Authors of the IPCC Fifth Assessment Report on Consistent Treatment of Uncertainties.
Masunaga, H., Schröder, M., Furuzawa, F. A., Kummerow, C., Rustemeier, E., and Schneider, U. (2019). Inter-product biases in global precipitation extremes. *Environ. Res. Lett.* 14, 125016. doi:10.1088/1748-9326/ab5da9.
Mathbout, S., Lopez-Bustins, J. A., Martin-Vide, J., Bech, J., and Rodrigo, F. S. (2018a). Spatial and temporal analysis of drought variability at several time scales in Syria during 1961–2012. *Atmos. Res.* 200, 153–168. doi:10.1016/j.atmosres.2017.09.016.
Mathbout, S., Lopez-Bustins, J. A., Royé, D., Martin-Vide, J., Bech, J., and Rodrigo, F. S. (2018b). Observed Changes in Daily Precipitation Extremes at Annual Timescale Over the Eastern Mediterranean During 1961–2012. *Pure Appl. Geophys.* 175, 3875–3890. doi:10.1007/s00024-017-1695-7.
Matthes, H., Rinke, A., and Dethloff, K. (2015). Recent changes in Arctic temperature extremes: Warm and cold spells during winter and summer. *Environ. Res. Lett.* 10. doi:10.1088/1748-9326/10/11/114020.
Matthews, T. K. R., Wilby, R. L., and Murphy, C. (2017). Communicating the deadly consequences of global warming for human heat stress. *Proc. Natl. Acad. Sci. U. S. A.* 114, 3861–3866. doi:10.1073/pnas.1617526114.
Matthews, T., Wilby, R. L., and Murphy, C. (2019). An emerging tropical cyclone–deadly heat compound hazard. *Nat. Clim. Chang.* 9, 602–606. doi:10.1038/s41558-019-0525-6.
Matti, B., Dahlke, H. E., Dieppois, B., Lawler, D. M., and Lyon, S. W. (2017). Flood seasonality across Scandinavia—Evidence of a shifting hydrograph? *Hydrol. Process.* 31, 4354–4370. doi:10.1002/hyp.11365.
Mátyás, C., and Sun, G. (2014). Forests in a water limited world under climate change. *Environ. Res. Lett.* 9. doi:10.1088/1748-9326/9/8/085001.
Maúre, G., Pinto, I., Ndebele-Murisa, M., Muthige, M., Lennard, C., Nikulin, G., et al. (2018). The southern African climate under 1.5 °C and 2 °C of global warming as simulated by CORDEX regional climate models. *Environ. Res. Lett.* doi:10.1088/1748-9326/aab190.
Mba, W. P., Longandjo, G. N. T., Moufouma-Okia, W., Bell, J. P., James, R., Vondou, D. A., et al. (2018). Consequences of 1.5 °c and 2 °c global warming levels for temperature and precipitation changes over Central Africa. *Environ. Res. Lett.* 13. doi:10.1088/1748-9326/aab048.
McAneney, J., van den Honert, R., and Yeo, S. (2017). Stationarity of major flood frequencies and heights on the Ba River, Fiji, over a 122-year record. *Int. J. Climatol.* 37, 171–178. Available at: https://www.scopus.com/inward/record.uri?eid=2-s2.0-85028437680&doi=10.1002%2Fjoc.4989&partnerID=40&md5=19abcf3f5472ab629d2eac2d6033c553.
Mcbride, J. l., Sahany, S., Hassim, M. E. E., Nguyen, C. M., Lim, S.-Y., Rahmat, R., et al. (2015). The 2014 Record Dry Spell at Singapore: An Intertropical Convergence Zone (ITCZ) Drought. *Bull. Am. Meteorol. Soc.* 96, S126–S130. doi:10.1175/BAMS-D-15-00117.1.
McCabe, G. J., Clark, M. P., and Hay, L. E. (2007). Rain-on-Snow Events in the Western United States. *Bull. Am. Meteorol. Soc.* 88, 319–328. doi:10.1175/BAMS-88-3-319.
McEvoy, D. J., Huntington, J. L., Hobbins, M. T., Wood, A., Morton, C., Anderson, M., et al. (2016). The evaporative demand drought index. Part II: CONUS-wide assessment against common drought indicators. *J. Hydrometeorol.* 17, 1763–1779. doi:10.1175/JHM-D-15-0122.1.
McGree, S., Herold, N., Alexander, L., Schreider, S., Kuleshov, Y., Ene, E., et al. (2019). Recent changes in mean and extreme temperature and precipitation in the western Pacific Islands. *J. Clim.*, JCLI-D-18-0748.1. doi:10.1175/JCLI-D-18-0748.1.

McGree, S., Schreider, S., and Kuleshov, Y. (2016). Trends and variability in droughts in the Pacific islands and Northeast Australia. *J. Clim.* 29, 8377–8397. Available at: https://www.scopus.com/inward/record.uri?eid=2-s2.0-84996757857&doi=10.1175%2FJCLI-D-16-0332.1&partnerID=40&md5=f032ebd4745a65dcb2e0104b6432c0e2.
McInnes, K. L., Walsh, K. J. E., Hoeke, R. K., O'Grady, J. G., Colberg, F., and Hubbert, G. D. (2014). Quantifying storm tide risk in Fiji due to climate variability and change. *Glob. Planet. Change* 116, 115–129. doi:https://doi.org/10.1016/j.gloplacha.2014.02.004.
McInnes, K. L., White, C. J., Haigh, I. D., Hemer, M. A., Hoeke, R. K., Holbrook, N. J., et al. (2016). Natural hazards in Australia: sea level and coastal extremes. *Clim. Change* 139, 69–83. doi:10.1007/s10584-016-1647-8.
McKenzie, D., and Littell, J. S. (2017). Climate change and the eco-hydrology of fire: Will area burned increase in a warming western USA. *Ecol. Appl.* 27, 26–36. doi:10.1002/eap.1420.
McLean, N. M., Stephenson, T. S., Taylor, M. A., and Campbell, J. D. (2015). Characterization of Future Caribbean Rainfall and Temperature Extremes across Rainfall Zones. *Adv. Meteorol.* 2015, 1–18. doi:10.1155/2015/425987.
McMahon, T. A., Peel, M. C., Lowe, L., Srikanthan, R., and McVicar, T. R. (2013). Estimating actual, potential, reference crop and pan evaporation using standard meteorological data: A pragmatic synthesis. *Hydrol. Earth Syst. Sci.* 17, 1331–1363. doi:10.5194/hess-17-1331-2013.
McNamara, K. E., and Prasad, S. S. (2014). Coping with extreme weather: Communities in Fiji and Vanuatu share their experiences and knowledge. *Clim. Change* 123, 121–132. Available at: https://www.scopus.com/inward/record.uri?eid=2-s2.0-84895741033&doi=10.1007%2Fs10584-013-1047-2&partnerID=40&md5=ccd50885affa9416c79169dbe6c08201.
McVicar, T. R., Roderick, M. L., Donohue, R. J., Li, L. T., Van Niel, T. G., Thomas, A., et al. (2012). Global review and synthesis of trends in observed terrestrial near-surface wind speeds: Implications for evaporation. *J. Hydrol.* 416–417, 182–205. doi:10.1016/j.jhydrol.2011.10.024.
Mcvicar, T. R., Roderick, M. L., Donohue, R. J., and Van Niel, T. G. (2012). Less bluster ahead? ecohydrological implications of global trends of terrestrial near-surface wind speeds. *Ecohydrology* 5, 381–388. doi:10.1002/eco.1298.
Mediero, L., Kjeldsen, T. R., Macdonald, N., Kohnova, S., Merz, B., Vorogushyn, S., et al. (2015). Identification of coherent flood regions across Europe by using the longest streamflow records. *J. Hydrol.* 528, 341–360. doi:10.1016/j.jhydrol.2015.06.016.
Meehl, Gerald A, Hu, A., Arblaster, J. M., Fasullo, J., and Trenberth, K. E. (2013). Externally Forced and Internally Generated Decadal Climate Variability Associated with the Interdecadal Pacific Oscillation. *J. Clim.* 26, 7298–7310.
Meehl, G. A., Tebaldi, C., and Adams-Smith, D. (2016). US daily temperature records past, present, and future. *Proc. Natl. Acad. Sci.* 113, 13977–13982. doi:10.1073/pnas.1606117113.
Meehl, G. A., Tebaldi, C., Tilmes, S., Lamarque, J.-F., Bates, S., Pendergrass, A., et al. (2018). Future heat waves and surface ozone. *Environ. Res. Lett.* 13, 064004. doi:10.1088/1748-9326/aabcdc.
Mei, W., and Xie, S. P. (2016). Intensification of landfalling typhoons over the northwest Pacific since the late 1970s. *Nat. Geosci.* 9, 753–757. doi:10.1038/ngeo2792.
Mekis, É., Vincent, L. A., Shephard, M. W., and Zhang, X. (2015). Observed Trends in Severe Weather Conditions Based on Humidex, Wind Chill, and Heavy Rainfall Events in Canada for 1953–2012. *Atmosphere-Ocean* 53, 383–397. doi:10.1080/07055900.2015.1086970.
Menéndez, C., Zaninelli, P., Carril, A., and Sánchez, E. (2016). Hydrological cycle, temperature, and land surface-atmosphere interaction in the La Plata Basin during summer: response to climate change. *Clim. Res.* 68, 231–241. doi:10.3354/cr01373.
Menezes-Silva, P. E., Loram-Lourenço, L., Alves, R. D. F. B., Sousa, L. F., Almeida, S. E. da S., and Farnese, F. S. (2019). Different ways to die in a changing world: Consequences of climate change for tree species performance and survival through an ecophysiological perspective. *Ecol. Evol.* 0. doi:10.1002/ece3.5663.
Meredith, E. P., Semenov, V. A., Maraun, D., Park, W., and Chernokulsky, A. V. (2015). Crucial role of Black Sea warming in amplifying the 2012 Krymsk precipitation extreme. *Nat. Geosci.* 8, 615. Available at: http://dx.doi.org/10.1038/ngeo2483.
Mernild, S. H., Hanna, E., Yde, J. C., Cappelen, J., and Malmros, J. K. (2014). Coastal Greenland air temperature extremes and trends 1890-2010: annual and monthly analysis. *Int. J. Climatol.* 34. doi:10.1002/joc.3777.
Merrifield, M. A., Becker, J. M., Ford, M., and Yao, Y. (2014). Observations and estimates of wave-driven water level extremes at the Marshall Islands. *Geophys. Res. Lett.* 41, 7245–7253. Available at: https://www.scopus.com/inward/record.uri?eid=2-s2.0-84911371526&doi=10.1002%2F2014GL061005&partnerID=40&md5=3bf849ef2bd99411bc78f72c7c7671fa.
Merz, R., and Blöschl, G. (2003). A process typology of regional floods. *Water Resour. Res.* 39. doi:10.1029/2002WR001952.
Meseguer-Ruiz, O., Ponce-Philimon, P. I., Quispe-Jofré, A. S., Guijarro, J. A., and Sarricolea, P. (2018). Spatial

behaviour of daily observed extreme temperatures in Northern Chile (1966–2015): data quality, warming trends, and its orographic and latitudinal effects. *Stoch. Environ. Res. Risk Assess.* 32, 3503–3523. doi:10.1007/s00477-018-1557-6.
Michaelis, A. C., Willison, J., Lackmann, G. M., and Robinson, W. A. (2017). Changes in winter North Atlantic extratropical cyclones in high-resolution regional pseudo-global warming simulations. *J. Clim.* 30, 6905–6925. doi:10.1175/JCLI-D-16-0697.1.
Milly, P. C. D., and Dunne, K. A. (2016). Potential evapotranspiration and continental drying. *Nat. Clim. Chang.* 6, 946–949. doi:10.1038/nclimate3046.
Min, E., Hazeleger, W., van Oldenborgh, G. J., and Sterl, A. (2013). Evaluation of trends in high temperature extremes in north-western Europe in regional climate models. *Environ. Res. Lett.* 8, 014011. doi:10.1088/1748-9326/8/1/014011.
Min, S.-K., Zhang, X., Zwiers, F. W., and Hegerl, G. C. (2011). Human contribution to more-intense precipitation extremes. *Nature* 470, 378–381. doi:10.1038/nature09763.
Min, S., Kim, Y.-H., Lee, S.-M., Sparrow, S., Li, S., Lott, F. C., et al. (2020). Quantifying human impact on the 2018 summer longest heat wave in south korea. *Bull Am Meteorol Soc*. doi:10.1175/BAMS-D-19-0151.1.
Minetti, J. L., Poblete, A. G., Vargas, W. M., and Ovejero, D. P. (2014). Trends of the Drought Indices in Southern Hemisphere Subtropical Regions. *J. Earth Sci. Res.* 2, 36–47. Available at: http://www.labclisud.com.ar/wp-content/uploads/2014/09/Trends-of-the-Drought-Indices-in-Southern-Hemisphere-Subtropical-Regions.pdf [Accessed July 12, 2018].
Miralles, D. G., Gentine, P., Seneviratne, S. I., and Teuling, A. J. (2019). Land-atmospheric feedbacks during droughts and heatwaves: state of the science and current challenges. *Ann. N. Y. Acad. Sci.* 8, 469.
Miralles, D. G., Teuling, A. J., Van Heerwaarden, C. C., and De Arellano, J. V. G. (2014). Mega-heatwave temperatures due to combined soil desiccation and atmospheric heat accumulation. *Nat. Geosci.* 7, 345–349. doi:10.1038/ngeo2141.
Mishra, V., Kumar, D., Ganguly, A. R., Sanjay, J., Mujumdar, M., Krishnan, R., et al. (2014a). Reliability of regional and global climate models to simulate precipitation extremes over India. *J. Geophys. Res. Atmos.* 119, 9301–9323. doi:10.1002/2014JD021636.
Mishra, V., Shah, R., and Thrasher, B. (2014b). Soil Moisture Droughts under the Retrospective and Projected Climate in India. *J. Hydrometeorol.* 15, 2267–2292. doi:10.1175/JHM-D-13-0177.1.
Mitchell, D., Davini, P., Harvey, B., Massey, N., Haustein, K., Woollings, T., et al. (2017). Assessing mid-latitude dynamics in extreme event attribution systems. *Clim. Dyn.* 48, 3889–3901. doi:10.1007/s00382-016-3308-z.
Mizuta, R., Murata, A., Ishii, M., Shiogama, H., Hibino, K., Mori, N., et al. (2017). Over 5,000 years of ensemble future climate simulations by 60-km global and 20-km regional atmospheric models. *Bull. Am. Meteorol. Soc.* 98, 1383–1398. doi:10.1175/BAMS-D-16-0099.1.
Mo, K. C., and Lettenmaier, D. P. (2018). Drought variability and trends over the central United States in the instrumental record. *J. Hydrometeorol.* 19, 1149–1166. doi:10.1175/JHM-D-17-0225.1.
Modarres, R., Sarhadi, A., and Burn, D. H. (2016). Changes of extreme drought and flood events in Iran. *Glob. Planet. Change* 144, 67–81. doi:10.1016/j.gloplacha.2016.07.008.
Moftakhari, H. R., Salvadori, G., AghaKouchak, A., Sanders, B. F., and Matthew, R. A. (2017). Compounding effects of sea level rise and fluvial flooding. *Proc. Natl. Acad. Sci.* 114, 9785–9790. doi:10.1073/pnas.1620325114.
Mohajerani, A., Bakaric, J., and Jeffrey-Bailey, T. (2017). The urban heat island effect, its causes, and mitigation, with reference to the thermal properties of asphalt concrete. *J. Environ. Manage.* 197, 522–538. doi:10.1016/j.jenvman.2017.03.095.
Möller, I., Kudella, M., Rupprecht, F., Spencer, T., Paul, M., van Wesenbeeck, B. K., et al. (2014). Wave attenuation over coastal salt marshes under storm surge conditions. *Nat. Geosci.* 7, 727. Available at: http://dx.doi.org/10.1038/ngeo2251.
Monjo, R., Gaitán, E., Pórtoles, J., Ribalaygua, J., and Torres, L. (2016). Changes in extreme precipitation over Spain using statistical downscaling of CMIP5 projections. *Int. J. Climatol.* 36, 757–769. doi:10.1002/joc.4380.
Montero-Martínez, M. J., Santana-Sepúlveda, J. S., Pérez-Ortiz, N. I., Pita-Díaz, Ó., and Castillo-Liñan, S. (2018). Comparing climate change indices between a northern (arid) and a southern (humid) basin in Mexico during the last decades. *Adv. Sci. Res.* 15, 231–237. doi:10.5194/asr-15-231-2018.
Moon, H., Gudmundsson, L., and Seneviratne, S. I. (2018). Drought Persistence Errors in Global Climate Models. *J. Geophys. Res. Atmos.* 123, 3483–3496. doi:10.1002/2017JD027577.
Moon, H., Guillod, B. P., Gudmundsson, L., and Seneviratne, S. I. (2019). Soil Moisture Effects on Afternoon Precipitation Occurrence in Current Climate Models. *Geophys. Res. Lett.* 46, 1861–1869. doi:10.1029/2018GL080879.
Moon, I.-J., Kim, S.-H., Klotzbach, P., and Chan, J. C. L. (2015). Roles of interbasin frequency changes in the poleward shifts of the maximum intensity location of tropical cyclones. *Environ. Res. Lett.* 10, 104004. doi:10.1088/1748-9326/10/10/104004.

Moon, I.-J., Kim, S.-H., Klotzbach, P., and Chan, J. C. L. (2016). Reply to Comment on 'Roles of interbasin frequency changes in the poleward shifts of maximum intensity location of tropical cyclones.' *Environ. Res. Lett.* 11, 068002. doi:10.1088/1748-9326/11/6/068002.

Mora, C., Spirandelli, D., Franklin, E. C., Lynham, J., Kantar, M. B., Miles, W., et al. (2018). Broad threat to humanity from cumulative climate hazards intensified by greenhouse gas emissions. *Nat. Clim. Chang.* 8, 1062–1071. doi:10.1038/s41558-018-0315-6.

Moravec, V., Markonis, Y., Rakovec, O., Kumar, R., and Hanel, M. (2019). A 250-Year European Drought Inventory Derived From Ensemble Hydrologic Modeling. *Geophys. Res. Lett.* 46, 5909–5917. Available at: https://www2.scopus.com/inward/record.uri?eid=2-s2.0-85067642187&doi=10.1029%2F2019GL082783&partnerID=40&md5=11193733551462f1ea05603f7c24f53e.

Morgan, J. A., LeCain, D. R., Pendall, E., Blumenthal, D. M., Kimball, B. A., Carrillo, Y., et al. (2011). C4 grasses prosper as carbon dioxide eliminates desiccation in warmed semi-arid grassland. *Nature* 476, 202–205. doi:10.1038/nature10274.

Morgan, J. A., Pataki, D. E., Körner, C., Clark, H., Del Grosso, S. J., Grünzweig, J. M., et al. (2004). Water relations in grassland and desert ecosystems exposed to elevated atmospheric CO2. *Oecologia* 140, 11–25. doi:10.1007/s00442-004-1550-2.

Moron, V., Oueslati, B., Pohl, B., Rome, S., and Janicot, S. (2016). Trends of mean temperatures and warm extremes in northern tropical Africa (1961-2014) from observed and PPCA-reconstructed time series. *J. Geophys. Res. Atmos.* 121, 5298–5319. doi:10.1002/2015JD024303.

Mostafa, A. N., Wheida, A., El Nazer, M., Adel, M., El Leithy, L., Siour, G., et al. (2019). Past (1950–2017) and future (−2100) temperature and precipitation trends in Egypt. *Weather Clim. Extrem.* doi:10.1016/j.wace.2019.100225.

Mote, P. W., Rupp, D. E., Li, S., Sharp, D. J., Otto, F., Uhe, P. F., et al. (2016). Perspectives on the causes of exceptionally low 2015 snowpack in the western United States. *Geophys. Res. Lett.* 43, 10,910-980,988. doi:10.1002/2016GL069965.

Mouhamed, L., Traore, S. B., Alhassane, A., and Sarr, B. (2013). Evolution of some observed climate extremes in the West African Sahel. *Weather Clim. Extrem.* doi:10.1016/j.wace.2013.07.005.

Mourão, C., Chou, S. C., and Marengo, J. (2016). Downscaling Climate Projections over La Plata Basin. *Atmos. Clim. Sci.* 06, 1–12. doi:10.4236/acs.2016.61001.

Mudersbach, C., Bender, J., and Netzel, F. (2017). An analysis of changes in flood quantiles at the gauge Neu Darchau (Elbe River) from 1875 to 2013. *Stoch. Environ. Res. Risk Assess.* 31, 145–157. doi:10.1007/s00477-015-1173-7.

Mueller, B., and Seneviratne, S. (2014). Systematic land climate and evapotranspiration biases in CMIP5 simulations. *Geophys. Res. Lett.* 41, 128–134. doi:10.1002/2013GL058055.

Mueller, B., and Seneviratne, S. I. (2012). Hot days induced by precipitation deficits at the global scale. *Proc. Natl. Acad. Sci.* 109, 12398–12403. doi:10.1073/pnas.1204330109.

Mueller, B., and Zhang, X. (2016). Causes of drying trends in northern hemispheric land areas in reconstructed soil moisture data. *Clim. Change* 134, 255–267. doi:10.1007/s10584-015-1499-7.

Mueller, B., Zhang, X., and Zwiers, F. W. (2016a). Historically hottest summers projected to be the norm for more than half of the world's population within 20 years. *Environ. Res. Lett.* 11, 1–15. doi:10.1088/1748-9326/11/4/044011.

Mueller, N. D., Butler, E. E., McKinnon, K. A., Rhines, A., Tingley, M., Holbrook, N. M., et al. (2016b). Cooling of US Midwest summer temperature extremes from cropland intensification. *Nat. Clim. Chang.* 6, 317–322. doi:10.1038/nclimate2825.

Muerth, M. J., Gauvin St-Denis, B., Ricard, S., Velázquez, J. A., Schmid, J., Minville, M., et al. (2013). On the need for bias correction in regional climate scenarios to assess climate change impacts on river runoff. *Hydrol. Earth Syst. Sci.* 17, 1189–1204. doi:10.5194/hess-17-1189-2013.

Muis, S., Güneralp, B., Jongman, B., Aerts, J. C. J. H., and Ward, P. J. (2015). Flood risk and adaptation strategies under climate change and urban expansion: A probabilistic analysis using global data. *Sci. Total Environ.* 538, 445–457. Available at: https://www.scopus.com/inward/record.uri?eid=2-s2.0-84956719059&doi=10.1016%2Fj.scitotenv.2015.08.068&partnerID=40&md5=38327aac4b086162c03830e8e2f695be.

Muis, S., Verlaan, M., Winsemius, H. C., Aerts, J. C. J. H., and Ward, P. J. (2016). A global reanalysis of storm surges and extreme sea levels. *Nat. Commun.* 7, 11969. Available at: http://dx.doi.org/10.1038/ncomms11969.

Mukherjee, S., Aadhar, S., Stone, D., and Mishra, V. (2018). Increase in extreme precipitation events under anthropogenic warming in India. *Weather Clim. Extrem.* 20, 45–53. doi:10.1016/J.WACE.2018.03.005.

Muller, J., Collins, J. M., Gibson, S., and Paxton, L. (2017). "Recent Advances in the Emerging Field of Paleotempestology," in *Hurricanes and Climate Change: Volume 3*, eds. J. M. Collins and K. Walsh (Cham: Springer International Publishing), 1–33. doi:10.1007/978-3-319-47594-3_1.

Murakami, H. (submitted). Detected Climatic Change in Global Tropical Cyclone Frequency of Occurrence. (submitted).

Murakami, H., Levin, E., Delworth, T. L., Gudgel, R., and Hsu, P.-C. (2018). Dominant effect of relative tropical

Atlantic warming on major hurricane occurrence. *Science* Available at: http://science.sciencemag.org/content/early/2018/09/26/science.aat6711.abstract.
Murakami, H., Li, T., and Hsu, P. C. (2014). Contributing factors to the recent high level of accumulated cyclone energy (ACE) and power dissipation index (PDI) in the North Atlantic. *J. Clim.* 27, 3023–3034. doi:10.1175/JCLI-D-13-00394.1.
Murakami, H., Vecchi, G. A., Delworth, T. L., Paffendorf, K., Jia, L., Gudgel, R., et al. (2015a). Investigating the Influence of Anthropogenic Forcing and Natural Variability on the 2014 Hawaiian Hurricane Season. *Bull. Am. Meteorol. Soc.* 96, S115–S119. doi:10.1175/BAMS-D-15-00119.1.
Murakami, H., Vecchi, G. A., Delworth, T. L., Wittenberg, A. T., Underwood, S., Gudgel, R., et al. (2017). Dominant Role of Subtropical Pacific Warming in Extreme Eastern Pacific Hurricane Seasons: 2015 and the Future. *J. Clim.* 30, 243–264. doi:10.1175/JCLI-D-16-0424.1.
Murakami, H., Vecchi, G. A., Underwood, S., Delworth, T. L., Wittenberg, A. T., Anderson, W. G., et al. (2015b). Simulation and prediction of category 4 and 5 hurricanes in the high-resolution GFDL HiFLOR coupled climate model. *J. Clim.* 28, 9058–9079. doi:10.1175/JCLI-D-15-0216.1.
Muramatsu, T., Kato, T., Nakazato, M., Endo, H., and Kitoh, A. (2016). Future Change of Tornadogenesis-Favorable Environmental Conditions in Japan Estimated by a 20-km-Mesh Atmospheric General Circulation Model. *J. Meteorol. Soc. Japan. Ser. II* 94A, 105–120. doi:10.2151/jmsj.2015-053.
Murari, K. K., Ghosh, S., Patwardhan, A., Daly, E., and Salvi, K. (2015). Intensification of future severe heat waves in India and their effect on heat stress and mortality. *Reg. Environ. Chang.* 15. doi:10.1007/s10113-014-0660-6.
Murata, A., Sasaki, H., Kawase, H., and Nosaka, M. (2017). Evaluation of precipitation over an oceanic region of Japan in convection-permitting regional climate model simulations. *Clim. Dyn.* 48, 1779–1792. doi:10.1007/s00382-016-3172-x.
Murata, A., Sasaki, H., Kawase, H., Nosaka, M., Oh'izumi, M., Kato, T., et al. (2015). Projection of Future Climate Change over Japan in Ensemble Simulations with a High-Resolution Regional Climate Model. *SOLA* 11, 90–94. doi:10.2151/sola.2015-022.
Muschinski, T., and Katz, J. I. (2013). Trends in hourly rainfall statistics in the United States under a warming climate. *Nat. Clim. Chang.* 3, 577. Available at: https://doi.org/10.1038/nclimate1828.
Myhre, G., Alterskjær, K., Stjern, C. W., Hodnebrog, Ø., Marelle, L., Samset, B. H., et al. (2019). Frequency of extreme precipitation increases extensively with event rareness under global warming. *Sci. Rep.* 9, 16063. doi:10.1038/s41598-019-52277-4.
Najafi, M. R., and Moazami, S. (2016). Trends in total precipitation and magnitude–frequency of extreme precipitation in Iran, 1969–2009. *Int. J. Climatol.* 36, 1863–1872. doi:10.1002/joc.4465.
Nakamura, J., Camargo, S. J., Sobel, A. H., Henderson, N., Emanuel, K. A., Kumar, A., et al. (2017). Western North Pacific Tropical Cyclone Model Tracks in Present and Future Climates. *J. Geophys. Res. Atmos.* 122, 9721–9744. doi:10.1002/2017JD027007.
Nakano, M., Wada, A., Sawada, M., Yoshimura, H., Onishi, R., Kawahara, S., et al. (2017). Global 7km mesh nonhydrostatic Model Intercomparison Project for improving TYphoon forecast (TYMIP-G7): Experimental design and preliminary results. *Geosci. Model Dev.* 10, 1368–1381. doi:10.5194/gmd-10-1363-2017.
Nakayama, T., and Shankman, D. (2013). Impact of the Three-Gorges Dam and water transfer project on Changjiang floods. *Glob. Planet. Change* 100, 38–50. doi:10.1016/j.gloplacha.2012.10.004.
Nangombe, S., Zhou, T., Zhang, W., Wu, B., Hu, S., Zou, L., et al. (2018). Record-breaking climate extremes in Africa under stabilized 1.5 °C and 2 °C global warming scenarios. *Nat. Clim. Chang.* 8, 375–380. doi:10.1038/s41558-018-0145-6.
Nasim, W., Amin, A., Fahad, S., Awais, M., Khan, N., Mubeen, M., et al. (2018). Future risk assessment by estimating historical heat wave trends with projected heat accumulation using SimCLIM climate model in Pakistan. *Atmos. Res.* 205, 118–133. doi:https://doi.org/10.1016/j.atmosres.2018.01.009.
Nasrollahi, N., Aghakouchak, A., Cheng, L., Damberg, L., Phillips, T. J., Miao, C., et al. (2015). How well do CMIP5 climate simulations replicate historical trends and patterns of meteorological droughts? *Water Resour. Res.* 51, 2847–2864. doi:10.1002/2014WR016318.
Nastos, P. T., and Kapsomenakis, J. (2015). Regional climate model simulations of extreme air temperature in Greece. Abnormal or common records in the future climate? *Atmos. Res.* 152, 43–60. doi:10.1016/j.atmosres.2014.02.005.
National Academies of Sciences, Engineering, and M. (2016). *Attribution of Extreme Weather Events in the Context of Climate Change*. Washington, D.C.: National Academies Press doi:10.17226/21852.
Naumann, G., Alfieri, L., Wyser, K., Mentaschi, L., Betts, R. A., Carrao, H., et al. (2018). Global Changes in Drought Conditions Under Different Levels of Warming. *Geophys. Res. Lett.* 45, 3285–3296. doi:10.1002/2017GL076521.
Nayak, S., Dairaku, K., Takayabu, I., Suzuki-Parker, A., and Ishizaki, N. N. (2017). Extreme precipitation linked to temperature over Japan: current evaluation and projected changes with multi-model ensemble downscaling. *Clim. Dyn.* 51, 1–17. doi:10.1007/s00382-017-3866-8.
Naz, B. S., Kao, S.-C., Ashfaq, M., Rastogi, D., Mei, R., and Bowling, L. C. (2016). Regional hydrologic response to

climate change in the conterminous United States using high-resolution hydroclimate simulations. *Glob. Planet. Change* 143, 100–117. doi:10.1016/j.gloplacha.2016.06.003.
Nazrul Islam, M., Almazroui, M., Dambul, R., Jones, P. D., and Alamoudi, A. O. (2015). Long-term changes in seasonal temperature extremes over Saudi Arabia during 1981-2010. *Int. J. Climatol.* 35, 1579–1592. doi:10.1002/joc.4078.
Neu, U., Akperov, M. G., Bellenbaum, N., Benestad, R., Blender, R., Caballero, R., et al. (2013). Imilast: A community effort to intercompare extratropical cyclone detection and tracking algorithms. *Bull. Am. Meteorol. Soc.* doi:10.1175/BAMS-D-11-00154.1.
Neukom, R., Gergis, J., Karoly, D. J., Wanner, H., Curran, M., Elbert, J., et al. (2014). Inter-hemispheric temperature variability over the past millennium. *Nat. Clim. Chang.* 4, 362–367. doi:10.1038/nclimate2174.
Neumann, B., Vafeidis, A. T., Zimmermann, J., and Nicholls, R. J. (2015). Future coastal population growth and exposure to sea-level rise and coastal flooding - A global assessment. *PLoS One* 10. doi:10.1371/journal.pone.0118571.
Newman, M., Wittenberg, A. T., Cheng, L., Compo, G. P., and Smith, C. A. (2018). The Extreme 2015/16 El Niño, in the Context of Historical Climate Variability and Change. *Bull. Am. Meteorol. Soc.* 99, S16–S20. doi:10.1175/BAMS-D-17-0116.1.
Nguyen, H., Lucas, C., Evans, A., Timbal, B., and Hanson, L. (2015). Expansion of the Southern Hemisphere hadley cell in response to greenhouse gas forcing. *J. Clim.* 28, 8067–8077. doi:10.1175/JCLI-D-15-0139.1.
Nicholls, R. J., Brown, S., Goodwin, P., Wahl, T., Lowe, J., Solan, M., et al. (2018). Stabilization of global temperature at 1.5°C and 2.0°C: implications for coastal areas. *Philos. Trans. R. Soc. A Math. Phys. Eng. Sci.* 376, 20160448. doi:10.1098/rsta.2016.0448.
Nicholson, S. E. (2017). Climate and climatic variability of rainfall over eastern Africa. *Rev. Geophys.* 55, 590–635.
Nicolai-Shaw, N., Hirschi, M., Mittelbach, H., and Seneviratne, S. I. (2015). Spatial representativeness of soil moisture using in situ, remote sensing, and land reanalysis data. *J. Geophys. Res. Atmos.* 120, 9955–9964. doi:10.1002/2015JD023305.
Nie, J., Sobel, A. H., Shaevitz, D. A., and Wang, S. (2018). Dynamic amplification of extreme precipitation sensitivity. *Proc. Natl. Acad. Sci.* 115, 9467 LP – 9472. doi:10.1073/pnas.1800357115.
Nied, M., Pardowitz, T., Nissen, K., Ulbrich, U., Hundecha, Y., and Merz, B. (2014). On the relationship between hydro-meteorological patterns and flood types. *J. Hydrol.* 519, 3249–3262. doi:10.1016/j.jhydrol.2014.09.089.
Nikulin, G., Lennard, C., Dosio, A., Kjellström, E., Chen, Y., Hänsler, A., et al. (2018). The effects of 1.5 and 2 degrees of global warming on Africa in the CORDEX ensemble. *Environ. Res. Lett.* 13, 065003. doi:10.1088/1748-9326/aab1b1.
Nilsen, I. B., Stagge, J. H., and Tallaksen, L. M. (2017). A probabilistic approach for attributing temperature changes to synoptic type frequency. *Int. J. Climatol.* 37, 2990–3002. doi:10.1002/joc.4894.
Niranjan Kumar, K., Rajeevan, M., Pai, D. S., Srivastava, A. K., and Preethi, B. (2013). On the observed variability of monsoon droughts over India. *Weather Clim. Extrem.* 1, 42–50. doi:10.1016/J.WACE.2013.07.006.
Nissen, K. M., Leckebusch, G. C., Pinto, J. G., and Ulbrich, U. (2014). Mediterranean cyclones and windstorms in a changing climate. *Reg. Environ. Chang.* 14, 1873–1890. doi:10.1007/s10113-012-0400-8.
Nissen, K. M., and Ulbrich, U. (2017). Increasing frequencies and changing characteristics of heavy precipitation events threatening infrastructure in Europe under climate change. *Nat. Hazards Earth Syst. Sci.* 17, 1177–1190. doi:10.5194/nhess-17-1177-2017.
Niu, X., Wang, S., Tang, J., Lee, D.-K., Gutowski, W., Dairaku, K., et al. (2018). Ensemble evaluation and projection of climate extremes in China using RMIP models. *Int. J. Climatol.* 38, 2039–2055. doi:10.1002/joc.5315.
NIWA (2018). *Climate change projections for New Zealand*. Available at: http://www.mfe.govt.nz/sites/default/files/media/Climate Change/climate-projections-snapshot.pdf.
Nka, B. N., Oudin, L., Karambiri, H., Paturel, J. E., and Ribstein, P. (2015). Trends in floods in West Africa: Analysis based on 11 catchments in the region. *Hydrol. Earth Syst. Sci.* 19, 4707–4719. doi:10.5194/hess-19-4707-2015.
Norris, J., Chen, G., and David Neelin, J. (2019a). Thermodynamic versus dynamic controls on extreme precipitation in a warming climate from the Community Earth System Model Large Ensemble. *J. Clim.* 32, 1025–1045. doi:10.1175/JCLI-D-18-0302.1.
Norris, J., Chen, G., and Neelin, J. D. (2019b). Changes in Frequency of Large Precipitation Accumulations over Land in a Warming Climate from the CESM Large Ensemble: The Roles of Moisture, Circulation, and Duration. *J. Clim.* 32, 5397–5416. doi:10.1175/JCLI-D-18-0600.1.
Nott, J., Smithers, S., Walsh, K., and Rhodes, E. (2009). Sand beach ridges record 6000 year history of extreme tropical cyclone activity in northeastern Australia. *Quat. Sci. Rev.* 28, 1511–1520. doi:10.1016/j.quascirev.2009.02.014.
Nyaupane, N., Thakur, B., Kalra, A., and Ahmad, S. (2018). Evaluating future flood scenarios using CMIP5 climate projections. *Water (Switzerland)* 10. Available at: https://www.scopus.com/inward/record.uri?eid=2-s2.0-85059003046&doi=10.3390%2Fw10121866&partnerID=40&md5=243a8e5f0af3cae0835b9ab2109e5b03.
O'Gorman, P. A. (2015). Precipitation Extremes Under Climate Change. *Curr. Clim. Chang. Reports* 1, 49–59.

doi:10.1007/s40641-015-0009-3.
O'Gorman, P. A., and Schneider, T. (2009). The physical basis for increases in precipitation extremes in simulations of 21st-century climate change. *Proc. Natl. Acad. Sci.* 106, 14773–14777. doi:10.1073/pnas.0907610106.
O'Neill, B. C., Oppenheimer, M., Warren, R., Hallegatte, S., Kopp, R. E., Pörtner, H. O., et al. (2017). IPCC reasons for concern regarding climate change risks. *Nat. Clim. Chang.* 7, 28. Available at: https://doi.org/10.1038/nclimate3179.
OB, C., Yang, S., Boberg, F., C, F. M., Thejll, P., Olesen, M., et al. (2015). Scalability of regional climate change in Europe for high-end scenarios . *Clim. Res.* 64, 25–38. Available at: https://www.int-res.com/abstracts/cr/v64/n1/p25-38/.
Odoulami, R. C., Abiodun, B. J., and Ajayi, A. E. (2019). Modelling the potential impacts of afforestation on extreme precipitation over West Africa. *Clim. Dyn.* 52, 2185–2198. doi:10.1007/s00382-018-4248-6.
Oey, L.-Y., and Chou, S. C. (2016). Evidence of rising and poleward shift of storm surge in western North Pacific in recent decades. *J. Geophys. Res. Ocean.* 121, 5181–5192. doi:10.1002/2015JC011516.
Ogata, T., Mizuta, R., Adachi, Y., Murakami, H., and Ose, T. (2015). Effect of air-sea coupling on the frequency distribution of intense tropical cyclones over the northwestern Pacific. *Geophys. Res. Lett.* 42, 10,410-415,421. doi:10.1002/2015GL066774.
Ogata, T., Mizuta, R., Adachi, Y., Murakami, H., and Ose, T. (2016). Atmosphere-Ocean Coupling Effect on Intense Tropical Cyclone Distribution and its Future Change with 60 km-AOGCM. *Sci. Rep.* 6, 29800. Available at: https://doi.org/10.1038/srep29800.
Oh, H., Ha, K.-J., and Timmermann, A. (2018). Disentangling Impacts of Dynamic and Thermodynamic Components on Late Summer Rainfall Anomalies in East Asia. *J. Geophys. Res. Atmos.* 123, 8623–8633. doi:10.1029/2018JD028652.
Ohba, M., and Sugimoto, S. (2019). Differences in climate change impacts between weather patterns: possible effects on spatial heterogeneous changes in future extreme rainfall. *Clim. Dyn.* 52, 4177–4191. doi:10.1007/s00382-018-4374-1.
Oizumi, T., Saito, K., Ito, J., Kuroda, T., Doc, L., DUC, L., et al. (2018). Ultra-High-Resolution Numerical Weather Prediction with a Large Domain Using the K Computer: A Case Study of the Izu Oshima Heavy Rainfall Event on October 15-16, 2013. *J. Meteorol. Soc. Japan. Ser. II* 96, 25–54. doi:10.2151/jmsj.2018-006.
Oleson, K. W., Bonan, G. B., and Feddema, J. (2010). Effects of white roofs on urban temperature in a global climate model. *Geophys. Res. Lett.* 37, n/a-n/a. doi:10.1029/2009GL042194.
Oliver, E. C. J., Benthuysen, J. A., Bindoff, N. L., Hobday, A. J., Holbrook, N. J., Mundy, C. N., et al. (2017). The unprecedented 2015/16 Tasman Sea marine heatwave. *Nat. Commun.* 8, 16101. doi:10.1038/ncomms16101.
Oliver, R. J., Mercado, L. M., Sitch, S., Simpson, D., Medlyn, B. E., Lin, Y.-S., et al. (2018). Large but decreasing effect of ozone on the European carbon sink. *Biogeosciences* 15, 4245–4269. doi:10.5194/bg-15-4245-2018.
Olson, R., Evans, J., Di Luca, A., and Argüeso, D. (2016). The NARCliM project: model agreement and significance of climate projections. *Clim. Res.* 69, 209–227. doi:10.3354/cr01403.
Ongoma, V., Chen, H., and Gao, C. (2018). Projected changes in mean rainfall and temperature over East Africa based on CMIP5 models. *Int. J. Climatol.* 38, 1375–1392.
ONOGI, K., TSUTSUI, J., KOIDE, H., SAKAMOTO, M., KOBAYASHI, S., HATSUSHIKA, H., et al. (2007). The JRA-25 Reanalysis. *J. Meteorol. Soc. Japan. Ser. II* 85, 369–432. doi:10.2151/jmsj.85.369.
Oppenheimer, M., Campos, M., Warren, R., Birkmann, J., Luber, G., and O'Neill, B. (2014). Emergent risks and key vulnerabilities. In: Climate Change 2014: Impacts, Adaptation, and Vulnerability. Part A: Global and Sectoral Aspects. Contribution of Working Group II to the Fifth Assessment Report of the Intergovernmental Panel on Climate Change.
Orlowsky, B., and Seneviratne, S. I. (2013). Elusive drought: Uncertainty in observed trends and short-and long-term CMIP5 projections. *Hydrol. Earth Syst. Sci.* 17, 1765–1781. doi:10.5194/hess-17-1765-2013.
Ortega, J. A., Razola, L., and Garzón, G. (2014). Recent human impacts and change in dynamics and morphology of ephemeral rivers. *Nat. Hazards Earth Syst. Sci.* 14, 713–730. doi:10.5194/nhess-14-713-2014.
Orth, R., Vogel, M. M., Luterbacher, J., Pfister, C., and Seneviratne, S. I. (2016a). Did European temperatures in 1540 exceed present-day records? *Environ. Res. Lett.* 11, 114021. doi:10.1088/1748-9326/11/11/114021.
Orth, R., Zscheischler, J., and Seneviratne, S. I. (2016b). Record dry summer in 2015 challenges precipitation projections in Central Europe. *Sci. Rep.* 6, 28334. Available at: http://dx.doi.org/10.1038/srep28334.
Osima, S., Indasi, V. S., Zaroug, M., Endris, H. S., Gudoshava, M., Misiani, H. O., et al. (2018). Projected climate over the Greater Horn of Africa under 1.5 °C and 2 °C global warming. *Environ. Res. Lett.* 13, 065004. doi:10.1088/1748-9326/aaba1b.
Otkin, J. A., Anderson, M. C., Hain, C., Svoboda, M., Johnson, D., Mueller, R., et al. (2016). Assessing the evolution of soil moisture and vegetation conditions during the 2012 United States flash drought. *Agric. For. Meteorol.* 218–219, 230–242. doi:10.1016/j.agrformet.2015.12.065.
Otkin, J. A., Svoboda, M., Hunt, E. D., Ford, T. W., Anderson, M. C., Hain, C., et al. (2018). Flash droughts: A review

and assessment of the challenges imposed by rapid-onset droughts in the United States. *Bull. Am. Meteorol. Soc.* 99, 911–919. doi:10.1175/BAMS-D-17-0149.1.
Otto, F. E. L. (2017). Attribution of Weather and Climate Events. *Annu. Rev. Environ. Resour.* 42, null. doi:10.1146/annurev-environ-102016-060847.
Otto, F. E. L., Boyd, E., Jones, R. G., Cornforth, R. J., James, R., Parker, H. R., et al. (2015a). Attribution of extreme weather events in Africa: a preliminary exploration of the science and policy implications. *Clim. Change* 132, 531–543. doi:10.1007/s10584-015-1432-0.
Otto, F. E. L., Harrington, L. J., Frame, D., Boyd, E., Lauta, K. C., Wehner, M. F., et al. (submitted, a). Towards an inventory of the impacts of human-induced climate change. *Nat. Clim. Chang.* submitted.
Otto, F. E. L., Haustein, K., Uhe, P., Coelho, C. A. S., Aravequia, J. A., Almeida, W., et al. (2015b). Factors Other Than Climate Change, Main Drivers of 2014/15 Water Shortage in Southeast Brazil. *Bull. Am. Meteorol. Soc.* 96, S35–S40. doi:10.1175/BAMS-D-15-00120.1.
Otto, F. E. L., Jones, R. G., Halladay, K., and Allen, M. R. (2013). Attribution of changes in precipitation patterns in African rainforests. *Philos. Trans. R. Soc. B Biol. Sci.* 368, 20120299. doi:10.1098/rstb.2012.0299.
Otto, F. E. L., Massey, N., van Oldenborgh, G. J., Jones, R. G., and Allen, M. R. (2012). Reconciling two approaches to attribution of the 2010 Russian heat wave. *Geophys. Res.\ Lett.* 39, L04702. doi:10.1029/2011GL050422.
Otto, F. E. L., Philip, S., Kew, S., Li, S., King, A., and Cullen, H. (2018a). Attributing high-impact extreme events across timescales—a case study of four different types of events. *Clim. Change* 149, 399–412. doi:10.1007/s10584-018-2258-3.
Otto, F. E. L., Rosier, S. M., Allen, M. R., Massey, N. R., Rye, C. J., and Quintana, J. I. (2015c). Attribution analysis of high precipitation events in summer in England and Wales over the last decade. *Clim. Change* 132, 77–91. doi:10.1007/s10584-014-1095-2.
Otto, F. E. L., van der Wiel, K., van Oldenborgh, G. J., Philip, S., Kew, S. F., Uhe, P., et al. (2018b). Climate change increases the probability of heavy rains in Northern England/Southern Scotland like those of storm Desmond—a real-time event attribution revisited. *Environ. Res. Lett.* 13, 024006. doi:10.1088/1748-9326/aa9663.
Otto, F. E. L., van Oldenborgh, G. J., Eden, J., Stott, P. A., Karoly, D. J., and Allen, M. R. (2016). The attribution question. *Nat. Clim. Chang.* 6, 813–816. doi:10.1038/nclimate3089.
Otto, F. E. L., Wolski, P., Lehner, F., Tebaldi, C., van Oldenborgh, G. J., Hogesteeger, S., et al. (2018c). Anthropogenic influence on the drivers of the Western Cape drought 2015–2017. *Environ. Res. Lett.* 13, 124010. doi:10.1088/1748-9326/aae9f9.
Otto, F., Harrington, L., Philip, S., Schmitt, K., Kew, S., van Oldenborgh, G. J., et al. (submitted, b). Challenges to understanding extreme weather changes in lower income countries. *Bull. Am. Meteorol. Soc.*(submitted).
Ozturk, T., Ceber, Z. P., Türkeş, M., and Kurnaz, M. L. (2015). Projections of climate change in the Mediterranean Basin by using downscaled global climate model outputs. *Int. J. Climatol.* 35, 4276–4292. doi:10.1002/joc.4285.
Paciorek, C. J., Stone, D. A., and Wehner, M. F. (2018). Quantifying statistical uncertainty in the attribution of human influence on severe weather. *Weather Clim. Extrem.* 20, 69–80. doi:10.1016/j.wace.2018.01.002.
Padrón, R. S., Gudmundsson, L., and Seneviratne, S. I. (2019). Observational Constraints Reduce Likelihood of Extreme Changes in Multidecadal Land Water Availability. *Geophys. Res. Lett.* 46, 736–744. doi:10.1029/2018GL080521.
Pai, D. S., Sridhar, L., Badwaik, M. R., and Rajeevan, M. (2015). Analysis of the daily rainfall events over India using a new long period (1901–2010) high resolution (0.25° × 0.25°) gridded rainfall data set. *Clim. Dyn.* 45, 755–776. doi:10.1007/s00382-014-2307-1.
Paik, S. et al. (submitted). Determining the greenhouse gas contribution to the observed intensification of extreme precipitation. *Geophys. Res. Lett.*(submitted).
Paik, S., and Min, S.-K. (2018). Assessing the Impact of Volcanic Eruptions on Climate Extremes Using CMIP5 Models. *J. Clim.* 31, 5333–5349. doi:10.1175/JCLI-D-17-0651.1.
Pakalidou, N., and Karacosta, P. (2018). Study of very long-period extreme precipitation records in Thessaloniki, Greece. *Atmos. Res.* 208, 106–115. doi:https://doi.org/10.1016/j.atmosres.2017.07.029.
Palazzi, E., Hardenberg, J., and Provenzale, A. (2013). Precipitation in the Hindu-Kush Karakoram Himalaya: Observations and future scenarios. *J. Geophys. Res. Atmos.* 118, 85–100. doi:10.1029/2012JD018697.
Palipane, E., and Grotjahn, R. (2018). Future Projections of the Large-Scale Meteorology Associated with California Heat Waves in CMIP5 Models. *J. Geophys. Res. Atmos.* 123, 8500–8517. doi:10.1029/2018JD029000.
Pall, P., Patricola, C. M., Wehner, M. F., Stone, D. A., Paciorek, C. J., and Collins, W. D. (2017). Diagnosing conditional anthropogenic contributions to heavy Colorado rainfall in September 2013. *Weather Clim. Extrem.* 17, 1–6. doi:https://doi.org/10.1016/j.wace.2017.03.004.
Paltan, H., Allen, M., Haustein, K., Fuldauer, L., and Dadson, S. (2018). Global implications of 1.5 °C and 2 °C warmer worlds on extreme river flows. *Environ. Res. Lett.* 13, 94003. doi:10.1088/1748-9326/aad985.
Panisset, J. S., Libonati, R., Gouveia, C. M. P., Machado-Silva, F., França, D. A., França, J. R. A., et al. (2018). Contrasting patterns of the extreme drought episodes of 2005, 2010 and 2015 in the Amazon Basin. *Int. J.*

Climatol. 38, 1096–1104. doi:10.1002/joc.5224.
Panthou, G., Lebel, T., Vischel, T., Quantin, G., Sane, Y., Ba, A., et al. (2018). Rainfall intensification in tropical semi-arid regions: The Sahelian case. *Environ. Res. Lett.* 13, 64013.
Panthou, G., Vischel, T., and Lebel, T. (2014). Recent trends in the regime of extreme rainfall in the Central Sahel. *Int. J. Climatol.* 34, 3998–4006. doi:10.1002/joc.3984.
Paprotny, D., Morales-Nápoles, O., Vousdoukas, M. I., Jonkman, S. N., and Nikulin, G. (2019). Accuracy of pan-European coastal flood mapping. *J. Flood Risk Manag.* 12. Available at: https://www.scopus.com/inward/record.uri?eid=2-s2.0-85047732612&doi=10.1111%2Fjfr3.12459&partnerID=40&md5=c17f6a9c0706cd822c9a992b0f9dbc99.
Park, C., and Min, S.-K. (2018). Multi-RCM near-term projections of summer climate extremes over East Asia. *Clim. Dyn.* 0, 1–16. doi:10.1007/s00382-018-4425-7.
Park, C., Min, S.-K., Lee, D., Cha, D.-H., Suh, M.-S., Kang, H.-S., et al. (2016). Evaluation of multiple regional climate models for summer climate extremes over East Asia. *Clim. Dyn.* 46, 2469–2486. doi:10.1007/s00382-015-2713-z.
Park Williams, A., Cook, B. I., Smerdon, J. E., Bishop, D. A., Seager, R., and Mankin, J. S. (2017). The 2016 Southeastern U.S. Drought: An Extreme Departure From Centennial Wetting and Cooling. *J. Geophys. Res. Atmos.* 122, 10,810-888,905. doi:10.1002/2017JD027523.
Park Williams, A., Seager, R., Berkelhammer, M., Macalady, A. K., Crimmins, M. A., Swetnam, T. W., et al. (2014). Causes and implications of extreme atmospheric moisture demand during the record-breaking 2011 wildfire season in the southwestern United States. *J. Appl. Meteorol. Climatol.* 53, 2671–2684. Available at: https://www.scopus.com/inward/record.uri?eid=2-s2.0-84928337240&doi=10.1175%2FJAMC-D-14-0053.1&partnerID=40&md5=128549cb260844d6d9831955d8e16a91.
Parker, H. R., Lott, F. C., Cornforth, R. J., Mitchell, D. M., Sparrow, S., and Wallom, D. (2017). A comparison of model ensembles for attributing 2012 West African rainfall. *Environ. Res. Lett.* 12, 14019. doi:10.1088/1748-9326/aa5386.
Parker, T. J., Berry, G. J., Reeder, M. J., and Nicholls, N. (2014). Modes of climate variability and heat waves in Victoria, southeastern Australia. *Geophys. Res. Lett.* 41, 6926–6934. doi:10.1002/2014GL061736.
Parsons, D. J., Rey, D., Tanguy, M., and Holman, I. P. (2019). Regional variations in the link between drought indices and reported agricultural impacts of drought. *Agric. Syst.* 173, 119–129. Available at: https://www.scopus.com/inward/record.uri?eid=2-s2.0-85062028592&doi=10.1016%2Fj.agsy.2019.02.015&partnerID=40&md5=6a5bf6a43f0090eaa777c3421d6f9017.
Pascale, S., Lucarini, V., Feng, X., Porporato, A., and ul Hasson, S. (2016). Projected changes of rainfall seasonality and dry spells in a high greenhouse gas emissions scenario. *Clim. Dyn.* 46, 1331–1350. doi:10.1007/s00382-015-2648-4.
Paschalis, A., Fatichi, S., Molnar, P., Rimkus, S., and Burlando, P. (2014). On the effects of small scale space-time variability of rainfall on basin flood response. *J. Hydrol.* 514, 313–327. doi:10.1016/j.jhydrol.2014.04.014.
Patarčić, M., Gajić-Čapka, M., Cindrić, K., and Branković, C. (2014). Recent and near-future changes in precipitationextreme indices over the Croatian Adriatic coast. *Clim. Res.* 61, 157–176. doi:10.3354/cr01250.
Patra, P. K., Crisp, D., Kaiser, J. W., Wunch, D., Saeki, T., Ichii, K., et al. (2017). The Orbiting Carbon Observatory (OCO-2) tracks 2-3 peta-gram increase in carbon release to the atmosphere during the 2014-2016 El Niño. *Sci. Rep.* 7, 1–12. doi:10.1038/s41598-017-13459-0.
Patricola, C. M., Saravanan, R., and Chang, P. (2018). The Response of Atlantic Tropical Cyclones to Suppression of African Easterly Waves. *Geophys. Res. Lett.* 45, 471–479. doi:10.1002/2017GL076081.
Patricola, C. M., and Wehner, M. F. (2018). Anthropogenic influences on major tropical cyclone events. *Nature* 563, 339–346. doi:10.1038/s41586-018-0673-2.
Paul, S., Ghosh, S., Mathew, M., Devanand, A., Karmakar, S., and Niyogi, D. (2018). Increased Spatial Variability and Intensification of Extreme Monsoon Rainfall due to Urbanization. *Sci. Rep.* 8, 3918. doi:10.1038/s41598-018-22322-9.
Paxian, A., Hertig, E., Seubert, S., Vogt, G., Jacobeit, J., and Paeth, H. (2014). Present-day and future mediterranean precipitation extremes assessed by different statistical approaches. *Clim. Dyn.* 44, 845–860. doi:10.1007/s00382-014-2428-6.
Pearce, T., Currenti, R., Mateiwai, A., and Doran, B. (2018). Adaptation to climate change and freshwater resources in Vusama village, Viti Levu, Fiji. *Reg. Environ. Chang.* 18, 501–510. Available at: https://www.scopus.com/inward/record.uri?eid=2-s2.0-85029587549&doi=10.1007%2Fs10113-017-1222-5&partnerID=40&md5=79e6c1d6a7ed706a375aca15b28e6de9.
Pedersen, S. H., Liston, G. E., Tamstorf, M. P., Westergaard-Nielsen, A., and Schmidt, N. M. (2015). Quantifying Episodic Snowmelt Events in Arctic Ecosystems. *Ecosystems* 18, 839–856. doi:10.1007/s10021-015-9867-8.
Pedron, I. T., Silva Dias, M. A. F., de Paula Dias, S., Carvalho, L. M. V., and Freitas, E. D. (2017). Trends and variability in extremes of precipitation in Curitiba - Southern Brazil. *Int. J. Climatol.* 37, 1250–1264. doi:10.1002/joc.4773.

Pellikka, H., Leijala, U., Johansson, M. M., Leinonen, K., and Kahma, K. K. (2018). Future probabilities of coastal floods in Finland. *Cont. Shelf Res.* 157, 32–42. Available at: https://www.scopus.com/inward/record.uri?eid=2-s2.0-85042739233&doi=10.1016%2Fj.csr.2018.02.006&partnerID=40&md5=ad04e0e85a31b38aba0386b5e8f23c4a.

Peña-Gallardo, M., SM, V.-S., Domínguez-Castro, F., Quiring, S., Svoboda, M., Beguería, S., et al. (2018a). Effectiveness of drought indices in identifying impacts on major crops across the USA . *Clim. Res.* 75, 221–240. Available at: https://www.int-res.com/abstracts/cr/v75/n3/p221-240/.

Peña-Gallardo, M., Vicente-Serrano, S. M., Camarero, J. J., Gazol, A., Sánchez-Salguero, R., Domínguez-Castro, F., et al. (2018b). Drought Sensitiveness on Forest Growth in Peninsular Spain and the Balearic Islands. *Forests* 9.

Pendergrass, A. G. (2018). What precipitation is extreme? *Science* 360, 1072–1073. doi:10.1126/science.aat1871.

Pendergrass, A. G., Lehner, F., Sanderson, B. M., and Xu, Y. (2015). Does extreme precipitation intensity depend on the emissions scenario? *Geophys. Res. Lett.* 42, 8767–8774. doi:10.1002/2015GL065854.

Pepler, A., Ashcroft, L., and Trewin, B. (2018). The relationship between the subtropical ridge and Australian temperatures. *J. South. Hemisph. Earth Syst. Sci.* 68, 201–214. doi:10.22499/3.6801.011.

Pepler, A. S. A. S., Di Luca, A., Ji, F., Alexander, L. V. L. V., Evans, J. P. J. P., and Sherwood, S. C. S. C. (2015). Impact of Identification Method on the Inferred Characteristics and Variability of Australian East Coast Lows. *Mon. Weather Rev.* 143, 864–877. doi:10.1175/MWR-D-14-00188.1.

Pepler, A. S., Luca, A. Di, Ji, F., Alexander, L. V, Evans, J. P., and Sherwood, S. C. (2016). Projected changes in east Australian midlatitude cyclones during the 21st century. *Geophys. Res. Lett.* 43, 334–340. doi:10.1002/2015GL067267.Received.

Pereira, L. S., Allen, R. G., Smith, M., and Raes, D. (2015). Crop evapotranspiration estimation with FAO56: Past and future. *Agric. Water Manag.* 147, 4–20. doi:10.1016/j.agwat.2014.07.031.

Perkins-Kirkpatrick, S. E., and Gibson, P. B. (2018). Changes in regional heatwave characteristics as a function of increasing global temperature. *Sci. Rep.*, 1–12.

Perkins-Kirkpatrick, S. E., White, C. J., Alexander, L. V, Argüeso, D., Boschat, G., Cowan, T., et al. (2016). Natural hazards in Australia: heatwaves. *Clim. Change* 139, 101–114. doi:10.1007/s10584-016-1650-0.

Perkins, S. E. (2015). A review on the scientific understanding of heatwaves their measurement, driving mechanisms, and changes at the global scale. *Atmos. Res.* 164–165, 242–267.

Perkins, S. E., Lewis, S. C., King, A. D., and Alexander, L. V (2014a). Increased simulated risk of the hot Australian summer of 2012-2013 due to anthropogenic activity as measured by heatwave frequency and intensity [in "Explaining Extremes of 2013 from a Climate Perspective"]. *Bull. Am. Meteorol. Soc.* 95, S34--S37.

Perkins, S. E., Moise, A., Whetton, P., and Katzfey, J. (2014b). Regional changes of climate extremes over Australia - A comparison of regional dynamical downscaling and global climate model simulations. *Int. J. Climatol.* 34, 3456–3478. doi:10.1002/joc.3927.

Persad, G. G., and Caldeira, K. (2018). Divergent global-scale temperature effects from identical aerosols emitted in different regions. *Nat. Commun.* 9, 3289. doi:10.1038/s41467-018-05838-6.

Peterson, T. C., Folland, C., Gruza, G., Hogg, W., Mokssit, A., and Plummer, N. (2001). Report on the activities of the Working Group on Climate Change Detection and Related Rapporteurs 1998–2001.

Peterson, T. C., Heim, R. R., Hirsch, R., Kaiser, D. P., Brooks, H., Diffenbaugh, N. S., et al. (2013a). Monitoring and Understanding Changes in Heat Waves, Cold Waves, Floods, and Droughts in the United States: State of Knowledge. *Bull. Am. Meteorol. Soc.* 94, 821–834. doi:10.1175/BAMS-D-12-00066.1.

Peterson, T. C., Hoerling, M. P., Stott, P. A., and Herring, S. C. (2013b). Explaining Extreme Events of 2012 from a Climate Perspective. *Bull. Am. Meteorol. Soc.* 94, S1–S74. doi:10.1175/BAMS-D-13-00085.1.

Peterson, T. C., Stott, P. A., and Herring, S. (2012). Explaining Extreme Events of 2011 from a Climate Perspective. *Bull. Am. Meteorol. Soc.* 93, 1041–1067. doi:10.1175/BAMS-D-12-00021.1.

Pfahl, S., O'Gorman, P. A., and Fischer, E. M. (2017). Understanding the regional pattern of projected future changes in extreme precipitation. *Nat. Clim. Chang.* 7, 423. Available at: http://dx.doi.org/10.1038/nclimate3287.

Pfahl, S., and Wernli, H. (2012). Quantifying the relevance of cyclones for precipitation extremes. *J. Clim.* 25, 6770–6780. doi:10.1175/JCLI-D-11-00705.1.

Phelan, P. E., Kaloush, K., Miner, M., Golden, J., Phelan, B., Silva, H., et al. (2015). Urban Heat Island: Mechanisms, Implications, and Possible Remedies. *Annu. Rev. Environ. Resour.* 40, 285–307. doi:10.1146/annurev-environ-102014-021155.

Phibbs, S., and Toumi, R. (2016). The dependence of precipitation and its footprint on atmospheric temperature in idealized extratropical cyclones. *J. Geophys. Res.* 121, 8743–8754. doi:10.1002/2015JD024286.

Philip, S., Kew, S. F., Jan van Oldenborgh, G., Otto, F., O'Keefe, S., Haustein, K., et al. (2018a). Attribution Analysis of the Ethiopian Drought of 2015. *J. Clim.* 31, 2465–2486. doi:10.1175/JCLI-D-17-0274.1.

Philip, S., Kew, S. F., van Oldenborgh, G. J., Aalbers, E., Vautard, R., Otto, F., et al. (2018b). Validation of a rapid attribution of the May/June 2016 flood-inducing precipitation in France to climate change. *J. Hydrometeorol.* 19, 1881–1898. Available at: https://www.scopus.com/inward/record.uri?eid=2-s2.0-

85058133394&doi=10.1175%2FJHM-D-18-0074.1&partnerID=40&md5=dd30b70613a4a8eb8aa9d7ded1d0389e.
Philip, S., Kew, S., van Oldenborgh, G. J., Otto, F., Vautard, R., van der Wiel, K., et al. (submitted). A protocol for probabilistic extreme event attribution analyses. *Adv. Stat. Climatol. Meteorol. Oceanogr.*(submitted).
Philip, S., Sparrow, S., Kew, S. F., van der Wiel, K., Wanders, N., Singh, R., et al. (2019). Attributing the 2017 Bangladesh floods from meteorological and hydrological perspectives. *Hydrol. Earth Syst. Sci.* 23, 1409–1429. doi:10.5194/hess-23-1409-2019.
Piaget, N., Froidevaux, P., Giannakaki, P., Gierth, F., Martius, O., Riemer, M., et al. (2015). Dynamics of a local Alpine flooding event in October 2011: moisture source and large-scale circulation. *Q. J. R. Meteorol. Soc.* 141, 1922–1937. doi:10.1002/qj.2496.
Pinto, I., Jack, C., and Hewitson, B. (2018). Process-based model evaluation and projections over southern Africa from Coordinated Regional Climate Downscaling Experiment and Coupled Model Intercomparison Project Phase 5 models. *Int. J. Climatol.*, 1–11. doi:https://doi.org/10.1002/joc.5666.
Pinto, I., Lennard, C., Tadross, M., Hewitson, B., Dosio, A., Nikulin, G., et al. (2016). Evaluation and projections of extreme precipitation over southern Africa from two CORDEX models. *Clim. Change* 135. doi:10.1007/s10584-015-1573-1.
Pinto, J. G., Bellenbaum, N., Karremann, M. K., and Della-Marta, P. M. (2013). Serial clustering of extratropical cyclones over the North Atlantic and Europe under recent and future climate conditions. *J. Geophys. Res. Atmos.* 118, 12,476-12,485. doi:10.1002/2013JD020564.
Pisaniello, J. D., Tingey-Holyoak, J., and Burritt, R. L. (2012). Appropriate small dam management for minimizing catchment-wide safety threats: International benchmarked guidelines and demonstrative cases studies. *Water Resour. Res.* 48. doi:10.1029/2011WR011155.
Pithan, F., and Mauritsen, T. (2014). Arctic amplification dominated by temperature feedbacks in contemporary climate models. *Nat. Geosci.* 7, 181–184. doi:10.1038/ngeo2071.
Pithan, F., Shepherd, T. G., Zappa, G., and Sandu, I. (2016). Climate model biases in jet streams, blocking and storm tracks resulting from missing orographic drag. *Geophys. Res. Lett.* 43, 7231–7240. doi:10.1002/2016GL069551.
Piticar, A., Mihăilă, D., Lazurca, L. G., Bistricean, P.-I., Puţuntică, A., and Briciu, A.-E. (2016). Spatiotemporal distribution of reference evapotranspiration in the Republic of Moldova. *Theor. Appl. Climatol.* 124, 1133–1144. doi:10.1007/s00704-015-1490-2.
Pitman, A. J., de Noblet-Ducoudré, N., Avila, F. B., Alexander, L. V, Boisier, J.-P., Brovkin, V., et al. (2012). Effects of land cover change on temperature and rainfall extremes in multi-model ensemble simulations. *Earth Syst. Dyn.* 3, 213–231. doi:10.5194/esd-3-213-2012.
Poli, P., Hersbach, H., Dee, D. P., Berrisford, P., Simmons, A. J., Vitart, F., et al. (2016). ERA-20C: An Atmospheric Reanalysis of the Twentieth Century. *J. Clim.* 29, 4083–4097. doi:10.1175/JCLI-D-15-0556.1.
Poli, P., Hersbach, H., Tan, D. G. H., Dee, D. P., Thepaut, J. N., Simmons, A. J., et al. (2013). The data assimilation system and initial performance evaluation of the ECMWF pilot reanalysis of the 20th-century assimilating surface observations only (ERA-20C).
Poschlod, B., Hodnebrog Øand Wood, R. R., Alterskjær, K., Ludwig, R., Myhre, G., and Sillmann, J. (2018). Comparison and Evaluation of Statistical Rainfall Disaggregation and High-Resolution Dynamical Downscaling over Complex Terrain. *J. Hydrometeorol.* 19, 1973–1982.
Poschlod, B., Zscheischler, J., Sillmann, J., Wood, P. J., and Ludwig, R. (submitted). Climate change effects on hydrometeorological compound events over southern Norway. *Weather Clim. Extrem.*(submitted).
Poshtiri, M. P., and Pal, I. (2016). Patterns of hydrological drought indicators in major U.S. River basins. *Clim. Change* 134, 549–563. doi:10.1007/s10584-015-1542-8.
Post, V. E. A., Bosserelle, A. L., Galvis, S. C., Sinclair, P. J., and Werner, A. D. (2018). On the resilience of small-island freshwater lenses: Evidence of the long-term impacts of groundwater abstraction on Bonriki Island, Kiribati. *J. Hydrol.* 564, 133–148. Available at: https://www.scopus.com/inward/record.uri?eid=2-s2.0-85049873611&doi=10.1016%2Fj.jhydrol.2018.06.015&partnerID=40&md5=7ff04cfcc05d2aaa902c1d1349d38829.
Potopová, V., Štěpánek, P., Možný, M., Türkott, L., and Soukup, J. (2015). Performance of the standardised precipitation evapotranspiration index at various lags for agricultural drought risk assessment in the Czech Republic. *Agric. For. Meteorol.* 202, 26–38. doi:10.1016/J.AGRFORMET.2014.11.022.
Potopová, V., Štěpánek, P., Zahradníček, P., Farda, A., Türkott, L., and Soukup, J. (2018). Projected changes in the evolution of drought on various timescales over the Czech Republic according to Euro-CORDEX models. *Int. J. Climatol.* 38, e939–e954. doi:10.1002/joc.5421.
Prein, A. F., Gobiet, A., Suklitsch, M., Truhetz, H., Awan, N. K., Keuler, K., et al. (2013). Added value of convection permitting seasonal simulations. *Clim. Dyn.* 41, 2655–2677. doi:10.1007/s00382-013-1744-6.
Prein, A. F., Gobiet, A., Truhetz, H., Keuler, K., Goergen, K., Teichmann, C., et al. (2016a). Precipitation in the EURO-CORDEX 0.11∘ and 0.44∘ simulations: high resolution, high benefits? *Clim. Dyn.* 46, 383–412.

doi:10.1007/s00382-015-2589-y.
Prein, A. F., and Holland, G. J. (2018). Global estimates of damaging hail hazard. *Weather Clim. Extrem.* 22, 10–23. doi:10.1016/j.wace.2018.10.004.
Prein, A. F., Langhans, W., Fosser, G., Ferrone, A., Ban, N., Goergen, K., et al. (2015). A review on regional convection-permitting climate modeling: Demonstrations, prospects, and challenges. *Rev. Geophys.* 53, 323–361. doi:10.1002/2014RG000475.
Prein, A. F., Liu, C., Ikeda, K., Bullock, R., Rasmussen, R. M., Holland, G. J., et al. (2017a). Simulating North American mesoscale convective systems with a convection-permitting climate model. *Clim. Dyn.* 0, 1–16. doi:10.1007/s00382-017-3993-2.
Prein, A. F., Liu, C., Ikeda, K., Trier, S. B., Rasmussen, R. M., Holland, G. J., et al. (2017b). Increased rainfall volume from future convective storms in the US. *Nat. Clim. Chang.* 7, 880–884. doi:10.1038/s41558-017-0007-7.
Prein, A. F., Rasmussen, R. M., Ikeda, K., Liu, C., Clark, M. P., and Holland, G. J. (2016b). The future intensification of hourly precipitation extremes. *Nat. Clim. Chang.* 7, 48. doi:10.1038/nclimate3168.
Prein, A. F., Rasmussen, R., and Stephens, G. (2017c). Challenges and Advances in Convection-Permitting Climate Modeling. *Bull. Am. Meteorol. Soc.* 98, 1027–1030. doi:10.1175/BAMS-D-16-0263.1.
Priya, P., Krishnan, R., Mujumdar, M., and Houze, R. A. (2017). Changing monsoon and midlatitude circulation interactions over the Western Himalayas and possible links to occurrences of extreme precipitation. *Clim. Dyn.* 49, 2351–2364. doi:10.1007/s00382-016-3458-z.
Prudhomme, C., Giuntoli, I., Robinson, E. L., Clark, D. B., Arnell, N. W., Dankers, R., et al. (2014). Hydrological droughts in the 21st century, hotspots and uncertainties from a global multimodel ensemble experiment. *Proc. Natl. Acad. Sci. U. S. A.* 111, 3262–3267. doi:10.1073/pnas.1222473110.
Púčik, T., Groenemeijer, P., Rädler, A. T., Tijssen, L., Nikulin, G., Prein, A. F., et al. (2017). Future Changes in European Severe Convection Environments in a Regional Climate Model Ensemble. *J. Clim.* 30, 6771–6794. doi:10.1175/JCLI-D-16-0777.1.
Qian, C., Wang, J., Dong, S., Yin, H., Burke, C., Ciavarella, A., et al. (2018). Human Influence on the Record-breaking Cold Event in January of 2016 in Eastern China. *Bull. Am. Meteorol. Soc.* 99, S118–S122. doi:10.1175/BAMS-D-17-0095.1.
Qian, C., Zhang, X., and Li, Z. (2019). Linear trends in temperature extremes in China, with an emphasis on non-Gaussian and serially dependent characteristics. *Clim. Dyn.* 53, 533–550. doi:10.1007/s00382-018-4600-x.
Qin, N., Wang, J., Yang, G., Chen, X., Liang, H., and Zhang, J. (2015a). Spatial and temporal variations of extreme precipitation and temperature events for the Southwest China in 1960–2009. *Geoenvironmental Disasters* 2. doi:10.1186/s40677-015-0014-9.
Qin, Y., Yang, D., Lei, H., Xu, K., and Xu, X. (2015b). Comparative analysis of drought based on precipitation and soil moisture indices in Haihe basin of North China during the period of 1960-2010. *J. Hydrol.* 526, 55–67. Available at: https://www.scopus.com/inward/record.uri?eid=2-s2.0-84936358867&doi=10.1016%2Fj.jhydrol.2014.09.068&partnerID=40&md5=ae4eb78cd5b3ad64742205cf5d329ea2.
Qiu, J., Gao, Q., Wang, S., and Su, Z. (2016). Comparison of temporal trends from multiple soil moisture data sets and precipitation: The implication of irrigation on regional soil moisture trend. *Int. J. Appl. Earth Obs. Geoinf.* 48, 17–27. Available at: https://www.scopus.com/inward/record.uri?eid=2-s2.0-84994087939&doi=10.1016%2Fj.jag.2015.11.012&partnerID=40&md5=13e6a69fa3dba90fc32f554410cf1af4.
Quan, X.-W., Hoerling, M., Smith, L., Perlwitz, J., Zhang, T., Hoell, A., et al. (2018). Extreme California Rains During Winter 2015/16: A Change in El Niño Teleconnection? *Bull. Am. Meteorol. Soc.* 99, S49–S53. doi:10.1175/BAMS-D-17-0118.1.
Quesada, B., Vautard, R., Yiou, P., Hirschi, M., and Seneviratne, S. I. (2012). Asymmetric European summer heat predictability from wet and dry southern winters and springs. *Nat. Clim. Chang.* 2, 736–741. doi:10.1038/nclimate1536.
Quiring, S. M., Ford, T. W., Wang, J. K., Khong, A., Harris, E., Lindgren, T., et al. (2016). The north American soil moisture database development and applications. *Bull. Am. Meteorol. Soc.* 97, 1441–1460. Available at: https://www.scopus.com/inward/record.uri?eid=2-s2.0-84963561455&doi=10.1175%2FBAMS-D-13-00263.1&partnerID=40&md5=bb485e48e429895e99ea61fc00f94446.
Ragone, F., Mariotti, M., Parodi, A., von Hardenberg, J., and Pasquero, C. (2018). A Climatological Study of Western Mediterranean Medicanes in Numerical Simulations with Explicit and Parameterized Convection. *Atmosphere (Basel).* 9, 397. doi:10.3390/atmos9100397.
Rahimi, M., and Fatemi, S. S. (2019). Mean versus Extreme Precipitation Trends in Iran over the Period 1960–2017. *Pure Appl. Geophys.* 176, 3717–3735. doi:10.1007/s00024-019-02165-9.
Rahimi, M., and Hejabi, S. (2018). Spatial and temporal analysis of trends in extreme temperature indices in Iran over the period 1960–2014. *Int. J. Climatol.* 38, 272–282. doi:10.1002/joc.5175.
Rai, P., Choudhary, A., and Dimri, A. P. (2019). Future precipitation extremes over India from the CORDEX-South

Asia experiments. *Theor. Appl. Climatol.* doi:10.1007/s00704-019-02784-1.
Rajbhandari, R., Shrestha, A. B., Kulkarni, A., Patwardhan, S. K., and Bajracharya, S. R. (2015). Projected changes in climate over the Indus river basin using a high resolution regional climate model (PRECIS). *Clim. Dyn.* 44, 339–357. doi:10.1007/s00382-014-2183-8.
Rajczak, J., Pall, P., and Schär, C. (2013). Projections of extreme precipitation events in regional climate simulations for Europe and the Alpine Region. *J. Geophys. Res. Atmos.* 118, 3610–3626. doi:10.1002/jgrd.502972013.
Rajczak, J., and Schär, C. (2017). Projections of Future Precipitation Extremes Over Europe: A Multimodel Assessment of Climate Simulations. *J. Geophys. Res. Atmos.* 122, 10,773-10,800. doi:10.1002/2017JD027176.
Rajsekhar, D., and Gorelick, S. M. (2017). Increasing drought in Jordan: Climate change and cascading Syrian land-use impacts on reducing transboundary flow. *Sci. Adv.* 3, 1–15. doi:10.1126/sciadv.1700581.
Ralph, F. M., Dettinger, M. D., Cairns, M. M., Galarneau, T. J., and Eylander, J. (2018). Defining "Atmospheric River": How the Glossary of Meteorology Helped Resolve a Debate. *Bull. Am. Meteorol. Soc.* 99, 837–839. doi:10.1175/BAMS-D-17-0157.1.
Ralph, F. M., Rutz, J. J., Cordeira, J. M., Dettinger, M., Anderson, M., Reynolds, D., et al. (2019). A Scale to Characterize the Strength and Impacts of Atmospheric Rivers. *Bull. Am. Meteorol. Soc.* 100, 269–289. doi:10.1175/BAMS-D-18-0023.1.
Ramos, A. M., Tomé, R., Trigo, R. M., Liberato, M. L. R., and Pinto, J. G. (2016). Projected changes in atmospheric rivers affecting Europe in CMIP5 models. *Geophys. Res. Lett.* 43, 9315–9323. doi:10.1002/2016GL070634.
Rasmijn, L. M., Van Der Schrier, G., Bintanja, R., Barkmeijer, J., Sterl, A., and Hazeleger, W. (2018). Future equivalent of 2010 Russian heatwave intensified by weakening soil moisture constraints. *Nat. Clim. Chang.* 8, 381–385. doi:10.1038/s41558-018-0114-0.
Rasmussen, K. L., and Houze, R. A. (2011). Orogenic Convection in Subtropical South America as Seen by the TRMM Satellite. *Mon. Weather Rev.* 139, 2399–2420. doi:10.1175/MWR-D-10-05006.1.
Rasmussen, K. L., Prein, A. F., Rasmussen, R. M., Ikeda, K., and Liu, C. (2017). Changes in the convective population and thermodynamic environments in convection-permitting regional climate simulations over the United States. *Clim. Dyn.* doi:10.1007/s00382-017-4000-7.
Ratnam, J. V., Behera, S. K., Ratna, S. B., Rajeevan, M., and Yamagata, T. (2016). Anatomy of Indian heatwaves. *Sci. Rep.* 6, 1–11. doi:10.1038/srep24395.
Raymond, F., Ullmann, A., Camberlin, P., Oueslati, B., and Drobinski, P. (2018). Atmospheric conditions and weather regimes associated with extreme winter dry spells over the Mediterranean basin. *Clim. Dyn.* 50, 4437–4453. doi:10.1007/s00382-017-3884-6.
Raymond, F., Ullmann, A., Tramblay, Y., Drobinski, P., and Camberlin, P. (2019). Evolution of Mediterranean extreme dry spells during the wet season under climate change. *Reg. Environ. Chang.* Available at: https://www.scopus.com/inward/record.uri?eid=2-s2.0-85069442607&doi=10.1007%2Fs10113-019-01526-3&partnerID=40&md5=68ab2c97f6366bf7c6d90f01bcc50ca3.
Reboita, M. S., da Rocha, R. P., Ambrizzi, T., and Gouveia, C. D. (2015). Trend and teleconnection patterns in the climatology of extratropical cyclones over the Southern Hemisphere. *Clim. Dyn.* 45, 1929–1944. doi:10.1007/s00382-014-2447-3.
Reed, A. J., Mann, M. E., Emanuel, K. A., Lin, N., Horton, B. P., Kemp, A. C., et al. (2015a). Increased threat of tropical cyclones and coastal flooding to New York City during the anthropogenic era. *Proc. Natl. Acad. Sci.* doi:10.1073/pnas.1513127112.
Reed, K. A., Bacmeister, J. T., Rosenbloom, N. A., Wehner, M. F., Bates, S. C., Lauritzen, P. H., et al. (2015b). Impact of the dynamical core on the direct simulation of tropical cyclones in a high-resolution global model. *Geophys. Res. Lett.* 42, 3603–3608. doi:10.1002/2015GL063974.
Reed, K. A., and Jablonowski, C. (2011). Impact of physical parameterizations on idealized tropical cyclones in the Community Atmosphere Model. *Geophys. Res. Lett.* 38. doi:10.1029/2010GL046297.
Reed, K. A., Stansfield, A. M., Wehner, M. F., and Zarzycki, C. M. (2020). Forecasted attribution of the human influence on Hurricane Florence. *Sci. Adv.* 6, eaaw9253. doi:10.1126/sciadv.aaw9253.
Rehbein, A., Ambrizzi, T., and Mechoso, C. R. (2018). Mesoscale convective systems over the Amazon basin. Part I: climatological aspects. *Int. J. Climatol.* 38, 215–229. doi:10.1002/joc.5171.
Rehman, S. (2013). Long-term wind speed analysis and detection of its trends using Mann-Kendall test and linear regression method. *Arab. J. Sci. Eng.* 38, 421–437. doi:10.1007/s13369-012-0445-5.
Reichle, R. H., Draper, C. S., Liu, Q., Girotto, M., Mahanama, S. P. P., Koster, R. D., et al. (2017). Assessment of MERRA-2 Land Surface Hydrology Estimates. *J. Clim.* 30, 2937–2960. doi:10.1175/JCLI-D-16-0720.1.
Rhee, J., and Cho, J. (2016). Future changes in drought characteristics: Regional analysis for South Korea under CMIP5 projections. *J. Hydrometeorol.* 17, 437–451. Available at: https://www.scopus.com/inward/record.uri?eid=2-s2.0-84957875467&doi=10.1175%2FJHM-D-15-0027.1&partnerID=40&md5=269d694e394916fcb552a891141d79cd.
Ribal, A., and Young, I. R. (2019). 33 Years of Globally Calibrated Wave Height and Wind Speed Data Based on

Altimeter Observations. *Sci. data* 6, 77. doi:10.1038/s41597-019-0083-9.

Ribeiro, I. O., Andreoli, R. V., Kayano, M. T., Sousa, T. R., Medeiros, A. S., Godoi, R. H. M., et al. (2018). Biomass burning and carbon monoxide patterns in Brazil during the extreme drought years of 2005, 2010, and 2015. *Environ. Pollut.* 243, 1008–1014. doi:10.1016/j.envpol.2018.09.022.

Ribes, A., Thao, S., Vautard, R., Dubuisson, B., Somot, S., Colin, J., et al. (2019). Observed increase in extreme daily rainfall in the French Mediterranean. *Clim. Dyn.* 52, 1095–1114. doi:10.1007/s00382-018-4179-2.

Ridder, N., de Vries, H., and Drijfhout, S. (2018). The role of atmospheric rivers in compound events consisting of heavy precipitation and high storm surges along the Dutch coast. *Nat. Hazards Earth Syst. Sci.* 18, 3311–3326. doi:10.5194/nhess-18-3311-2018.

Ridley, J., Wiltshire, A., and Mathison, C. (2013). More frequent occurrence of westerly disturbances in Karakoram up to 2100. *Sci. Total Environ.* 468–469, S31–S35. doi:10.1016/J.SCITOTENV.2013.03.074.

Ringard, J., Dieppois, B., Rome, S., Diedhiou, A., Pellarin, T., Konaré, A., et al. (2016). The intensification of thermal extremes in west Africa. *Glob. Planet. Change* 139, 66–77. doi:10.1016/j.gloplacha.2015.12.009.

Risser, M. D., and Wehner, M. F. (2017). Attributable Human-Induced Changes in the Likelihood and Magnitude of the Observed Extreme Precipitation during Hurricane Harvey. *Geophys. Res. Lett.* 44, 12,412-457,464. doi:10.1002/2017GL075888.

Rivera, J. A., Penalba, O. C., and Betolli, M. L. (2013). Inter-annual and inter-decadal variability of dry days in Argentina. *Int. J. Climatol.* 33, 834–842. doi:10.1002/joc.3472.

Roberts, K. J., Colle, B. A., and Korfe, N. (2017). Impact of simulated twenty-first-century changes in extratropical cyclones on coastal flooding at the Battery, New York City. *J. Appl. Meteorol. Climatol.* 56, 415–432. Available at: https://www.scopus.com/inward/record.uri?eid=2-s2.0-85013168682&doi=10.1175%2FJAMC-D-16-0088.1&partnerID=40&md5=1c47a35d1ccda8ff9ebd8cb5d293dbc6.

Roberts, M. J., Baker, A., Blockley, E. W., Calvert, D., Coward, A., Hewitt, H. T., et al. (2019). Description of the resolution hierarchy of the global coupled HadGEM3-GC3.1 model as used in CMIP6 HighResMIP experiments. *Geosci. Model Dev. Discuss.* 2019, 1–47. doi:10.5194/gmd-2019-148.

Roberts, M. J., Camp, J., Seddon, J., Vidale, P. L., Hodges, K., Vanniere, B., et al. (submitted, a). Future change of tropical cyclones simulated using the HighResMIP-PRIMAVERA multi-model ensemble. (submitted).

Roberts, M. J., Camp, J., Seddon, J., Vidale, P. L., Hodges, K., Vanniere, B., et al. (submitted, b). Impact of model resolution on tropical cyclone simulation using the HighResMIP PRIMAVERA multi-model ensemble. *J. Clim.*(submitted).

Roberts, M. J., Vidale, P. L., Senior, C., Hewitt, H. T., Bates, C., Berthou, S., et al. (2018). The Benefits of Global High Resolution for Climate Simulation: Process Understanding and the Enabling of Stakeholder Decisions at the Regional Scale. *Bull. Am. Meteorol. Soc.* 99, 2341–2359. doi:10.1175/BAMS-D-15-00320.1.

Roca, R., Alexander, L. V., Potter, G., Bador, M., Jucá, R., Contractor, S., et al. (2019). FROGS: a daily 1° × 1° gridded precipitation database of rain gauge, satellite and reanalysis products. *Earth Syst. Sci. Data* 11, 1017–1035. doi:10.5194/essd-11-1017-2019.

Rodell, M., Famiglietti, J. S., Wiese, D. N., Reager, J. T., Beaudoing, H. K., Landerer, F. W., et al. (2018). Emerging trends in global freshwater availability. *Nature* 557, 651–659. doi:10.1038/s41586-018-0123-1.

Roderick, M. L., Greve, P., and Farquhar, G. D. (2015). On the assessment of aridity with changes in atmospheric CO<inf>2</inf> *Water Resour. Res.* 51, 5450–5463. doi:10.1002/2015WR017031.

Rogger, M., Agnoletti, M., Alaoui, A., Bathurst, J. C., Bodner, G., Borga, M., et al. (2017). Land use change impacts on floods at the catchment scale: Challenges and opportunities for future research. *Water Resour. Res.* 53, 5209–5219. doi:10.1002/2017WR020723.

Rohini, P., Rajeevan, M., and Srivastava, A. K. (2016). On the Variability and Increasing Trends of Heat Waves over India. *Sci. Rep.*, 1–9.

Rohrer, M., Brönnimann, S., Martius, O., Raible, C. C., Wild, M., and Compo, G. P. (2018). Representation of extratropical cyclones, blocking anticyclones, and alpine circulation types in multiple reanalyses and model simulations. *J. Clim.* doi:10.1175/JCLI-D-17-0350.1.

Rojas, O., Mardones, M., Martínez, C., Flores, L., Sáez, K., and Araneda, A. (2018). Flooding in central Chile: Implications of tides and sea level increase in the 21st century. *Sustain.* 10. Available at: https://www.scopus.com/inward/record.uri?eid=2-s2.0-85057082648&doi=10.3390%2Fsu10124335&partnerID=40&md5=7aa09ed7149c20609e28a276c0635211.

Romera, R., Gaertner, M. Á., Sánchez, E., Domínguez, M., González-Alemán, J. J., and Miglietta, M. M. (2017). Climate change projections of medicanes with a large multi-model ensemble of regional climate models. *Glob. Planet. Change* 151, 134–143. doi:10.1016/j.gloplacha.2016.10.008.

Romero, R., and Emanuel, K. (2013). Medicane risk in a changing climate. *J. Geophys. Res. Atmos.* 118, 5992–6001. doi:10.1002/jgrd.50475.

Romero, R., and Emanuel, K. (2017). Climate change and hurricane-like extratropical cyclones: Projections for North Atlantic polar lows and medicanes based on CMIP5 models. *J. Clim.* 30, 279–299. doi:10.1175/JCLI-D-16-

0255.1.
Rosier, S., Dean, S., Stuart, S., Carey-Smith, T., Black, M. T., and Massey, N. (2015). Extreme rainfall in early July 2014 in northland, New Zealand-was there an anthropogenic influence? *Bull. Am. Meteorol. Soc.* 96, S136–S140. doi:10.1175/BAMS-D-15-00105.1.
Roth, M., Buishand, T. A., Jongbloed, G., Klein Tank, A. M. G., and van Zanten, J. H. (2014). Projections of precipitation extremes based on a regional, non-stationary peaks-over-threshold approach: A case study for the Netherlands and north-western Germany. *Weather Clim. Extrem.* 4, 1–10. doi:10.1016/j.wace.2014.01.001.
Roth, M., Jongbloed, G., and Buishand, A. (2018). Monotone trends in the distribution of climate extremes. *Theor. Appl. Climatol.* doi:10.1007/s00704-018-2546-x.
Roudier, P., Andersson, J. C. M., Donnelly, C., Feyen, L., Greuell, W., and Ludwig, F. (2016). Projections of future floods and hydrological droughts in Europe under a +2°C global warming. *Clim. Change* 135, 341–355. doi:10.1007/s10584-015-1570-4.
Rowell, D. P., Booth, B. B. B., Nicholson, S. E., and Good, P. (2015). Reconciling Past and Future Rainfall Trends over East Africa. *J. Clim.* 28, 9768–9788. doi:10.1175/JCLI-D-15-0140.1.
Roxy, M. K. K., Ghosh, S., Pathak, A., Athulya, R., Mujumdar, M., Murtugudde, R., et al. (2017). A threefold rise in widespread extreme rain events over central India. *Nat. Commun.* 8, 708. doi:10.1038/s41467-017-00744-9.
Roy, S. Sen (2019). Spatial patterns of trends in seasonal extreme temperatures in India during 1980–2010. *Weather Clim. Extrem.* 24, 100203. doi:10.1016/j.wace.2019.100203.
Ruckert, K. L., Oddo, P. C., and Keller, K. (2017). Impacts of representing sea-level rise uncertainty on future flood risks: An example from San Francisco Bay. *PLoS One* 12. Available at: https://www.scopus.com/inward/record.uri?eid=2-s2.0-85016287133&doi=10.1371%2Fjournal.pone.0174666&partnerID=40&md5=3925844a6f24055e3827fed84da5fba4.
Ruffault, J., Curt, T., Martin-Stpaul, N. K., Moron, V., and Trigo, R. M. (2018). Extreme wildfire events are linked to global-change-type droughts in the northern Mediterranean. *Nat. Hazards Earth Syst. Sci.* 18, 847–856. doi:10.5194/nhess-18-847-2018.
Ruml, M., Gregorić, E., Vujadinović, M., Radovanović, S., Matović, G., Vuković, A., et al. (2017). Observed changes of temperature extremes in Serbia over the period 1961 − 2010. *Atmos. Res.* 183, 26–41. doi:10.1016/j.atmosres.2016.08.013.
Ruosteenoja, K., Markkanen, T., Venäläinen, A., Räisänen, P., and Peltola, H. (2018). Seasonal soil moisture and drought occurrence in Europe in CMIP5 projections for the 21st century. *Clim. Dyn.* 50, 1177–1192. doi:10.1007/s00382-017-3671-4.
Rupp, D. E., Li, S., Massey, N., Sparrow, S. N., Mote, P. W., and Allen, M. (2015). Anthropogenic influence on the changing likelihood of an exceptionally warm summer in Texas, 2011. *Geophys. Res. Lett.* 42, 2392–2400. doi:10.1002/2014GL062683.
Rupp, D. E., Mote, P. W., Massey, N., Otto, F. E. L., and Allen, M. R. (2013). Human influence on the probability of low precipitation in the central United States in 2012. *Bull. Am. Meteorol. Soc.* 94, S2–S6. doi:http://dx.doi.org/10.1108/17506200710779521.
Ruprich-Robert, Y., Delworth, T., Msadek, R., Castruccio, F., Yeager, S., and Danabasoglu, G. (2018). Impacts of the Atlantic Multidecadal Variability on North American Summer Climate and Heat Waves. *J. Clim.* 31, 3679–3700. doi:10.1175/JCLI-D-17-0270.1.
Russo, S., Marchese, A. F., Sillmann, J., and Immé, G. (2016). When will unusual heat waves become normal in a warming Africa? *Environ. Res. Lett.* 11, 054016. doi:10.1088/1748-9326/11/5/054016.
Russo, S., Sillmann, J., and Fischer, E. M. (2015). Top ten European heatwaves since 1950 and their occurrence in the coming decades. *Environ. Res. Lett.* 10, 124003. doi:10.1088/1748-9326/10/12/124003.
Rusticucci, M., Barrucand, M., and Collazo, S. (2017). Temperature extremes in the Argentina central region and their monthly relationship with the mean circulation and ENSO phases. *Int. J. Climatol.* 37, 3003–3017. doi:10.1002/joc.4895.
Rutz, J. J., Shields, C. A., Lora, J. M., Payne, A. E., Guan, B., Ullrich, P., et al. (2019). The Atmospheric River Tracking Method Intercomparison Project (ARTMIP): Quantifying Uncertainties in Atmospheric River Climatology. *J. Geophys. Res. Atmos.*, 2019JD030936. doi:10.1029/2019JD030936.
Saha, S., Moorthi, S., Pan, H.-L., Wu, X., Wang, J., Nadiga, S., et al. (2010). The NCEP Climate Forecast System Reanalysis. *Bull. Am. Meteorol. Soc.* 91, 1015–1058. doi:10.1175/2010BAMS3001.1.
Salinger, J. (2013). New Zealand Climate : Patterns of Drought 1941 - 2013. *New Zeal. Clim. Patterns Drought 1941 - 2013* 32, 2–19.
Salnikov, V., Tutulina, G., Polyakova, S., Petrova, Y., and Skakova, A. (2015). Climate change in Kazakhstan during the past 70 years. *Quat. Int.* 358, 77–82. doi:10.1016/j.quaint.2014.09.008.
Salvi, K., and Ghosh, S. (2016). Projections of Extreme Dry and Wet Spells in the 21st Century India Using Stationary and Non-stationary Standardized Precipitation Indices. *Clim. Change* 139, 667–681. doi:10.1007/s10584-016-

1824-9.
Samaniego, L., Kumar, R., Breuer, L., Chamorro, A., Flörke, M., Pechlivanidis, I. G., et al. (2017). Propagation of forcing and model uncertainties on to hydrological drought characteristics in a multi-model century-long experiment in large river basins. *Clim. Change* 141, 435–449. doi:10.1007/s10584-016-1778-y.
Samaniego, L., Thober, S., Kumar, R., Wanders, N., Rakovec, O., Pan, M., et al. (2018). Anthropogenic warming exacerbates European soil moisture droughts. *Nat. Clim. Chang.* 8, 421–426. doi:10.1038/s41558-018-0138-5.
Samuels, R., Hochman, A., Baharad, A., Givati, A., Levi, Y., Yosef, Y., et al. (2018). Evaluation and projection of extreme precipitation indices in the Eastern Mediterranean based on CMIP5 multi-model ensemble. *Int. J. Climatol.* 38, 2280–2297. doi:10.1002/joc.5334.
Sanderson, B. M., Xu, Y., Tebaldi, C., Wehner, M., O'Neill, B., Jahn, A., et al. (2017a). Community climate simulations to assess avoided impacts in 1.5 and 2C futures. *Earth Syst. Dyn.* 8, 827–847. doi:10.5194/esd-8-827-2017.
Sanderson, M., Economou, T., Salmon, K., and Jones, S. (2017b). Historical Trends and Variability in Heat Waves in the United Kingdom. *Atmosphere (Basel).* 8, 117–191.
Sandvik, M. I., Sorteberg, A., and Rasmussen, R. (2018). Sensitivity of historical orographically enhanced extreme precipitation events to idealized temperature perturbations. *Clim. Dyn.* 50, 143–157. doi:10.1007/s00382-017-3593-1.
Sanginés de Cárcer, P., Vitasse, Y., Peñuelas, J., Jassey, V. E. J., Buttler, A., and Signarbieux, C. (2018). Vapor–pressure deficit and extreme climatic variables limit tree growth. *Glob. Chang. Biol.* 24, 1108–1122. Available at: https://www.scopus.com/inward/record.uri?eid=2-s2.0-85042151870&doi=10.1111%2Fgcb.13973&partnerID=40&md5=2707aef5820da66240718ff621b68f14.
Sanogo, S., Fink, A. H., Omotosho, J. A., Ba, A., Redl, R., and Ermert, V. (2015). Spatio-temporal characteristics of the recent rainfall recovery in West Africa. *Int. J. Climatol.* 35, 4589–4605. doi:10.1002/joc.4309.
Santer, B. D., Fyfe, J. C., Pallotta, G., Flato, G. M., Meehl, G. A., England, M. H., et al. (2017). Causes of differences in model and satellite tropospheric warming rates. *Nat. Geosci.* 10, 478.
Sarangi, C., Tripathi, S. N., Kanawade, V. P., Koren, I., and Pai, D. S. (2017). Investigation of the aerosol–cloud–rainfall association over the Indian summer monsoon region. *Atmos. Chem. Phys.* 17, 5185–5204. doi:10.5194/acp-17-5185-2017.
Satoh, M., Stevens, B., Judt, F., Khairoutdinov, M., Lin, S., and Putman, W. M. (2019). Global Cloud-Resolving Models. *Curr. Clim. Chang. Reports*. doi:10.1007/s40641-019-00131-0.
Satoh, M., Tomita, H., Yashiro, H., Kajikawa, Y., Miyamoto, Y., Yamaura, T., et al. (2017). Outcomes and challenges of global high-resolution non-hydrostatic atmospheric simulations using the K computer. *Prog. Earth Planet. Sci.* 4, 13. doi:10.1186/s40645-017-0127-8.
Satoh, M., Yamada, Y., Sugi, M., Komada, C., and Noda, A. T. (2015). Constraint on Future Change in Global Frequency of Tropical Cyclones due to Global Warming. *J. Meteorol. Soc. Japan. Ser. II* 93, 489–500. doi:10.2151/jmsj.2015-025.
Saurral, R. I., Camilloni, I. A., and Barros, V. R. (2017). Low-frequency variability and trends in centennial precipitation stations in southern South America. *Int. J. Climatol.* 37, 1774–1793. doi:10.1002/joc.4810.
Scaini, A., Sánchez, N., Vicente-Serrano, S. M., and Martínez-Fernández, J. (2015). SMOS-derived soil moisture anomalies and drought indices: A comparative analysis using in situ measurements. *Hydrol. Process.* 29. doi:10.1002/hyp.10150.
Scanlon, B. R., Zhang, Z., Save, H., Sun, A. Y., Müller Schmied, H., van Beek, L. P. H., et al. (2018). Global models underestimate large decadal declining and rising water storage trends relative to GRACE satellite data. *Proc. Natl. Acad. Sci.* 115, E1080–E1089. doi:10.1073/pnas.1704665115.
Schaaf, B., and Feser, F. (2018). Is there added value of convection-permitting regional climate model simulations for storms over the German Bight and Northern Germany? *Meteorol. Hydrol. Water Manag.* 6, 21–37. doi:10.26491/mhwm/85507.
Schaller, N., Kay, A. L., Lamb, R., Massey, N. R., van Oldenborgh, G. J., Otto, F. E. L., et al. (2016). Human influence on climate in the 2014 southern England winter floods and their impacts. *Nat. Clim. Chang.* 6, 627–634. doi:10.1038/nclimate2927.
Schaller, N., Otto, F. E. L., van Oldenborgh, G. J., Massey, N. R., Sparrow, S., and Allen, M. R. (2014). The heavy precipitation event of May-June 2013 in the upper Danube and Elbe basins. *Bull. Amer. Meteor. Soc.* 95, S69–S72.
Schaller, N., Sillmann, J., Anstey, J., Fischer, E. M., Grams, C. M., and Russo, S. (2018). Influence of blocking on Northern European and Western Russian heatwaves in large climate model ensembles. *Environ. Res. Lett.* 13. doi:10.1088/1748-9326/aaba55.
Schär, C., Ban, N., Fischer, E. M., Rajczak, J., Schmidli, J., Frei, C., et al. (2016). Percentile indices for assessing changes in heavy precipitation events. *Clim. Change* 137, 201–216. doi:10.1007/s10584-016-1669-2.
Scheff, J. (2018). Drought Indices, Drought Impacts, CO2, and Warming: a Historical and Geologic Perspective. *Curr.*

Clim. Chang. Reports 4, 202–209. doi:10.1007/s40641-018-0094-1.
Scheff, J., and Frierson, D. M. W. (2015). Terrestrial aridity and its response to greenhouse warming across CMIP5 climate models. *J. Clim.* 28, 5583–5600. doi:10.1175/JCLI-D-14-00480.1.
Scheff, J., Seager, R., Liu, H., and Coats, S. (2017). Are glacials dry? Consequences for paleoclimatology and for greenhouse warming. *J. Clim.* 30, 6593–6609. doi:10.1175/JCLI-D-16-0854.1.
Scherrer, S. C., Fischer, E. M., Posselt, R., Liniger, M. A., Croci-Maspoli, M., and Knutti, R. (2016). Emerging trends in heavy precipitation and hot temperature extremes in Switzerland. *J. Geophys. Res. Atmos.* 121, 2626–2637. doi:10.1002/2015JD024634.
Schewe, J., Heinke, J., Gerten, D., Haddeland, I., Arnell, N. W., Clark, D. B., et al. (2014). Multimodel assessment of water scarcity under climate change. *Proc. Natl. Acad. Sci. U. S. A.* 111, 3245–3250. doi:10.1073/pnas.1222460110.
Schleussner, C.-F., Pfleiderer, P., and Fischer, E. M. (2017). In the observational record half a degree matters. *Nat. Clim. Chang.* 7, 460–462. doi:10.1038/nclimate3320.
Schleussner, C. F., Vogel, M. M., Pfleiderer, P., Andrijevic, M., Otto, F. E. L., and Seneviratne, S. I. (submitted). Outpacing climate change ? – Development vs the emergence of extreme heat. *Proc. Natl. Acad. Sci.*(submitted).
Schmid, P. E., and Niyogi, D. (2017). Modeling Urban Precipitation Modification by Spatially Heterogeneous Aerosols. *J. Appl. Meteorol. Climatol.* 56, 2141–2153. doi:10.1175/JAMC-D-16-0320.1.
Schneider, D., Huggel, C., Cochachin, A., Guillén, S., and García, J. (2013). Mapping hazards from glacier lake outburst floods based on modelling of process cascades at Lake 513, Carhuaz, Peru. *Adv. Geosci.* 35, 145–155. doi:10.5194/adgeo-35-145-2014.
Schoetter, R., Cattiaux, J., and Douville, H. (2015). Changes of western European heat wave characteristics projected by the CMIP5 ensemble. *Clim. Dyn.* 45, 1601–1616. doi:10.1007/s00382-014-2434-8.
Schreck, C. J., Knapp, K. R., and Kossin, J. P. (2014). The impact of best track discrepancies on global tropical cyclone climatologies using IBTrACS. *Mon. Weather Rev.* 142, 3881–3899. doi:10.1175/MWR-D-14-00021.1.
Schubert, S. D., Stewart, R. E., Wang, H., Barlow, M., Berbery, E. H., Cai, W., et al. (2016). Global Meteorological Drought: A Synthesis of Current Understanding with a Focus on SST Drivers of Precipitation Deficits. *J. Clim.* 29, 3989–4019. doi:10.1175/JCLI-D-15-0452.1.
Schubert, S. D., Wang, H., Koster, R. D., Suarez, M. J., and Groisman, P. Y. (2014). Northern Eurasian heat waves and droughts. *J. Clim.* 27, 3169–3207. doi:10.1175/JCLI-D-13-00360.1.
Schumacher, D. L., Keune, J., van Heerwaarden, C. C., Vilà-Guerau de Arellano, J., Teuling, A. J., and Miralles, D. G. (2019). Amplification of mega-heatwaves through heat torrents fuelled by upwind drought. *Nat. Geosci.* 12, 712–717. doi:10.1038/s41561-019-0431-6.
Schumacher, R. S., and Johnson, R. H. (2005). Organization and Environmental Properties of Extreme-Rain-Producing Mesoscale Convective Systems. *Mon. Weather Rev.* 133, 961–976. doi:10.1175/MWR2899.1.
Schwanghart, W., Worni, R., Huggel, C., Stoffel, M., and Korup, O. (2016). Uncertainty in the Himalayan energy–water nexus: estimating regional exposure to glacial lake outburst floods. *Environ. Res. Lett.* 11, 074005. doi:10.1088/1748-9326/11/7/074005.
Schwingshackl, C., Davin, E. L., Hirschi, M., Sørland, S. L., Wartenburger, R., and Seneviratne, S. I. (2019). Regional climate model projections underestimate future warming due to missing plant physiological CO 2 response. *Environ. Res. Lett.* 14, 114019. doi:10.1088/1748-9326/ab4949.
Scoccimarro, E., Villarini, G., Vichi, M., Zampieri, M., Fogli, P. G., Bellucci, A., et al. (2015). Projected Changes in Intense Precipitation over Europe at the Daily and Subdaily Time Scales. *J. Clim.* 28, 6193–6203. doi:10.1175/JCLI-D-14-00779.1.
Seager, R., and Hoerling, M. (2014). Atmosphere and ocean origins of North American droughts. *J. Clim.* 27, 4581–4606. doi:10.1175/JCLI-D-13-00329.1.
Seager, R., Hooks, A., Williams, A. P., Cook, B., Nakamura, J., and Henderson, N. (2015). Climatology, variability, and trends in the U.S. Vapor pressure deficit, an important fire-related meteorological quantity. *J. Appl. Meteorol. Climatol.* 54, 1121–1141. Available at: https://www.scopus.com/inward/record.uri?eid=2-s2.0-84944111544&doi=10.1175%2FJAMC-D-14-0321.1&partnerID=40&md5=9260cd39519d65575e832323cc8f9002.
Seager, R., Nakamura, J., and Ting, M. (2019). Mechanisms of seasonal soil moisture drought onset and termination in the southern Great Plains. *J. Hydrometeorol.* 20, 751–771. doi:10.1175/JHM-D-18-0191.1.
Sedlmeier, K., Feldmann, H., and Schädler, G. (2018). Compound summer temperature and precipitation extremes over central Europe. *Theor. Appl. Climatol.* 131, 1493–1501. doi:10.1007/s00704-017-2061-5.
Seiler, C., Hutjes, R. W. A., and Kabat, P. (2013). Likely Ranges of Climate Change in Bolivia. *J. Appl. Meteorol. Climatol.* 52, 1303–1317. doi:10.1175/JAMC-D-12-0224.1.
Seiler, C., and Zwiers, F. W. (2016a). How well do CMIP5 climate models reproduce explosive cyclones in the extratropics of the Northern Hemisphere? *Clim. Dyn.* 46, 1241–1256. doi:10.1007/s00382-015-2642-x.
Seiler, C., and Zwiers, F. W. (2016b). How will climate change affect explosive cyclones in the extratropics of the

Northern Hemisphere? *Clim. Dyn.* 46, 3633–3644. doi:10.1007/s00382-015-2791-y.
Seiler, C., Zwiers, F. W., Hodges, K. I., and Scinocca, J. F. (2018). How does dynamical downscaling affect model biases and future projections of explosive extratropical cyclones along North America's Atlantic coast? *Clim. Dyn.* 50, 677–692. doi:10.1007/s00382-017-3634-9.
Sekizawa, S., Miyasaka, T., Nakamura, H., Shimpo, A., Takemura, K., and Maeda, S. (2019). Anomalous Moisture Transport and Oceanic Evaporation during a Torrential Rainfall Event over Western Japan in Early July 2018. *SOLA* 15A, 25–30. doi:10.2151/sola.15A-005.
Sen Roy, S., and Rouault, M. (2013). Spatial patterns of seasonal scale trends in extreme hourly precipitation in South Africa. *Appl. Geogr.* 39, 151–157. doi:https://doi.org/10.1016/j.apgeog.2012.11.022.
Şen, Z. (2018). *Flood Modeling, Prediction and Mitigation*. Cham: Springer International Publishing doi:10.1007/978-3-319-52356-9.
Senatore, A., Hejabi, S., Mendicino, G., Bazrafshan, J., and Irannejad, P. (2019). Climate conditions and drought assessment with the Palmer Drought Severity Index in Iran: evaluation of CORDEX South Asia climate projections (2070–2099). *Clim. Dyn.* 52, 865–891. doi:10.1007/s00382-018-4171-x.
Seneviratne, S. I., Corti, T., Davin, E. L., Hirschi, M., Jaeger, E. B., Lehner, I., et al. (2010). Investigating soil moisture-climate interactions in a changing climate: A review. *Earth-Science Rev.* 99, 125–161. doi:10.1016/j.earscirev.2010.02.004.
Seneviratne, S. I., Donat, M. G., Mueller, B., and Alexander, L. V. (2014). No pause in the increase of hot temperature extremes. *Nat. Clim. Chang.* 4, 161–163. doi:10.1038/nclimate2145.
Seneviratne, S. I., Donat, M. G., Pitman, A. J., Knutti, R., and Wilby, R. L. (2016). Allowable CO2emissions based on regional and impact-related climate targets. *Nature* 529, 477–483. doi:10.1038/nature16542.
Seneviratne, S. I., and Hauser, M. (submitted). Regional climate sensitivity of climate extremes in CMIP6 and CMIP5 multi-model ensembles. *Earth's Futur.*(submitted).
Seneviratne, S. I., Lehner, I., Gurtz, J., Teuling, A. J., Lang, H., Moser, U., et al. (2012a). Swiss prealpine Rietholzbach research catchment and lysimeter: 32 year time series and 2003 drought event. *Water Resour. Res.* 48. doi:10.1029/2011WR011749.
Seneviratne, S. I., Nicholls, N., Easterling, D., Goodess, C. M., Kanae, S., Kossin, J., et al. (2012b). "Changes in Climate Extremes and their Impacts on the Natural Physical Environment," in *Managing the Risks of Extreme Events and Disasters to Advance Climate Change Adaptation*, eds. C. B. Field, V. Barros, T. F. Stocker, and Q. Dahe (Cambridge, UK, and New York, NY, USA: Cambridge University Press), 109–230. doi:10.1017/CBO9781139177245.006.
Seneviratne, S. I., Phipps, S. J., Pitman, A. J., Hirsch, A. L., Davin, E. L., Donat, M. G., et al. (2018a). Land radiative management as contributor to regional-scale climate adaptation and mitigation. *Nat. Geosci.* 11, 88–96. doi:10.1038/s41561-017-0057-5.
Seneviratne, S. I., Rogelj, J., Séférian, R., Wartenburger, R., Allen, M. R., Cain, M., et al. (2018b). The many possible climates from the Paris Agreement's aim of 1.5 °C warming. *Nature* 558, 41–49. doi:10.1038/s41586-018-0181-4.
Seneviratne, S. I., Wartenburger, R., Guillod, B. P., Hirsch, A. L., Vogel, M. M., Brovkin, V., et al. (2018c). Climate extremes, land–climate feedbacks and land-use forcing at 1.5°C. *Philos. Trans. R. Soc. A Math. Phys. Eng. Sci.* 376, 20160450. doi:10.1098/rsta.2016.0450.
Seneviratne, S. I., Wilhelm, M., Stanelle, T., Van Den Hurk, B., Hagemann, S., Berg, A., et al. (2013). Impact of soil moisture-climate feedbacks on CMIP5 projections: First results from the GLACE-CMIP5 experiment. *Geophys. Res. Lett.* 40, 5212–5217. doi:10.1002/grl.50956.
Seo, Y.-W., Kim, H., Yun, K.-S., Lee, J.-Y., Ha, K.-J., and Moon, J.-Y. (2014). Future change of extreme temperature climate indices over East Asia with uncertainties estimation in the CMIP5. *Asia-Pacific J. Atmos. Sci.* 50, 609–624. doi:10.1007/s13143-014-0050-5.
Seo, Y.-W., Yun, K.-S., Lee, J.-Y., Lee, Y.-W., Ha, K.-J., and Jhun, J.-G. (2018). Future changes due to model biases in probabilities of extreme temperatures over East Asia using CMIP5 data. *Int. J. Climatol.* 38, 1177–1188. doi:10.1002/joc.5233.
Seong, M.-G., Min, S.-K., Kim, Y.-H., Zhang, X., and Sun, Y. (submitted). Anthropogenic greenhouse gas and aerosol contributions to extreme temperature changes during 1951-2015. *J. Clim.*(submitted).
Seth, A., Giannini, A., Rojas, M., Rauscher, S. A., Bordoni, S., Singh, D., et al. (2019). Monsoon Responses to Climate Changes—Connecting Past, Present and Future. *Curr. Clim. Chang. Reports*. doi:10.1007/s40641-019-00125-y.
Shaevitz, D. A., Camargo, S. J., Sobel, A. H., Jonas, J. A., Kim, D., Kumar, A., et al. (2014). Characteristics of tropical cyclones in high-resolution models in the present climate. *J. Adv. Model. Earth Syst.* 6, 1154–1172. doi:10.1002/2014MS000372.
Shanas, P. R., and Kumar, V. S. (2015). Trends in surface wind speed and significant wave height as revealed by ERA-Interim wind wave hindcast in the Central Bay of Bengal. *Int. J. Climatol.* 35, 2654–2663. doi:10.1002/joc.4164.
Sharma, A., Wasko, C., and Lettenmaier, D. P. (2018). If Precipitation Extremes Are Increasing, Why Aren't Floods?

Water Resour. Res. 54, 8545–8551. doi:10.1029/2018WR023749.
Sharma, S., and Mujumdar, P. (2017). Increasing frequency and spatial extent of concurrent meteorological droughts and heatwaves in India. *Sci. Rep.* 7, 15582. doi:10.1038/s41598-017-15896-3.
Sharmila, S., and Walsh, K. J. E. (2018). Recent poleward shift of tropical cyclone formation linked to Hadley cell expansion. *Nat. Clim. Chang.* doi:10.1038/s41558-018-0227-5.
Shashikanth, K., Ghosh, S., H, V., and Karmakar, S. (2018). Future projections of Indian summer monsoon rainfall extremes over India with statistical downscaling and its consistency with observed characteristics. *Clim. Dyn.* 51, 1–15. doi:10.1007/s00382-017-3604-2.
Shastri, H., Paul, S., Ghosh, S., and Karmakar, S. (2015). Impacts of urbanization on Indian summer monsoon rainfall extremes. *J. Geophys. Res. Atmos.* 120, 496–516. doi:10.1002/2014JD022061.
Shaw, T. A. A., Baldwin, M., Barnes, E. A. A., Caballero, R., Garfinkel, C. I. I., Hwang, Y.-T., et al. (2016). Storm track processes and the opposing influences of climate change. *Nat. Geosci.* 9, 656–664. doi:10.1038/ngeo2783.
Sheffield, J., Barrett, A. P., Colle, B., Fernando, D. N., Fu, R., Geil, K. L., et al. (2013). North American Climate in CMIP5 experiments. Part I: Evaluation of historical simulations of continental and regional climatology. *J. Clim.* 26, 9209–9245. doi:10.1175/JCLI-D-12-00592.1.
Sheffield, J., Wood, E. F., and Roderick, M. L. (2012). Little change in global drought over the past 60 years. *Nature* 491, 435–438. doi:10.1038/nature11575.
Sheikh, M. M., Manzoor, N., Ashraf, J., Adnan, M., Collins, D., Hameed, S., et al. (2015). Trends in extreme daily rainfall and temperature indices over South Asia. *Int. J. Climatol.* 35, 1625–1637. doi:10.1002/joc.4081.
Shekhar, A., and Shapiro, C. A. (2019). What do meteorological indices tell us about a long-term tillage study? *Soil Tillage Res.* 193, 161–170. Available at: https://www.scopus.com/inward/record.uri?eid=2-s2.0-85067273290&doi=10.1016%2Fj.still.2019.06.004&partnerID=40&md5=1f20cc15f8e93fe3625fd9af80b90003.
Shephard, M. W., Mekis, E., Morris, R. J., Feng, Y., Zhang, X., Kilcup, K., et al. (2014). Trends in Canadian Short-Duration Extreme Rainfall: Including an Intensity–Duration–Frequency Perspective. *Atmosphere-Ocean* 52, 398–417. doi:10.1080/07055900.2014.969677.
Shepherd, J. M. (2013). Impacts of Urbanization on Precipitation and Storms: Physical Insights and Vulnerabilities. *Clim. Vulnerability*, 109–125. doi:10.1016/B978-0-12-384703-4.00503-7.
Shepherd, T. G. (2014). Atmospheric circulation as a source of uncertainty in climate change projections. *Nat. Geosci.* 7, 703–708. doi:10.1038/NGEO2253.
Shepherd, T. G. (2016). A Common Framework for Approaches to Extreme Event Attribution. *Curr. Clim. Chang. Reports* 2, 28–38. doi:10.1007/s40641-016-0033-y.
Shepherd, T. G., Boyd, E., Calel, R. A., Chapman, S. C., Dessai, S., Dima-West, I. M., et al. (2018). Storylines: an alternative approach to representing uncertainty in physical aspects of climate change. *Clim. Change* 151, 555–571. doi:10.1007/s10584-018-2317-9.
Sherwood, S. C., Bony, S., and Dufresne, J.-L. (2014). Spread in model climate sensitivity traced to atmospheric convective mixing. *Nature* 505, 37–42. doi:10.1038/nature12829.
Sherwood, S., and Fu, Q. (2014). A Drier Future? *Science* 343, 737–739. doi:10.1126/science.1247620.
Shevchenko, O., Lee, H., Snizhko, S., and Mayer, H. (2014). Long-term analysis of heat waves in Ukraine. *Int. J. Climatol.* 34, 1642–1650. doi:10.1002/joc.3792.
Shi, Y., Wang, G., and Gao, X. (2017). Role of resolution in regional climate change projections over China. *Clim. Dyn.* 51, 2375–2396. doi:10.1007/s00382-017-4018-x.
Shimpo, A., Takemura, K., Wakamatsu, S., Togawa, H., Mochizuki, Y., Takekawa, M., et al. (2019). Primary Factors behind the Heavy Rain Event of July 2018 and the Subsequent Heat Wave in Japan. *SOLA* 15A, 13–18. doi:10.2151/sola.15A-003.
Shiogama, H., Imada, Y., Mori, M., Mizuta, R., Stone, D., Yoshida, K., et al. (2016). Attributing Historical Changes in Probabilities of Record-Breaking Daily Temperature and Precipitation Extreme Events. *SOLA* 12, 225–231. doi:10.2151/sola.2016-045.
Shiogama, H., Watanabe, M., Imada, Y., Mori, M., Ishii, M., and Kimoto, M. (2013). An event attribution of the 2010 drought in the South Amazon region using the MIROC5 model. *Atmos. Sci. Lett.* 14, 170–175. doi:10.1002/asl2.435.
Shkolnik, I. M., and Efimov, S. V. (2013). Cyclonic activity in high latitudes as simulated by a regional atmospheric climate model: Added value and uncertainties. *Environ. Res. Lett.* 8. doi:10.1088/1748-9326/8/4/045007.
Shkolnik, I., Pavlova, T., Efimov, S., and Zhuravlev, S. (2018). Future changes in peak river flows across northern Eurasia as inferred from an ensemble of regional climate projections under the IPCC RCP8.5 scenario. *Clim. Dyn.* 50, 215–230. doi:10.1007/s00382-017-3600-6.
Shope, J. B., Storlazzi, C. D., Erikson, L. H., and Hegermiller, C. A. (2016). Changes to extreme wave climates of islands within the Western Tropical Pacific throughout the 21st century under RCP 4.5 and RCP 8.5, with implications for island vulnerability and sustainability. *Glob. Planet. Change* 141, 25–38. Available at: https://www.scopus.com/inward/record.uri?eid=2-s2.0-

84964320719&doi=10.1016%2Fj.gloplacha.2016.03.009&partnerID=40&md5=c2d6b5e52bcd26af381f18e77406 2302.
Shukla, S., Safeeq, M., Aghakouchak, A., Guan, K., and Funk, C. (2015). Temperature impacts on the water year 2014 drought in California. *Geophys. Res. Lett.* 42, 4384–4393. doi:10.1002/2015GL063666.
Sigmond, M., Fyfe, J. C., and Swart, N. C. (2018). Ice-free Arctic projections under the Paris Agreement. *Nat. Clim. Chang.* 8, 404–408. doi:10.1038/s41558-018-0124-y.
Sikorska, A. E., Viviroli, D., and Seibert, J. (2015). Flood-type classification in mountainous catchments using crisp and fuzzy decision trees. *Water Resour. Res.* 51, 7959–7976. doi:10.1002/2015WR017326.
Sillmann, J., Donat, M. G., Fyfe, J. C., and Zwiers, F. W. (2014). Observed and simulated temperature extremes during the recent warming hiatus. *Environ. Res. Lett.* 9, 64023–64029.
Sillmann, J., Kharin, V. V., Zhang, X., Zwiers, F. W., and Bronaugh, D. (2013a). Climate extremes indices in the CMIP5 multimodel ensemble: Part 1. Model evaluation in the present climate. *J. Geophys. Res. Atmos.* 118, 1716–1733. doi:10.1002/jgrd.50203.
Sillmann, J., Kharin, V. V, Zwiers, F. W., Zhang, X., and Bronaugh, D. (2013b). Climate extremes indices in the CMIP5 multimodel ensemble: Part 2. Future climate projections. *J. Geophys. Res. Atmos.* 118, 2473–2493. doi:10.1002/jgrd.50188.
Sillmann, J., Stjern, C. W., Myhre, G., and Forster, P. M. (2017a). Slow and fast responses of mean and extreme precipitation to different forcing in CMIP5 simulations. *Geophys. Res. Lett.* 44, 6383–6390. doi:10.1002/2017GL073229.
Sillmann, J., Stjern, C. W., Myhre, G., Samset, B. H., Hodnebrog, Ø., Andrews, T., et al. (2019). Extreme wet and dry conditions affected differently by greenhouse gases and aerosols. *npj Clim. Atmos. Sci.* 2, 24. doi:10.1038/s41612-019-0079-3.
Sillmann, J., Thorarinsdottir, T., Keenlyside, N., Schaller, N., Alexander, L. V., Hegerl, G., et al. (2017b). Understanding, modeling and predicting weather and climate extremes: Challenges and opportunities. *Weather Clim. Extrem.* 18, 65–74. doi:10.1016/j.wace.2017.10.003.
Simmons, A. J., Willett, K. M., Jones, P. D., Thorne, P. W., and Dee, D. P. (2010). Low-frequency variations in surface atmospheric humidity, temperature, and precipitation: Inferences from reanalyses and monthly gridded observational data sets. *J. Geophys. Res. Atmos.* 115. doi:10.1029/2009JD012442.
Singh, D., Horton, D. E., Tsiang, M., Haugen, M., Ashfaq, M., Mei, R., et al. (2014). Severe precipitaiton in northern India in June 2013: Causes, historical context, and changes in probability. *Bull. Am. Meteorol. Soc.* 95, S58–S61.
Singh, D., Seager, R., Cook, B. I., Cane, M., Ting, M., Cook, E., et al. (2018). Climate and the Global Famine of 1876–78. *J. Clim.* 31, 9445–9467. doi:10.1175/JCLI-D-18-0159.1.
Singh, S., Ghosh, S., Sahana, A. S., Vittal, H., and Karmakar, S. (2017). Do dynamic regional models add value to the global model projections of Indian monsoon? *Clim. Dyn.* 48, 1375–1397. doi:10.1007/s00382-016-3147-y.
Singh, V., and Goyal, M. K. (2016). Changes in climate extremes by the use of CMIP5 coupled climate models over eastern Himalayas. *Environ. Earth Sci.* 75, 839. doi:10.1007/s12665-016-5651-0.
Sippel, S., El-Madany, T. S., Migliavacca, M., Mahecha, M. D., Carrara, A., Flach, M., et al. (2018a). Warm Winter, Wet Spring, and an Extreme Response in Ecosystem Functioning on the Iberian Peninsula. *Bull. Am. Meteorol. Soc.* 99, S80–S85. doi:10.1175/BAMS-D-17-0135.1.
Sippel, S., and Otto, F. E. L. (2014). Beyond climatological extremes - assessing how the odds of hydrometeorological extreme events in South-East Europe change in a warming climate. *Clim. Change* 125, 381–398. doi:10.1007/s10584-014-1153-9.
Sippel, S., Otto, F. E. L., Flach, M., and van Oldenborgh, G. J. (2016). The role of anthropogenic warming in 2015 central european heat waves. *Bull. Am. Meteorol. Soc.* 97, S51–S56. doi:10.1175/BAMS-D-16-0150.1.
Sippel, S., Reichstein, M., Ma, X., Mahecha, M. D., Lange, H., Flach, M., et al. (2018b). Drought, Heat, and the Carbon Cycle: a Review. *Curr. Clim. Chang. Reports* 4, 266–286. doi:10.1007/s40641-018-0103-4.
Sippel, S., Zscheischler, J., Heimann, M., Lange, H., Mahecha, M. D., van Oldenborgh, G. J., et al. (2017). Have precipitation extremes and annual totals been increasing in the world's dry regions over the last 60 years? *Hydrol. Earth Syst. Sci.* 21, 441–458. doi:10.5194/hess-21-441-2017.
Sippel, S., Zscheischler, J., Heimann, M., Otto, F. E. L., Peters, J., and Mahecha, M. D. (2015). Quantifying changes in climate variability and extremes: Pitfalls and their overcoming. *Geophys. Res. Lett.* 42, 9990–9998.
Siswanto, Jan van Oldenborgh, G., van der Schrier, G., Lenderink, G., and van den Hurk, B. (2015). Trends in High-Daily Precipitation Events in Jakarta and the Flooding of January 2014. *Bull. Am. Meteorol. Soc.* 96, S131–S135. doi:10.1175/BAMS-D-15-00128.1.
Skansi, M. de los M., Brunet, M., Sigró, J., Aguilar, E., Arevalo Groening, J. A., Bentancur, O. J., et al. (2013). Warming and wetting signals emerging from analysis of changes in climate extreme indices over South America. *Glob. Planet. Change* 100, 295–307. doi:10.1016/j.gloplacha.2012.11.004.
Smerdon, J. E., and Pollack, H. N. (2016). Reconstructing Earth's surface temperature over the past 2000 years: the science behind the headlines. *Wiley Interdiscip. Rev. Clim. Chang.* 7, 746–771. doi:10.1002/wcc.418.

Smith, B. K., Smith, J. A., Baeck, M. L., Villarini, G., and Wright, D. B. (2013). Spectrum of storm event hydrologic response in urban watersheds. *Water Resour. Res.* 49, 2649–2663. doi:10.1002/wrcr.20223.
Sobel, A. H., Camargo, S. J., Hall, T. M., Lee, C.-Y., Tippett, M. K., and Wing, A. A. (2016). Human influence on tropical cyclone intensity. *Science* 353, 242 LP – 246. doi:10.1126/science.aaf6574.
Sohn, B. J., Ryu, G.-H., Song, H.-J., and Ou, M.-L. (2013). Characteristic Features of Warm-Type Rain Producing Heavy Rainfall over the Korean Peninsula Inferred from TRMM Measurements. *Mon. Weather Rev.* 141, 3873–3888. doi:10.1175/MWR-D-13-00075.1.
Sohrabi, M. M., Ryu, J. H., Abatzoglou, J., and Tracy, J. (2015). Development of soil moisture drought index to characterize droughts. *J. Hydrol. Eng.* 20. doi:10.1061/(ASCE)HE.1943-5584.0001213.
Soltani, M., Laux, P., Kunstmann, H., Stan, K., Sohrabi, M. M., Molanejad, M., et al. (2016). Assessment of climate variations in temperature and precipitation extreme events over Iran. *Theor. Appl. Climatol.* 126. doi:10.1007/s00704-015-1609-5.
Song, J., and Klotzbach, P. J. (2018). What Has Controlled the Poleward Migration of Annual Averaged Location of Tropical Cyclone Lifetime Maximum Intensity Over the Western North Pacific Since 1961? *Geophys. Res. Lett.* 45, 1148–1156. doi:10.1002/2017GL076883.
Sonkoué, D., Monkam, D., Fotso-Nguemo, T. C., Yepdo, Z. D., and Vondou, D. A. (2019). Evaluation and projected changes in daily rainfall characteristics over Central Africa based on a multi-model ensemble mean of CMIP5 simulations. *Theor. Appl. Climatol.* 137, 2167–2186. doi:10.1007/s00704-018-2729-5.
Sorribas, M. V., Paiva, R. C. D., Melack, J. M., Bravo, J. M., Jones, C., Carvalho, L., et al. (2016). Projections of climate change effects on discharge and inundation in the Amazon basin. *Clim. Change* 136, 555–570. doi:10.1007/s10584-016-1640-2.
Sousa, P. M., Trigo, R. M., Barriopedro, D., Soares, P. M. M., Ramos, A. M., and Liberato, M. L. R. (2017). Responses of European precipitation distributions and regimes to different blocking locations. *Clim. Dyn.* 48, 1141–1160. doi:10.1007/s00382-016-3132-5.
Sparrow, S., Su, Q., Tian, F., Li, S., Chen, Y., Chen, W., et al. (2018). Attributing human influence on the July 2017 Chinese heatwave: the influence of sea-surface temperatures. *Environ. Res. Lett.* 13, 114004. doi:10.1088/1748-9326/aae356.
Spinoni, J., Barbosa, P., De Jager, A., McCormick, N., Naumann, G., Vogt, J. V., et al. (2019). A new global database of meteorological drought events from 1951 to 2016. *J. Hydrol. Reg. Stud.* 22, 100593. doi:10.1016/J.EJRH.2019.100593.
Spinoni, J., Naumann, G., Carrao, H., Barbosa, P., and Vogt, J. (2014). World drought frequency, duration, and severity for 1951-2010. *Int. J. Climatol.* 34, 2792–2804. doi:10.1002/joc.3875.
Spinoni, J., Naumann, G., and Vogt, J. (2015). Spatial patterns of European droughts under a moderate emission scenario. *Adv. Sci. Res.* 12, 179–186. doi:10.5194/asr-12-179-2015.
Spinoni, J., Naumann, G., and Vogt, J. V. (2017). Pan-European seasonal trends and recent changes of drought frequency and severity. *Glob. Planet. Change* 148, 113–130. doi:10.1016/j.gloplacha.2016.11.013.
Spinoni, J., Vogt, J. V, Barbosa, P., Dosio, A., McCormick, N., Bigano, A., et al. (2018a). Changes of heating and cooling degree-days in Europe from 1981 to 2100. *Int. J. Climatol.* 38, e191–e208. doi:10.1002/joc.5362.
Spinoni, J., Vogt, J. V, Naumann, G., Barbosa, P., and Dosio, A. (2018b). Will drought events become more frequent and severe in Europe? *Int. J. Climatol.* 38, 1718–1736. doi:10.1002/joc.5291.
Srivastava, A., Grotjahn, R., and Ullrich, P. A. (submitted). Evaluation of historical CMIP6 model simulations of extreme precipitation over contiguous US regions. *Weather Clim. Extrem.*(submitted).
Stagge, J. H., Kingston, D. G., Tallaksen, L. M., and Hannah, D. M. (2017). Observed drought indices show increasing divergence across Europe. *Sci. Rep.* 7. doi:10.1038/s41598-017-14283-2.
Staten, P. W., Lu, J., Grise, K. M., Davis, S. M., and Birner, T. (2018). Re-examining tropical expansion. *Nat. Clim. Chang.* 8, 768–775. doi:10.1038/s41558-018-0246-2.
Staudinger, M., Weiler, M., and Seibert, J. (2015). Quantifying sensitivity to droughts-an experimental modeling approach. *Hydrol. Earth Syst. Sci.* 19, 1371–1384. doi:10.5194/hess-19-1371-2015.
Stéfanon, M., Drobinski, P., D'Andrea, F., Lebeaupin-Brossier, C., and Bastin, S. (2014). Soil moisture-temperature feedbacks at meso-scale during summer heat waves over Western Europe. *Clim. Dyn.* 42, 1309–1324. doi:10.1007/s00382-013-1794-9.
Stegall, S. T., and Kunkel, K. E. (2017). Monthly Extreme Temperature Trends in CMIP5 Hindcast/Prediction Simulations, 1981–2010 and 2006–35. *J. Appl. Meteorol. Climatol.* 56, 1141–1154. doi:10.1175/JAMC-D-16-0281.1.
Stegehuis, A. I., Vautard, R., Ciais, P., Teuling, A. J., Jung, M., and Yiou, P. (2013). Summer temperatures in Europe and land heat fluxes in observation-based data and regional climate model simulations. *Clim. Dyn.* 41, 455–477. doi:10.1007/s00382-012-1559-x.
Stennett-Brown, R. K., Jones, J. J. P., Stephenson, T. S., and Taylor, M. A. (2017). Future Caribbean temperature and rainfall extremes from statistical downscaling. *Int. J. Climatol.* 37, 4828–4845. doi:10.1002/joc.5126.

Stephens, C. M., McVicar, T. R., Johnson, F. M., and Marshall, L. A. (2018). Revisiting Pan Evaporation Trends in Australia a Decade on. *Geophys. Res. Lett.* 45, 11,111-164,172. doi:10.1029/2018GL079332.
Sterling, S. M., Ducharne, A., and Polcher, J. (2013). The impact of global land-cover change on the terrestrial water cycle. *Nat. Clim. Chang.* 3, 385–390. doi:10.1038/nclimate1690.
Stillman, S., Zeng, X., and Bosilovich, M. G. (2016). Evaluation of 22 Precipitation and 23 Soil Moisture Products over a Semiarid Area in Southeastern Arizona. *J. Hydrometeorol.* 17, 211–230. doi:10.1175/JHM-D-15-0007.1.
Stocker, B. D., Zscheischler, J., Keenan, T. F., Prentice, I. C., Peñuelas, J., and Seneviratne, S. I. (2018). Quantifying soil moisture impacts on light use efficiency across biomes. *New Phytol.* 218, 1430–1449. doi:10.1111/nph.15123.
Stocker, B. D., Zscheischler, J., Keenan, T. F., Prentice, I. C., Seneviratne, S. I., and Peñuelas, J. (2019). Drought impacts on terrestrial primary production underestimated by satellite monitoring. *Nat. Geosci.* 12, 264–270. doi:10.1038/s41561-019-0318-6.
Stoelzle, M., Stahl, K., and Weiler, M. (2013). Are streamflow recession characteristics really characteristic? *Hydrol. Earth Syst. Sci.* 17, 817–828. Available at: https://www.scopus.com/inward/record.uri?eid=2-s2.0-84879034008&doi=10.5194%2Fhess-17-817-2013&partnerID=40&md5=f8848ffbb6dcccc1767bad5a017d9ca7.
Stoffel, M., and Corona, C. (2018). Future winters glimpsed in the Alps. *Nat. Geosci.* 11, 458–460. doi:10.1038/s41561-018-0177-6.
Stott, P. A., Christidis, N., Otto, F. E. L., Sun, Y., Vanderlinden, J.-P., van Oldenborgh, G. J., et al. (2016). Attribution of extreme weather and climate-related events. *Wiley Interdiscip. Rev. Clim. Chang.* 7, 23–41. doi:10.1002/wcc.380.
Stratton, R. A., Senior, C. A., Vosper, S. B., Folwell, S. S., Boutle, I. A., Earnshaw, P. D., et al. (2018). A Pan-African Convection-Permitting Regional Climate Simulation with the Met Office Unified Model: CP4-Africa. *J. Clim.* 31, 3485–3508. doi:10.1175/JCLI-D-17-0503.1.
Strauch, A. M., MacKenzie, R. A., Giardina, C. P., and Bruland, G. L. (2015). Climate driven changes to rainfall and streamflow patterns in a model tropical island hydrological system. *J. Hydrol.* 523, 160–169. Available at: https://www.scopus.com/inward/record.uri?eid=2-s2.0-84922311736&doi=10.1016%2Fj.jhydrol.2015.01.045&partnerID=40&md5=869acaef8fbc8a3615f3bc26a59dab91.
Strong, J. D. O., Vecchi, G. A., and Ginoux, P. (2018). The Climatological Effect of Saharan Dust on Global Tropical Cyclones in a Fully Coupled GCM. *J. Geophys. Res. Atmos.* 123, 5538–5559. doi:10.1029/2017JD027808.
Studholme, J., and Gulev, S. (2018). Concurrent Changes to Hadley Circulation and the Meridional Distribution of Tropical Cyclones. *J. Clim.* 31, 4367–4389. doi:10.1175/JCLI-D-17-0852.1.
Sugi, M., Murakami, H., and Yoshida, K. (2017). Projection of future changes in the frequency of intense tropical cyclones. *Clim. Dyn.* 49, 619–632. doi:10.1007/s00382-016-3361-7.
Sugi, M., Murakami, H., and Yoshimura, J. (2012). On the Mechanism of Tropical Cyclone Frequency Changes Due to Global Warming. *J. Meteorol. Soc. Japan* 90A, 397–408. doi:10.2151/jmsj.2012-A24.
Sugi, M., Yamada, Y., Yoshida, K., Mizuta, R., Nakano, M., Kodama, C., et al. (submitted). Future changes in frequency of tropical cyclone seeds. *SOLA*(submitted).
Sui, C., Zhang, Z., Yu, L., Li, Y., and Song, M. (2017). Investigation of Arctic air temperature extremes at north of 60N in winter. *Acta Oceanol. Sin.* 36, 51–60. doi:10.1007/s13131-017-1137-5.
Sui, Y., Lang, X., and Jiang, D. (2018). Projected signals in climate extremes over China associated with a 2 °C global warming under two RCP scenarios. *Int. J. Climatol.* 38, e678–e697. doi:10.1002/joc.5399.
Sun, J., Wang, D., Hu, X., Ling, Z., and Wang, L. (2019a). Ongoing Poleward Migration of Tropical Cyclone Occurrence Over the Western North Pacific Ocean. *Geophys. Res. Lett.* 46, 9110–9117. doi:10.1029/2019GL084260.
Sun, Q., and Miao, C. (2018). Extreme Rainfall (R20mm, RX5day) in Yangtze–Huai, China, in June–July 2016: The Role of ENSO and Anthropogenic Climate Change. *Bull. Am. Meteorol. Soc.* 99, S102–S106. doi:10.1175/BAMS-D-17-0091.1.
Sun, Q., Zhang, X., Zwiers, F., Westra, S., and Alexander, L. (submitted). A Global, continental and regional analysis of changes in extreme precipitation. *J. Clim.*(submitted).
Sun, Q., Zwiers, F., Zhang, X., and Li, G. (2019b). A comparison of intra-annual and long-term trend scaling of extreme precipitation with temperature in a large-ensemble regional climate simulation. *J. Clim.* Under Revi.
Sun, X. B., Ren, G. Y., Shrestha, A. B., Ren, Y. Y., You, Q. L., Zhan, Y. J., et al. (2017). Changes in extreme temperature events over the Hindu Kush Himalaya during 1961–2015. *Adv. Clim. Chang. Res.* 8, 157–165. doi:10.1016/j.accre.2017.07.001.
Sun, Y., Hu, T., and Zhang, X. (2018a). Substantial Increase in Heat Wave Risks in China in a Future Warmer World. *Earth's Futur.* 6, 1528–1538. doi:10.1029/2018EF000963.
Sun, Y., Hu, T., Zhang, X., Li, C., Lu, C., Ren, G., et al. (2019c). Contribution of Global warming and Urbanization to Changes in Temperature Extremes in Eastern China. *Geophys. Res. Lett.* 46, 11426–11434.

doi:10.1029/2019GL084281.
Sun, Y., Hu, T., Zhang, X., Wan, H., Stott, P., and Lu, C. (2018b). Anthropogenic Influence on the Eastern China 2016 Super Cold Surge. *Bull. Am. Meteorol. Soc.* 99, S123–S127. doi:10.1175/BAMS-D-17-0092.1.
Sun, Y., Zhang, X., Zwiers, F. W., Song, L., Wan, H., Hu, T., et al. (2014). Rapid increase in the risk of extreme summer heat in Eastern China. *Nat. Clim. Chang.* 4, 1082–1085. doi:10.1038/nclimate2410.
Sun, Z., Ouyang, Z., Zhao, J., Li, S., Zhang, X., and Ren, W. (2018c). Recent rebound in observational large-pan evaporation driven by heat wave and droughts by the Lower Yellow River. *J. Hydrol.* 565, 237–247. doi:10.1016/J.JHYDROL.2018.08.014.
Sunyer, M. A., Hundecha, Y., Lawrence, D., Madsen, H., Willems, P., Martinkova, M., et al. (2015). Inter-comparison of statistical downscaling methods for projection of extreme precipitation in Europe. *Hydrol. Earth Syst. Sci.* 19, 1827–1847. doi:10.5194/hess-19-1827-2015.
Supari, Tangang, F., Juneng, L., and Aldrian, E. (2017). Observed changes in extreme temperature and precipitation over Indonesia. *Int. J. Climatol.* 37, 1979–1997. doi:10.1002/joc.4829.
Sutton, R. T. (2018). ESD Ideas: a simple proposal to improve the contribution of IPCC WGI to the assessment and communication of climate change risks. *Earth Syst. Dynam.* 9, 1155–1158. doi:10.5194/esd-9-1155-2018.
Sutton, R. T. (2019). Climate Science Needs to Take Risk Assessment Much More Seriously. *Bull. Am. Meteorol. Soc.* 100, 1637–1642. doi:10.1175/BAMS-D-18-0280.1.
Swain, D. L., Langenbrunner, B., Neelin, J. D., and Hall, A. (2018). Increasing precipitation volatility in twenty-first-century California. *Nat. Clim. Chang.* 8, 427–433. doi:10.1038/s41558-018-0140-y.
Swain, D. L., Tsiang, M., Haugen, M., Singh, D., Charland, A., Rajaratnam, B., et al. (2014). The Extraordinary California Drought of 2013 / 2014 : Character , Context , and the Role of Climate Change. *Bull. Amer. Meteor. Soc.* 95, S3–S7.
Swain, S., and Hayhoe, K. (2015). CMIP5 projected changes in spring and summer drought and wet conditions over North America. *Clim. Dyn.* 44, 2737–2750. doi:10.1007/s00382-014-2255-9.
Swann, A. L. S. (2018). Plants and Drought in a Changing Climate. *Curr. Clim. Chang. Reports* 4, 192–201. doi:10.1007/s40641-018-0097-y.
Swann, A. L. S., Hoffman, F. M., Koven, C. D., and Randerson, J. T. (2016). Plant responses to increasing CO2 reduce estimates of climate impacts on drought severity. *Proc. Natl. Acad. Sci.* 113, 10019–10024. doi:10.1073/pnas.1604581113.
Swierczynski, T., Lauterbach, S., Dulski, P., Delgado, J., Merz, B., and Brauer, A. (2013). Mid- to late Holocene flood frequency changes in the northeastern Alps as recorded in varved sediments of Lake Mondsee (Upper Austria). *Quat. Sci. Rev.* 80, 78–90. doi:10.1016/j.quascirev.2013.08.018.
Syafrina, A. H., Zalina, M. D., and Juneng, L. (2015). Historical trend of hourly extreme rainfall in Peninsular Malaysia. *Theor. Appl. Climatol.* 120, 259–285. doi:10.1007/s00704-014-1145-8.
Sylla, M. B., Elguindi, N., Giorgi, F., and Wisser, D. (2016). Projected robust shift of climate zones over West Africa in response to anthropogenic climate change for the late 21st century. *Clim. Change* 134, 241–253. doi:10.1007/s10584-015-1522-z.
Szeto, K., Gysbers, P., Brimelow, J., and Stewart, R. (2015). The 2014 Extreme Flood on the Southeastern Canadian Prairies. *Bull. Am. Meteorol. Soc.* 96, S20–S24. doi:10.1175/BAMS-D-15-00110.1.
Szeto, K., Zhang, X., White, R. E., and Brimelow, J. (2016). The 2015 Extreme Drought in Western Canada. *Bull. Am. Meteorol. Soc.* 97, S42–S46. doi:10.1175/BAMS-D-16-0147.1.
Tabari, H., and Aghajanloo, M.-B. (2013). Temporal pattern of aridity index in Iran with considering precipitation and evapotranspiration trends. *Int. J. Climatol.* 33, 396–409. doi:10.1002/joc.3432.
Tabari, H., and Willems, P. (2018). More prolonged droughts by the end of the century in the Middle East. *Environ. Res. Lett.* 13. doi:10.1088/1748-9326/aae09c.
Tai, A. P. K., Martin, M. V., and Heald, C. L. (2014). Threat to future global food security from climate change and ozone air pollution. *Nat. Clim. Chang.* 4, 817–821. doi:10.1038/nclimate2317.
Tai, A. P. K., and Val Martin, M. (2017). Impacts of ozone air pollution and temperature extremes on crop yields: Spatial variability, adaptation and implications for future food security. *Atmos. Environ.* 169, 11–21. doi:10.1016/j.atmosenv.2017.09.002.
Takagi, H., Esteban, M., Mikami, T., and Fujii, D. (2016). Projection of coastal floods in 2050 Jakarta. *Urban Clim.* 17, 135–145. Available at: https://www.scopus.com/inward/record.uri?eid=2-s2.0-84977591169&doi=10.1016%2Fj.uclim.2016.05.003&partnerID=40&md5=f5064f1b585cfbc247b5e5e3305175f6.
Takahashi, C., Watanabe, M., and Mori, M. (2017). Significant Aerosol Influence on the Recent Decadal Decrease in Tropical Cyclone Activity Over the Western North Pacific. *Geophys. Res. Lett.* 44, 9496–9504. doi:10.1002/2017GL075369.
Takahashi, C., Watanabe, M., Shiogama, H., Imada, Y., and Mori, M. (2016). A Persistent Japanese Heat Wave in Early August 2015: Roles of Natural Variability and Human-Induced Warming. *Bull. Am. Meteorol. Soc.* 97,

S107–S112. doi:10.1175/BAMS-D-16-0157.1.
Takayabu, I., Hibino, K., Sasaki, H., Shiogama, H., Mori, N., Shibutani, Y., et al. (2015). Climate change effects on the worst-case storm surge: a case study of Typhoon Haiyan. *Environ. Res. Lett.* 10, 064011. doi:10.1088/1748-9326/10/6/064011.
Takemi, T., and Unuma, T. (2019). Diagnosing Environmental Properties of the July 2018 Heavy Rainfall Event in Japan. *SOLA* 15A, 60–65. doi:10.2151/sola.15A-011.
Takemura, K., Wakamatsu, S., Togawa, H., Shimpo, A., Kobayashi, C., Maeda, S., et al. (2019). Extreme Moisture Flux Convergence over Western Japan during the Heavy Rain Event of July 2018. *SOLA* 15A, 49–54. doi:10.2151/sola.15A-009.
Tallaksen, L. M., and Stahl, K. (2014). Spatial and temporal patterns of large-scale droughts in Europe: Model dispersion and performance. *Geophys. Res. Lett.* 41, 429–434. doi:10.1002/2013GL058573.
Tam, B. Y., Szeto, K., Bonsal, B., Flato, G., Cannon, A. J., and Rong, R. (2019). CMIP5 drought projections in Canada based on the Standardized Precipitation Evapotranspiration Index. *Can. Water Resour. J.* 44, 90–107. Available at: https://www.scopus.com/inward/record.uri?eid=2-s2.0-85057759729&doi=10.1080%2F07011784.2018.1537812&partnerID=40&md5=c2eefdd0899ddc96d76ea4f4996417a9.
Tamarin-Brodsky, T., Hodges, K., Hoskins, B. J., and Shepherd, T. G. (2019). A dynamical perspective on atmospheric temperature variability and its response to climate change. *J. Clim.* 32, 1707–1724. doi:10.1175/JCLI-D-18-0462.1.
Tamura, T., Nicholas, W. A., Oliver, T. S. N., and Brooke, B. P. (2018). Coarse-sand beach ridges at Cowley Beach, north-eastern Australia: Their formative processes and potential as records of tropical cyclone history. *Sedimentology* 65, 721–744. doi:10.1111/sed.12402.
Tandon, N. F., Nie, J., and Zhang, X. (2018a). Strong Influence of Eddy Length on Boreal Summertime Extreme Precipitation Projections. *Geophys. Res. Lett.* 45, 10,665-10,672. doi:10.1029/2018GL079327.
Tandon, N. F., Zhang, X., and Sobel, A. H. (2018b). Understanding the Dynamics of Future Changes in Extreme Precipitation Intensity. *Geophys. Res. Lett.* 45, 2870–2878. doi:10.1002/2017GL076361.
Tangang, F., Supari, S., Chung, J. X., Cruz, F., Salimun, E., Ngai, S. T., et al. (2018). Future changes in annual precipitation extremes over Southeast Asia under global warming of 2°C. *APN Sci. Bull.* 8, 6–11. doi:10.30852/sb.2018.436.
Tauvale, L., and Tsuboki, K. (2019). Characteristics of Tropical Cyclones in the Southwest Pacific. *J. Meteorol. Soc. Japan. Ser. II* 97, 711–731. doi:10.2151/jmsj.2019-042.
Taylor, C. M., Belusic, D., Guichard, F., Parker, D. J., Vischel, T., Bock, O., et al. (2017). Frequency of extreme Sahelian storms tripled since 1982 in satellite observations. *Nature* 544, 475–478. doi:10.1038/nature22069.
Taylor, C. M., de Jeu, R. A. M., Guichard, F., Harris, P. P., and Dorigo, W. A. (2012). Afternoon rain more likely over drier soils. *Nature* 489, 423–426. doi:10.1038/nature11377.
Tebaldi, C., and Knutti, R. (2018). Evaluating the accuracy of climate change pattern emulation for low warming targets. *Environ. Res. Lett.* 13, 055006. doi:10.1088/1748-9326/aabef2.
Tebaldi, C., and Wehner, M. F. (2018). Benefits of mitigation for future heat extremes under RCP4.5 compared to RCP8.5. *Clim. Change* 146, 349–361. doi:10.1007/s10584-016-1605-5.
Tehrany, M. S., Pradhan, B., and Jebur, M. N. (2014). Flood susceptibility mapping using a novel ensemble weights-of-evidence and support vector machine models in GIS. *J. Hydrol.* 512, 332–343. Available at: https://www.scopus.com/inward/record.uri?eid=2-s2.0-84897880041&doi=10.1016%2Fj.jhydrol.2014.03.008&partnerID=40&md5=be57dac3cb7a11af98e53b00264dd9b5.
Tennille, S. A., and Ellis, K. N. (2017). Spatial and temporal trends in the location of the lifetime maximum intensity of tropical cyclones. *Atmosphere (Basel).* 8, 1–9. doi:10.3390/atmos8100198.
Teufel, B., Diro, G. T., Whan, K., Milrad, S. M., Jeong, D. I., Ganji, A., et al. (2017). Investigation of the 2013 Alberta flood from weather and climate perspectives. *Clim. Dyn.* 48, 2881–2899. Available at: https://www.scopus.com/inward/record.uri?eid=2-s2.0-84976273794&doi=10.1007%2Fs00382-016-3239-8&partnerID=40&md5=9c9076640b8072728cead900dec1b8c3.
Teufel, B., Sushama, L., Huziy, O., Diro, G. T., Jeong, D. I., Winger, K., et al. (2019). Investigation of the mechanisms leading to the 2017 Montreal flood. *Clim. Dyn.* 52, 4193–4206. doi:10.1007/s00382-018-4375-0.
Teuling, A. J. (2018). A hot future for European droughts. *Nat. Clim. Chang.* 8, 364–365. doi:10.1038/s41558-018-0154-5.
Teuling, A. J., de Badts, E., Jansen, F. A., Fuchs, R., Buitink, J., van Dijke, A. J., et al. (2019). Climate change, re-/afforestation, and urbanisation impacts on evapotranspiration and streamflow in Europe. *Hydrol. Earth Syst. Sci. Discuss.* 2019, 1–30. doi:10.5194/hess-2018-634.
Teuling, A. J., Van Loon, A. F., Seneviratne, S. I., Lehner, I., Aubinet, M., Heinesch, B., et al. (2013). Evapotranspiration amplifies European summer drought. *Geophys. Res. Lett.* 40, 2071–2075.

doi:10.1002/grl.50495.
Thackeray, C. W., DeAngelis, A. M., Hall, A., Swain, D. L., and Qu, X. (2018). On the Connection Between Global Hydrologic Sensitivity and Regional Wet Extremes. *Geophys. Res. Lett.* 45. doi:10.1029/2018GL079698.
Thiery, W., Davin, E. L., Lawrence, D. M., Hirsch, A. L., Hauser, M., and Seneviratne, S. I. (2017). Present-day irrigation mitigates heat extremes. *J. Geophys. Res. Atmos.* 122, 1403–1422. doi:10.1002/2016JD025740.
Thiery, W., Visser, A. J., Fischer, E. M., Hauser, M., Hirsch, A. L., Lawrence, D. M., et al. (in press). Warming of hot extremes alleviated by expanding irrigation. *Nat. Commun.* (in press).
Thober, S., Kumar, R., Wanders, N., Marx, A., Pan, M., Rakovec, O., et al. (2018). Multi-model ensemble projections of European river floods and high flows at 1.5, 2, and 3 degrees global warming. *Environ. Res. Lett.* 13, 014003. doi:10.1088/1748-9326/aa9e35.
Thorne, P. W., and Vose, R. S. (2010). Reanalyses Suitable for Characterizing Long-Term Trends. *Bull. Am. Meteorol. Soc.* 91, 353–361. doi:10.1175/2009BAMS2858.1.
Tian, L., Yuan, S., and Quiring, S. M. (2018). Evaluation of six indices for monitoring agricultural drought in the south-central United States. *Agric. For. Meteorol.* 249, 107–119. doi:10.1016/J.AGRFORMET.2017.11.024.
Tian, X., Shu, L., Wang, M., and Zhao, F. (2017). The impact of climate change on fire risk in Daxing'anling, China. *J. For. Res.* 28, 997–1006. doi:10.1007/s11676-017-0383-x.
Tijdeman, E., Hannaford, J., and Stahl, K. (2018). Human influences on streamflow drought characteristics in England and Wales. *Hydrol. Earth Syst. Sci.* 22, 1051–1064. doi:10.5194/hess-22-1051-2018.
Tilinina, N., Gulev, S. K., Rudeva, I., and Koltermann, P. (2013). Comparing cyclone life cycle characteristics and their interannual variability in different reanalyses. *J. Clim.* doi:10.1175/JCLI-D-12-00777.1.
Timmermans, B., Patricola, C., and Wehner, M. (2018). Simulation and analysis of extremehurricane-drivenwave climate under two ocean warming scenarios. *Oceanography* 31, 88–99. doi:10.5670/oceanog.2018.218.
Timmermans, B., Stone, D., Wehner, M., and Krishnan, H. (2017). Impact of tropical cyclones on modeled extreme wind-wave climate. *Geophys. Res. Lett.* 44, 1393–1401. doi:10.1002/2016GL071681.
Timmermans, B., Wehner, M., Cooley, D., O'Brien, T., and Krishnan, H. (2019). An evaluation of the consistency of extremes in gridded precipitation data sets. *Clim. Dyn.* 52, 6651–6670. doi:10.1007/s00382-018-4537-0.
Ting, M., Kossin, J. P., Camargo, S. J., and Li, C. (2019). Past and Future Hurricane Intensity Change along the U.S. East Coast. *Sci. Rep.* 9, 7795. doi:10.1038/s41598-019-44252-w.
Tochimoto, E., and Niino, H. (2018). Structure and Environment of Tornado-Spawning Extratropical Cyclones around Japan. *J. Meteorol. Soc. Japan* 96, 355–380. doi:10.2151/jmsj.2018-043.
Tokinaga, H., and Xie, S.-P. (2010). Wave- and Anemometer-Based Sea Surface Wind (WASWind) for Climate Change Analysis. *J. Clim.* 24, 267–285. doi:10.1175/2010JCLI3789.1.
Tölle, M. H., Schefczyk, L., and Gutjahr, O. (2018). Scale dependency of regional climate modeling of current and future climate extremes in Germany. *Theor. Appl. Climatol.* 134, 829–848. doi:10.1007/s00704-017-2303-6.
Tomas-Burguera, M., Vicente-Serrano, S. M., Grimalt, M., and Beguería, S. (2017). Accuracy of reference evapotranspiration (ETo) estimates under data scarcity scenarios in the Iberian Peninsula. *Agric. Water Manag.* 182, 103–116. doi:10.1016/j.agwat.2016.12.013.
Toreti, A., Belward, A., Perez-Dominguez, I., Naumann, G., Luterbacher, J., Cronie, O., et al. (2019). The Exceptional 2018 European Water Seesaw Calls for Action on Adaptation. *Earth's Futur.* 7, 652–663. doi:10.1029/2019EF001170.
Touma, D., Ashfaq, M., Nayak, M. A., Kao, S.-C., and Diffenbaugh, N. S. (2015). A multi-model and multi-index evaluation of drought characteristics in the 21st century. *J. Hydrol.* 526, 196–207. doi:10.1016/j.jhydrol.2014.12.011.
Tous, M., Zappa, G., Romero, R., Shaffrey, L., and Vidale, P. L. (2016). Projected changes in medicanes in the HadGEM3 N512 high-resolution global climate model. *Clim. Dyn.* 47, 1913–1924. doi:10.1007/s00382-015-2941-2.
Tozer, C., Risbey, J. S., Grose, M. R., Monselesan, D., Squire, D., Black, A., et al. (2020). A 1-day extreme rainfall event in Tasmania: Process evaluation and long tail attribution. *Bull. Am. Meteorol. Soc.* Available at: http://ametsoc.net/eee/2018/21_Tozer0219_w.pdf.
Trapp, R. J., Tessendorf, S. A., Godfrey, E. S., and Brooks, H. E. (2005). Tornadoes from Squall Lines and Bow Echoes. Part I: Climatological Distribution. *Weather Forecast.* 20, 23–34. doi:10.1175/WAF-835.1.
Trenary, L., DelSole, T., Doty, B., and Tippett, M. K. (2015). Was the Cold Eastern US Winter of 2014 Due to Increased Variability? *Bull. Am. Meteorol. Soc.* 96, S15–S19. doi:10.1175/BAMS-D-15-00138.1.
Trenary, L., DelSole, T., Tippett, M. K., and Doty, B. (2016). Extreme Eastern U.S. Winter of 2015 Not Symptomatic of Climate Change. *Bull. Am. Meteorol. Soc.* 97, S31–S35. doi:10.1175/BAMS-D-16-0156.1.
Trenberth, K. E. (1999). Conceptual Framework for Changes of Extremes of the Hydrological Cycle with Climate Change. *Clim. Change* 42, 327–339. doi:10.1023/A:1005488920935.
Trenberth, K. E., Dai, A., van der Schrier, G., Jones, P. D., Barichivich, J., Briffa, K. R., et al. (2014). Global warming and changes in drought. *Nat. Clim. Chang.* 4, 17. Available at: http://dx.doi.org/10.1038/nclimate2067.

Trenberth, K. E., Fasullo, J. T., and Shepherd, T. G. (2015). Attribution of climate extreme events. *Nat. Clim. Chang.* 5, 725–730. doi:10.1038/nclimate2657.
Trenberth, K., Lijing, C., Peter, J., Yongxin, Z., and John, F. (2018). Hurricane Harvey Links to Ocean Heat Content and Climate Change Adaptation. *Earth's Futur.* 6, 730–744. doi:10.1029/2018EF000825.
Trigg, M. A., Birch, C. E., Neal, J. C., Bates, P. D., Smith, A., Sampson, C. C., et al. (2016). The credibility challenge for global fluvial flood risk analysis. *Environ. Res. Lett.* 11, 094014. doi:10.1088/1748-9326/11/9/094014.
Trigo, R. M., Añel, J. A., Barriopedro, D., García-Herrera, R., Gimeno, L., Nieto, R., et al. (2013). The Record Winter Drought of 2011 – 12 in the Iberian Peninsula. *Bull. Am. Meteorol. Soc.*, S41–S45.
Trismidianto, and Satyawardhana, H. (2018). Mesoscale Convective Complexes (MCCs) over the Indonesian Maritime Continent during the ENSO events. *IOP Conf. Ser. Earth Environ. Sci.* 149, 12025. Available at: http://stacks.iop.org/1755-1315/149/i=1/a=012025.
Trnka, M., Brázdil, R., Balek, J., Semerádová, D., Hlavinka, P., Možný, M., et al. (2015a). Drivers of soil drying in the Czech Republic between 1961 and 2012. *Int. J. Climatol.* 35, 2664–2675. Available at: https://www.scopus.com/inward/record.uri?eid=2-s2.0-84937039492&doi=10.1002%2Fjoc.4167&partnerID=40&md5=40f69929dcfa3e119672d0aef8c5bddf.
Trnka, M., Brázdil, R., Možný, M., Štěpánek, P., Dobrovolný, P., Zahradníček, P., et al. (2015b). Soil moisture trends in the Czech Republic between 1961 and 2012. *Int. J. Climatol.* 35, 3733–3747. Available at: https://www2.scopus.com/inward/record.uri?eid=2-s2.0-84945483088&doi=10.1002%2Fjoc.4242&partnerID=40&md5=2ad52cdd58f682ea973d9032b5ea659f.
Troccoli, A., Muller, K., Coppin, P., Davy, R., Russell, C., and Hirsch, A. L. (2012). Long-term wind speed trends over Australia. *J. Clim.* 25, 170–183. doi:10.1175/2011JCLI4198.1.
Trzeciak, T. M., Knippertz, P., Pirret, J. S. R., and Williams, K. D. (2016). Can we trust climate models to realistically represent severe European windstorms? *Clim. Dyn.* 46, 3431–3451. doi:10.1007/s00382-015-2777-9.
Tsuboki, K., Yoshioka, M. K., Shinoda, T., Kato, M., Kanada, S., and Kitoh, A. (2015). Future increase of supertyphoon intensity associated with climate change. *Geophys. Res. Lett.* 42, 646–652. doi:10.1002/2014GL061793.
Tsuguti, H., Seino, N., Kawase, H., Imada, Y., Nakaegawa, T., and Takayabu, I. (2018). Meteorological overview and mesoscale characteristics of the Heavy Rain Event of July 2018 in Japan. *Landslides* 16, 363–371. doi:10.1007/s10346-018-1098-6.
Tsuji, H., Yokoyama, C., and Takayabu, Y. N. (2019). Contrasting features of the July 2018 heavy rainfall event and the 2017 Northern Kyushu rainfall event in Japan. *J. Meteorol. Soc. Japan* in review.
Türkeş, M., and Erlat, E. (2018). Variability and trends in record air temperature events of Turkey and their associations with atmospheric oscillations and anomalous circulation patterns. *Int. J. Climatol.* 38, 5182–5204. doi:10.1002/joc.5720.
Tuttle, S., and Salvucci, G. (2016). Atmospheric science: Empirical evidence of contrasting soil moisture-precipitation feedbacks across the United States. *Science* 352, 825–828. doi:10.1126/science.aaa7185.
Twardosz, R., and Kossowska-Cezak, U. (2013). Exceptionally hot summers in Central and Eastern Europe (1951-2010). *Theor. Appl. Climatol.* 112, 617–628. doi:10.1007/s00704-012-0757-0.
U.S. Department of Agriculture Economic Research Service (2016). Bulletin of the American Meteorological Society. Available at: http://hdl.handle.net/10261/110100 [Accessed August 21, 2018].
Udall, B., and Overpeck, J. (2017). The twenty-first century Colorado River hot drought and implications for the future. *Water Resour. Res.* 53, 2404–2418. doi:10.1002/2016WR019638.
Uhe, P., Otto, F. E. L., Haustein, K., van Oldenborgh, G. J., King, A. D., Wallom, D. C. H., et al. (2016). Comparison of methods: Attributing the 2014 record European temperatures to human influences. *Geophys. Res. Lett.* 43, 8685–8693. doi:10.1002/2016GL069568.
Uhe, P., Sjoukje, P., Sarah, K., Kasturi, S., Joyce, K., Emmah, M., et al. (2017). Attributing drivers of the 2016 Kenyan drought. *Int. J. Climatol.* 38, e554–e568. doi:10.1002/joc.5389.
Ukkola, A. M., Pitman, A. J., De Kauwe, M. G., Abramowitz, G., Herger, N., Evans, J. P., et al. (2018). Evaluating CMIP5 model agreement for multiple drought metrics. *J. Hydrometeorol.* 19, 969–988. doi:10.1175/JHM-D-17-0099.1.
UNFCCC (2015). Adoption of the Paris agreement. in Available at: http://unfccc.int/resource/docs/2015/cop21/eng/l09r01.pdf.
Uppala, S. M., KÅllberg, P. W., Simmons, A. J., Andrae, U., Bechtold, V. D. C., Fiorino, M., et al. (2005). The ERA-40 re-analysis. *Q. J. R. Meteorol. Soc.* 131, 2961–3012. doi:10.1256/qj.04.176.
Utsumi, N., Kim, H., Kanae, S., and Oki, T. (2017). Relative contributions of weather systems to mean and extreme global precipitation. *J. Geophys. Res.* 122, 152–167. doi:10.1002/2016JD025222.
Valverde, M. C., and Marengo, J. A. (2014). Extreme Rainfall Indices in the Hydrographic Basins of Brazil. *Open J. Mod. Hydrol.* 04, 10–26. doi:10.4236/ojmh.2014.41002.
van den Besselaar, E. J. M., Klein Tank, A. M. G., and Buishand, T. A. (2013). Trends in European precipitation

extremes over 1951–2010. *Int. J. Climatol.* 33, 2682–2689. doi:10.1002/joc.3619.
van den Hurk, B., Meijgaard, E. van, Valk, P. de, Heeringen, K.-J. van, and Gooijer, J. (2015). Analysis of a compounding surge and precipitation event in the Netherlands. *Environ. Res. Lett.* 10. Available at: http://iopscience.iop.org/article/10.1088/1748-9326/10/3/035001/meta.
Van Der Linden, E. C., Haarsma, R. J., and Van Der Schrier, G. (2019). Impact of climate model resolution on soil moisture projections in central-western Europe. *Hydrol. Earth Syst. Sci.* 23, 191–206. Available at: https://www.scopus.com/inward/record.uri?eid=2-s2.0-85060026642&doi=10.5194%2Fhess-23-191-2019&partnerID=40&md5=6b91a3e1ef86e3c131b169d92b0575f4.
van der Schrier, G., Barichivich, J., Briffa, K. R., and Jones, P. D. (2013). A scPDSI-based global data set of dry and wet spells for 1901-2009. *J. Geophys. Res. Atmos.* 118, 4025–4048. doi:10.1002/jgrd.50355.
van der Wiel, K., Kapnick, S. B., van Oldenborgh, G. J., Whan, K., Philip, S., Vecchi, G. A., et al. (2017). Rapid attribution of the August 2016 flood-inducing extreme precipitation in south Louisiana to climate change. *Hydrol. Earth Syst. Sci.* 21, 897–921. doi:10.5194/hess-21-897-2017.
van Dijk, A. I. J. M., Beck, H. E., Crosbie, R. S., de Jeu, R. A. M., Liu, Y. Y., Podger, G. M., et al. (2013). The Millennium Drought in southeast Australia (2001-2009): Natural and human causes and implications for water resources, ecosystems, economy, and society. *Water Resour. Res.* 49, 1040–1057. doi:10.1002/wrcr.20123.
Van Huijgevoort, M. H. J., Hazenberg, P., Van Lanen, H. A. J., Teuling, A. J., Clark, D. B., Folwell, S., et al. (2013). Global multimodel analysis of drought in runofffor the second half of the twentieth century. *J. Hydrometeorol.* 14, 1535–1552. doi:10.1175/JHM-D-12-0186.1.
Van Lanen, H. A. J., Wanders, N., Tallaksen, L. M., and Van Loon, A. F. (2013). Hydrological drought across the world: Impact of climate and physical catchment structure. *Hydrol. Earth Syst. Sci.* 17, 1715–1732. doi:10.5194/hess-17-1715-2013.
Van Loon, A. F., and Laaha, G. (2015). Hydrological drought severity explained by climate and catchment characteristics. *J. Hydrol.* 526, 3–14. doi:10.1016/j.jhydrol.2014.10.059.
Van Loon, A. F., Stahl, K., Di Baldassarre, G., Clark, J., Rangecroft, S., Wanders, N., et al. (2016). Drought in a human-modified world: Reframing drought definitions, understanding, and analysis approaches. *Hydrol. Earth Syst. Sci.* 20, 3631–3650. doi:10.5194/hess-20-3631-2016.
Van Loon, A. F., and Van Lanen, H. A. J. (2012). A process-based typology of hydrological drought. *Hydrol. Earth Syst. Sci.* 16, 1915–1946. Available at: https://www.scopus.com/inward/record.uri?eid=2-s2.0-84863846961&doi=10.5194%2Fhess-16-1915-2012&partnerID=40&md5=8642052ccee3e7a602304835ec5903ec.
van Oldenborgh, G. J., Mitchell-Larson, E., Vecchi, G. A., de Vries, H., Vautard, R., and Otto, F. (2019). Cold waves are getting milder in the northern midlatitudes. *Environ. Res. Lett.* 14, 114004. doi:10.1088/1748-9326/ab4867.
van Oldenborgh, G. J., Otto, F. E. L., Haustein, K., and AchutaRao, K. (2016). The Heavy Precipitation Event of December 2015 in Chennai, India. *Bull. Am. Meteorol. Soc.* 97, S87–S91. doi:10.1175/BAMS-D-16-0129.1.
van Oldenborgh, G. J., Philip, S., Kew, S., van Weele, M., Uhe, P., Otto, F., et al. (2018). Extreme heat in India and anthropogenic climate change. *Nat. Hazards Earth Syst. Sci.* 18, 365–381. doi:10.5194/nhess-18-365-2018.
van Oldenborgh, G. J., van der Wiel, K., Kew, S., Philip, S., Otto, F., Vautard, R., et al. (submitted). Pathways and pitfalls in extreme event attribution: reflections based on the WWA experience. *Bull. Am. Meteorol. Soc.*(submitted).
van Oldenborgh, G. J., van der Wiel, K., Sebastian, A., Singh, R., Arrighi, J., Otto, F., et al. (2017). Attribution of extreme rainfall from Hurricane Harvey, August 2017. *Environ. Res. Lett.* 12, 124009. Available at: http://stacks.iop.org/1748-9326/12/i=12/a=124009.
Vanden Broucke, S., Wouters, H., Demuzere, M., and van Lipzig, N. P. M. (2019). The influence of convection-permitting regional climate modeling on future projections of extreme precipitation: dependency on topography and timescale. *Clim. Dyn.* 52, 5303–5324. doi:10.1007/s00382-018-4454-2.
Varino, F., Arbogast, P., Joly, B., Riviere, G., Fandeur, M. L., Bovy, H., et al. (2018). Northern Hemisphere extratropical winter cyclones variability over the 20th century derived from ERA-20C reanalysis. *Clim. Dyn.* doi:10.1007/s00382-018-4176-5.
Vautard, R., Aalst, M. van, Boucher, O., Drouin, A., Haustein, K., Kreienkamp, F., et al. (submitted). Human contribution to the record-breaking June and July 2019 heat waves in Western Europe. *Environ. Res. Lett.*(submitted).
Vautard, R., Gobiet, A., Jacob, D., Belda, M., Colette, A., Déqué, M., et al. (2013). The simulation of European heat waves from an ensemble of regional climate models within the EURO-CORDEX project. *Clim. Dyn.* 41, 2555–2575. doi:10.1007/s00382-013-1714-z.
Vautard, R., Yiou, P., D'Andrea, F., de Noblet, N., Viovy, N., Cassou, C., et al. (2007). Summertime European heat and drought waves induced by wintertime Mediterranean rainfall deficit. *Geophys. Res. Lett.* 34. doi:10.1029/2006GL028001.
Vautard, R., Yiou, P., Otto, F., Stott, P., Christidis, N., Oldenborgh, G. J. van, et al. (2016). Attribution of human-

induced dynamical and thermodynamical contributions in extreme weather events. *Environ. Res. Lett.* 11, 114009. doi:10.1088/1748-9326/11/11/114009.
Veale, L., and Endfield, G. H. (2016). Situating 1816, the 'year without summer', in the UK. *Geogr. J.* 182, 318–330. doi:10.1111/geoj.12191.
Vecchi, G. A., Delworth, T. L., Murakami, H., Underwood, S. D., Wittenberg, A. T., Zeng, F., et al. (2019). Tropical cyclone sensitivities to CO2 doubling: roles of atmospheric resolution, synoptic variability and background climate changes. *Clim. Dyn.* doi:10.1007/s00382-019-04913-y.
Vecchi, G. A., and Soden, B. J. (2007a). Global warming and the weakening of the tropical circulation. *J. Clim.* 20, 4316–4340. doi:10.1175/JCLI4258.1.
Vecchi, G. A., and Soden, B. J. (2007b). Increased tropical Atlantic wind shear in model projections of global warming. *Geophys. Res. Lett.* 34. doi:10.1029/2006GL028905.
Vecchi, G. A., Soden, B. J., Wittenberg, A. T., Held, I. M., Leetmaa, A., and Harrison, M. J. (2006). Weakening of tropical Pacific atmospheric circulation due to anthropogenic forcing. *Nature* 441, 73–76. doi:10.1038/nature04744.
Velázquez, J. A., Schmid, J., Ricard, S., Muerth, M. J., Gauvin St-Denis, B., Minville, M., et al. (2013). An ensemble approach to assess hydrological models' contribution to uncertainties in the analysis of climate change impact on water resources. *Hydrol. Earth Syst. Sci.* 17, 565–578. Available at: https://www.scopus.com/inward/record.uri?eid=2-s2.0-84873691070&doi=10.5194%2Fhess-17-565-2013&partnerID=40&md5=2c31d16ac5a22caf88a656ff5f942688.
Veldkamp, T. I. E., Wada, Y., Aerts, J. C. J. H., Döll, P., Gosling, S. N. N., Liu, J., et al. (2017). Water scarcity hotspots travel downstream due to human interventions in the 20th and 21st century. *Nat. Commun.* 8, 15697. doi:10.1038/ncomms15697.
Vemula, S., Raju, K. S., Veena, S. S., and Kumar, A. S. (2019). Urban floods in Hyderabad, India, under present and future rainfall scenarios: a case study. *Nat. Hazards* 95, 637–655. Available at: https://www.scopus.com/inward/record.uri?eid=2-s2.0-85055866373&doi=10.1007%2Fs11069-018-3511-9&partnerID=40&md5=fc48f87908a0f3b7e436acd4c3b8b9ac.
Venkataraman, K., Tummuri, S., Medina, A., and Perry, J. (2016). 21st century drought outlook for major climate divisions of Texas based on CMIP5 multimodel ensemble: Implications for water resource management. *J. Hydrol.* 534, 300–316. Available at: https://www.scopus.com/inward/record.uri?eid=2-s2.0-84961313927&doi=10.1016%2Fj.jhydrol.2016.01.001&partnerID=40&md5=8efa9b18ec725eb88db452f7b489b18b.
Vera, C. S., and Díaz, L. (2015). Anthropogenic influence on summer precipitation trends over South America in CMIP5 models. *Int. J. Climatol.* 35, 3172–3177. doi:10.1002/joc.4153.
Vetter, T., Reinhardt, J., Flörke, M., van Griensven, A., Hattermann, F., Huang, S., et al. (2017). Evaluation of sources of uncertainty in projected hydrological changes under climate change in 12 large-scale river basins. *Clim. Change* 141, 419–433. Available at: https://www.scopus.com/inward/record.uri?eid=2-s2.0-84990909781&doi=10.1007%2Fs10584-016-1794-y&partnerID=40&md5=4560b7de04ebf79f7f2c2984dfbaf73b.
Vicente-Serrano, S., Domínguez-Castro, F., Murphy, C., Hannaford, J., Reig, F., Peña-Angulo, D., et al. (submitted). Long term variability and trends of droughts in Western Europe (1851-2018). *Int. J. Climatol.*(submitted).
Vicente-Serrano, S. M., Azorin-Molina, C., Sanchez-Lorenzo, A., Revuelto, J., Morán-Tejeda, E., Lõpez-Moreno, J. I., et al. (2014a). Sensitivity of reference evapotranspiration to changes in meteorological parameters in Spain (1961-2011). *Water Resour. Res.* 50. doi:10.1002/2014WR015427.
Vicente-Serrano, S. M., Bidegain, M., Tomas-Burguera, M., Dominguez-Castro, F., El Kenawy, A., McVicar, T. R., et al. (2018a). A comparison of temporal variability of observed and model-based pan evaporation over Uruguay (1973–2014). *Int. J. Climatol.* 38. doi:10.1002/joc.5179.
Vicente-Serrano, S. M., Lopez-Moreno, J.-I., Beguería, S., Lorenzo-Lacruz, J., Sanchez-Lorenzo, A., García-Ruiz, J. M., et al. (2014b). Evidence of increasing drought severity caused by temperature rise in southern Europe. *Environ. Res. Lett.* 9, 044001. doi:10.1088/1748-9326/9/4/044001.
Vicente-Serrano, S. M., McVicar, T., Miralles, D., Yang, Y., and Tomas-Burguera, M. (2020). Unravelling the influence of atmospheric evaporative demand on drought under climate dynamics. *Wiley Interdiscip. Rev. Clim. Chang.* doi:10.1002/wcc.632.
Vicente-Serrano, S. M., Nieto, R., Gimeno, L., Azorin-Molina, C., Drumond, A., El Kenawy, A., et al. (2018b). Recent changes of relative humidity: Regional connections with land and ocean processes. *Earth Syst. Dyn.* 9, 915–937. doi:10.5194/esd-9-915-2018.
Vicente-Serrano, S. M., Peña-Gallardo, M., Hannaford, J., Murphy, C., Lorenzo-Lacruz, J., Dominguez-Castro, F., et al. (2019a). Climate, irrigation, and land-cover change explain streamflow trends in countries bordering the Northeast Atlantic. *Geophys. Res. Lett.* 46, 10821–10833. Available at: https://doi.org/10.1029/2019GL084084.
Vicente-Serrano, S. M., Quiring, S., Peña-Gallardo, M., Domínguez-castro, F., and Yuan, S. (2019b). A review of environmental droughts: Increased risk under global warming? *Earth Sci.*

*Rev.*doi:https://doi.org/10.1016/j.earscirev.2019.102953.
Vicente-Serrano, S. M., Van der Schrier, G., Beguería, S., Azorin-Molina, C., Lopez-Moreno, J.-I. J.-I., der Schrier, G., et al. (2015). Contribution of precipitation and reference evapotranspiration to drought indices under different climates. *J. Hydrol.* 526, 42–54. doi:10.1016/j.jhydrol.2014.11.025.
Vicente-Serrano, S. M., Zabalza-Martínez, J., Borràs, G., López-Moreno, J. I., Pla, E., Pascual, D., et al. (2017a). Effect of reservoirs on streamflow and river regimes in a heavily regulated river basin of Northeast Spain. *Catena* 149. doi:10.1016/j.catena.2016.03.042.
Vicente-Serrano, S. M., Zabalza-Martínez, J., Borràs, G., López-Moreno, J. I., Pla, E., Pascual, D., et al. (2017b). Extreme hydrological events and the influence of reservoirs in a highly regulated river basin of northeastern Spain. *J. Hydrol. Reg. Stud.* 12, 13–32. doi:10.1016/j.ejrh.2017.01.004.
Vicente-Serrano, S. M., Domínguez-Castro, F., McVicar, T. R., Tomas-Burguera, M., Peña-Gallardo, M., Noguera, I., et al. (2019). Global characterization of hydrological and meteorological droughts under future climate change: The importance of timescales, vegetation-CO2 feedbacks and changes to distribution functions. *Int. J. Climatol.*, joc.6350. doi:10.1002/joc.6350.
Vikhamar-Schuler, D., Isaksen, K., Haugen, J. E., Tømmervik, H., Luks, B., Schuler, T. V., et al. (2016). Changes in Winter Warming Events in the Nordic Arctic Region. *J. Clim.* 29, 6223–6244. doi:10.1175/JCLI-D-15-0763.1.
Villafuerte, M. Q., and Matsumoto, J. (2015). Significant Influences of Global Mean Temperature and ENSO on Extreme Rainfall in Southeast Asia. *J. Clim.* 28, 1905–1919. doi:10.1175/JCLI-D-14-00531.1.
Villarini, G., Smith, J. A., and Vecchi, G. A. (2012). Changing Frequency of Heavy Rainfall over the Central United States. *J. Clim.* 26, 351–357. doi:10.1175/JCLI-D-12-00043.1.
Vimont, D. J., and Kossin, J. P. (2007). The Atlantic Meridional Mode and hurricane activity. *Geophys. Res. Lett.* 34. doi:10.1029/2007GL029683.
Vincent, L. A., Zhang, X., Mekis, É., Wan, H., and Bush, E. J. (2018). Changes in Canada's Climate: Trends in Indices Based on Daily Temperature and Precipitation Data. *Atmosphere-Ocean* 56, 332–349. doi:10.1080/07055900.2018.1514579.
Vogel, M. M., Hauser, M., and Seneviratne, S. I. (submitted, a). Projected changes in hot, dry and wet extreme events' clusters in CMIP6 multi-model ensemble. *Environ. Res. Lett.*(submitted).
Vogel, M. M., Orth, R., Cheruy, F., Hagemann, S., Lorenz, R., van den Hurk, B. J. J. M., et al. (2017). Regional amplification of projected changes in extreme temperatures strongly controlled by soil moisture-temperature feedbacks. *Geophys. Res. Lett.* 44, 1511–1519. doi:10.1002/2016GL071235.
Vogel, M. M., Zscheischler, J., Fischer, E., and Seneviratne, S. I. (submitted, b). Development of future heatwaves under different adaptation levels. *J. Geophys. Res. Atmos.*(submitted).
Vogel, M. M., Zscheischler, J., and Seneviratne, S. I. (2018). Varying soil moisture–atmosphere feedbacks explain divergent temperature extremes and precipitation projections in central Europe. *Earth Syst. Dyn.* 9, 1107–1125. doi:10.5194/esd-9-1107-2018.
Vogel, M. M., Zscheischler, J., Wartenburger, R., Dee, D., and Seneviratne, S. I. (2019). Concurrent 2018 Hot Extremes Across Northern Hemisphere Due to Human-Induced Climate Change. *Earth's Futur.* 7, 2019EF001189. doi:10.1029/2019EF001189.
Volosciuk, C., Maraun, D., Semenov, V. A., Tilinina, N., Gulev, S. K., and Latif, M. (2016). Rising Mediterranean Sea Surface Temperatures Amplify Extreme Summer Precipitation in Central Europe. *Sci. Rep.* 6, 32450. Available at: https://doi.org/10.1038/srep32450.
von Buttlar, J., Zscheischler, J., Rammig, A., Sippel, S., Reichstein, M., Knohl, A., et al. (2018). Impacts of droughts and extreme-temperature events on gross primary production and ecosystem respiration: a systematic assessment across ecosystems and climate zones. *Biogeosciences* 15, 1293–1318. doi:10.5194/bg-15-1293-2018.
Vose, R. S., Easterling, D. R., Kunkel, K. E., LeGrande, A. N., and Wehner, M. F. (2017). Ch. 6: Temperature Changes in the United States. Climate Science Special Report: Fourth National Climate Assessment, Volume I. , eds. D. J. Wuebbles, D. W. Fahey, K. A. Hibbard, D. J. Dokken, B. C. Stewart, and T. K. Maycock Washington, DC, DC, USA: U.S. Global Change Research Program doi:10.7930/J0N29V45.
Vousdoukas, M. I., Mentaschi, L., Voukouvalas, E., Bianchi, A., Dottori, F., and Feyen, L. (2018a). Climatic and socioeconomic controls of future coastal flood risk in Europe. *Nat. Clim. Chang.* 8, 776–780. Available at: https://www.scopus.com/inward/record.uri?eid=2-s2.0-85051428825&doi=10.1038%2Fs41558-018-0260-4&partnerID=40&md5=2e6095feaa9602099d15a1b4cd030c00.
Vousdoukas, M. I., Mentaschi, L., Voukouvalas, E., Verlaan, M., Jevrejeva, S., Jackson, L. P., et al. (2018b). Global probabilistic projections of extreme sea levels show intensification of coastal flood hazard. *Nat. Commun.* 9, 2360. doi:10.1038/s41467-018-04692-w.
Vousdoukas, M. I., Voukouvalas, E., Mentaschi, L., Dottori, F., Giardino, A., Bouziotas, D., et al. (2016). Developments in large-scale coastal flood hazard mapping. *Nat. Hazards Earth Syst. Sci.* 16, 1841–1853. Available at: https://www.scopus.com/inward/record.uri?eid=2-s2.0-84981495374&doi=10.5194%2Fnhess-16-1841-2016&partnerID=40&md5=6e156cc19d10d6fac4f0f8605d728fe2.

Vries, H., Lenderink, G., and Meijgaard, E. (2014). Future snowfall in western and central Europe projected with a high-resolution regional climate model ensemble. *Geophys. Res. Lett.* 41, 4294–4299. doi:10.1002/2014GL059724.
Wada, Y., van Beek, L. P. H., Wanders, N., and Bierkens, M. F. P. (2013). Human water consumption intensifies hydrological drought worldwide. *Environ. Res. Lett.* 8, 034036. doi:10.1088/1748-9326/8/3/034036.
Wadey, M., Brown, S., Nicholls, R. J., and Haigh, I. (2017). Coastal flooding in the Maldives: an assessment of historic events and their implications. *Nat. Hazards* 89, 131–159. Available at: https://www.scopus.com/inward/record.uri?eid=2-s2.0-85020740618&doi=10.1007%2Fs11069-017-2957-5&partnerID=40&md5=333b1d8235a8e8ed4c52f8b8373ba29d.
Wahl, T., Haigh, I. D., Nicholls, R. J., Arns, A., Dangendorf, S., Hinkel, J., et al. (2017). Understanding extreme sea levels for broad-scale coastal impact and adaptation analysis. *Nat. Commun.* 8. doi:10.1038/ncomms16075.
Wahl, T., Jain, S., Bender, J., Meyers, S. D., and Luther, M. E. (2015). Increasing risk of compound flooding from storm surge and rainfall for major US cities. *Nat. Clim. Chang.* 5, 1093. Available at: http://dx.doi.org/10.1038/nclimate2736.
Waliser, D., and Guan, B. (2017). Extreme winds and precipitation during landfall of atmospheric rivers. *Nat. Geosci.* 10, 179. Available at: http://dx.doi.org/10.1038/ngeo2894.
Walsh, K. J. E. E., Camargo, S. J., Vecchi, G. A., Daloz, A. S., Elsner, J., Emanuel, K., et al. (2015). Hurricanes and climate: The U.S. Clivar working group on hurricanes. *Bull. Am. Meteorol. Soc.* 96, 997–1017. doi:10.1175/BAMS-D-13-00242.1.
Walsh, K. J. E., McBride, J. L., Klotzbach, P. J., Balachandran, S., Camargo, S. J., Holland, G., et al. (2016). Tropical cyclones and climate change. *Wiley Interdiscip. Rev. Clim. Chang.* 7, 65–89. doi:10.1002/wcc.371.
Wan, H., Zhang, X., and Zwiers, F. (2019). Human influence on Canadian temperatures. *Clim. Dyn.* 52, 479–494. doi:10.1007/s00382-018-4145-z.
Wanders, N., and Van Lanen, H. A. J. (2015). Future discharge drought across climate regions around the world modelled with a synthetic hydrological modelling approach forced by three general circulation models. *Nat. Hazards Earth Syst. Sci.* 15, 487–504. doi:10.5194/nhess-15-487-2015.
Wanders, N., and Wada, Y. (2015). Human and climate impacts on the 21st century hydrological drought. *J. Hydrol.* 526, 208–220. doi:10.1016/j.jhydrol.2014.10.047.
Wang, H., Chen, Y., Xun, S., Lai, D., Fan, Y., and Li, Z. (2013a). Changes in daily climate extremes in the arid area of northwestern China. *Theor. Appl. Climatol.* 112, 15–28. doi:10.1007/s00704-012-0698-7.
Wang, H., Rogers, J. C., and Munroe, D. K. (2015). Commonly used drought indices as indicators of soil moisture in China. *J. Hydrometeorol.* 16, 1397–1408. Available at: https://www.scopus.com/inward/record.uri?eid=2-s2.0-84941275386&doi=10.1175%2FJHM-D-14-0076.1&partnerID=40&md5=6fa5738a4b53662c4ce9f2ccbc39b0fe.
Wang, H., and Schubert, S. (2014). 2 . CAUSES OF THE EXTREME DRY CONDITIONS OVER CALIFORNIA DURING EARLY 2013. *Bull. Amer. Meteor. Soc.*, S7–S11.
Wang, H., Vicente-serrano, S. M., Tao, F., Zhang, X., Wang, P., Zhang, C., et al. (2016a). Monitoring winter wheat drought threat in Northern China using multiple climate-based drought indices and soil moisture during 2000–2013. *Agric. For. Meteorol.* 228–229. doi:10.1016/j.agrformet.2016.06.004.
Wang, K., Dickinson, R. E., and Liang, S. (2012). Global atmospheric evaporative demand over land from 1973 to 2008. *J. Clim.* 25, 8353–8361. doi:10.1175/JCLI-D-11-00492.1.
Wang, P., Tang, J., Sun, X., Liu, J., and Juan, F. (2018a). Spatiotemporal characteristics of heat waves over China in regional climate simulations within the CORDEX-EA project. *Clim. Dyn.* doi:10.1007/s00382-018-4167-6.
Wang, S.-Y. S., Zhao, L., Yoon, J.-H., Klotzbach, P., and Gillies, R. R. (2018b). Quantitative attribution of climate effects on Hurricane Harvey's extreme rainfall in Texas. *Environ. Res. Lett.* 13, 54014.
Wang, X., Jiang, D., and Lang, X. (2017a). Future extreme climate changes linked to global warming intensity. *Sci. Bull.* 62, 1673–1680. doi:10.1016/j.scib.2017.11.004.
Wang, X. L., Feng, Y., Chan, R., and Isaac, V. (2016b). Inter-comparison of extra-tropical cyclone activity in nine reanalysis datasets. *Atmos. Res.* doi:10.1016/j.atmosres.2016.06.010.
Wang, X. L., Feng, Y., Compo, G. P., Swail, V. R., Zwiers, F. W., Allan, R. J., et al. (2013b). Trends and low frequency variability of extra-tropical cyclone activity in the ensemble of twentieth century reanalysis. *Clim. Dyn.* 40, 2775–2800. doi:10.1007/s00382-012-1450-9.
Wang, X. L., Trewin, B., Feng, Y., and Jones, D. (2013c). Historical changes in Australian temperature extremes as inferred from extreme value distribution analysis. *Geophys. Res. Lett.* 40, 573–578. doi:10.1002/grl.50132.
Wang, Y., Lee, K.-H., Lin, Y., Levy, M., and Zhang, R. (2014). Distinct effects of anthropogenic aerosols on tropical cyclones. *Nat. Clim. Chang.* 4, 368.
Wang, Y., Xie, Y., Dong, W., Ming, Y., Wang, J., and Shen, L. (2017b). Adverse effects of increasing drought on air quality via natural processes. *Atmos. Chem. Phys.* 17, 12827–12843. doi:10.5194/acp-17-12827-2017.
Wang, Y., Zhou, B., Qin, D., Wu, J., Gao, R., and Song, L. (2017c). Changes in mean and extreme temperature and precipitation over the arid region of northwestern China: Observation and projection. *Adv. Atmos. Sci.* 34, 289–

305. doi:10.1007/s00376-016-6160-5.
Wang, Z., Jiang, Y., Wan, H., Yan, J., and Zhang, X. (2017d). Detection and Attribution of Changes in Extreme Temperatures at Regional Scale. *J. Clim.* 30, 7035–7047. doi:10.1175/JCLI-D-15-0835.1.
Wang, Z., Lin, L., Zhang, X., Zhang, H., Liu, L., and Xu, Y. (2017e). Scenario dependence of future changes in climate extremes under 1.5 °C and 2 °C global warming. *Sci. Rep.* 7, 46432. doi:10.1038/srep46432.
Wang, Z., Zhong, R., Lai, C., Zeng, Z., Lian, Y., and Bai, X. (2018c). Climate change enhances the severity and variability of drought in the Pearl River Basin in South China in the 21st century. *Agric. For. Meteorol.* 249, 149–162. Available at: https://www.scopus.com/inward/record.uri?eid=2-s2.0-85036671028&doi=10.1016%2Fj.agrformet.2017.12.077&partnerID=40&md5=90eaeacdda0135ffb53d5ad72eb9d9f1.
Ward, K., Lauf, S., Kleinschmit, B., and Endlicher, W. (2016). Heat waves and urban heat islands in Europe: A review of relevant drivers. *Sci. Total Environ.* 569–570, 527–539. doi:10.1016/j.scitotenv.2016.06.119.
Ward, P. J., Couasnon, A., Eilander, D., Haigh, I. D., Hendry, A., Muis, S., et al. (2018). Dependence between high sea-level and high river discharge increases flood hazard in global deltas and estuaries. *Environ. Res. Lett.* 13, 084012. doi:10.1088/1748-9326/aad400.
Wartenburger, R., Hirschi, M., Donat, M. G., Greve, P., Pitman, A. J., and Seneviratne, S. I. (2017). Changes in regional climate extremes as a function of global mean temperature: an interactive plotting framework. *Geosci. Model Dev. Discuss.*, 1–30. doi:10.5194/gmd-2017-33.
Watterson, I. G., J. Bathols, and Heady, C. (2014). What influences the skill of climate models over the continents? *Bull. Amer. Meteor. Soc.* 95, 689–700. doi:http://dx.doi.org/10.1175/BAMS-D-12-00136.1.
Wehner, M. F. (submitted). Characterization of long period return values of extreme daily temperature and precipitation in the CMIP6 models: Part 2, projections of future change. *Weather Clim. Extrem.*(submitted).
Wehner, M. F., Arnold, J. R., Knutson, T., Kunkel, K. E., and LeGrande, A. N. (2017). Ch. 8: Droughts, Floods, and Wildfires. Climate Science Special Report: Fourth National Climate Assessment, Volume I. , eds. D. J. Wuebbles, D. W. Fahey, K. A. Hibbard, D. J. Dokken, B. C. Stewart, and T. K. Maycock Washington, DC, DC, USA: U.S. Global Change Research Program doi:10.7930/J0CJ8BNN.
Wehner, M. F., Gleckler, P., and Lee, J. (submitted). Characterization of long period return values of extreme daily temperature and precipitation in the CMIP6 models: Part 1, model evaluation. *Weather Clim. Extrem.*(submitted).
Wehner, M. F., Reed, K. A., Li, F., Prabhat, Bacmeister, J., Chen, C.-T., et al. (2014). The effect of horizontal resolution on simulation quality in the Community Atmospheric Model, CAM5.1. *J. Adv. Model. Earth Syst.* 6, 980–997. doi:10.1002/2013MS000276.
Wehner, M. F., Reed, K. A., Loring, B., Stone, D., and Krishnan, H. (2018a). Changes in tropical cyclones under stabilized 1.5 and 2.0 °C global warming scenarios as simulated by the Community Atmospheric Model under the HAPPI protocols. *Earth Syst. Dyn.* 9, 187–195. doi:10.5194/esd-9-187-2018.
Wehner, M., Prabhat, Reed, K. A., Stone, D., Collins, W. D., and Bacmeister, J. (2015). Resolution Dependence of Future Tropical Cyclone Projections of CAM5.1 in the U.S. CLIVAR Hurricane Working Group Idealized Configurations. *J. Clim.* 28, 3905–3925. doi:10.1175/JCLI-D-14-00311.1.
Wehner, M., Stone, D., Krishnan, H., AchutaRao, K., and Castillo, F. (2016). The Deadly Combination of Heat and Humidity in India and Pakistan in Summer 2015. *Bull. Am. Meteorol. Soc.* 97, S81–S86. doi:10.1175/BAMS-D-16-0145.1.
Wehner, M., Stone, D., Mitchell, D., Shiogama, H., Fischer, E., Graff, L. S., et al. (2018b). Changes in extremely hot days under stabilized 1.5 and 2.0°C global warming scenarios as simulated by the HAPPI multi-model ensemble. *Earth Syst. Dyn.* 9, 299–311. doi:10.5194/esd-9-299-2018.
Wehner, M., Stone, D., Shiogama, H., Wolski, P., Ciavarella, A., Christidis, N., et al. (2018c). Early 21st century anthropogenic changes in extremely hot days as simulated by the C20C+ detection and attribution multi-model ensemble. *Weather Clim. Extrem.* 20, 1–8. doi:10.1016/j.wace.2018.03.001.
Wehner, M., Zarzycki, C. M., and Patricola, C. (2018d). "Estimating the human influence on tropical cyclone intensity as the climate changes.," in *Hurricanes and climate change, volume 4*, ed. J. Collins.
Wehrli, K., Guillod, B. P., Hauser, M., Leclair, M., and Seneviratne, S. I. (2019). Identifying Key Driving Processes of Major Recent Heat Waves. *J. Geophys. Res. Atmos.* 124, 11746–11765. doi:10.1029/2019JD030635.
Wehrli, K., Hauser, M., and Seneviratne, S. I. (submitted). Storylines of the 2018 Northern Hemisphere heatwave at pre-industrial and higher global warming levels. *Earth Syst. Dynam.*(submitted).
Weir, T., Dovey, L., and Orcherton, D. (2017). Social and cultural issues raised by climate change in Pacific Island countries: an overview. *Reg. Environ. Chang.* 17, 1017–1028. Available at: https://www.scopus.com/inward/record.uri?eid=2-s2.0-84977072788&doi=10.1007%2Fs10113-016-1012-5&partnerID=40&md5=936fbf8002170cb8cb08d043e70b42bf.
Weldon, D., and Reason, C. J. C. (2014). Variability of rainfall characteristics over the South Coast region of South Africa. *Theor. Appl. Climatol.* 115, 177–185.
Wen, Q. H., Zhang, X., Xu, Y., and Wang, B. (2013). Detecting human influence on extreme temperatures in China.

Geophys. Res. Lett. 40, 1171–1176. doi:10.1002/grl.50285.
Westra, S., Alexander, L. V., and Zwiers, F. W. (2013). Global Increasing Trends in Annual Maximum Daily Precipitation. *J. Clim.* 26, 3904–3918. doi:10.1175/JCLI-D-12-00502.1.
Westra, S., Fowler, H. J., Evans, J. P., Alexander, L. V, Berg, P., Johnson, F., et al. (2014). Future changes to the intensity and frequency of short-duration extreme rainfall. *Rev. Geophys.* 52, 522–555. doi:10.1002/2014RG000464.
Westra, S., White, C. J., and Kiem, A. S. (2016). Introduction to the special issue: historical and projected climatic changes to Australian natural hazards. *Clim. Change* 139, 1–19. doi:10.1007/s10584-016-1826-7.
Wetter, O., and Pfister, C. (2013). An underestimated record breaking event – why summer 1540 was likely warmer than 2003. 41–56. doi:10.5194/cp-9-41-2013.
Wetter, O., Pfister, C., Werner, J. P., Zorita, E., Wagner, S., Seneviratne, S. I., et al. (2014). The year-long unprecedented European heat and drought of 1540 - a worst case. *Clim. Change* 125, 349–363. doi:10.1007/s10584-014-1184-2.
Wever, N. (2012). Quantifying trends in surface roughness and the effect on surface wind speed observations. *J. Geophys. Res. Atmos.* 117, 1–14. doi:10.1029/2011JD017118.
Whan, K., Alexander, L. V., Imielska, A., Mcgree, S., Jones, D., Ene, E., et al. (2014). Trends and variability of temperature extremes in the tropical Western Pacific. *Int. J. Climatol.* 34, 2585–2603. doi:10.1002/joc.3861.
Whan, K., Zscheischler, J., Orth, R., Shongwe, M., Rahimi, M., Asare, E. O., et al. (2015). Impact of soil moisture on extreme maximum temperatures in Europe. *Weather Clim. Extrem.* 9, 57–67. doi:10.1016/j.wace.2015.05.001.
Whan, K., and Zwiers, F. (2016). Evaluation of extreme rainfall and temperature over North America in CanRCM4 and CRCM5. *Clim. Dyn.* 46, 3821–3843. doi:10.1007/s00382-015-2807-7.
Wilcox, L. J., Yiou, P., Hauser, M., Lott, F. C., van Oldenborgh, G. J., Colfescu, I., et al. (2018). Multiple perspectives on the attribution of the extreme European summer of 2012 to climate change. *Clim. Dyn.* 50, 3537–3555. doi:10.1007/s00382-017-3822-7.
Wild, M., Gilgen, H., Roesch, A., Ohmura, A., Long, C. N., Dutton, E. G., et al. (2005). From Dimming to Brightening: Decadal Changes in Solar Radiation at Earth's Surface. *Science* 308, 847–850. doi:10.1126/science.1103215.
Wilhelm, B., Ballesteros Canovas, J. A., Corella Aznar, J. P., Kämpf, L., Swierczynski, T., Stoffel, M., et al. (2018). Recent advances in paleoflood hydrology: From new archives to data compilation and analysis. *Water Secur.* 3, 1–8. doi:10.1016/j.wasec.2018.07.001.
Wilhelm, B., Ballesteros Cánovas, J. A., Macdonald, N., Toonen, W. H. J., Baker, V., Barriendos, M., et al. (2019). Interpreting historical, botanical, and geological evidence to aid preparations for future floods. *Wiley Interdiscip. Rev. Water* 6, e1318. doi:10.1002/wat2.1318.
Wilhelm, M., Davin, E. L., and Seneviratne, S. I. (2015). Climate engineering of vegetated land for hot extremes mitigation: An Earth system model sensitivity study. *J. Geophys. Res. Atmos.* 120, 2612–2623. doi:10.1002/2014JD022293.
Wilhite, D. A., and Pulwarty, R. S. (2017). "Drought as Hazard: Understanding the Natural and Social Context," in *Drought and Water Crises: Integrating Science, Management, and Policy*, 3–22.
Willems, P. (2013). Multidecadal oscillatory behaviour of rainfall extremes in Europe. *Clim. Change* 120, 931–944. doi:10.1007/s10584-013-0837-x.
Willett, K. M., Dunn, R. J. H., Thorne, P. W., Bell, S., de Podesta, M., Parker, D. E., et al. (2014). HadISDH land surface multi-variable humidity and temperature record for climate monitoring. *Clim. Past* 10, 1983–2006.
Williams, A. P., Abatzoglou, J. T., Gershunov, A., Guzman-Morales, J., Bishop, D. A., Balch, J. K., et al. (2019). Observed Impacts of Anthropogenic Climate Change on Wildfire in California. *Earth's Futur.* 7, 892–910. doi:10.1029/2019EF001210.
Williams, A. P., Allen, C. D., Macalady, A. K., Griffin, D., Woodhouse, C. A., Meko, D. M., et al. (2013). Temperature as a potent driver of regional forest drought stress and tree mortality. *Nat. Clim. Chang.* 3, 292–297. doi:10.1038/nclimate1693.
Willison, J., Robinson, W. A., and Lackmann, G. M. (2013). The Importance of Resolving Mesoscale Latent Heating in the North Atlantic Storm Track. *J. Atmos. Sci.* 70, 2234–2250. doi:10.1175/JAS-D-12-0226.1.
Winter, H. C., Brown, S. J., and Tawn, J. A. (2017). Characterising the changing behaviour of heatwaves with climate change. *Dyn. Stat. Clim. Syst.*, dzw006. doi:10.1093/climsys/dzw006.
Wobus, C., Gutmann, E., Jones, R., Rissing, M., Mizukami, N., Lorie, M., et al. (2017). Climate change impacts on flood risk and asset damages within mapped 100-year floodplains of the contiguous United States. *Nat. Hazards Earth Syst. Sci.* 17, 2199–2211. doi:10.5194/nhess-17-2199-2017.
Woldemichael , Abel, T., Hossain, F., Pielke, R., and Beltrán-Przekurat, A. (2012). Understanding the impact of dam-triggered land use/land cover change on the modification of extreme precipitation. *Water Resour. Res.* 48. doi:10.1029/2011WR011684.
Wolski, P., Stone, D., Tadross, M., Wehner, M., and Hewitson, B. (2014). Attribution of floods in the Okavango basin, Southern Africa. *J. Hydrol.* 511, 350–358. doi:10.1016/j.jhydrol.2014.01.055.

Wolter, K., Eischeid, J. K., Quan, X.-W., Chase, T. n., Hoerling, M., Dole, R. M., et al. (2015). How Unusual was the Cold Winter of 2013/14 in the Upper Midwest? *Bull. Am. Meteorol. Soc.* 96, S10–S14. doi:10.1175/BAMS-D-15-00126.1.
Woodruff, J. D., Irish, J. L., and Camargo, S. J. (2013). Coastal flooding by tropical cyclones and sea-level rise. *Nature* 504, 44. Available at: https://doi.org/10.1038/nature12855.
Woodward, C., Shulmeister, J., Larsen, J., Jacobsen, G. E., and Zawadzki, A. (2014). The hydrological legacy of deforestation on global wetlands. *Science* 346, 844–847. doi:10.1126/science.1260510.
Wooster, M. J., Perry, G. L. W., and Zoumas, A. (2012). Fire, drought and El Niño relationships on Borneo (Southeast Asia) in the pre-MODIS era (1980-2000). *Biogeosciences* 9, 317–340. doi:10.5194/bg-9-317-2012.
World Meteorological Organization (2016). WMO Statement on the Status of the Global Climate in 2015.
Wu, J., Liu, Z., Yao, H., Chen, X., Chen, X., Zheng, Y., et al. (2018a). Impacts of reservoir operations on multi-scale correlations between hydrological drought and meteorological drought. *J. Hydrol.* 563, 726–736. Available at: https://www.scopus.com/inward/record.uri?eid=2-s2.0-85048990177&doi=10.1016%2Fj.jhydrol.2018.06.053&partnerID=40&md5=e87c15bb8f177c3325432fa96178d40e.
Wu, J., Xu, Y., and Gao, X.-J. (2017). Projected changes in mean and extreme climates over Hindu Kush Himalayan region by 21 CMIP5 models. *Adv. Clim. Chang. Res.* 8, 176–184. doi:10.1016/j.accre.2017.03.001.
Wu, M., Nikulin, G., Kjellström, E., Belušić, D., Jones, C., and Lindstedt, D. (2019a). The impact of RCM formulation and resolution on simulated precipitation in Africa. *Earth Syst. Dyn. Discuss.* 2019, 1–40. doi:10.5194/esd-2019-55.
Wu, S.-Y. (2015). Changing characteristics of precipitation for the contiguous United States. *Clim. Change* 132, 677–692. doi:10.1007/s10584-015-1453-8.
Wu, W., McInnes, K., O'Grady, J., Hoeke, R., Leonard, M., and Westra, S. (2018b). Mapping Dependence Between Extreme Rainfall and Storm Surge. *J. Geophys. Res. Ocean.* 123, 2461–2474. doi:10.1002/2017JC013472.
Wu, Y., and Polvani, L. M. (2017). Recent Trends in Extreme Precipitation and Temperature over Southeastern South America: The Dominant Role of Stratospheric Ozone Depletion in the CESM Large Ensemble. *J. Clim.* 30, 6433–6441. doi:10.1175/JCLI-D-17-0124.1.
Wu, Z., Yu, L., Du, Z., Zhang, H., Fan, X., and Lei, T. (2019b). Recent changes in the drought of China from 1960 to 2014. *Int. J. Climatol.* doi:10.1002/joc.6397.
Xia, Y., Ek, M. B., Wu, Y., Ford, T., and Quiring, S. M. (2015). Comparison of NLDAS-2 Simulated and NASMD Observed Daily Soil Moisture. Part I: Comparison and Analysis. *J. Hydrometeorol.* 16, 1962–1980. doi:10.1175/JHM-D-14-0096.1.
Xia, Y., Sheffield, J., Ek, M. B., Dong, J., Chaney, N., Wei, H., et al. (2014). Evaluation of multi-model simulated soil moisture in NLDAS-2. *J. Hydrol.* 512, 107–125. doi:10.1016/j.jhydrol.2014.02.027.
Xiao, M., Udall, B., and Lettenmaier, D. P. (2018). On the Causes of Declining Colorado River Streamflows. *Water Resour. Res.* 54, 6739–6756. doi:10.1029/2018WR023153.
Xie, P., Joyce, R., Wu, S., Yoo, S.-H., Yarosh, Y., Sun, F., et al. (2017). Reprocessed, Bias-Corrected CMORPH Global High-Resolution Precipitation Estimates from 1998. *J. Hydrometeorol.* 18, 1617–1641. doi:10.1175/JHM-D-16-0168.1.
Xu, L., Chen, N., and Zhang, X. (2019a). Global drought trends under 1.5 and 2 °C warming. *Int. J. Climatol.* 39, 2375–2385. doi:10.1002/joc.5958.
Xu, Y., Wu, J., Shi, Y., Zhou, B., Li, R., and Wu, J. (2016). Change in Extreme Climate Events over China Based on CMIP5 Change in Extreme Climate Events over China Based on CMIP5. *Atmos. Ocean. Sci. Lett.* 8, 185–192. doi:10.3878/AOSL20150006.
Xu, Y., Zhang, X., Wang, X., Hao, Z., Singh, V. P., and Hao, F. (2019b). Propagation from meteorological drought to hydrological drought under the impact of human activities: A case study in northern China. *J. Hydrol.* 579. doi:10.1016/j.jhydrol.2019.124147.
Xu, Y., Zhou, B. T., Wu, J., Han, Z. Y., Zhang, Y. X., and Wu, J. (2017). Asian climate change under 1.5–4 °C warming targets. *Adv. Clim. Chang. Res.* 8, 99–107. doi:10.1016/j.accre.2017.05.004.
Xue, M., Schleif, J., Kong, F., Thomas, K. W., Wang, Y., and Zhu, K. (2013). Track and Intensity Forecasting of Hurricanes: Impact of Convection-Permitting Resolution and Global Ensemble Kalman Filter Analysis on 2010 Atlantic Season Forecasts. *Weather Forecast.* 28, 1366–1384. doi:10.1175/WAF-D-12-00063.1.
Yamada, Y., Kodama, C., Satoh, M., Nakano, M., Nasuno, T., and Sugi, M. (2019). High-Resolution Ensemble Simulations of Intense Tropical Cyclones and Their Internal Variability During the El Niños of 1997 and 2015. *Geophys. Res. Lett.* 46, 7592–7601. doi:10.1029/2019GL082086.
Yamada, Y., Kodama, C., Satoh, M., and Sugi, M. (submitted). Future changes in tropical cyclone activities due to global warming projected by high-resolution climate simulations of the HighResMIP multi-model and multi-resolution experiments. *Prog. Earth Planet. Sci.*(submitted).
Yamada, Y., Oouchi, K., Satoh, M., Tomita, H., and Yanase, W. (2010). Projection of changes in tropical cyclone

activity and cloud height due to greenhouse warming: global cloud-system-resolving approach. *Geophys Res Lett* 37.

Yamada, Y., Satoh, M., Sugi, M., Kodama, C., Noda, A. T., Nakano, M., et al. (2017). Response of Tropical Cyclone Activity and Structure to Global Warming in a High-Resolution Global Nonhydrostatic Model. *J. Clim.* 30, 9703–9724. doi:10.1175/JCLI-D-17-0068.1.

Yamaguchi, M., Chan, J. C. L., Moon, I.-J., Yoshida, K., and Mizuta, R. (2020). Global warming changes tropical cyclone translation speed. *Nat. Commun.* 11, 47. doi:10.1038/s41467-019-13902-y.

Yamaguchi, M., and Maeda, S. (submitted). Increase in the number of tropical cyclones approaching Tokyo since 1980. *J. Meteorol. Soc. Japan*(submitted).

Yang, C., Li, L., and Xu, J. (2018a). Changing temperature extremes based on CMIP5 output via semi-parametric quantile regression approach. *Int. J. Climatol.* 38, 3736–3748. doi:10.1002/joc.5524.

Yang, M.-Z., Zhong, P. A., Li, J.-Y., Chen, J., Wang, W.-Z., Zhu, F.-L., et al. (2018b). Spatial and temporal characteristics of pan evaporation in the Huaihe river basin during 1951-2015. *Appl. Ecol. Environ. Res.* 16, 7635–7655. doi:10.15666/aeer/1606_76357655.

Yang, S.-H., Kang, N.-Y., Elsner, J. B., and Chun, Y. (2018c). Influence of Global Warming on Western North Pacific Tropical Cyclone Intensities during 2015. *J. Clim.* 31, 919–925. doi:10.1175/JCLI-D-17-0143.1.

Yang, Y., Guan, H., Batelaan, O., McVicar, T. R., Long, D., Piao, S., et al. (2016). Contrasting responses of water use efficiency to drought across global terrestrial ecosystems. *Sci. Rep.* 6. doi:10.1038/srep23284.

Yang, Y., Roderick, M. L., Zhang, S., McVicar, T. R., and Donohue, R. J. (2019). Hydrologic implications of vegetation response to elevated CO2 in climate projections. *Nat. Clim. Chang.* 9, 44–48. doi:10.1038/s41558-018-0361-0.

Yang, Y., Zhang, S., McVicar, T. R., Beck, H. E., Zhang, Y., and Liu, B. (2018d). Disconnection Between Trends of Atmospheric Drying and Continental Runoff. *Water Resour. Res.* 54, 4700–4713. doi:10.1029/2018WR022593.

Yao, N., Li, Y., Lei, T., and Peng, L. (2018). Drought evolution, severity and trends in mainland China over 1961–2013. *Sci. Total Environ.* 616–617, 73–89. Available at: https://www.scopus.com/inward/record.uri?eid=2-s2.0-85032823626&doi=10.1016%2Fj.scitotenv.2017.10.327&partnerID=40&md5=706350570fb2eeeac96135337334d074.

Yatagai, A., Minami, K., Masuda, M., and Sueto, N. (2019). Development of Intensive APHRODITE Hourly Precipitation Data for Assessment of the Moisture Transport That Caused Heavy Precipitation Events. *SOLA* 15A, 43–48. doi:10.2151/sola.15A-008.

Ye, Z., and Li, Z. (2017). Spatiotemporal variability and trends of extreme precipitation in the Huaihe river basin, a climatic transitional zone in East China. *Adv. Meteorol.* 2017. doi:10.1155/2017/3197435.

Yeh, S.-W. W., Cai, W., Min, S.-K. K., McPhaden, M. J., Dommenget, D., Dewitte, B., et al. (2018). ENSO Atmospheric Teleconnections and Their Response to Greenhouse Gas Forcing. *Rev. Geophys.* 56, 185–206. doi:10.1002/2017RG000568.

Yettella, V., and Kay, J. E. (2017). How will precipitation change in extratropical cyclones as the planet warms? Insights from a large initial condition climate model ensemble. *Clim. Dyn.* 49, 1765–1781. doi:10.1007/s00382-016-3410-2.

Yin, H., Donat, M. G., Alexander, L. V, and Sun, Y. (2015). Multi-dataset comparison of gridded observed temperature and precipitation extremes over China. *Int. J. Climatol.* 35, 2809–2827. doi:10.1002/joc.4174.

Yin, H., and Sun, Y. (2018). Detection of Anthropogenic Influence on Fixed Threshold Indices of Extreme Temperature. *J. Clim.* 31, 6341–6352. doi:10.1175/JCLI-D-17-0853.1.

Yin, H., Sun, Y., and Donat, M. G. (2019a). Changes in temperature extremes on the Tibetan Plateau and their attribution. *Environ. Res. Lett.* 14, 124015. doi:10.1088/1748-9326/ab503c.

Yin, H., Sun, Y., Wan, H., Zhang, X., and Lu, C. (2017). Detection of anthropogenic influence on the intensity of extreme temperatures in China. *Int. J. Climatol.* 37, 1229–1237. doi:10.1002/joc.4771.

Yin, J., Zhao, Q., Yu, D., Lin, N., Kubanek, J., Ma, G., et al. (2019b). Long-term flood-hazard modeling for coastal areas using InSAR measurements and a hydrodynamic model: The case study of Lingang New City, Shanghai. *J. Hydrol.* 571, 593–604. Available at: https://www.scopus.com/inward/record.uri?eid=2-s2.0-85061773417&doi=10.1016%2Fj.jhydrol.2019.02.015&partnerID=40&md5=501379d8844bde0ffa404f3f9ed360b6.

Yiou, P., Jézéquel, A., Naveau, P., Otto, F. E. L., Vautard, R., and Vrac, M. (2017). A statistical framework for conditional extreme event attribution. *Adv. Stat. Climatol. Meteorol. Oceanogr.* 3, 17–31. doi:10.5194/ascmo-3-17-2017.

YOKOYAMA, C., TSUJI, H., and TAKAYABU, Y. N. (2020). The Effects of an Upper-Tropospheric Trough on the Heavy Rainfall Event in July 2018 over Japan. *J. Meteorol. Soc. Japan. Ser. II.* doi:10.2151/jmsj.2020-013.

Yoshida, K., Sugi, M., Mizuta, R., Murakami, H., and Ishii, M. (2017). Future Changes in Tropical Cyclone Activity in High-Resolution Large-Ensemble Simulations. *Geophys. Res. Lett.* 44, 9910–9917. doi:10.1002/2017GL075058.

You, Q., Jiang, Z., Kong, L., Wu, Z., Bo, Y., Kang, S., et al. (2017). A comparison of heat wave climatologies and

trends in China based on multiple definitions. *Clim. Dyn.* 48, 3975–3989.
Young, I. R., Vinoth, J., Zieger, S., and Babanin, A. V. (2012). Investigation of trends in extreme value wave height and wind speed. *J. Geophys. Res. Ocean.* 117, 1–13. doi:10.1029/2011JC007753.
Yu, B., Lin, H., Kharin, V. V., and Wang, X. L. (2019). Interannual variability of North American winter temperature extremes and its associated circulation anomalies in observations and CMIP5 simulations. *J. Clim.*, JCLI-D-19-0404.1. doi:10.1175/JCLI-D-19-0404.1.
Yu, E., Sun, J., Chen, H., and Xiang, W. (2015). Evaluation of a high-resolution historical simulation over China: climatology and extremes. *Clim. Dyn.* 45, 2013–2031. doi:10.1007/s00382-014-2452-6.
Yu, L., Zhong, S., Heilman, W. E., and Bian, X. (2018). Trends in seasonal warm anomalies across the contiguous United States: Contributions from natural climate variability. *Sci. Rep.* 8, 1–13. doi:10.1038/s41598-018-21817-9.
Yu, M., Li, Q., Hayes, M. J., Svoboda, M. D., and Heim, R. R. (2014). Are droughts becoming more frequent or severe in China based on the Standardized Precipitation Evapotranspiration Index: 1951-2010? *Int. J. Climatol.* 34, 545–558. doi:10.1002/joc.3701.
Yu, R., and Li, J. (2012). Hourly Rainfall Changes in Response to Surface Air Temperature over Eastern Contiguous China. *J. Clim.* 25, 6851–6861. doi:10.1175/JCLI-D-11-00656.1.
Yuan, S., and Quiring, S. M. (2017). Evaluation of soil moisture in CMIP5 simulations over the contiguous United States using in situ and satellite observations. *Hydrol. Earth Syst. Sci.* 21, 2203–2218. doi:10.5194/hess-21-2203-2017.
Yuan, W., Zheng, Y., Piao, S., Ciais, P., Lombardozzi, D., Wang, Y., et al. (2019). Increased atmospheric vapor pressure deficit reduces global vegetation growth. *Sci. Adv.* 5. Available at: https://www.scopus.com/inward/record.uri?eid=2-s2.0-85070882807&doi=10.1126%2Fsciadv.aax1396&partnerID=40&md5=accc4ceca4db1b9313b80ffb5f57dfec.
Yuan, X., Wang, L., and Wood, E. F. (2018a). Anthropogenic Intensification of Southern African Flash Droughts as Exemplified by the 2015/16 Season. *Bull. Am. Meteorol. Soc.* 99, S86–S90. doi:10.1175/BAMS-D-17-0077.1.
Yuan, X., Wang, S., and Hu, Z.-Z. (2018b). Do Climate Change and El Niño Increase Likelihood of Yangtze River Extreme Rainfall? *Bull. Am. Meteorol. Soc.* 99, S113–S117. doi:10.1175/BAMS-D-17-0089.1.
Zaherpour, J., Gosling, S. N., Mount, N., Schmied, H. M., Veldkamp, T. I. E., Dankers, R., et al. (2018). Worldwide evaluation of mean and extreme runoff from six global-scale hydrological models that account for human impacts. *Environ. Res. Lett.* 13. Available at: https://www.scopus.com/inward/record.uri?eid=2-s2.0-85049770640&doi=10.1088%2F1748-9326%2Faac547&partnerID=40&md5=cf821e490e0905cb3a4d732a54a6f3f1.
Zahid, M., Blender, R., Lucarini, V., and Bramati, M. C. (2017). Return levels of temperature extremes in southern Pakistan. *Earth Syst. Dyn.* 8, 1263–1278. doi:10.5194/esd-8-1263-2017.
Zahid, M., and Rasul, G. (2012). Changing trends of thermal extremes in Pakistan. *Clim. Change*. doi:10.1007/s10584-011-0390-4.
Zampieri, M., Ceglar, A., Dentener, F., and Toreti, A. (2017). Wheat yield loss attributable to heat waves, drought and water excess at the global, national and subnational scales. *Environ. Res. Lett.* 12, 064008. doi:10.1088/1748-9326/aa723b.
Zandonadi, L., Acquaotta, F., Fratianni, S., and Zavattini, J. A. (2016). Changes in precipitation extremes in Brazil (Paraná River Basin). *Theor. Appl. Climatol.* 123, 741–756. doi:10.1007/s00704-015-1391-4.
Zaninelli, P. G., Menéndez, C. G., Falco, M., López-Franca, N., and Carril, A. F. (2019). Future hydroclimatological changes in South America based on an ensemble of regional climate models. *Clim. Dyn.* 52, 819–830. doi:10.1007/s00382-018-4225-0.
Zappa, G., Hawcroft, M. K., Shaffrey, L., Black, E., and Brayshaw, D. J. (2015). Extratropical cyclones and the projected decline of winter Mediterranean precipitation in the CMIP5 models. *Clim. Dyn.* doi:10.1007/s00382-014-2426-8.
Zappa, G., Shaffrey, L. C., and Hodges, K. I. (2013a). The Ability of CMIP5 Models to Simulate North Atlantic Extratropical Cyclones*. *J. Clim.* 26, 5379–5396. doi:10.1175/JCLI-D-12-00501.1.
Zappa, G., Shaffrey, L. C., Hodges, K. I., Sansom, P. G., and Stephenson, D. B. (2013b). A multimodel assessment of future projections of north atlantic and european extratropical cyclones in the CMIP5 climate models. *J. Clim.* 26, 5846–5862. doi:10.1175/JCLI-D-12-00573.1.
Zappa, G., and Shepherd, T. G. (2017). Storylines of Atmospheric Circulation Change for European Regional Climate Impact Assessment. *J. Clim.* 30, 6561–6577. doi:10.1175/JCLI-D-16-0807.1.
Zarzycki, C. M., and Ullrich, P. A. (2017). Assessing sensitivities in algorithmic detection of tropical cyclones in climate data. *Geophys. Res. Lett.* 44, 1141–1149. doi:10.1002/2016GL071606.
Zhan, R., Chen, B., and Ding, Y. (2018). Impacts of SST anomalies in the Indian-Pacific basin on Northwest Pacific tropical cyclone activities during three super El Niño years. *J. Oceanol. Limnol.* 36, 20–32. doi:10.1007/s00343-018-6321-8.
Zhan, R., and Wang, Y. (2017). Weak Tropical Cyclones Dominate the Poleward Migration of the Annual Mean

Location of Lifetime Maximum Intensity of Northwest Pacific Tropical Cyclones since 1980. *J. Clim.* 30, 6873–6882. doi:10.1175/JCLI-D-17-0019.1.
Zhan, Y. J., Ren, G. Y., Shrestha, A. B., Rajbhandari, R., Ren, Y. Y., Sanjay, J., et al. (2017). Changes in extreme precipitation events over the Hindu Kush Himalayan region during 1961–2012. *Adv. Clim. Chang. Res.* 8, 166–175. doi:10.1016/j.accre.2017.08.002.
Zhang, C., Liu, F., and Shen, Y. (2018a). Attribution analysis of changing pan evaporation in the Qinghai-Tibetan Plateau, China: Pan Evaporation in the Qinghai-Tibetan Plateau. *Int. J. Climatol.* 38. doi:10.1002/joc.5431.
Zhang, C., and Wang, Y. (2018). Why is the simulated climatology of tropical cyclones so sensitive to the choice of cumulus parameterization scheme in the WRF model? *Clim. Dyn.* 51, 3613–3633. doi:10.1007/s00382-018-4099-1.
Zhang, D., Zhang, Q., Qiu, J., Bai, P., Liang, K., and Li, X. (2018b). Intensification of hydrological drought due to human activity in the middle reaches of the Yangtze River, China. *Sci. Total Environ.* 637–638, 1432–1442. doi:10.1016/j.scitotenv.2018.05.121.
Zhang, G., Murakami, H., Knutson, T. R., Mizuta, R., and Yoshida, K. (submitted). Tropical motion in a changing climate. *Sci. Adv.*(submitted).
Zhang, J., Chen, H., and Zhang, Q. (2019a). Extreme drought in the recent two decades in northern China resulting from Eurasian warming. *Clim. Dyn.* 52, 2885–2902. doi:10.1007/s00382-018-4312-2.
Zhang, J., Gao, Y., Luo, K., Leung, L. R., Zhang, Y., Wang, K., et al. (2018c). Impacts of compound extreme weather events on ozone in the present and future. *Atmos. Chem. Phys.* 18, 9861–9877. doi:10.5194/acp-18-9861-2018.
Zhang, M., Chen, Y., Shen, Y., and Li, B. (2019b). Tracking climate change in Central Asia through temperature and precipitation extremes. *J. Geogr. Sci.* 29, 3–28. doi:10.1007/s11442-019-1581-6.
Zhang, M., Chen, Y., Shen, Y., and Li, Y. (2017). Changes of precipitation extremes in arid Central Asia. *Quat. Int.* 436, 16–27. doi:10.1016/j.quaint.2016.12.024.
Zhang, P., Ren, G., Xu, Y., Wang, X. L., Qin, Y., Sun, X., et al. (2019c). Observed Changes in Extreme Temperature over the Global Land Based on a Newly Developed Station Daily Dataset. *J. Clim.* 32, 8489–8509. doi:10.1175/JCLI-D-18-0733.1.
Zhang, Q., Gu, X., Singh, V. P., Kong, D., and Chen, X. (2015a). Spatiotemporal behavior of floods and droughts and their impacts on agriculture in China. *Glob. Planet. Change* 131, 63–72. doi:10.1016/j.gloplacha.2015.05.007.
Zhang, Q., Gu, X., Singh, V. P., Xiao, M., and Xu, C.-Y. (2015b). Flood frequency under the influence of trends in the Pearl River basin, China: Changing patterns, causes and implications. *Hydrol. Process.* 29, 1406–1417. doi:10.1002/hyp.10278.
Zhang, R., Su, F., Jiang, Z., Gao, X., Guo, D., Ni, J., et al. (2015c). An overview of projected climate and environmental changes across the Tibetan Plateau in the 21st century. *Chinese Sci. Bull.* doi:10.1360/N972014-01296.
Zhang, W., Vecchi, G. A., Murakami, H., Delworth, T. L., Paffendorf, K., Jia, L., et al. (2016a). Influences of Natural Variability and Anthropogenic Forcing on the Extreme 2015 Accumulated Cyclone Energy in the Western North Pacific. *Bull. Am. Meteorol. Soc.* 97, S131–S135. doi:10.1175/BAMS-D-16-0146.1.
Zhang, W., Vecchi, G. A., Murakami, H., Villarini, G., and Jia, L. (2016b). The Pacific meridional mode and the occurrence of tropical Cyclones in the western North Pacific. *J. Clim.* 29, 381–398. doi:10.1175/JCLI-D-15-0282.1.
Zhang, W., Villarini, G., Vecchi, G. A., and Smith, J. A. (2018d). Urbanization exacerbated the rainfall and flooding caused by hurricane Harvey in Houston. *Nature* 563, 384–388. doi:10.1038/s41586-018-0676-z.
Zhang, X., Flato, G., Kirchmeier-Young, M., Vincent, L. A., Wan, H., Wang, X., et al. (2019d). Changes in Temperature and Precipitation Across Canada. , eds. E. Bush and D. S. Lemmen Ottawa: Government of Canada Available at: https://changingclimate.ca/CCCR2019/.
Zhang, X., Wan, H., Zwiers, F. W., Hegerl, G. C., and Min, S.-K. (2013). Attributing intensification of precipitation extremes to human influence. *Geophys. Res. Lett.* 40, 5252–5257. doi:10.1002/grl.51010.
Zhang, Y., Pang, X., Xia, J., Shao, Q., Yu, E., Zhao, T., et al. (2019e). Regional Patterns of Extreme Precipitation and Urban Signatures in Metropolitan Areas. *J. Geophys. Res. Atmos.* 124, 641–663. doi:10.1029/2018JD029718.
Zhang, Y., Wang, H., Sun, J., and Drange, H. (2010). Changes in the tropical cyclone genesis potential index over the western north pacific in the SRES A2 scenario. *Adv. Atmos. Sci.* 27, 1246–1258. doi:10.1007/s00376-010-9096-1.
Zhang, Y., Wang, Y., Chen, Y., Liang, F., and Liu, H. (2019f). Assessment of future flash flood inundations in coastal regions under climate change scenarios—A case study of Hadahe River basin in northeastern China. *Sci. Total Environ.* 693. Available at: https://www.scopus.com/inward/record.uri?eid=2-s2.0-85069659648&doi=10.1016%2Fj.scitotenv.2019.07.356&partnerID=40&md5=70a4bf0b33466510f062d2c060fa45ae.
Zhang, Z., and Colle, B. A. (2017). Changes in Extratropical Cyclone Precipitation and Associated Processes during the Twenty-First Century over Eastern North America and the Western Atlantic Using a Cyclone-Relative Approach. *J. Clim.* 30, 8633–8656. doi:10.1175/JCLI-D-16-0906.1.

Zhang, Z., Li, Y., Chen, F., Barlage, M., and Li, Z. (2018e). Evaluation of convection-permitting WRF CONUS simulation on the relationship between soil moisture and heatwaves. *Clim. Dyn.* doi:10.1007/s00382-018-4508-5.
Zhang, Z., Ralph, F. M., and Zheng, M. (2019g). The Relationship Between Extratropical Cyclone Strength and Atmospheric River Intensity and Position. *Geophys. Res. Lett.* 46, 1814–1823. doi:10.1029/2018GL079071.
Zhang, Z., Wang, K., Chen, D., Li, J., and Dickinson, R. (2019h). Increase in Surface Friction Dominates the Observed Surface Wind Speed Decline during 1973–2014 in the Northern Hemisphere Lands. *J. Clim.* 32, 7421–7435. doi:10.1175/JCLI-D-18-0691.1.
Zhao, C., Lin, Y., Wu, F., Wang, Y. Y., Li, Z., Rosenfeld, D., et al. (2018a). Enlarging Rainfall Area of Tropical Cyclones by Atmospheric Aerosols. *Geophys. Res. Lett.* 45, 8604–8611. doi:10.1029/2018GL079427.
Zhao, L., Oppenheimer, M., Zhu, Q., Baldwin, J. W., Ebi, K. L., Bou-Zeid, E., et al. (2018b). Interactions between urban heat islands and heat waves. *Environ. Res. Lett.* 13. doi:10.1088/1748-9326/aa9f73.
Zhao, M., and Held, I. M. (2011). TC-Permitting GCM Simulations of Hurricane Frequency Response to Sea Surface Temperature Anomalies Projected for the Late-Twenty-First Century. *J. Clim.* 25, 2995–3009. doi:10.1175/JCLI-D-11-00313.1.
Zhao, M., Held, I. M., and Lin, S.-J. (2012). Some Counterintuitive Dependencies of Tropical Cyclone Frequency on Parameters in a GCM. *J. Atmos. Sci.* 69, 2272–2283. doi:10.1175/JAS-D-11-0238.1.
Zhao, M., Held, I. M., Lin, S. J., and Vecchi, G. A. (2009). Simulations of global hurricane climatology, interannual variability, and response to global warming using a 50-km resolution GCM. *J. Clim.* 22, 6653–6678. doi:10.1175/2009JCLI3049.1.
Zhao, S., Deng, Y., and Black, R. X. (2016). Warm season dry spells in the Central and Eastern United States: Diverging skill in climate model representation. *J. Clim.* 29, 5617–5624. Available at: https://www.scopus.com/inward/record.uri?eid=2-s2.0-85012284490&doi=10.1175%2FJCLI-D-16-0321.1&partnerID=40&md5=cd50b744a1f419404dc0a895e2daea26.
Zhao, T., and Dai, A. (2015). The magnitude and causes of global drought changes in the twenty-first century under a low-moderate emissions scenario. *J. Clim.* 28, 4490–4512. doi:10.1175/JCLI-D-14-00363.1.
Zhao, T., and Dai, A. (2017). Uncertainties in historical changes and future projections of drought. Part II: model-simulated historical and future drought changes. *Clim. Change* 144, 535–548. doi:10.1007/s10584-016-1742-x.
Zheng, C., Zhang, R., Shi, W., Li, X., and Chen, X. (2017). Trends in significant wave height and surface wind speed in the China Seas between 1988 and 2011. *J. Ocean Univ. China* 16, 717–726. doi:10.1007/s11802-017-3213-z.
Zheng, F., Westra, S., and Sisson, S. A. (2013). Quantifying the dependence between extreme rainfall and storm surge in the coastal zone. *J. Hydrol.* 505, 172–187. doi:10.1016/j.jhydrol.2013.09.054.
Zhou, B., Wang, Z., Shi, Y., Xu, Y., and Han, Z. (2018a). Historical and future changes of snowfall events in China under a warming background. *J. Clim.* 31, 5873–5889. doi:10.1175/JCLI-D-17-0428.1.
Zhou, B., Wen, Q. H., Xu, Y., Song, L., and Zhang, X. (2014). Projected changes in temperature and precipitation extremes in China by the CMIP5 multimodel ensembles. *J. Clim.* 27, 6591–6611. doi:10.1175/JCLI-D-13-00761.1.
Zhou, B., Xu, Y., Wu, J., Dong, S., and Shi, Y. (2016a). Changes in temperature and precipitation extreme indices over China: Analysis of a high-resolution grid dataset. *Int. J. Climatol.* 36, 1051–1066. doi:10.1002/joc.4400.
Zhou, C., Wang, K., and Qi, D. (2017). 21. Attribution of the July 2016 Extreme Precipitation Event Over China's Wuhang. *Bull. Am. Meteorol. Soc.* 99, 107–111. doi:10.1175/BAMS-D-17-0090.1.
Zhou, Q., Leng, G., and Huang, M. (2018b). Impacts of future climate change on urban flood volumes in Hohhot in northern China: benefits of climate change mitigation and adaptations. *Hydrol. Earth Syst. Sci.* 22, 305–316. Available at: https://www.scopus.com/inward/record.uri?eid=2-s2.0-85044786289&doi=10.5194%2Fhess-22-305-2018&partnerID=40&md5=64b367c755f667ab843e054c7cfa5c93.
Zhou, S., Williams, A. P., Berg, A. M., Cook, B. I., Zhang, Y., Hagemann, S., et al. (2019). Land–atmosphere feedbacks exacerbate concurrent soil drought and atmospheric aridity. *Proc. Natl. Acad. Sci.* 116, 18848–18853. doi:10.1073/pnas.1904955116.
Zhou, W., Tang, J., Wang, X., Wang, S., Niu, X., and Wang, Y. (2016b). Evaluation of regional climate simulations over the CORDEX-EA-II domain using the COSMO-CLM model. *Asia-Pacific J. Atmos. Sci.* 52, 107–127. doi:10.1007/s13143-016-0013-0.
Zieger, S., Babanin, A. V., and Young, I. R. (2014). Changes in ocean surface wind with a focus on trends in regional and monthly mean values. *Deep. Res. Part I Oceanogr. Res. Pap.* 86, 56–67. doi:10.1016/j.dsr.2014.01.004.
Zipper, S. C., Qiu, J., and Kucharik, C. J. (2016). Drought effects on US maize and soybean production: spatiotemporal patterns and historical changes. *Environ. Res. Lett.* 11, 094021. doi:10.1088/1748-9326/11/9/094021.
Zipser, E. J., Cecil, D. J., Liu, C., Nesbitt, S. W., and Yorty, D. P. (2006). Where are the most: Intense thunderstorms on Earth? *Bull. Am. Meteorol. Soc.* 87, 1057–1071. doi:10.1175/BAMS-87-8-1057.
Zittis, G. (2017). Observed rainfall trends and precipitation uncertainty in the vicinity of the Mediterranean, Middle East and North Africa. *Theor. Appl. Climatol.* doi:10.1007/s00704-017-2333-0.
Zkhiri, W., Tramblay, Y., Hanich, L., Jarlan, L., and Ruelland, D. (2019). Spatiotemporal characterization of current

and future droughts in the High Atlas basins (Morocco). *Theor. Appl. Climatol.* 135, 593–605. doi:10.1007/s00704-018-2388-6.

Zolina, O., Simmer, C., Belyaev, K., Gulev, S. K., and Koltermann, P. (2013). Changes in the duration of European wet and dry spells during the last 60 years. *J. Clim.* 26, 2022–2047. doi:10.1175/JCLI-D-11-00498.1.

Zollo, A. L., Rillo, V., Bucchignani, E., Montesarchio, M., and Mercogliano, P. (2016). Extreme temperature and precipitation events over Italy: assessment of high-resolution simulations with COSMO-CLM and future scenarios. *Int. J. Climatol.* 36, 987–1004. doi:10.1002/joc.4401.

Zscheischler, J., Fischer, E. M., and Lange, S. (2018a). The effect of bias adjustment on impact modeling. *Earth Syst. Dyn. Discuss.*, 1–17. doi:10.5194/esd-2018-68.

Zscheischler, J., Michalak, A. M., Schwalm, C., Mahecha, M. D., Huntzinger, D. N., Reichstein, M., et al. (2014). Impact of large-scale climate extremes on biospheric carbon fluxes: An intercomparison based on MsTMIP data. *Global Biogeochem. Cycles* 28, 585–600. doi:10.1002/2014GB004826.

Zscheischler, J., and Seneviratne, S. I. (2017). Dependence of drivers affects risks associated with compound events. *Sci. Adv.* 3. Available at: http://advances.sciencemag.org/content/3/6/e1700263.abstract.

Zscheischler, J., Westra, S., van den Hurk, B. J. J. M., Seneviratne, S. I., Ward, P. J., Pitman, A., et al. (2018b). Future climate risk from compound events. *Nat. Clim. Chang.* 8, 469–477. doi:10.1038/s41558-018-0156-3.

Zulkafli, Z., Buytaert, W., Manz, B., Rosas, C. V., Willems, P., Lavado-Casimiro, W., et al. (2016). Projected increases in the annual flood pulse of the Western Amazon. *Environ. Res. Lett.* 11, 014013. doi:10.1088/1748-9326/11/1/014013.

Appendix 11.A

[START TABLE 11.A.1 HERE]

Table 11.A.1: This table gives an overview of the attribution studies of individual extreme events in the IPCC regions that have been published since 2013, the cut-off date of the AR5 report. The third column provides an assessment of the confidence of the signals of anthropogenic climate change that have been found in the different regions (column 1) for different types of extreme events (column 2) for which studies exist. The final column provides the references and column 4 gives an assessment of the quality of the evidence provided in these references following the assessment steps described in Section 11.2.5 and the flow diagram included in Fig. 11.4.

Region	Type of event	Anthropogenic Signal	Confidence	Quality of evidence	Reference
CNA	drought	No sig change	Medium (because of other studies in same region)	low	(Rupp et al., 2013)
CNA & ENA	Heat wave	increase	medium	medium	(Diffenbaugh & Scherer 2013) , (Cattiaux & Yiou 2013)(Knutson et al., 2014a)
ENA	Hurricane Sandy	Increase in inundation	low	low	(Peterson et al., 2013b; Garner et al., 2017)
ARO	Sea ice extend	decrease	medium	low	(Peterson et al., 2013b)
NEU	Summer extreme rainfall	No change	medium		(Peterson et al., 2013b)
MED	Winter drought	increase	medium	Medium	(Peterson et al., 2013b)
NEAF/CEAF	drought	No change	low	medium	(Funk et al., 2013, 2015c; Marthews et al., 2015)(Funk et al., 2016)(Uhe et al., 2017; Philip et al., 2018a; Kew et al., 2019a)
EAS	Extreme precip	Mixed signal	low	low	(Peterson et al., 2013b)
SAU	Extreme precip	No change/small increase	low	medium	(Peterson et al., 2013b)
NCA	drought	No change/	Low, Signal depends on definition	high	(Swain et al., 2014; Wang and Schubert, 2014) Funk et al., in (Herring et al., 2014)
CNA	Extreme rainfall	Mixed signal	low		Hoerling in (Herring et al., 2014) Wolter et

					al., in (Herring et al., 2016)
ENA	Snowfall	decrease	low	low	Edwards in (Herring et al., 2014)
NAU	Heat wave	Increase	high	High	(Knutson et al., 2014c; Lewis and Karoly, 2014b; Perkins et al., 2014a) Arblaster et al. in (Herring et al., 2014)(King et al., 2014)king et al., in (Herring et al., 2015) Hope et al. in, Perkins & Gibson in (Herring et al., 2015) Black & Karoly in , Hope et al in (Herring et al., 2016)
SAU	Heat wave	Increase	high	high	(Knutson et al., 2014c) Black et al., in; Hope et al. in, Perkins & Gibson in (Herring et al., 2015) Black & Karoly in , Hope et al in (Herring et al., 2016)
SAU	drought	increase	medium	medium	(Harrington et al. 2014) Karoly et al., in (Herring et al., 2016)
EAS	Heat wave	increase	high	high	Min et al.; Imada et al.; Zhou et al., in (Herring et al., 2014) Min et al., in, Song et al., in (Herring et al., 2015) Miao et al., in , Sun et al., in , Takahashi et al., in (Herring et al., 2016)
SAS	Extreme precipitation	No change	medium	Medium	Singh et al., in (Herring et al., 2014)(van Oldenborgh et al., 2016)
CEU	Heat wave	increase	high	high	Dong et al., in (Herring et al., 2014)(Sippel et al., 2016) Dong et al., in (Herring et al., 2016)

					Jezequel et al., in (Herring et al., 2018)(Christidis et al., 2015; Cattiaux and Ribes, 2018; Wilcox et al., 2018)
SAS	floods	increase	low	low	(Philip et al. 2019)
CEU	Extreme summer precip	increase	low	low	(Schaller et al., 2014; Philip et al., 2018b)
NEU	Cold wave	decrease	high	medium	(Christidis et al., 2014; Christiansen et al., 2018)
CNA	Fire risk	increase	low	low	Yoon et al., in (Herring et al., 2015)
CNA	Cold wave	decrease	high	medium	(Wolter et al., 2015)
NES	drought	No change	medium	low	(Otto et al. 2015) Martins et al., in (Herring et al., 2018)
SES	Heat wave	increase	medium	low	(Hannart et al., 2015)
NEU	Winter extreme rainfall	increase	medium	high	Christidis & Stott in (Herring et al. 2015)(Schaller et al., 2016; Vautard et al., 2016; Yiou et al., 2017; Otto et al., 2018b)
CEU	Extreme wingter precip	increase	medium	low	Vautard et al., in (Herring et al., 2015)
MED	drought	increase	low	low	(Bergaoui et al., 2015)
WCA	Drought	No change	Low sing. Dep. On def	low	(Barlow and Hoell, 2015)
EEU	drought	No change	low	Low	(Barlow and Hoell, 2015)
TIB	Snow storm	increase	low	low	Simon Wang et al., in (Herring et al., 2015)
NEA	drought	No signal	low	low	Wilcox et al., in (Herring et al., 2015)
NPO	Hurricane activity	Increase	low	low	(Murakami et al., 2015a)

SEA	drought	increase	low	low	(Mcbride et al., 2015)(King et al., 2016c) ch 25 in (Herring et al., 2018)
SEA	Extreme precip	increase	medium	low	(Siswanto et al., 2015)
SAU	Winter extreme precip	increase	low	low	(Rosier et al., 2015)
SAU	High pressure	increase	low	low	(Grose et al., 2015)
WNA	Extreme rainfall	Increase	medium	Low	Walter et al., in (Herring et al., 2016)
SWN	Extreme rainfall	Increase	Medium	Low	Walter et al., in (Herring et al., 2016)
ENA	Extreme rainfall	increase	Medium	low	Walter et al., in (Herring et al., 2016)
NWN	fire	increase	low	low	Partain et al., in (Herring et al., 2016)
WNA	drought	increase	low	low	Fosu et al., in (Herring et al., 2016)(Szeto et al., 2016)
ENA	Cold wave	decrease	high	medium	(Trenary et al., 2016; van Oldenborgh et al., 2019)
NEU	Sunshine hours	increase	medium	low	Christidis et al., in (Herring et al., 2016)
WAF	Low precip/ drought	No change	low	low	(Lawal et al., 2016)
MED	heatwave	increase	high	medium	Mitchell in (Herring et al., 2016)
SAS	Heat wave	Mixed signal	low	medium	(Wehner et al., 2016)
EAS	Extreme precip	Mixed signal	low	low	(Burke et al., 2016)
SEA	Heat wave	increase	medium	medium	(King et al., 2016c) Christidis et al., in (Herring et al., 2018)
ARO	Heat wave	increase	medium	low	Quian et al., in (Herring et al., 2018)

EAS	Cold wave	decrease	high	medium	Qian et al., & Sun et al., in (Herring et al., 2018)
SWAF	Drought	increase	medium	Medium	Yuan et al., & Funk et al., in (Herring et al., 2018) (Otto, Wolski, et al. 2018)
SEAF	drought	Increase	medium	low	Yuan et al., & Funk et al., in (Herring et al., 2018)
CEU	Stagnant air	No change	low	low	Vautard et al., in (Herring et al., 2018)
WNA	Fire	increase	low	medium	Tett et al., in (Herring et al., 2018) (Kirchmeier-Young et al., 2017)
SAU/NAU/CAU	Fire	increase	low	low	Tett et al. in (Herring et al., 2018)
CAU/NAU	Fire	increase	low	low	(Lewis et al., 2019a)
SEA	Extreme rainfall	increase	medium	medium	(Otto et al., 2018a)
NWS	Cold wave	decrease	high	medium	(Otto et al., 2018a)
CEAF	drought	No signal	low	low	(Otto, Philip, et al. 2018)
NWS	Extreme rainfall	decrease	low	medium	(Otto et al., 2018a)
CNA	Extreme rainfall (in land)	No signal	low	high	(Eden et al., 2016; Pall et al., 2017; Cattiaux and Ribes, 2018)
CNA	Hurricane associated rainfall	increase	medium	high	(Risser and Wehner, 2017; van der Wiel et al., 2017; van Oldenborgh et al.,

					2017; Wang et al., 2018b)
CEU	drought	No change	medium	Medium	(Hauser et al., 2017)
CAR	Tropical cyclone	increase	medium	low	(Patricola and Wehner, 2018)
EEU	Heat wave	increase	high	high	(Otto et al., 2012; Sippel and Otto, 2014; Hauser et al., 2016)
SWN	flood	increase	low	low	(Huang et al., 2018c)
NZE	drought	increase	low	low	(Harrington et al., 2016)
NZE	Marine heatwave	increase	high	medium	(Oliver et al., 2017)
WAF	Extreme rainfall	No signal	low	low	(Parker et al., 2017)
CAM	Heat wave	increase	low	low	(Rupp et al., 2015)
SWN	fire	increase	low	low	(Abatzoglou and Williams, 2016)
CEU	Cold wave	decrease	high	low	(Christiansen et al., 2018)
SOO/NPO/AROO	Marine heat wave	increase	high	low	(Frölicher et al., 2018)
CAF	Extreme precipitation	No signal	low	low	(Otto et al. 2013)
CAF	drought	No signal	low	low	(Otto et al. 2013)
SAS	Cold wave	decrease	high	Medium	(Kumar and Kumar, 2017)
NAU	Extreme rainfall	No signal	low	low	(Dey et al., 2019)
NZE	Extreme rainfall	increase	medium	low	(Rosier et al., 2015)
NZE	drought	increase	low	Low	(Harrington et al., 2014)
CEU	drought	increase	medium	low	(García-Herrera et al., 2019)
MED	Extreme snowfall	No signal	low	low	(Añel et al., 2014)
NEU	drought	decrease	low	low	(Gudmundsson and Seneviratne, 2016)
NSA	Extreme rainfall	increase	medium	low	(Li et al., 2019)
SAM	Extreme rainfall	increase	medium	low	(Li et al., 2019)
NES	Extreme rainfall	increase	medium	low	(Li et al., 2019)
SWS	Extreme rainfall	increase	medium	low	(Li et al., 2019)
NWS	Extreme rainfall	increase	medium	low	(Li et al., 2019)
SES	Extreme rainfall	increase	medium	medium	(Li et al., 2019; Díaz and Vera 2018)

SSA	Extreme rainfall	increase	medium	medium	(Li et al., 2019; Díaz and Vera 2018)
SWS	drought	increase	medium	low	(Minetti et al., 2014)
SWN	fire	increase	medium	low	(Brown et al., 2020)
SEAF	Extreme rainfall	decrease	low	medium	(Fuckar et al., 2020)

[END TABLE 11.A.1 HERE]

[START FIGURE 11.A.1 HERE]

Figure 11.A.1 : Regional mean changes in annual minimum nighttime temperature (TNn) for land regions, the global land and global ocean, against changes in global mean surface temperature (Tglob) as simulated by CMIP5 models for historical conditions (black) and different forcing scenarios including RCP2.6 (light blue), RCP4.5 (blue), RCP6.0 (light red), and (red) RCP8.5. The black line indicates the 1:1 reference scaling. The grey shading indicates the range over all RCPs. [Note to reviewers: the figure will be updated to include CMIP6 simulations for the FGD, as well as the final selected AR6 regions].

[END FIGURE 11.A.1 HERE]

[START FIGURE 11.A.2 HERE]

Figure 11.A.2. : Regional mean changes in regional mean warming (Tmean) for land regions, the global land and global ocean, against changes in global mean surface temperature (Tglob) as simulated by CMIP5 models for historical conditions (black) and different forcing scenarios including RCP2.6 (light blue), RCP4.5 (blue), RCP6.0 (light red), and (red) RCP8.5. The black line indicates the 1:1 reference scaling. The grey shading indicates the range over all RCPs. [Note to reviewers: the figure will be updated to include CMIP6 simulations for the FGD, as well as the final selected AR6 regions].

[END FIGURE 11.A.2 HERE]

Figures

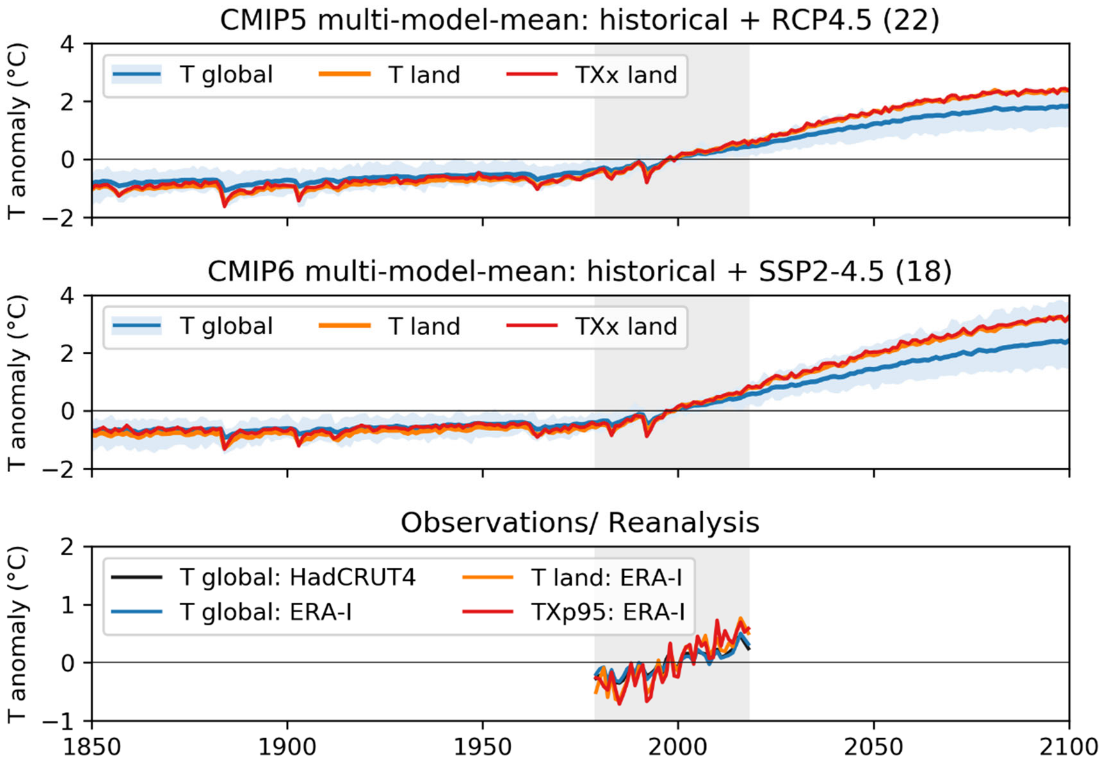

Figure 11.1: Time series of temperature anomalies (relative to 1979-2018 mean) for global average annual mean temperature (T_global), land average annual mean temperature (T_land) and extreme temperatures from CMIP5 and CMIP6 simulations, and from observations and a reanalysis data product. Extreme temperatures include annual maximum daily maximum temperature (TXx) and the annual 95th percentile of daily maximum temperature (TXp95). Grey shading mark the reference period 1979-2018. (a) and (b), temperatures from CMIP5 and CMIP6 simulations, respectively. Solid lines are multi-model averages while the blue shading shows the multiple range of global mean temperature by all models. CMIP5 temperatures include the models' historical simulations and future projection under RCP4.5 forcing scenario. CMIP6 temperatures include the models' historical simulations and future projections under the SSP2-4.5 forcing scenario (note that RCP4.5 and SSP2-4.5 do not share the same forcing). (c) Observed temperatures based on HadCRUT4 and temperatures computed from ERA–Interim reanalysis.

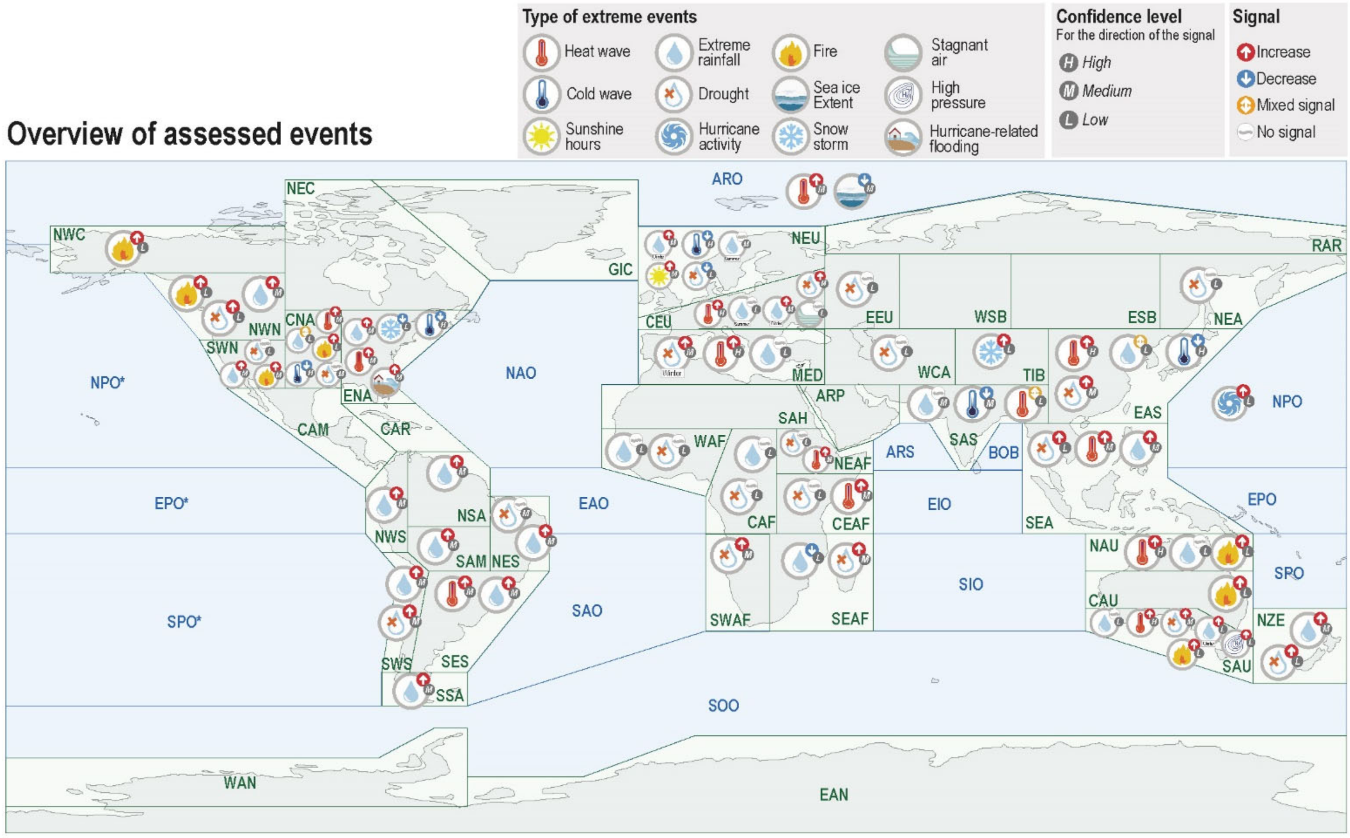

Figure 11.2: Synthesis of event attribution literature. The symbols depict types of extreme events for which one or more such events have been studied in the event attribution framework (see Appendix Table 11.A.1). The location of symbols does not indicate the places of the event occurrence as the symbols represent the synthesized assessment of all studies for the same type of events occurring in the region. The arrows indicate the direction of changes in the intensity and likelihood of the events due to anthropogenic climate change. A "mixed signal" indicates that different studies found different results regarding the direction of changes in magnitude and frequency, depending on the definition of the event (Section 11.2.5).

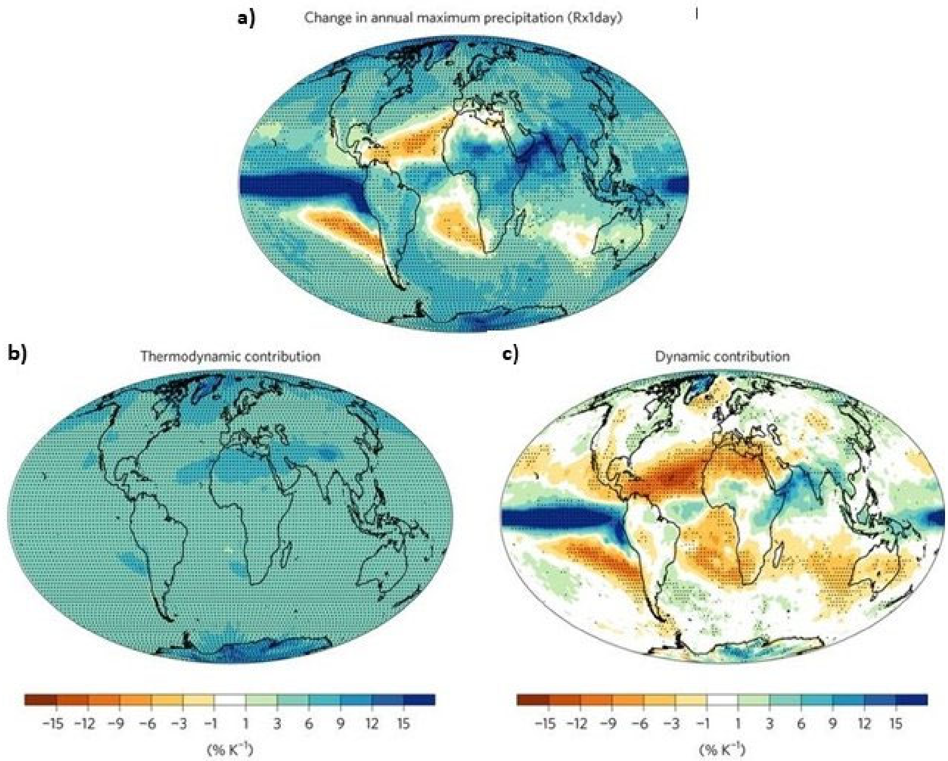

Box 11.1, Figure 1: Multi-model mean fractional changes in % per degree of warming for (a) annual maximum precipitation (Rx1day), (b) thermodynamic contributions and (c) dynamic contributions estimated using the difference between full changes and changes in thermodynamic contributions. Changes were derived from a linear regression for the period 1950–2100. Stippling indicates that at least 80% of the models agree on the sign of the signal. A more detailed description of the estimation of dynamic and thermodynamic contributions is given in Pfahl et al. (2017).

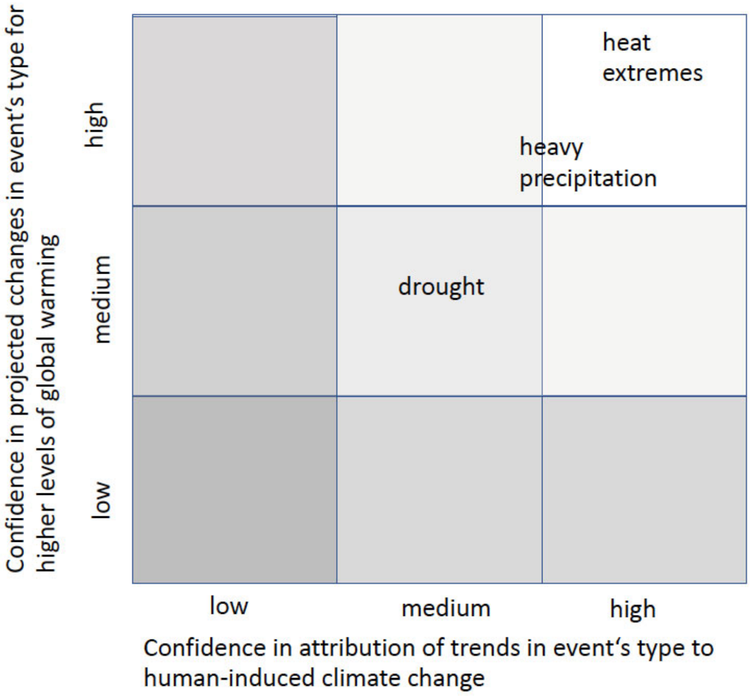

Idea: 1 symbol per extreme
Distinguish between:
*response at 1.5, 2 and 4?
*response on global scale vs regional scale

Figure 11.3: Synthesis of confidence in attribution of extremes vs confidence in projection of extremes

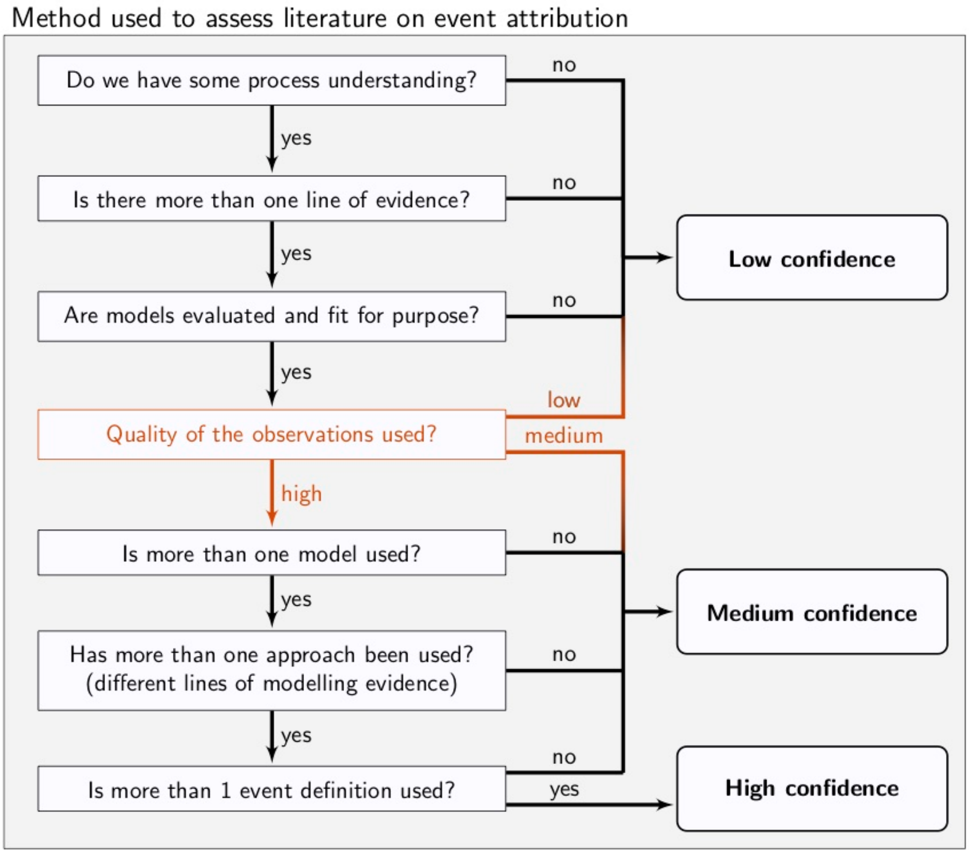

Figure 11.4: Flowchart, adapted from (Otto et al., submitted), depicting the assessment process to identify the quality of evidence in attribution studies and illustrating the different decision steps when assing the quality of evidence.

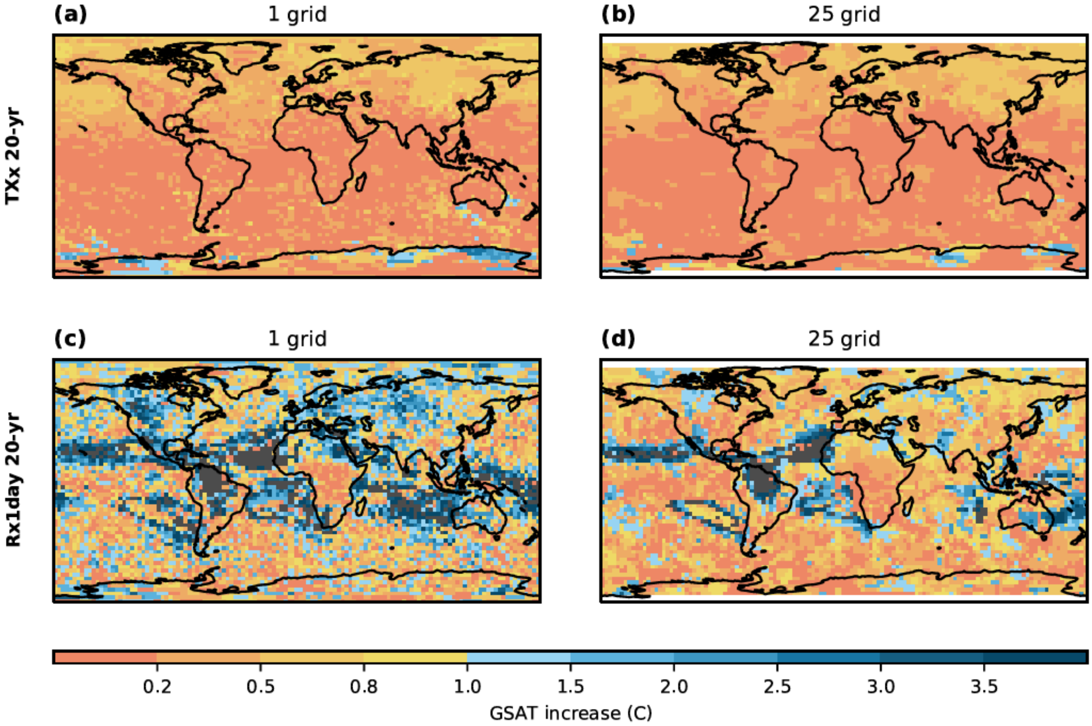

Figure 11.5: Global warming level (°C) for the emergence of a robust increase in the probability of extremes attributable to anthropogenic forcing. The temperature displayed is from the 10-year period when the lower bound (5th percentile) of the risk ratio for 20-year TXx (a,b) and Rx1day (c,d) events first exceeds 1.0 and remains above 1.0 for all subsequent periods. The first column calculates extremes from each grid box, while the second column first calculates the mean of the surrounding 25 grid boxes (5 x 5) to represent larger-scale extremes. A perfect-model approach was used with the CanESM2 large ensemble and areas in grey indicate emergence did not occur before +4.7 °C. Adapted from Kirchmeier-Young et al. (2019).

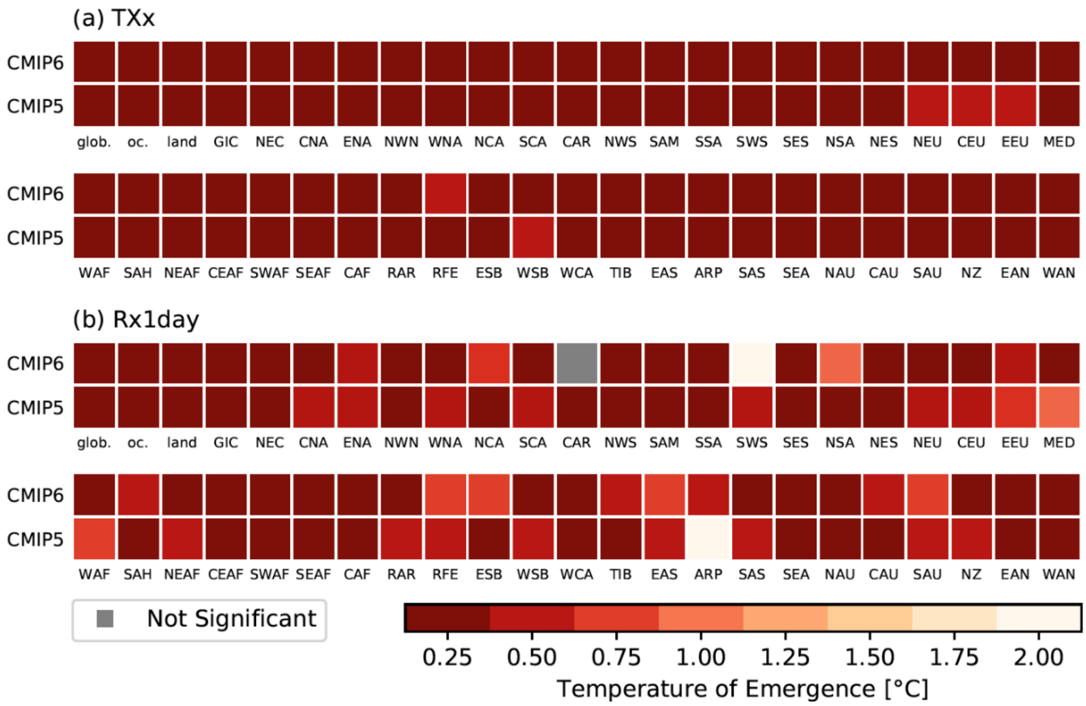

Figure 11.6: Regional-scale analysis of the global mean temperature of emergence for temperature extremes and precipitation extremes based on the CMIP5 and CMIP6 ensembles. For definition of regions, see Atlas [adapted from Seneviratne and Hauser (submitted)], for a detection compared to pre-industrial time rather than late 20th century conditions].

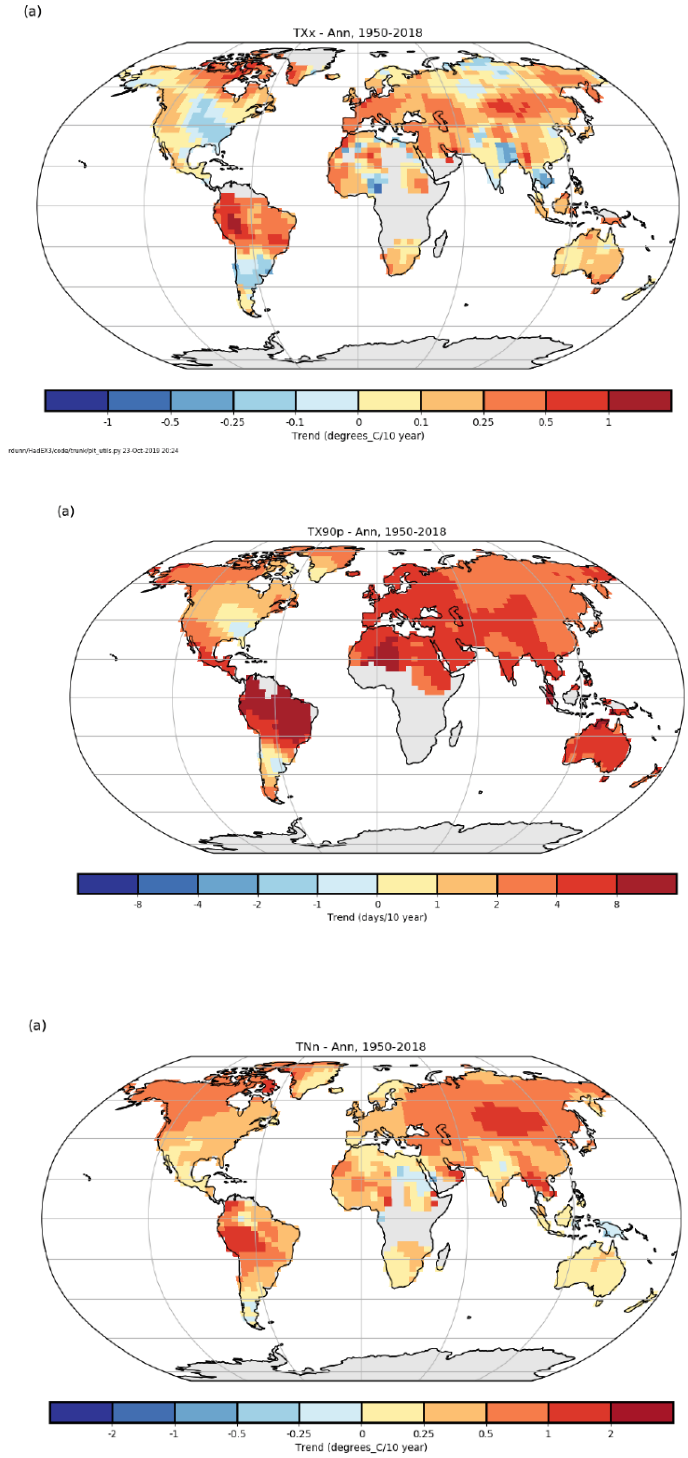

Figure 11.7: Linear trends over 1950-2018 in the annual maximum daily maximum temperature (TXx, top), the annual number of days when daily maximum temperature exceeds its 90th percentile during a base period 1961-1990 (TX90p, middle), and the annual minimum daily minimum temperature (TNn, bottom) based on the HadEX3 data set. Units are °C/decade for TXx and TNn and days/decade fir TX90p. HadEX3 is gridded product at 2.5° latitude x 3.75 ° longitude resolution. Linear trends are calculated only for grids with at least 66% annual values over the period. Areas without sufficient data are shown in grey. (adapted from Dunn et al. submitted)

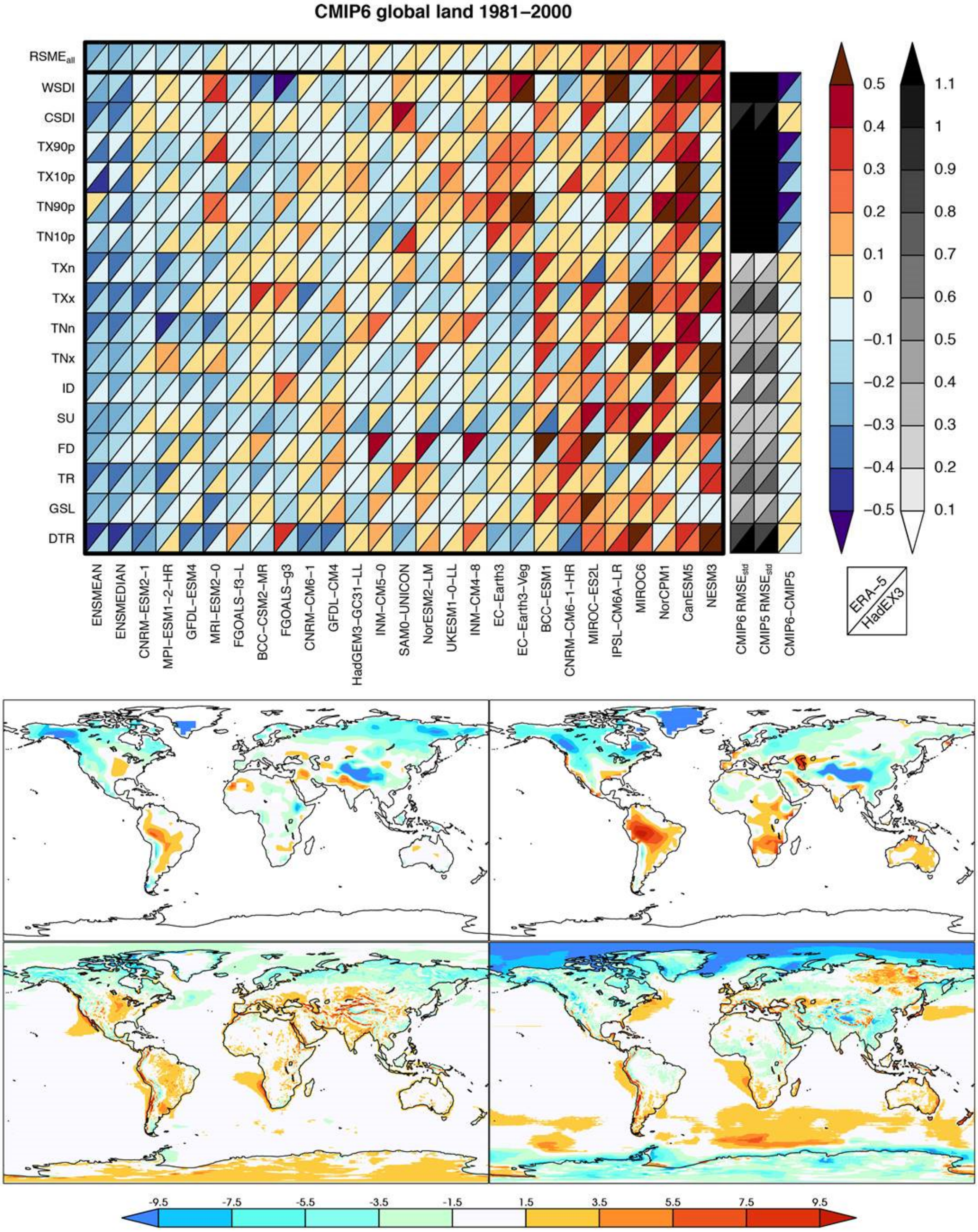

Figure 11.8: Top panel: A portrait diagram of relative spatially averaged root mean square errors (RMSEs) in the 1981–2000 climatologies of temperature indices simulated by the CMIP6 models with respect to the ERA-5 reanalysis (upper triangle), and HadEX3 (right triangle). The RMSEs are spatially averaged over global land 531 grid points. The top row indicates the mean relative RMSE across all indices for a particular model. The grey-shaded columns and blue-red columns on the right side indicates the standardized median RMSEmedian,std for CMIP6 and CMIP5 and their differences. Adapted from Kim et al., (submitted). Middle panel: Difference between CMIP6 multi-model average and ERA5 in their respective averages over 1979-2014. Bottom panel: Difference between CMIP6 multi-model average and HadEX3 in their respective averages over 1979-2014. The left in both middle and bottom panels is for TXx and the right for TNn. Unit is °C. Adapted from Kim et al., (submitted), Li et al., (submitted) and

Wehner et al., (submitted).

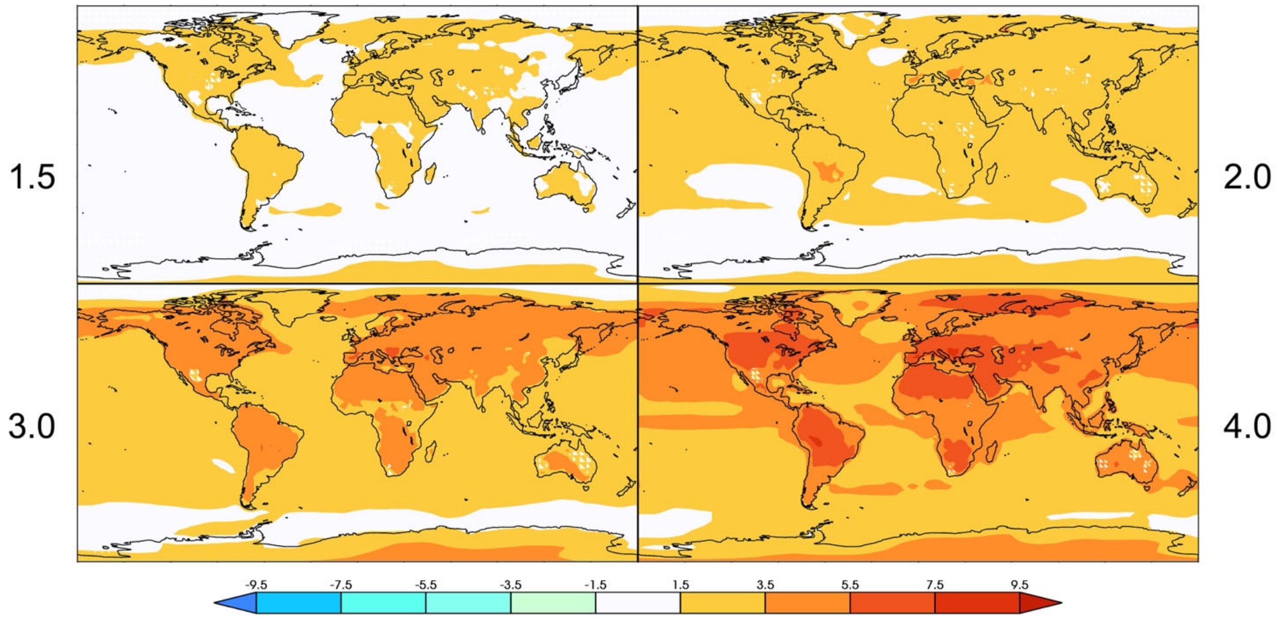

Figure 11.9: Projected changes (°C) in annual maximum daily maximum temperature (TXx) at 1.5°C, 2°C, 3°C, and 4°C of global warming compared to the early-industrial baseline (1851-1900), based on simulations by 21 CMIP5 and 11 CMIP6 models. Stippling indicates where the multi-model average change is larger than the across-model standard deviation (Note to reviewers: stippling scheme will be changed in the FGD to be consistent with other chapters, maps will be updated if additional simulations from CMIP6 models become available).

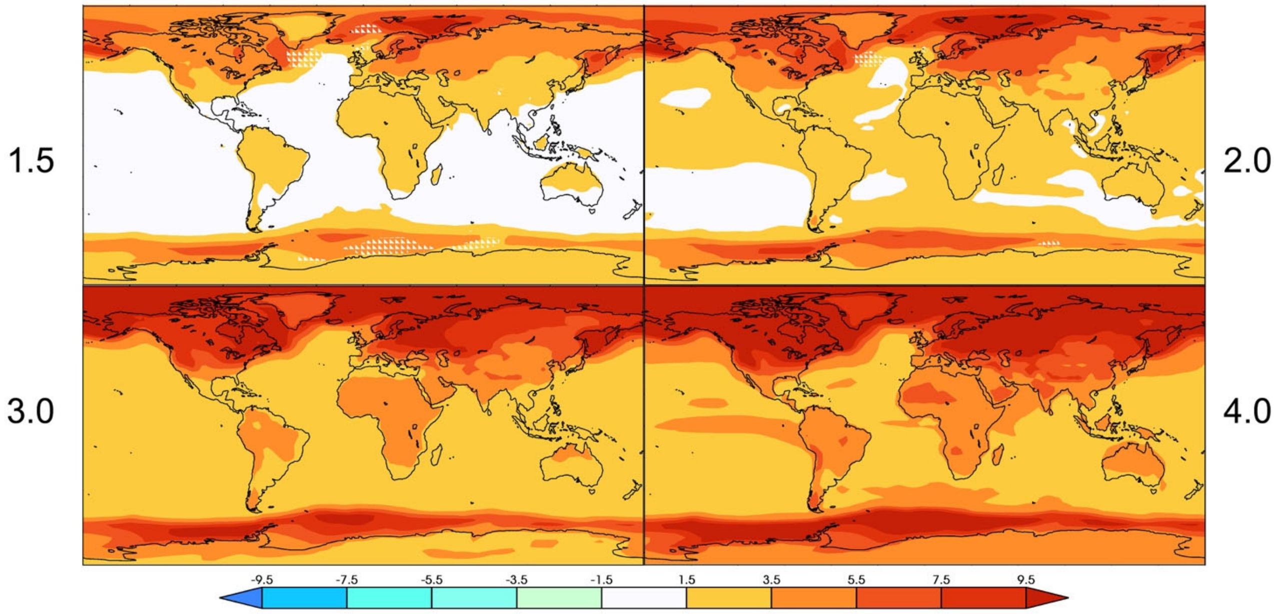

Figure 11.10: Projected changes (°C) in annual minimum daily minimum temperature (TNn) at 1.5°C, 2°C, 3°C, and 4°C of global warming compared to the early-industrial baseline (1851-1900), based on simulations by 21 CMIP5 and 11 CMIP6 models. Stippling indicates where the multi-model average change is larger than the across-model standard deviation (Note to reviewers: stippling scheme will be changed in the FGD to be consistent with other chapters, maps will be updated if additional simulations from CMIP6 models become available).

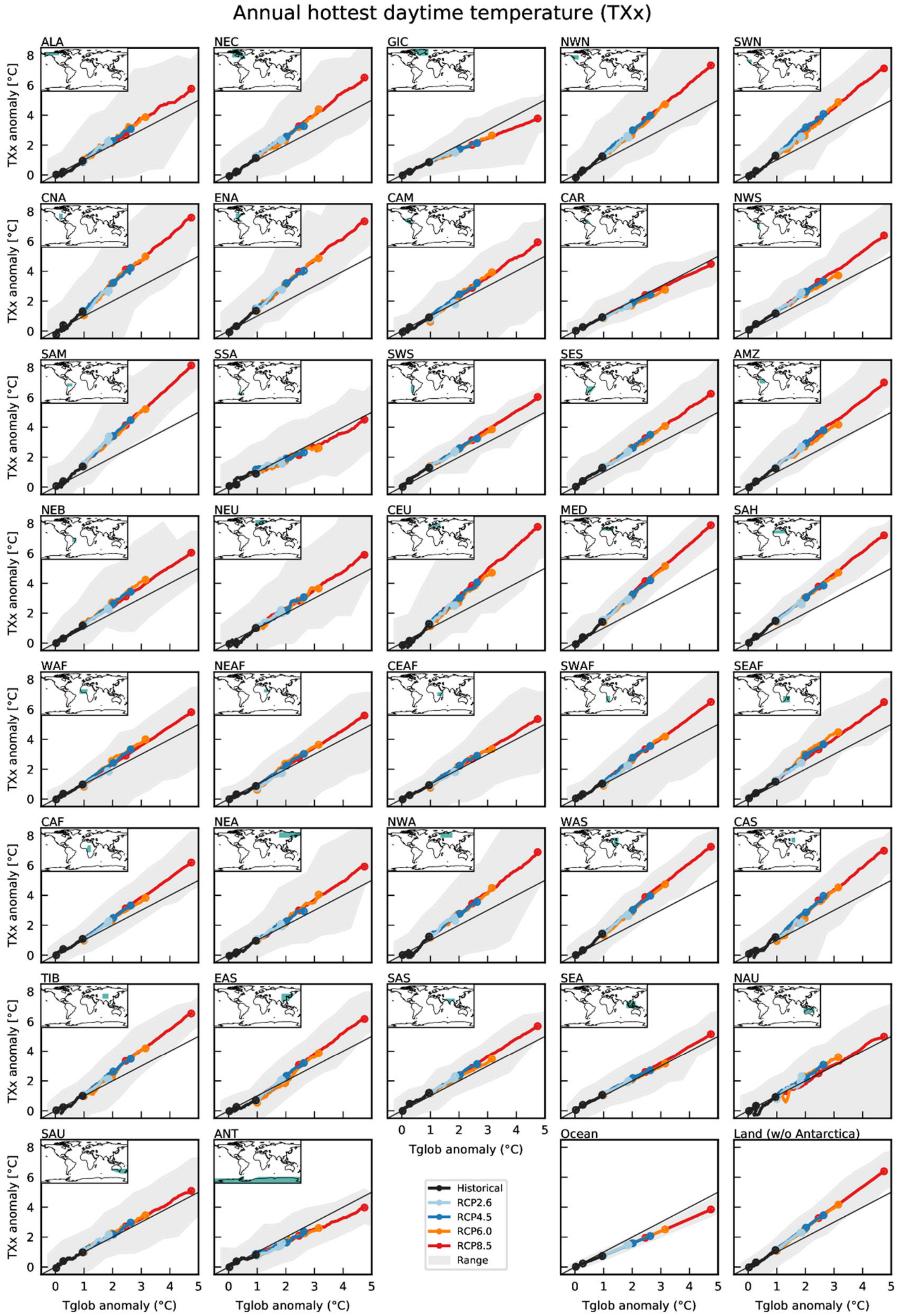

Figure 11.11: Regional mean changes in annual maximum daily temperature (TXx) for land regions, the global land and global ocean, against changes in global mean surface temperature (Tglob) as simulated by CMIP5 models for historical conditions (black) and under different forcing scenarios including RCP2.6 (light blue), RCP4.5 (blue), RCP6.0 (light red), and (red) RCP8.5. The black line indicates the 1:1 reference scaling. The grey shading indicates the range over all RCPs. [Note to reviewers: the plot will be updated to include CMIP6 simulations for the FGD, as well as the final selected AR6 regions].

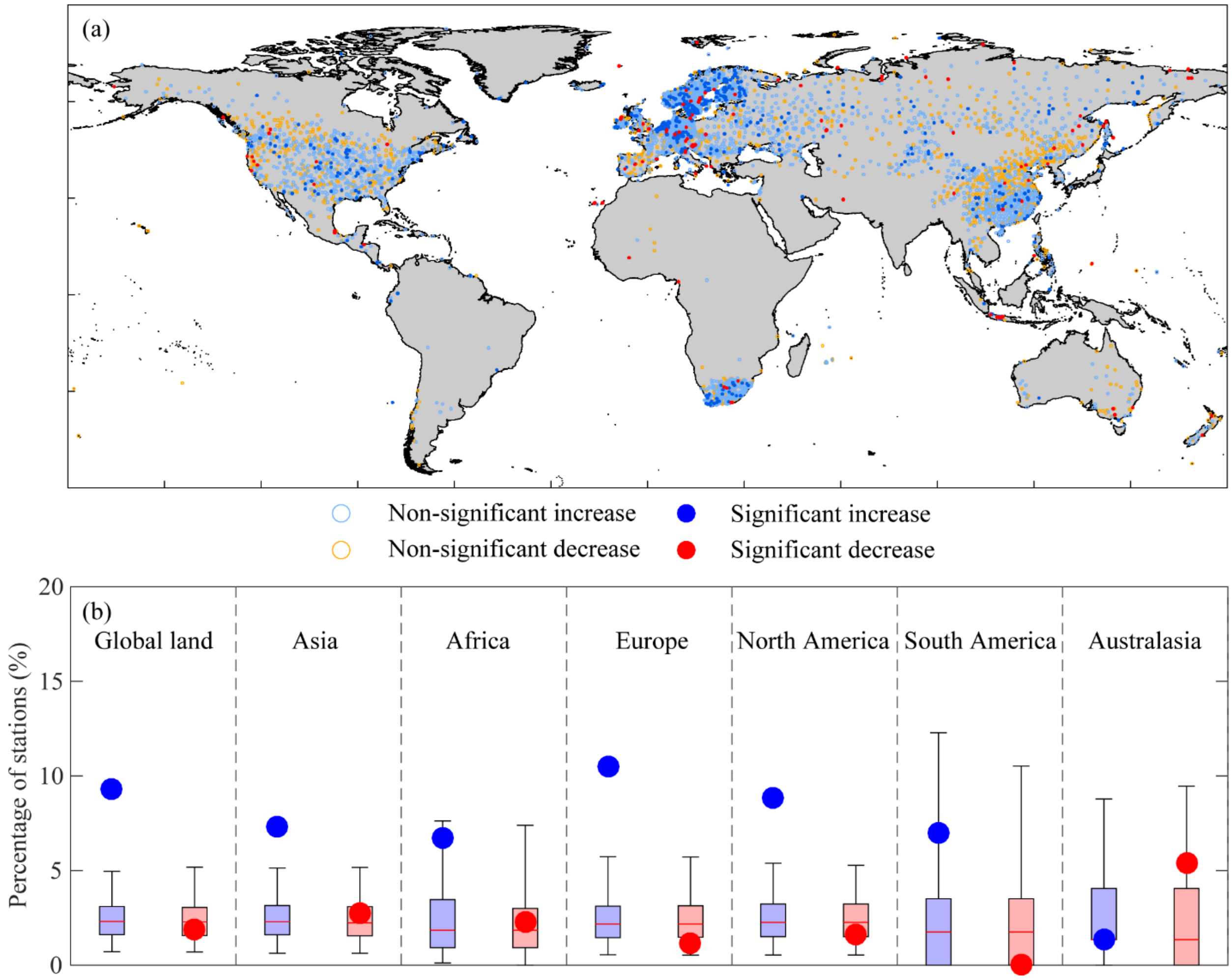

Figure 11.12: (a) Trends in annual maximum amount of one-day precipitation (Rx1day) during 1950–2018 at 8345 stations with sufficient data for the calculate data to estimate. Light blue dots indicate increases and light red dots mark decreases. Solid blue and red dots indicate statistically significant increases and decreases, respectively, as determined by a two-tailed test conducted at the 5% level. (b) Summary statistics of the percentage of stations with statistically significant trends in Rx1day in the observations during the same period and in 1000 bootstrap samples. The blue and red colors indicate significant positive and negative trends, respectively, in the observations. Box-and-whisker plots summarize the breadth of the distribution from 1000 bootstrap realizations under the no-trend null hypothesis. In the plots, the upper and lower edges of the boxes mark the 25th and the 75th percentiles and the red lines indicate the median values. The upper and lower whiskers show the 97.5th and the 2.5th percentiles, respectively. Adapted from (Sun et al., submitted).

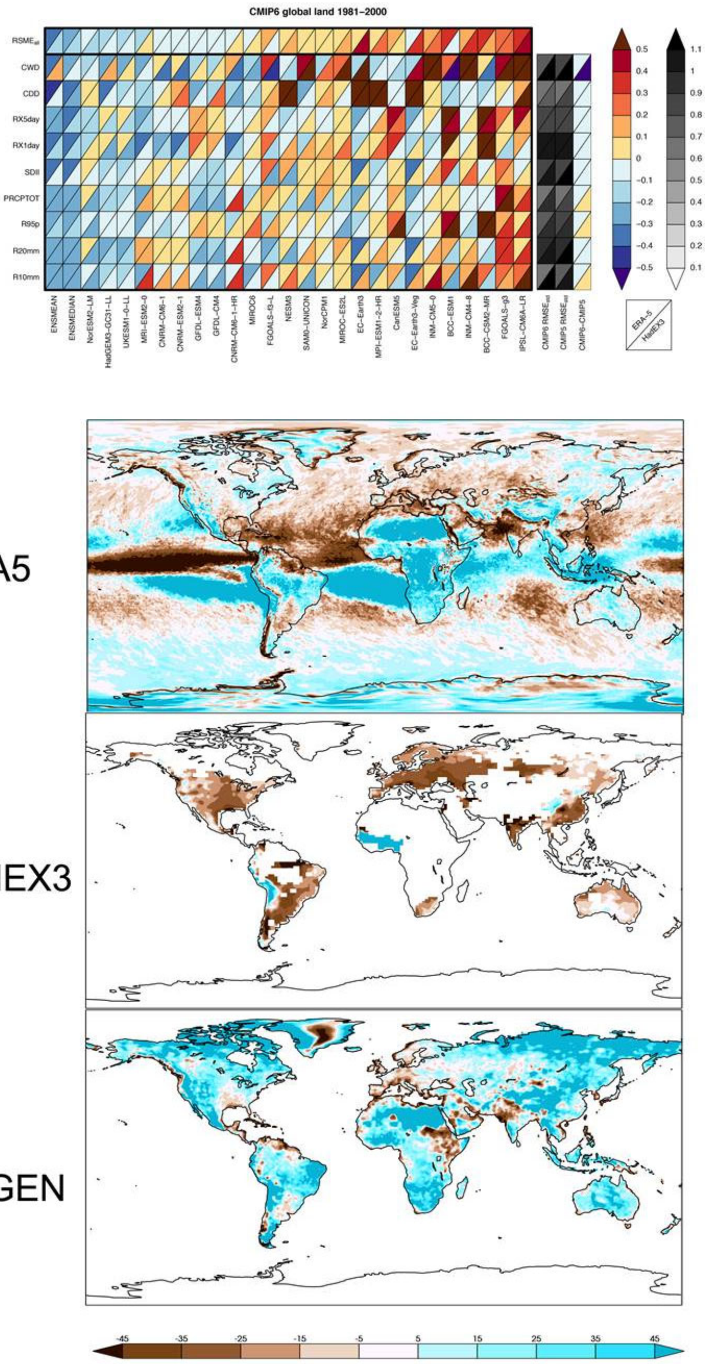

Figure 11.13: Top panel (matrix): A portrait diagram of relative spatially averaged root mean square errors (RMSEs) in the 1981–2000 climatologies of precipitation indices simulated by the CMIP6 models with respect to the ERA-5 reanalysis (upper triangle), and HadEX3 (right triangle). The RMSEs are spatially averaged over global land 531 grid points. The top row indicates the mean relative RMSE across all indices for a particular model. The grey-shaded columns and blue-red columns on the right side indicates the standardized median RMSEmedian,std for CMIP6 and CMIP5 and their differences. Adapted from Kim et al., (submitted). Other panels (maps): Percent errors in the CMIP6 multimodel mean Rx1day (1979-2014) relative to ERA5 (top), HadEX3 (middle) and REGEN (bottom). Brown indicate that models are too dry, while blue indicates that they are too wet. Adapted from Kim et al., (submitted), Li et al., (submitted) and Wehner et al., (submitted). (top), HadEX3 (middle), and REGEN (bottom)

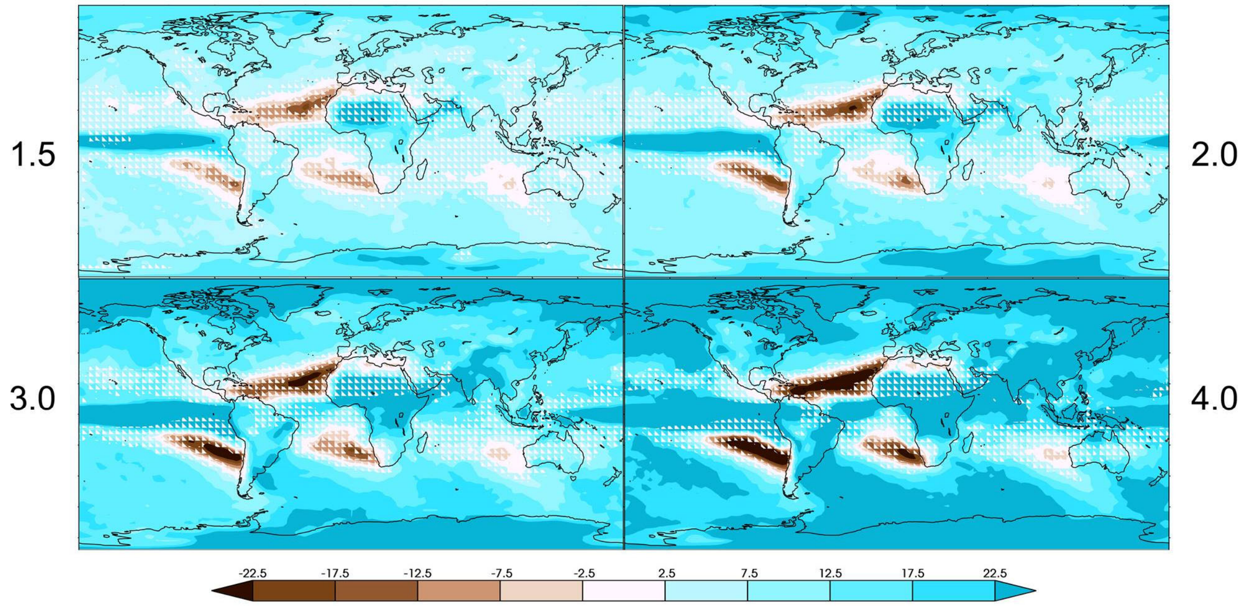

Figure 11.14: Projected percentage changes (%) in annual maximum one-day precipitation at 1.5°C, 2°C, 3°C, and 4°C of global warming compared to the early-industrial baseline (1851-1900), based on simulations by 21 CMIP5 and 11 CMIP6 models. Stippling indicates where the multi-model average change is larger than the across-model standard deviation (Note to reviewers: stippling scheme will be changed in the FGD to be consistent with other chapters, maps will be updated if additional simulations from CMIP6 models become available)

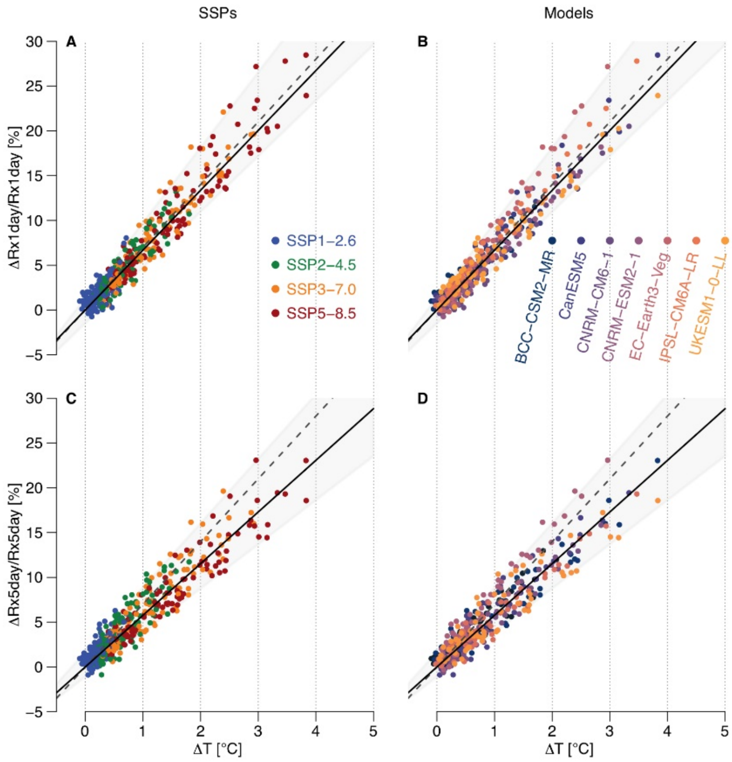

Figure 11.15: Global land median changes in the 50-year return values of annual maximum 1-day precipitation (Rx1day; A-B) and 5-day precipitation (Rx5day; C-D) against changes in global annual mean surface air temperature (GMST) in the CMIP6 multi-model ensemble projections under different future forcing scenarios. At each land grid cell, the corresponding return values are first estimated in each of the six overlapping 30-year periods (i.e., 2021-2050, 2031-2060, …, 2071-2100) for each model and forcing scenario. Then the global land median relative changes in the estimated return values from one period to a later period and the corresponding GMST changes are plotted as scatter points, with these scatter points marked according to forcing scenarios (A and C) or climate models (B and C). The black solid lines mark the median regression lines of the scatter points, while the grey shading bounds the 5-95% regression lines of the scatter points. The black dashed lines show the 7% per °C (CC-scaling rate) reference line. Adapted from (Li et al., submitted).

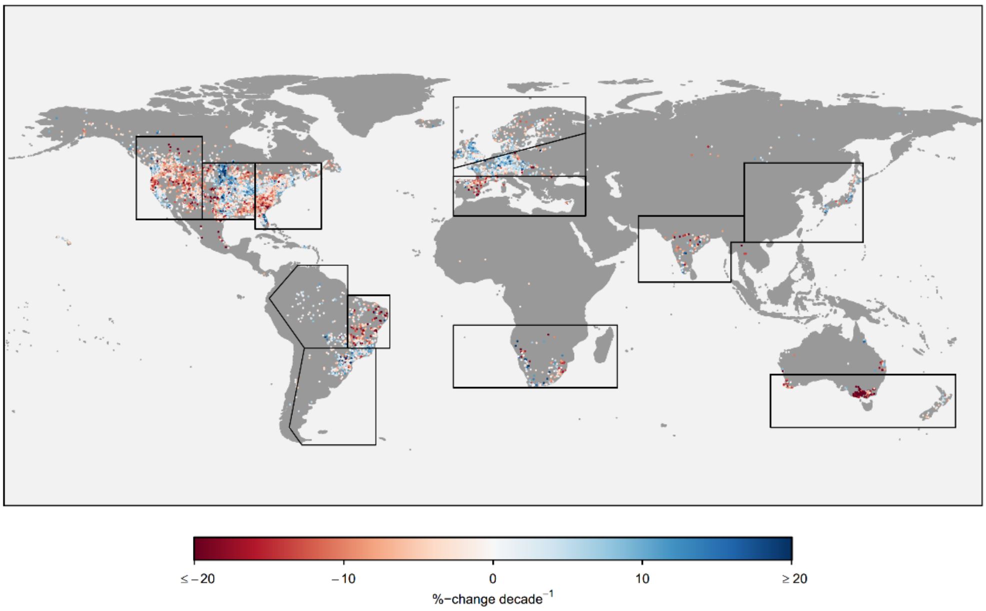

Figure 11.16: Trends in annual maximum daily streamflow during 1971-2010 for SREX regions with at least 50 streamflow gauge stations with sufficient data (from Gudmundsson et al. 2019).

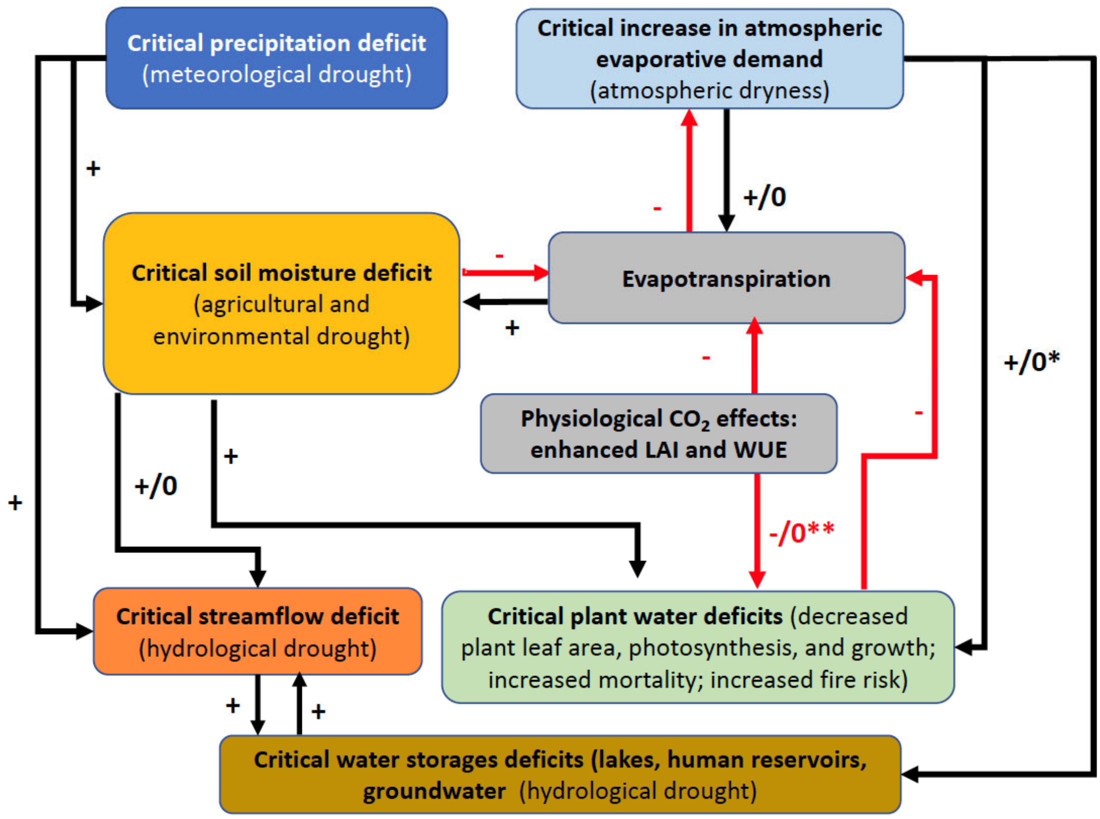

Figure 11.17: Sketch of processes and drivers related to different drought types. Note that all relationships are indicated under the dry range of the given variable and may not apply to humid conditions (e.g. impacts of soil moisture on evapotranspiration). The asterisk (*) denotes that under conditions of critical soil moisture deficits, plant water deficits are generally critically affected by high levels of atmospheric evaporative demand (only a + relationship); however the effects can be limited outside the growing season and under humid soil moisture but dry atmospheric conditions (see text for details). The double asterisk (**) denotes that under critical soil moisture deficits CO_2 effects on plant water savings can be limited as evidenced by experimental studies in which water and CO_2 effects are controlled (see text for details).

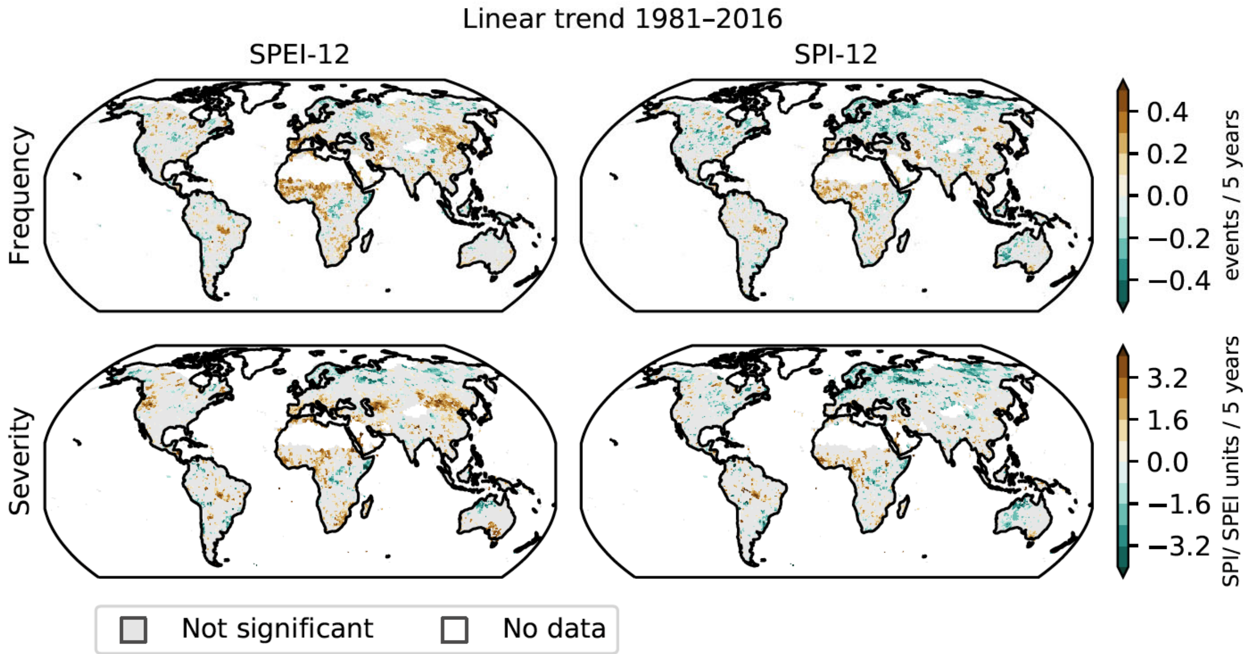

Figure 11.18: Observed trends in drought severity and frequency obtained from 3-month SPEI and SPI based on Global Precipitation Climatology Centre (GPCC) precipitation using the Climate Research Unit (CRU) Epot datasets from 1981 to 2016. The threshold to identify drought episodes was set at -1 SPI/SPEI units, which represents 20% of probability (1 event in 5 years). Based on (Spinoni et al., 2019).

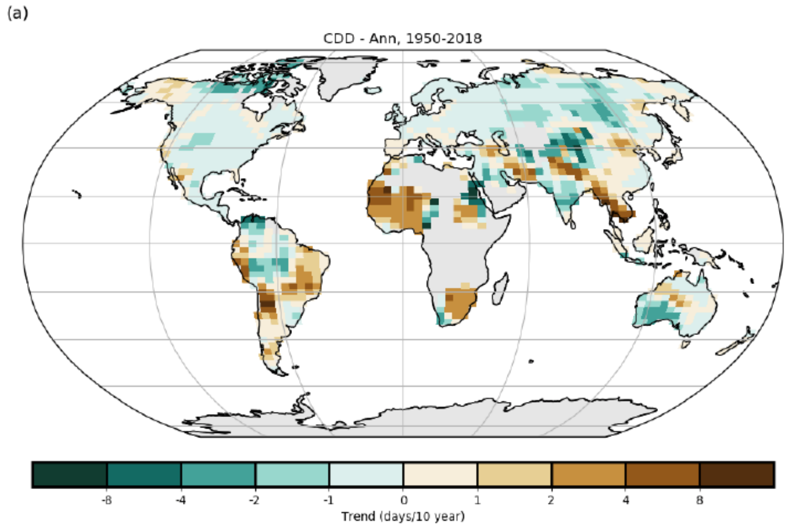

Figure 11.19: Observed linear trend over 1951-2018 in the annual consecutive dry days (CDD) from the most recent HadEX3 data set. Units: days/decade. (from Dunn et al., submitted)

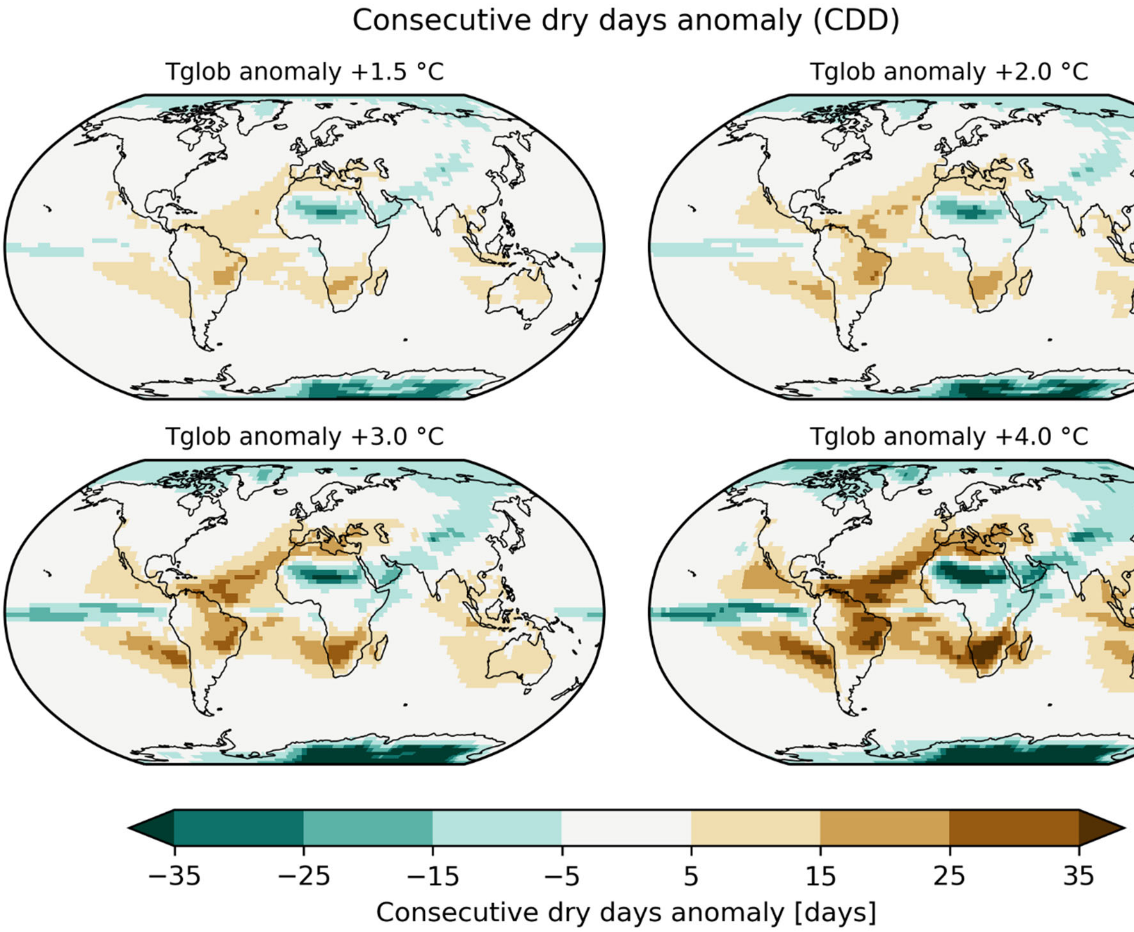

Figure 11.20: Projected changes in Consecutive Dry Days for projections at 1.5°C, 2°C, 3°C and 4°C of global warming compared to pre-industrial conditions (1850-1900), using empirical scaling relationship based on transient CMIP6 simulations. [Stippling will be added for FGD]

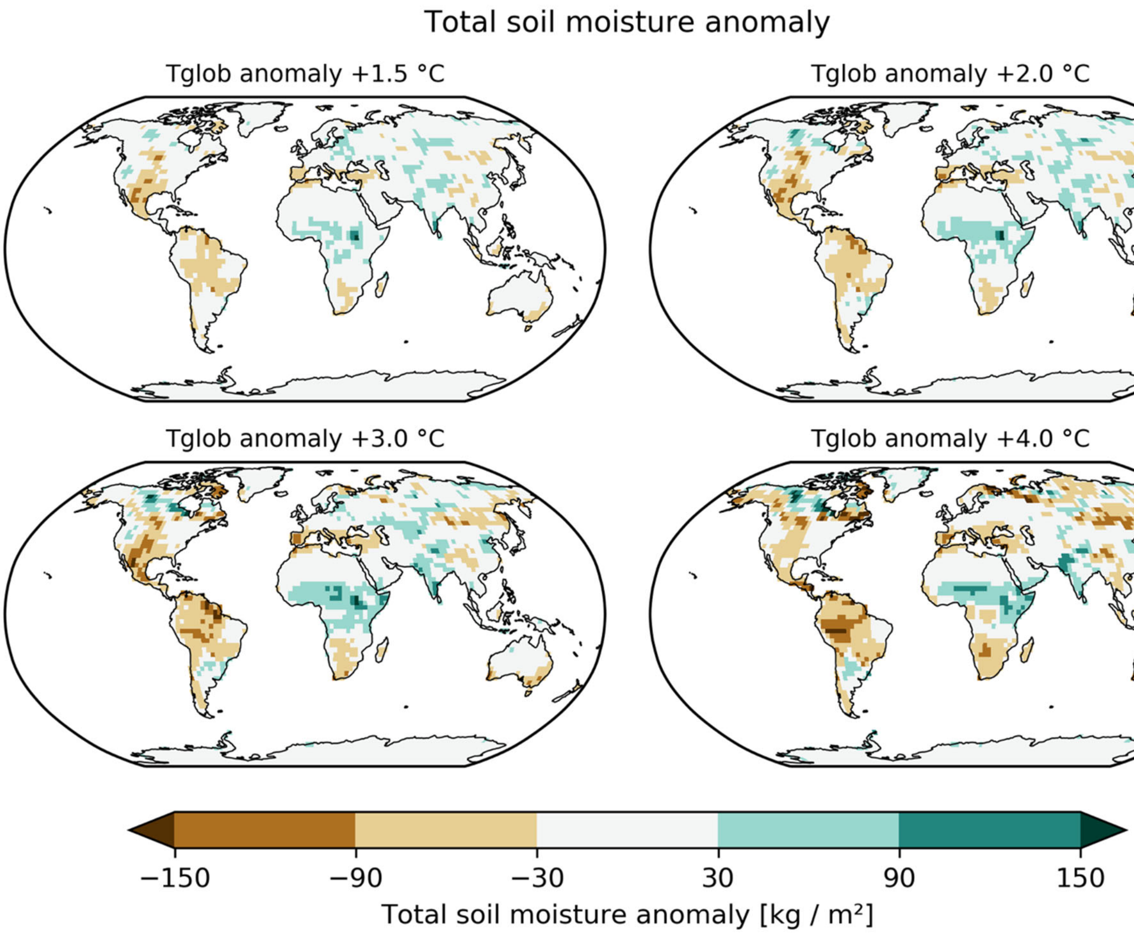

Figure 11.21: Projected changes in surface soil moisture for projections at 1.5°C, 2°C, 3°C and 4°C of global warming compared to pre-industrial conditions (1850-1900), using empirical scaling relationship based on transient CMIP6 simulations. [Stippling will be added for FGD]

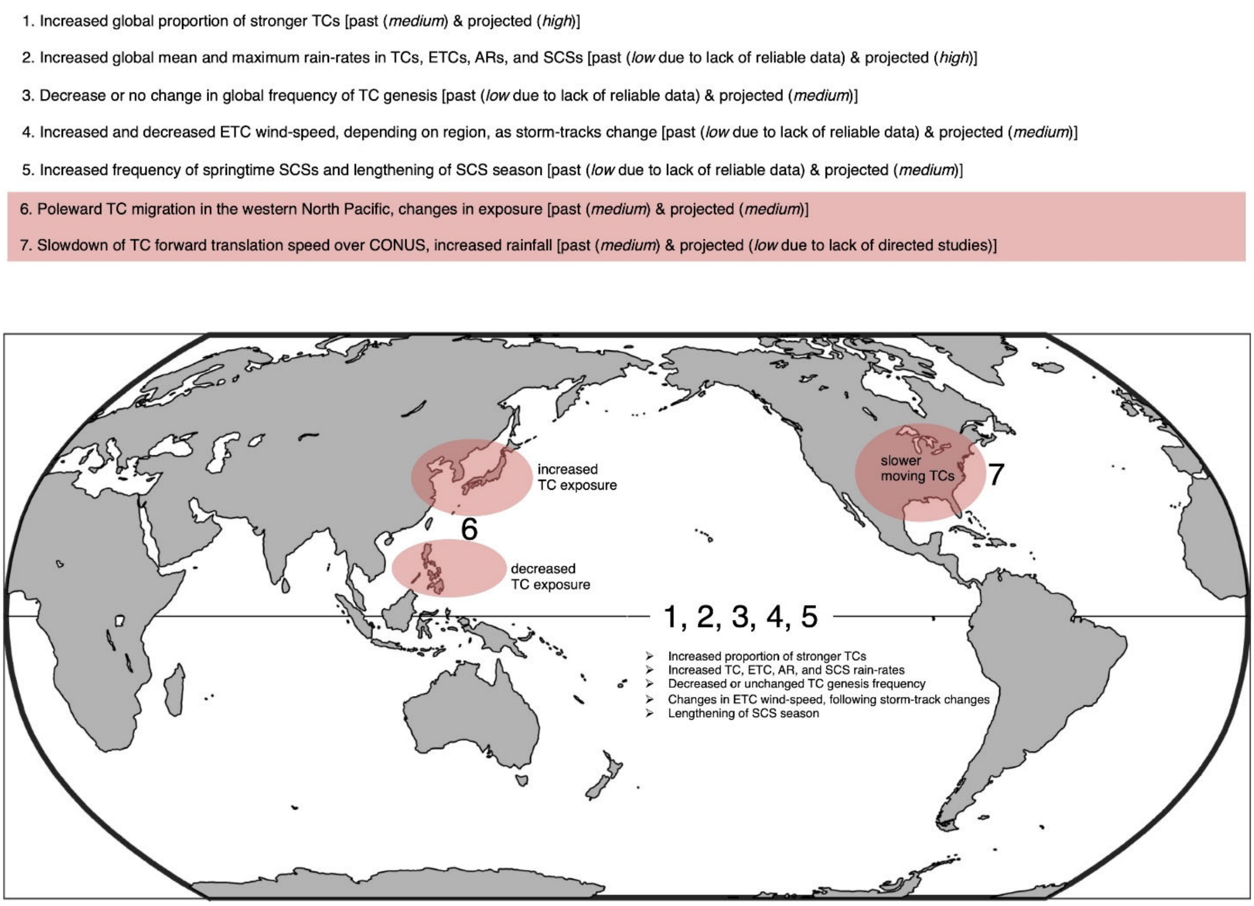

Figure 11.22: Summary schematic of past and projected changes in tropical cyclone (TC), extra-tropical cyclone (ETC), atmospheric river (AR), and severe convective storm (SCS) behaviour and their associated confidence levels. Changes are shown at the global scale (statements 1–5) and regional scale (statements 6, 7).

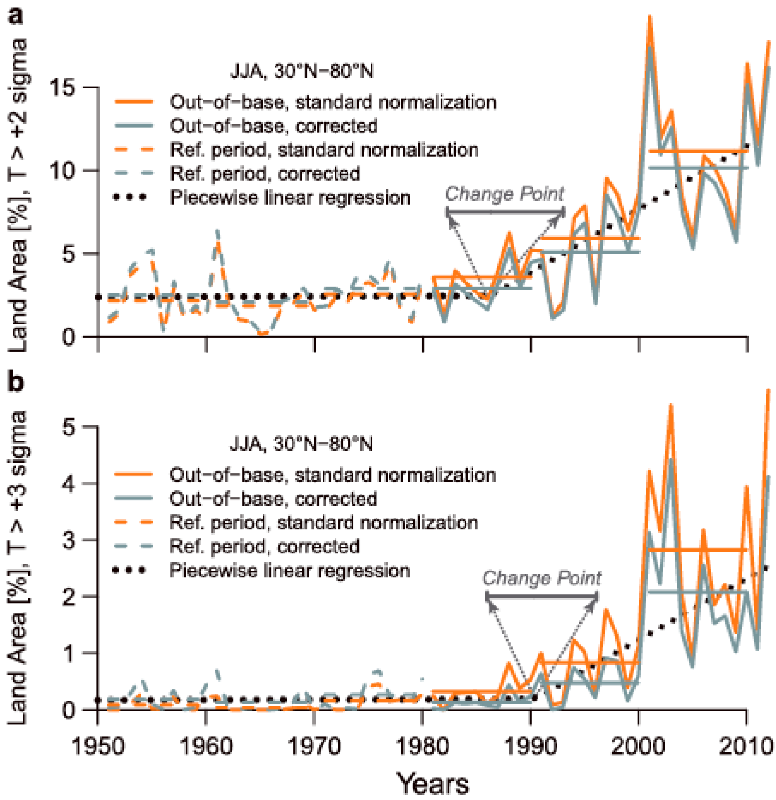

Box 11.3, Figure 1: Analysis of the percentage of land area affected by temperature extremes larger than a) two or b) three standard deviations in June-July-August (JJA) between 30°N and 80°N using an approach using a standard normalization (orange) and a corrected normalization (grey). The more appropriate estimate is the corrected normalization. These panels show for both estimates a substantial increase in the overal land area affected by very high hot extremes since 1990 onward. From Sippel et al.

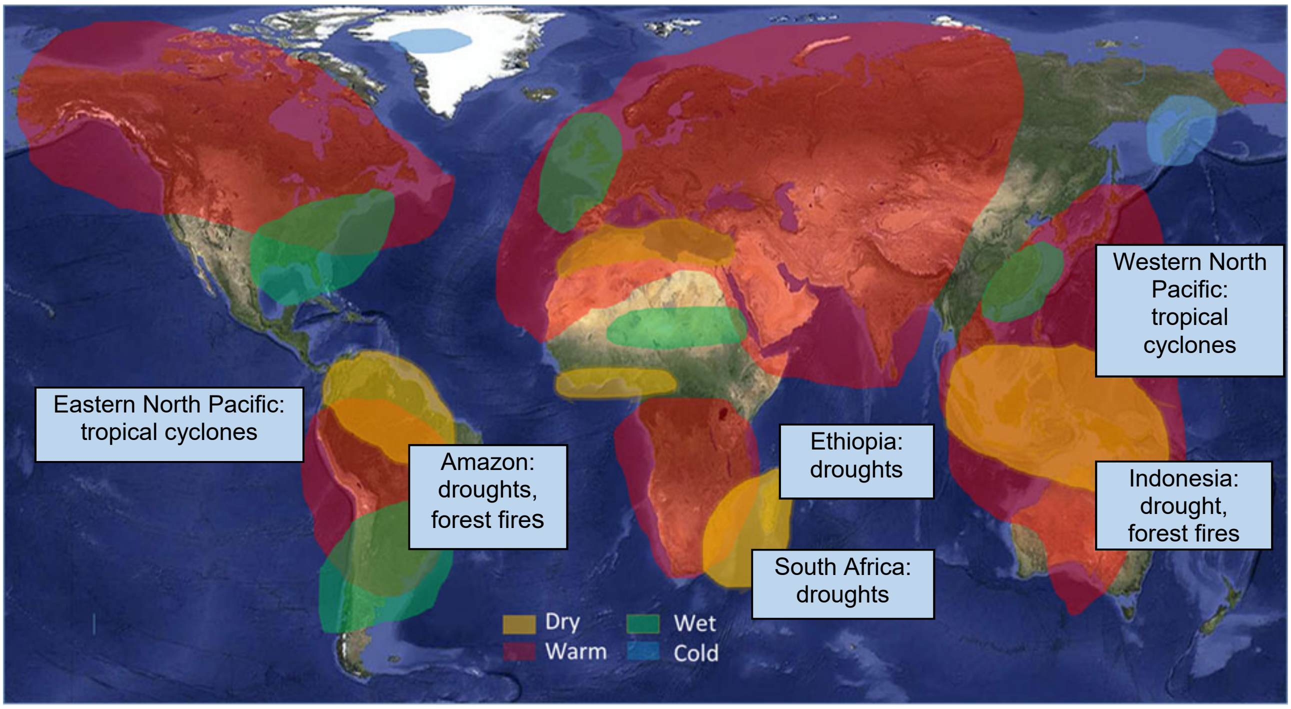

Box 11.3, Figure 2: Geographical distribution of notable climate anomalies and events occurring around the world in 2015. The warm/cold/dry/wet categories are defined according to precipitation and temperature anomalies for the period DJF 2015/2016 which coincides with the highest magnitude of ENSO.

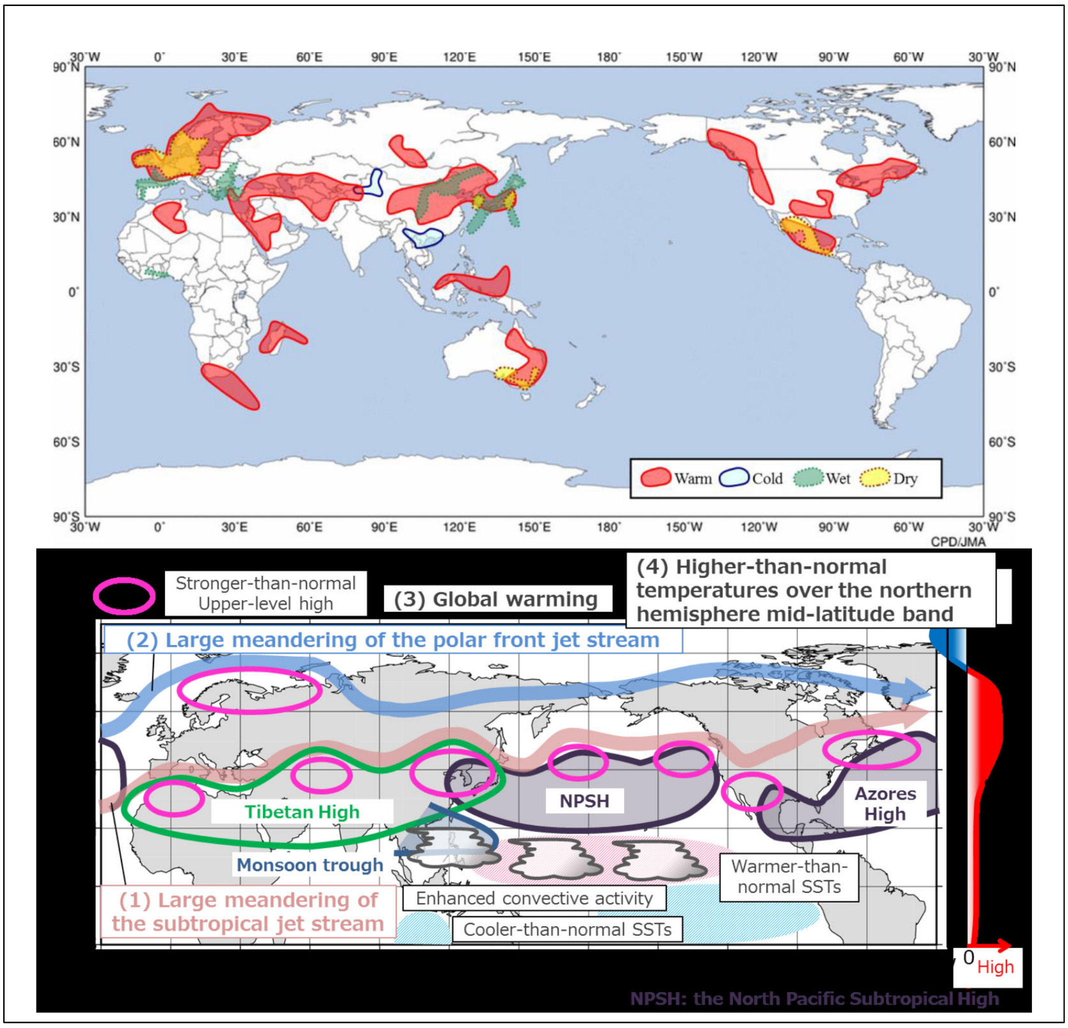

Box 11.3, Figure 3: Global extreme climate events in July 2018 (Japan Meteorological Agency, 2018). This figure shows overlaid climate extremes (warm, cold, wet and dry) from weekly reports for July 2018. [FGD PLACEHOLDER: WILL INCLUDE AN UPDATED FIGURE PROVIDING ANOMALIES OVER THE WHOLE DURATION OF THE EVENT, I.E. AT LEAST MAY-AUGUST 2018]

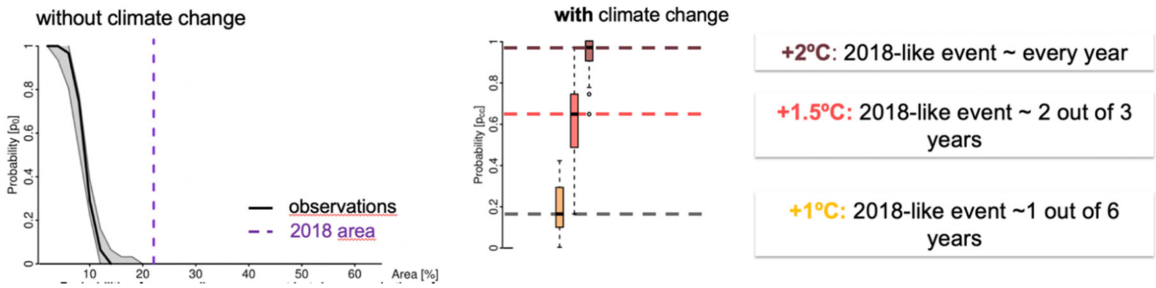

Box 11.3, Figure 4: (left) Probabilities for exceeding concurrent hot day areas in the reference period 1958–1988 (p_0) for the multimodel ensemble (gray range) and observations (black line). The 2018 area is highlighted by a purple vertical dashed line in each subpanel. (right) CMIP5-based multi-model range of probabilities for exceeding concurrent hot days areas experienced in May-July 2018 for global warming of +1°C (orange), +1.5°C (red) and +2°C (dark red) with respect to 1870-1900. From Vogel et al. (2019).

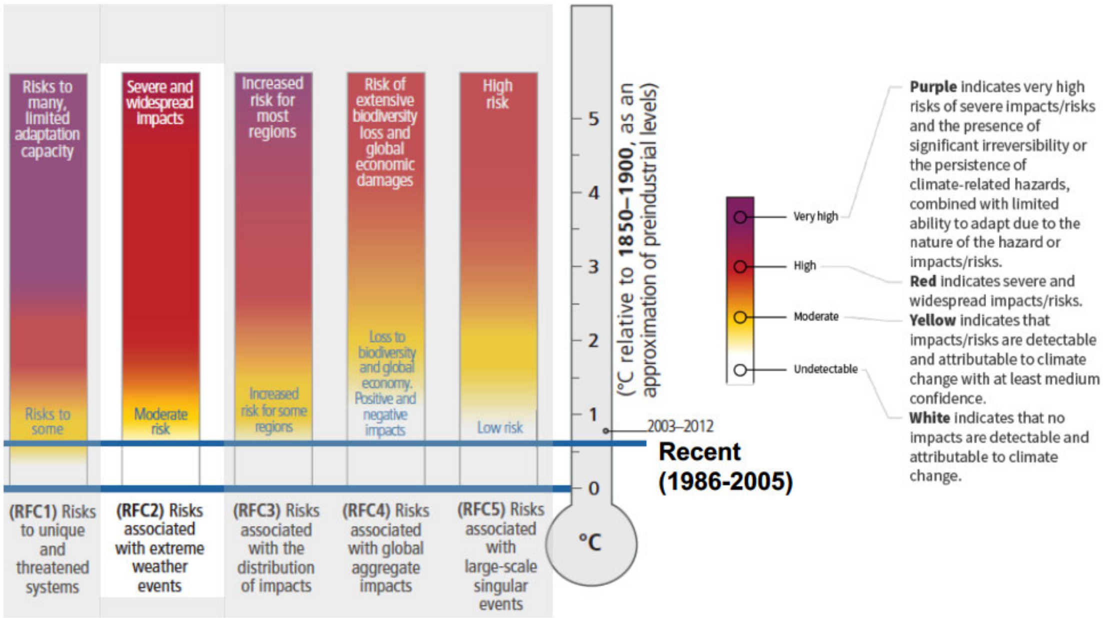

Box 11.4, Figure 1:“Reasons for concerns” (RFCs), highlighting RFC2 on “Risks associated with extreme weather events. From Oppenheimer, M. et al (2014), IPCC AR5 WG2).

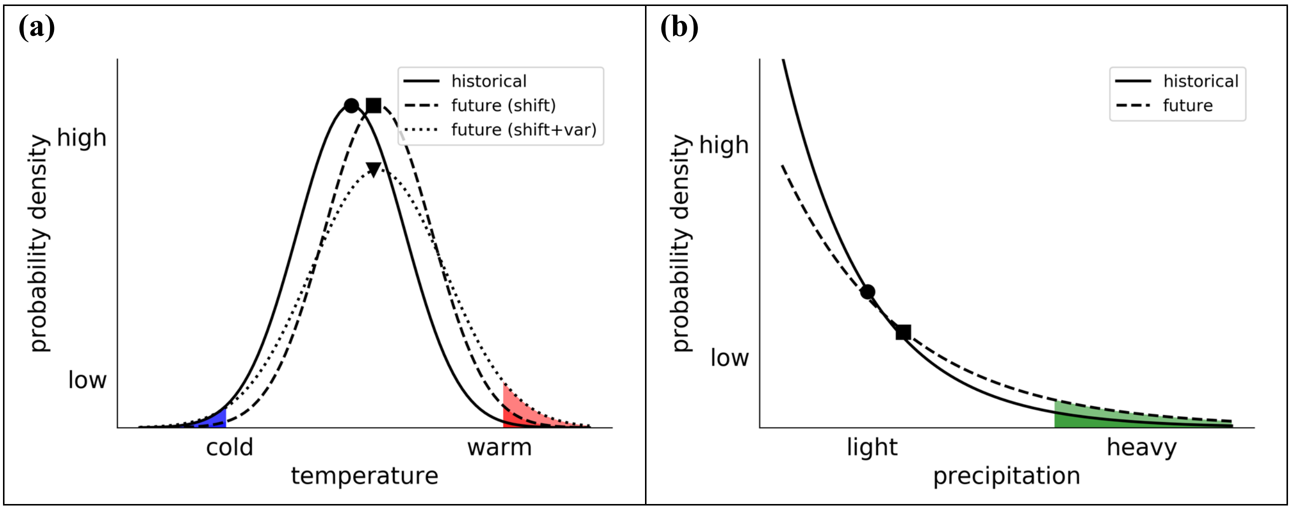

FAQ 11.1, Figure 1: Schematic representations of the probability density function of (a) daily temperature, which tends to be approximately Gaussian, and (b) daily precipitation, which has a skewed distribution. Solid lines represent a previous (historical) distribution and dashed lines a changed (future) distribution. The probability of occurrence, or frequency, of extremes is denoted by the shaded areas. In the case of temperature (red and blue shade), changes in the frequencies of extremes can be affected either by changes only in the mean, or average (shift) or in both the mean and the variance, or shape (shift+var). For example, the wider distribution of the shift+var case means that both cold and warm extremes are more common relative to the average than in the historical or future (shift) cases. But combined with the increase in average, this increase in variability means a higher probability of extremely warm temperatures compared to the future (shift) case, where the variability does not increase. Similarly, in a skewed distribution such as that of precipitation (green shaded), a change in the mean of the distribution generally affects its variability or spread, and thus an increase in mean precipitation would also imply an increase in heavy precipitation extremes, and vice-versa. In addition, the shape of the right-hand tail could also change, affecting extremes. Furthermore, climate change may alter the frequency of precipitation and the duration of dry spells between precipitation events. (Parts a–c modified from Folland et al., 2001, and modified from Peterson et al., 2008, as in Zhang and Zwiers, 2012.)

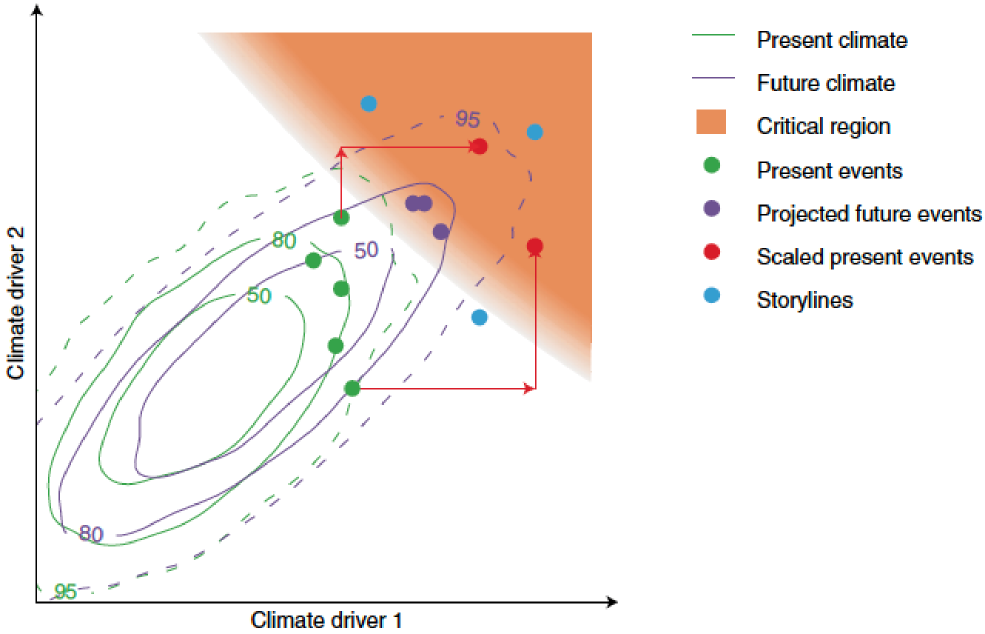

FAQ 11.2, Figure 1.: Illustration of enhanced risks associated with compound events (from Zscheischler et al., 2018b), The hypothetical present-day distribution of two climatic drivers and their potential future distribution, together with a critical region in which impacts are induced. Continuous lines depict the 50th and 80th percentiles, dashed lines denote the 95th percentiles. The coloured points denote different possibilities to generate potentially critical events. The critical region is shown in orange with a blurred border to illustrate uncertainty in the estimation of its extent. The critical region can only be known if enough critical events have occurred (or can be simulated) to characterize it. This figure illustrates that climate change is modifying the envelope of the distribution of climate extremes we have at the moment, which possibly could yield new unprecedented extremes which are within some "critical region" in which new impacts could happen.

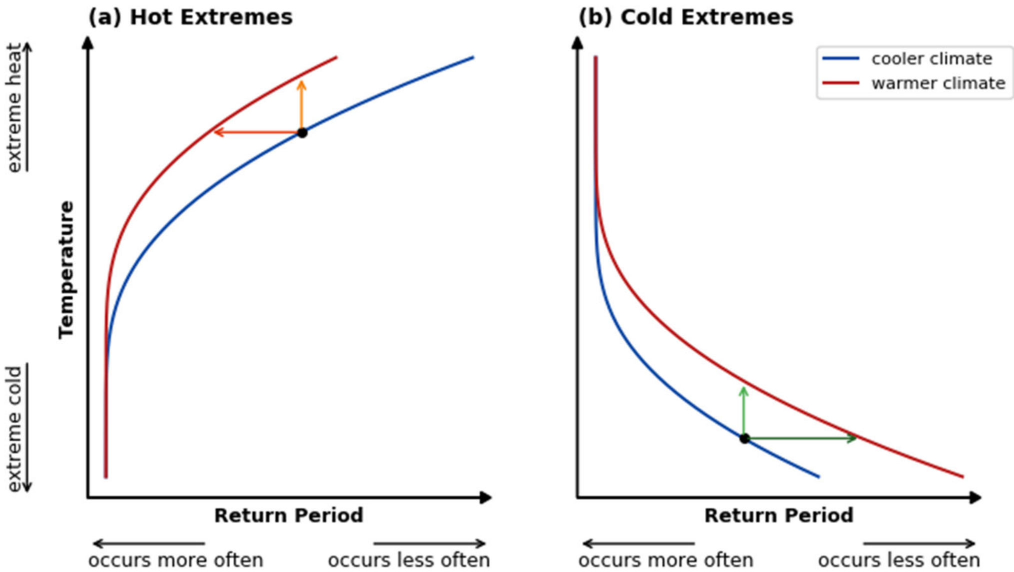

FAQ 11.3, Figure 1: Examples of how temperature extremes differ in cooler and warmer climates. Changes in extreme events can be thought of as either changes in the frequency of events of a given magnitude or as changes in the magnitude of events that occur at the same frequency. These two concepts are closely related, as illustrated in this example for (a) hot extremes and (b) cold extremes. The vertical axis shows the range of extreme temperatures on a logarithmic scale, while the horizontal axis shows the estimated average time between events, referred to as the return period of an event. In a warmer climate, extreme hot events of the same magnitude occur more frequently (that is, the return period for a given temperature decreases) and cooler events occur less frequently (return period increases) as indicated by the horizontal arrows between curves. If we look at events of a fixed rarity (constant return period), we see that in a warmer climate, both hot and cold extreme temperature events of a given return period are warmer (vertical arrows), although not necessarily by the same amount.

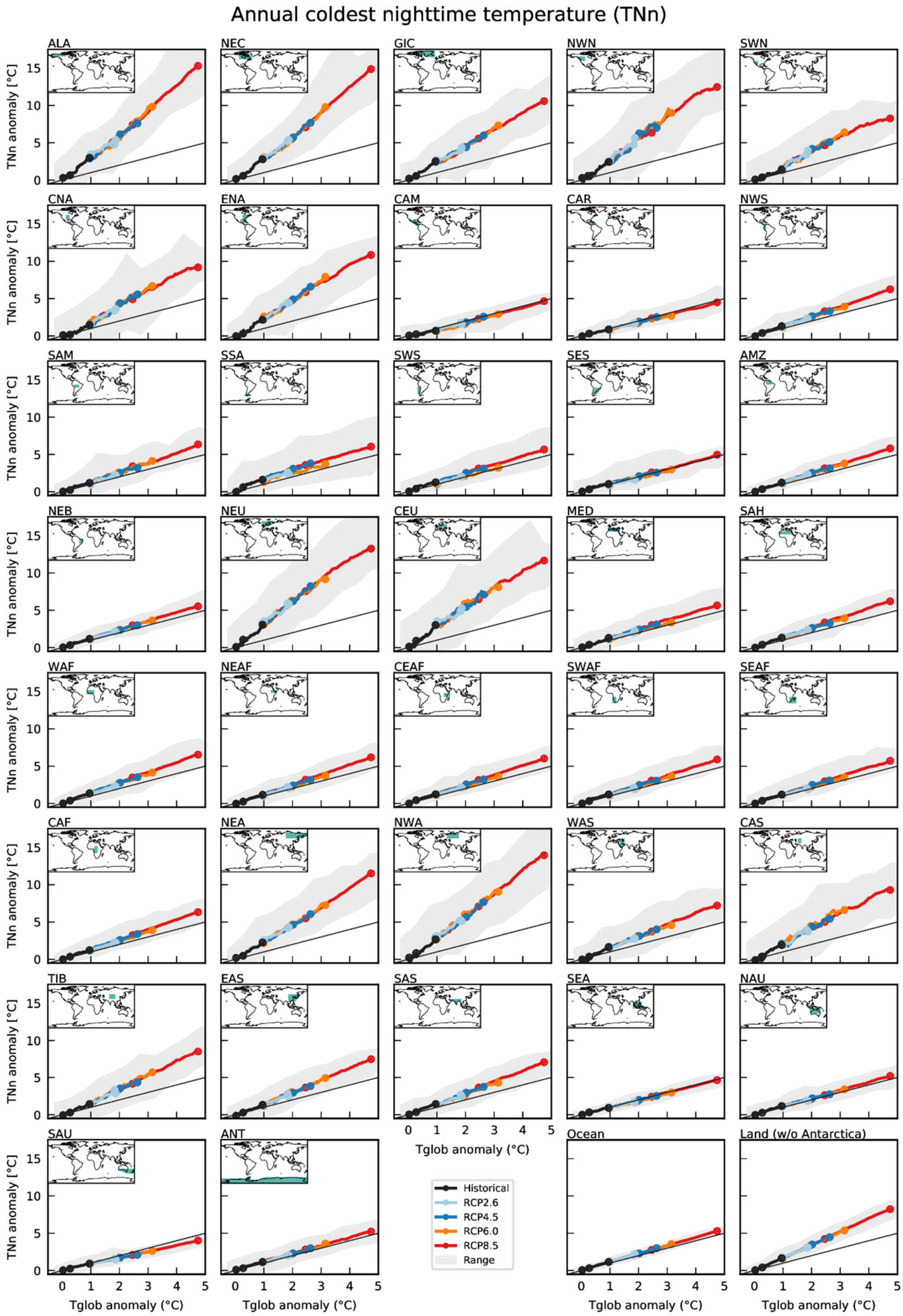

Figure 11.A.1.: Regional mean changes in annual minimum nighttime temperature (TNn) for land regions, the global land and global ocean, against changes in global mean surface temperature (Tglob) as simulated by CMIP5 models for historical conditions (black) and different forcing scenarios including RCP2.6 (light blue), RCP4.5 (blue), RCP6.0 (light red), and (red) RCP8.5. The black line indicates the 1:1 reference scaling. The grey shading indicates the range over all RCPs. [Note to reviewers: the figure will be updated to include CMIP6 simulations for the FGD, as well as the final selected AR6 regions].

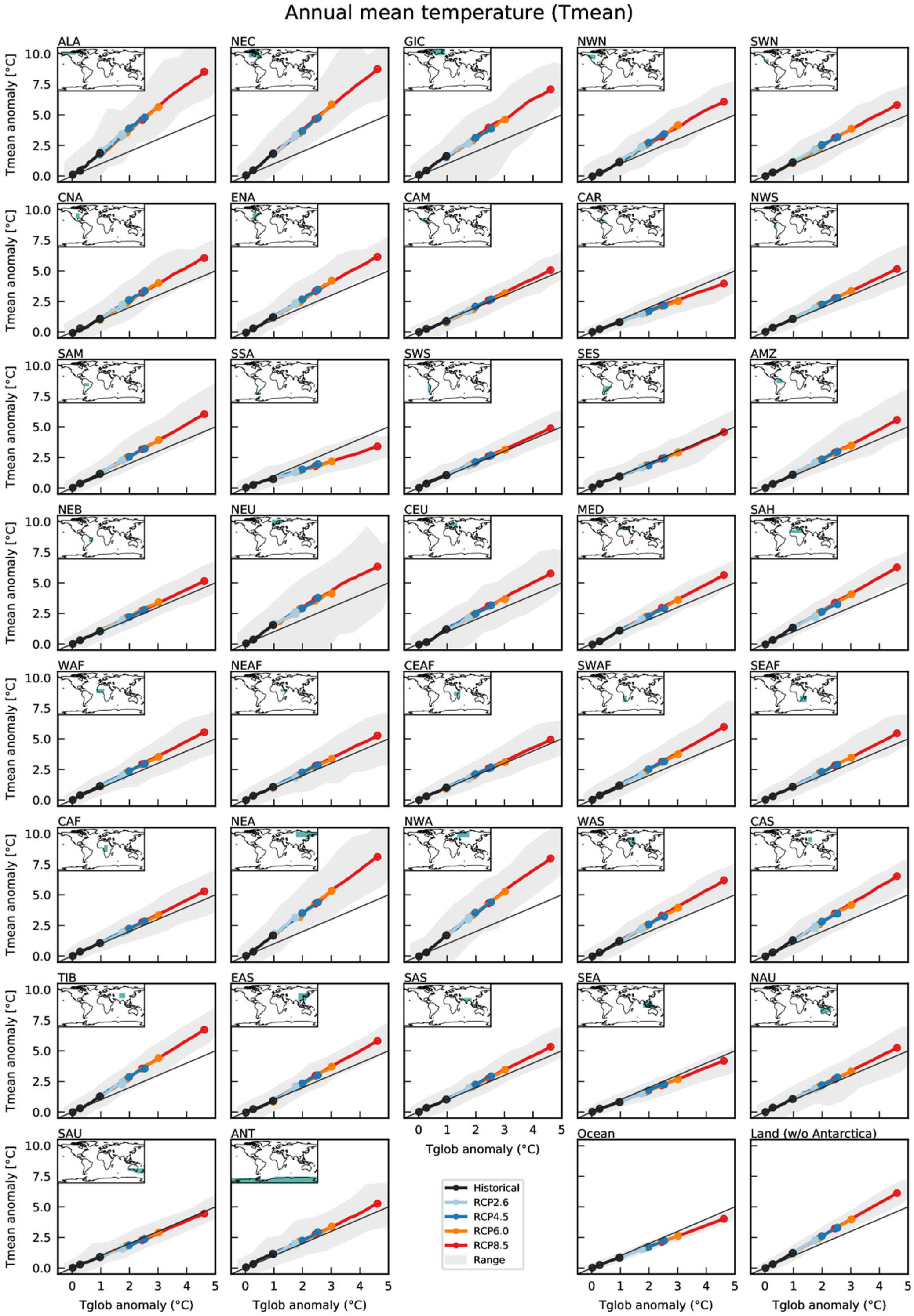

Figure 11.A.2.: Regional mean changes in regional mean warming (Tmean) for land regions, the global land and global ocean, against changes in global mean surface temperature (Tglob) as simulated by CMIP5 models for historical conditions (black) and different forcing scenarios including RCP2.6 (light blue), RCP4.5 (blue), RCP6.0 (light red), and (red) RCP8.5. The black line indicates the 1:1 reference scaling. The grey shading indicates the range over all RCPs. [Note to reviewers: the figure will be updated to include CMIP6 simulations for the FGD, as well as the final selected AR6 regions].